

# Landslide modelling & applications : proceedings of the 5th Regional Symposium on Landslides in the Adriatic-Balkan Region

---

**Edited book / Urednička knjiga**

*Publication status / Verzija rada:* **Published version / Objavljena verzija rada (izdavačev PDF)**

*Publication year / Godina izdavanja:* **2022**

*Permanent link / Trajna poveznica:* <https://urn.nsk.hr/urn:nbn:hr:169:271422>

*Rights / Prava:* [In copyright](#) / [Zaštićeno autorskim pravom.](#)

*Download date / Datum preuzimanja:* **2024-07-26**



*Repository / Repozitorij:*

[Faculty of Mining, Geology and Petroleum Engineering Repository, University of Zagreb](#)

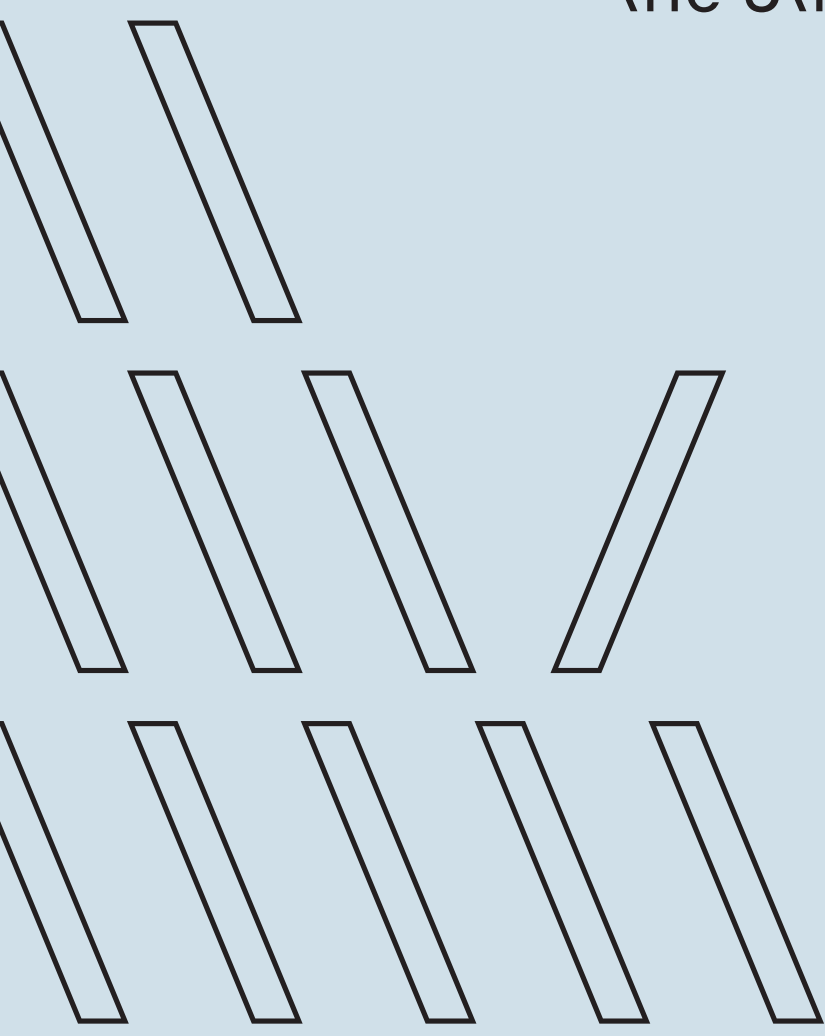


Re /  
Sy //  
LAB /—

5TH REGIONAL SYMPOSIUM ON LANDSLIDES  
IN ADRIATIC-BALKAN REGION

# Landslide Modelling & Applications

Proceedings of  
the 5th ReSyLAB



## **Editors**

Josip Peranić  
Martina Vivoda Prodan  
Sanja Bernat Gazibara  
Martin Krkač  
Snježana Mihalić Arbanas  
Željko Arbanas

---

# Landslide Modelling & Applications



---

Josip Peranić • Martina Vivoda Prodan  
Sanja Bernat Gazibara • Martin Krkač  
Snježana Mihalić Arbanas • Željko Arbanas  
Editors

# Landslide Modelling & Applications

Proceedings of the  
5<sup>th</sup> Regional Symposium on Landslides  
in the Adriatic-Balkan Region

**Croatian Landslide Group**

University of Rijeka, Faculty of Civil Engineering

University of Zagreb, Faculty of Mining, Geology and Petroleum  
Engineering

Under the sponsorship of International Consortium on Landslides  
(ICL)

---

### Symposium Chairs

Željko Arbanas  
University of Rijeka, Faculty of Civil Engineering, Rijeka,  
Croatia

Snježana Mihalić Arbanas  
University of Zagreb, Faculty of Mining, Geology and  
Petroleum Engineering, Zagreb, Croatia

### Editors

Josip Peranić  
University of Rijeka, Faculty of Civil Engineering, Rijeka,  
Croatia

Martina Vivoda Prodan  
University of Rijeka, Faculty of Civil Engineering, Rijeka,  
Croatia

Sanja Bernat Gazibara  
University of Zagreb, Faculty of Mining, Geology and  
Petroleum Engineering, Zagreb, Croatia

Martin Krkač  
University of Zagreb, Faculty of Mining, Geology and  
Petroleum Engineering, Zagreb, Croatia

Snježana Mihalić Arbanas  
University of Zagreb, Faculty of Mining, Geology and  
Petroleum Engineering, Zagreb, Croatia

Željko Arbanas  
University of Rijeka, Faculty of Civil Engineering, Rijeka,  
Croatia

### Organizing Committee

Željko Arbanas  
University of Rijeka, Faculty of Civil Engineering, Rijeka,  
Croatia

Josip Peranić  
University of Rijeka, Faculty of Civil Engineering, Rijeka,  
Croatia

Martina Vivoda Prodan  
University of Rijeka, Faculty of Civil Engineering, Rijeka,  
Croatia

Sanja Bernat Gazibara  
University of Zagreb, Faculty of Mining, Geology and  
Petroleum Engineering, Zagreb, Croatia

Martin Krkač  
University of Zagreb, Faculty of Mining, Geology and  
Petroleum Engineering, Zagreb, Croatia

Snježana Mihalić Arbanas  
University of Zagreb, Faculty of Mining, Geology and  
Petroleum Engineering, Zagreb, Croatia

Vedran Jagodnik  
University of Rijeka, Faculty of Civil Engineering, Rijeka,  
Croatia Slovenia

Petra Jagodnik  
University of Rijeka, Faculty of Civil Engineering, Rijeka,  
Croatia

### Technical Committee

Marko Sinčić  
University of Zagreb, Faculty of Mining, Geology and  
Petroleum Engineering, Zagreb, Croatia

Hrvoje Lukačić  
University of Zagreb, Faculty of Mining, Geology and  
Petroleum Engineering, Zagreb, Croatia

Sara Pajalić  
University of Rijeka, Faculty of Civil Engineering, Rijeka,  
Croatia

Davor Plazonić  
University of Rijeka, Faculty of Civil Engineering, Rijeka,  
Croatia

ISBN 978-953-6953-55-4, ISBN 978-953-6953-56-1 (eBook) - Faculty of Civil Engineering, University of Rijeka

ISBN 978-953-6923-47-2, ISBN 978-953-6923-46-5 (eBook) - Faculty of Mining, Geology and Petroleum Engineering, University of Zagreb

**Published by:** Faculty of Civil Engineering, University of Rijeka and Faculty of Mining, Geology and Petroleum Engineering, University of Zagreb

**For publisher:** Mladen Bulić and Vladislav Brkić

**Cover design:** Mikser

**Issued:** March 2022, 200 copies

---

## Scientific Programme Committee

Biljana Abolmasov  
University of Belgrade, Faculty  
of Mining and Geology,  
Belgrade, Serbia

Željko Arbanas  
University of Rijeka, Faculty of  
Civil Engineering, Rijeka,  
Croatia

Sanja Bernat Gazibara  
University of Zagreb, Faculty  
of Mining, Geology and  
Petroleum Engineering,  
Zagreb, Croatia

Julijana Bojadijeva  
Ss. Cyril and Methodius  
University, Faculty of Natural  
Sciences and Mathematics,  
Skopje, North Macedonia

Michele Calvello  
University of Salerno,  
Department of Civil  
Engineering, Fisciano, Italy

Nicola Casagli  
University of Florence,  
Department of Earth Sciences,  
Florence, Italy

Sabatino Cuomo  
University of Salerno,  
Department of Civil  
Engineering, Fisciano, Italy

Matteo Del Soldato  
University of Florence, Earth  
Sciences Department,  
Florence, Italy

Uroš Đurić  
University of Belgrade, Faculty  
for Civil Engineering, Belgrade,  
Serbia

Kemal Edip  
Ss. Cyril and Methodius  
University, Faculty of Natural  
Sciences and Mathematics,  
Skopje, North Macedonia

Mirko Grošić  
Geotech Ltd, Rijeka, Croatia

Michel Jaboyedoff  
University of Lausanne,  
Institute of Earth Sciences,  
University of Lausanne,  
Switzerland

Petra Jagodnik  
University of Rijeka, Faculty of  
Civil Engineering, Rijeka,  
Croatia

Vedran Jagodnik  
University of Rijeka, Faculty of  
Civil Engineering, Rijeka,  
Croatia Slovenia

Mateja Jemec Auflič  
Geological Survey of Slovenia,  
Ljubljana, Slovenia

Milorad Jovanovski  
Ss. Cyril and Methodius  
University, Faculty of Natural  
Sciences and Mathematics,  
Skopje, North Macedonia

Martin Krkač  
University of Zagreb, Faculty  
of Mining, Geology and  
Petroleum Engineering,  
Zagreb, Croatia

Matej Maček  
University of Ljubljana, Faculty  
of Civil and Geodetic  
Engineering, Ljubljana,  
Slovenia

Miloš Marjanović  
University of Belgrade, Faculty  
of Mining and Geology,  
Belgrade, Serbia

Snježana Mihalić Arbanas  
University of Zagreb, Faculty  
of Mining, Geology and  
Petroleum Engineering,  
Zagreb, Croatia

Matjaž Mikoš  
University of Ljubljana, Faculty  
of Civil and Geodetic  
Engineering, Ljubljana,  
Slovenia

Toni Nikolić  
University Džemal Bijedić  
Mostar, Faculty of Civil  
Engineering, Mostar, Bosnia  
and Herzegovina

Jovan Papić  
Ss. Cyril and Methodius  
University, Faculty of Natural  
Sciences and Mathematics,  
Skopje, North Macedonia

Josip Peranić  
University of Rijeka, Faculty of  
Civil Engineering, Rijeka,  
Croatia

Igor Peshevski  
Ss. Cyril and Methodius  
University, Faculty of Natural  
Sciences and Mathematics,  
Skopje, North Macedonia

Tina Peternel  
Geological Survey of Slovenia,  
Ljubljana, Slovenia

Tomislav Popit  
University of Ljubljana, Faculty  
of Natural Sciences and  
Engineering, Ljubljana,  
Slovenia

Vlatko Sheshov  
Ss. Cyril and Methodius  
University, Faculty of Natural  
Sciences and Mathematics,  
Skopje, North Macedonia

Jasna Smolar  
University of Ljubljana, Faculty  
of Civil and Geodetic  
Engineering, Ljubljana,  
Slovenia

Binod Tiwari  
California State University,  
Fullerton, California, USA

Veronica Tofani  
University of Florence,  
Department of Earth Sciences,  
Florence, Italy

Timotej Verbovšek  
University of Ljubljana, Faculty  
of Natural Sciences and  
Engineering, Ljubljana,  
Slovenia

Martina Vivoda Prodan  
University of Rijeka, Faculty of  
Civil Engineering, Rijeka,  
Croatia

Sabid Zekan  
University of Tuzla, Faculty of  
Mining, Geology and Civil  
Engineering, Tuzla, Bosnia and  
Herzegovina





---

## Foreword

The Regional Symposium on Landslides in the Adriatic-Balkan Region (ReSyLAB), organized under the auspices of the International Consortium on Landslides (ICL), has reached its fifth edition. This is an important milestone for ICL and for its Adriatic-Balkan Network (ABN).

Ten years ago, the ICL has encouraged the establishment of thematic and regional networks in the framework of its ten-year strategic Plan. The ABN was promptly launched in 2012, gathering together scientists, researchers, engineers, professionals and decision-makers, from the Adriatic and Balkan region and elsewhere, concerned with landslide hazard and risk, their reduction and impact on society.

Today we can say that this has proved to be a successful strategy and the ABN is perhaps the best example of successful regional network. Since its foundation in the year 2012, the ABN has regularly organized its regional symposium every two years, dedicated to specific issues, in various countries of the Adriatic-Balkan area: Croatia, Serbia, Slovenia, Bosnia and Herzegovina and Croatia again.

Participation has gradually expanded to other countries, throughout Europe and elsewhere. This year the Symposium sees the participation of scientists from ten countries, providing an effective platform to achieve fruitful cooperation among landslide researchers.

The ReSyLAB represents a successful contribution to the Kyoto Landslide Commitment (KLC2020) launched by ICL in the year 2020 for the global promotion of understanding and reducing landslide disaster risk. The main purpose of the KLC2020 is to build a common platform for sharing ideas, good practices and policies with key actors and stakeholders concerned with landslide risk at the global level. One of the main priority actions of KLC2020 is to facilitate and assess progresses through the organization of meetings at the regional and national level, to take place in respective countries, in order to show deliveries and performances made towards the achievement of objectives for landslide risk reduction on a global scale.

The general theme of the 5<sup>th</sup> ReSyLAB is “Landslide Modelling & Applications”, which clearly shows the close interplay between scientific research and its application in the engineering practice and for supporting risk reduction policies.

For these reasons, I am convinced that the example of the ABN and the ReSyLAB should be valued and exported in other geographical contexts.



Nicola Casagli  
President of the International Consortium on Landslides  
Florence, Italy



---

## Foreword

The International Consortium on Landslides (ICL) was established in January 2002 in Kyoto, Japan, to promote landslide research for the benefit of society and the environment, and capacity building, including education, notably in developing countries.

In January 2005, the second UN World Conference for Disaster Reduction was organized in Kobe, Japan. ICL, UNESCO, WMO, UNU, IAHS etc. jointly organized a thematic session on Landslides (IPL) and Floods (IFI). The Letter of Intent on Earth System Risk Analysis and Sustainable Disaster Management was agreed in the session and signed by global partners (ICL, UNESCO, WMO, FAO, UNU, UN-ISDR, ICSU, WFEO within 2005. Participants included Professors Ognjen Bonacci from Croatia, Kyoji Sassa, Hideaki Marui, and Kaoru Takara from Japan.

In January 2006, ICL and its global partners (UNESCO, WMO, FAO, UNU, UN-ISDR, ICSU, WFEO etc.) organized the Round Table Discussion for the IPL and adopted the 2006 Tokyo Action Plan strengthening research and learning on landslides and related earth system disasters for global risk preparedness. In 2007, Science and Technology Research Partnership for Sustainable Development (SATREPS) program to promote international joint research for global issues based on the needs of developing countries was founded by the Government of Japan. This programme was very timely to promote the 2006 Tokyo Action Plan. The Croatia-Japan Joint SATREPS Project “Risk identification and land-use planning for disaster mitigation of landslide and floods in Croatia” was proposed in 2007 and accepted as one of the initial SATREPS projects in 2008.

In order to support this SATREPS project, the Ministry of Foreign Affairs of Japan organized a workshop in Tokyo aiming at regional cooperation in South-Eastern Europe on disaster management by inviting Professors Željko Arbanas, Matjaž Mikoš, Snježana Mihalić, Biljana Abolmasov, Sabid Zekan and others from Adriatic-Balkan Region on 14-17 December 2010. This workshop contributed to the establishment of the Adriatic-Balkan Network of International Consortium on Landslides (ICL ABN) in January 2012 and also its biannual regional symposium; the 1<sup>st</sup> ReSyLAB in March 2013 in Zagreb (Croatia), the 2<sup>nd</sup> in May 2015 in Belgrade (Serbia), the 3<sup>rd</sup> in October 2017 in Ljubljana (Slovenia) and the 4<sup>th</sup> in October 2019 in Sarajevo (Bosnia and Herzegovina), and 5<sup>th</sup> in March 2022 in Rijeka (Croatia). The ICL has launched the Open Access Book Series “Progress in Landslide Research and Technology” for Kyoto Landslide Commitment 2020 which is published twice a year. I wish to invite all participants of this symposium to contribute articles to this new open access book series. The target readers of the book series are practitioners and other stakeholders who apply in practice the most advanced knowledge of science and technology for landslide disaster risk reduction. Articles must be written in a simplified way easily understandable by practitioners and stakeholders.

The Adriatic-Balkan Network of International Consortium on Landslides (ICL ABN) is the most successful network of the ICL and its biennial symposium and its publication contributed to boost the regional potentials for reducing landslide disaster risk. I am very grateful for this tremendous effort to organize the fifth regional symposium of the International Consortium on Landslides. I wish the Adriatic-Balkan network a very successful meeting and a very good publication.



Kyoji Sassa  
Secretary-General of the International Consortium on Landslides  
and the Kyoto Landslide Commitment 2020  
Editor-in-Chief of the Open Access Book Series of the ICL  
Kyoto, Japan



---

## Preface

The 5<sup>th</sup> Regional Symposium on Landslides in Adriatic-Balkan Region (ReSyLAB) will be held in the year of two important anniversaries: 20 years of establishing of International Consortium on Landslides (ICL) and 10 years of establishing regional and thematic networks of ICL. The regional Adriatic-Balkan Network (ABN) is one of the most active networks and this 5<sup>th</sup> ReSyLab2015 will contribute to regional cooperation and widening the Network by the new members in the region. Just for reminder, the 1<sup>st</sup> ReSyLAB was held in Zagreb, Croatia, 2013; 2<sup>nd</sup> ReSyLAB in Belgrade, Serbia; 3<sup>rd</sup> ReSyLAB in Ljubljana, Slovenia and 4<sup>th</sup> ReSyLAB in Sarajevo, Bosnia and Herzegovina. The 5<sup>th</sup> ReSyLAB will be held three years after the last Symposium, disrupting the biannual schedule due to Covid-19 pandemic and will be held as hybrid event, but we believe that this will not diminish the significance of this Symposium.

This book contains peer-reviewed papers that will be presented at the 5<sup>th</sup> Regional Symposium on Landslides in the Adriatic-Balkan Region entitled “Landslide Modelling & Applications”. The Symposium will be held in Rijeka, Croatia from March 23<sup>th</sup> to 26<sup>th</sup>, 2022. A wide range of landslide topics are presented in the Symposium sessions that include landslide monitoring, landslide investigation, landslide mapping, landslide susceptibility zonation, laboratory testing, physical and numerical modelling of landslides and landslide case studies. This collection of papers is beneficial to practitioners, researchers and other professionals dealing with landslides. The proceedings reflect the ongoing response of researchers and practitioners from 10 countries from the region and around the world. Unfortunately, the Covid-19 pandemic situation disables landslide scientists from Japan that were present at all previous ReSyLABs, to join us in Rijeka.

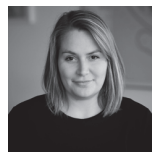
We would like to thank all authors and participants for sharing their ideas and research results in the area of landslide science and practice. We wish to acknowledge the help from all the reviewers in advising and refining the contributions to their final version published in this book.



Josip Peranić  
University of Rijeka  
Faculty of Civil Engineering  
Rijeka, Croatia



Martina Vivoda Prodan  
University of Rijeka  
Faculty of Civil Engineering  
Rijeka, Croatia



Sanja Bernat Gazibara  
University of Zagreb  
Faculty of Mining, Geology  
and Petroleum Engineering  
Zagreb, Croatia



Martin Krkač  
University of Zagreb  
Faculty of Mining, Geology  
and Petroleum Engineering  
Zagreb, Croatia



Snježana Mihalić Arbanas  
University of Zagreb  
Faculty of Mining, Geology  
and Petroleum Engineering  
Zagreb, Croatia



Željko Arbanas  
University of Rijeka  
Faculty of Civil Engineering  
Rijeka, Croatia



---

## Contents

### Invited Lectures

<b>Failure hazard of rockfall sources: some aspects of the hazard quantification</b> .....	1
Michel Jaboyedoff	
<b>Rainfall-induced landslides and debris flows under the influence of climate change: review of recent Slovenian studies</b> .....	7
Nejc Bezak, Matjaž Mikoš, Mateja Jemec Auflič	

### Landslide Investigation

<b>Mountain slopes above Koroška Bela (NW Slovenia) – A landslide prone area</b> .....	13
Tina Peternel, Jernej Jež, Mitja Janža, Ela Šegina, Matija Zupan, Anže Markelj, Ana Novak, Mateja Jemec Auflič, Janko Logar, Matej Maček, Nejc Bezak, Jošt Sodnik, Matjaž Mikoš	
<b>Recent large-scale gravitational collapses in the Madonna di Puianello mud-volcanoes field calderas (Northern Apennines, Modena, Italy)</b> .....	19
Giuseppe Ciccacese, Marco Mulas, Francesco Ronchetti, Marco Aleotti, Alessandro Corsini	
<b>Paroxysmal reactivation of a large-scale earth flow documented by multitemporal UAV photo surveys and Robotic Total Station</b> .....	23
Giuseppe Ciccacese, Marco Mulas, Francesco Ronchetti, Marco Aleotti, Alessandro Corsini	
<b>Field investigation of the landslide that occurred during the construction of the dam “Svráčkovo”</b> .....	29
Nemanja Babović, Aleksandar Miladinović, Dajana Biorac	
<b>Probabilistic modelling of HVSr results for 3D mapping of rock-slides subsurface</b> .....	35
Vincenzo Critelli, Alessandro Corsini, Matteo Berti, Anna Rita Bernardi, Matteo Bernardi, Giuseppe Caputo, Giuseppe Ciccacese, Gianluigi Di Paola, Marco Mulas, Francesco Ronchetti	
<b>Statistical relationships for characterising rock avalanche mobility: state of the art and perspectives</b> .....	41
Alexander Strom	

### Landslide Monitoring

<b>Statistical literature analysis of combined GNSS-InSAR landslide investigation</b> .....	47
Matteo Del Soldato, Camilla Medici, Pierluigi Confuorto, Silvia Bianchini	
<b>Ground deformation monitoring service of Veneto region (NE Italy) by means of Sentinel-1 data</b> .....	53
Pierluigi Confuorto, Silvia Bianchini, Matteo Del Soldato, Davide Festa, Federico Raspini, Nicola Casagli	
<b>Monitoring the Slano blato mudflow using InSAR and UAV photogrammetry (preliminary results)</b> .....	59
Galena Jordanova, Marko Vrabc, Krištof Oštir, Timotej Verbovšek	
<b>Validation of innovative mitigation strategy through long-term landslide and structural monitoring</b> .....	65
Giulia Bossi, Gianluca Marcato, Filippo Tommaso Catelan	

<b>Long-term monitoring of active large-scale landslides based on integrated systems in South Tyrol (SoLoMon project).....</b>	<b>71</b>
Giulia Bossi, Alessandro Corsini, Giuseppe Ciccarese, Gianluca Marcato, Marco Mulas, Luca Schenato, David Tonidandel, Volkmar Mair	
<b>Monitoring of rockfall prone areas in eastern Slovenia.....</b>	<b>75</b>
Mateja Jemec Auflič, Ela Šegina, Tina Peternel, Matija Zupan, Jernej Jež, Manja Žebre, Polona Kralj, Marjana Zajc, Matjaž Mikoš, Nejc Bezak, Milan Kobal	
 <b>Landslide Mapping</b>	
<b>Landslide inventory mapping based on LiDAR data: case study from Hrvatsko Zagorje (Croatia) .....</b>	<b>81</b>
Martin Krkač, Sanja Bernat Gazibara, Marko Sinčić, Hrvoje Lukačić, Snježana Mihalić Arbanas	
<b>Influence of expert knowledge on completeness and accuracy of landslide inventory maps - Example from Istria, Croatia .....</b>	<b>87</b>
Hrvoje Lukačić, Sanja Bernat Gazibara, Marko Sinčić, Martin Krkač, Željko Arbanas, Petra Jagodnik, Vedran Damjanović, Snježana Mihalić Arbanas	
<b>Slope gradient anomalies as indicators of potential slope instabilities .....</b>	<b>93</b>
Ela Šegina, Gorazd Žibret	
 <b>Landslide Susceptibility, Hazard and Risk Modelling</b>	
<b>LandSlidePlan - Scientific research project on landslide susceptibility assessment in large scale .....</b>	<b>99</b>
Sanja Bernat Gazibara, Snježana Mihalić Arbanas, Marko Sinčić, Martin Krkač, Hrvoje Lukačić, Petra Jagodnik, Željko Arbanas	
<b>Shallow landslide susceptibility assessment for the Polog region (North Macedonia) .....</b>	<b>107</b>
Natasha Nedelkovska, Igor Peshevski, Milorad Jovanovski, Jovan Papić, Ivan Radevski, Svemir Gorin	
<b>MASPREM – Slovenian landslide forecasting and warning system .....</b>	<b>113</b>
Tina Peternel, Jasna Šinigoj, Mateja Jemec Auflič, Špela Kumelj, Matija Krivic	
<b>Harmonized approach for mapping the earthquake-induced landslide hazard at the cross-border region between North Macedonia, Greece and Albania .....</b>	<b>119</b>
Julijana Bojadjeva, Vlatko Sheshov, Kemal Edip, Radmila Shalic, Marta Stojmanovska, Roberta Apostolska, Stavroula Fotopoulou, Dimitris Pitolakis, Neritan Shkodrani, Markel Babaleku, Francesca Bozzoni, Antonella di Meo	
<b>A proposal for the landslide damage questionnaire in suburban areas.....</b>	<b>125</b>
Uroš Đurić, Biljana Ablomasov, Miloš S. Marjanović, Sanja Jocković, Miloš D. Marjanović	
<b>Slopes of higher protection priority rating using modified Colorado Rockfall Hazard Rating System - Case study.....</b>	<b>131</b>
Valentina Kocijan, Mirko Grošič, Lovro Blažok	
<b>Rock frost weathering and rockfall activity assessment in Slovenia .....</b>	<b>137</b>
Matjaž Mikoš, Mateja Jemec Auflič, Jernej Jež, Nejc Bezak	
<b>Regional rockfall exposure assessment, experience from Serbia.....</b>	<b>145</b>
Miloš Marjanović, Biljana Abolmasov, Uroš Đurić, Jelka Krušič, Snežana Bogdanović	



---

## **Laboratory Testing, Physical and Numerical Modelling of Landslides**

<b>Numerical simulations of landslide physical model results</b> .....	151
Sabatino Cuomo	
<b>Physical modelling investigation and integrated analysis of landslides for defining risk scenarios</b> .....	157
Giovanna Capparelli, Gennaro Spolverino, Irasema Alcántara-Ayala, Noemi Sharon Ruiz-Cortés	
<b>Role of stratigraphy for rainfall-induced shallow instabilities in volcanic soils: a case study</b> .....	165
Luca Crescenzo, Michele Calvello	
<b>Small-scale physical landslide models under 1g infiltration conditions and the role of hydrological monitoring</b> .....	171
Josip Peranić, Vedran Jagodnik, Nina Čeh, Martina Vivoda Prodan, Sara Pajalić, Željko Arbanas	
<b>Digital image correlation and the use of high-speed cameras for 3D displacement monitoring in 1g small-scale landslide models</b> .....	181
Nina Čeh, Josip Peranić, Vedran Jagodnik, Sara Pajalić, Martina Vivoda Prodan, Željko Arbanas	
<b>Mechanism of rainfall induced landslides in small-scale models built of different materials</b> .....	187
Martina Vivoda Prodan, Josip Peranić, Sara Pajalić, Vedran Jagodnik, Nina Čeh, Željko Arbanas	
<b>Impact of gravity retaining wall on the stability of a sandy slope in small-scale physical model</b> .....	193
Željko Arbanas, Josip Peranić, Vedran Jagodnik, Martina Vivoda Prodan, Nina Čeh, Sara Pajalić, Davor Plazonić	
<b>Preliminary results on the undrained cyclic behavior of uniform sand at low confining stress</b> .....	201
Vedran Jagodnik, Martina Turković, Željko Arbanas	
<b>Laboratory rheology measurements of natural debris material</b> .....	207
Timotej Jurček, Matjaž Mikoš, Matej Maček	
<b>A use of similarity laws in landslide physical modelling: preliminary considerations</b> .....	213
Sara Pajalić, Josip Peranić, Vedran Jagodnik, Martina Vivoda Prodan, Željko Arbanas	

## **Landslide Case Studies**

<b>The Kravec bottom cabin lift station protection against torrential hazards by a new slit check dam and a series of flexible net barriers</b> .....	219
Jošt Sodnik, Matjaž Mikoš	
<b>Design of rockfall protection at the Špičunak location, Gorski kotar, Croatia</b> .....	225
Maroje Sušac, Mirjana Vugrinski, Dalibor Udovič, Davor Marušić, Željko Arbanas	
<b>The Ladiser Landslide mitigation project with a flexible high tensile steel mesh protection system</b> .....	231
Vjekoslav Budimir, Helene Lanter, Armin Roduner, Ronald Steinlechner	

---

<b>Highway construction in fossil landslides zones – Lessons learned from the Grdelica Gorge, Serbia</b> .....	237
Biljana Abolmasov, Marinos Skempas, Svetozar Milenković, Janko Radovanović, Miloš Marjanović	
<b>Remediation measures of landslides on State roads in the Republic of Croatia – Presentation of case studies</b> .....	243
Mirko Grošić, Ivan Volf, Ivana Blagdan	
<b>Deep landslide in the jointed flysch sediments on the Bar-Boljare Highway, Montenegro</b> .....	249
Slobodan Živaljević, Nikola Međedović, Miodrag Bujišić, Zvonko Tomanović	
<b>Author Index</b> .....	255

# Failure hazard of rockfall sources: some aspects of the hazard quantification

Michel Jaboyedoff<sup>(1)</sup>

1) Risk-group, Institut des Sciences de la Terre, Université de Lausanne, CH-1015 Lausanne, Suisse  
([michel.jaboyedoff@unil.ch](mailto:michel.jaboyedoff@unil.ch))

**Abstract** This paper presents two attempts to improve rockfall failure hazards assessment. The first is based on the matrix hazard approach, it tries to assess the failure of medium size rock instability based on two parameters the rockfall activity and the deformation. It assumes that if a rock mass starts to be deformed, which is measured as the displacement divided by the length of the landslide in the direction of displacement. When it is larger 0.001% per year, it starts to be significant. If this is coupled with rockfall temporal frequency above 0.1 per year for boulders larger than 1 m<sup>3</sup>, the hazard is significant. The matrix is created with four classes numbered 1 to 4 for both activity parameters and higher is the sum of both higher is the hazard level. The second attempt is a validation of the volume temporal frequency cumulative distribution obtained by comparing the result of inventory of fallen rock volumes and the distribution obtained using the potential unstable volumes. The volume distributions may be obtained by comparing point clouds for the fallen volumes and by using structures or other methods to define the unstable volume and their limits. These methodologies are in an early stage, the results are not yet confirmed, but they may be tested and used in the case of fast risk hazard and risk assessment.

**Keywords** rockfall source, hazard, volume, activity

## Introduction

In its simplest form rockfall hazard  $H$  is composed of two terms:

$$H = \lambda \times P_p \quad [1]$$

$\lambda$  is the temporal frequency or hazard failure and  $P_p$  the probability of propagation, which ranges from 0 to 1. Here we will deal only with the  $\lambda$  variable. Up to now there has been no simple method that permits to evaluate this value in all cases. Its evaluation is mainly dependent on the available data (Jaboyedoff et al. 2021).

The best case is to get an inventory in a region, which allows to obtain a cumulative distribution such as power law (Hungre et al. 1999; Dussauge-Peisser et al. 2002; Hantz 2011). It means that larger the volume is the smaller the temporal frequency of failure. The question can be how to

validate this approach. Here we propose to compare the distribution of the released volumes with the potential unstable volume distribution to verify if the distributions possess the same trend.

This also means that large volumes can be released, albeit rarely. As observed by several authors, the failure of a larger volume can be preceded by smaller rockfalls (Guerin et al. 2020a; Rosser et al. 2015). Using this argument with an estimation of the deformation it seems possible to provide a ranking of failure hazard for medium volume from 100 m<sup>3</sup> to several 1,000,000 m<sup>3</sup> in a quick and simple way.

## Temporal frequency for rockfall using power laws

Inventory of fallen rockfall volume can be obtained from the differences of cloud points either provided by Laser scanning of Structure or Motion techniques (SfM).

### Volume power laws

A power law distribution of the rockfall volume sources were first shown in Yosemite Valley (Wieczorek et al. 1995) and confirmed by a recent study (Guerin et al. 2020b). The temporal frequency of failure of volume larger or equal to  $V$  is given by (Dussauge-Peisser et al. 2003):

$$N(v \geq V) = \frac{N_0}{\Delta t} \left( \frac{V}{V_0} \right)^{-b} = a V^{-b} \quad [2]$$

where  $N_0$  is the number of failures larger or equal to  $V_0$  that occurred during a period  $\Delta t$  and  $b$  is the exponent that can be deduced from the cumulative volume distribution taken from an inventory (Fig. 1). The return period  $\tau$  is given by:

$$\tau(v > V) = \frac{1}{N(v \geq V)} \quad [3]$$

This method permits to assess rockfall hazards (Hungre et al. 1999; Dussauge-Peisser et al. 2002; Hantz 2011). This allows to obtain the probability that  $n$  instabilities of volume larger or equal to  $V$  are produced during a period  $T$ , with  $\lambda = 1/\tau$ , (Hantz et al. 2003):

$$P(n, \Delta t) = \frac{(\lambda T)^n}{n!} e^{-\lambda T} \quad [4]$$

For instance, the probability that during the period T at least one event occurs (Hantz et al. 2003):

$$P(n > 0) = 1 - e^{-\lambda T} \quad [5]$$

Other types of distribution laws may be used, as for instance the generalised Pareto distribution (De Biagi et al. 2017).

Hantz et al. (2020) propose to normalise per unit of surface the parameter a, which is given in rockfall number per unit of surface area and year [ $\text{hm}^{-1} \text{year}^{-1}$ ].

It must be noticed that the b value increases with diminishing the interval of time between point clouds

acquisitions (Van Veen et al. 2017; Williams et al. 2018; 2019). This means that larger volumes are apparently more frequent if the inventory of volumes is based on the difference between two acquisitions with a longer time separating them. Often power laws show rollovers for a small value, which means that small volumes are not fully identified. In addition, there are some maximum limits for the volume because of the size of the rock wall, and then the distribution starts to be steeper for large volumes.

Recently Hantz et al. (2020) have used geological strength index (GSI) and joints spacing to characterise the parameter a and b of the power law applied to unlocalized hazard in a rock wall.

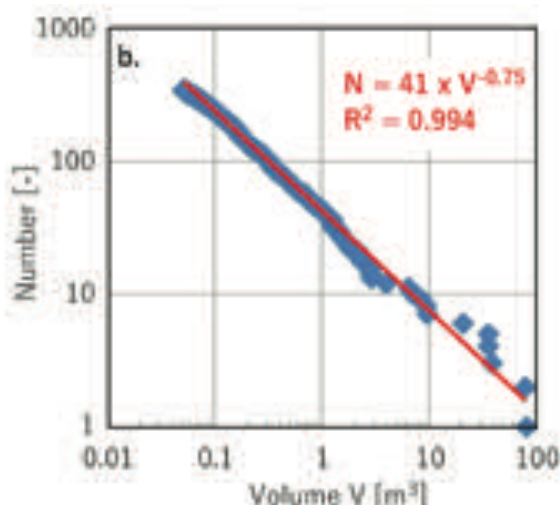
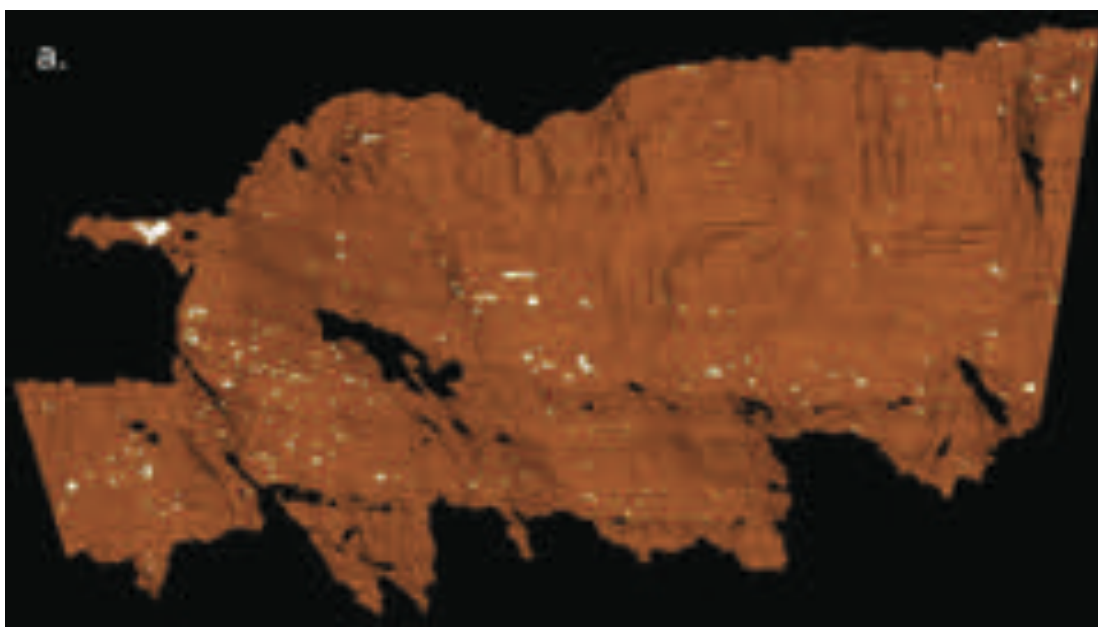


Fig. 1 (a) Example of rockfall source area detected using terrestrial laser scanner data in the Mont Saint-Eynard cliff (France). Comparison of point cloud in August 2009 and November 2012. (b) Power law obtained from 344 scars > 0.05 m<sup>3</sup> (modified after Guerin et al. 2014).

### Large rockfall hazard of failure

The hazards of failure of large rockfall source areas can be estimated using a simple method, based on activity assessment, especially in the case of the situation of rock slopes close to of equilibrium.

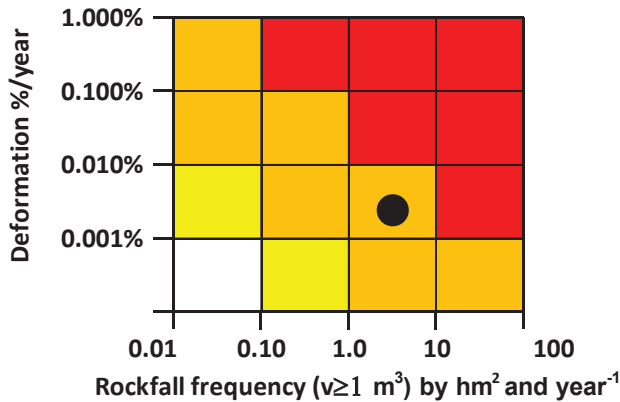


Fig. 2. Failure hazard levels based on rockfall frequency and deformations. Red = high, orange = medium, yellow = low and white = null. The black point corresponds to the cliff of Fig. 1.

The activity of a rock instability of medium size, leading to failure can be characterised based on deformation, either by the ratio of the observed movement of the length of the instability in the direction of the deformation (Chigira 2009), or by the activity of block falls (Jaboyedoff et al. 2012). Thus, when the deformation of a rock mass is accompanied by rockfall activity, then the higher the deformation and/or rockfall are, the more likely the instability is to fail. So, a matrix can be constructed with the deformation and the rockfall frequency per unit of surface. The latter can be defined by the a parameter of the power law with the units [ $\text{hm}^{-1} \text{year}^{-1}$ ].

Fig 3. shows a cliff made of carbonates, the rockfall temporal frequency or a  $\geq 1$  events  $\text{hm}^{-1} \text{year}^{-1}$  (in fact, it corresponds to the number of rockfalls equal or larger than  $1 \text{ m}^3$  because  $\log(1)=0$ ). For the observed deformation are low, it can be estimated to be lower than 0.01% per year, but most probably more than 0.001% per year (Fig. 4). So, in that case the observed activity is medium. This result can be compared to the result we can obtain for this cliff area using the data of Dussauge-Peisser et al. (2002) which gives a temporal frequency of 0.002 events per year for rockfall sources greater or equal to  $1000 \text{ m}^3$  for the  $1 \text{ km}$  wide cliff of Fig. 1.

### Validation of power laws

Creating good linear fitting in graphs in log-log scale is often rather easy but it does not mean that the results are relevant (Fig. 1), it means that it is important to check the validity of the results.

First it can be confirmed by performing several years of surveys comparing the a and b values for each year. The year is important to avoid the impact of seasons on activity, or the same season must be chosen for comparison.

Another solution is to create a distribution of the potential volumes that are potentially unstable and can fall and compare the b-value of both distributions.

The instability volume can be either defined by simple calculation of using the structures as limits or using the sloping local base level (SLBL) (Jaboyedoff et al. 2020).

### Volume estimations

The first technique is to use the surface area of the instability multiplied by its average thinness or to use predefined shape parallelepipeds.

The second technique is to use the structure to define planes following traces of discontinuities on a 3D point cloud to define volumes.

The third method is the SLBL, which can be summarised as follows. SLBL construction is rather simple. The perimeter of the instability must be defined. The principle is based on an iterative process. The SLBL routine dig “numerically” a gridded DEM ( $z(t)_{ij}$ ) inside the defined limits perimeter.

At each iteration  $t$ , each grid node of the digital elevation model (DEM) an “average”  $z_{temp}(t)_{ij}$  of all the altitudes of the neighbours of the previous iteration  $z(t-1)_{ij}$ , i.e. ( $f(z_n(t-1))$ ) are estimated.  $z_n$  means the neighbours nodes. A positive or null constant  $C$  (tolerance) is subtracted to the average, i.e.:

$$z_{temp}(t)_{ij} = (f(z_n(t-1)) - C) \quad [6]$$

This step generates a new grid assuming that if  $z_{temp}(t)_{ij} < z(t-1)_{ij}$ , then  $z(t)_{ij} = z_{temp}(t)_{ij}$ ; otherwise, the value is unchanged.  $z(t)_{ij}$  value can also be limited for instance by another DEM or by assuming a lower limiting slope angle of the failure surface. The iteration is repeated until all the differences over the grid ( $z_{temp}(k-1)_{ij} - z(t)_{ij}$ ) reach a given threshold. It must be underlined that  $C$  depends on the grid cell size  $\Delta x$ , but this can be considered (see Jaboyedoff et al. 2020).

### Method

If the observed fallen volumes follow a power law distribution, it can be compared to the volumes that can potentially fail, which can be defined by the previous methods.

If the b values are similar by less than  $\pm 0.1$ , this may prove that the fallen volumes characterize the morphology of the rock wall well and it can be concluded that the hazard of failure possess a good confidence level.

This have been shown in a quarry that suffer landslides, for which we cannot reproduce data.

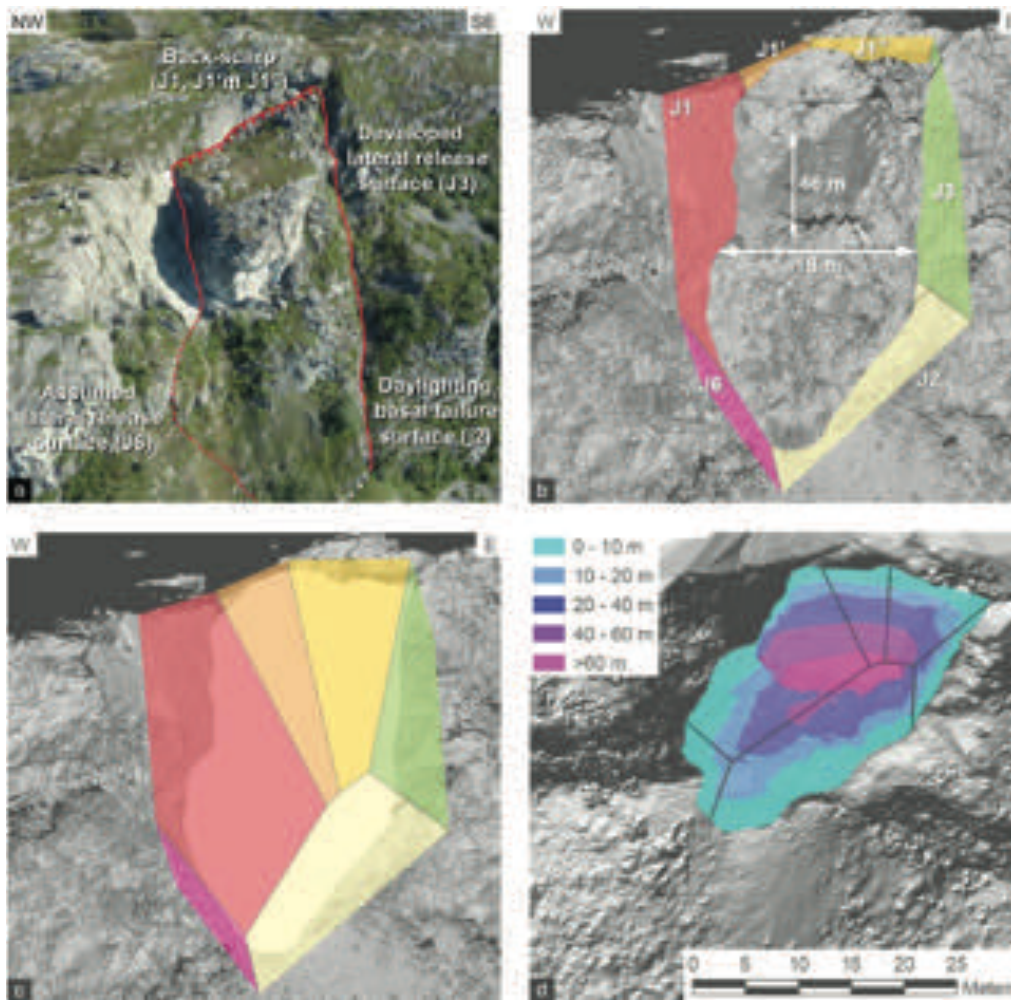


Fig 3. Example of construction in 3D of the basal failure surface of an instability at Lausefjellet in western Norway: a) photograph of the instability; b) prolongation of discontinuity traces by planes; c) result for failure surface under the instability; d) elevation differences between the present topography and the surface in (b) (from Jaboyedoff et al. 2020).

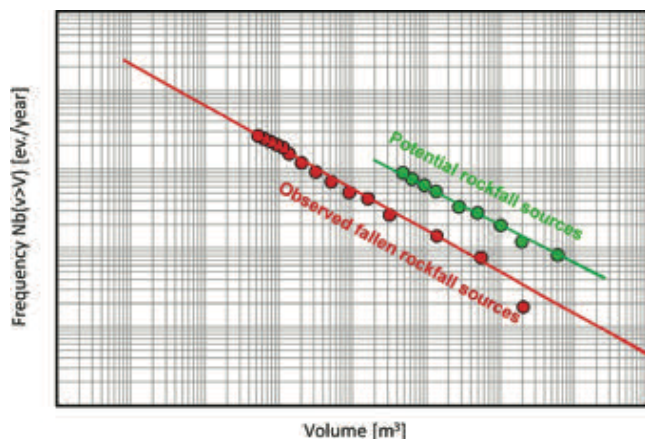


Fig 4. Synthetic example of the method, both observed and potential volumes possess similar b values.

### Discussion and conclusion

This short communication presented tools to better characterize the failure hazards of sources of rockfalls. The first method is an attempt to obtain a hazard level observing both types of activities deformation (movements) and rockfalls activity. It assumes that when both are present, the hazard of failure is increased, which has been observed in several examples. This first attempt uses limits proposed by Hantz et al. (2020) for the activity and extend it, based on a logarithmic scale. Concerning the deformation levels, it used the values proposed for large landslides (Jaboyedoff et al. 2012). All must be improved by using more case studies to set the limits of both logarithmic scale of the matrix. Its application is probably useful for assessing failure near the limit equilibrium.

The second method tries to make the failure hazard based on power law volume – temporal frequency relationship more objective. Indeed, there exist no real validation of power-law distribution, because the

variability of the  $b$  factor can be large. For that purpose, the potential unstable volumes are estimated using volume estimations based on various method methods such as SLBL. The agreement of both  $b$  values may be a test for the quality of the power law hypothesis for the volume. But this must be applied in many other cases to be validated. Such behaviours have already been observed partially verified at the level of the entire slope (Jaboyedoff and Evans 2005), showing that it needs further developments.

## References

- Chigira M (2009) September 2005 rain-induced catastrophic rockslides on slopes affected by deep-seated gravitational deformations, Kyushu, southern Japan. *Engineering Geology*. 108: 1–15.
- De Biagi V, Napoli ML, Barbero M, Peila D (2017) Estimation of the return period of rockfall blocks according to their size. *Nat. Hazards Earth Syst. Sci.* 17(1): 103-113.
- Dussauge C, Grasso J-R, Helmstetter A (2003) Statistical analysis of rockfall volume distributions: Implications for rockfall dynamics. *Journal of Geophysical Research: Solid Earth*. 108(B6).
- Dussauge-Peisser C, Helmstetter A, Grasso J-R, Hantz D, Desvarreux P, Jeannin M, Giraud A (2002) Probabilistic approach to rock fall hazard assessment: potential of historical data analysis. *Nat. Hazards Earth Syst. Sci.* 2: 15–26. doi:10.5194/nhess-2-15-2002.
- Guérin A, Ravanel L, Matasci B, Jaboyedoff M, Deline P (2020a): The three-stage rock failure dynamics of the Drus (Mont Blanc massif, France) since the June 2005 large event. *Scientific Reports*. 10: 17330. doi: 10.1038/s41598-020-74162-1.
- Guérin A, Stock GM, Radue MJ, Jaboyedoff M, Collins BD, Matasci B, Avdievitch N, Derron M-H (2020b) Quantifying 40 years of rockfall activity in Yosemite Valley with historical Structure-from-Motion photogrammetry and terrestrial laser scanning. *Geomorphology*. 107069. doi: <https://doi.org/10.1016/j.geomorph.2020.107069>.
- Guérin A, Hantz D, Rossetti J-P, Jaboyedoff M (2014) Brief communication "Estimating rockfall frequency in a mountain limestone cliff using terrestrial laser scanner". *Nat. Hazards Earth Syst. Sci. Discuss.* 2: 123–135. <https://doi.org/10.5194/nhessd-2-123-2014>.
- Guérin A, Stock GM, Radue MJ, Jaboyedoff M, Collins BD, Matasci B, Avdievitch N, Derron M-H (2020) Quantifying 40 years of rockfall activity in Yosemite Valley with historical Structure-from-Motion photogrammetry and terrestrial laser scanning. *Geomorphology*. 356: 107069.
- Hantz D, Colas B, Dewez T, Lévy C, Rossetti J-P, Guérin A, Jaboyedoff M (2020) Caractérisation quantitative des aléas rocheux de départ diffus. *Rev. Fr. Geotech.* 163, 2.
- Hantz, D., 2011. Quantitative assessment of diffuse rock fall hazard along a cliff foot. *Natural Hazards and Earth System Science*, 11(5), 1303-1309.
- Hantz, D., Vengeon, J. M., and Dussauge-Peisser, C. 2003. An historical, geomechanical and probabilistic approach to rock-fall hazard assessment, *Nat. Hazards Earth Syst. Sci.*, 3, 693–701, <https://doi.org/10.5194/nhess-3-693-2003>.
- Hungro O, Evans SG, Hazzard J (1999) Magnitude and frequency of rock falls along the main transportation corridors of southwestern British Columbia. *Can. Geotech. J.* 36: 224–238.
- Jaboyedoff M, Derron M-H, Pedrazzini A, Blikra L, Crosta GB, Froese C, Hermanns R, Oppikofer T, Stead D (2012) Fast assessment of susceptibility of massive rock instabilities. *Landslides and Engineered Slopes. Protecting Society through Improved Understanding. Proceedings of the 11th International and 2nd North American Symposium on Landslides.* 3-8 June 2012. Banff, Canada. pp. 459-465.
- Jaboyedoff M, Carrea D, Derron M-H, Oppikofer T, Penna IM, Rudaz B (2020) A review of methods used to estimate initial landslide failure surface depths and volumes. *Engineering Geology*. 267, 105478. doi: <https://doi.org/10.1016/j.enggeo.2020.105478>.
- Jaboyedoff M, Ben Hammouda M, Derron MH, Guérin A, Hantz D, Noel F (2021) The Rockfall Failure Hazard Assessment: Summary and New Advances. *Understanding and Reducing Landslide Disaster Risk. WLF 2020. ICL Contribution to Landslide Disaster Risk Reduction.* Springer, Cham. [https://doi.org/10.1007/978-3-030-60196-6\\_3](https://doi.org/10.1007/978-3-030-60196-6_3)
- Jaboyedoff M, Evans SG (2005) Self-similar distribution of the cumulative number of potential landslides volumes. *Geophysical Research Abstracts*. 7, 05815. SRef-ID: 1607-7962/gra/EGU05-A-05815, EGU.
- Rosser N, Lim M, Petley D, Dunning S, Allison R (2007) Patterns of precursory rockfall prior to slope failure. *Journal of Geophysical Research: Earth Surface*. 112 (4): F04014. doi: 10.1029/2006JF000642.
- van Veen M, Hutchinson DJ, Bonneau DA, Sala Z, Ondercin M, Lato M (2018) Combining temporal 3-D remote sensing data with spatial rockfall simulations for improved understanding of hazardous slopes within rail corridors. *Nat. Hazards Earth Syst. Sci.* 18(8): 2295-2308.
- Wieczorek GF, Nishenko SP, Varnes DJ (1995) Analysis of rock falls in the Yosemite Valley, California, *Proc. U.S. Symp. Rock Mech.*, 35th, 85–89.
- Williams JG, Rosser NJ, Hardy RJ, Brain MJ (2019) The Importance of Monitoring Interval for Rockfall Magnitude - Frequency Estimation. *Journal of Geophysical Research: Earth Surface*. 124(12), 2841-2853.
- Williams JG, Rosser NJ, Hardy RJ, Brain MJ, Afana AA (2018) Optimising 4-D surface change detection: an approach for capturing rockfall magnitude–frequency. *Earth Surface Dynamics*. 6(1): 101-119.





# Rainfall-induced landslides and debris flows under the influence of climate change: review of recent Slovenian studies

Nejc Bezak<sup>(1)</sup>, Matjaž Mikoš<sup>(1)</sup>, Mateja Jemec Auflič<sup>(2)</sup>

1) University of Ljubljana, Faculty of Civil and Geodetic Engineering, UNESCO Chair on Water-related Disaster Risk Reduction, Ljubljana, Jamova cesta 2, Slovenia, +386 4768 685 (nejc.bezak@fgg.uni-lj.si)

2) Geological Survey of Slovenia, Ljubljana, Slovenia

**Abstract** Climate changes are expected to increase the frequency and magnitude of the most intense precipitation events. In addition, the elements of the hydrological cycle and the seasonal characteristics of climatological and hydrological processes are expected to change in the future. Therefore, these changes will also affect the frequency, magnitude, and impact of landslides, debris flows, rockfalls, and similar natural hazards. This paper reviews recent studies conducted by Slovenian researchers, focusing on Slovenia and other European countries. Special emphasis is placed on the characteristics of precipitation events responsible for triggering mass movements and on an overview of the effects of climate change.

**Keywords** Rainfall characteristics, landslides, debris flows, rock falls, climate change, Slovenia.

## Introduction

It is clear that global warming and the associated effects of climate change affect the stability of slopes and have consequences for landslides, rock falls, debris flows, and similar phenomena (Gariano and Guzzetti 2016). However, it is not clear to what extent climate change will affect the frequency and magnitude of mass movements in different parts of the world (Gariano and Guzzetti 2016). It can be seen that mass movements activity is or will increase in many parts of the world including parts of Asia, Africa, North and South America (Gariano and Guzzetti 2016). Among all continents, Europe is the most diverse in its response to climate change in terms of mass movement activity (Gariano and Guzzetti 2016). Hence, additional attention should be paid to this part of the world to better identify climate change's changing patterns and impacts. Therefore, this paper provides an overview of recent studies conducted by Slovenian researchers focusing on precipitation characteristics related to the triggering of landslides, debris flows and rock falls.

## Larger-scale studies

### Rainfall event characteristics above the empirical global rainfall thresholds at the continental scale

Bezak and Mikoš (2021) investigated characteristics of rainfall events positioned above the empirical global

rainfall thresholds for landslides triggering. The focus of the study was to analyse the magnitude and frequency of rainfall events. Changes for the areas classified as at least moderately susceptible to landslides (according to the ELSUS v2 map;  $1.8 \cdot 10^6$  km<sup>2</sup>) were evaluated for the 1961-2018 period where precipitation reanalysis data was used as input (Bezak and Mikoš 2021). It was found that around 15% more rainfall events were detected above the selected thresholds for 1991-2018 period compared to the 1961-1990 period (Bezak and Mikoš 2021). Additionally, several regions across Europe were detected where these changes were positive and statistically significant with the selected significance level of 5% (Bezak and Mikoš 2021). Such examples are Italy or the Carpathian Mountains, where landslides frequently occur (Fig. 1). There were also regions where the detected changes were negative (and statistically significant) such as the Alps or Pyrenees (Fig. 1). Moreover, no significant change could be detected for around 50% of the area. Hence, it can be seen that climate change already has an effect, in some parts of Europe, on the rainfall characteristics that could trigger landslides or debris flows.

### Human exposure to landslides

Recent study also investigated human exposure to landslides. Modugno et al. (2022) used a GIS-based and multi-scale approach to indicate when and where a country is affected by a high probability of landslide occurrence (Modugno et al. 2022). It was shown that most of the people living in landslide hazard areas are located in Asia in countries such as Nepal, India, Philippines, etc. Exposure in Europe is generally smaller than some other parts of the world. However, countries like Italy, Switzerland, and Slovenia have quite high exposure. A recent study showed that 48 million people are exposed to landslides in Europe (Mateos et al. 2020). While the number of fatalities in Europe is relatively small (i.e. 39 in the 2015-2017 period by 3,907 landslides (Mateos et al. 2020) or 1,370 deaths in 1995-2014 (Haque et al. 2016)), the number of fatalities is much higher in other parts of the world, exceeding 1,000 in the 2007-2018 period in countries such as Brazil, India, Philippines, China, etc (Modugno et al. 2022). Therefore, a novel methodological approach, such as the one proposed by Modugno et al. (2022), will need to be developed in the future to predict landslides better, debris flows, and rock falls.

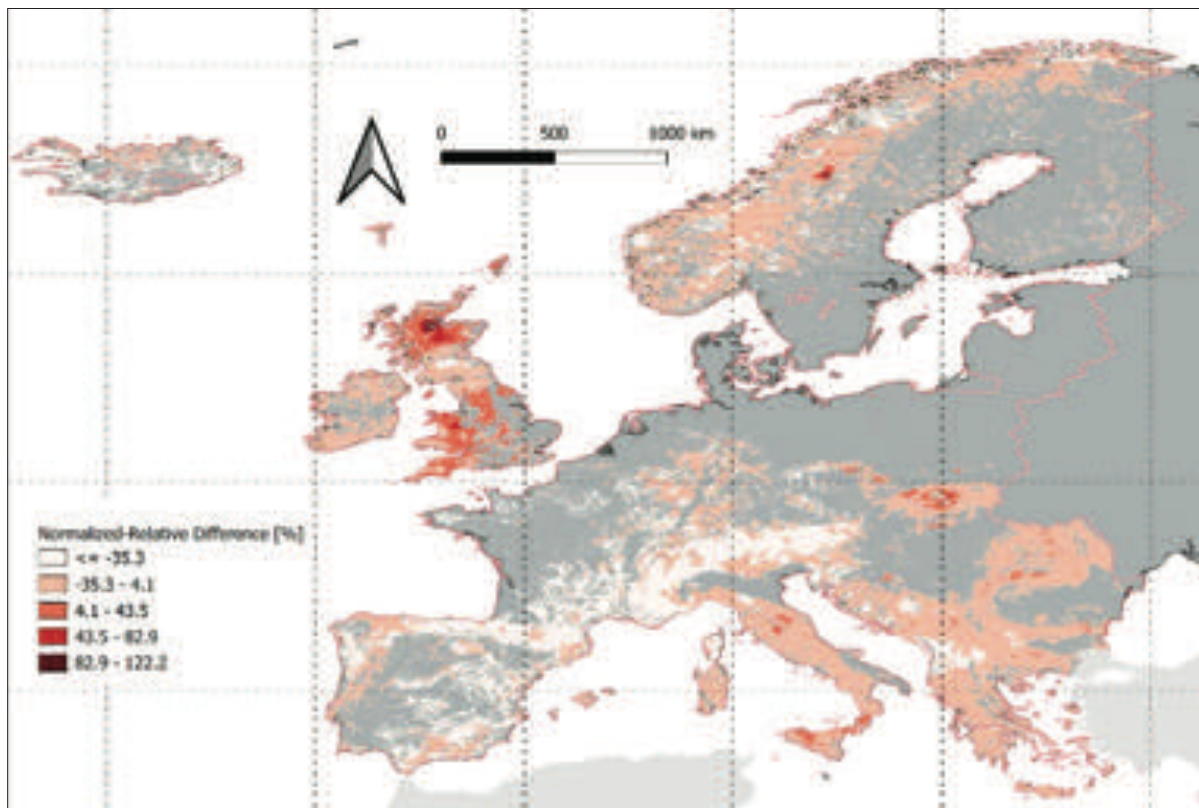


Figure 1 Relative difference between recent and historic periods (1991-2018 and 1961-1990) based on the consideration of the normalized threshold. Pink line shows the area at least moderately susceptible to landslides. Adopted after (Bezak and Mikoš 2021).

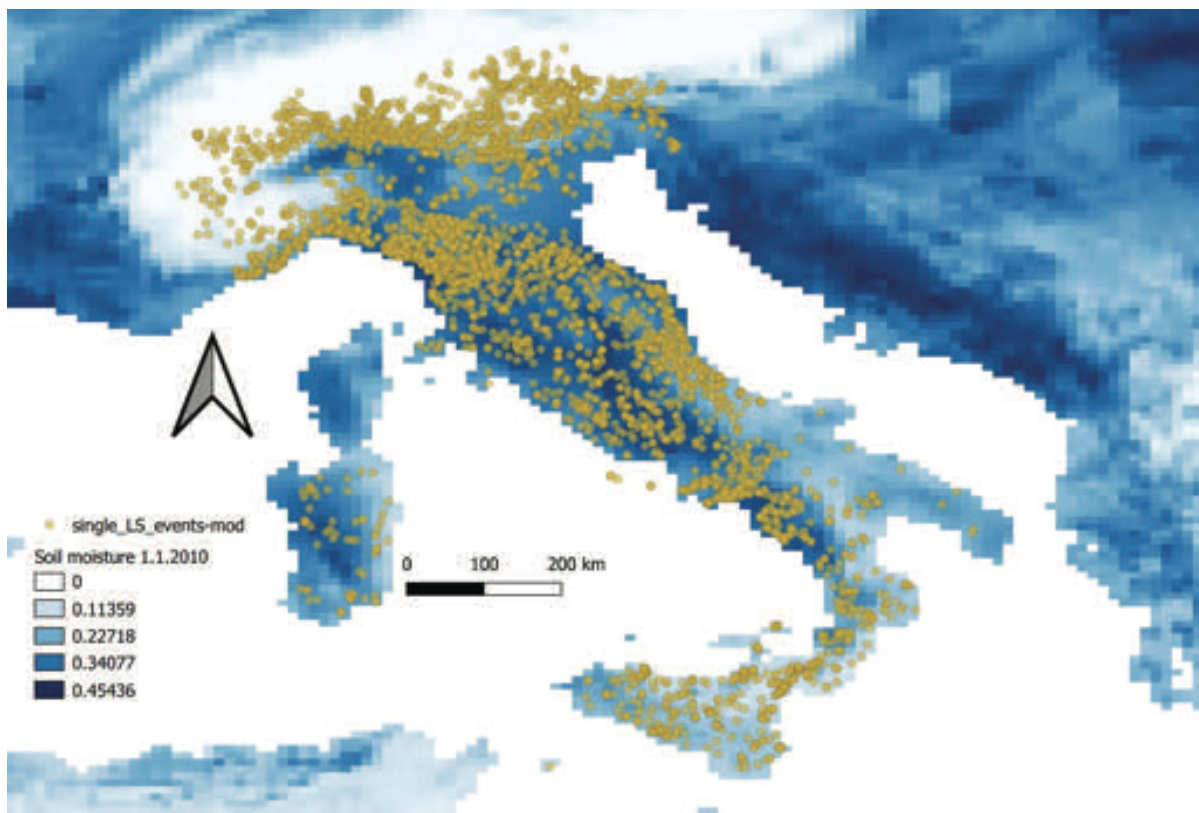


Figure 2 Soil moisture reanalysis data ( $m^3/m^3$ ) on a specific date (i.e. 1.1.2010) and all the landslides included in the FranEItalia database. Adopted after Bezak et al. (2021).

### Improving landslides predictions

Recently, Bezak et al. (2021) tested the added value of the reanalysis soil moisture data (i.e. Copernicus Uncertainties in Ensembles of Regional Reanalyses (UERRA)) in predicting historical landslides events in Italy (Fig. 2). It was found that precipitation is much better predictor of landslides occurrence compared to soil moisture data. Moreover, using only soil moisture data (without precipitation) a small fraction of landslides could be predicted. However, other more detailed satellite-based soil moisture data should be tested to additionally evaluate the added value of the soil moisture data.

### Slovenian case studies

Besides global and continental studies, Slovenian researchers have also focused on the smaller-scale studies including national ones with focus on Slovenia.

### Rainfall events characteristics

Bezak and Mikoš (2019) investigated trends and temporal changes in intensity-duration-frequency (IDF) and extreme rainfall events that can also trigger landslides and other mass movements (Bezak et al. 2016). Using high-frequency data for 10 rainfall stations with 44 years of data (i.e. 1975-2018) it was found that no clear pattern could be

detected in precipitation trends. Minimal changes in the seasonal characteristics of 5- and 30-minutes rainfall events (tend to occur a few days earlier, Fig. 3) and of 360- and 720-minutes events (tend to occur a few days later) were detected. Moreover, Bezak et al. (2016) also investigated the possibility to use copula functions for the definition of the IDF curves and compared these curves with empirical global rainfall thresholds that are used for the shallow-landslides triggering.

Jordanova et al. (2020) reconstructed the cumulated event rainfall and the duration of the rainfall conditions responsible for landslide occurrences for the period of 2007 and 2018 in order to obtain reliable thresholds that could be implemented in a landslide early warning system.

### Climate change studies

Several recent studies have investigated a direct climate change impact on conditions related to landslides triggering. Jemec Auflič et al. (2021) studied climate change impact on landslides in the mid of the 21<sup>st</sup> century in Slovenia. They used the Representative Concentration Pathway climate scenario (RCP4.5) and MASPREM (landslide prediction system) system for modelling. They found that extreme rainfall events are likely to occur more frequently in the future (2041-2070; Fig. 4), which may lead to a higher frequency of landslides in some areas in Slovenia.

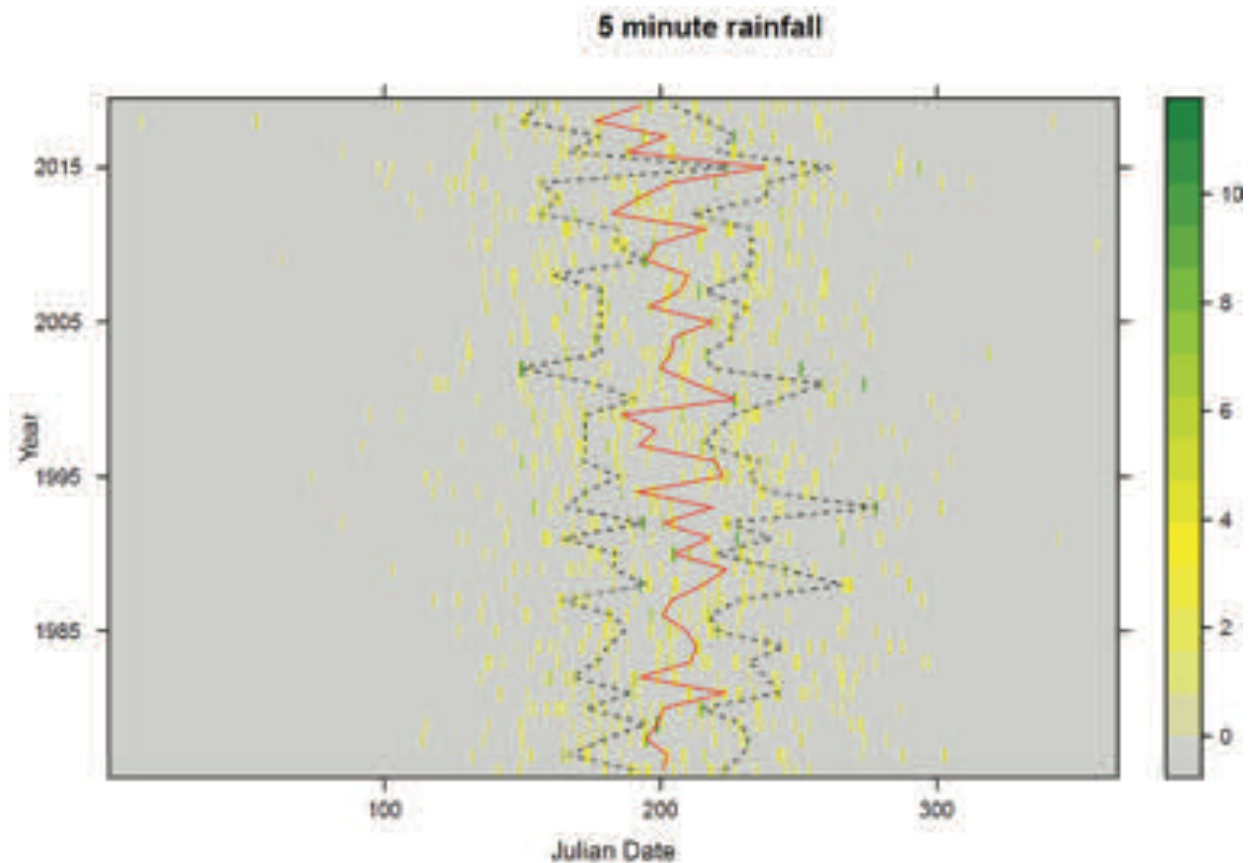


Figure 3 Temporal clustering of the annual maximum rainfall events with the duration of 5 minutes. Red line indicates the median Julian date and the dotted black lines indicate 25% and 75% Julian date. Adopted after Bezak and Mikoš (2019).

Bezak et al. (2021b) also investigated impact of climate change on the water balance elements of the Koroška Bela area (Jemec Auflič et al. 2017; Sodnik et al. 2017; Janža et al. 2018; Bezak et al. 2021c). The results indicated that total and effective rainfall could increase in future. Due to the air temperature increase we could also expect an increase in the evapotranspiration. However, these changes does not linearly translate in the water balance elements of the Koroška Bela area (Bezak et al. 2021b). More specifically, projected changes in the total runoff, percolation, etc. are within the range of 5% compared to the baseline period (Bezak et al. 2021b). Additionally, mGROWA water balance model was also used to evaluate possible changes in the water balance elements (Bertalančič et al. 2018) for the Koroška Bela area. An example of such modelling results is shown in Fig. 5 for the groundwater recharge variable. Moreover, changes in the IDF curves were also evaluated (Fig. 6) and also no significant changes between future and baseline periods could be detected (Fig. 6). In general the climate change evaluation in Slovenia was conducted by the Slovenian Environment Agency (ARSO) (Bertalančič et al. 2018) but

they did not focus specifically on mass movements such as landslides or debris flows.

### Modelling improvements

Several improvements have also been made with respect to landslides-related modelling. The landslide prediction system for modelling the probability of landslides through time in Slovenia (MASPREM, Fig. 7) has been in operation since 2013 (Jemec Auflič et al. 2016). Since then, the system has been updated at the national level with new rainfall thresholds. At the municipal level, the system now makes predictions for 25 municipalities in the scale of 1:25,000 and at the local level for one landslide-prone area (Koroška Bela). A very important part of the system is also the data collection, which is done through the application e-Plaz (<https://www.e-plaz.si/>). Also hydrological models have been suggested to be applied for the prediction of the shallow landslides at the catchment level in Slovenia (Bezak et al. 2019a). Moreover, recently several modelling applications have been conducted using the RAMMS debris flow module at various locations across the country (Bezak et al. 2019b, 2020, 2021c; Mikoš and Bezak 2021). Example of such simulations are shown in Fig. 8.

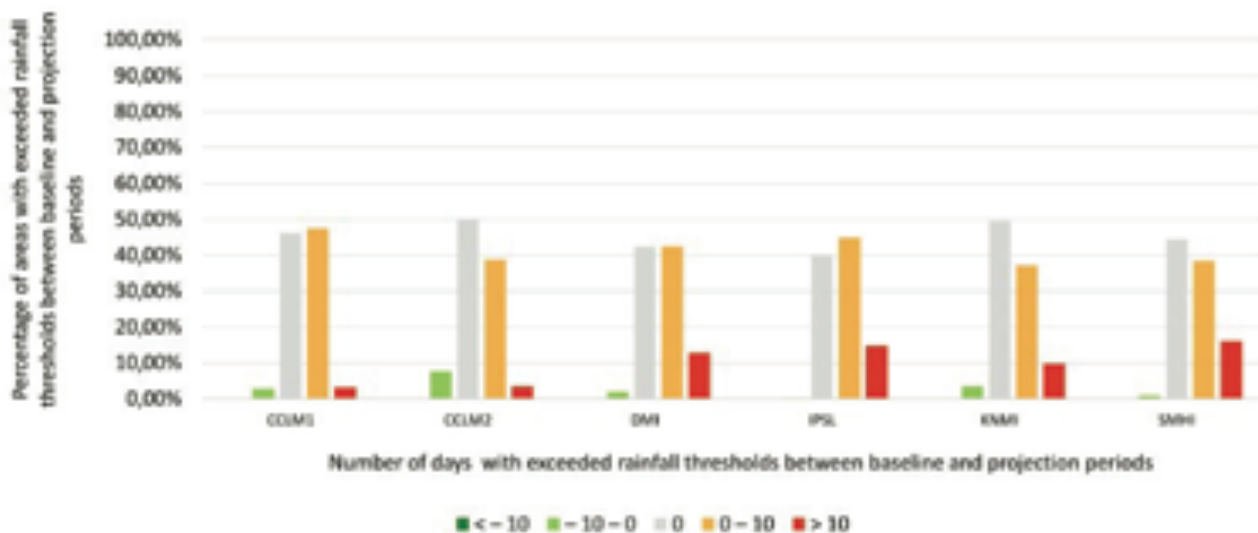


Figure 4 Percentage of areas for which rainfall thresholds between baseline and future periods was exceeded. Six RCP4.5 model runs are shown (i.e. one per column). Adopted after Jemec Auflič et al. (2021).

### Conclusions

This contribution provides a short overview of recent studies conducted by Slovenian researchers related to the triggering and prediction of landslides and debris flows under the impact of climate change. As can be seen quite some number of studies have been conducted in this field. Some of the studies also investigated global and large regional scales while others were conducted at national scale. However, further research is needed and will be conducted in Slovenia. For example, in the scope of the

on-going basic research project “Deciphering the sensitivity of rock faces to climatic changes and freeze-thaw cycles in permafrost-free regions (J1-3024)” climate change impact on the rock fall triggering will be investigated. Further work is also needed to continuously fill landslide inventory with new landslide cases to be able to validate susceptibility and triggering models and better predict potential climate change impact.

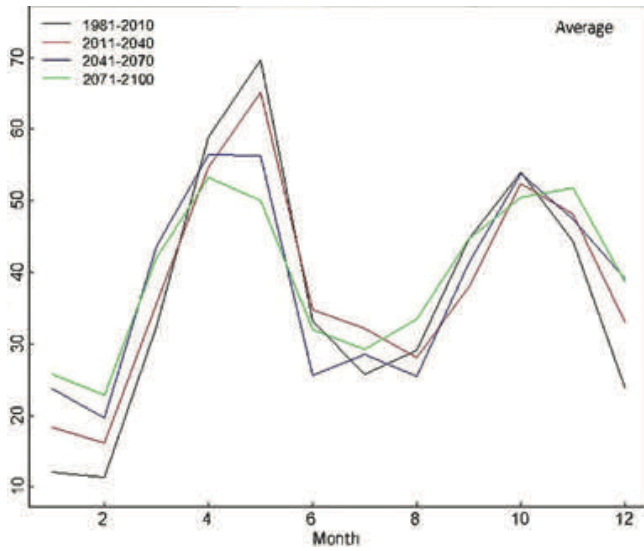


Figure 5 Monthly (x-axis) variations in the monthly groundwater recharge (y-axis; in mm) for a baseline (1981-2010) and three future periods for the Koroška Bela area based on the simulations using the mGROWA water balance model. Average values for the six GCM/RCMs are shown.

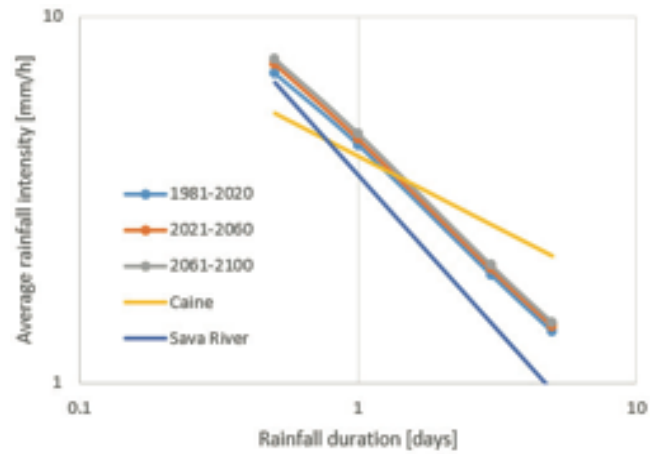


Figure 6 Comparison of the empirical rainfall thresholds (one for Sava River basin and one Global threshold) and IDF curves for the 2-year return period for the Koroška Bela area. Adopted after Bezak et al. (2021b).

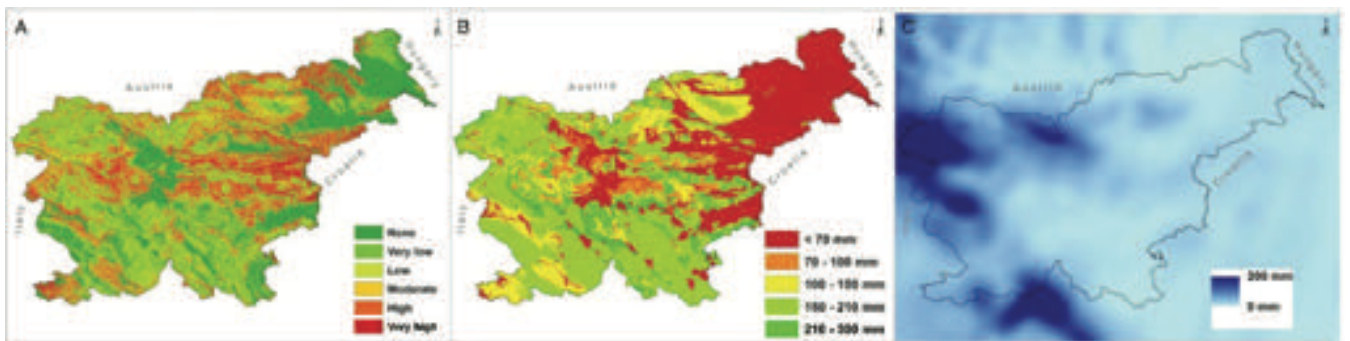


Figure 7 Three major elements of the MASPREM system: landslide susceptibility model, triggering rainfall thresholds and precipitation forecasting model. Adopted after Jemec Auflič et al. (2016).

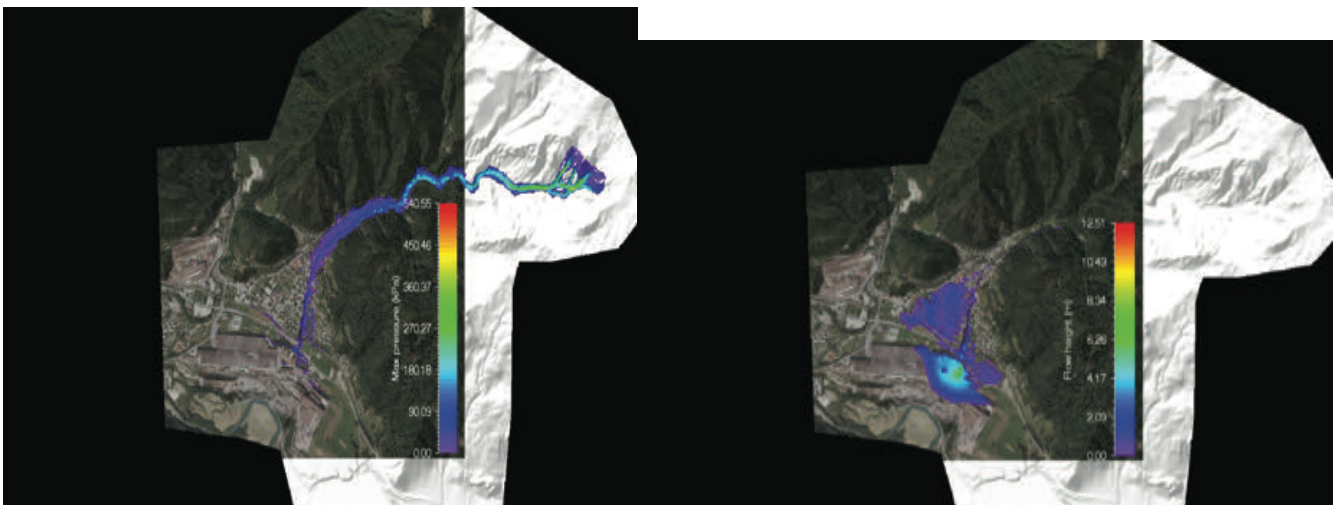


Figure 8 Example of RAMMS debris flow modelling results for the Koroška Bela area using hydrograph as input (peak of around 3,000 m<sup>3</sup>/s and magnitude of around 340,000 m<sup>3</sup>). Flow height at the end of simulation and maximum pressure are shown for the RAMMS model parameters  $\mu = 0.075$  and  $\xi = 200$  m/s<sup>2</sup>.

## Acknowledgments

The authors would like to thank Slovenian Research Agency (ARRS) for financial support through core financing P2-0180 and P1-0011, and two research projects J1-2477 and J1-3024, respectively.

## References

- Bertalanč R, Mojca D, Andrej D et al. (2018) Estimation of climate change impact in Slovenia until 2100, 1st edn. Slovenian Environment Agency, Ljubljana. (in Slovenian)
- Bezak N, Jemec Auflič M, Mikoš M (2019a) Application of hydrological modelling for temporal prediction of rainfall-induced shallow landslides. *Landslides*. 16: 1273–1283. <https://doi.org/10.1007/s10346-019-01169-9>
- Bezak N, Jemec Auflič M, Mikoš M (2021a) Reanalysis of Soil Moisture Used for Rainfall Thresholds for Rainfall-Induced Landslides: The Italian Case Study. *Water*. 13(14): 1977. <https://doi.org/10.3390/w13141977>
- Bezak N, Jež J, Sodnik J et al. (2020) An extreme May 2018 debris flood case study in northern Slovenia: analysis, modelling, and mitigation. *Landslides*. 17: 2373–2383. <https://doi.org/10.1007/s10346-019-01325-1>
- Bezak N, Mikoš M (2021) Changes in the rainfall event characteristics above the empirical global rainfall thresholds for landslide initiation at the pan-European level. *Landslides*. 18: 1859–1873. <https://doi.org/10.1007/s10346-020-01579-0>
- Bezak N, Mikoš M (2019) Investigation of trends, temporal changes in Intensity-Duration-Frequency (IDF) curves and extreme rainfall events clustering at regional scale using 5 min rainfall data. *Water (Switzerland)*. 11(10): 2167. <https://doi.org/10.3390/w11102167>
- Bezak N, Peternel T, Medved A, Mikoš M (2021b) Climate Change Impact Evaluation on the Water Balance of the Koroška Bela Area, NW Slovenia. In: Vilimek V, Wang F, Storm A et al. (eds) *Understanding and Reducing Landslide Disaster Risk*. Springer
- Bezak N, Sodnik J, Maček M et al. (2021c) Investigation of potential debris flows above the Koroška Bela settlement, NW Slovenia, from hydro-technical and conceptual design perspectives. *Landslides*. 18: 3891–3906. <https://doi.org/10.1007/s10346-021-01774-7>
- Bezak N, Sodnik J, Mikoš M (2019b) Impact of a random sequence of Debris flows on torrential fan formation. *Geosci*. 9(2): 64. <https://doi.org/10.3390/geosciences9020064>
- Bezak N, Šraj M, Mikoš M (2016) Copula-based IDF curves and empirical rainfall thresholds for flash floods and rainfall-induced landslides. *J Hydrol*. 541(Part A): 272–284. <https://doi.org/10.1016/j.jhydrol.2016.02.058>
- Gariano SL, Guzzetti F (2016) Landslides in a changing climate. *Earth-Science Rev* 162: 227–252. <https://doi.org/10.1016/j.earscirev.2016.08.011>
- Haque U, Blum P, da Silva PF, et al. (2016) Fatal landslides in Europe. *Landslides*. 13: 1545–1554. <https://doi.org/10.1007/s10346-016-0689-3>
- Janža M, Serianz L, Šram D, Klasinc M (2018) Hydrogeological investigation of landslides Urbas and Čikla above the settlement of Koroška Bela (NW Slovenia). *Geologija* 61:191–203. (in Slovenian) <https://doi.org/10.5474/geologija.2018.013>
- Jemec Auflič M, Bokal G, Kumelj Š et al. (2021) Impact of climate change on landslides in Slovenia in the mid-21st century. *Geologija*. 64: 159–171. <https://doi.org/10.5474/geologija.2021.009>
- Jemec Auflič M, Jež J, Popit T et al (2017) The variety of landslide forms in Slovenia and its immediate NW surroundings. *Landslides*. 14: 1537–1546. <https://doi.org/10.1007/s10346-017-0848-1>
- Jemec Auflič M, Šinigoj J, Krivic M et al. (2016) Landslide prediction System for rainfall induced landslides in Slovenia (Masprem). *Geologija*. 59: 259–271. <https://doi.org/10.5474/geologija.2016.016>
- Jordanova G, Gariano SL, Melillo M, et al. (2020) Determination of empirical rainfall thresholds for shallow landslides in Slovenia using an automatic tool. *Water (Switzerland)*. 12(5): 1449. <https://doi.org/10.3390/w12051449>
- Mateos RM, López-Vinielles J, Poyiadji E et al. (2020) Integration of landslide hazard into urban planning across Europe. *Landsc Urban Plan* 196: 103740. <https://doi.org/https://doi.org/10.1016/j.landurbplan.2019.103740>
- Mikoš M, Bezak N (2021) Debris Flow Modelling Using RAMMS Model in the Alpine Environment With Focus on the Model Parameters and Main Characteristics. *Front Earth Sci*. 8: 605061. <https://doi.org/10.3389/feart.2020.605061>
- Modugno S, Johnson SCM, Borrelli P et al. (2022) Analysis of human exposure to landslides with a GIS multiscale approach. *Nat Hazards*. <https://doi.org/10.1007/s11069-021-05186-7>
- Sodnik J, Kumelj Š, Peternel T et al. (2017) Identification of Landslides as Debris Flow Sources Using a Multi-model Approach Based on a Field Survey---Koroška Bela, Slovenia. In: Mikos M, Tiwari B, Yin Y, Sassa K (eds) *Advancing Culture of Living with Landslides*. Springer International Publishing, Cham, pp 1119–1126.

# Mountain slopes above Koroška Bela (NW Slovenia) – a landslide prone area

Tina Peternel<sup>(1)</sup>, Jernej Jež<sup>(1)</sup>, Mitja Janža<sup>(1)</sup>, Ela Šegina<sup>(1)</sup>, Matija Zupan<sup>(1)</sup>, Anže Markelj<sup>(1)</sup>, Ana Novak<sup>(1)</sup>, Mateja Jemec Auflič<sup>(1)</sup>, Janko Logar<sup>(2)</sup>, Matej Maček<sup>(2)</sup>, Nejc Bezak<sup>(3)</sup>, Jošt Sodnik<sup>(3)</sup>, Matjaž Mikoš<sup>(3)</sup>

1) Geological Survey of Slovenia, Dimičeva ulica 14, Ljubljana, Slovenia. +386 1 2809 813 ([tina.peternel@geo-zs.si](mailto:tina.peternel@geo-zs.si))

2) University of Ljubljana, Faculty of Civil and Geodetic Engineering, Chair of Geotechnical Engineering, Ljubljana, Slovenia

3) University of Ljubljana, Faculty of Civil and Geodetic Engineering, Chair of Hydraulic Engineering, Ljubljana, Slovenia

**Abstract** The paper deals with landslides in the hinterland of the Koroška Bela settlement, located in northwestern Slovenia at the foothills of the Karavanke mountain ridge. This area is known for numerous landslides. The settlement itself is built on the deposits of past debris flows, which indicates that its hinterland is prone to slope mass movements, which pose a threat to the settlement of Koroška Bela, which is very densely populated (about 2000 inhabitants) and has a well-developed industry and infrastructure. In this regard, the hinterland of Koroška Bela has been investigated since 2006 within the framework of various national and European projects. The main geological and geotechnical investigations were implemented after April 2017, when part of the Čikla landslide collapsed and mobilized into a debris flow with an estimated volume of 5,000 m<sup>3</sup>. The trigger was heavy rainfall with 200 mm of precipitation in 48 hours. Activities following this event focused mainly on identifying and understanding the landslide dynamics in order to design and implement mitigation measures. To achieve this, geological, geotechnical, and geodetic investigations were essential. In 2017 and 2019, several boreholes were drilled and equipped as inclinometers or piezometers. During drilling, we also conducted in-situ geotechnical and hydrogeological measurements. Cores samples were taken for geomechanical laboratory tests, and geophysical surveys were carried out along several cross-sections. This paper reports the main engineering geological descriptions based on field investigations of landslides in the hinterland of Koroška Bela.

**Keywords** monitoring, modelling, landslide, debris flow, Slovenia

## Introduction

Koroška Bela is a densely populated settlement located in the Upper Carniola region in the northwestern part of Slovenia. It was built on the deposits of past debris flow and covers an area of about 1.02 km<sup>2</sup> (Jež et al. 2008; Bezak et al. 2021b). Beyond the settlement of Koroška Bela, there

are mountain slopes that belong to the Karavanke mountain ridge. There are numerous landslide areas. Some of them could represent the source area of a potential debris flow, which could pose a threat to the underlying densely populated settlement with about 2000 inhabitants and well-developed industry and infrastructure.

Historical records also describe that there have been several debris flows in the hinterland of Koroška Bela in the recent geological past. The most recent event occurred in the 18th century and caused the partial or complete destruction of more than 40 buildings and cultivated areas in the village of Koroška Bela (Lavtižar 1897; Zupan 1937). Since we cannot completely avoid the effects of landslides and must adapt to them, it is important to understand their dynamics in space and time. Landslide monitoring and research on landslide dynamics provide the basis for landslide prevention and serve as a prerequisite for establishing prevention and mitigation measures.

In this respect, the mountain slopes above Koroška Bela have been studied since 2008 within the framework of various national and European projects (Jež et al. 2008; Komac et al. 2014; Peternel 2017; Peternel et al. 2017a; Peternel et al. 2017b; Peternel et al. 2018; Janža et al. 2018; Šegina et al. 2020; Peternel et al. 2021; Bezak et al. 2021). This paper presents investigations conducted after the April 2017 debris flow event and their results with the focus on the geological and hydrogeological characterization of landslides.

## Methodology

### Study area

The study area has complex geological and tectonic conditions. The geological units in this area are mainly represented by Jež et al. (2008) and Peternel et al. (2018):

- Quaternary clastic rocks, colluvium, slope and fluvial deposits (dry gravel, clayey gravel, silt, clay);
- Triassic to Lower Jurassic carbonate rocks (predominantly limestone);
- Permian carbonates (predominantly dolomite);

- Upper Carboniferous and Permian clastic and carbonate rocks (predominantly alternation of siltstone, claystone, sandstone, conglomerate).

The slope instabilities are mainly related to the tectonic contacts between the Upper Carboniferous to Permian clastic rocks and different Permian and Triassic carbonate and clastic rocks.

Tectonically, the area is part of the Košuta fault zone and is dissected by numerous NW-SE faults linking two major fault zones (the Sava and Periadriatic fault zones) (Jež et al. 2008). Detailed engineering geological mapping showed that there are more than 20 landslides, five of which are larger than 8,000 m<sup>2</sup>: Urbas, Čikla, Potoška planina, Malnež and Obešnik (Fig. 1). Based on previous research and field observations, the Urbas and Čikla landslides are considered the most active among them.

Landslide activity can be evidenced by hummocky terrain comprised of protrusions and depressions, curved pine trees, longitudinal tension cracks, erosion slumps and ponds on the surface, as well as the common deformation of local roads (Jež et al. 2008; Peternel 2017; Peternel et al. 2017a; Peternel et al. 2018; Peternel et al. 2020).

### Investigations

Recently, in April 2017, part of the Čikla landslide body collapsed and mobilized into mass flow with a large amount of debris and vegetation. The sliding material

flowed several hundred meters along the Čikla stream. This event and historical facts have shown that this area requires detailed observation and monitoring to prevent or mitigate the consequences of future events that pose a direct risk to the settlement of Koroška Bela. Consequently, numerous investigations were initiated to provide data for the design and implementation of mitigation measures. To address this need, geologic (including hydrogeologic, geophysical) and geotechnical investigations were conducted and used for stability analysis. All investigations performed are shown in Tab. 1 and Fig. 1. For landslide modelling and volume calculation, the GOCAD-SKUA software was used.

In addition to the listed investigations, climate change impact analysis and modelling of potential debris flows were performed (Bezak et al. 2021a; Bezak et al. 2021b). The result of debris-flow monitoring revealed that the magnitude of a previous debris flow ranged from 100,000 to 400,000 m<sup>3</sup>. In addition, more than 15,000 m<sup>3</sup> of material was deposited in the Bela and Čikla watercourses as a result of previous debris flows. Potential torrential floods could mobilize this material and increase the magnitude of the potential mass flow (Bezak et al. 2021b).

Climate change impact analysis indicates that the amount of precipitation, and thus effective precipitation, in the area of the Bela stream (hinterland) is expected to increase compared to the previous period (Bezak et al. 2021a). This may increase landslide activity in the future.

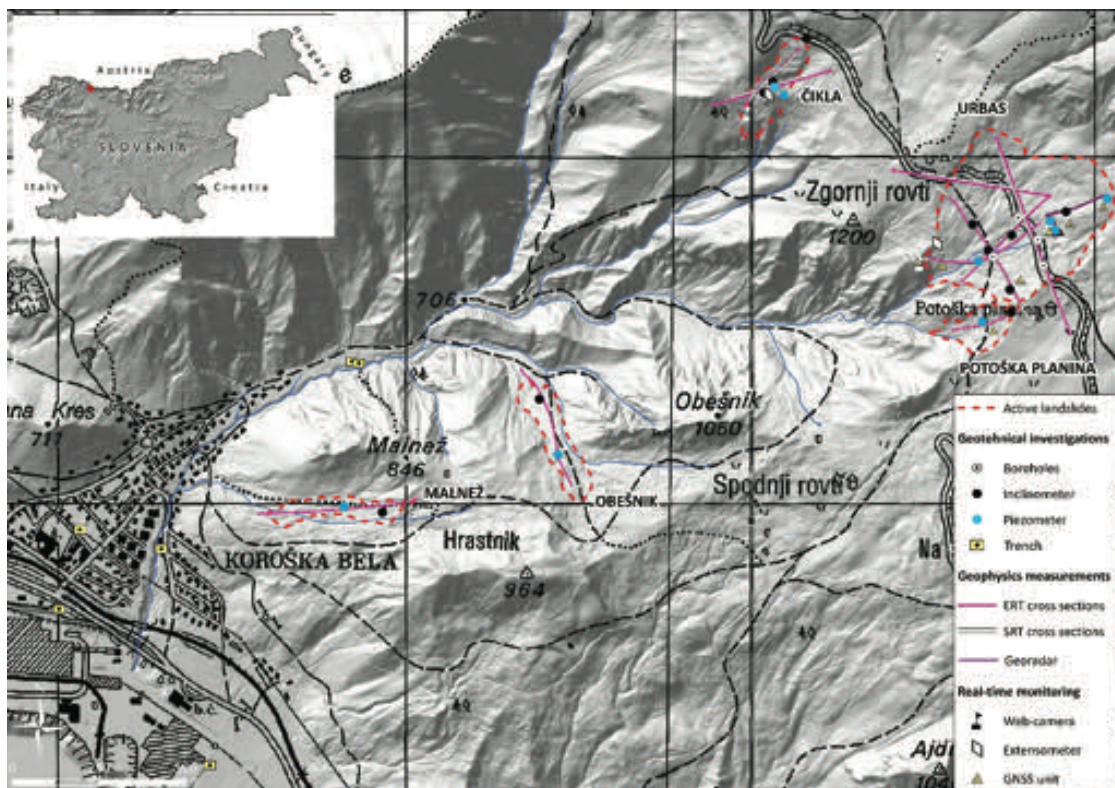


Figure 1 Location of study case and spatial distribution of applied methods.



Table 1: An overview of implemented recent investigations.

Landslide	Geotechnical investigations				Hydrogeological in-situ tests			Geophysical surveys (No. of cross-sections)			Real-time monitoring	
	Boreholes	Incl.	Piez.	Trench	Slug	Pumping	Tracking	ERT	SRT	GPR	GNSS	Exten.
Urbas	15	6	6	1	9	1	4	6	6	3	5	1
Potoška planina	2	1	1	/	/	/	/	1	1	/	1	/
Čikla	5	3	2	1	8	/	/	5	5	/	/	1
Malnež	2	1	1	/	1	/	/	1	/	/	/	/
Obešnik	2	1	1	/	1	/	/	1	/	/	/	/
Koroška Bela	/	/	/	7	/	/	/	/	/	/	/	/
<b>Sum</b>	<b>26</b>	<b>12</b>	<b>11</b>	<b>9</b>	<b>19</b>	<b>1</b>	<b>4</b>	<b>14</b>	<b>12</b>	<b>3</b>	<b>6</b>	<b>2</b>

**Results and discussion**

**Engineering geological characteristics of major landslides**

The Urbas landslide was recognized as the largest landslide in the hinterland of Koroška Bela. The landslide has a length of 500 m and a width of about 440 m. The landslide covers an area of 177,000 m<sup>2</sup>. The results of geological and geotechnical investigations revealed that the volume of the sliding mass is about 1,578,700 m<sup>3</sup>. A total of the 15 boreholes with a depth ranging from 21 m to 40 m were drilled (Tab.1, Fig.1). The six boreholes were equipped as inclinometers and piezometers.

The formation of the Urbas landslide is related to complex geological and tectonic conditions. It is defined as a rotational landslide and was formed at the tectonic contact between the Triassic carbonate and Carboniferous clastic rocks, mainly composed of siltstone and claystone. The main scarp was formed at the contact between the Carboniferous clastic rocks and dry talus material accumulated below the steep limestone ridge. In this part, the sliding surface was estimated to be 23 m deep.

The central part of the landslide consists of tectonically deformed and weathered clastic rocks with very low geomechanical properties and permeability. In this part, the depth of the landslide is about 10 m.

The most active part of the landslide is the lowest part. It consists of tectonically deformed and weathered clastic rocks mixed with a large amount of carbonate talus material. In addition, the Bela stream causes erosion and contributes significantly to the mobilization of the sliding material downstream (Fig.2).

The strong activity of the landslide can also be evidenced by the fact that 3 out of 5 inclinometers were sheared during the monitoring period of about six months.

Separated by a stable limestone ridge, a smaller landslide Potoška planina was formed south of the Urbas landslide. The Potoška planina landslide covers an area of 19,000 m<sup>2</sup>. The transverse width of the landslide at the widest part is about 120 m, and the length from the upper to the lower edge of the landslide is about 270 m.

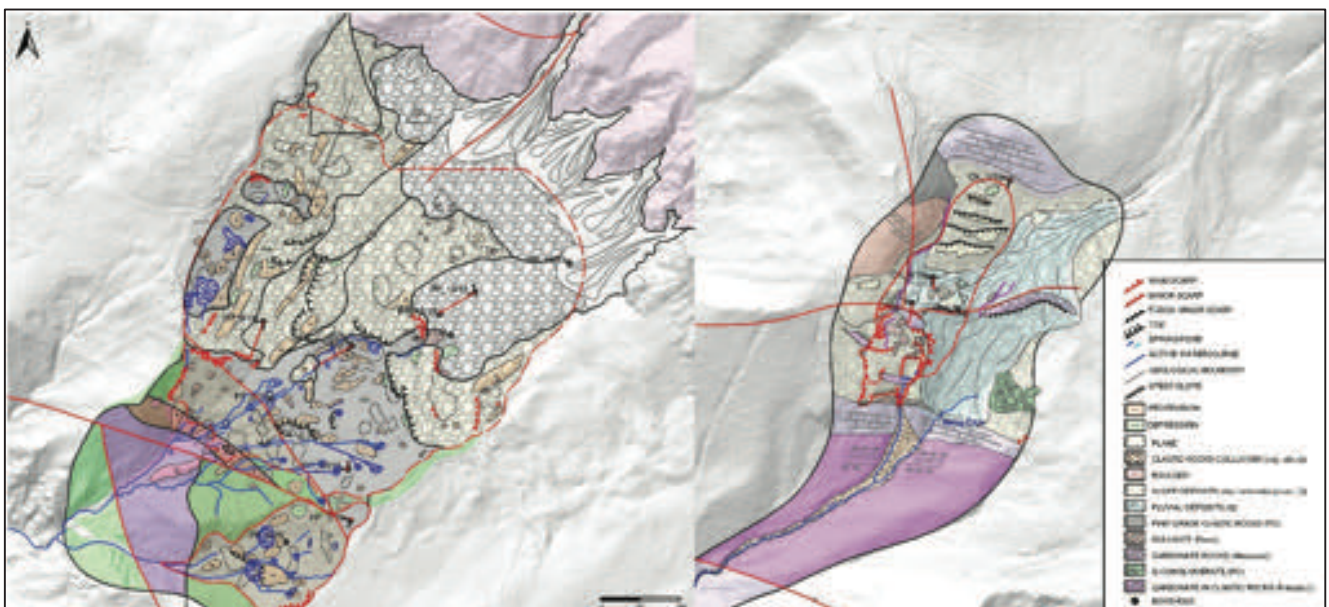


Figure 2 Engineering geological maps of Urbas (left) and Čikla (right) landslides.

Together with the Urbas landslide, the Čikla landslide is one of the most active landslides in the wider hinterland. Compared to the Urbas landslide, the Čikla landslide is much smaller, but much more active, which is also known from past debris flow events. Moreover, the path from the landslide to the settlement is shorter and narrower compared to the Urbas landslide. The Čikla landslide is 330 m long and 105 m wide. It covers an area of 26,000 m<sup>2</sup> and its volume was estimated to be about 330,500 m<sup>3</sup>. The Čikla landslide was investigated with 5 boreholes, two of which were equipped as piezometers and three as inclinometers (Tab. 1, Fig. 1). The depth of the boreholes was 40 m.

Like the Urbas landslide, the Čikla landslide is also defined by complex geological and tectonic conditions. The sliding mass of the Čikla landslide consists mainly of debris material deposited as a result of fossil mass flows. This material consists of silty gravel mixed with limestone blocks.

The main scarp was formed in debris material. In the central part of the Čikla landslide is a large limestone block that is tectonically deformed and highly weathered. This limestone block is very prone to instability and is also a source of debris material.

Boreholes and inclinometers indicate that the maximum shear surface occurs at a depth of 28 m, while the average sliding surface is about 23 m deep (Peternel et

al. 2018; Peternel et al. 2020). The groundwater level is at the contact between the debris deposits and the weathered bedrock. In this case, all inclinometers are still operative, although the measurements detect a constant displacement at a depth of 23.5 m.

The Malnež landslide was first identified in 2017 in the frame of detailed geological mapping of the Koroška Bela hinterland. The landslide was investigated with two boreholes (1 inclinometer, 1 piezometer) with depths of 25 and 17 m, respectively (Tab. 1, Fig. 1).

Detailed geological mapping revealed that this area could pose a threat to the settlement due to (Fig.3): the location and orientation of the landslide, which gravitates towards the settlement of Koroška Bela; short distance between the Koroška Bela settlement and the lower part of the landslide Malnež (less than 250 m); the presence of strong erosion in the torrent channels that gravitate directly towards the settlement of Koroška Bela.

The Malnež landslide covers an area of 21,200 m<sup>2</sup>. The geotechnical measurements showed that the depth of the sliding surface was determined to be 2.5 to 3 m in the upper part of the landslide, while the sliding surface in the middle part was estimated to be 10 m deep. Compared to the Urbas and Čikla landslides, this landslide is shallower. It consists of several successive rotational landslides related to the layer of weathered bedrock and the groundwater table (Fig. 3).

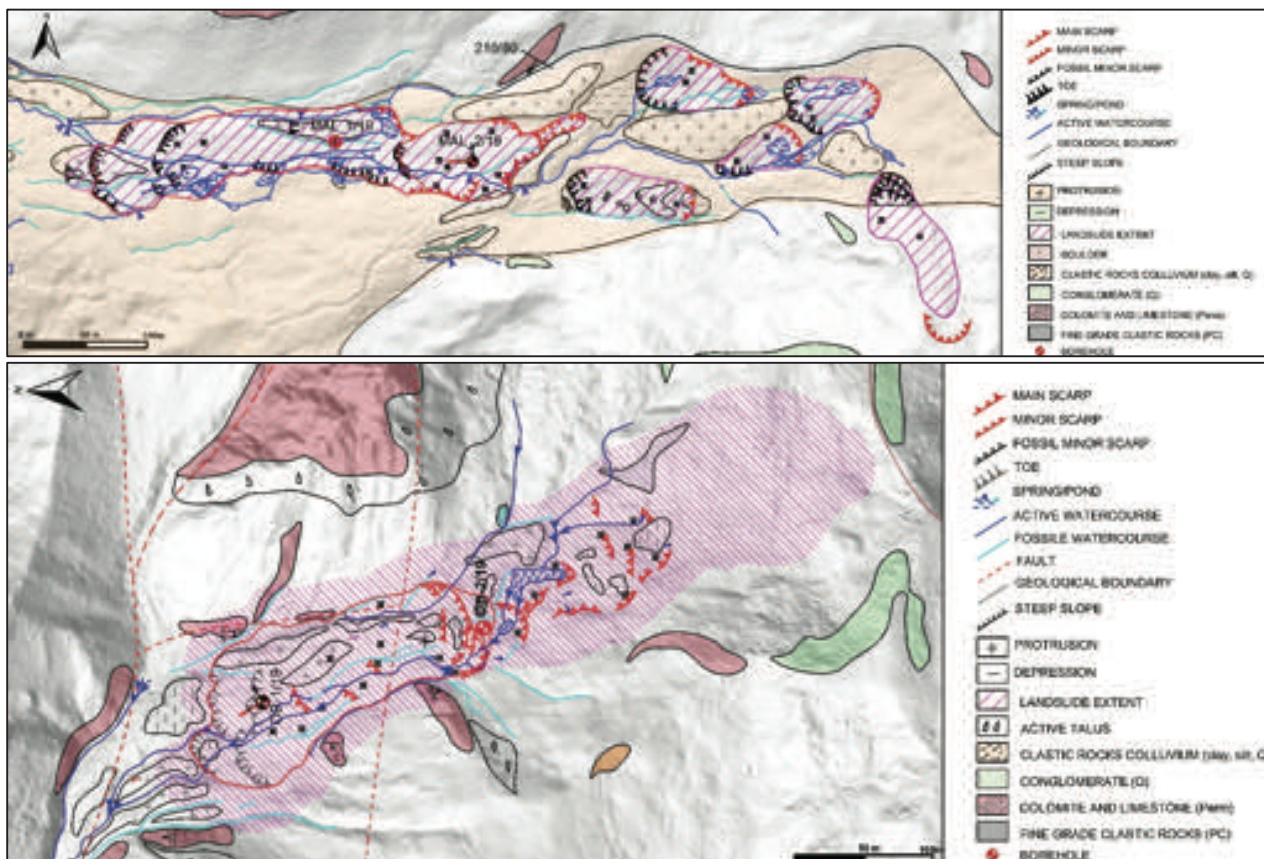


Figure 3 Engineering geological maps of Malnež (upper) and Obešnik (lower) landslides.

The Obešnik landslide was also identified in 2017 during the detailed engineering geological mapping. It was investigated with two boreholes (Tab. 1, Fig. 1). The depths of both boreholes were 25 m.

Detailed geological mapping showed that this landslide is active and potentially dangerous due to its size, steep slope and strong erosion. The landslide is moving towards the torrent channel, which is a left tributary of the Bela stream. The sliding material could dam the confluence or reach the settlement as a debris flow. The landslide is about 400 m long and about 80 m wide. It covers an area of 28,150 m<sup>2</sup>. The maximum depth of the sliding surface was estimated to be 20 m (Fig. 3). The sliding material consists of weathered bedrock of clastic rocks. Clayey gravel and sand with clay and silt layers are predominant.

### Hydrogeological conditions of landslides

The landslides above Koroška Bela have heterogeneous hydrogeological conditions and cannot be characterised uniformly due to complex geological and tectonic conditions.

In the case of the Urbas, Potoška planina and Čikla landslides, groundwater is recharged by the infiltration of precipitation and subsurface flow from carbonate hinterland. In the upper parts of the landslides, the groundwater occurs at the contact of slope deposits and weathered clastic rocks. Because of the steep slope, the water flows rapidly, especially during heavy precipitation. The bedrock morphology contributes significantly to the groundwater dynamics and the formation of local aquifers. The temporary and permanent springs are mainly located in the middle and lower parts of the landslides, where the weathered clastic rocks outcrop.

In the case of the Manež and Obešnik landslides, groundwater is recharged by infiltration of precipitation. In the case of the Malnež landslide, the groundwater level is just below the surface, while in the case of the Obešnik landslide, the groundwater level was measured at a depth of 6 m.

### Conclusions

The main outcomes are:

- The mechanisms of landslides are determined by complex geologic structures, intense tectonics, and hydrogeologic predispositions. Consequently, the lithological units of the study area are heavily deformed and prone to weathering. This leads to weak geomechanical properties of the bedrock.
- The Čikla and Urbas landslides are the most active in the hinterland of the Koroška Bela settlement. The formation of both landslides is attributed to complex geological and tectonic conditions. The dynamics of both landslides depends on hydrogeological conditions.

- The most active part of the Urbas landslide is its lower part. The sliding mass consists of tectonically deformed and weathered clastic rocks covered with a large amount of carbonate talus material. The Bela stream causes erosion and mobilization of the sliding material downstream.
- The Čikla landslide is known for past debris flows. The most recent one occurred in April 2017 due to heavy precipitation.
- The review of recent meteorological data shows that there has been no rainfall event on the scale of the one in April 2017 (app. 200 mm/48 h).
- The historical evidence, recent events and investigations confirmed that the landslides Urbas and Čikla are a source area for debris flows and could pose a direct threat to the settlement of Koroška Bela.
- Implementation of structural mitigation measures is essential to protect the population and infrastructure. Remediation measures need to be taken primarily on the Čikla and Urbas landslides and in the torrents.
- Potoška planina, Malnež and Obešnik landslides with their current state and dynamics do not pose a direct risk to the settlement. Nevertheless, monitoring should be continued and improved.
- In the future, regular and continuous monitoring of all landslides is essential to observe the landslide dynamics and to evaluate the effectiveness of structural mitigation measures.

### Acknowledgements

The research was funded by the Slovenian Research Agency (project Z1-2638 and Research Program P1-0419), the Ministry of Environment and Spatial Planning, and the Municipality of Jesenice.

### References

- Bezak N, Peternel T, Medved A, Mikoš M (2021a) Climate Change Impact Evaluation on the Water Balance of the Koroška Bela Area, NW Slovenia. Understanding and Reducing Landslide Disaster Risk. Vilímek V et al. (eds). Springer. pp. 221-228.
- Bezak N, Sodnik J, Maček M, Jurček T, Jež J, Peternel T, Mikoš M (2021b) Investigation of potential debris flows above the Koroška Bela settlement, NW Slovenia, from hydro-technical and conceptual design perspectives. *Landslides*. 18: 3891–3906.
- Jež J, Mikoš M, Trajanova M, Kumelj Š, Budkovič T, Bavec M (2008) Koroška Bela alluvial fan - The result of the catastrophic slope events (Karavanke Mountains, NW Slovenia). *Geologija*. 51(2):219-227. (in Slovenian)
- Komac M, Holly R, Mahapatra P, Van der Marel H, Bavec M (2014) Coupling of GPS/GNSS and radar interferometric data for a 3D surface displacement monitoring of landslides. *Landslides*. 12/2:241-257
- Lavtižar J (1897) History of parishes and bells in Radolica deanery. Self-published, Ljubljana. (in Slovenian)
- Peternel T (2017) Dynamics of the slope mass movements in the Potoška planina with analyses of results of remote sensing and terrestrial surveys techniques and in-situ measurements. PhD Thesis, University of Ljubljana, Ljubljana. (in Slovenian)

- Peternel T, Kumelj Š, Oštir K, Komac M (2017a) Monitoring the Potoška planina landslide (NW Slovenia) using UAV photogrammetry and tachymetric measurements. *Landslides*. 14(1): 395-406.
- Peternel T, Jež J, Milanič B et al. (2017b) Conducting urgent engineering geological, hydrogeological, geophysical and geomechanical and geodetic surveys to determine the objective risk to the population due to landslides in the area of Potoška planina and preparing expert bases with proposals for remedial measures. Geological Survey of Slovenia, Ljubljana. (in Slovenian)
- Peternel T, Jež J, Milanič B, Markelj A, Jemec Auflič M (2018) Engineering-geological conditions of landslides above the settlement of Koroška Bela (NW Slovenia). *Geologija*. 61(2): 177–189.
- Peternel T, Jež J, Janža M (2020) Detailed geological-geotechnical and hydrogeological characterization of large landslides in the hinterland of Koroška Bela settlement for the purpose of stability analyses and study of mitigation and remediation measures. Geological Survey of Slovenia, Faculty of Civil and Geodetic Engineering, Ljubljana. (in Slovenian)
- Peternel T, Šegina E, Zupan M, Jemec Auflič M, Jež J (2021) Preliminary result of real-time landslide monitoring in the case of the hinterland of Koroška Bela, NW Slovenia. *Understanding and Reducing Landslide Disaster Risk*. Tiwari et al (eds). Springer. pp. 459-464.
- Šegina E, Peternel T, Urbančič T, Realini E, Zupan M, Jež J, Caldera S, Gatti A, Tagliaferro G, Consoli A, González J, Jemec Auflič M (2020) Monitoring Surface Displacement of a Deep-Seated Landslide by a Low-Cost and near Real-Time GNSS System. *Remote Sensing*. 12(20): 3375.
- Zupan G (1937) *The local lexicon of Dravske banovine*. Uprava Krajevnega leksikona dravske banovine, Ljubljana. (in Slovenian)

# Recent large-scale gravitational collapses in the Madonna di Puianello mud-volcanoes field calderas (Northern Apennines, Modena, Italy)

Giuseppe Ciccacese<sup>(1)</sup>, Marco Mulas<sup>(1)</sup>, Francesco Ronchetti<sup>(1)</sup>, Marco Aleotti<sup>(2)</sup>, Alessandro Corsini<sup>(1)</sup>

1) University of Modena and Reggio Emilia, Department of Chemical and Geological Sciences, Modena, via G. Campi 103, Italy, +39 059 205 8498 (marco.mulas@unimore.it)

2) Emilia-Romagna Region—Regional Agency for Civil Protection and Territorial Security, Modena, Italy

**Abstract** This contribution aims to describe the geomorphic and kinematic characteristics of gravitational collapses that occurred on two different locations in the Madonna di Puianello mud-volcanoes field calderas (Northern Apennines, Modena, Italy) in February 2015 and in December 2020. These phenomena are studied on the basis of Global Navigation Satellites System periodic and permanent monitoring, SAR-Multi-Temporal Interferometry processing, field and Uncrewed Aerial Vehicle multi-temporal surveys. Observations and monitoring data are discussed with respect to the geological setting and geochemical constraints to identify potential causes of such events.

**Keywords** Northern Apennines, mud volcanoes, monitoring

## Introduction

Mud volcanoes are quite widespread phenomena in the front “Pede-Apennine margin” of the Northern Apennines within the Emilia-Romagna region (Bonini 2007). The upward migration of overpressure fluids and/or hydrocarbons can manifest on the surface with the formation of mud volcanoes up to 2-3 m high or gas vents. A mud volcano field is characterized by different eruptive phases alternating with calm phases and it can evolve by sinking into a caldera-like circular pattern (Bonini 2012). Eventually, mud volcanoes can evolve into paroxysmal eruptions with destructive consequences as happened in 91 BC in the Montegibbio settlement (Modena province), not distant from these mud-volcanoes field calderas (Borgatti et al. 2010).



Figure 1 Field impressions of Madonna di Puianello field calderas. a) Active mud volcanoes in the Possessione field; b) Houses damaged within the Traino caldera; c) and d) normal rimming fractures in the Possessione and Traino fields. Picture (c) courtesy of G. Bertolini.

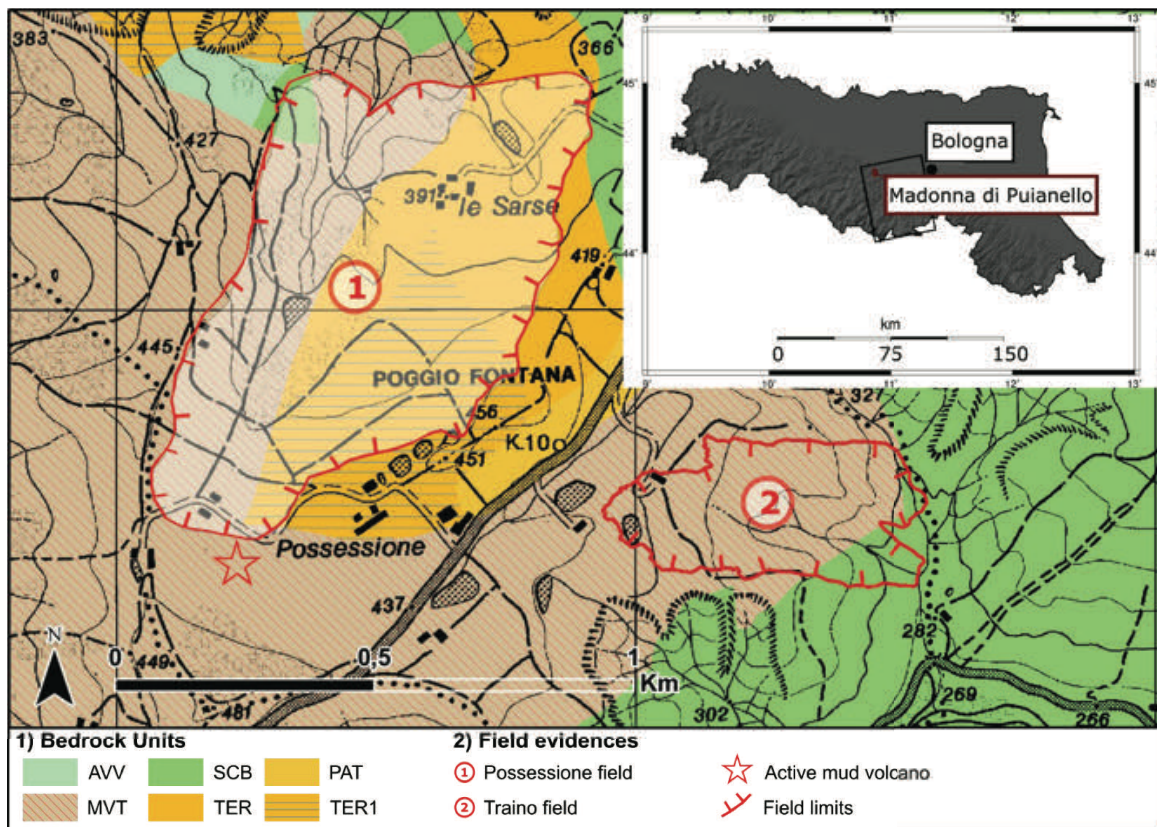


Figure 2 Geographical and geological setting of Madonna di Puianello mud-volcanoes field calderas.

From the geochemical point of view, the mud volcano fluids are characterized by the absence of Tritium content ( $T < 0.5$  TU) and by depleted oxygen ( $\delta^{18}\text{O}$ ) and hydrogen ( $\delta\text{D}$ ) stable isotope content ( $\delta^{18}\text{O}$  between 0.0 and 6.0‰ and  $\delta\text{D}$  between -30.0 and -10.0‰) and they are characterized by an isotope content completely different from the precipitation and the normally groundwater (Cervi et al. 2012).

### Case study and geological setting

Active mud volcanoes are present within the Possessione field (Fig. 1a): they are characterised by 2 gryphons up to 2.5 m tall with fluids emissions and intermittent gas bubbles emerging from the saline muddy water. Manga and Bonini (2012) reported, at this same site, an increase of activity characterised by the extrusion of mud flows containing several clasts with max size of 2.5 cm a few days after the 20 May 2012 Emilia seismic sequence. The Madonna di Puianello mud volcanoes field has recently experienced two major large-scale gravitational collapses of significant magnitude in two different locations in 2015 and 2020 (Fig. 2). Both events started suddenly and developed rapidly during less than 12 hours. In February 2015, at the Possessione field, normal fractures with up to 25 cm (Fig. 1) of vertical displacement rimmed an area as large as 0,5 km<sup>2</sup> area (Mulas et al. 2016). At first the uphill

normal fractures (located at south) were identified as the crown of a deep-seated landslide. Later, thanks to field surveys, aerial photo interpretation, the phenomenon was better identified as a gravitational collapse feature. Recently, in December 2020, in the Traino field located less than 1 km eastward, another similar event took place affecting an area of 0,15 km<sup>2</sup>. In this second case, sub-vertical fractures rimming the collapsed area showed displacements as high as 5-7 m, evidencing the caldera-like collapse nature of the phenomenon (Fig. 1).

The geology of the area (Fig. 2) consists of the Ligurian units and the overlying Epiligurian. Within the Ligurian units outcrop the “Arenarie di Scabiazza” (SCB) (Late Turonian-Campanian), formed of thin-bedded sandstone turbidites and the “Argille Varicolori di Cassio” (AVV) (Late Cenomanian-Late Campanian). While the Epiligurian Succession is represented by four units: the “Brecce Argillose della Val Tiepido-Canossa” (MVT) (Chattian-Aquitania), a thick chaotic body of shales with dispersed clasts of heterogeneous sizes and types; the “Pantano” (PAT) formation (late Burdigalian- Langhian), mainly composed of fine-grained shallow-water sandstones; the Termina (TER) formation (Tortonian-Messinian) represented by mudstones and turbidite sandy limestones, and the “Membro di Montardone” (TER<sub>1</sub>) of the same age formed of shaly argillaceous polygenic breccias (Fig. 2).

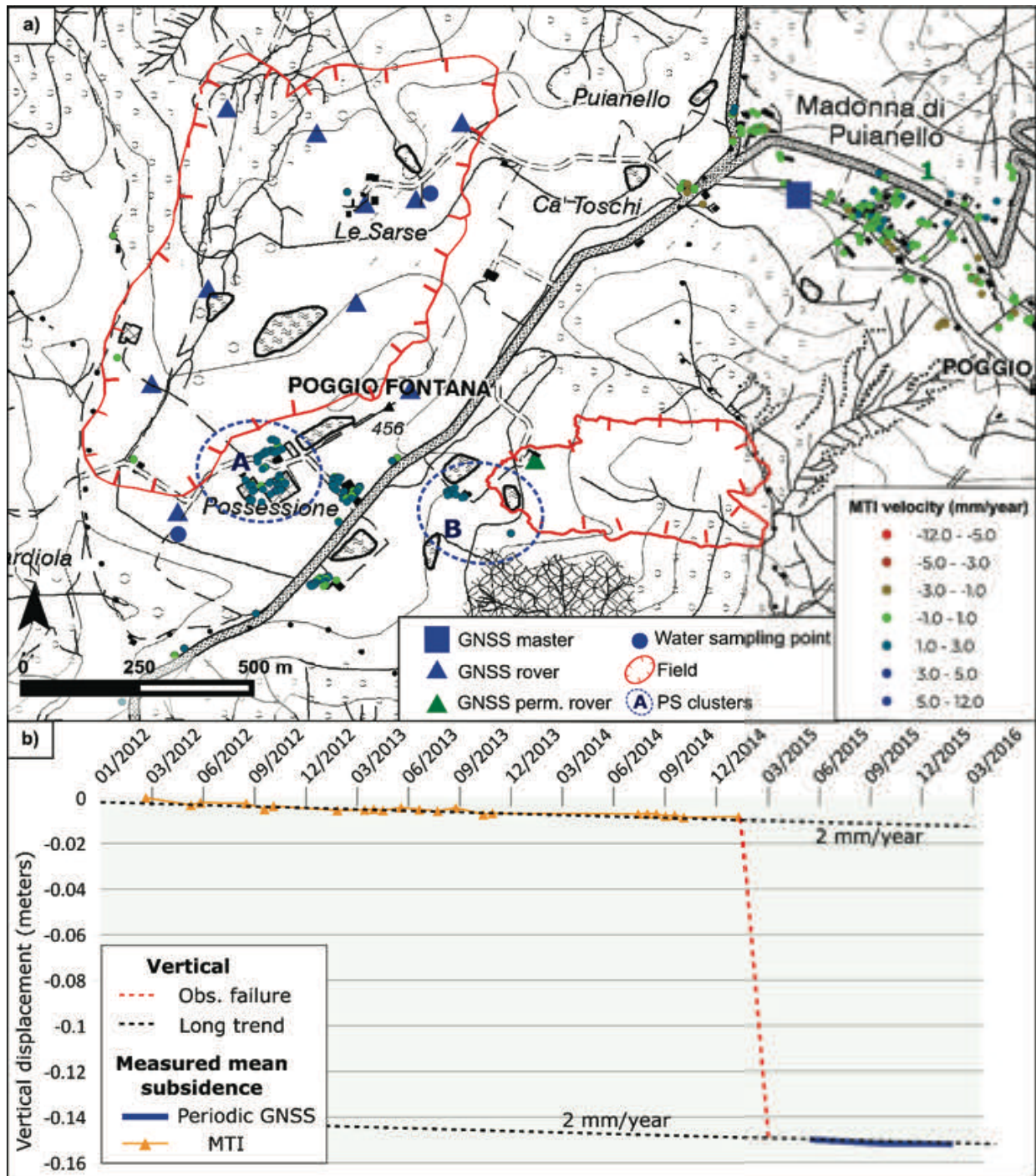


Figure 3 Monitoring data collected at the Madonna di Puianello mud-volcanoes field calderas. MTI time-series presented in Fig. 3b are representative of mean velocities of points selected within clusters “A” and “B” of Fig. 3a.

### Monitoring data

Periodic Global Navigation Satellite System (GNSS) surveys, Permanent GNSS and SAR Multi-Temporal Interferometry (MTI) are the technique applied for surface displacement monitoring. SAR scenes obtained from archives represent a key tool to determine displacements in an area in the past (Mulas et al. 2015). Using the Small baseline implementation of the STaMPS method (Hooper et al. 2007) 23 X-band COSMO-SkyMed (CSK) scenes were

processed. SAR data cover a two-year period (January 2013 to January 2015), refer to the Ascending orbit and were acquired in Stripmap HIMAGE mode.

In the Possessione field, with respect to the timing of the evolution of these phenomena, both periodic GNSS surveys (Possessione field) and permanent GNSS monitoring (Traino field) and MTI analysis, evidenced that movements had substantially return to extremely slow rates after the main events. Quantitatively, displacement rates returned in the order of 2 mm/year that MTI SAR

interferometry shows as long-term trend in both areas (Fig. 3b). Planimetric displacements, in the Traino field, derived from UAV orthophoto, referred to the Jan. 2021 survey (Tab. 1), compared to the pre-event AGEA-2018 orthophoto confirm the metric magnitude observed by field surveys (Fig. 4).

Table 1 Topographic monitoring data

Technology	Date	Site
MTI	01/2012-01/2015	Possessione field
Periodic GNSS	05/2015-01/2016	Possessione field
Perm. GNSS	03/2021-11/2021	Traino field
UAV surveys	03/01/2021;08/03/2021	Traino field

Isotopes analysis of water samples collected within the Possessione field (see location in Fig.3) after the 2015 event shows negative values for the  $\delta^{18}\text{O}$  (-9.0‰) and  $\delta\text{D}$  (-61.01‰) and a Tritium content of 5.3 TU. These results excluded the migration of fluids from the Puianello mud volcano to the deformed area and highlighted a meteoric origin of the groundwater inside the caldera.

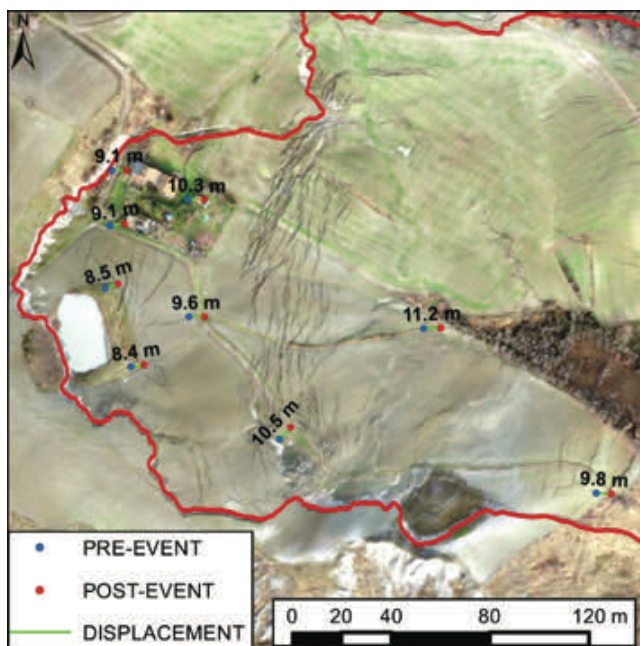


Figure 4. Planimetric displacements occurred in the Traino field during the Dec. 2020 event: quantitatively measured by comparing the UAV derived orthophoto of Jan. 2021 and AGEA-2018 orthophoto.

## Discussion

Actually, the possible causes of these sudden impulsive evolutions are still substantially unknown. The geological setting of the area is highly complex, and for a number of tectonic reasons highly fractured sandstones of the Pantano formation lay in depth underneath clay shales of

Ligurian and Epi-ligurian sequence. Thus, at least in principle, a rapid degasification or reduction of deep water fluxes inside the sandstones, could trigger normal faulting inside the clay shales cap and determine the caldera-like shape observed in the field. Nevertheless, there is no direct evidence of any sudden degasification before the events, and as a matter of fact, the mud-volcanoes in the field did not show any increased activity prior to the collapses. Furthermore, water sampled in wells located in the area have mostly a gravitational origin, since they do not show the distinctive isotopic signature of mud-volcanoes fluids (i.e. absence of Tritium and depleted oxygen  $\delta^{18}\text{O}$  and hydrogen  $\delta\text{D}$  stable isotopes). Nevertheless, this does not exclude possible changes of pressure in deep fluids.

## Acknowledgments

This work was supported by the Civil Protection Agency of the Emilia-Romagna Region under the framework agreement “Special activities on support to the forecast and emergency planning of Civil Protection with respect to hydrogeological risk” (ASPER-RER, 2016-2021)

## References

- Bonini M (2007) Interrelations of mud volcanism, fluid venting, and thrust-anticline folding: Examples from the external northern Apennines (Emilia-Romagna, Italy). *J Geophys Res* 112:B08413. <https://doi.org/10.1029/2006JB004859>
- Bonini M (2012) Mud volcanoes: Indicators of stress orientation and tectonic controls. *Earth-Science Rev* 115:121–152. <https://doi.org/10.1016/j.earscirev.2012.09.002>
- Borgatti L., Cervi F., Corsini A., Guandalini F., Ronchetti F., Pellegrini M. (2010). Ipotesi sugli eventi distruttivi rilevati nell’abitato romano di Montegibbio. In: Guandalini F. & Labate D. (eds.), *L’insediamento di Montegibbio*. Quaderni di Archeologia dell’Emilia Romagna, 26, 95-109.
- Cervi F, Ronchetti F, Martinelli G, et al (2012) Origin and assessment of deep groundwater inflow in the Ca’ Lita landslide using hydrochemistry and in situ monitoring. *Hydrol Earth Syst Sci* 16:4205–4221. <https://doi.org/10.5194/hess-16-4205-2012>
- Hooper A., Segall P, Zebker H (2007) Persistent scatterer interferometric synthetic aperture radar for crustal deformation analysis, with application to Volcán Alcedo, Galápagos. *J Geophys Res Solid Earth* 112:1–21. <https://doi.org/10.1029/2006JB004763>
- Manga M, Bonini M (2012) Large historical eruptions at subaerial mud volcanoes, Italy. *Nat Hazards Earth Syst Sci* 12:3377–3386. <https://doi.org/10.5194/nhess-12-3377-2012>
- Mulas M, Bayer B, Bertolini G, et al (2016) Impulsive ground movements in the mud volcanoes area of “Le Sarse” di Puianello (Northern Apennines, Modena, Italy): field evidence and multi-approach monitoring. *Rend Online della Soc Geol Ital* 41:251–254. <https://doi.org/10.3301/ROL.2016.141>
- Mulas M, Petitta M, Corsini A, et al (2015) Long-term monitoring of a deep-seated, slow-moving landslide by mean of C-band and X-band advanced interferometric products: the Corvara in Badia case study (Dolomites, Italy). *ISPRS - Int Arch Photogramm Remote Sens Spat Inf Sci* XL-7/W3:827–829. <https://doi.org/10.5194/isprsarchives-XL-7-W3-827-2015>



# Paroxysmal reactivation of a large-scale earth flow documented by multitemporal UAV photo surveys and Robotic Total Station

Giuseppe Ciccarese<sup>(1)</sup>, Marco Mulas<sup>(1)</sup>, Francesco Ronchetti<sup>(1)</sup>, Marco Aleotti<sup>(2)</sup>, Alessandro Corsini<sup>(1)</sup>

1) University of Modena and Reggio Emilia, Department of Chemical and Geological Sciences, Modena, via G. Campi 103, Italy, +39 059 205 8498 (marco.mulas@unimore.it)

2) Emilia-Romagna Region—Regional Agency for Civil Protection and Territorial Security, Modena, Italy

**Abstract** Monitoring the evolution of large earth flows can be a difficult task when a rapid paroxysmal reactivation occurs. When studying landslides that can have a total length of several kilometres, it is difficult to select the suitable technique to provide reliable and rapidly available data to local authorities that are managing the emergency. Nowadays, Uncrewed Aerial Vehicle shows strength not only for field emergency inspections but also to deliver high resolution multitemporal orthophotos. These can represent the starting point to obtain spatialised displacement maps that could be of great use to support decision makers during emergency scenarios. In this contribution, we present the application of Uncrewed Aerial Vehicle structure from motion tool to images acquired in the visible spectrum by comparing the results obtained from Robotic Total Station monitoring.

**Keywords**, Monitoring, Earth slide, Earth flow, Uncrewed Aerial Vehicle, Robotic Total Station, Photogrammetry, Northern Apennines

## Introduction

Large earth flows can alternate long dormant periods to phases characterised by paroxysmal reactivations involving partially or entirely the landslide body (Bertolini and Pizziolo 2008; Mulas et al. 2018; Mulas et al. 2020a). Once a reactivation event occurs, it is crucial to rapidly assess the portion of the landslide involved and then set up the proper monitoring system if infrastructures or human activities are at risk. Given the accuracy and precision of Robotic Total Stations (RTS) it is considered an established technique for monitoring active landslides (Giordan et al. 2013; Corsini et al. 2015; Corsini and Mulas 2016). More recently, the advent of Uncrewed Aerial Vehicle (UAV) based photogrammetry represented a complementary tool to study and monitor landslides (Niethammer et al. 2012; Peternel et al. 2017; Meng et al. 2021).

The aim of this contribution is to describe the recent reactivation of the Valoria landslide, pointing out the peculiarities of the displacement patterns evidenced by RTS monitoring and by highlighting possible multiple applications of UAV as a tool for an effective landslide evolution characterization. This is tentatively done by using UAV rapid mode surveys and quantitative estimation of displacements by using UAV photogrammetric mode surveys.

## Case study

The Valoria landslide is a complex earth flow located in the Northern Apennines of Italy, in the upper Secchia River basin of the Emilia Romagna Region. It is a rainfall triggered and well-characterised landslide (Corsini et al. 2009; Ronchetti et al. 2007; Tonnellier et al. 2013). It affects flysh rock masses and clayey shales for a surface of 1.6 km<sup>2</sup> over a length of 3.5 km. It has a vertical development of about 900 m, with the source area at 1,413 m above sea level. Between 2001 and 2009, landslide reactivations caused repeated interruptions to traffic on a local road. This led local authorities to build an overpass bridge in the track zone in 2009 to preserve the viability in case of further reactivation. From October 2020 to March 2021, the Valoria landslide experienced the first paroxysmal reactivation since overpass bridge construction, which has caused concern for the infrastructure itself. This last reactivation is considered as paroxysmal since it involved the entire landslide, from crown to toe over a length of 3 km and with cumulative displacements as large as 300 m. This event, like previous ones, has started as a retrogressive rotational landslide in the source zone and then the masses evolved into an earth flow along the track and accumulation zone, so it can be classified as a complex landslide (*sensu* Cruden and Varnes 1996). The downhill propagation was characterised by repeated accelerations within the period from October 2020 to March 2021.

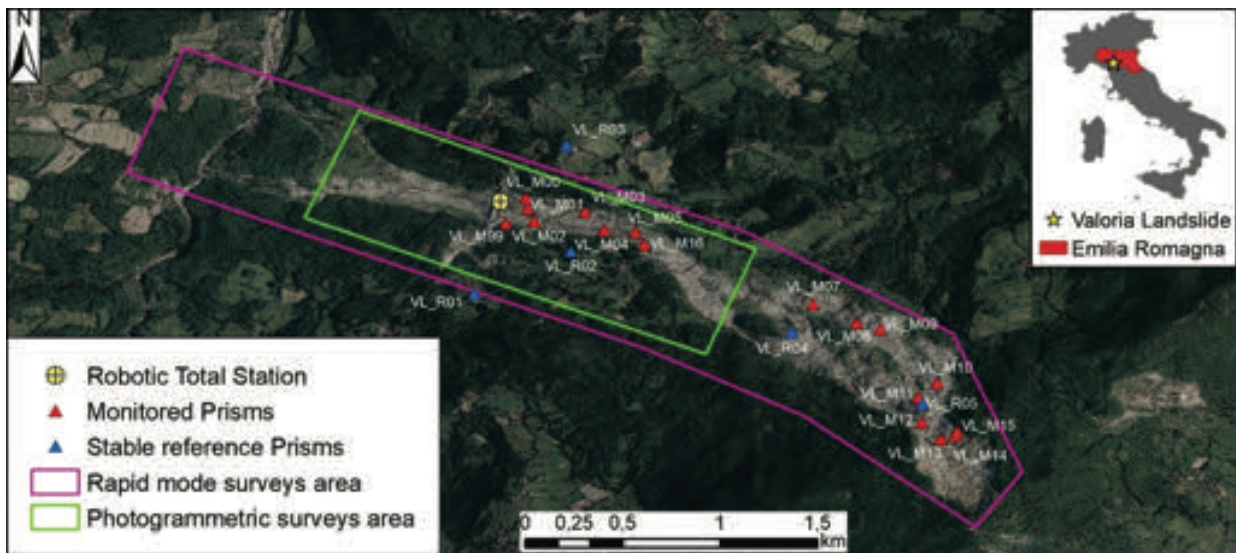


Figure 1 Valoria landslide with marked RTS monitoring prisms and UAV survey modes coverage.

## Materials and Method

### Robotic Total Station

To monitor the evolution of the phenomenon, from November 2020 onward a total of 18 prisms (see location in Fig. 1) have been continuously monitored (1 hour frequency) using an RTS installed on the overpass bridge itself (Fig. 2). More in detail, the RTS in use is characterised by vertical and horizontal angular accuracy of 0.5", maximum range up to 3.5 km and distance accuracy of 0.6 mm + 1 ppm. Monitoring points are located uphill of the overpass bridge in-between the source and track areas. The RTS is remotely controlled to perform hourly monitoring cycles (two strata in direct and reverse positions) but during the most active phases, frequency acquisition was manually increased to 30 minutes to preserve target identification.

### UAV surveys strategies

As is common in this field, repeated UAV surveys were performed to obtain updated georeferenced orthophotos (Thiebes et al. 2016), which would allow to follow the evolution of the landslide in unmonitored sectors and, eventually, quantify movements. Two acquisition strategies have been used: i) *rapid mode surveys* (RS), which cover the entire re-activated landslide area characterised by low resolution and accuracy but useful to map the landslide evolution; ii) *photogrammetric mode surveys* (P), which cover smaller areas but deliver highly reliable results that can be coupled to pointwise data obtained by the contextual RTS results.

More in detail, RS surveys are performed by manually capturing the images and manually flying the UAV. It is characterised by a relatively low quantity of pictures taken with respect to very large areas covered. This will lead to the Structure from Motion (SfM) elaboration to lower dense cloud outputs with respect to P surveys (Tab. 1).

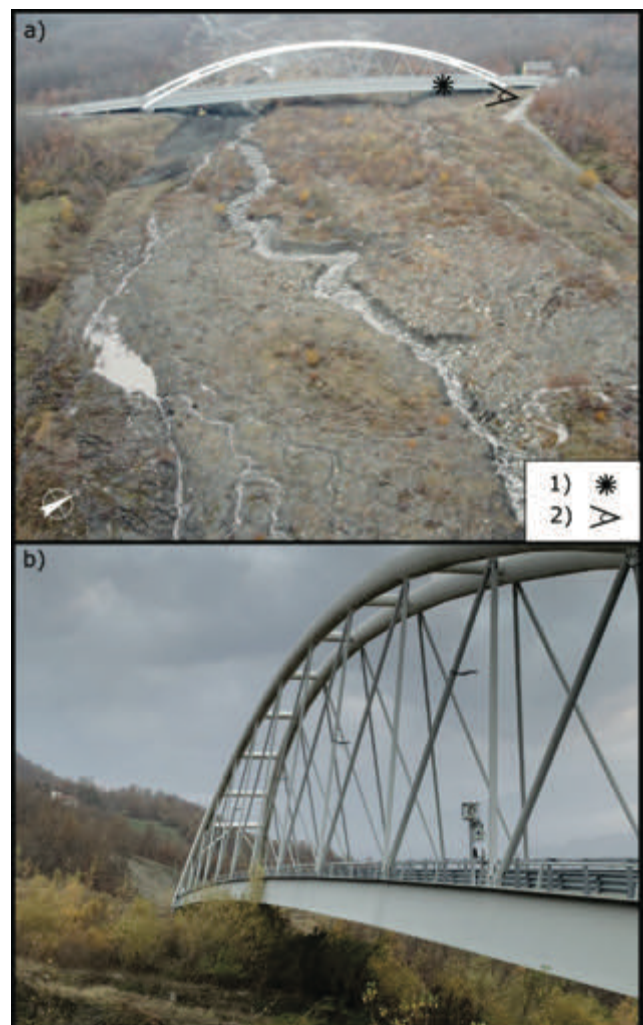


Figure 2 RTS location. a) Valoria landslide overpass bridge, 1) RTS location; 2) picture take position of Fig.2b. b) RTS installation.

Table 1 UAV surveys results. Survey strategies: P) Photogrammetric; RS) Rapid Survey.

Date	Survey strategy	Pictures	Dense cloud (pts)	Resolution (cm)
08/11/2020	RS	73	10,527,473	10
21/11/2020	RS	101	14,076,446	10
21/12/2020	RS	201	14,868,148	10
23/12/2020	P	496	34,798,151	3.5
14/01/2021	RS	198	12,391,355	10
30/01/2021	RS	204	17,507,519	10
20/02/2021	RS	198	18,314,550	10
04/03/2021	P	487	51,124,553	3.5
05/03/2021	RS	207	13,525,463	10
16/04/2021	P	545	11,537,949	3.5
19/04/2021	RS	241	11,185,398	10
18/05/2021	P	535	53,720,054	3.5

Photogrammetric surveys are performed by programming automatic photogrammetric missions with the following characteristics: flight height 100 m, side overlap 70%, front overlap 80%, ground sample distance 2.74 cm/pixel, flight speed: 5.5 m/s, area: 0.8 km<sup>2</sup> and flight time ~35 minutes. In order to allow replication of the SfM workflow performed these are the settings used in Agisoft Metashape environment: Photo alignment (Accuracy: Medium), dense cloud building (Quality: Medium), DEM building (Interpolation: Enabled) and orthomosaic building (Blending mode: Mosaic).

**Results**

The cumulative time-series of displacements resulting from RTS monitoring (Fig. 3) depict an initial rapid phase (Stage 1) characterised by maximum mean velocities of up to 1.3 m/day (period within November to December 2020), followed by a less active period (Stage 2) with maximum mean velocities of 0.75 m/day (from December 2020 to March 2021). Finally, from the end of March 2021, the landslide decelerated to several cm/day (Stage 3). Some monitored prisms (VL\_Mo4, VL\_o6 and VL\_M16) located in the track zone closely uphill the bridge bypass scored a total cumulative displacement up to 300 m and showed distinctive acceleration and deceleration patterns in response to changing geomorphic triggering conditions (i.e. mass accumulation/depletion) and meteorological forcing factors.

UAV RS orthophoto outputs, even if characterised by lower geometric resolution and less dense cloud points than photogrammetric surveys (see Tab. 1), allowed to determine and map the evolution of the landslide. In Fig. 4 it is depicted the area progressively involved by the reactivation as interpreted using relevant rapid survey orthophotos acquired on 08/11/2020, 21/11/2020, 21/12/2020 and 30/01/2021. It presents the initial retrogressive style of activity in the source area characterised by rotational movements that evolved into earth slides (within the steepest slopes) and earth flows with downslope enlarging style of activity sensu Cruden and Varnes (1996).

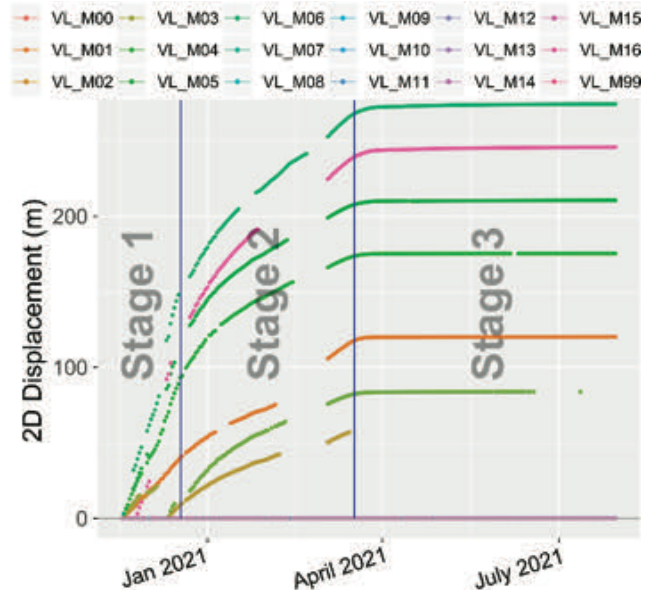


Figure 3 RTS cumulative displacements. Prisms VL\_Moo, VL\_Mo7, VL\_Mo8, VL\_Mo9, VL\_M1o, VL\_M11, VL\_M12, VL\_M13, VL\_M14, VL\_M15 and VL\_M99 have total cumulative displacements lower than 0.4 m resulting flattened on the horizontal axe.

The high resolution (3.5 cm) of orthophotos obtained by P surveys allowed to perform the validation of displacements derived from feature tracking at four different dates (23/12/2020, 04/03/2021, 16/04/2021 and 18/05/2021) in comparison to those measured by RTS. In detail, we have compared planimetric displacements of prisms VL\_Mo1 and VL\_Mo4 derived from RTS monitoring and feature tracking (prisms location identification) operated on the photogrammetric orthophotos. Results, presented in Fig. 5, confirm the good accuracy of cumulative displacements derived from UAV photogrammetric surveys.

**Conclusions**

In this contribution, we presented the application of UAV SfM algorithms applied to images acquired with two different survey strategies (P and RS modes) and distinct aims to characterise the recent Valoria landslide reactivation. The RS survey mode is characterised by rapid execution and large area coverage but at cost of the lower resolution of the resulting orthophoto. This strategy proved to be of help when the first goal is to deliver updated maps to support decision makers during emergency scenarios. On the other hand, P surveys proved their reliability as a quantitative tool and represent the starting point for the application of automated spatially distributed offset tracking algorithms for landslide monitoring (Dahene et al. 2013; Mulas et al. 2016; Mulas et al. 2020b).

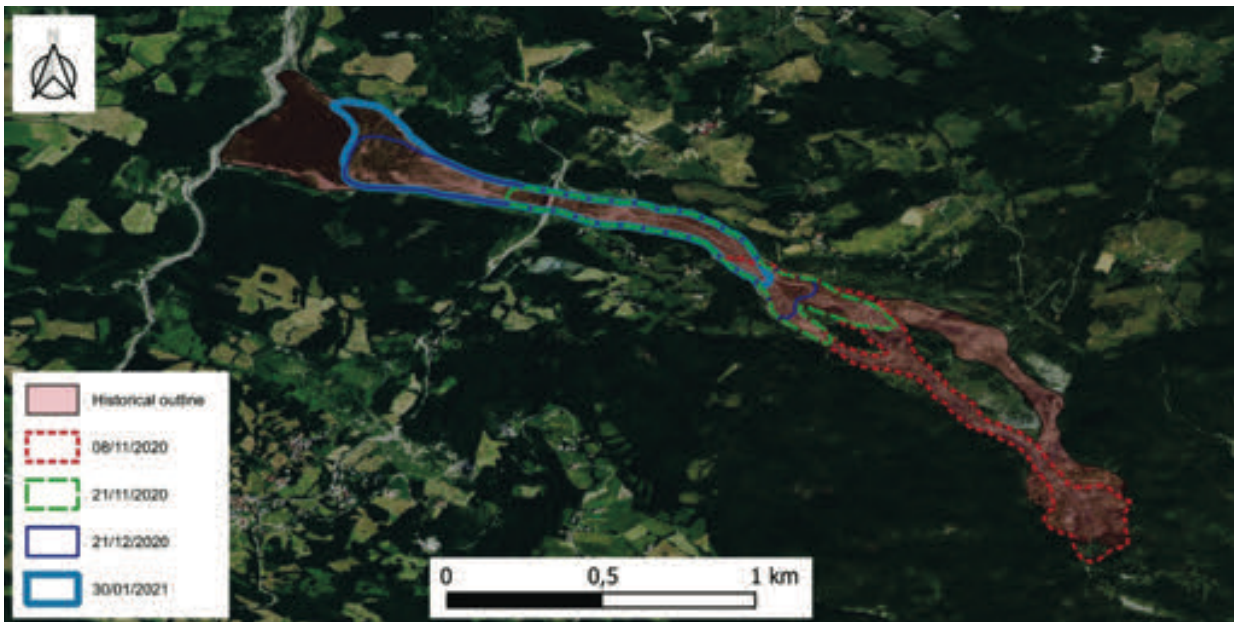


Figure 4 Relevant UAV Rapid survey outputs. Historical outline represents the maximum extension of the landslide area involved in previous reactivations.

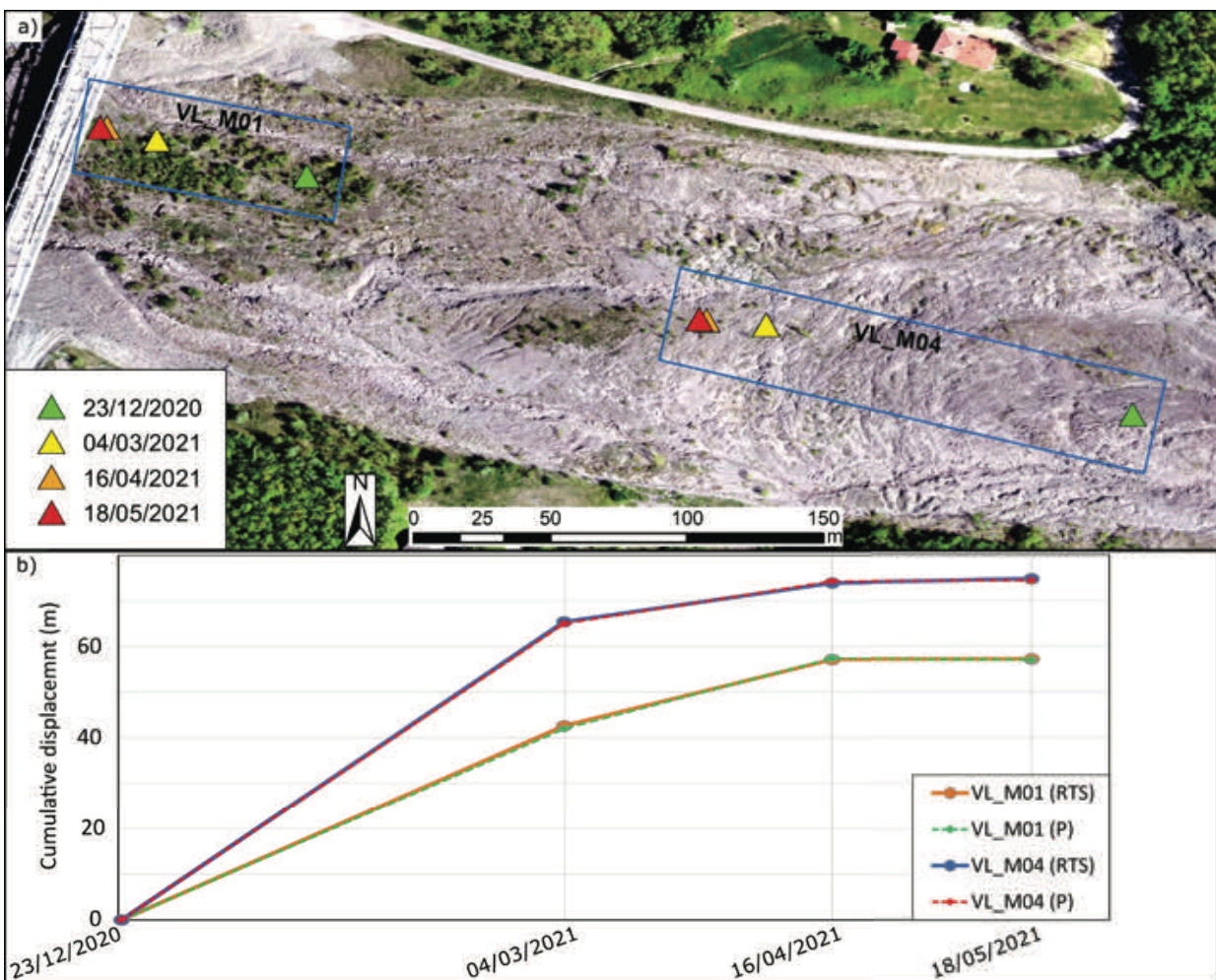


Figure 5 Photogrammetric survey output vs RTS. a) Prisms VL\_M01 and VL\_M04 tracking (base map: orthophoto acquired on 18/05/2021). b) Relative cumulative planimetric displacement comparison between RTS and UAV feature tracking on photogrammetric orthophotos.

## Acknowledgements

This work was supported by the Civil Protection Agency of the Emilia-Romagna Region under the framework agreement “Special activities on support to the forecast and emergency planning of Civil Protection with respect to hydrogeological risk” (ASPER-RER, 2016-2021)

## References

- Bertolini G, Pizziolo M (2008) Risk assessment strategies for the reactivation of earth flows in the Northern Apennines (Italy). *Eng Geol.* 102: 178–192.  
<https://doi.org/10.1016/j.enggeo.2008.03.017>
- Corsini A, Bonacini F, Mulas M et al (2015) Long-Term Continuous Monitoring of a Deep-Seated Compound Rock Slide in the Northern Apennines (Italy). *Engineering Geology for Society and Territory - Volume 2*. Springer International Publishing, Cham. pp 1337–1340.
- Corsini A, Borgatti L, Cervi F et al (2009) Estimating mass-wasting processes in active earth slides – earth flows with time-series of High-Resolution DEMs from photogrammetry and airborne LiDAR. *Nat Hazards Earth Syst Sci.* 9: 433–439.  
<https://doi.org/10.5194/nhess-9-433-2009>
- Corsini A, Mulas M (2016) Use of ROC curves for early warning of landslide displacement rates in response to precipitation (Piagneto landslide, Northern Apennines, Italy). *Landslides.* 14: 1241. <https://doi.org/10.1007/s10346-016-0781-8>
- Cruden DN, Varnes DJ (1996) Landslides types and processes. *Landslides: Investigation and Mitigation*, Special Re. Turner AK, Shuster RL (eds). Transportation Research Board. pp 36–75.
- Daehne A, Corsini A (2013) Kinematics of active earthflows revealed by digital image correlation and DEM subtraction techniques applied to multi-temporal LiDAR data. *Earth Surf Process Landforms.* 38: 640–654. <https://doi.org/10.1002/esp.3351>
- Giordan D, Allasia P, Manconi A et al (2013) Morphological and kinematic evolution of a large earthflow: The Montaguto landslide, southern Italy. *Geomorphology.* 187: 61–79.  
<https://doi.org/10.1016/j.geomorph.2012.12.035>
- Meng Q, Li W, Raspini F et al (2021) Time-series analysis of the evolution of large-scale loess landslides using InSAR and UAV photogrammetry techniques : a case study in Hongheyan , Gansu Province , Northwest China. *Landslides.* 18: 251–265.  
<https://doi.org/10.1007/s10346-020-01490-8>
- Mulas M, Ciccacese G, Ronchetti F et al (2018) Slope dynamics and streambed uplift during the Pergalla landslide reactivation in March 2016 and discussion of concurrent causes (Northern Apennines, Italy). *Landslides.* 15: 1881–1887.  
<https://doi.org/10.1007/s10346-018-1039-4>
- Mulas M, Ciccacese G, Truffelli G, Corsini A (2020a) Integration of Digital Image Correlation of Sentinel-2 Data and Continuous GNSS for Long-Term Slope Movements Monitoring in Moderately Rapid Landslides. *Remote Sens.* 12: 2605.  
<https://doi.org/10.3390/rs12162605>
- Mulas M, Ciccacese G, Truffelli G, Corsini A (2020b) Displacements of an Active Moderately Rapid Landslide—A Dataset Retrieved by Continuous GNSS Arrays. *Data.* 5: 71.  
<https://doi.org/10.3390/data5030071>
- Mulas M, Corsini A, Cuzzo G et al (2016) Quantitative monitoring of surface movements on active landslides by multi-temporal, high-resolution X-Band SAR amplitude information: Preliminary results. *Landslides and Engineered Slopes. Experience, Theory and Practice*. Aversa S, Cascini L, Picarelli L, Scavia C (eds). CRC Press, London. pp 1511–1516.
- Niethammer U, James MR, Rothmund S, Travelletti J, Joswig M (2012) UAV-based remote sensing of the super-Sauze landslide: evaluation and results. *Eng Geol.* 128: 2–11
- Ronchetti F, Borgatti L, Cervi F et al (2007) The Valoria landslide reactivation in 2005–2006 (Northern Apennines, Italy). *Landslides.* 4: 189–195. <https://doi.org/10.1007/s10346-006-0073-9>
- Thiebes B, Tomelleri E, Mejia-Aguilar A et al (2016) Assessment of the 2006 to 2015 Corvara landslide evolution using a UAV-derived DSM and orthophoto. *Landslides and Engineered Slopes. Experience, Theory and Practice*. Aversa S, Cascini L, Picarelli L, Scavia C (eds). CRC Press, London. pp 1897–1902
- Tonnellier A, Helmstetter A, Malet JP et al (2013) Seismic monitoring of soft-rock landslides: The Super-Sauze and Valoria case studies. *Geophys J Int.* 193(3): 1515–1536.  
<https://doi.org/10.1093/gji/ggt039>



# Field Investigation of the Landslide that Occurred During the Construction of the Dam "Svrackovo"

Nemanja Babović<sup>(1)</sup>, Aleksandar Miladinović<sup>(1)</sup>, Dajana Biorac<sup>(2)</sup>

1) ENERGOPROJEKT-HIDROINŽENJERING, Department for geology, hydrogeology, geophysics, geodesy, GIS & roads, Belgrade, 12 Mihailo Pupin Boulevard, Serbia, +381 11 310 1136 (nbabovic@ephydro.com)

2) ENERGOPROJEKT-HIDROINŽENJERING, Department for Dams, structures, geomechanics and organization of construction, Belgrade, 12 Mihailo Pupin Boulevard, Serbia

**Abstract** Svrackovo dam site is located in western Serbia, on the Rzav River, 8 km upstream of Arilje town. About 26 million m<sup>3</sup> reservoir capacity shall be formed by the construction of the embankment dam with the clay core - 60 m high and with the dam crest elevation of 423.60 m a.s.l. During construction of the S2 road slopes, contemporary scars resulting from the movement of the terrain were detected at the upper access road and in the surrounding terrain. The landslide affected the Middle Triassic rock complex, consisting of tectonic limestone blocks lying over completely altered tuffs, tuff breccias, porphyrites, and partially underlying marly limestone of the Lower Triassic. For the rehabilitation of this part of the terrain, multidisciplinary geotechnical investigation of the terrain had been conducted, which included: geological mapping of the terrain, drilling with coring, emplacement and monitoring of geodetic benchmarks and inclinometers, geophysical testing, and laboratory tests. Based on the conducted investigations and tests, complex geotechnical zoning of the terrain was conducted for the requirements of the stability analysis. As a rehabilitation measure, it was proposed to unburden moving rock material and to install preloaded geotechnical anchors.

**Keywords** Dam Svrackovo, landslide, investigations

## Introduction

The primary purpose of the "Svrackovo" dam construction is a safe, sustainable water supply of the wider area of this part of the Republic of Serbia, which includes cities of Arilje, Požega, Užice, and Ivanjica (Fig. 1). In addition to the basic hydro/technical purpose, this structure is also designed as a hydropower plant.

With the construction of the first access road to the location of the construction site in 2010, work began on the execution of the HPP Svrackovo. During the execution of excavation for structures adjacent to the dam, difficult working conditions were noted, primarily due to the stability of the executed slopes.

At the beginning of August 2018, the preparatory works for the access road S2 were continued. The works were executed from elevation 369,20 m a.s.l. exclusively



Figure 1 Geographical position of the dam Svrackovo.

by the use of machinery. After several metres of progress by this procedure, fresh scars were noted in the terrain, on several access roads that are hypsometric at higher elevations, access roads S3 and S1. The occurrences of terrain instability were not related to bad weather, since the initiation started in the dry period of the year. The works had to be stopped, and a detailed geological prospection was conducted, whereby all contemporary scars of terrain movement were geodetically surveyed (Fig. 2).

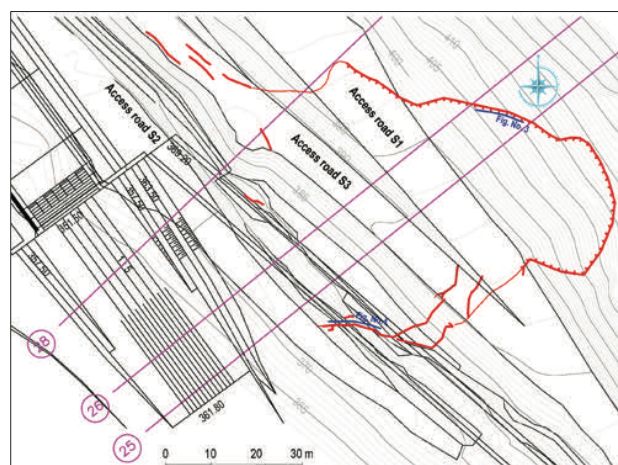


Figure 2 Active scars at the terrain.

The main scar of the landslide was detected in a wide arc above the access road S<sub>1</sub>, all the way to the elevation 420 m a.s.l. (Fig. 3). The left landslide boundary could be traced to the elevation 369.20 m a.s.l., with visible traces of movement within the part of bedrock, at the contact of two different geological formations (Fig. 4). The right landslide boundary could be traced downstream, up the access road S<sub>3</sub>, where it slowly disappears.



Figure 3 Frontal scar above the S<sub>1</sub> road.



Figure 4 Left boundary of an active landslide.

### Implemented geological/geotechnical investigations

After detection of newly created execution conditions and the instability, the Programme of geotechnical field investigations was prepared for the needs of rehabilitation and permanent protection of the slopes above the access road S<sub>2</sub>. Given the width of the instability area, additional investigations had to include the entire downstream slope of the left bank of Rzav river, from the exit of the future diversion tunnel, along the length of up to 120 m. Achieving the investigation goal imposed a multidisciplinary methodological approach, which would ensure that a credible presentation of the geological structure and other prevailing natural conditions are obtained, as well as gathering of representative samples.

The investigation consisted of the following works:

- detailed engineering-geological mapping
- borehole drilling survey with coring and installation of inclinometer structures
- installation of geodetic benchmarks with the monitoring program for the horizontal and vertical displacement vectors
- execution of geophysical investigations
- laboratory testing of samples.

The detailed engineering-geological mapping of the terrain had supplemented the discoveries related to the structure of terrain and helped in combining them with the already existing information collected during the previous detailed investigations of the executed slopes between the access roads S<sub>1</sub> and S<sub>3</sub>.

A total of 23 test boreholes were executed, with a total length of 784.1 m. Inclinometer structures were installed in 10 boreholes (Fig.5).

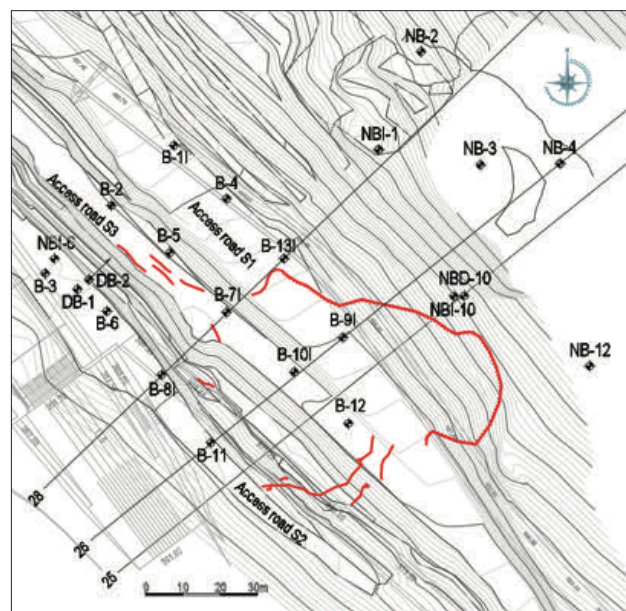


Figure 5 Topographical map of the area with locations of boreholes.

The drilling survey was executed by a rotary process with continuous coring. It was predominantly conducted within the active landslide area (between sections 25 and 30). A smaller part of the survey was implemented on limestone massif, above the elevation 420 m a.s.l. Given that the spatial position of the limestone outcrop is directly above the already formed active landslide, it was estimated that it could have a very large impact on the regressive spread of instability phenomenon along the slope.

The basic geodetic network for landslide monitoring has been installed as part of the already existing micro-trigonometric network to monitor the dam and associated structures during and after the construction. According to the quality and reliability analyses, the classical geodetic



methods (measuring lengths and directions) at the site measure the displacements of geodetic benchmarks with an accuracy of 5 mm, both horizontally and vertically. Eleven benchmarks were installed, and 1 to 4 series of measurements were performed.

With geophysical tests, two methods were used: refraction seismic and geoelectrical. A total of 8 refraction seismic sections were executed, perpendicular and parallel to the slope, of 720 m total length. Specific electric resistivity was measured by ten geo-electric probes.

Laboratory geotechnical tests of physical-mechanical characteristics in soft and medium strength rock masses included: tests of unconfined compressive and tensile strength in dry and water-saturated state, determination of natural density, and tests of peak and shear strengths on large samples.

### Investigation results

#### The geological composition of the terrain

The investigation area is structured from sedimentary rocks of the Lower and Middle Triassic, igneous rocks of the Middle Triassic, and Quaternary formations (Fig. 6).

The **Lower Triassic** is relatively poorly exposed, outcropping along the edge of the riverbed, and in some places near access roads. It is represented by *bioturbiditic formation*, composed of marly limestone of pronounced laminated structure. The rock mass is of medium to low strength, with pronounced fracture systems, whose walls are smooth and flat. At the Basic geological map of the sheet Čačak (Brkovic and Malešević 1977), it was believed for a long time that the Lower Triassic sediments were in a normal relationship with the Middle Triassic sediments, until an extensive investigation procedure was conducted for the requirements of rehabilitation of this instability. Namely, by execution of access roads to the hypsometrically higher test boreholes NBI-10 and NB-4, it was noted at fresh outcrops that the sediments of the

Lower Triassic are in a reverse relationship with the sediments of the Middle Triassic. The contacts are slightly inclined, with the obligatory presence of a thin layer of hydrothermal altered red rocks in the contact area. This data indicates high pressures during block overthrust of older geological formations over the younger ones. The described process was also identified on the borehole cores. Expert confirmation of such geological terrain composition, on the conditions of intensive block overthrust and supported by the results of the investigation procedure, is documented within the structural-tectonic Study (Trivić 2019). Based on mentioned Study, the block overthrusts are of the general inclination towards the north-east, with the average statistical elements of the inclination EPkr 21/44. In Fig.6, the sediments of the Lower Triassic are marked with T<sub>1</sub>.

**Sediments of the Middle Triassic** dominate in the zone of the investigation area, and are composed of limestone of sparite structure, massive texture, partially or completely recrystallized, in some places irregularly dolomitized, and in some places with lenticular intercalations of sedimentary breccias. The slopes structured from massive limestone are steep, and in some places they turn into vertical sections, for example, immediately above the main scarp of the active landslide. On the limestone outcrops, sets of fractures stand out, by which the rock is divided into monoliths of different dimensions. Massive limestones are divided into four units, in relation to the degree of jointing and the degree of karstification:

- K<sub>1</sub> – limestone and limestone breccia, fractured and highly karstified;
- K<sub>2</sub> – limestone extremely fractured and karstified;
- K<sub>3</sub> – limestone slightly fractured;
- K<sub>4</sub> – limestone strong, compact, and slightly fractured.

In Fig.6, massive limestone is marked with designations from K<sub>1</sub> to K<sub>4</sub>.

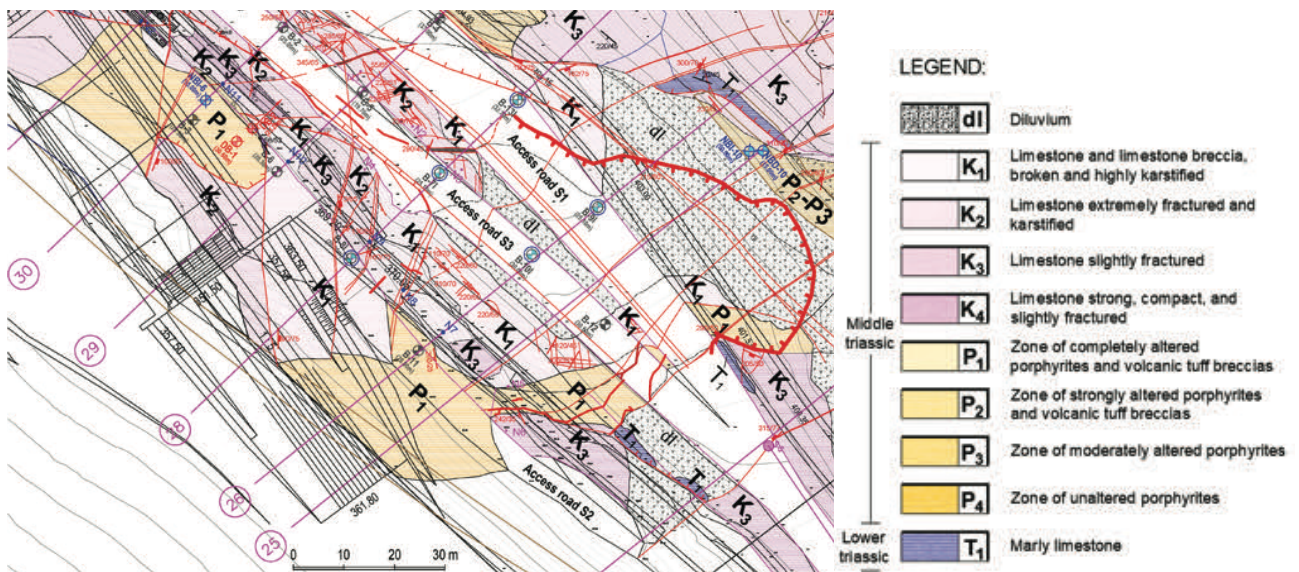


Figure 6. Engineering geological map of the investigation area.

**Porphyrites (Middle Triassic)** are present in the central and south-western parts of the investigation area. Their genesis is related to submarine-type volcanism in synsedimentation conditions. According to most authors, these volcanic rocks are the product of Triassic rift area. According to the Basic Geological Map, sheet Užice (Mojsilovic and Baklaic 1977), they were treated as an integral part of the volcanogenic-sedimentary unit, where it was noted that they occur in the form of porphyritic tuffs, breccias, and porphyrites in alteration with crystalloclastic tuffs. Based on additional petrologic tests, it was concluded that these volcanogenic-sedimentary masses are present at the investigated location. Porphyrites are volcanic rocks formed by lava flow, thus they are initially of higher strength than volcanic tuff breccias, while volcanic tuff breccias, as softer rocks, are more susceptible to the process of hydrothermal modifications. Chlorination and calcitization were registered on the majority of volcanic tuff breccia samples, and sericitization on one sample.

Based on the degree of alteration, these volcanogenic-sedimentary rock masses are divided into four categories:

- P<sub>1</sub> – zone of completely altered porphyrites and volcanic tuff breccias;
- P<sub>2</sub> – zone of strongly altered porphyrites and volcanic tuff breccias;
- P<sub>3</sub> – zone of moderately altered porphyrites;
- P<sub>4</sub> – zone of unaltered porphyrites.

It can be noted that the zones of completely (P<sub>1</sub>) and partially altered porphyrites (P<sub>2</sub>) are mixed with tuff breccias, whereby the processes of hydrothermal modifications have masked the mutual geological cross-sections and borders. The processes of chlorination, calcitization, and especially sericitization have a key role in the degradation of rock material. Values of very low physical-mechanical characteristics were obtained on representative samples from these materials.

When it comes to jointing, the systems of fractures were observed, which belong to shear fractures by their genetic type. A summary statistical diagram of all shear fractures (D7 sm), collected during these investigations, is presented in Fig. 7. The statistics had included almost 240 elements of shear fracture inclinations. Two maximums are clearly distinguished, the first in the NE-quadrant EPsm<sub>1</sub> 225/68 and the second along the eastern and western periphery of the EPsm<sub>2</sub> 100/85-90, i.e. 280/85-90 diagrams. In addition to these two systems, the system of fractures that marks the sub-maximum along the northern edge of the diagram with statistical EPsm<sub>3</sub> 191/85 is of extreme importance.

Fracture set (EPsm<sub>1</sub>) with mean dip elements 225/68 are considered highly unfavourable regarding the slope stability. This fracture sets stretch almost in parallel with the formed slopes. Apart from that, the fractures of this set are slickenside at the dip angle and as a result, they can be expected to form highly unfavourable sliding planes in relation to other fracture sets.

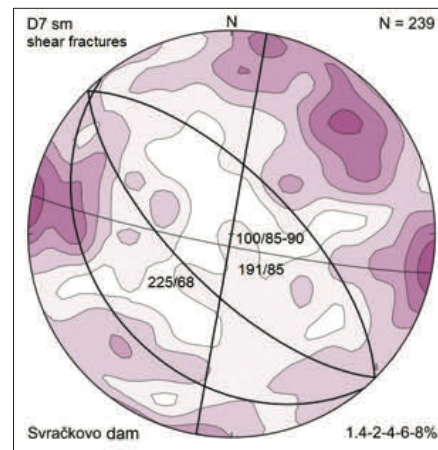


Figure 7 Statistical diagram of jointing.

### Analysis of the results of geological/geotechnical investigations

After the executed investigation, the Synthesis geotechnical/geological Study was prepared. The most important observations on the natural conditions prevailing at this terrain are presented below.

The results of the drilling survey with coring at the top elevations of this investigation area had indicated that there was a well-founded suspicion related to a massive limestone outcrop, which is directly above the active landslide area, that it is actually a block. Test borehole NBI-10, executed right next to the mentioned outcrop and up to a depth of 25 m, had been executed in altered porphyries. Inclined borehole NBD-10, which was executed perpendicularly to the outcrop, was also drilled in porphyries. The results of this executed investigation procedure are presented in Fig. 8.

The results of the drilling survey within the area of active landslide showed complex engineering geological conditions. Even in the early phase of the investigation, it was discovered that the rock mass is heterogeneous and anisotropic in depth, i.e. in the vertical and horizontal directions. Each next new test borehole had presented new

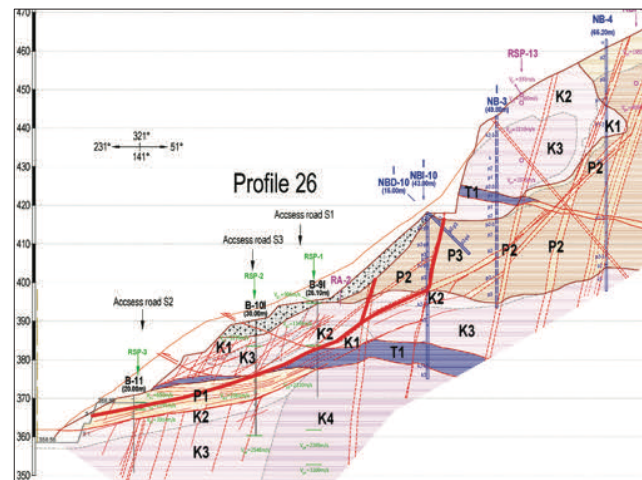


Figure 8 Detail from geological cross-section 26.

geological information, so it was increasingly difficult to prepare a geologically logical cross-section. In addition to the above, in the conditions of irregular relations between the geological formations of the Middle Triassic, limestone, and porphyries with tuff breccias, the heterogeneous geological terrain structure was further complicated by the overthrust, i.e. block overthrust of the Lower Triassic sediments. The summary conclusion concerning the executed investigations of the active landslide area is that irregular relations between lithological members within the complex are the rule, rather than the exception at this locality. Two geological cross-sections of the terrain 26 and 28 (Figs. 8 and 9), were prepared by comprehensive analysis of detailed geological mapping of the terrain and borehole data.

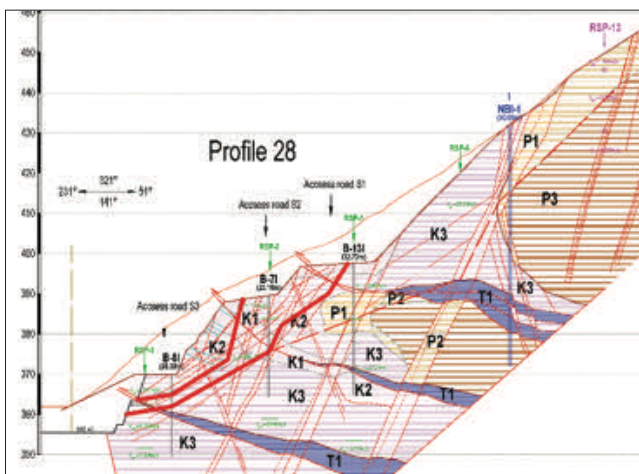


Figure 9 Detail from geological section 28.

On the basis of geological information, at section 26 it is assumed that the sliding plane is formed by unfavourable fractures of EPsm1 set (225/68), as well as in weakened geological areas of completely altered porphyrites with tuff breccias, and laminated marly limestone of the Lower Triassic. In section 28, the instability phenomena are exclusively related to jointing in massive limestone. These geological assumptions needed to be confirmed by other geological/geotechnical investigations.

Monitoring of geodetic benchmarks was conducted with a total of four series of monitoring at six geodetic benchmarks, and only one series of monitoring on the other benchmarks. The period between two series of monitoring is up to three months. A displacement was noted on 10 geodetic benchmarks (Fig. 10).

The largest increase in displacement is at geodetic benchmark N5, a total of 99 mm. In addition to the above, the negative trend of the displacement vector (down the slope and in the direction of sliding rock masses) was also noted at the benchmarks N1, N2, N3, N4 and N9. The geodetic benchmark N6 was executed on massive limestone, i.e. on a stable part of the terrain, and it does

not show any displacements, i.e. movements within the limits of determination accuracy.

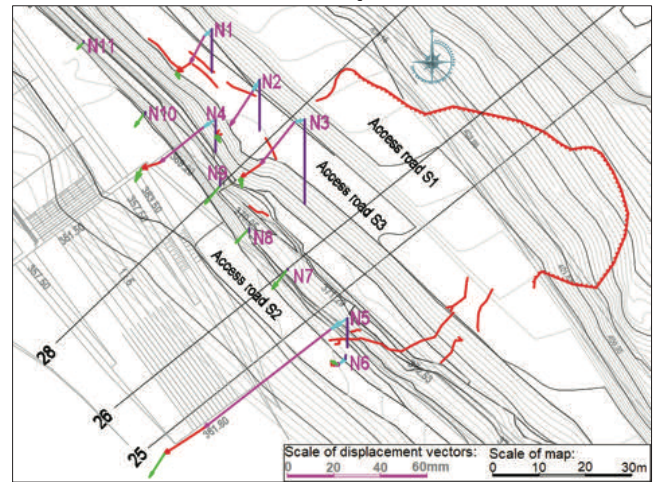


Figure 10 Total displacement vectors of geodetic benchmarks.

In general, it can be concluded that the surface displacement of geodetic benchmarks corresponds to the scars in the terrain, which were detected by mid-2018, with geodetic benchmarks N1 and N2 indicating a regressive spread of instability phenomena uphill from the detected landslide boundaries.

For the requirements of depth displacement verification, the analysis of inclinometer displacements within the area of sections 26 and 28 is presented below. Inclinometer borehole B-10I (Fig. 11.) was executed within the area of section 26.

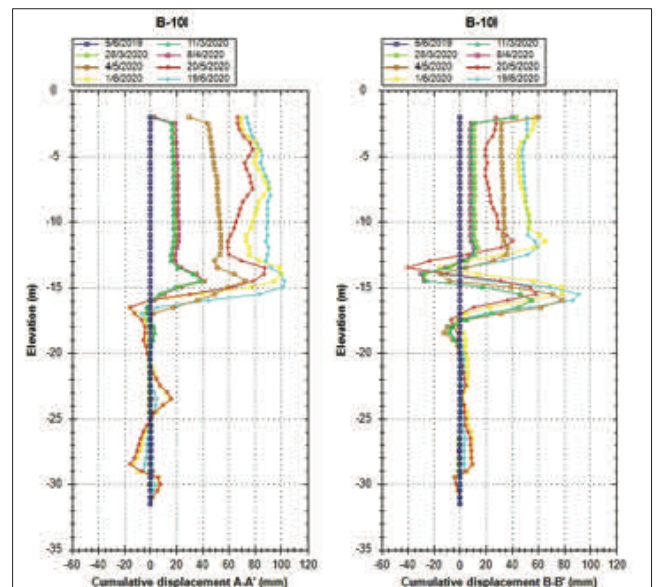


Figure 11 Cumulative displacement results at B-10I.

A displacement of 14 – 17 m response depth to the assumed sliding plane as was noted in section 26. The inclinometer casing on the B-9I borehole was relatively

quickly damaged at 9 m depth, due to the displacement of the terrain.

The inclinometer borehole B-7I was executed in the area of section 28, and its results are presented in Fig. 12. The displacement results are in accordance to the assumed sliding plane, which was defined in cross-section 28. The inclinometer B-8I had been monitored for a relatively long time, almost as long as the inclinometer B-7I, and before a displacement was detected at 5 and 8 m of depth.

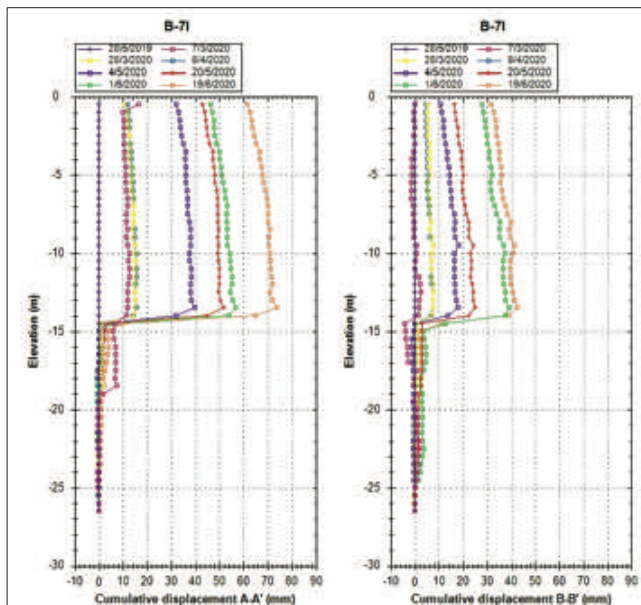


Figure 12 Cumulative displacement results at B-7I.

In order to obtain relevant parameters of physical-mechanical characteristics in geological mediums that can be potential sliding planes, undisturbed samples were gathered to determine peak and residual strengths. Shearing tests were executed on large samples according to the regulations defined by the Programme of geotechnical field investigations. The results of these tests are presented in Tab. 1.

Table 1 Results of laboratory tests on a large scale

No.	EG rock description	Ultimate strength		Residual strength	
		$\varphi$ (°)	c (kPa)	$\varphi$ (°)	c(kPa)
1	Laminated marly limestone (T1)	27,85	168,98	19,39	10,23
2	Laminated and ringed marly limestone (T1)	33,32	83,20	26,34	3,50
3	Laminated and ringed marly limestone (T1)	31,74	49,42	23,82	6,02
4	Porphyry completely altered with tuff breccias (P1)	27,32	40,95	21,23	8,05
5	Porphyry strongly altered with tuff breccias (P2)	32,62	44,50	18,08	4,23
6	Limestone completely karstified (K1)	29,00	9,00	-	-

## Conclusions

The conducted field investigations and tests for the requirements of the active landslide within the area of stilling basin of the embankment dam “Svračkovo” had demonstrated that the rock masses in the investigation area are heterogeneous and anisotropic.

The most important conclusion is that the results could not be observed/treated individually but exclusively integrally. On the basis of conducted investigations and tests, a complex geotechnical terrain zoning was conducted for the requirements of stability analysis.

Based on the conducted analysis of terrain stability, as a measure of rehabilitation, it is proposed to unload the displaced rock material in a combination of pre-stressed geotechnical anchors executed in phases along with the excavation floors.

## Acknowledgements

We want to thank the Public Water Management Company „Srbija vode“ of Serbia, which provided support during the field investigation process and approved the publication of data and conclusions of the analysis.

## References

- Brkovic T, Malesevic M (1977) Basic geological map, Sheet Čačak 1:100 000 – K34-05. Department for Geological Investigations, Belgrade. (in Serbian)
- Mojsilovic S, Baklaic D (1977) Basic geological map, Sheet Titovo Užice 1:100 000 – K34-04. Department for Geological Investigations, Belgrade. (in Serbian)
- Trivic B (2019) Structural – tectonic analysis of the area within the zone of the embankment dam “Svračkovo“ with special reference to the tectonic structure within the area of stilling basin. Faculty of Mining and Geology, Belgrade. (in Serbian)

# Probabilistic modelling of HVSR results for 3D mapping of rock-slides subsurface

Vincenzo Critelli<sup>(1)</sup>, Alessandro Corsini<sup>(1)</sup>, Matteo Berti<sup>(2)</sup>, Anna Rita Bernardi<sup>(3)</sup>, Matteo Bernardi<sup>(3)</sup>, Giuseppe Caputo<sup>(3)</sup>, Giuseppe Ciccarese<sup>(1)</sup>, Gianluigi Di Paola<sup>(2)</sup>, Marco Mulas<sup>(1)</sup>, Francesco Ronchetti<sup>(1)</sup>

1) University of Modena and Reggio Emilia, Department of Chemical and Geological Sciences, Modena, via G. Campi 103, Italy (vcritell@unimore.it)

2) University of Bologna, Department of Biological, Geological and Environmental Sciences, Bologna, Italy

3) Regional Agency for Civil Protection and Territorial Security, Emilia-Romagna Region, Italy

**Abstract** In this study we show a probabilistic model based on HVSR recordings dataset collected on a large-scale, deep-seated rock-slide in Northern Apennines (Italy). We addressed the representativeness and performance of the model by comparing it with the interpretation of existing surveys and by the means of cross-validation analysis. We first defined a reference landslide kinematic model based on the interpretation of 1000 m of P-wave seismic refraction tomography and 900 m of DC electrical resistivity tomography. We constrained the interpretation by evidence provided by boreholes and an airborne Lidar survey. We then performed an indicator kriging 3D interpolation of 129 S-wave velocity vertical profiles obtained by inversion of HVSR surveys, in order to obtain a probabilistic model of subsurface S-wave velocity distribution. As required by indicator kriging, we modelled three significant velocity cut-offs (300, 450 and 600 m/sec), chosen by comparison between borehole stratigraphy logs and nearest S-wave velocity vertical profiles. Cross-validation analysis was employed to optimize the kriging settings. As result, we obtained three interpolations expressed in terms of a probability for the velocity value at a given location of being below the given cut-off. The interpolation based on the 600 m/sec cut-off showed the best match with the reference model, providing a good estimate of the subsurface distribution of low rigidity rock-slide material. Despite being an indirect observation, HVSR recordings proved to be a good way to extend information from existing boreholes and the probabilistic analysis approach provides a basis to assess the uncertainty in the conceptual model.

**Keywords** HVSR, Indicator Kriging, deep-seated rock-slide, Flysch

## Introduction

When dealing with the structural mapping of large landslides, high heterogeneity and a limited number of direct observations lead to uncertainties in the definition of a suitable geological conceptual model. In recent years,

geophysical surveys were widely employed in the subsurface characterisation (Bichler et al. 2004; Jongmans and Garambois 2007; Thirard et al. 2022). Among them, horizontal to vertical spectral ratio or HVSR surveys (Nakamura 1989) are also employed to locate the sliding surface (Méric et al. 2007; Berti et al. 2017).

In this article, a probabilistic model of subsurface S-wave velocity distribution based on indicator kriging of 129 HVSR surveys is carried out to map the slide inner structure and basal sliding surface. We addressed the representativeness and performance of the model by cross-validation analysis with respect to a reference subsurface model derived by the interpretation of other existing geophysical and boreholes surveys.

The aim of the study is to provide a way to assimilate the sub-surface's geomechanical insights within a kinematic/structural model to support the parameterization of a geotechnical numerical model.

## The “Camugnano” landslide

### Study area

The “Camugnano” landslide is an active, deep-seated rotational rock-slide involving flysch rock materials located in Northern Apennines (Italy, Province of Bologna). The slide's activity is characterized mainly by slow continuous movements and occasional acceleration events reported since 1934. Damages to the buildings and roads of Camugnano led authorities in the last years to perform investigations aimed to a substantial understanding of the slide's kinematics and geometry (Fig. 1). A total of eight boreholes equipped with inclinometer casing have been installed, together with piezometers. The inclinometer records indicate a sliding surface reaching the maximum depth of 64 meters in the central part of the slide (22-I). Furthermore, electrical resistivity tomography profiles show the presence of relatively high electrical resistivity volumes ( $\sim 700 \Omega \cdot m$ ) separated by narrow areas of lower resistivity ( $\sim 100 \Omega \cdot m$ ). Seismic refraction/reflection profiles aimed to locate the sliding surface in between the boreholes, show velocity gradients that match inclinometer data and suggest inner differentiation within the landslide body. Finally, the

interpretation of a Lidar-derived DEM of the study area provides morphological constraints to the landslide areal extension and its inner structure as well.

**Reference sub-surface kinematic units model**

From the joint interpretation of the existing geophysical surveys, boreholes and morphological evidence, a reference sub-surface kinematic model is defined (Fig. 2),

in which the slide is depicted as a nested roto-translational structure. The upper and central parts of the slide are characterized by the presence of relatively intact rock masses dislocated with each other by intersecting sliding surfaces. On the other hand, the lower part is characterized by highly damaged materials and the presence of a former landslide deposit.

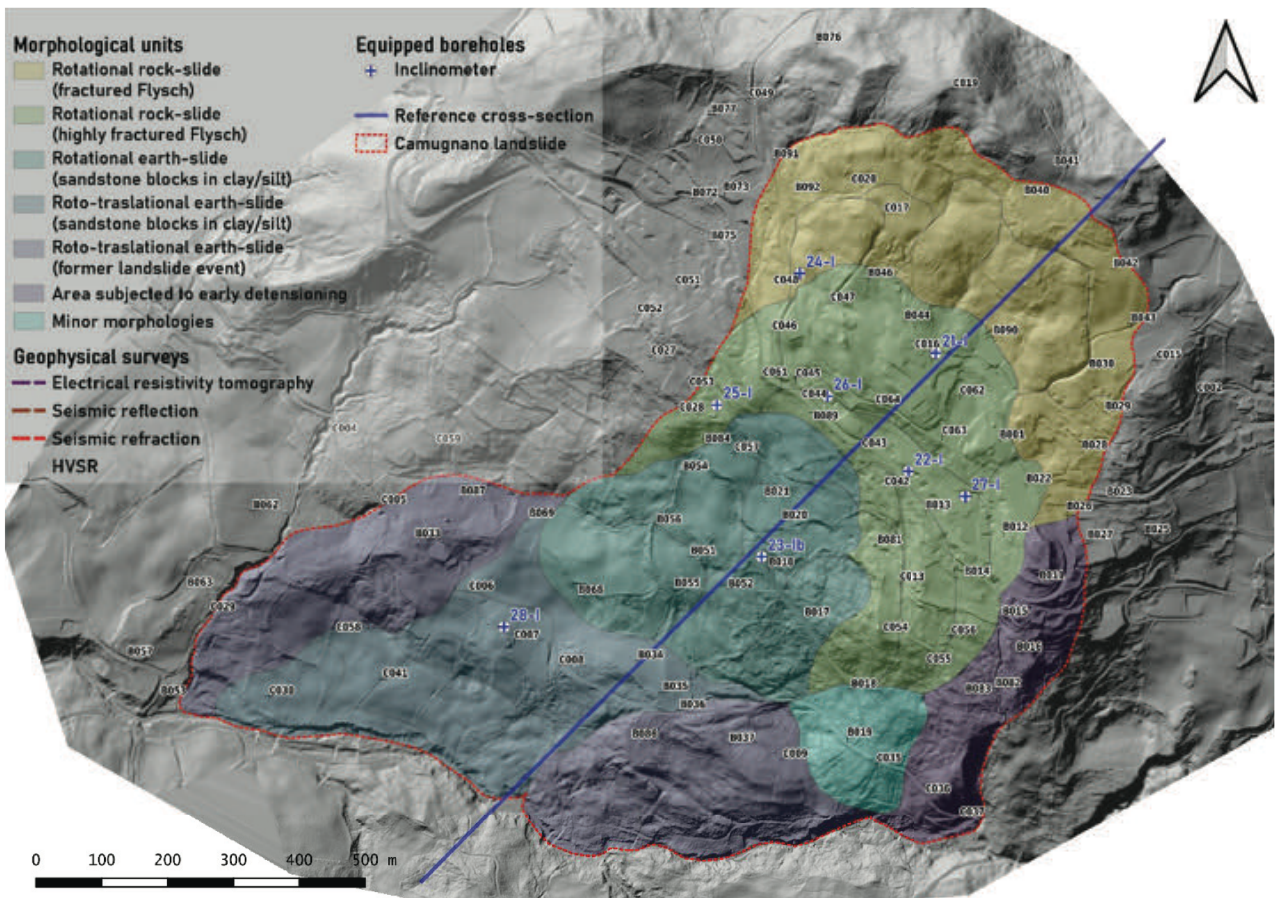


Figure 1- Geomorphological map for the Camugnano landslide over Lidar-supported DEM.

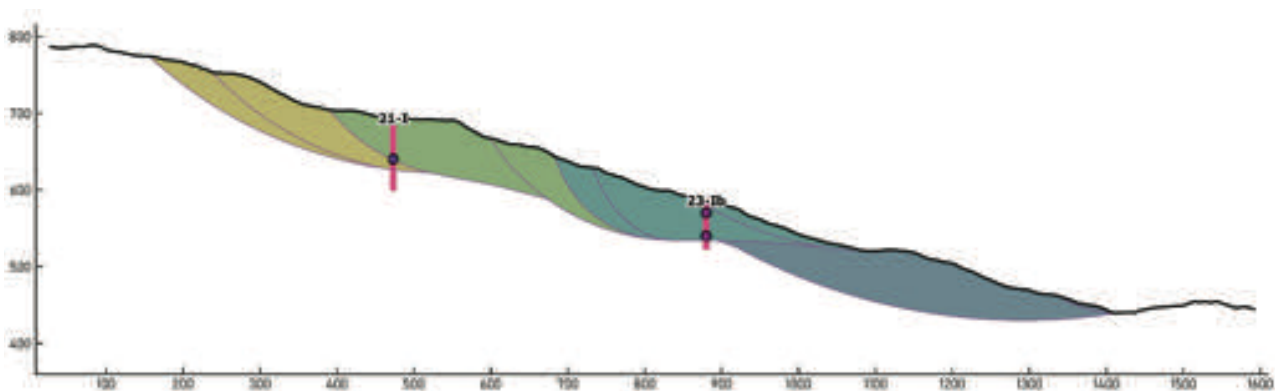


Figure 2 - Reference kinematics units sub-surface model.

## Probabilistic model

### Seismic noise and HVSR method

Horizontal to vertical spectral ratio (HVSR) passive seismic techniques are based on the recording of ambient vibrations (e.g., seismic noise) by a three-component seismometer. The average Fourier spectrum ratio between horizontal (H) and vertical (V) components is maximum at the fundamental resonance frequency of the investigated site (Nakamura 1989), which in turn depends upon the seismic velocity ( $V_s$ ) and the thickness of the investigated underground strata. The frequencies at which the H/V peaks can consequently be correlated, using regression models, to the depth of the main acoustic impedance interfaces. HVSR can be applied in seismic site-response analysis and in coseismic landslides studies (Bourdeau et al. 2017; Ma et al. 2019). Furthermore, it can also be used in sub-surface characterization (Méric et al. 2007; Berti et al. 2017; Delgado et al. 2021), by a velocity inversion of the spectrum itself, providing a multi-layer model of the site in terms of S-wave velocity profiles (Herak 2008).

### HVRS surveys

In June 2020 the existing investigation were integrated with 129 HVSR recordings. The surveys were done with an acquisition time of 12 minutes at 128 Hz sampling frequency. Their inversion led to the generation of the same number of one-dimensional vertical S-wave velocity profiles involved in the next step of the analysis.

The comparison between the vertical profiles with the core of the nearest borehole provided the basis to choose the relevant velocity cut-offs required by indicator kriging and were namely 300, 450 and 600 m/s. In Fig. 3 the variogram models for each cut-off is reported.

### Indicator Kriging

Inside each kinematics unit in the reference model, a differentiation of the of landslide body according to the rigidity of the involved rock and debris masses is to be expected. To depict such differentiation, S-wave velocities are employed as spatial variable to be modelled. Moreover, rock volumes showing higher S-wave velocities (e.g., undamaged rock masses beneath the basal surface) are expected to be characterized by a higher horizontal spatial continuity when compared to the spatial continuity of lower S-wave velocities. To deal with such complex structure the indicator kriging paradigm is employed (Isaaks and Srivastava 1989; Pyrcz and Deutsch 2014), which allows the modeler to define different variogram models for different cut-offs value.

The method requires the coding of the continuous variable (S-wave velocity) into an indicator variable  $i(u, z_k)$  according to the following rule:

$$i(u, z_k) = \begin{cases} 1, & \text{if } z(u) \leq z_k \\ 0, & \text{otherwise} \end{cases}$$

where  $z(u)$  is the value of the continuous variable at location  $u$ , while  $z_k$  is one of a series of cut-off values. Once the indicator variables are coded, a variogram model for each of the cut-offs must be defined. The main output of the indicator kriging are maps showing the probability for the variable at a given location in the three-dimensional space to be less or equal to a given cut-off.

### Model validation

The output of the indicator kriging can be easily processed in terms of contingency matrices. This analysis is performed by *jack-knifing* (Pyrcz and Deutsch 2014), a procedure which requires each vertical log to be removed in turn and using the remaining ones to estimate the values on the removed log locations. A traditional cross-validation in this case is not suitable since each value in the log are closely adjacent and the analysis would have led to unrealistically good results.

This validation procedure is applied to optimize the kriging settings and to compare the results derived by employing both simple and ordinary indicator kriging. Only the best results are shown in Fig. 4 which depicts the ROC curves derived by the procedure previously outlined for the optimized simple indicator kriging algorithm.

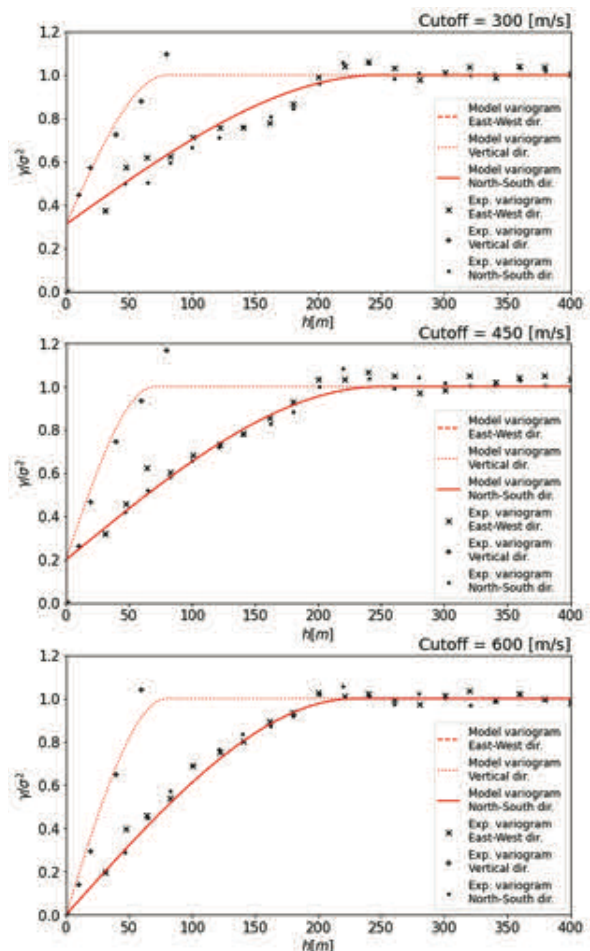


Figure 3 - Experimental and modelled variograms.

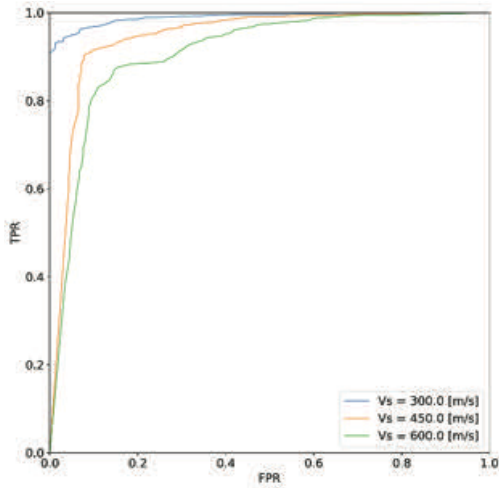


Figure 4 - ROC curves for optimized simple indicator kriging settings.

## Results and conclusions

The comparison with a reference model derived by joint interpretation of past surveys showed that indicator kriging can differentiate inner volumes while achieving a good match between high probability values and sliding surface locations detected by inclinometer readings, moreover, as showed by ROC curves, indicator kriging performs well, especially in estimating low value cut-offs ( $AUC_{300}=0.990$ ,  $AUC_{450}=0.934$ ,  $AUC_{600}=0.877$ ).

The methodology applied in this study can allow relevant information regarding the mechanical behaviour of landslide' masses to be coupled with a kinematic reference model. Both the elements can support the implementation and parameterization of complex geotechnical numerical models.

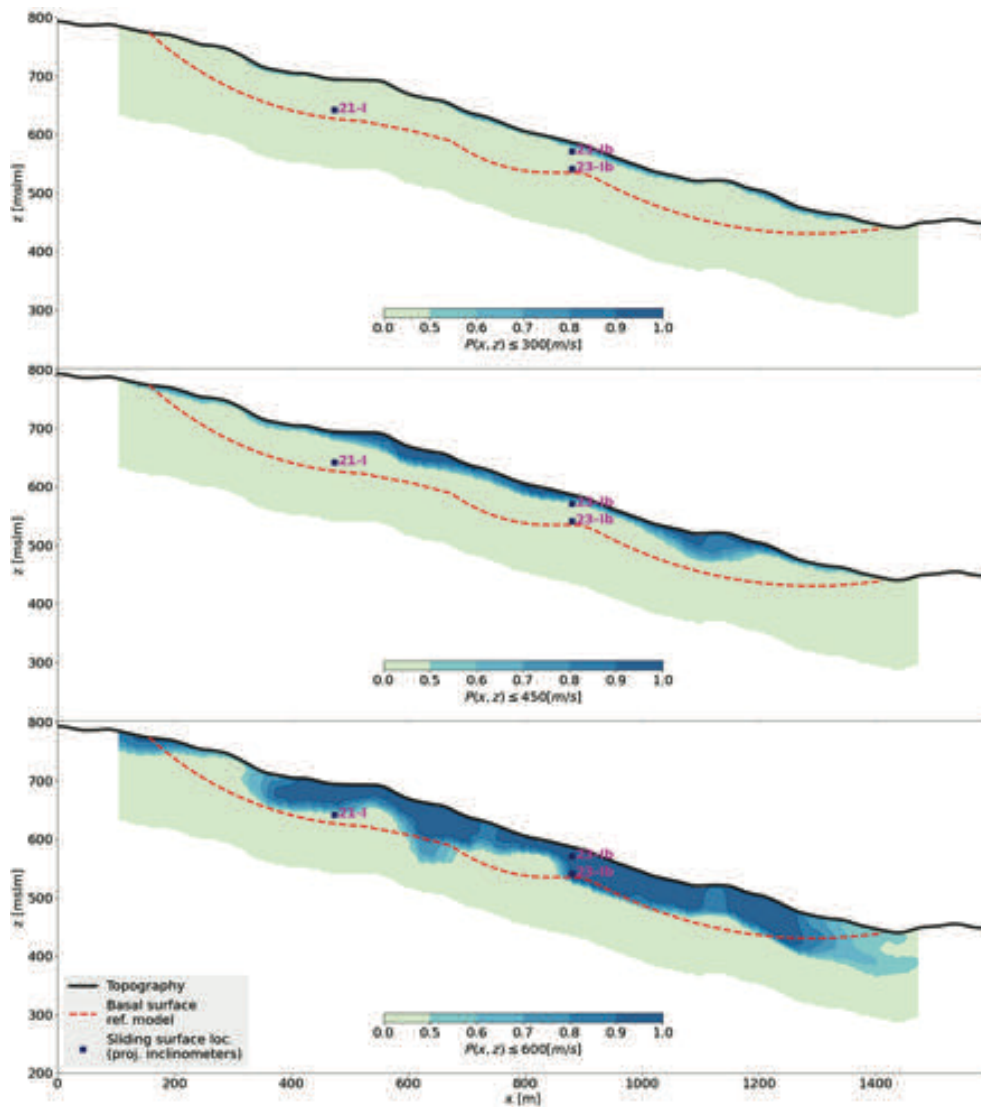


Figure 5 - Comparison between indicator kriging results and reference sub-surface model. The square blue dots represent the sliding surface's location detected by inclinometers, while the dashed red line is the basal surface depicted in Fig. 2. The map corresponding to the 450 m/s cut-off shows a good match with the first sliding surface, while the map for 600 m/s cut-off best describes the deepest sliding surface.



## References

- Berti M *et al.* (2017) Back analysis of a large landslide in a flysch rock mass. *Landslides*. 14(6): 2041–2058. doi: 10.1007/s10346-017-0852-5.
- Bichler A *et al.* (2004) Three-dimensional mapping of a landslide using a multi-geophysical approach: The Quesnel Forks landslide. *Landslides*. 1(1): 29–40. doi: 10.1007/s10346-003-0008-7.
- Bourdeau C *et al.* (2017) Comprehensive analysis of the local seismic response in the complex Büyükçekmece landslide area (Turkey) by engineering-geological and numerical modelling. *Engineering Geology*. 218: 90–106. doi: 10.1016/j.enggeo.2017.01.005.
- Delgado J *et al.* (2021) Ambient noise measurements to constrain the geological structure of the güevéjar landslide (S Spain). *Applied Sciences (Switzerland)*. 11(4): 1–18. doi: 10.3390/app11041454.
- Herak M (2008) ModelHVSR-A Matlab® tool to model horizontal-to-vertical spectral ratio of ambient noise. *Computers and Geosciences*. 34(11): 1514–1526. doi: 10.1016/j.cageo.2007.07.009.
- Isaaks EH, Srivastava RM (1989) *An Introduction to Applied Geostatistics*. 1st edn. New York: Oxford University Press.
- Jongmans D, Garambois S (2007) Geophysical investigation of landslides: A review. *Bulletin de la Societe Geologique de France*. 178(2): 101–112. doi: 10.2113/gssgfbull.178.2.101.
- Ma N *et al.* (2019) Amplification of seismic response of a large deep-seated landslide in Tokushima, Japan. *Engineering Geology*. 249: 218–234. doi: 10.1016/j.enggeo.2019.01.002.
- Méric O *et al.* (2007) Seismic noise-based methods for soft-rock landslide characterization. *Bulletin de la Societe Geologique de France*. 178(2): 137–148. doi: 10.2113/gssgfbull.178.2.137.
- Nakamura Y (1989) Method for Dynamic Characteristics of Subsurface using Microtremor on the Ground Surface. *Quarterly Report of Railway Technical Research Institute (RTRI)*. 30(1): 25–33.
- Pyrzc JM, Deutsch VC (2014) *Geostatistical reservoir modeling*. 2nd edn. New York: Oxford University Press.
- Thirard G *et al.* (2022) Hydromechanical assessment of a complex landslide through geophysics and numerical modeling: Toward an upgrade for the Villerville landslide (Normandy, France). *Engineering Geology*. 297: 106516. doi: 10.1016/j.enggeo.2022.106516.



# Statistical relationships for characterising rock avalanche mobility: state of the art and perspectives

Alexander Strom <sup>(1)</sup>

1) Geodynamics Research Centre LLC, 125008, 3<sup>rd</sup> Novomikhalkovsky passage 9, Moscow, Russia, +7 910 4553405  
([strom.alexandr@yandex.ru](mailto:strom.alexandr@yandex.ru))

**Abstract** Statistical analysis of various rock avalanche databases provides relationships that link parameters, characterizing the collapsing slope (volume, slope height, maximal height drop), and parameters characterizing rock avalanche mobility (runout, angle of reach, total affected area, area of the deposits). Judgment on these relationships' reliability and the preferability of their use for practical applications can be based on comparing the correlation coefficients of corresponding regression equations. Obviously, such analysis is most efficient not for the entire database but for samples that consider some important factors influencing rock avalanche motion. The most relevant relationships were derived for three samples selected according to the confinement conditions – for unconfined, laterally confined and frontally confined cases. The best correlations with  $R^2$  exceeding 0.9 were derived from samples from the Central Asian database, between total affected area (dependant parameter) and product of rock avalanche volume and its maximal height drop (independent parameter). The latter is proportional to the potential energy released during emplacement. Further progress in this research field could be achieved if a larger rock avalanche database, ideally, the global one, will be used. Besides higher representativeness of regressions derived according to the same sampling criteria as described above, it will allow selecting samples with more strict characteristics based on some additional classification criteria.

**Keywords** rock avalanche, mobility, volume, runout, affected area

## Introduction: state of the art and some unsolved problems

### General approaches

Statistical analysis of various rock avalanche databases provides relationships that link parameters, characterizing the collapsing slope (volume, slope height, maximal height drop), and parameters characterizing rock avalanche mobility (runout, angle of reach, total affected area, area of the deposits). Such analysis has been performed, first, by Sheidegger (1973), and by Howard (1973), Hsü (1975), Davies (1982), Li (1983), Nicoletti and Sorriso-Valvo (1991), Shaller (1991), Kobayashi (1993, 1997), Corominas (1996).

Kilburn and Sørrensen (1998), Legros (2002, 2006), Hungri (2006), Griswold and Iverson (2008), Strom and Abdrakhmatov (2018), Strom et al. (2019), Mitchell et al. (2020), Yu and Su (2021), Liu et al. (under review).

Despite the conclusion made by Legros in 2002 that angle of reach or  $H/L$ , where  $H$  is the height drop (vertical difference between the headscarp crown and the deposits tip), and  $L$  is runout (horizontal projection of the distance between these points), does not have physical meaning, most of the researchers still use this ratio as a measure of rock avalanche mobility.

All these studies demonstrate an increase of the runout ( $L$ ) and a decrease of the  $H/L$  ratio with growing rockslide volume ( $V$ ). However, according to relationships based on the statistical analysis of a large database from the Central Asia region (Strom and Abdrakhmatov 2018; Strom et al. 2019),  $R^2$  values (coefficient of determination) of all  $L$  vs.  $V$  regressions are 1.63 – 2.44 times higher than those of the  $H/L$  vs.  $V$  regressions derived for the same samples. It supports the conclusion made by Legros (2002) about the preferableness of just runout to characterize rock avalanche mobility.

Runout, however, is the unidimensional parameter that cannot characterize debris motion in the transverse direction, which can be critical for hazard and risk assessment. Indeed, what rock avalanche can affect a larger area with more objects at risk – one that moves strictly forward forming a narrow tongue of debris (Fig. 1a), or another one that covers a wider area even if its travel distance ( $L$ ) is shorter (Fig. 1b, c)?

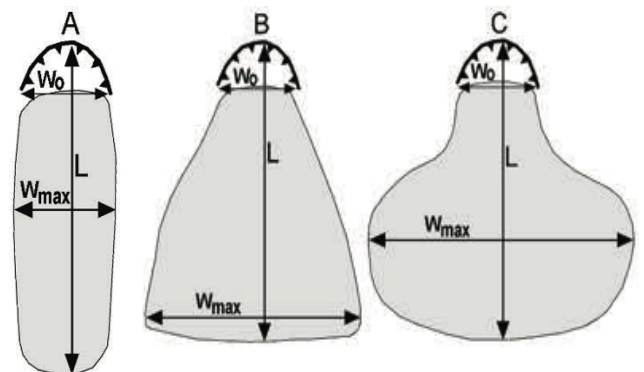


Figure 1 Morphological types of rock avalanches.  $L$  – runout,  $W_0$  – headscarp base width,  $W_{max}$  – maximal width of deposits (after Strom and Abdrakhmatov 2018, with permission of Elsevier).

**Sampling according to confinement conditions**

It is evident that statistical analysis is more efficient not for the entire database, but for samples that take into consideration some important external factors influencing rock avalanche motion. The most obvious sampling criterion is the confinement conditions, according to which unconfined, laterally confined, and frontally confined cases can be selected (Nicoletti and Sorriso-Valvo, 1991; Shaller 1991; Strom and Abdrakhmatov 2018; Strom et al. 2019). Indeed, it is almost useless to compare, for example, the runout of an unconfined or laterally confined rock avalanche that came to a halt due to basal friction and some internal processes evolving in moving debris and causing energy and momentum consumption, with that of a frontally confined event where some portion of the kinetic energy and momentum is consumed to overcome gravity force when moving upslope (Fig. 2) and, moreover, during direct impact against the steep opposite slope of the valley.

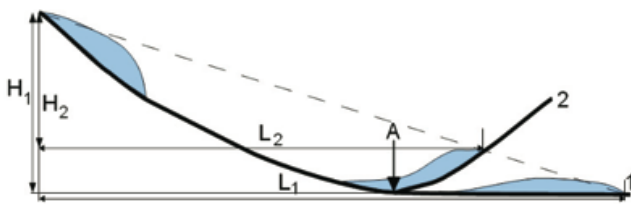


Figure 2 Scheme of rock avalanches without (1) and with (2) frontal confinement. H/L ratio is the same for both cases (after Strom and Abdrakhmatov 2018, with permission of Elsevier).

Similarly, how can we compare the deposits' area of unconfined and frontally confined rock avalanches that can spread in the transverse direction freely, with the same parameter of the laterally confined events that can move only ahead being bounded by valley slopes?

This paper presents some approaches how to get more relevant and physically-based relationships between parameters characterizing the unstable slope and those characterizing rock avalanche mobility. They are illustrated by relationships derived from the analysis of the Central Asia rockslide database (Strom and Abdrakhmatov 2018).

**Relationships derived from Central Asia database and some problematic issues**

Statistical analysis performed for samples from Central Asian database selected according to confinement conditions (Strom and Abdrakhmatov 2018; Strom et al. 2019) demonstrates that the highest R<sup>2</sup> values ranging from 0.9258 to 0.9361 characterize regressions between total area affected by rock avalanches (A<sub>total</sub>) and product of volume (V) and H<sub>max</sub> – the elevation difference between the headscarp crown and the lowermost point of the deposits (Fig. 3).

Besides statistical significance indicating that the affected area characterizes mobility better than just the

runout, it should be pointed out that V×H<sub>max</sub> is somehow proportional to the potential energy released during rock avalanche emplacement and, thus, has clear and easily understandable physical meaning.

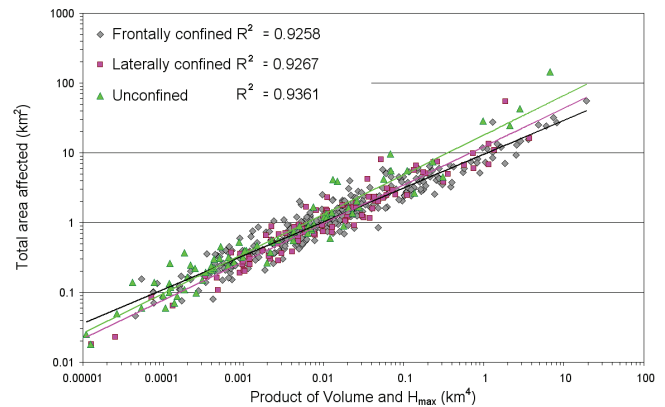


Figure 3 Relationships between total affected area and product of rock avalanche volume and maximal height drop derived for samples with different confinement and their R<sup>2</sup> values (after Strom and Abdrakhmatov 2018, with permission of Elsevier)

It is interesting that relationships between total affected area (A<sub>total</sub>) and runout (L) are almost similar for rockslides that moved in frontally confined (339 cases) and in unconfined (79 cases) conditions, while average A<sub>total</sub> value for 92 laterally confined rockslides is about 2 times smaller practically within the entire runout range (Fig. 4). It looks as that transverse spreading of unconfined and frontally confined rock avalanches is governed by the same laws, despite the significant difference in their motion mechanics, and that results in the similar increase of the affected area compared with laterally confined cases for which widening of rock avalanche debris is limited by the valley slopes.

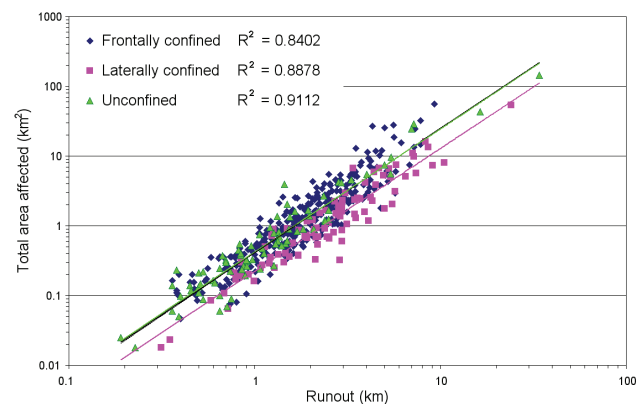


Figure 4 Relationships between total area affected and runout for rockslide samples with different confinement and corresponding R<sup>2</sup> values (after Strom and Abdrakhmatov, 2018, with permission of Elsevier).

This comparison, however, does not take into account that unconfined and frontally confined rock avalanches that affect the same area, should have a

significant difference in their volumes – unconfined features that usually form rather thin blankets should be much thinner than natural blockages formed in relatively narrow valleys with pronounced frontal confinement. Multi-parameter correlation analysis is required to characterize these relationships adequately.

Laterally confined cases provide also the anomalous relationship between the product of slope failure volume and maximal height drop ( $V \times H_{max}$ ) on the one hand and runout ( $L$ ) on the other hand. Unlike rock avalanches of two other confinement types (unconfined and frontally confined) whose regressions have rather high  $R^2$  values – not as high as for  $A_{total}$  vs.  $V \times H_{max}$  regressions, but slightly higher than for corresponding  $L \pm V$  regressions, runout of laterally confined cases practically does not correlate with  $V \times H_{max}$  (Fig. 5). Analysis performed in Strom et al. (2019) showed that it is due to a lack of correlation between runout and maximal height drop for rock avalanches of such confinement type ( $R^2$  is even lower – compare Figs. 5 and 6). It should be pointed out that, unlike Figs. 3 or 5 where independent parameter ( $V \times H_{max}$ ) varies for about 6 orders,  $H_{max}$  itself varies less than for 1.5 order – from ca. 100 m to ca. 3000 m only.

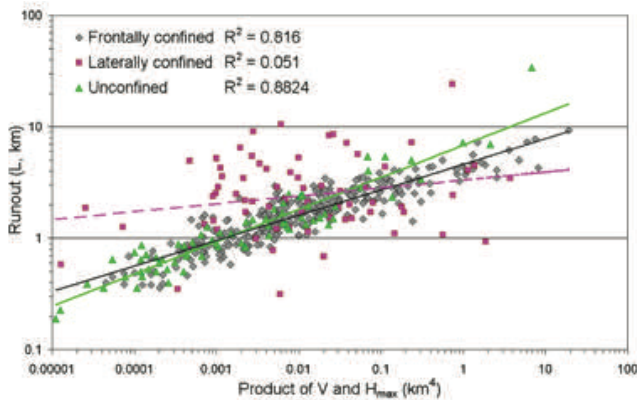


Figure 5 Relationships and corresponding  $R^2$  values of log-log regressions between runout ( $L$ ) and product of rockslide volume and maximal height drop ( $V \times H_{max}$ ) for rock avalanches with different confinement (after Strom and Abdrakhmatov, 2018, with permission of Elsevier).

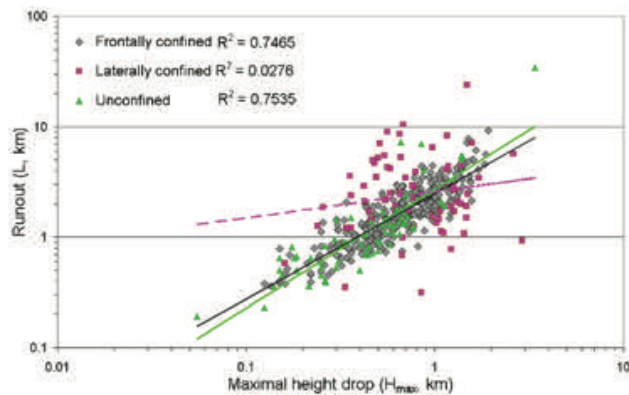


Figure 6 Relationships and corresponding  $R^2$  values of log-log regressions between runout ( $L$ ) and maximal height drop ( $H_{max}$ ) for rock avalanches with different confinement (after Strom and Abdrakhmatov, 2018, with permission of Elsevier).

Perspectives of further statistical analysis allowing better understanding of rock avalanches mobility and their more adequate hazards and risk assessment are discussed in brief hereafter

### Additional sampling criteria

Multilevel classification proposed in (Strom 2021) allows selecting rock avalanche types and subtypes that takes into consideration not only confinement conditions described above, but also some additional criteria. The latter are the deposits' spreading in the direction transverse to that of the initial motion (see Fig. 1), and debris distribution along the rock avalanche path that can be used as sampling criteria for the statistical analysis.

### Subdivision of unconfined and frontally confined types

Unconfined rock avalanches can be subdivided into mono-directional, fan-shaped and isometric subtypes illustrated by Fig. 1. Similarly, frontally confined features can be subdivided into compact and widened subtypes (Fig. 7). A similar classification of the laterally confined features according to this criterion is useless since they are strictly bounded by valley slopes that exclude the transverse debris spreading.

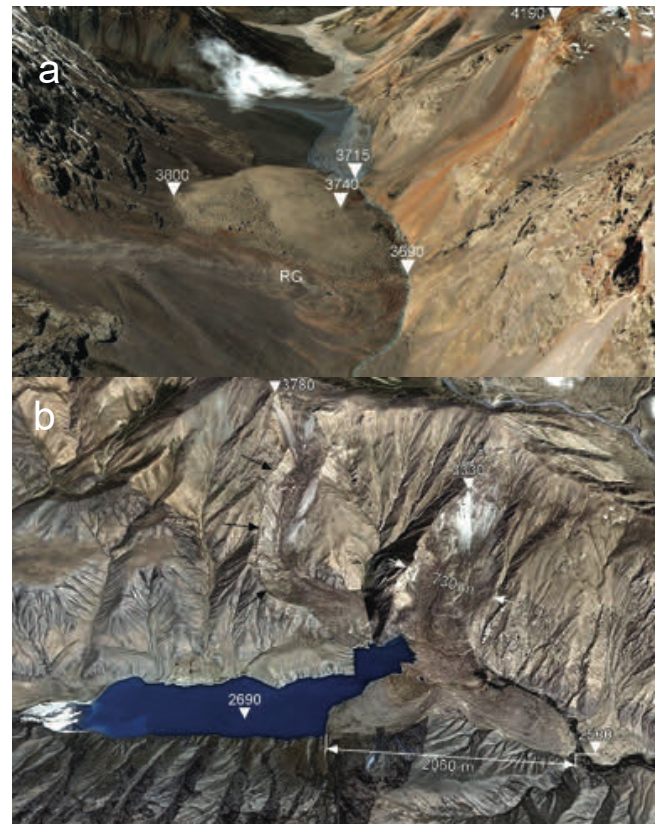


Figure 7 Two subtypes of frontally confined rock avalanches. a – compact Kainar dam, Central Tien Shan; b – widened rock avalanche dam in the Sarmin-Ula Range, Eastern Tien Shan, China (after Strom and Abdrakhmatov, 2018, with permission of Elsevier).

The formation of each of these subtypes is governed by interrelations of moving rock avalanche debris with the topographic obstacles and/or substrate. It can be assumed that statistical analysis can provide some insights into the nature of such interrelations.

For the frontally confined cases, effect of the topography of the opposite valley slope with which rapidly moving debris collides, or on which it climbs, is more or less obvious (see, e.g., Strom 2010). In the case shown in Fig. 7a, the momentum gained during the initial descent was released by rock avalanche upslope climbing. In contrast, the collision of rock avalanche in the Sarmin-Ula Range (Fig. 7b) with the triangular spur of the opposite valley slope had cut it into two parts that spread up- and downstream the valley.

For frontally confined cases it would be reasonable to subdivide the database into samples considering such additional parameters as the width of the valley floor (or its ratio to the valley depth), straightness or curvature of the collision zone, the overall shape of the valley (V-type or U-type).

Variability of the shapes of the unconfined rock avalanche deposits can be explained assuming that presence or absence of the sidewise debris spreading depend on the shear strength of the base over which rock avalanche moves (Strom 2006; Strom and Abdrakhmatov 2018).

Indeed, distinct sidewise spreading took place at large-scale rock avalanches that moved either on glaciers like the 1964 Serman Glacier rock avalanche (McSaveney 1978) or rock avalanches triggered by the 2002 Denali Fault earthquake (Jibson et al. 2006), or on well saturated flood plains such as the 2006 Leyte rock avalanche in Philippines (Sassa et al. 2010). Similar lateral spreading took place at the prehistoric Atdjailau rock avalanche in eastern Kyrgyzstan that moved over the kilometre-wide flat flood plain of the Inylchek River valley formed by a glacier (Fig. 8).



Figure 8 Remnants of the strongly eroded isometric body of the Atdjailau rock avalanche (simplified from Strom and Abdrakhmatov, 2018, with permission from Elsevier).

Strong vibrations produced by the dynamic loading of rock avalanche debris rapidly moving over the substrate could cause some liquefaction of the saturated alluvium that, in its turn, could reduce basal friction significantly.

Most of the rock avalanches, when they just escape from the source zone, move as a rather thick body undergoing gradual thinning during its further motion. Such gravity-governed thinning produce lateral forces directed both forward and sidewise (similar to the behaviour of liquid) and, thus, debris spreading in all directions. However, the 'additional' forces produced by such thinning should be not as high as forces inherited from the directed motion under rock avalanche own momentum gained during the initial descent.

If the material of the substrate over which rock avalanche moves is strong enough, as it can be expected for dry gravelly alluvial fans, the additional forces produced by debris thinning and acting in the transverse direction, might be too small to overcome basal friction that requires some shearing of the material (Grigorian 1979). In such case thinning would lead to rock avalanche body elongation in the same direction as it moves under its own momentum only, increasing the runout.

If, however, rock avalanche moves over glacier ice, or snow-covered plain or over liquefiable flood plain with the shallow groundwater table, the basal friction can be very low. In such cases, the flattening debris can overcome this friction force and spread sidewise as well as forward. Snow cover can explain the formation of fan-shaped bodies of rock avalanches that moved over depression bottoms composed of alluvial fans such as an extremely mobile 16.36 km long Yimake rock avalanche at the eastern foot of the Pamir (Yuan et al. 2013).

Of course, additional analysis is necessary to prove or disprove this assumption. In particular, many rock avalanches that collapsed on the glaciers have quite elongated shape (see Figs. 9 and 10). However, most of such rock slope failures were rather small – less than one million cubic meters in volume (Strom 2014; Dokukin et al. 2019), and, probably there was not enough material to produce laterally directed forces large enough to overcome even low basal friction.

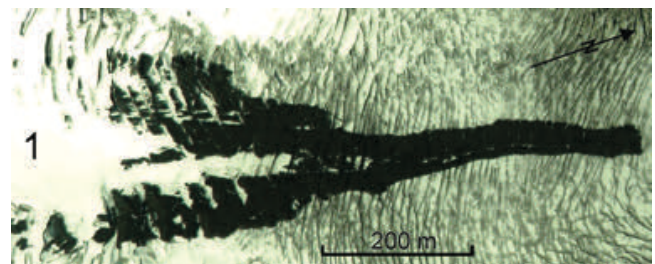


Figure 9 Small elongated rock avalanche about 0.3 Mm<sup>3</sup> in volume at the upper part of the Korpsay glacier (Xingiang, China) (after Strom and Abdrakhmatov, 2018, with permission from Elsevier).

### Debris distribution along the rock avalanche path

This criterion allows classifying rock avalanches regardless of the confinement conditions. Three main types have been selected according to it – primary, secondary and jumping (Fig. 11) (Strom 2006, 2010, 2021; Strom and Abdrakhmatov 2018).

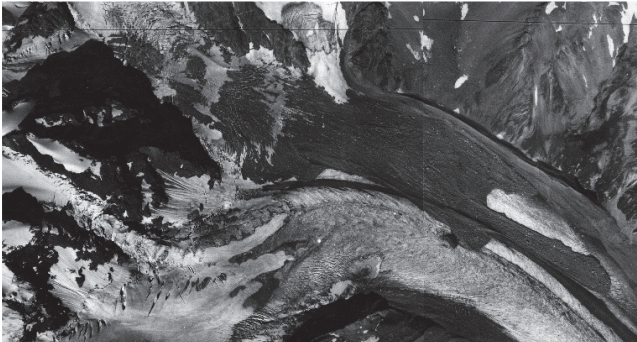


Figure 10 Small elongated rock avalanche about 1.5 km long at the upper part of the glacier in the Uruk River Basin (Northern Caucasus, Russia). Fragment of an aerial photo made in 1959.

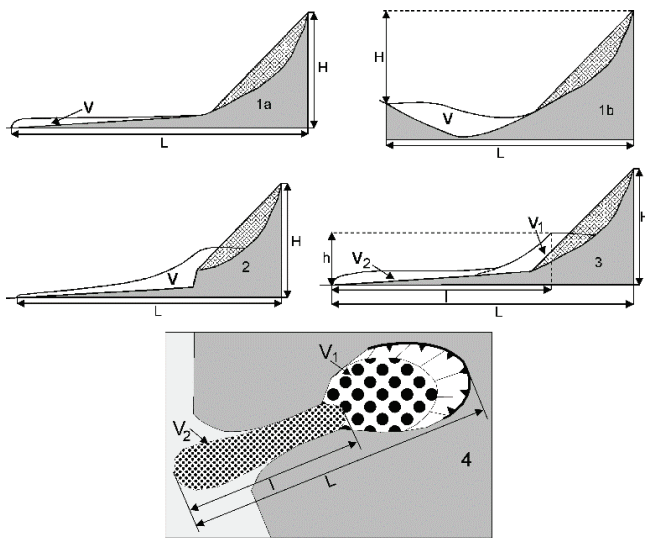


Figure 11 Rock avalanche types. 1: Primary rock avalanche. The entire rock mass is involved in the avalanche-like motion. 1a: in unconfined or laterally confined conditions, ignoring transverse debris spreading that can be significant for unconfined events; 1b: in frontally confined conditions. 2: Jumping rock avalanche with compact proximal and gradually thinning avalanche-like parts. 3 and 4: Secondary rock avalanches. H: height drop (vertical distance between the headscarp crown and the deposits tip); h: that of the secondary rock avalanche; L: runout; l: secondary rock avalanche runout; V: entire volume;  $V_1$ : volume of the compact part of the secondary rock avalanche;  $V_2$ : that of its avalanche-like part. 3: Secondary rock avalanche of the “classical” subtype characterized by compact proximal accumulation with the prominent secondary scar above the avalanche-like part. 4: Secondary rock avalanche of the “bottleneck” subtype, which bipartition occurs when the rapidly moving rock mass meets sharp valley constriction (after Strom and Abdrakhmatov, 2018, with permission from Elsevier).

Preliminary statistical analysis, which results are presented in (Strom and Abdrakhmatov 2018), proved that secondary rock avalanches associated with momentum transfer from rapidly decelerating part of debris to its part retaining the possibility of further motion, are more mobile than those of the primary type.

Further statistical analysis could be performed separately for unconfined and laterally confined cases that can be attributed to primary and secondary types.

### Conclusions

The regression analysis of various parameters characterizing rock avalanche mobility such as runout, angle of reach, affected area, etc., allows a better understanding of the processes governing their motion and derives relationships that can be used to estimate the shape and dimensions of the harmed area.

The most relevant statistical discrimination requires analysis of samples selected according to several criteria that reflect factors affecting debris motion. To ensure the statistical representativeness of such samples, a compilation of a much larger database, than it has been used up to now, is necessary. It should be compiled according to the strict, well-defined principles that will guarantee the similarity of all measured parameters throughout the entire database.

### References

- Corominas J (1996) The angle of reach as a mobility index for small and large landslides. *Can Geotech J.* 33: 260–271.
- Davies T R (1982) Spreading of rock avalanche debris by mechanical fluidization. *Rock Mech.* 15: 9–24.
- Dokukin MD, Kalov HM, Saverniuk EA, (2019) Activation of rock fall processes in the high-mountain zone of Western Caucasus in XXI Century (analysis of space images obtained at a different time). *Proceedings of the 1<sup>st</sup> International scientific conference. Karachaev-Cherkessk State University. Karachaevsk pp. 61-66. ISBN 978-5-8307-0594-3 (in Russian).*
- Grigorian SS (1979) New friction law and mechanism of large-scale rockfalls and landslides. *Proceedings of Academy of Sciences of USSR.* 244: 846-849 (in Russian).
- Griswold JP, Iverson RM (2008) Mobility statistics and automated hazard mapping for debris flows and rock avalanches (ver. 1.1, April 2014). *Scientific Investigations Report 2007–5276. U.S. Geological Survey.* pp 1–59.
- Howard K (1973) Avalanche mode of motion: implications from lunar examples. *Science, New Series.* 180: 1052–1055.
- Hsü KJ, (1975) Catastrophic debris streams (sturzstroms) generated by rock falls. *Geological Society of America Bulletin.* 86: 129-140.
- Hung O (2006) Rock avalanche occurrence, process and modeling. *Landslides from Massive Rock Slope Failure.* Evans S G, Scarascia Mugnozza G, Strom A, Hermanns RL (eds.). NATO Science Series: IV: Earth and Environmental Sciences, vol 49. Springer, Dordrecht. 243-266.
- Jibson RW, Harp EL, Schulz W, Keefer DK (2006) Large rock avalanches triggered by the M 7.9 Denali Fault, Alaska, earthquake of 3 November 2002. *Eng. Geol.* 83:144–160.
- Kilburn CRJ, Sørensen S-A, (1998) Runout length of sturzstroms: the control of initial conditions and of fragment dynamics. *J. Geophys. Res.* 103(B8):17877–17884.

- Kobayashi Y (1993) A hypothesis for reduced resistance in large landslides. *Safety and Environmental Issues in Rock Engineering. Proc. of the ISRM Int. Symp. Lisboa, 21–24 June 1993*. Balkema Rotterdam. pp 335–339.
- Kobayashi Y (1997) Long runout landslides riding on basal guided wave. *Engineering geology and the environment*. Marinis K, Tsiambaos S (eds). Balkema, Rotterdam. pp. 761–766.
- Li T (1983) A mathematical model for predicting the extent of a major rockfall. *Z. Geomorphol.* 27: 473–482.
- Liu H, Zhao X, Xiao D (under review) Effects of local topography on the mobility of rock avalanches: a preliminary statistical analysis. *Engineering Geology*.
- McSaveney MJ (1978) Sherman glacier rock avalanche. *Rockslides and Avalanches 1, Natural Phenomena*. Voight B (ed). Elsevier, Amsterdam. pp. 197–258.
- Mitchell A, McDougall S, Aaron J, Brideau M-A (2020) Rock Avalanche-Generated Sediment Mass Flows: Definitions and Hazard. *Frontiers in Earth Science.* 8: 1-18, Article 543937.
- Nicoletti P G, Sorriso-Valvo M (1991) Geomorphic controls of the shape and mobility of rock avalanches. *Geol Soc Am Bull.* 103: 1365–1373.
- Legros F (2002) The mobility of long-runout landslides. *Eng Geol.* 63:301–331.
- Legros F (2006) Landslide mobility and the role of water. *Landslides from massive rock slope failure*. Evans S G, Scarascia Mugnozza G, Strom A, Hermanns R L (eds.). NATO Science Series: IV: Earth and Environmental Sciences, vol 49. Springer, Dordrecht. pp. 233–242.
- Sassa K, Nagai O, Solidum R, Yamazaki Y, Ohta H (2010) An integrated model simulating the initiation and motion of earthquake and rain induced rapid landslides and its application to the 2006 Leyte landslide. *Landslides.* 7: 219-236.
- Shaller PJ, (1991) Analysis and implications of large Martian and Terrestrial landslides. Ph.D. Thesis, California Institute of Technology.
- Strom A, (1996) Some morphological types of long-runout rockslides: effect of the relief on their mechanism and on the rockslide deposits distribution. *Landslides. Proc. Of the Seventh International Symposium on Landslides*. Balkema, Rotterdam. pp. 1977-1982.
- Strom A (2006) Morphology and internal structure of rockslides and rock avalanches: grounds and constraints for their modelling. *Landslides from massive rock slope failure*. Evans SG, Scarascia Mugnozza G, Strom A, Hermanns RL (eds.). NATO Science Series: IV: Earth and Environmental Sciences. Springer, Dordrecht. 49:305-328.
- Strom A (2010) Evidence of momentum transfer during large-scale rockslides' motion. *Geologically Active. Proc. of the 11th IAEG Congress, Auckland, New Zealand, 5-10 September 2010*. Taylor & Francis Group, London. pp. 73-86.
- Strom A (2014) Catastrophic Slope Processes in Glaciated Zones of Mountainous Regions. *Landslides in Cold Regions in the Context of Climate Change, Environmental Science and Engineering*. Shan W et al. (eds). Springer International Publishing, Switzerland. pp. 3-10.
- Strom A, Abdrakhmatov K (2018) Rockslides and rock avalanches of Central Asia: distribution, morphology, and internal structure. Elsevier, Netherlands, UK, USA. ISBN: 978-0-12-803204-6. 449 p.
- Strom A, Li L, Lan H (2019) Rock avalanche mobility: optimal characterization and the effects of confinement. *Landslides.* 16: 1437–1452.
- Yu F, Su L (2021) Experimental investigation of mobility and deposition characteristics of dry granular flow. *Landslides.* 18. <https://doi.org/10.1007/s10346-020-01593-2>.
- Yuan Z, Chen J, Owen LA, Hedrick KA, Caffee MW, Li W, Schoenbohm LM, Robinson AC (2013) Nature and timing of large landslides within an active orogen, Eastern Pamir, China. *Geomorphology.* 182: 49–65.



# Statistical literature analysis of combined GNSS-InSAR landslide investigation

Matteo Del Soldato<sup>(1)</sup>, Camilla Medici<sup>(1)</sup>, Pierluigi Confuorto<sup>(1)</sup>, Silvia Bianchini<sup>(1)</sup>

1) University of Firenze, Earth Sciences Department, Firenze, Via G. La Pira 4, Italy (matteo.delsoldato@unifi.it)

**Abstract** The Synthetic Aperture Radar Interferometry (InSAR) is a technique capable to detect ground deformation, by comparing the phase difference between two radar images over the same area. The GNSS (Global Navigation Satellite System) approach permits to retrieve precise worldwide information about the positioning, timing and navigation of elements. Considering the strength and drawbacks of both techniques, they were combined several times for investigating, analysing and monitoring natural hazards. Landslides are one of the main damaging and diffuse natural hazards in Europe and the scientific community took advantage of the combination of InSAR and GNSS approaches for their investigations. A literature analysis conducted using Google Scholar, a freely accessible web search engine, allowed gathering 40 scientific contributions published since 2006 over 15 European countries, i.e. peer-reviewed articles, book chapters, proceedings of international congresses, that considered both InSAR and GNSS data for landslide investigation. The research was conducted using keywords recalling the use of the two combined techniques over European countries. The collected scientific contributions were critically analysed to identify the scope, the used radar satellite constellations as well as the spatial and temporal distribution of publications.

**Keywords** landslide, InSAR, GNSS, review, Europe

## Introduction

The GNSS (Global Navigation Satellite System) family is composed of several constellations that provide global information about position, timing and navigation data of elements equipped with GNSS receivers that automatically commute this information in precise location and velocity of movement. Since the 1980's (Gabriel et al. 1989), the InSAR (Interferometry Synthetic Aperture Radar) approach is used and became widely exploited for detecting, investigating and monitoring ground deformations (Del Soldato et al. 2021). The phase difference between two SAR satellite images acquired at two different times over the same area, DInSAR (Differential InSAR), allows estimating the cumulative displacement that occurred. The InSAR approach has evolved over time and several algorithms for elaborating more than two images have been developed, namely

Multi-Temporal InSAR (MT-InSAR), allowing the analysis of ground deformation evolution (Crosetto et al. 2016).

GNSS approach is (i) accurate to determine the position in time, and consequently, the velocity of movement, (ii) reliable thanks to the ability to work constantly, maintaining high precision and integrity, (iii) 3-dimensional, able to calculate horizontal (East-West and North-South) and vertical (Up-Down) motion components. On the other hand, it is station-dependent (Zulkifli et al. 2018) and some inaccessible areas cannot be covered by GNSS receivers. Europe has more than 300 distributed multi-GNSS reference stations (Bruyninx et al. 2019). Differently, the InSAR approaches do not require any receiver at the ground but only reflecting elements, e.g., urban areas, outcrops, artificial elements, for returning a spread and dense network of measurement points (MP) collecting accurate and high precise values of the velocity of movement and cumulative displacement over time. In addition, it allows a short-time repetitiveness of measure, the possibility to reach inaccessible areas with a high benefits/cost ratio. Nevertheless, the InSAR measurements are relative, thus referred to a Reference Point accurately chosen, and the MP can be affected by (i) geometrical effects due to the combination between LoS the topography, (ii) atmospheric and aliasing artefacts and (iii) errors due to land covers.

The combined use of GNSS and InSAR datasets were made for several purposes, from the InSAR processing, e.g., atmospheric corrections (e.g., Catalão et al. 2011; Heublein et al. 2015; Mateus et al. 2012), to a longer investigation of ground deformations, e.g. subsidence or uplift phenomena (e.g., Béjar-Pizarro et al. 2016; Catalão et al. 2009; Del Soldato et al. 2018; Heimlich et al. 2015), landslide investigation (e.g., Bardi et al. 2016), glacial analysis (e.g., Gudmundsson et al. 2002), volcanic (e.g., Currenti et al. 2011; Fernández et al. 2004) and seismic activity investigation (e.g., Ganas et al. 2019; Stramondo et al. 1999) or infrastructure analysis (e.g., Bignami and Stramondo 2015; Gheorghe et al. 2020), and more general and theoretical applications (e.g., Ge 2003; Simonetto et al. 2014).

Landslides are one of the main damaging and diffuse natural hazards in Europe and several times the scientific community took advantage of the combination of InSAR and GNSS approaches for their investigations. The proposed literature analysis focus on the scientific contribution for the landslide investigation that combined

the use of the two datasets, indifferently on the whole European continent, including the European Turkey, Thrace, but excluding Russia.

In this review, the DInSAR and MTInSAR approaches were considered separately, while GNSS, GPS, cGPS (continuous GPS) and DGPS (Differential GPS) were taken into account as unique approach, namely GNSS, in order to have an overview of the landslide analysis combining these two remote techniques.

The state-of-the-art of InSAR and GNSS data integration for landslide investigation can be a relevant starting point considering that the EPN (European REferences - EUREF - Permanent GNSS Network) freely provides GNSS data of more than 300 continuously operating stations referenced to the ETRS89 (European Terrestrial Reference System) benchmarks over the European territory and that in the mid of 2022 MT-InSAR data, yearly updated, will be freely available over Europe thanks to the European Ground Motion Service (EGMS).

### Data collection

The collection of the scientific contributions combining InSAR and GNSS data for the landslide investigation was conducted exploiting the freely accessible web search engine Google Scholar. It is considered “*essentially a superset of WoS and Scopus, with substantial extra coverage*” (Martín-Martín et al. 2018). In fact, approximately 95% and 92% of the citations are comparable to those contained in Web of Science (WoS) and Scopus databases. On the other hand, the research of the contributions cannot be automatized as in other web search engines. The gathering of the documents was conducted combining two lists of keywords with each European country: (i) one list based on the InSAR approaches, e.g., “InSAR”, and related words as “DInSAR”, “MT-InSAR”, “A-DInSAR” (Advanced DInSAR), and “PSI” (Persistent Scatterers Interferometry) and related words; (ii) one focused on the GNSS family and techniques, e.g., “GNSS”, “GPS” and related terms as “cGPS” (continuous GPS) and “DGPS” (Differential GPS).

All the collected scientific contributions were critically analysed for realizing a database by considering:

- Title of the scientific contribution
- List of authors
- Type of submission
- Year of publication
- Country and location of the area of interest
- Investigated period
- Type of SAR processing (InSAR or MT-InSAR)
- Satellite sensor band (C- X- L-band) and name
- Use of other techniques (e.g., inclinometers)

### Spatial distribution and temporal evolution

Forty scientific contributions on the combined use of GNSS and InSAR data for landslide investigation, considering peer-reviewed international scientific articles, book chapters, and conference abstracts, were collected by

Google Scholar. Taking into consideration the little less than 200 scientific contributions combining the use of GNSS and InSAR data over Europe for several aims collected by Del Soldato et al. (2021), the landslide investigation is approximately 20% of the total works. The spatial distribution and the temporal evolution of these publications were examined.

### Spatial distribution

The 40 collected scientific contributions investigate landslides localized in 15 countries (Tab. 1). The countries with the most contributions are Italy and Norway with a total number of 8 – 7 peer-reviewed international scientific journals (e.g., Carlà et al. 2019; Cenni et al. 2021; Crippa et al. 2020; Pappalardo et al. 2021) and 1 proceeding (Radicioni et al. 2012), and 5 journal articles (e.g., Bardi et al. 2016; Eckerstorfer et al. 2018; Rouyet et al. 2017), 2 peer-reviewed book chapters (Böhme et al. 2016; Dehls et al. 2012) and 1 proceeding of a congress (Dehls et al. 2008), respectively. All the contributions referred to Italy are focused on local areas and single landslides, e.g., Assisi landslide (Bovenga et al. 2013; Radicioni et al. 2012) or Corvara landslide (Darvishi et al. 2020), except one that analyses at regional scale the Northern Apennines (Bayer et al. 2017), while the Norwegian contributions are divided between landslide investigations at regional (e.g., Lauknes et al. 2010) and local scale (e.g., Booth et al. 2015).

Table 1 Spatial distribution of scientific contributions combining GNSS and InSAR data for landslide analysis.

Country	Num. articles	Years of publications
Bulgary	1	2018
Cyprus	1	2021
France	1	2013
Greece	1	2014
Hungary	1	2020
Italy	8	2012-2013-2017-2019-2020-2021
Liechtenstein	1	2006
Malta	2	2015
Norway	8	2008-2010-2012-2015-2016-2017-2018
Portugal	1	2015
Slovakia	1	2018
Slovenia	3	2012-2013-2015
Spain	5	2011-2013-2014-2021
Switzerland	5	2007-2010-2013-2015-2016
Turkey (Thrace)	1	2021

Spain and Switzerland follow Italy and Norway with 5 contributions, all scientific articles on international peer-reviewed journals (e.g., Gili et al. 2021; Herrera et al. 2011), and 3 publications in international journals (e.g., Strozzi et al. 2013) and 2 peer-reviewed book chapters (e.g., Kenner et al. 2016), respectively. The landslide analyses over Spain with GNSS and InSAR datasets was focused on the Tena Valley at a regional scale (García-Davalillo et al. 2014; Herrera et al. 2013) or the Vallecambre (e.g., Crosetto et al.

2013) and Portalet (Herrera, et al. 2011) at a local scale. Scientific contributions about Swiss territory investigated regional areas (e.g., Barboux et al. 2015) or single rock glacier phenomena (e.g., Delaloye et al. 2008) and mass movements (Strozzi et al. 2010).

Three publications, 2 articles (e.g., Komac et al. 2015; Mahapatra et al. 2013) and 1 book chapter (Mahapatra et al. 2012) in peer-reviewed international journals focus on the Potoška Planina, Slovenia. The last country with more than one publication is Malta with two regional scale peer-reviewed articles published in international scientific journals (Mantovani et al. 2016; Piacentini et al. 2015).

Only one scientific contribution was gathered for Bulgaria, Trifon Zarezan landslide (Atanasova and Nikolov 2018), Cyprus, Choirokotia case study (Themistocleous et al. 2021), France, La Valette landslide (Raucoules et al. 2013), Greece (Elias et al. 2014), Hungary (Bozsó et al. 2020), Liechtenstein, the first landslide investigation combining GNSS and InSAR data (Colesanti and Wasowski 2006), Portugal, Grande da Pipa River basin, (Oliveira et al. 2015), Slovakia, Tatra Mountains (Czikhardt et al. 2018) and Turkey, landslides in Beylikdüzü-Esenyurt Districts of Istanbul (Bayik et al. 2021).

### Temporal distribution

The first scientific contribution combining the GNSS and InSAR data was published in 1999 (Stramondo et al. 1999) focused on the September 26, 1997 Colfiorito (Italy) earthquakes, but the first one outlining this approach for landslide investigation dates back 2006 (Colesanti and Wasowski 2006). The scientific production shows an increment in 2012, with 2 conference proceedings and 1 book chapter, and in 2013 with the higher number of 6 peer-reviewed articles in international scientific journals (Fig. 1).

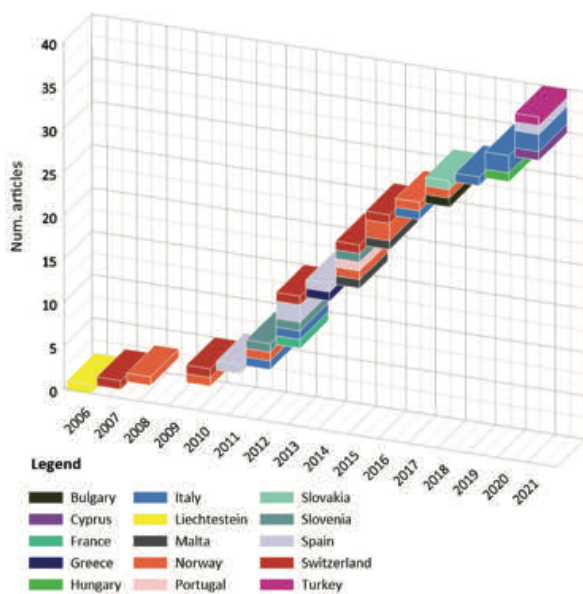


Figure 1 Temporal evolution of the scientific contribution of GNSS-InSAR landslide analysis.

More than 3 contributions can be highlighted in: (i) 2015 and 2021, with 5 articles in international scientific journals, and (ii) in 2016, the year in which 4 scientific contributions were collected.

It is worth noting that the research of scientific contributions was made in autumn 2021, and articles, book chapters or extended abstracts and proceedings published in the late 2021 cannot be collected. For this reason, the number of publications in 2021 could be higher than 5. In addition, there is only one year without scientific contributions, the 2009, so that allows confirming the continuous use of combined GNSS and InSAR data as a valuable approach by the scientific community for the landslide investigation.

### Discussions

For each work, the GNSS and InSAR datasets used for the landslide investigation are visually synthesized in Fig. 2. The oldest scientific contributions used ERS1/2 dataset since it was the only available in that period, and the GNSS data cover a previous period from '80 to '90 (Colesanti and Wasowski 2006). Then, starting from 2010 (Strozzi et al. 2010), the Envisat data were used alone or combined with other datasets. In the following years, the ERS1/2 datasets were not used in this type of approach for landslide analysis, but some works (Booth et al. 2015; Mantovani et al. 2016; Piacentini et al. 2015; Strozzi et al. 2013) used more than one dataset, including ERS1/2, for investigating longer periods. The 58% of the scientific contributions used only one dataset, the 28% two datasets, only the 5% investigated landslides with 3 datasets and only one, 1%, (Strozzi et al. 2010) 5 datasets in C-band (~5.6 cm), X-band (~3.1), and L-band (~23.5 cm). In these counts, two abstracts that do not report the investigated period of the GNSS and InSAR data were considered since information about the band used were present. The use of more datasets helps the investigation on a longer period, and if the datasets used were acquired by satellites mounting sensors with different wavelengths, the landslide investigation could be improved indifferently in urban areas, peri-urban or cultivated and vegetated zones. Considering that, 17 scientific contributions combined more than one dataset in landslide investigation, 11 of these use at least two different wavelengths and only 2 datasets acquired by sensors in three different bands.

It is relevant to note as since 2018 the landslide analysis combining GNSS and InSAR data used only Sentinel-1 dataset in C-band, alone or combined with constellations with other wavelengths. It allows demonstrating the crucial role covered by the Sentinel-1 constellation in this field, as the interest of the scientific community in the back analysis is limited, or forced for the costs of older datasets. Another information that can be extrapolated by the graph of the temporal comparison of GNSS and InSAR datasets used for each contribution, is that from 2014, with few exceptions recently published, both datasets covered approximately the same time-span.

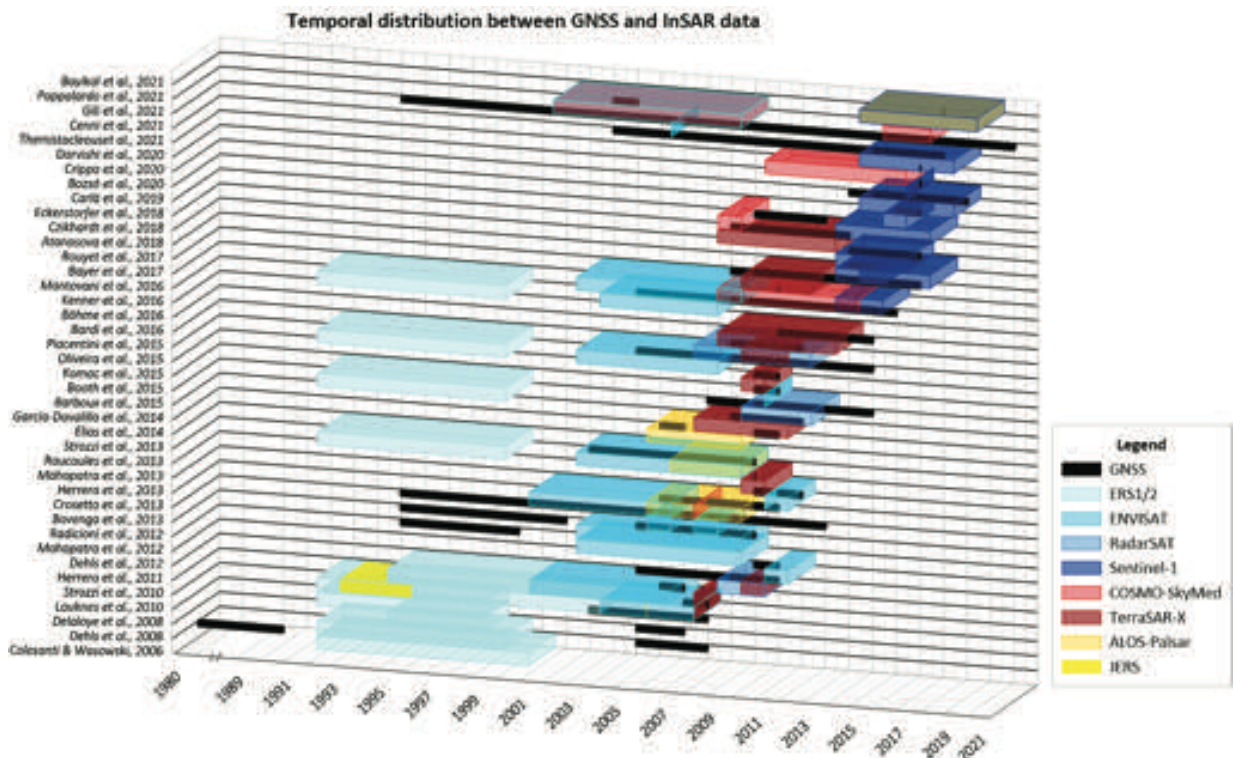


Figure 2 Temporal distribution between GNSS and InSAR datasets of each scientific contribution. It is worth highlighting that for some contributions the GNSS dataset is reported the words “since”, in this case, it was considered the time span from the specified year until the date of submission (Booth et al. 2015; Crosetto et al. 2013; Dehls et al. 2012; Mantovani et al. 2016; Piacentini et al. 2015; Rouyet et al. 2017); in two cases, instead, there was not written the exact period of the GNSS dataset and it was assumed to be the same of the InSAR (Eckerstorfer et al. 2018; Oliveira et al. 2015); and for two abstracts it was not possible to extract the information on the period covered by the GNSS and InSAR used datasets (Elias et al. 2014; Kenner et al. 2016).

The remaining 78% of the publications show the combination with other topographic, atmospheric and satellite datasets. More in detail, 15 scientific contributions (22% of the total) combined or compared the GNSS and InSAR data with direct measurements as inclinometers (e.g., Colesanti and Wasowski 2006; Gili et al. 2021), piezometers (e.g., Crosetto et al. 2013), extensometers (e.g., Rouyet et al. 2017), seismic analysis (Bayer et al. 2017), Terrestrial Laser Scanning (e.g., Booth, et al. 2015, Dehls, et al. 2012) or levelling (e.g., Mahapatra et al. 2013; Radicioni et al. 2012); 11 publications (16% of the total) use also a dataset of aerial optical images (e.g., Cenni et al.

2021; Eckerstorfer et al. 2018; Themistocleous et al. 2021). Eight scientific contributions show the use of the GBInSAR (Ground Based InSAR) data (e.g., Carlà et al. 2019) as other 8 field surveys for validating the remote sensed data (e.g., Lauknes et al. 2010; Oliveira et al. 2015). Some authors used more particular datasets for comparing or validating the results obtained by the landslide investigations performed combining GNSS and InSAR data, to which MODIS (Moderate Resolution Imaging Spectroradiometer) data (Darvishi et al. 2020), atmospheric and rainfall data (e.g., Herrera et al. 2011), and infrared images (Pappalardo et al. 2021).

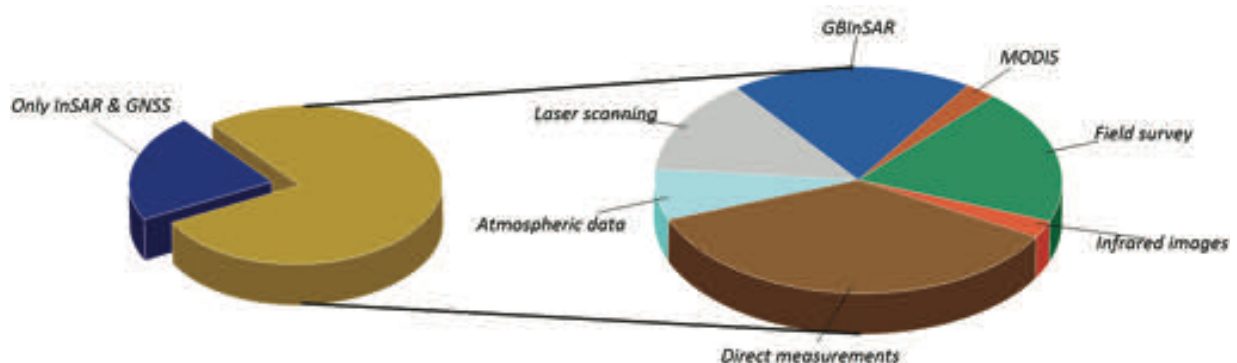


Figure 3 Landslide investigation techniques with GNSS and InSAR.

## References

- Atanasova M, Nikolov H (2018) Ground displacements detection in Trifon Zarezan landslide based on GNSS and SAR data. *MMM Geo Information*: 7-15.
- Barboux C, Strozzi T, Delaloye R, Wegmüller U, Collet C (2015) Mapping slope movements in Alpine environments using TerraSAR-X interferometric methods. *ISPRS Journal of Photogrammetry Remote Sensing*. 109: 178-192.
- Bardi F, Raspini F, Ciampalini A, Kristensen L, Rouyet L, Lauknes TR, Frauenfelder R, Casagli N (2016) Space-Borne and Ground-Based InSAR Data Integration: The Åknes Test Site. *Remote Sensing*. 8: 237.
- Bayer B, Simoni A, Schmidt D, Bertello L (2017) Using advanced InSAR techniques to monitor landslide deformations induced by tunneling in the Northern Apennines, Italy. *Engineering Geology*. 226: 20-32.
- Bayik C, Abdikan S, Ozdemir A, Arıkan M, Sanlı FB, Dogan U (2021) Investigation of the landslides in Beylikdüzü-Eesenyurt districts of Istanbul from InSAR and GNSS observations. *Natural Hazards*. 109: 1201–1220.
- Béjar-Pizarro M, Guardiola-Albert C, García-Cárdenas RP, Herrera G, Barra A, López Molina A, Tessitore S, Staller A, Ortega-Becerril JA and García-García RP (2016) Interpolation of GPS and geological data using InSAR deformation maps: method and application to land subsidence in the alto Guadalentín aquifer (SE Spain). *Remote Sensing*. 8(11): 965.
- Bignami C, Stramondo S (2015) Ground deformation observed at Kozloduy (Bulgaria) and Akkuyu (Urkey) NPPS by means of multitemporal SAR inteferometry. *Πανελλήνια και Διεθνή Γεωγραφικά Συνέδρια, Συλλογή Πρακτικών*. 1337-1355.
- Böhme M, Bunkholt H, Oppikofer T, Dehls J, Hermanns R, Eriksen H, Lauknes T, Eiken T (2016) Using 2D InSAR, dGNSS and structural field data to understand the deformation mechanism of the unstable rock slope Gamanjunni 3, northern Norway. *Landslides and Engineered Slopes Experience, Theory and Practice Proceedings of the 12th International Symposium on Landslides, 12-19 June 2016, Napoli, Italy*. CRC Press. pp 443-449.
- Booth AM, Dehls J, Eiken T, Fischer L, Hermanns RL, Oppikofer T (2015) Integrating diverse geologic and geodetic observations to determine failure mechanisms and deformation rates across a large bedrock landslide complex: The Osmundneset landslide, Sogn og Fjordane, Norway. *Landslides*. 12: 745-756.
- Bovenga F, Nitti DO, Fornaro G, Radicioni F, Stoppini A, Brigante R (2013) Using C/X-band SAR interferometry and GNSS measurements for the Assisi landslide analysis. *International Journal of Remote Sensing*. 34: 4083-4104.
- Bozsó I, Bányai L, Hooper A, Sz E, Wesztergom V (2020) Integration of sentinel-1 interferometry and GNSS networks for derivation of 3-D surface changes. *IEEE Geoscience Remote Sensing Letters*. 18(4): 692-696.
- Bruyninx C, Legrand J, Fabian A, Pottiaux E (2019) GNSS metadata and data validation in the EUREF Permanent Network. *GPS Solutions*. 23: 1-14.
- Carlà T, Tofani V, Lombardi L, Raspini F, Bianchini S, Bertolo D, Thuegaz P, Casagli N (2019) Combination of GNSS, satellite InSAR, and GBInSAR remote sensing monitoring to improve the understanding of a large landslide in high alpine environment. *Geomorphology*. 335: 62-75.
- Catalão J, Nico G, Hanssen R, Catita C (2009) Integration of InSAR and GPS for vertical deformation monitoring: A case study in Faial and Pico Islands. *Proceedings of the Fringe 2009 Workshop, Frascati, Italy*. pp 1-7.
- Catalão J, Nico G, Hanssen R, Catita C (2011) Merging GPS and atmospherically corrected InSAR data to map 3-D terrain displacement velocity. *IEEE Transactions on Geoscience Remote Sensing*. 49: 2354-2360.
- Cenni N, Fiaschi S, Fabris M (2021) Integrated use of archival aerial photogrammetry, GNSS, and InSAR data for the monitoring of the Patigno landslide (Northern Apennines, Italy). *Landslides*. 18: 2247-2263.
- Colesanti C, Wasowski J (2006) Investigating landslides with space-borne Synthetic Aperture Radar (SAR) interferometry. *Engineering geology*. 88: 173-199.
- Crippa C, Franzosi F, Zonca M, Manconi A, Crosta GB, Dei Cas L, Agliardi F (2020) Unraveling spatial and temporal heterogeneities of very slow rock-slope deformations with targeted DInSAR analyses. *Remote Sensing*. 12: 1329.
- Crosetto M, Gili J, Monserrat O, Cuevas-González M, Corominas J, Serral D (2013) Interferometric SAR monitoring of the Vallcebre landslide (Spain) using corner reflectors. *Natural Hazards Earth System Sciences*. 13: 923-933.
- Crosetto M, Monserrat O, Cuevas-González M, Devanthery, Crippa B (2016) Persistent scatterer interferometry: A review. *ISPRS Journal of Photogrammetry and Remote Sensing*. 115: 78-89.
- Currenti G, Napoli R, Del Negro C (2011) Toward a realistic deformation model of the 2008 magmatic intrusion at Etna from combined DInSAR and GPS observations. *Earth Planetary Science Letters*. 312: 22-27.
- Czikhhardt R, Papčo J, Bakoň M (2018) Feasibility of the Sentinel-1 Multi-temporal InSAR system based on the SNAP and StaMPS: Case study from the Tatras Mts., Slovakia. *Procedia computer science*. 138: 366-373.
- Darvishi M, Cuzzo G, Bruzzone L, Nilfouroushan F (2020) Performance evaluation of phase and weather-based models in atmospheric correction with Sentinel-1 data: Corvara landslide in the Alps. *IEEE Journal of Selected Topics in Applied Earth Observations and Remote Sensing*. 13: 1332-1346.
- Dehls J, Fischer L, Böhme M, Saintot A, Hermanns R, Oppikofer T, Lauknes T, Larsen Y, Blikra L (2012) Landslide monitoring in western Norway using high resolution TerraSAR-X and Radarsat-2 InSAR. *Landslides and Engineered Slopes: Protecting Society through improved Understanding*. Eberhardt et al. (eds). pp 1321-1325.
- Dehls J, Henderson I, Lauknes T, Larsen Y (2008) Regional landslide mapping and detailed site characterization using InSAR. *Proceedings of "GeoEdmonton"*. pp 21-24.
- Del Soldato M, Confuorto P, Bianchini S, Sbarra P, Casagli N (2021) Review of works combining GNSS and InSAR in Europe. *Remote Sensing* 13: 1684.
- Del Soldato M, Farolfi G, Rosi A, Raspini F, Casagli N (2018) Subsidence evolution of the Firenze–Prato–Pistoia plain (central Italy) combining psi and GNSS data. *Remote Sensing*. 10: 1146.
- Delaloye R, Strozzi T, Lambiel C, Perruchoud E (2008) Landslide-like development of rockglaciers detected with ERS-1/2 SAR interferometry. *Proceedings ESA FRINGE Symposium 2007, Workshop, Frascati, Italy*. pp 1-6.
- Eckerstorfer M, Eriksen HØ, Rouyet L, Christiansen HH, Lauknes TR, Blikra LH (2018) Comparison of geomorphological field mapping and 2D-InSAR mapping of periglacial landscape activity at Nordnesfjellet, northern Norway. *Earth Surface Processes Landforms*. 43: 2147-2156.
- Elias P, Sykioti O, Drakatos G, Paronis D, Chousianitis K, Sabatakakis N, Anastasopoulos V, Briole P (2014) Landslides modelling and monitoring by exploiting satellite SAR acquisitions, optical imagery, GPS and in-situ measurements in Greece. *Preliminary results. EGU General Assembly Conference Abstracts*. id. 4402.
- Fernández J, González-Matesanz F, Prieto J, Rodríguez-Velasco G, Staller A, Alonso-Medina A, Charco M (2004) GPS monitoring in

- the NW part of the volcanic island of Tenerife, Canaries, Spain: Strategy and results. *Pure Applied Geophysics*. 161: 1359-1377.
- Gabriel AK, Goldstein RM, Zebker HA (1989) Mapping small elevation changes over large areas: Differential radar interferometry. *Journal of Geophysical Research: Solid Earth*. 94: 9183-9191.
- Ganas A, Elias P, Kapetanidis V, Valkaniotis S, Briole P, Kassaras I, Argyrakis P, Barberopoulou A, Moshou A (2019) The July 20, 2017 M6. 6 Kos earthquake: Seismic and geodetic evidence for an active north-dipping normal fault at the western end of the Gulf of Gökova (SE Aegean Sea). *Pure Applied Geophysics*. 176: 4177-4211.
- García-Davalillo JC, Herrera G, Notti D, Strozzi T, Álvarez-Fernández I (2014) DInSAR analysis of ALOS PALSAR images for the assessment of very slow landslides: The Tena valley case study. *Landslides*. 11: 225-246.
- Ge L (2003) Integration of GPS and radar interferometry. *GPS Solutions*. 7: 52-54.
- Gheorghie M, Armaş I, Dumitru P, Călin A, Bădescu O, Necsoiu M (2020) Monitoring subway construction using Sentinel-1 data: A case study in Bucharest, Romania. *International Journal of Remote Sensing*. 41: 2644-2663.
- Gili JA, Moya J, Corominas J, Crosetto M, Monserrat O (2021) Past, present and future monitoring at the Vallcebre landslide (Eastern Pyrenees, Spain). *Applied Sciences*. 11: 571.
- Gudmundsson S, Gudmundsson MT, Björnsson H, Sigmundsson F, Rott H, Carstensen JM (2002) Three-dimensional glacier surface motion maps at the Gjalp eruption site, Iceland, inferred from combining InSAR and other ice-displacement data. *Annals of Glaciology*. 34: 315-322.
- Heimlich C, Gourmelen N, Masson F, Schmittbuhl J, Kim S-W, Azzola J (2015) Uplift around the geothermal power plant of Landau (Germany) as observed by InSAR monitoring. *Geothermal Energy*. 3: 1-12.
- Herrera G, Gutiérrez F, García-Davalillo J, Guerrero J, Notti D, Galve J, Fernández-Merodo J, Cooksley G (2013) Multi-sensor advanced DInSAR monitoring of very slow landslides: The Tena valley case study (central Spanish Pyrenees). *Remote Sensing of Environment*. 128: 31-43.
- Herrera G, Notti D, García-Davalillo JC, Mora O, Cooksley G, Sánchez M, Arnaud A, Crosetto M (2011) Analysis with C-and X-band satellite SAR data of the Portalet landslide area. *Landslides*. 8: 195-206.
- Heublein M, Zhu XX, Alshawaf F, Mayer M, Bamler R, Hinz S (2015) Compressive sensing for neutrospheric water vapor tomography using GNSS and InSAR observations. 2015 IEEE international geoscience and remote sensing symposium (IGARSS). IEEE. pp 5268-5271.
- Kenner R, Phillips M, Beutel J, Limpach P, Papke J, Hasler A, Raetzo H (2016) Investigating the dynamics of a rock glacier using terrestrial laser scanning, time-lapse photography, in situ GPS measurements and satellite SAR interferometry: Ritigraben rock glacier, Switzerland. *Proceedings of the International Conference on Permafrost*. Potsdam, Germany, pp 20-24
- Komac M, Holley R, Mahapatra P, van der Marel H, Bavec M (2015) Coupling of GPS/GNSS and radar interferometric data for a 3D surface displacement monitoring of landslides. *Landslides*. 12: 241-257.
- Lauknes T, Shanker AP, Dehls J, Zebker H, Henderson I and Larsen Y (2010) Detailed rockslide mapping in northern Norway with small baseline and persistent scatterer interferometric SAR time series methods. *Remote Sensing of Environment* 114: 2097-2109.
- Mahapatra P, van der Marel H, Hanssen R, Holley R, Samiei-Esfahany S, Komac M, Fromberg A (2012) Radar transponders and their combination with GNSS for deformation monitoring. 2012 IEEE International Geoscience and Remote Sensing Symposium. IEEE. pp 3891-3894
- Mahapatra PS, Samiei-Esfahany S, van der Marel H, Hanssen RF (2013) On the use of transponders as coherent radar targets for SAR interferometry. *IEEE Transactions on Geoscience Remote Sensing*. 52: 1869-1878.
- Mantovani M, Devoto S, Piacentini D, Prampolini M, Soldati M, Pasuto A (2016) Advanced SAR interferometric analysis to support geomorphological interpretation of slow-moving coastal landslides (Malta, Mediterranean Sea). *Remote Sensing*. 8: 443.
- Martín-Martín A, Orduna-Malea E, Thelwall M, López-Cózar ED (2018) Google scholar, web of science, and Scopus: A systematic comparison of citations in 252 subject categories. *Journal of Informetrics*. 12: 1160-1177.
- Mateus P, Nico G, Tomé R, Catalão J, Miranda PM (2012) Experimental study on the atmospheric delay based on GPS, SAR interferometry, and numerical weather model data. *IEEE Transactions on Geoscience Remote Sensing*. 51: 6-11.
- Oliveira S, Zêzere J, Catalão J, Nico G (2015) The contribution of PSInSAR interferometry to landslide hazard in weak rock-dominated areas. *Landslides*. 12: 703-719.
- Pappalardo G, Mineo S, Cappadonia C, Di Martire D, Calcaterra D, Tammaro U, Rotigliano E, Agnesi V (2021) A combined GNSS-DInSAR-IRT study for the characterization of a deep-seated gravitational slope deformation. *Ital. J. Eng. Geol. Environ. Special Issue*: 151-162
- Piacentini D, Devoto S, Mantovani M, Pasuto A, Prampolini M, Soldati M (2015) Landslide susceptibility modeling assisted by Persistent Scatterers Interferometry (PSI): An example from the northwestern coast of Malta. *Natural Hazards*. 78: 681-697.
- Radicioni F, Stoppini A, Brigante R, Fornaro G, Bovenga F, Nitti DO (2012) Long-term GNSS and SAR data comparison for the deformation monitoring of the Assisi landslide. *Proceedings of the FIG Working Week*.
- Raucoules D, De Michele M, Malet J-P, Ulrich P (2013) Time-variable 3D ground displacements from high-resolution Synthetic Aperture Radar (SAR). Application to la Valette landslide (south French Alps). *Remote Sensing of Environment*. 139: 198-204.
- Rouyet L, Kristensen L, Derron M-H, Michoud C, Blikra LH, Jaboyedoff M, Lauknes TR (2017) Evidence of rock slope breathing using ground-based InSAR. *Geomorphology*. 289: 152-169.
- Simonetto E, Durand S, Burdack J, Polidori L, Morel L, Nicolas-Duroy J (2014) Combination of InSAR and GNSS measurements for ground displacement monitoring. *Proc. Technology*. 16: 192-198.
- Stramondo S, Tesauro M, Briole P, Sansosti E, Salvi S, Lanari R, Anzidei M, Baldi P, Fornaro G, Avallone A (1999) The September 26, 1997 Colfiorito, Italy, earthquakes: Modeled coseismic surface displacement from SAR interferometry and GPS. *Geophysical research letters*. 26: 883-886.
- Strozzi T, Ambrosi C, Raetzo H (2013) Interpretation of aerial photographs and satellite SAR interferometry for the inventory of landslides. *Remote Sensing*. 5: 2554-2570.
- Strozzi T, Delaloye R, Kääb A, Ambrosi C, Perruchoud E, Wegmüller U (2010) Combined observations of rock mass movements using satellite SAR interferometry, differential GPS, airborne digital photogrammetry, and airborne photography interpretation. *Journal of Geophysical Research: Earth Surface*. 115: 1-11.
- Themistocleous K, Danezis C, Gikas V (2021) Monitoring ground deformation of cultural heritage sites using SAR and geodetic techniques: The case study of Choroikoitia, Cyprus. *Applied Geomatics*. 13: 37-49.
- Zulkifli NA, Din AHM, Som ZAM (2018) Vertical land motion quantification using space-based geodetic methods: A review. *IOP Conference Series: Earth and Environmental Science*. IOP Publishing. 169: 1-10.

# Ground deformation monitoring service of Veneto region (NE Italy) by means of Sentinel-1 data

Pierluigi Confuorto <sup>(1)</sup>, Silvia Bianchini <sup>(1)</sup>, Matteo Del Soldato<sup>(1)</sup>, Davide Festa<sup>(1)</sup>, Federico Raspini<sup>(1)</sup>, Nicola Casagli <sup>(1)</sup>

1) University of Firenze, Earth Science Department, Via G. La Pira 4, Firenze - 50121 Firenze, Italy

**Abstract** Spaceborne Earth Observation represents nowadays consolidated tools for monitoring a wide range of natural and anthropogenic displacement events occurring on the Earth's surface. The use of SAR (Synthetic Aperture Radar) sensors, since the early '90s, and the development of Interferometric and Multi-Temporal Interferometric techniques (InSAR and MTInSAR) have enabled the constant and continuous worldwide observation for 30 years. In particular, Veneto region (NE Italy) implemented a continuous monitoring service based on the exploitation of MTInSAR Sentinel-1 data in 2020: the service benefits from regularly updated deformation maps (every 12 days) to detect trend variation in the time series of displacement, defined as anomalies of deformation. Anomalies collected between July 2019 and April 2021 on the Veneto territory were considered for the analysis conducted in this work, counting about 20,000 points. Each anomaly has been classified according to the cause of the velocity variation (mainly SI, Slope Instability, S, Subsidence and MA, Mining Activities, plus ND and N, Not Determined and Noise, respectively, i.e., anomalies without any real cause assigned). SI anomalies were intersected with several types of factors, such as the existing landslide inventory, slope gradient, slope aspect, and elevation to evaluate their impact over the Veneto territory. In the period of analysis, one main anomaly case was reported to Veneto regional authorities, related to the Lamosano landslide located in an urban setting in the Belluno province. Specific field surveys and further investigations followed up this warning report and regional authorities undertook the proper actions to mitigate the risk. Therefore, the continuous satellite radar interferometric information on terrain deformation rates along with ancillary data and the interpreter expertise is fundamental to correctly analyse the automatically highlighted anomalies.

**Keywords** monitoring, Sentinel-1, landslides, Veneto, InSAR.

## Introduction

Over the last decades, landslides annually cause severe losses, both in human and socio-economic terms (Schuster, 1996). Italy is a well-known landslide prone

country due to a peculiar geological configuration and, at times, improper land management. It is one of the countries of Europe affected the most, with more than 60% of the European landslides (Herrera et al. 2018). Nonetheless, Italy is a forefront country for the monitoring of the territory. Ground deformation monitoring consists of magnitude, rate, location, and displacement vector measurement. Monitoring has a fundamental role in the correct organization of strategies for first aid and risk mitigation. Among the different techniques and instruments for monitoring ground deformations, the satellite Advanced Differential Interferometry Synthetic Aperture Radar (ADInSAR) has demonstrated, in the last 30 years, to be a valuable tool for assessing displacements occurring on the Earth surface. Moreover, the launch of the Sentinel-1 (S-1) constellation by the European Space Agency (ESA) represented a breakthrough for terrain monitoring, providing an unprecedented operational capability for intensive radar mapping of the Earth surface (Lanari et al. 2020), also thanks to the reduced revisit time (6 days when in dual configuration), the open policy for data collection and the global coverage. Benefitting from the abovementioned S-1 imaging capabilities, a systematic and continuously updated monitoring system on a regional scale was implemented in Italy, overcoming previous projects based on static mapping or monitoring at a different scale, e.g., Boni et al. (2020), Aslan et al. (2020) at regional scale and Di Martire et al. (2017) at national scale for Italy, or Novellino et al. (2017) for Great Britain. Raspini et al. (2018) presented a routine based on regularly updated ground deformation maps (every 12 days) and detection of deformation anomalies, i.e., changes in the deformation trend as detected by a data-mining algorithm. Areas with persistent and significant anomalies are reported and notified to regional authorities to define further analysis and risk mitigation strategies (Del Soldato et al. 2019). Such an approach has been firstly implemented in the Tuscany region (Central Italy), hence in Valle d'Aosta (VdA) and Veneto regions (NW and NE Italy, respectively), as also described in Confuorto et al. (2021). Here, the anomalies collected over Veneto region between July 2019 and April 2021 were statistically analyzed, linking them with geomorphological and environmental triggering factors. A specific focus was carried out on the Slope Instability (SI) anomalies, since landslides are recurrent and dangerous phenomena, and

an example of successful application in Lamosano (Belluno province) is shown. Therefore, a balance of almost two years of analysis is shown, also evaluating the distribution and the impact of the anomalies in the operational chain in the Veneto region.

## Data and methods

### Veneto regional setting

Veneto is one of the largest Italian regions, extending for a total of about 18,000 km<sup>2</sup> along the NE flank of the Italian peninsula. It counts seven provinces, among which Venezia is the regional capital. The landscape of Veneto is very variegated, with a coastal sector and a very flat Southern part of the region (included in the Po plain and delta). Gentle slopes can be recognized in the western sector of Veneto, where Colli Euganei and Colli Berici are located (Padova and Vicenza provinces); finally, the northernmost part of the region is characterized by very high and steep morphologies, typical of Alpine environments, dominated by the presence of the Dolomites. From a geological perspective, Veneto territory is made up of three macro-sectors: the Alpine area at N, with mainly calcareous-dolomitic rocks and at times flysch deposits (Mesozoic and Eocene, respectively); a piedmont area, constituted by alluvial and morenic deposits of the Pleistocene; a great plain, with alluvial sediments belonging to the Po activity in the Holocene.

Veneto territory is strongly affected by either landsliding (as testified by the almost 10,000 landslides reported in the IFFI, *Inventario dei Fenomeni Franosi*, landslide inventory in Italy, Trigila et al. 2010, in which landslides were collected between 2005 and 2007) mainly located in the northern hilly and mountainous portion of the Region and subsidence, mainly occurring in the coastal area of Venice and in the Po plain (Tosi et al. 2007, 2013).

### InSAR data and time series analysis

Veneto region is covered by two Sentinel-1 tracks for each geometry of acquisition. The image stacks are processed by means of SqueeSAR algorithm (Ferretti et al. 2011), an approach capable of getting information of the ground displacement from both the PSs (Permanent Scatterers) and the DSs (Distributed Scatterers), getting in total a higher amount of data. PSs can be generated over coherent electromagnetically stable points over time, corresponding to man-made artefacts or rocky outcrops, while the DS's information is extracted by identifying and averaging, within a search window, the contribution from statistically homogeneous pixels. The main assumption of the SqueeSAR technique is to identify sets of pixels sharing the same radar back signal, i.e., statistically homogeneous pixels, through a Kolmogorov-Smirnov (KS) test, using the amplitude index of a co-registered (overlapped) and calibrated stack of SAR images. Specifically, DSs are identified according to five different steps: (i) selection and analysis of each pixel of the image; (ii) creation of a window around the pixel; (iii) comparison of adjacent

pixels with the KS test; (iv) further processing and analysis of statistically homogeneous pixels, while pixels with different distribution functions are discarded; (v) the DSs identified within statistically homogeneous areas are processed using the traditional PSInSAR algorithm (Ferretti et al. 2001) for the estimation of the deformation maps and the construction of displacement time series of each measurement point (MP). Once obtained a displacement map, time series are analysed. Anomalies are identified, through a time series screening activity, every 12 days, once two consecutive processed S<sub>1</sub> images are added to the existing archive through a parallelized and automatized chain. Therefore, anomalous trends are automatically identified when the point targets show a  $\Delta v$  (difference of velocity) value higher than a given threshold in a  $\Delta t$  (time interval). The  $\Delta t$  was set in 150-days and the velocity thresholds  $\Delta v$  in 10 mm/yr after a “tuning period” carried out on Tuscany region. Such values allow limiting false positives and negatives as much as possible, as tested by an iterative procedure considering different values. The final stage is related to interpreting the anomalous points through the support of ancillary information given by DEMs (Digital Elevation Models) and derived products, and by official inventories. Further information on the methodology for the detection of the anomalies can be found in Raspini et al. (2018) and Confuorto et al. (2021).

## Results

In the timespan, July 2019 – April 2021, a total of 19,889 anomalies were collected and analyzed. The anomalies were generated through a data-mining algorithm over about 6 million point targets derived from the Sentinel-1 ascending and descending processing (Fig. 1a). In order to differentiate the anomalies according to the main triggering factor, 6 six classes were distinguished: Slope Instability (SI), Subsidence (S), Mining Activity (MA), Uplift (U), plus Not Determined (ND) and R (noise), i.e., anomalies whose trigger cannot be determined or produced for some error or noise in the processing. The total number of anomalies classified as real movement on the ground (excluding ND and R anomalies) is 6,085. The distribution of each type of anomaly within the Veneto territory is led by the local geomorphological setting (Fig. 1). The Belluno province, the northernmost of the region, is characterized by mostly SI anomalies, counting 2,439 anomalies (95% of the total of the province). On the other hand, coastal and/or flat provinces such as Rovigo, Venezia, Padova and Treviso show exclusively or mainly subsidence anomalies. Indeed, Rovigo and Venezia area characterized by 99 and 100% of S anomalies, counting respectively 335 and 275 anomalies, while Padova and Treviso show the little percentage of SI and MA anomalies (less than 20% in both cases). Finally, Vicenza and Verona territories are more heterogeneous, with the prevalence of SI in the first case (65% of 1,258 anomalies) and of S in the second case (66% of 509 anomalies). The graph in Fig. 2 resumes the abovementioned numbers.



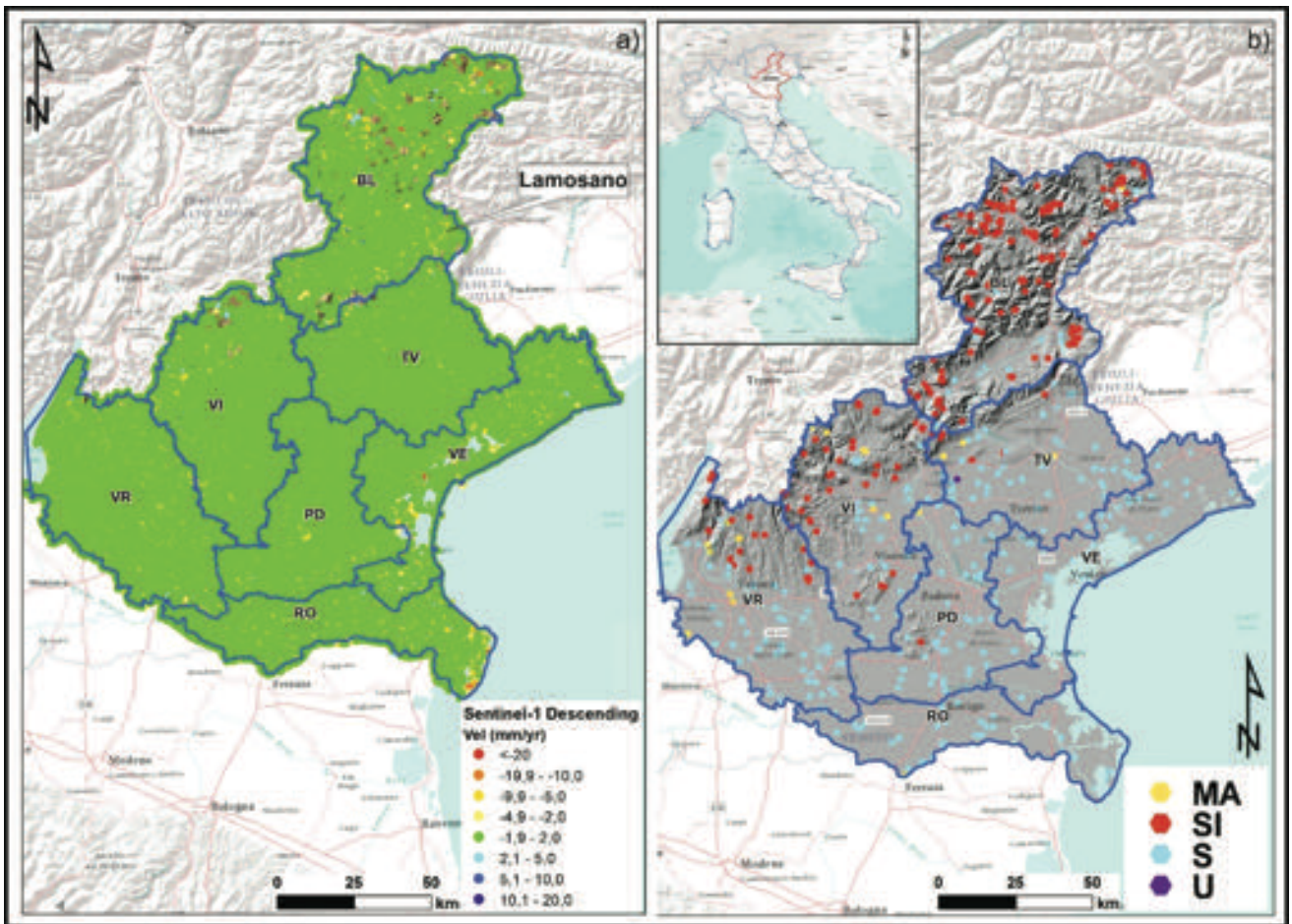


Figure 1 On the left, map of the PSs derived from the Sentinel-1 descending imagery between October 2014 and April 2021. On the right, map of the anomalies collected in Veneto between July 2019 and April 2021.

**Slope instability anomalies**

A special focus was dedicated to SI anomalies since they represent an important instability factor in the area (Fig. 3 and 4). In detail, SI anomalies distribution has been analysed by coupling it with the existing landslide inventories, derived from the IFFI project, with the elevation, slope gradient and the slope aspect, derived from the regional DEM.

From the total of 3,446 SI anomalies, only 4.3% are located within inventoried landslides, counting thus 148 anomalies. Of these, the majority of anomalies is within landslides classified as rotational/translational slides and complex (36 and 39%, respectively), while minor percentages correspond to slow and rapid flows and falls and landslides whose type cannot be determined (nd).

As concern the elevation, most of the SI anomalies are distributed among the 1,000 and 2,000 m a.s.l., with almost 80% of the total number (Fig. 3). In detail, the class with the highest percentage is that between 1,750 and 2,000 m a.s.l., with 22% ca. Furthermore, SI anomalies have been intersected with slope gradient and slope aspect (Fig. 4).

The distribution of the SI anomalies is homogeneous in all the classes of slope gradient, except for the class  $<10^\circ$ ,

with less than 10% of the total, followed by the class  $>50^\circ$ , with 13% of the total.

As regards the slope aspect, landslide-related anomalies are fairly distributed between east- and west-facing slopes, with about 40 and 37% of the total.

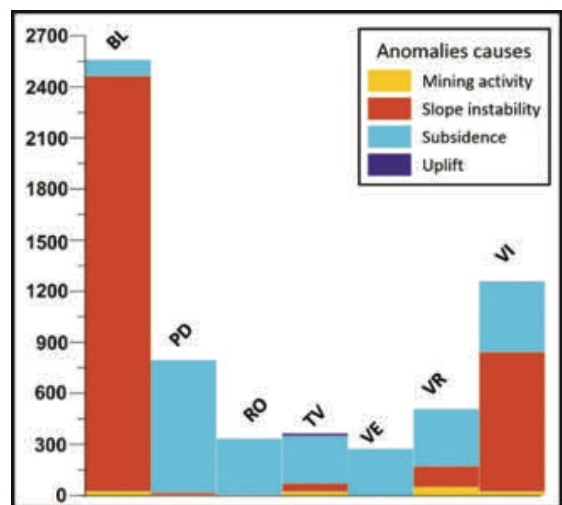


Figure 2 Distribution of anomalies for each Veneto province and according to the triggering factor. BL=Belluno; PD=Padova; RO=Rovigo; TV=Treviso; VE=Venezia; VR=Verona; VI=Vicenza.

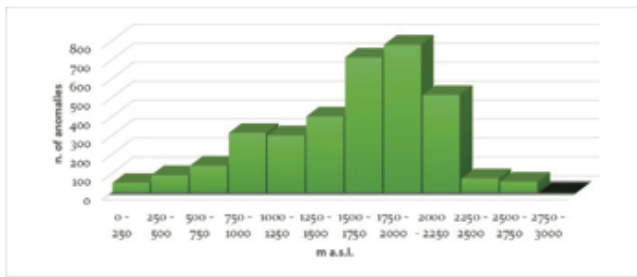


Figure 3 Anomalies distribution according to each elevation class.

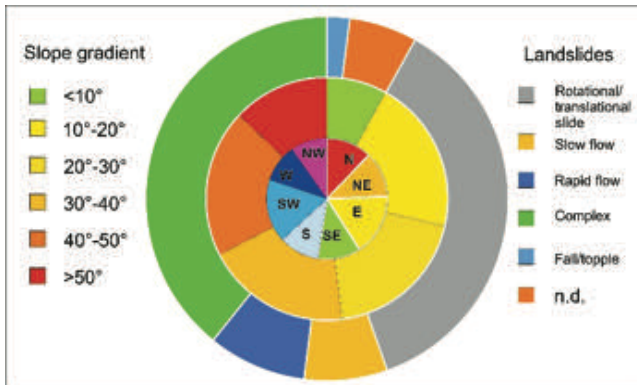


Figure 4 Pie and donut charts for SI anomalies. From the outside to the inside: Anomalies vs. Type of landslide; Anomalies vs. Slope gradient; Anomalies vs. Aspect.

### Anomalies warning

Critical situations highlighted by the anomaly detector have been reported to regional authorities. Here is an example of a warning due to SI anomalies in the area of

Lamosano (Belluno province, Fig. 5). Lamosano is a small hamlet located just beneath the well-known Tessina landslide (Mantovani et al. 2000; Tarchi et al. 2003; Cola et al. 2016), in the municipality of Chies d’Alpago (BL).

In the inhabited area of the hamlet, three anomalies were retrieved during satellite acquisition and analysis in December 2019. The three point-targets were localized within the boundary of a well-known roto-translational slide and placed over some houses and the main building within the centre of the hamlet, as computed by the elaboration of the Sentinel-1 descending dataset of January 2020.

The time series of the three points showed a changing deformation trend starting from the mid of November, with a clear acceleration pattern, which was detected by the anomaly algorithm. The average velocity of the TSs before the breaking point was generally 10 mm/year, while the average velocities between November 15, 2019, and January 2, 2020, were over 80 mm/year in the three points (with the point of the highest value, of 98 mm/yr), thus overcoming the selected threshold.

The ongoing situation of Lamosano was reported to regional authorities, which conducted further investigations on the field to have a clearer state of the art of the ongoing deformation and to undertake the necessary actions to mitigate the current risk. Indeed, despite the area being well known and periodically surveyed, the warning was useful for Veneto geologists, which cross-validated InSAR information with GPS (Global Positioning System) data and carried out several damage surveys to check the conservation status of the local buildings.

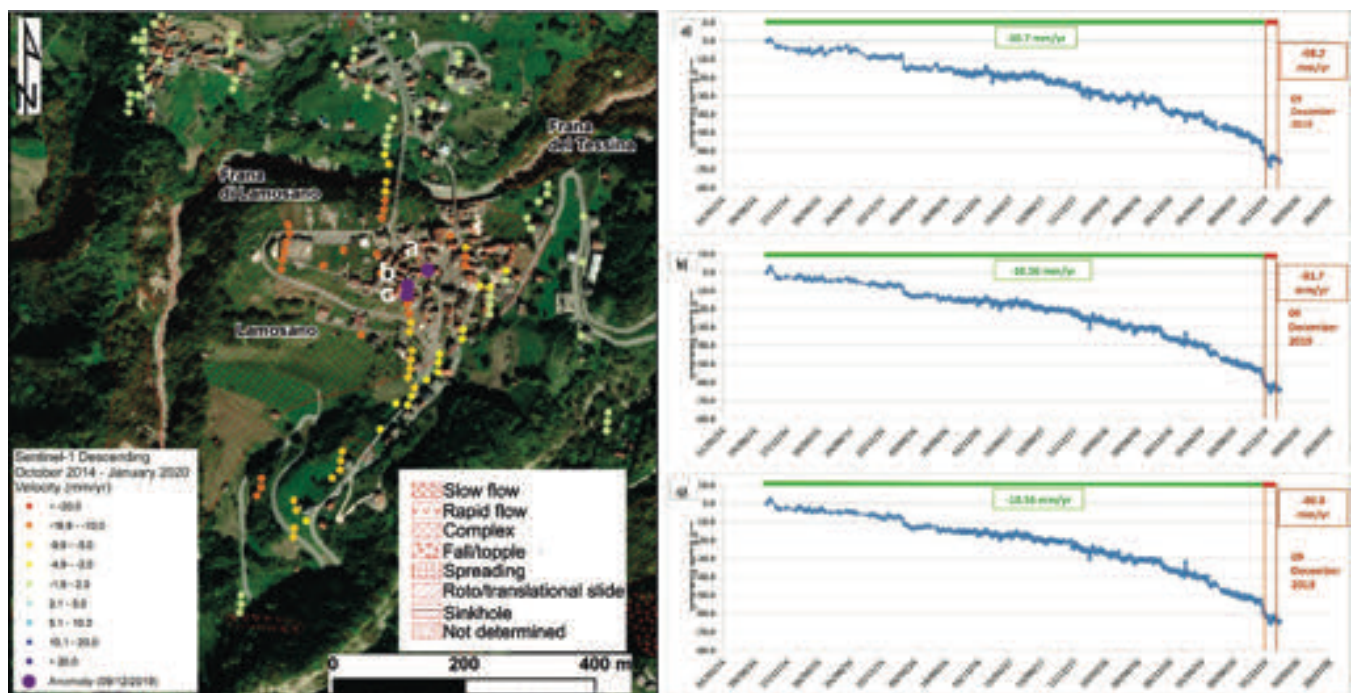


Figure 5 On the left, map of the PSs with the anomalies detected in Lamosano (Belluno province). On the right, the three Time Series belonging to the three anomalies detected in the period May 2014-December 2019.

## Discussion

The Sentinel-1 mission can be pictured as a breakthrough in the InSAR community due to the short revisit time of six days and the capacity to cover the world territory, along with the technical innovations that made the data provisioning faster and more reliable. One of the main objectives of the InSAR technique is mapping unstable areas at different scales of analysis (Rosi et al. 2018; Antonielli et al. 2019) or the characterization and modelling of deformation phenomena (Confuorto et al. 2017; Squarzoni et al. 2020).

The analysis and the detection of the trend changes has been made possible by implementing a continuous and regular acquisition plan, as one of the Sentinel-1 missions, as testified by the regional services in Italy. Indeed, the readiness of Sentinel-1 imagery and the possibility to cover large areas enabled the quasi-real time monitoring at the regional scale. Here, the results of almost two years of operational service over the Veneto region were shown. Since the generation of the anomalies of movement can be owed to several factors, such as geology, geomorphology or environment, a brief analysis of the anomalies collected between July 2019 and April 2021 is shown, by intersecting the anomalous points with geographical and geomorphological factors. In Veneto, a balance between SI and S anomalies can be found, since its territory is extremely variegated, with wide plains as well as extensive mountain sectors. Indeed, Belluno province shows almost exclusively SI anomalies, being located in the eastern sector of the Alps, while Venezia, Rovigo and Treviso provinces are characterized by the massive presence of S anomalies due to the flat configuration of their territory and to recurrent subsidence phenomena due to either sediment compaction or groundwater extraction. However, the number of ND and R anomalies highlights that false positives can be always generated by the automatic algorithm. For this reason, the human-supervised interpretation stage is fundamental to correctly address and categorize the signal detected. The intersection of SI anomalies with landslide inventories, instead, has highlighted that 5% of the anomalies are within redacted landslides, suggesting that very often landslide inventories are outdated or incomplete. Finally, SI anomalies have been analyzed through a correlation with slope gradient and slope aspect. As regards the first parameter, SI anomalies of Veneto are distributed in all slope classes, except for the  $<10^\circ$  class, coherently with the configuration of the alpine setting, with steep slopes; as concern slope aspect, there is a general homogeneity between west- and east-faced slopes. The efficacy of the operational service is testified also by the alerts delivered to the regional authorities. In the analysis's timespan, two landslides highlighted by anomalies were reported (including the Lamosano case). Consequently, field surveys and further investigations were carried out by regional authorities to define the best actions to reduce ongoing risks. As seen in Veneto, the anomalies

distribution is a reflection of the local setting and presents an important picture of the ongoing deformational scenario. Nonetheless, further improvements can be made aiming at the reduction of false positives or the improvement of the detector algorithm.

## Conclusions

An operational service based on the exploitation of Sentinel-1 data is active on the territory of Veneto region (NE Italy). Such service, based on the detection of variations in the time series of displacement, provides fundamental support to regional authorities, through the update every 12 days of the deformations ongoing as seen by the satellite. This work provides a summary of the results of almost two years of continuous monitoring over the Veneto region by analysing the anomalies obtained with geographical and geomorphological factors. The anomalies' distribution reflects the territory's physiography, showing large concentrations of Subsidence anomalies in the main plains and almost exclusively Slope Instability anomalies over the Alps. Specifically for the Slope Instability anomalies, they are more concentrated over steep slopes, and, at the same time, a very low percentage is located within inventoried landslides. This last aspect is relevant and highlights the need to update landslide mapping. The importance of the operational service is also testified by alerts delivered to regional authorities, as seen for the Lamosano (Belluno province) case. Indeed, after the warnings, further surveys and data collection activities were carried out to reduce the ongoing risks.

## Acknowledgements

The authors gratefully acknowledge TRE ALTAMIRA for having processed the S-1 data.

## References

- Antonielli B, Mazzanti P, Rocca A, Bozzano F, Dei Cas L (2019) A-Dinsar Performance For Updating Landslide Inventory In Mountain Areas: An Example From Lombardy Region (Italy). *Geosciences*. 9(9): 364.
- Aslan G, Fouvelis M, Raucoules D, De Michele M, Bernardie S, Cakir, Z (2020) Landslide mapping and monitoring using Persistent Scatterer Interferometry (PSI) technique in the French Alps. *Remote Sensing*. 12(8): 1305.
- Boni R, Bordoni M, Vivaldi V, Troisi C, Tarabra M, Lanteri L, Zucca F, Meisina C (2020) Assessment Of The Sentinel-1 Based Ground Motion Data Feasibility For Large Scale Landslide Monitoring. *Landslides*. 17: 2287-2299.
- Cola S, Gabrieli F, Marcato G, Pasuto A, Simonini P (2016) Evolutionary behaviour of the Tessina landslide. *Rivista italiana di Geotecnica*. 1: 51.
- Confuorto P, Del Soldato M, Solari L, Festa D, Bianchini S, Raspini F, Casagli N (2021) Sentinel-1-Based Monitoring Services At Regional Scale In Italy: State Of The Art And Main Findings. *International Journal Of Applied Earth Observation And Geoinformation*. 102:102448.

- Confuorto P, Di Martire D, Centolanza G, Iglesias R, Mallorqui JJ, Novellino A, Plank S, Ramondini M, Thuro K, Calcaterra D (2017) Post-Failure Evolution Analysis Of A Rainfall-Triggered Landslide By Multi-Temporal Interferometry Sar Approaches Integrated With Geotechnical Analysis. *Remote Sensing Of Environment*. 188: 51-72.
- Del Soldato M, Solari L, Raspini F, Bianchini S, Ciampalini A, Montalti R, Ferretti A, Pellegrineschi V, Casagli N (2019) Monitoring ground instabilities using SAR satellite data: A practical approach. *ISPRS International Journal of Geo-Information*. 8(7): 307.
- Di Martire D, Paci M, Confuorto P, Costabile S, Guastaferro F, Verta A, Calcaterra D (2017) A Nation-Wide System For Landslide Mapping And Risk Management In Italy: The Second Not-Ordinary Plan Of Environmental Remote Sensing *Int. J. Appl. Earth Obs. Geoinf.* 63: 143-157.
- Ferretti A, Prati C, Rocca F (2019) Permanent Scatterers In Sar Interferometry. *IEEE Transactions On Geoscience And Remote Sensing*. 39:8–20.
- Herrera G, Mateos RM, García-Davalillo JC, Grandjean G, Poyiadji E, Maftai R, Jensen, OA (2018) Landslide Databases In The Geological Surveys Of Europe. *Landslides*. 15(2): 359-379.
- Lanari R, Bonano M, Casu F, De Luca C, Manunta M, Manzo M, Onorato G, Zinno I (2020) Automatic Generation Of Sentinel-1 Continental Scale Dinsar Deformation Time Series Through An Extended P-Sbas Processing Pipeline In A Cloud Computing. *Environment Remote Sens*. 12: 2961
- Mantovani F, Pasuto A, Silvano S, Zannoni A (2000) Collecting data to define future hazard scenarios of the Tessina landslide. *International Journal of Applied Earth Observation and Geoinformation*. 2(1): 33-40.
- Novellino A, Cigna F, Brahmi M, Sowter A, Bateson L, Marsh S (2017) Assessing the feasibility of a national InSAR ground deformation map of Great Britain with Sentinel-1. *Geosciences*. 7(2): 19.
- Raspini F, Bianchini S, Ciampalini A, Del Soldato M, Solari L, Novali F, Del Conte S, Rucci A, Ferretti A, Casagli N (2018) Continuous, semi-automatic monitoring of ground deformation using Sentinel-1 satellites. *Scientific reports*. 8(1): 1-11.
- Rosi A, Tofani V, Tanteri L, Stefanelli CT, Agostini A, Catani F, Casagli N (2018) The New Landslide Inventory Of Tuscany (Italy) Updated With Ps-Insar: Geomorphological Features And Landslide Distribution. *Landslides*. 15: 5–19.
- Schuster RL (1996) Socioeconomic Significance Of Landslides. *Landslides: Investigation And Mitigation*. Special Report. 247. Turner AK, Schuster RL (eds). National Academy Press. Washington (Dc). 12-35.
- Squarzonni G, Bayer B, Franceschini S, Simoni A (2020) Pre-And Post-Failure Dynamics Of Landslides In The Northern Apennines Revealed By Space-Borne Synthetic Aperture Radar Interferometry (Insar). *Geomorphology*. 369.
- Tarchi D, Casagli N, Fanti R, Leva DD, Luzi G, Pasuto A, Pieraccini M, Silvano S (2003) Landslide monitoring by using ground-based SAR interferometry: an example of application to the Tessina landslide in Italy. *Engineering geology*. 68(1-2): 15-30.
- Tosi L, Teatini P, Carbognin L, Frankenfield J (2007) A New Project To Monitor Land Subsidence In The Northern Venice Coastland (Italy). *Environmental Geology*. 52(5): 889-898.
- Tosi L, Teatini P, Strozzi T (2013) Natural versus anthropogenic subsidence of Venice. *Scientific reports*. 3(1): 1-9.
- Trigila A, Iadanza C, Spizzichino D (2010) Quality assessment of the Italian Landslide Inventory using GIS processing. *Landslides*. 7(4): 455-470.

# Monitoring the Slano blato mudflow using InSAR and UAV photogrammetry (preliminary results)

Galena Jordanova<sup>(1)</sup>, Marko Vrabec<sup>(1)</sup>, Krištof Oštir<sup>(2)</sup>, Timotej Verbovšek<sup>(1)</sup>

1) University of Ljubljana, Faculty of Natural Sciences and Engineering, Department of Geology, Aškerčeva 12, 1000 Ljubljana, Slovenia, +386 1 77 72 734 (galena.jordanova@ntf.uni-lj.si)

2) University of Ljubljana, Faculty of Civil Engineering and Geodesy, Department of Geodesy and Geoinformatics, Jamova 2, 1000 Ljubljana, Slovenia

**Abstract** In this paper we have summarized some preliminary results of landslide monitoring using remote sensing – UAV photogrammetry and InSAR. The main area of interest is Slano blato mudflow (Western Slovenia) that is supposedly still active and threatens the buildings and citizens of Lokavec settlement. We used an unmanned aerial vehicle (UAV) to obtain surface images for the purpose of constructing 3D photogrammetric models and digital elevation models (DEM). Furthermore, we subtracted the models to calculate elevation difference between them. We also used Sentinel-1 images in time series analysis to extract surface displacement using the SBAS DInSAR processing method. The two methods are complementary and offer highly accurate results – the UAV photogrammetry reaches spatial resolution of 5 cm and InSAR's accuracy is 1 mm year<sup>-1</sup> in LOS direction. However, although the preliminary results show promising findings, more data is needed to draw conclusions and to evaluate the possibility of implementing this methodology into long-term monitoring of deep-seated complex landslides.

**Keywords** remote sensing, SBAS DInSAR, UAV photogrammetry, landslide monitoring, time-series analysis

## Introduction

A third of the Slovenian territory is highly susceptible to landslides (Komac and Ribičič 2006). One of the most hazardous areas in Slovenia is certainly the Vipava valley, where many different slope mass movements have been observed. Due to the distinctive geology and geomorphology of the valley, the settings were appropriate for the occurrence of many debris slides and landslides, rock slides and mudflows (Popit 2015). Many of them are fossil mass movements, and many still threaten the safety of residents and infrastructure.

One of the most hazardous events in the valley is Slano blato mudflow. It was reactivated in November 2000 (Ribičič 2003), during the same rainfall event that caused two other major landslides in Slovenia – Stože (Log pod Mangartom) debris flow (Mikoš et al. 2004) and Macesnik

mudflow. Slano blato is a direct threat to the safety of the residents in the settlement of Lokavec. The recent activity of the landslide is unknown since there have been no monitoring activities in the past decade. The last monitoring activity was reported by Petkovšek et al. (2013). Accordingly, monitoring its activity for the purpose of early warning and future remediation steps is of high importance.

In this paper we present preliminary results of using remote sensing for landslide monitoring. In Slovenia, photogrammetry using an UAV for the purpose of landslide monitoring was firstly introduced by Peternel et al. (2016) for monitoring the landslides of Potoška planina. They found the technique suitable for acquiring horizontal movements and defining volumes of moving soil. InSAR, on the other hand, has not been implemented into any long-term monitoring activities of slope mass movements.

## Study area

Slano blato mudflow is located in Vipava valley in western Slovenia (Fig. 1). Its outflow reaches the Grajšček spring bed that flows through the settlement of Lokavec near the city of Ajdovščina. The landslide is 1.3 km long with up to 250 m in width and 9–11 m in depth. The estimated volume of the landslide is more than 1 million m<sup>3</sup> (Jemec Auflič et al. 2017), and its velocity in the years following the reactivation in November 2000 reached up to 100 m/day during rainfall events (Ribičič 2003). The landslide's been a subject of interest of the authorities for more than 200 years, and since then it went through many phases of remediation (Logar et al. 2005).

The landslide occurred on weathered flysch slopes. Due to the Mesozoic carbonates lying above the flysch, the landslide is constantly soaked by the inflow of karst water (Placer et al. 2008). The flysch is highly susceptible to weathering, and the landslide mass is mud dominated with poor geomechanical properties, such as low shear angle and high water suction (Fifer Bizjak and Zupančič, 2009; Petkovšek et al. 2013; Maček et al. 2016). The remediation of the landslide included construction of 11 reinforced concrete wells – dowels, retaining walls and drainage system (Ribičič and Kočevar 2002; Logar et al.

2005; Fifer Bizjak and Zupančič 2009). The latter was partially renovated during the fall months in 2021.

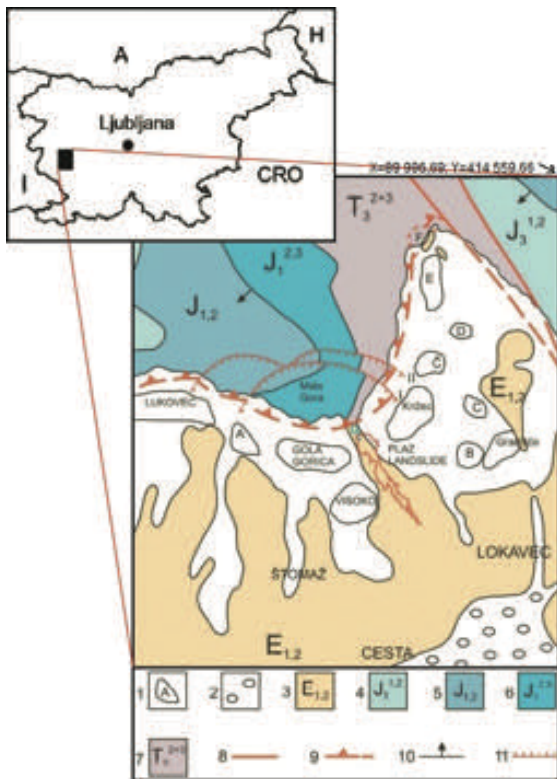


Figure 1 Location of Slano blato and simplified geological map; 1. Rotational blocks; 2. Alluvium; 3. Eocene flysch; 4-7. Mesozoic carbonates; 8. Fault; 9. Boundary of Trnovo nappe; 10. Dip of beds; 11. Curved shear surface (modified after Placer et al. 2008).

## Methodology

Due to the size and relatively steep slopes with little to no vegetation and instead of drilling new expensive inclinometers, we presumed remote sensing techniques would be suitable for precise monitoring of the landslide's activity. We chose two complementary methods:

(i) UAV photogrammetry - to be able to define eventual larger surface deformations which spatial resolution of 5 cm, and

(ii) InSAR with extremely high sensing precision of surface deformations ( $1 \text{ mm year}^{-1}$ ) and high temporal resolution of images (every 6 days), but low spatial resolution of 10–15 m (in the case of DInSAR).

### UAV photogrammetry

We use DJI Phantom 4 RTK quadcopter. It offers the possibility to shoot with in advance programmed missions, making it a fast and easy method to use. The campaign was divided into two sections - upper and lower (with two separate base points) due to the steep slope and the possible loss of connection between the drone and controller. The campaigns were programmed to capture the surface images twice - vertically and obliquely. That way we obtained images from different angles for the

purpose of constructing geometrically correct photogrammetric models and later on the digital elevation models – DEMs (Fig. 2). The image overlap was at least 60%. A whole campaign lasted less than 3 hours, including 5-6 battery changes (each lasting cca. 20 minutes). It is very important that the weather is suitable for image capturing, i.e., without wind or rainfall. We carried out our flight missions on calm sunny and cloudy days.

Each model was constructed from cca. 1300 images, georeferenced using 23 fixed GCP, which were precisely measured with fast-static GNSS method. We used Sokkia GRX2 GNSS equipment and reached 1 cm of accuracy. We have used the Agisoft Metashape software (Agisoft LLC) for generating the 3D photogrammetric terrain models.

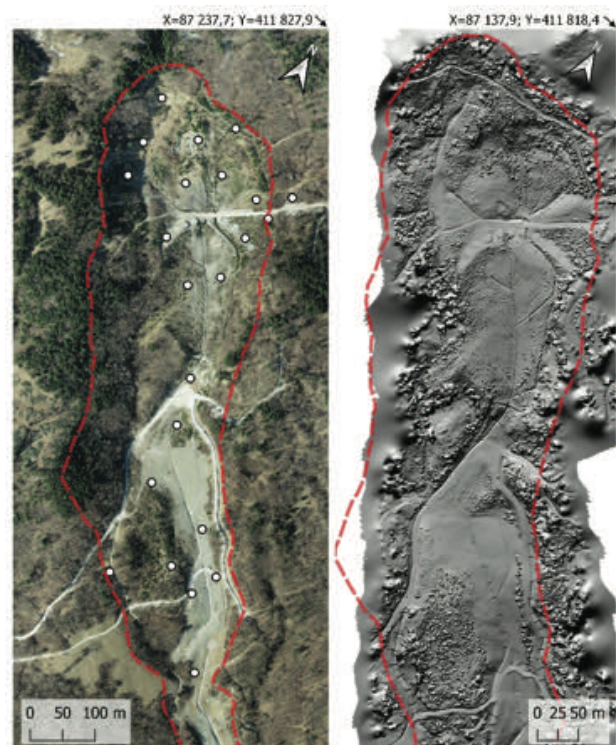


Figure 2 (A) Orthophoto mosaic of the landslide. The red hatched line presents approximate current landslide border and the white points present fixed GCP; (B) Hillshaded digital elevation model with 5 cm spatial resolution, constructed from aerial images.

### Interferometric SAR

InSAR is a powerful technique used for many purposes. One of them is monitoring the topography changes, which is extremely useful for flat areas, e.g., for estimating subsidence or uplift (e.g., Oštir and Komac 2007). Landslide monitoring using InSAR is widely spread, but its application must be done carefully, following strict criteria, such as spatial orientation of the landslide and direction of expected movements, rate of displacement and vegetation cover. It is important to comply with these criteria in order to obtain reliable results. The SAR satellites can only detect changes in their line of sight (LOS), which is roughly in E–W direction and inversely,

while the N-S direction is compromised due to the satellites' sub-polar trajectory. More information on SAR principles is available in e.g. Oštir and Komac (2007) or Zhou et al. (2009) for more mathematical background.

In this study we performed a time series analysis of 57 Sentinel-1 images of the descending orbit path 22 and frame 441. The latter is more appropriate for Slano blato than ascending orbit due to its azimuth of LOS, which is 280° (-80°), while the landslide is NW-SE oriented. We tested two different processing methods: PSInSAR and SBAS (*Small Baseline Subset*) DInSAR. The images were processed in ENVI SARscape (Exelis Visual Information Solutions).

### Results and discussion

For this study we created two photogrammetric models; one was made from images captured on 19 March 2021, before vegetation bloomed, and second one from images captured on 21 December 2021. We used them to calculate the difference in elevation (ED). The ED was calculated by

QGIS Raster calculator using the following simple equation (1):

$$ED = DEM_{NEWER} - DEM_{OLDER} \quad (1)$$

The results are shown in Fig. 3A along with the results from the InSAR processing. Note that the vegetation cover was not removed from the models.

We performed InSAR processing only for the year 2021 for the purpose of correlating the results with the UAV photogrammetry.

The permanent scatterer method (PSInSAR) proved inappropriate for use due to the lower coherence and thus a lower number of scatterers. We have obtained 32 scatterers. While this method offers accurate 1D results (regarding to the LOS) in certain points (scatterers), it is impossible to obtain results in areas without natural or artificial scatterers that occur in the whole set of images. On the other hand, SBAS DInSAR offers planar results as shown in Fig. 3B. Due to lack of vegetation, it was possible to obtain DInSAR time series results for large area.

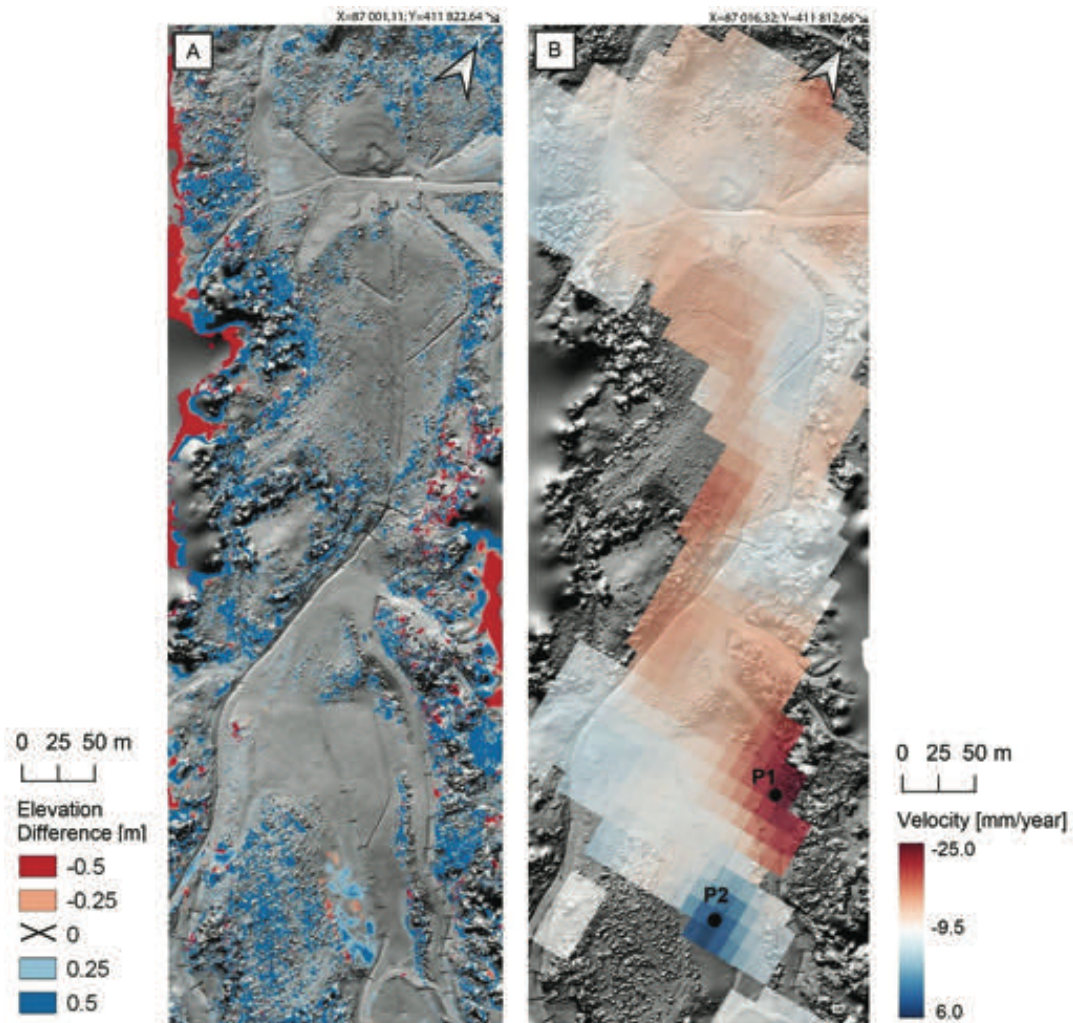


Figure 3 (A) Elevation difference (ED) between the two acquisitions by UAV photogrammetry, (B) velocity [mm year<sup>-1</sup>] of ground displacement obtained by SBAS DInSAR data processing; both on hillshaded background. Points P1 and P2 were chosen to present the areas with the highest deformation in LOS, their time-displacement plots are shown in Fig. 5 and 6.

On first sight, the Fig. 3A shows a lot of blue and red areas (zero values are transparent), especially on the edges of the model. The vegetation changes a lot through the year, which was recognized as elevation difference. The vegetation areas have noticeable sharply defined edges. However, there are multiple orange and blue areas with more blurred edges (see Fig. 4). These present changes in surface elevation.

Fig. 4B presents slope displacement. It clearly shows areas of erosion and deposition. This area was carefully inspected in the field, where we noticed newly occurred surface fractures and other signs of slope movements in the field, and these results were expected. Figures 4C and 4D also present changes in surface elevation, but as a consequence of civil (earth) works. In Fig. 4C it is evident where they surfaced the maintenance road, in the area shown in Fig. 4D there was maintenance work done on the ground drainage system. These results therefore present the areas of excavation and ground levelling. Here we emphasize the importance of field observations that are crucial for avoiding the possibility of interpretation bias.

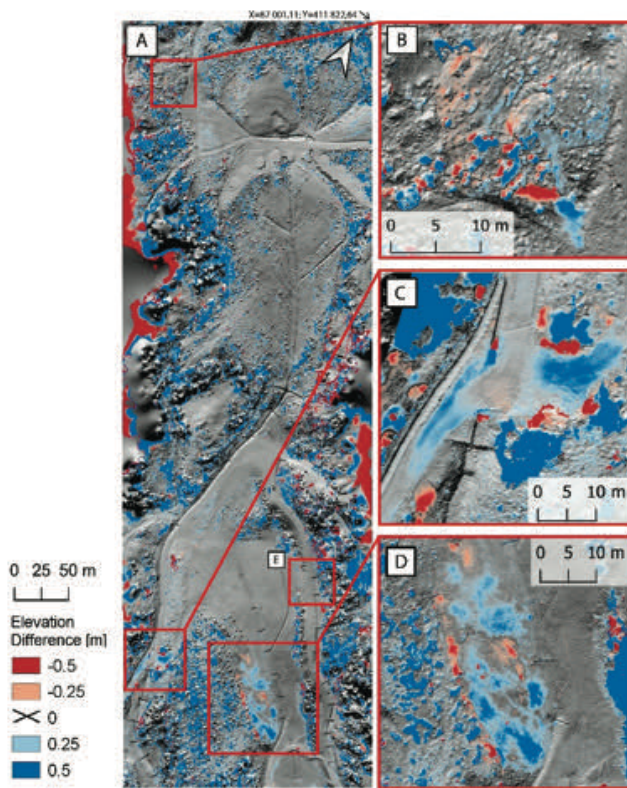


Figure 4 (A) Landslide area; (B) Slope displacement(C) and (D) maintenance work on a road and ground drainage system (results of excavation and ground levelling); (E) is presented in Fig. 7.

Fig. 3B presents the results of SBAS DInSAR time series analysis. The velocity of ground displacement means a yearly average of displacement in LOS in  $\text{mm year}^{-1}$ . At first, we clearly see many areas of displacement, especially in the lower part of the landslide. To better present the displacement in these areas, we chose points P1 and P2 as

the centre points of the areas with the highest deformation in positive and negative direction in LOS. It is very interesting to notice the dark blue area (P2), which correlates with the area of the maintenance work of the drainage system (Fig. 4C). If we present the surface displacement in point P2 (Fig. 3B) on a time-displacement plot (Fig. 5), it is even possible to define at what time they began and finished the constructional work. The construction company confirmed this statement.

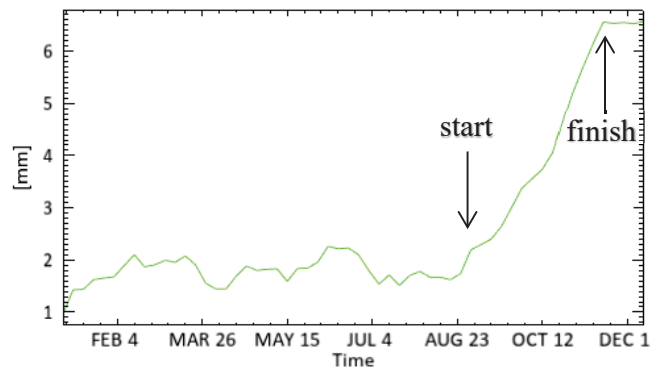


Figure 5 Displacement in point P2 (see Fig. 3B) over time for year 2021 based on SBAS DInSAR results. The start and finish arrows indicate the beginning and end of constructional work.

The plot of point P1 on the other hand presents a more constant ground subsidence up to 20 mm “away” from the satellite in LOS, which can be either a result of surface erosion or slope movements.

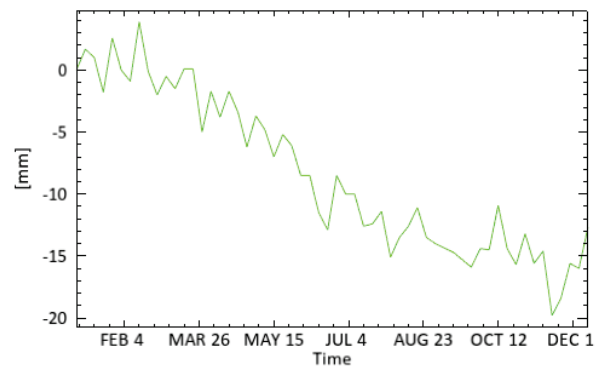


Figure 6 Displacement in point P1 (see Fig. 3B) over time for year 2021 based on SBAS DInSAR results.

Unfortunately, due to the low spatial resolution, it is relatively hard to define what does the dark red area in Fig. 3B. represent. We adjusted the scale for ED classification to better match the scale of calculated DInSAR deformation and presented the results in Fig. 7. Here it is clearly seen that there are elevation differences on the banks surrounding the maintenance road (red to orange blurred areas). This could be one of the reasons InSAR detects such surface changes.



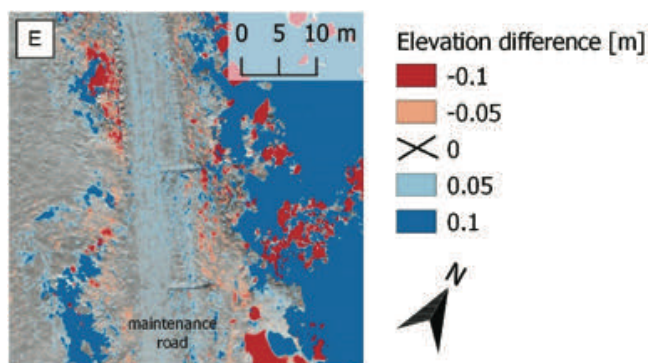


Figure 7 Elevation difference of maintenance road and its banks – detail. The blue and red areas on the right present vegetation.

The UAV photogrammetry also shows promising results, but the accuracy of the models is bound to accurate processing. A small shift in the referenced models can cause errors and bias in the results, therefore thresholds need to be considered when analysing surface displacements. Thresholds can be defined after a longer period of monitoring and more collected data.



Figure 8 Excavating work on the landslide in October 2021.

## Conclusions

In this paper, we presented the preliminary results of monitoring activities of Slano blato landslide using UAV photogrammetry and SBAS DInSAR. The results show promising findings about how to effectively monitor the landslide with both techniques used in the study. We found both techniques to be efficient and accurate enough to detect any topographic changes due to landslide activity, constructional work or even changes in vegetation cover in the case of UAV photogrammetry. Despite that fact, more work needs to be done to be able to draw solid conclusions regarding the accuracy of the methodology and the activity of the landslide itself. The monitoring will proceed further for a longer period of time; therefore we

will be able to improve it along with the interpretation of the results.

## Acknowledgments

This work was supported by the Slovenian Research Agency (“Young researcher” grant number 53536 and the research programs P1-0195: “Geoenvironment and Geomaterials” and P2-0406: “Earth Observation and Geoinformatics”). We are thankful to the reviewers for the constructive comments and suggestions for improvements of this paper.

## References

- Fifer Bizjak K, Zupančič A (2009) Site and laboratory investigation of the Slano blato landslide. *Engineering Geology*. 105(3–4):171–185. doi:10.1016/j.enggeo.2009.01.006
- Jemec Auflič M, Jež J, Popit T, Košir A, Maček M, Logar J, Petkovšek A, Mikoš M, Calligaris C, Boccali C, Zini L, Reitner J M, Verbovšek T (2017) The variety of landslide forms in Slovenia and its immediate NW surroundings. *Landslides*. 14:1537–1546. doi:10.1007/s10346-017-0848-1
- Komac M, Ribičič M (2006) Landslide susceptibility map of Slovenia at scale 1:250,000. *Geologija*. 49(2):295–309.
- Logar J, Fifer Bizjak K, Kočevar M, Mikoš M, Ribičič M, Majes B (2005) History and present state of the Slano Blato landslide. *Natural Hazards and Earth System Sciences*. 5:447–457.
- Maček M, Majes B, Petkovšek A (2016) Lessons learned from 6 years of suction monitoring of the Slano blato landslide. *Rivista Italiana di Geotecnica*. 1:21–33.
- Mikoš M, Četina M, Brilly M (2004) Hydrologic conditions responsible for triggering the Stože landslide, Slovenia. *Engineering Geology*. 73(3–4):193–213.
- Oštir K, Komac M (2007) PSInSAR and DInSAR methodology comparison and their applicability in the field of surface deformations – A case of NW Slovenia. *Geologija*. 50/1: 77–96. doi:10.5474/geologija.2007.007
- Peternel T, Kumelj Š, Oštir K, Komac M (2016). Monitoring the Potoška planina landslide (NW Slovenia) using UAV photogrammetry and tachymetric measurements. *Landslides*. 14:395–406. doi: doi.org/10.1007/s10346-016-0759-6
- Petkovšek A, Maček M, Mikoš M, Majes B (2013) Mechanism of active landslides in flysch. In: Sassa, K. et al. (eds) *Landslides: Global Risk Preparedness*. Springer-Verlag Berlin Heidelberg, pp. 149–165. doi:10.1007/978-3-642-22087-6\_10
- Placer L, Jež J, Atanackov J (2008) Strukturni pogled na plaz Slano blato = Structural aspect on the Slano blato landslide (Slovenia). *Geologija* 51/2:229–234. doi:10.5475/geologija.2008.023 (in Slovenian with English abstract)
- Popit T (2015) *Mehanizmi transporta in sedimentacijski procesi kvartarnih pobočnih sedimentov na območju Rebrnic=Transport mechanisms and depositional processes of quaternary slope deposit in Rebrnice area*. Doctoral thesis, University of Ljubljana, Faculty of Civil Engineering and Geodesy, Ljubljana, Slovenia. (in Slovenian with English abstract)
- Ribičič M (2003) Calculation of the moving landslide masses volume from air images. *Geologija*. 46/2: 413–418.
- Ribičič M, Kočevar M (2002) The final remediation of the landslide Slano blato above settlement Lokavec at Ajdovščina. *Geologija*. 45(2):525–530. (in Slovenian)
- Zhou X, Chang NB, Li S (2009). Applications of SAR Interferometry in Earth and Environmental Science Research. *Sensors*. 9: 1876–1912.



# Validation of innovative mitigation strategy through long-term landslide and structural monitoring

Giulia Bossi<sup>(1)</sup>, Gianluca Marcato<sup>(1)</sup>, Filippo Tommaso Catelan<sup>(1)</sup>

1) Research Institute for Geo-Hydrological Protection, National Research Council (CNR-IRPI), Padova, Corso Stati Uniti 4, Italy (giulia.bossi@irpi.cnr.it)

**Abstract** Long-term monitoring is a fundamental tool for the study of medium-to-large slow moving landslides that might be eligible for structural countermeasure works. Since in the design of geotechnical numerical models, uncertainties regarding the soil parameters are high, the possibility to rely on monitoring data to calibrate the model is a fundamental tool to check the robustness and overall value of the reference model. Sometimes, by analysing the signals between potential triggering factors and displacements on a long period, comprising also extreme meteo-climatic events, it can be possible to skip the numerical modelling step altogether by acting directly on the activating factors. In this case, a grey box model that needs to be validated on one additional dataset might be defined. In this work, we present a case study consisting of a complex shaped slope instability crossed by a stream called Rio Verde. The scarp of the slope cuts across a National Road that connects the Veneto and Friuli Venezia Giulia regions (Italy). The potential risk of road disruption with major impacts on the valley economic life is high. A dataset of continuous monitoring of several years is available for the landslide. It consists of Global Navigation Satellite System (GNSS) data, piezometer, in-place inclinometers, and a thin plate weir that continuously measure the Rio Verde's discharge. A grey box model linking the landslide displacements with the Rio Verde discharge has been proposed. Based on these results, new monitoring instruments have been installed, and a low-cost mitigation strategy consisting in the removal of the water from the stream is being implemented. Since the typology of the countermeasure work is unconventional, the protraction of the continuous monitoring is fundamental to assess and quantify the efficacy of the measure, to validate the conceptual grey box model, and to decide to proceed with an additional intervention if needed be.

**Keywords** mitigation, landslides, countermeasure works design, cost sustainability,

## Introduction

The increased urgency of knowledge about how to deal with landslides and their triggering factors is linked to the

constant growth of anthropic pressure, even in mountainous areas (Blaikie et al. 1994; Eisbacher 1982). In the framework of landslide risk mitigation, the effective prediction of slope movements is one of the most important challenges to be solved. To do this, there are different types of approaches. Examples are 3D numerical models that solve the physical equations that govern the process under study. These methods are certainly very sophisticated and theoretically reliable. However, they require a deep knowledge of the geotechnical characteristic of the soils and their distribution, which is extremely rare and difficult to gain. In fact, when accounting for all the possible uncertainties, the quality of 3D models can drop dramatically (Titti et al. 2021). That's why numerical models, despite their solid physical basis, are not always the best option in predictive terms. In fact, potential uncertainties are numerous, considering the groundwater regime, the subsoil reconstruction and rock/soil geotechnical parameters, all complex properties that may vary both in time and space.

Another solution are the grey box models. In this case the main objective is to identify a correlation between input and output with limited knowledge of the intrinsic process that produces the relation, e.g., the rheological properties of the landslide soil. In this case, data are approached as phenomenological entities, and the model should be a specific function able to produce the expected output based on selected inputs.

Grey box modelling requires a long time series of all the possible variables that can be hypothesized to have an effect on the landslide process (Angeli et al. 2000; Corominas et al. 2005). Once the correlation of the two signals has been established, a possible causal relationship between the two variables can be hypnotized (Du et al. 2013). The reference data can be split to validate and calibrate a linear-regression or complex machine learning function (Krkač et al. 2017; Zhou et al. 2016). If the output is the landslide displacement, after a procedure of calibration, the model may be considered for prediction purposes (Huang et al. 2017). As a matter of fact, it is possible to quantify the expected landslide movement mitigation as a function of the reduction of the input parameter.

## Case of study

Passo della Morte (46.396 N, 12.715 E) is located on the left flank of the upper Tagliamento valley. This area is crossed by a very important National road called SS52 “Carnica” that cuts across the Eastern Alps. It extends mainly in Friuli-Venezia Giulia Region, connecting the provinces of Udine and Bolzano, with a brief passage into the province of Belluno. To bypass a tortuous tract of the road that was subject to rockfalls and snow avalanches, in 1994 a two-kilometre long new road tunnel was built. Regrettably, the flank of the mountain in which the tunnel was constructed, and the tunnel entrance was later discovered to be affected by slow moving deep-seated landslides that nowadays are damaging the road infrastructure.

The eastern portal of the tunnel and 300 m of the aerial national road are affected by a  $2.1 \times 10^6 \text{ m}^3$  landslide that is damaging the small bridge crossing the Rio Verde torrent. The landslide is slow moving at about some cm per year but in the hypothetical event of a major activation of the landslide, the whole crossing traffic of the valley would be diverted since there would be no access also to the old road (Fig. 1). This scenario will have an important economic impact on the local municipalities. Despite Landslide 1 and Landslide 2 having different scarp, they can be considered as a unique slope instability with a rotational movement at the crown and translational behaviour at the toe (Sinigardi et al. 2015).

In the study area, rainfall play an important role and very intense events are not so rare. The mean annual accumulated precipitation (ARPA-OSMER 2008) is 1721 mm. In periods with more precipitation Landslide 1-2 activity increases, indicating a possible link between water runoff, snow melt and landslide displacement.

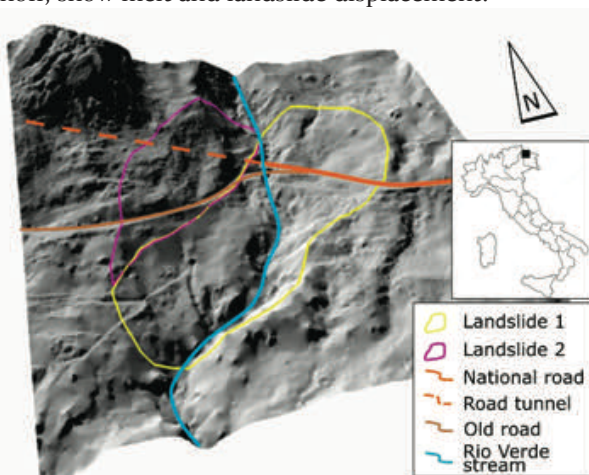


Figure 1 Study area of Passo della Morte.

## Hydrological Setting

The most important hydrological element in the area is the Rio Verde torrent (Fig. 2) that divides Landslide 1 from Landslide 2 by passing through this slope movement. The drainage basin of this element extends from 735 m a.s.l., where the hydrometer is placed, and the 2122 m of the summit of Mt. Tinisa for a total area of approximately

1.68 km<sup>2</sup>. Geologically, 1.52 km<sup>2</sup> is tectonized dolomitic limestone of Monte Tiarfin Formation affected by karst phenomena and 0.161 km<sup>2</sup> is dolomitic boulders and colluvial deposits (Fig. 2). The upper part of the Rio Verde torrent is mostly dry all over the year except during intense (higher than 150 mm/day) rainfall events. This is mainly due to the presence of a very permeable deposit located in the upper part of the basin. On the other hand, just above Landslide 1-2, the presence of springs must be highlighted. This element is very important because it guarantees, in the sector of the torrent that crosses the heart shaped landslide, a minimum flow rate of 40 l/s even in dry periods. The water supplies that keep this “dry baseflow” are connected to deep circulations with long residence time set in the dolomitic limestones. The springs are also sensitive to heavy rain events that rapidly increase the flow rate. This second component is due to the water infiltration in the high-permeability debris at the base of the Tinisa massif, in particular during sudden snowmelt (Cervi et al. 2017).

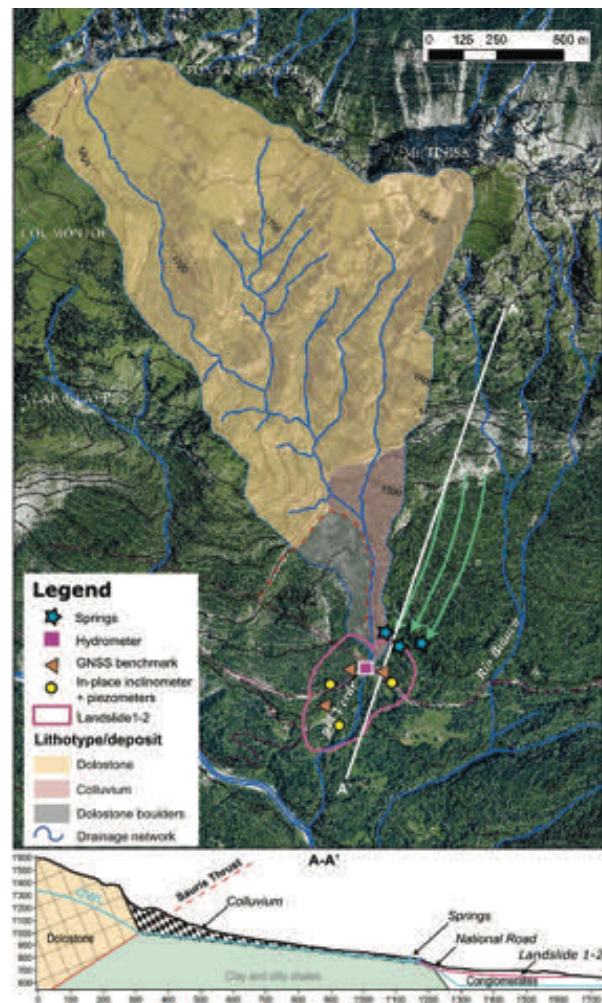


Figure 2 Lithotypes and deposits in the surface hydrological basin of the Rio Verde. The green arrows represent the groundwater flow circulation. In the hydrogeological section below, the process leading to the presence of the springs is clearly illustrated (modified from Bossi et al. 2019).

The structural element that justifies the occurrence of this system of springs is the local presence of the Sauris fault. The latter creates a geological setting that keeps the water table shallow near the contact between the clay and silty shales and the colluvium, as shown in Fig. 2.

**Monitoring Network and Data**

Monitoring in this area began in 2002 with the deployment of several inclinometers and piezometers. The installation of more and more sensors over the years has generated a complex system consisting of inclinometers (periodic and in-place), Global Navigation Satellite System (GNSS) surveys, quasi-real time piezometers, a thin plate weir to measure continuously the discharge of the Rio Verde, a rain gauge and temperature sensors. More than 20 boreholes were drilled and most of them were equipped with inclinometers. That allowed to gain lots of information about the location of the slip surface along the slope in order to be able to reconstruct the 3D slip surface of the phenomenon. At the moment, three series of in-place inclinometers, continuously acquiring data since 2010, are still active as shown in Fig. 2. Besides, in each borehole, a piezometer has been installed. It is important to note that according to the measurements, the water table on Landslide 1-2 has never reached the slip surface. GNSS survey consists of three benchmarks placed in the heart shaped landslide. It monitors the slope's surface movement through periodic surveys that show that the landslide moves at a rate of 1-2 cm/y in dry years and reaches 3-4 cm/y in years characterized by particularly long and intense rainfall events.

The monitoring system was integrated in 2012 with a very important element. It consists of a sharp crested thin plate weir installed in the Rio Verde to measure the water discharge of the torrent (Fig. 3). The weir is deployed in a regular 6 x 5 m concrete culvert that acts as a bridge for the SS 52 over the stream. The rating curve for the measuring station was assessed through periodic measurements with different flow rates and then interpolated using simple hydraulic equations considering the free fall setting of the streamflow (Fig. 3).



Figure 3 Thin plate weir, the hydrometer is installed behind the steel plate. Photo taken during one of the calibration campaigns.

**Modelling**

Using data from the continuous monitoring in-place inclinometers and discharge in the Rio Verde a sharp correlation between the velocity of the landslide and the Rio Verde discharge was found. Based on that, a grey box model able to reconstruct and effectively predict the landslide displacement rate on the sole input of the Rio Verde streamflow was produced (Bossi et al. 2019). The model was tested and validated (Fig. 4).

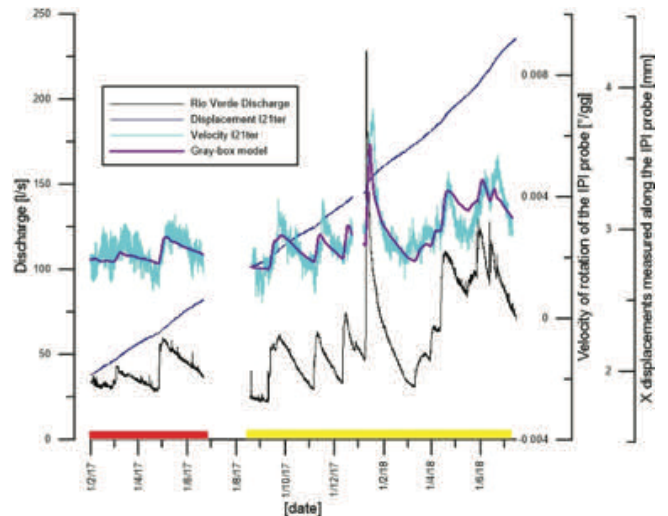


Figure 4 Velocity recorded in inclinometer compared with Rio Verde discharge and daily rainfall – from Bossi et al. (2019).

**Definition of the mitigation strategy**

Considering the strong correlation between the velocity of displacement of Landslide 1-2 and the discharge in Rio Verde stream, it seems a natural consequence that the mitigation strategy should have concentrated on reducing the flow rate in the torrent. For this reason, the sequestration of part of the water flowing in the Rio Verde was proposed to the local authorities (Civil Protection of the Friuli Venezia Giulia Region).

To measure the effectiveness of this countermeasure, some forecast simulations were performed. A maximum value of 100 l/s in the reduction of the discharge was considered. The results show a displacement decrease of more than 50% in the average rainy year and more than 75% in years characterized by extreme meteo-climatic events.

In view of these results, the personnel from Protezione Civile Friuli Venezia Giulia start the realization of the mitigation strategy. The catch box of the discharge is placed next to the existing check dam, under the Rio Verde road bridge at 735 m a.s.l (Fig. 5). At the present time is also under construction an HDPE (High Density Polyethylene) penstocks (Fig. 6). The latter will tunnel the intercepted water to the nearby Tagliamento River for an expected restitution altitude of 575 m a.s.l (Fig. 6). It is also under consideration the hypothesis to associate a micro-hydroelectric station to exploit the energy accumulated in the penstock.



Figure 5 Design of the intercepting structure: A view from downstream, below the road bridge; B view from above.

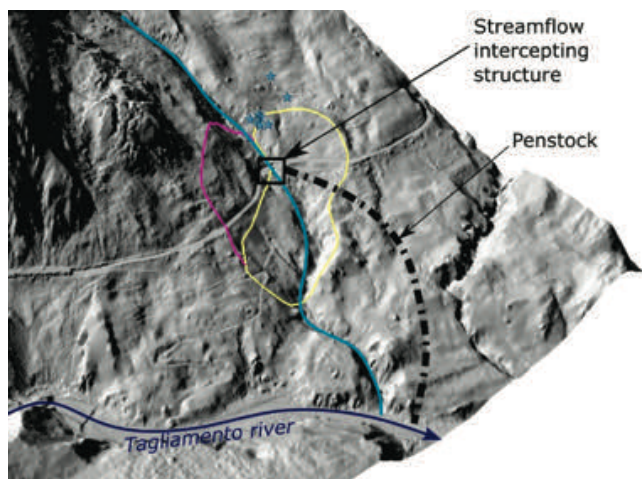


Figure 6 Synoptic scheme of the proposed mitigation solutions over shaded relief of the area.

Concurrently to the structural mitigation works, a new in-place inclinometer has been deployed in order to follow the landslide movements during construction and, more importantly, after the water sequestration starts. That would permit to assess directly if the mitigation strategy is working as planned.

## Conclusions

In this work, the importance of long-term monitoring system of a landslide, including the measure of river discharges in similar slope movement situations, was underlined. The analysis of this dataset can lead to the identification of possible correlations of the monitored parameters that can include also the potential triggering factors. In this study, a strong link between the velocity displacement of Landslide 1-2 and the discharge of the Rio Verde stream was found. Considering the hypothesis of causality, a grey-box model was developed, calibrated and validated with experimental inclinometers information. This model is a great tool to simulate expected velocities in the function of discharge. As consequence, a countermeasure was planned and proposed to local authorities. It consists of the subtraction of the water flowing in the Rio Verde by a catch box and to tunnel it away from the landslide affected area by using a penstock. This highlights that it is possible to produce a landslide structural mitigation strategy even without the rheological characterization of the process. That allows, to a certain degree, also avoiding all the uncertainties and simplifications linked with the definition of a numerical geotechnical model, especially if the prospective model is just bi-dimensional.

After the construction of the water intercepting structure, the hypothesis of the causal relationship between velocities and discharge will be re-tested, and hopefully validated through the prosecution of the monitoring activity in Landslide 1-2. Moreover, the economic perspective of providing these types of self-paying mitigation approaches in the framework of installing the hydroelectric power plant will be further investigated.

## Acknowledgements

We thank for the support of our twenty-year lasting activity in the Passo della Morte area, the Civil Protection of the Friuli Venezia Giulia region. We also want to thank the municipality of Forni di Sotto.

## References

- Angeli MG, Pasuto A, Silvano A (2000) Critical review of landslide monitoring experiences. *Eng. Geol.* 55: 133–147.
- ARPA-OSMER (2008) Climatic data from the Friuli Venezia Giulia Environmental Division. Available online: [https://www.meteo.fvg.it/clima/clima\\_fvg/01\\_elaborazioni\\_\(grafici\\_e\\_tabelle\)/01\\_precipitazioni/dati\\_elaborati/dati\\_idrografico\\_19612000/tabelle\\_e\\_grafici\\_stazioni/mensili/01\\_piogge\\_cumulate/tabella/AMPEZZOpiogge\\_tab.pdf](https://www.meteo.fvg.it/clima/clima_fvg/01_elaborazioni_(grafici_e_tabelle)/01_precipitazioni/dati_elaborati/dati_idrografico_19612000/tabelle_e_grafici_stazioni/mensili/01_piogge_cumulate/tabella/AMPEZZOpiogge_tab.pdf) (accessed on 5 April 2008).
- Blaikie P, Cannon T, Davis I, Wisner B (1994) *At risk: natural hazards, people's vulnerability and disasters*. Routledge.
- Bossi G, Marcato G (2019) Planning Landslide Countermeasure Works through Long Term Monitoring and Grey Box Modelling. *Geosciences*. 9(4): 185.
- Cervi F, Borgatti L, Dreossi G, Marcato G, Michelini M, Stenni B (2017) Isotopic features of precipitation and groundwater from the

- Eastern Alps of Italy: Results from the Mt. Tinisa hydrogeological system. *Environ. Earth Sci.* 76: 410.
- Corominas J, Moya J, Ledesma A, Lloret A, Gili JA (2005) Prediction of ground displacements and velocities from groundwater level changes at the Vallcebre landslide (Eastern Pyrenees, Spain). *Landslides*. 2: 83–96.
- Du J, Yin K, Lacasse S (2013) Displacement prediction in colluvial landslides, Three Gorges Reservoir, China. *Landslides*. 10: 203–218.
- Eisbacher RH (1982) Slope stability and land use in mountain valleys. *Geoscience Canada*. 9: 14-27.
- Huang F, Huang J, Jiang S, Zhou C (2017) Landslide displacement prediction based on multivariate chaotic model and extreme learning machine. *Eng. Geol.* 218: 173–186.
- Krkač M, Špoljarić D, Bernat S, Arbanas Mihalić S (2017) Method for prediction of landslide movements based on random forests. *Landslides*. 14: 947–960.
- Pasuto A, Soldati M (1999) The use of landslide units in geomorphological mapping: An example in the Italian Dolomites. *Geomorphology*. 30: 53–64.
- Petronici F, Borgatti L, Cervi F, Piccinini L, Bonaga G, Marcato G (2016) Hydrogeological monitoring and modelling in the S. Lorenzo road tunnel area (Passo della Morte, Udine) for the design of countermeasure works. *Rend. Online Soc. Geol. It.* 39: 93-96.
- Sinigardi G, Bossi G, Scuri A, Marcato G, Borgatti L (2015) Geological and numerical models as a tool to manage landslide risk: the Passo dell Morte case study (UD, Italy). *Rend. Online Soc. Geol. It.* 34: 46-53.
- Titti G, Bossi G, Zhou GG, Marcato G, Pasuto A (2021) Backward automatic calibration for three-dimensional landslide models. *Geoscience Frontiers*. 12(1): 231-241.
- Zhou C, Yin K, Cao Y, Ahmed B (2016) Application of time series analysis and PSO–SVM model in predicting the Bazimen landslide in the Three Gorges Reservoir, China. *Eng. Geol.* 204: 108–120.





# Long-term monitoring of active large-scale landslides based on integrated systems in South Tyrol (SoLoMon project)

Giulia Bossi<sup>(1)</sup>, Alessandro Corsini<sup>(2)</sup>, Giuseppe Ciccarese<sup>(2)</sup>, Gianluca Marcato<sup>(1)</sup>, Marco Mulas<sup>(2)</sup>, Luca Schenato<sup>(1)</sup>, David Tonidandel<sup>(3)</sup>, Volkmar Mair<sup>(3)</sup>

1) Research Institute for Geo-Hydrological Protection, National Research Council, Padova, Corso Stati Uniti 4, Italy (giulia.bossi@irpi.cnr.it)

2) Department of Chemical and Geological Sciences, University of Modena and Reggio Emilia, Modena, Italy

3) Geological service, Autonomous Province of Bolzano-South Tyrol, Bolzano, Italy

**Abstract** Active large-scale landslides alternate long-lasting “ordinary” semi-steady-state slow moving periods to short-lasting “non-ordinary” acceleration phases that can lead to major damaging events. As their complexity and dimensions determine serious technical difficulties in implementing cost-effective structural mitigation measures, long-term monitoring is crucial for risk reduction, as it allows for a better understanding of the spatial and temporal behaviour of the phenomenon and, therefore, to focus on the most risk-significant elements of the landslide. Nowadays, a large selection of methods is available for the integrated cross-validated multi-scale monitoring of such phenomena so to achieve a sound knowledge of slope movements on a continuous and time-lapsed basis. The EU Financed EFRE FESR project SoLoMon (Software for Longterm Monitoring; FESR4008) project aims to apply relevant remote, proximal and in-site monitoring techniques to representative case studies of large-scale landslides in South Tyrol. In the frame of SoLoMon project, the following monitoring techniques are applied in an integrated manner: (a) periodic (once per year) high-resolution (5 cm) airborne Lidar and Orthophotos surveys of the entire landslides analysed with DEM of Difference and Offset-tracking techniques (landslides 1, 2, 3); (b) Continuous Robotic Total Stations monitoring using reflectors (landslides 2, 3); Continuous in-place D-GPS (landslides 1, 2, 3). Monitoring data from these systems will be integrated into a single functional web-based platform that will handle and analyse data using machine learning algorithms

**Keywords** Monitoring, web-based platform, DEM of Differences, Offset-tracking, non-structural countermeasures

## Introduction

To mitigate large landslide related risk both structural and non-structural mitigation actions may be implemented. Non-structural mitigation measures are monitoring, policies, training and other types of actions that reduce the risk without physically interfering with the hazardous process. These approaches are usually chosen when the

landslide is too large to deal with construction works that would be either ineffective or too costly. Ineffectiveness is frequently linked with a large number of uncertainties regarding the landslide kinematic that may be too high to proceed with cost-effective structural works.

The upside of non-structural mitigation measures is a significantly minor impact on the environment and on the landscape than structural options, and, in general, a minor overall cost. The downside is the continued necessity of maintenance and updating of the system, the dependence on the compliance of the exposed population and the need for experts that can interpret data and retrofit the alert mechanism.

Active large-scale landslides alternate long-lasting “ordinary” semi-steady-state slow moving periods of activity to short-lasting “non-ordinary” acceleration phases that can lead to major damaging events. In this case, long-term monitoring is crucial for risk reduction, as it allows for a better understanding of the spatial and temporal behaviour of the phenomenon and, therefore, to focus on the most risk-significant elements of the landslide. Nowadays, a large selection of methods is available for the integrated cross-validated multi-scale multi-source monitoring of such phenomena in order to achieve a sound knowledge of slope movements on a continuous and time-lapsed basis.

The EFRE-FESR SoLoMon project aims to apply relevant remote, proximal and on-site monitoring techniques to representative case studies of large-scale landslides in the Autonomous Province of Bolzano (Italy), namely: (1) the Ganderberg Deep-seated Slope Deformation; (2) the Trafoi rockslide and (3) the Corvara earth slide-earth flow.

## Test sites

### The Ganderberg Deep-seated Slope Deformation

The Ganderberg Deep-seated Slope Deformation (DGSD) is located in the upper Passirio valley (46°51'34.5"N 11°10'18.3"E). The slope affected by the DGSD covers an area of about 4.7 km<sup>2</sup>, and is predominantly oriented toward SW. The mass movement develops for more than 1200 m,

from the crown at 2250-2450 m to the valley floor located at 1170-1300 m a.s.l (Fig. 1).

The Ganderberg slope is located at the boundary between the Schneeberg complex and Laas series, both consisting of metamorphic rocks of the Austroalpine domain of the Eastern Alps. The Schneeberg complex is composed by amphibolites, garnet-mica-shists and paragneiss. The Laas series differs from the Schneeberg complex mainly for the greater content of carbonates that induce a less plastic behavior of the rock under loading and a coarser colluvium. The contact between the two complexes crosses the DGSD area along a fault trending NE-SW.



Figure 1 The Ganderberg DGSD; in red the potential rock avalanche; in orange and yellow the secondary slides.

The slope movements have been monitored since 2007 through a network of 20 GNSS benchmarks. The slope instability moves at a velocity of several cm per year thus inducing secondary phenomena (Bossi 2015). One of these is a potential rock avalanche detaching from the northern scarp that can induce river damming (Bossi et al. 2013). Other two secondary instabilities of some million cubic meters at the toe threaten the valley road and the small village of Hahnebaum. During the last decade a “non-ordinary” acceleration phase of one of these slides, completely damaged the National Road 44bis, blocking its transibility and de facto isolating the upstream village of Rabenstein. Moreover, the road disruption interrupts the passage through Passo Rombo/Timmelsjoch towards Austria, a particularly scenic route that was the object of an Interreg project aimed at the touristic exploitation of the route.

#### The Trafoi Rockslide

The Trafoi deep-seated rockslide is located in the upper Venosta valley (46°33'16.4"N 10°29'50.4"E). The rockslide area covers an area of about 6.0 km<sup>2</sup>, and can be subdivided into two main units (A & B) (Fig. 2).

Geologically the landslide is characterized by a complex stratigraphic arrangement due to the presence of gypsum, anhydrite and cellular dolostone in the form of lenses of the permo-Mesozoic successions intercalated in the Dolomia Principale. These layers exhibit low mechanical load bearing capacity and high susceptibility to sliding.

The Trafoi Unit A (from 2950 to 2600 m a.s.l) shows double crested ridges and trenches in the upper part, a rockslide in the central part (from 2600 to 2000 m a.s.l). Unit A is morphologically very similar to the Val Pola landslide (located 20 km to the west of Trafoi) before it evolved into a catastrophic rock avalanche in 1987.

Since periodic D-GPS monitoring indicates that Unit A moves at a velocity from 2 to 7 cm/year, the phenomenon is certainly worth of attention (Corsini et al. 2013), and potential runout scenarios in case of the collapse of the Trafoi rockslide have been calculated (Iannacone et al. 2013). The Trafoi Unit B consists of a fairly developed rockslide phenomenon that, locally, evolves as earth slides damaging the “Hotel Tannenheim” and the National Road 38 to “Passo dello Stelvio”. Periodic inclinometric monitoring of unit B indicates a max velocity in the order of 3 cm/year.

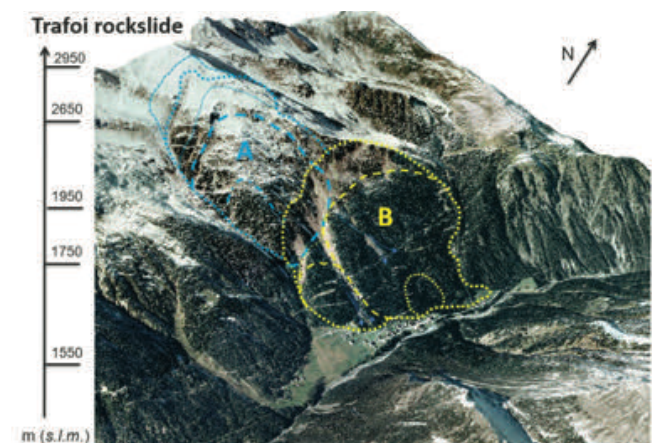


Figure 2 The Trafoi rockslide area (Unit A and Unit B).

#### The Corvara Earthslide-Earthflow

The Corvara rotational earth slide-earth flow is located in the upper Badia valley (46°32'31.8"N 11°53'09.7"E). It consists of weak clayey rock masses of the Triassic. Present-day movements, ranging from cm to m/year, cause damages to National Road 244 and ski infrastructures. Movements are also of some concern for buildings at the toe of the landslide (Fig.3).

The landslide has been extensively investigated over the past years, including studies on landslide characterization and field-based monitoring (Corsini et al. 2005), dating (Soldati et al. 2004), and modelling (Schädler et al. 2015). Monitoring of the Corvara landslide using D-GPS started in 2001 (Corsini et al. 2005) while monitoring with satellite-based PS-MTI started 2010 (Iasio et al. 2012; Mulas et al. 2015), which then evolved in integrated D-GPS



Figure 3 The Corvara earthslide-earthflow (modified after Corsini et al. 2005)

and Corner Reflectors monitoring (Mair et al. 2016; Schlögel et al. 2017). The active part involves approximately 25 million m<sup>3</sup> with major active shear surfaces ranging at depths between 10 and 48 m and movement rates ranging along the slope and over different years from cm to m/year.

### The SoLoMon project

#### Monitoring

Regarding in depth characterization of the investigated processes, monitoring is extremely useful when dealing with large and slow moving landslides as it may support the definition of a reference geological model and the identification of the most unstable sections along a slope, how they move and if there is some correlation with potential triggering factors.

Small displacements in large landslides can only be identified instrumentally since their geomorphological traces cannot otherwise be univocally associated with a present-day activity. In this framework, monitoring must be carried out for long periods because certain phenomena can present long phases of quiescence to which phases of activity are interspersed and usually consequent to particular climatic events with long return periods. A reliable risk mitigation strategy cannot ignore the observation of the slope behaviour during these phases, and in the context of the subsequent definition of a numerical model to update the risk scenarios.

On this basis, an effective monitoring system is inevitably influenced by the quality of the insightful planning of instrument installation. The instruments should be able to collect the physical and dynamic parameters in the most significant areas, extracting the most information from the measuring point. It is also fundamental that data should be gathered continuously, and along with the hypothesized triggering factors. Redundancy in monitoring and the availability of numerous measuring points are good starting points for a network. However, a training period of observation with

data interpretation by experts is also fundamental to establish an operational Early Warning System that should be activated when non-ordinary states are reached by the landslide itself or by its environment.

In Solomon project, the following new monitoring systems are being installed: (1) Ganderberg Deep-seated Slope Deformation: n<sub>3</sub> continuous D-GPS monitoring devices (Leica GM30); (2) Trafoi rockslide: n<sub>1</sub> continuous D-GPS monitoring devices (Leica GM30) and n<sub>1</sub> robotic Total Station (Leica TM60); and (3) Corvara earth slide - earth flow: n<sub>1</sub> robotic Total Station (Leica TM60).

#### Multi Temporal DEM of Difference and Offset-tracking

Recent improvements in topographical data acquisition techniques allow the production of high-resolution digital terrain models (DTMs). In particular, comparisons of LiDAR-derived DTMs obtained from successive surveys make it possible to produce DEM of differences (DoD) maps, which are a valuable tool to interpret the evolution of geomorphological processes and to quantitatively assess areas of accumulation, deposition or erosion along mountain slopes. However, DoD maps do not provide information regarding planar displacements but just highlight pointwise vertical variations of heights.

To get an insight into the horizontal displacement rate of landslides, offset tracking techniques based on optical images are particularly useful to bridge the gap with DoD analysis and to help provide 3d superficial displacement estimates for landslides with remotely acquired data.

Within the project, periodic (once per year) high-resolution (5 cm) airborne Lidar and Orthophotos surveys of the entire landslides will be analysed with Offset Tracking digital image correlation algorithms to provide maps of activity for each test site and to compare them with ground truth data from the monitoring equipment.

#### Web based platforms

Most monitoring techniques have undergone a continuous advancement in hardware and software platforms, improving the quality and significance of data collection, real-time processing and user interfaces. This means that lots of data need to be properly handled and interpreted, even considering the integration between remote sensing data and in situ measurements. When implementing a new monitoring network, it is necessary to provide the stakeholder with the tools to manage data combined and derived from different instruments on the same site.

Making data available on interactive web systems is not just a matter of access. Yes, data may be easily consulted and seen everywhere, but it may also be shared, compared and analysed with the tools implemented in the web platform. These algorithms will support the identification of events or thresholds that can trigger an alert. Collecting all data in a unique repository is also fundamental for the application of machine learning techniques. To do so, an important feature of up-to-date

web platforms is that they should integrate different types of sensors with different time bases, guaranteeing the system's scalability and allowing redundancy.

The web environment provides secure advantages: (1) data is collected from different data sources and matched on a single server-side framework avoiding complex data management; (2) a remote user-interface allows regular maintenance and direct access to the instruments for maintenance, calibration and synchronization; (3) a graphical interface in a browser provides an easy-to-use support system for decision-makers to interact with a system which is continuously updated.

### Machine learning

Machine learning techniques can support the definition of warning /alarm systems based on monitoring data. The ability to rely on a simple and automatic procedure to identify dangerous situations is of great help to risk management. As part of the project, new methodologies will be tested, and some algorithms already applied by CNR-IRPI in other contexts will be developed in parallel. Among these is a hierarchical clustering algorithm (Day 1984) to identify pattern changes in landslide displacements. The procedure makes it possible to group zones characterized by similar “movement patterns” based on data from automated total stations. The unsupervised definition of homogeneous areas from a kinematic perspective supports a landslide's impartial geomorphological characterization (not linked to an expert opinion). In addition, the method allows to trigger alerts if some monitored points change deformation patterns. In this way, identifying possible dangerous situations is carried out without imposing fixed and arbitrary thresholds and without calibration. The recognition of areas with new types of activities supports the definition of the volumes of the most active portions of the slope and therefore helps the definition of reliable risk scenarios (Titti et al. 2020).

### Final remarks

The SoLoMon project pipeline has been organized in order to produce reliable risk scenarios and warnings via multi-source multi-temporal analysis and monitoring. All the instruments that have been, and will be, deployed are of top-notch technology and will gather data for many years to come, well beyond the project timeline.

Given the different types and processes active in the three study areas, the integration of different techniques will be extremely valuable and will allow testing the effectiveness of each approach for different potential landslide hazards (i.e. rock avalanches, rockslides). A web-based platform with embedded machine learning algorithms to produce warnings will also be directly assessed by the stakeholders of the Autonomous Province of Bolzano (Italy). This will provide a first-hand assessment of the usability and reliability of the methods.

### Acknowledgements

The project is financed by the European Regional Development Fund FESR4008 “Monitoraggio a lungo termine di grandi frane basato su sistemi integrativi di sensori e reti” – Prorityaxis 4, Territorio sicuro – CUP B36D16000270009

### References

- Bossi G, Frigerio S, Mantovani M, Schenato L, Pasuto A, Marcato G (2013) Hazard assessment of a potential rock avalanche in south Tyrol, Italy: 3D modeling and risk scenarios. *Italian Journal of Engineering Geology and Environment*. 2:221-228.
- Bossi G, Frigerio S, Mantovani M, Marcato G, Schenato L, Pasuto A (2015) Ganderberg Landslide Characterization Through Monitoring. *Engineering Geology for Society and Territory*, Volume 2. Springer, Cham. pp. 1327-1331.
- Corsini A, Pasuto A, Soldati M, Zannoni A (2005) Field monitoring of the Corvara landslide (Dolomites, Italy) and its relevance for hazard assessment. *Geomorphology*. 66: 149–165.
- Corsini A, Iannacone J P, Ronchetti F, Salvini R, Mair V, Nossing L, Stefani M, Unterthiner G, Valentinotti G (2013) Hot spots for simplified risk scenarios of the Trafoi rockslide (South Tyrol). *Landslide Science and Practice - Volume 6: Risk Assessment, Management and Mitigation*. Springer, Berlin. pp. 739-745.
- Iannacone J P, Quan Luna B, Corsini A (2013) Forward simulation and sensitivity analysis of run out scenarios using MassMov2D at the Trafoi rockslide (South Tyrol, Italy). *GEORISK*. 7(4): pp. 240-249.
- Iasio C, Novali F, Corsini A, Mulas M, Branzanti M, Benedetti E, Giannico C, Tamburini A, Mair V (2012) COSMO SkyMed high frequency—High resolution monitoring of an alpine slow landslide, Corvara in Badia, Northern Italy. *Proceedings of the IEEE International Geoscience and Remote Sensing Symposium (IGARSS)*. 22–27 July 2012. Munich, Germany, pp. 7577–7580.
- Mulas M, Petitta M, Corsini A, Schneiderbauer S, Mair V, Iasio C (2015) Long-term monitoring of a deep-seated, slow-moving landslide by mean of C-band and X-band advanced interferometric products: The Corvara in Badia case study (Dolomites, Italy). *ISPRS Int. Arch. Photogramm. Remote Sens. Spat. Inf. Sci.* XL-7/W3: 827–829.
- Mair V, Mulas M, Chinellato G, Corsini A, Iasio C, Mosna D, Thiebes B (2016) Developing X-band corner reflectors for multi-technological monitoring of ground displacement in alpine environments. *Proceedings of the 13th Congress INTERPRAEVENT*. 30 May–2 June 2016. Lucerne, Switzerland.
- Schädler W, Borgatti L, Corsini A, Meier J, Ronchetti F, Schanz T, (2015) Geomechanical assessment of the Corvara earthflow through numerical modelling and inverse analysis. *Landslides*. 12: 495–510.
- Schlögel R, Thiebes B, Mulas M, Cuozzo G, Notarnicola C, Schneiderbauer S, Crespi M, Mazzoni A, Mair V, Corsini A (2017) Multi-Temporal X-Band Radar Interferometry Using Corner Reflectors: Application and Validation at the Corvara Landslide (Dolomites, Italy). *REMOTE SENSING*. 9: 739-758. doi: 10.3390/rs9070739.
- Soldati M, Corsini A, Pasuto A (2004) Landslides and climate change in the Italian Dolomites since the Lateglacial. *CATENA*.55(2): 141-161. doi: 10.1016/S0341-8162(03)00113-9.
- Titti G, Mantovani M, Bossi G (2020) Detecting Change of Patterns in Landslide Displacements Using Machine Learning, an Example Application. *Workshop on World Landslide Forum*. Springer, Cham. pp. 215-221.

# Monitoring of rockfall prone areas in eastern Slovenia

Mateja Jemec Auflič<sup>(1)</sup>, Ela Šegina<sup>(1)</sup>, Tina Peternel<sup>(1)</sup>, Matija Zupan<sup>(1)</sup>, Jernej Jež<sup>(1)</sup>, Manja Žebre<sup>(1)</sup>, Polona Kralj<sup>(1)</sup>, Marjana Zajc<sup>(1)</sup>, Matjaž Mikoš<sup>(2)</sup>, Nejc Bezak<sup>(2)</sup>, Milan Kobal<sup>(3)</sup>

1) Geological Information Centre, Geological Survey of Slovenia, Ljubljana, Slovenia (mateja.jemec-auflic@geo-zs.si)

2) University of Ljubljana, Faculty of Civil and Geodetic Engineering, Ljubljana, Slovenia

3) University of Ljubljana, Biotechnical faculty, Ljubljana, Slovenia

**Abstract** In recent years, about ten large rockfalls with a volume of more than 10,000 m<sup>3</sup> have been observed in the eastern part of Slovenia, causing damage to infrastructure, and resulting in two fatalities. Because rockfalls occur suddenly and usually without visible warning signs, they are extremely difficult (or impossible) to predict and thus pose a major potential risk to people and infrastructure. Within the framework of the project Development of Research Infrastructure for International Competitiveness of Slovenian Responsible Research and Innovation Space a set of pilot areas were equipped with meteorological and geotechnical sensors (rain gauges, air temperature and humidity sensors, tilt gauges, kit for measuring rock stress and deformability, laser distance metres, crackmeters and rock temperature sensors) providing real time monitoring data. In this paper, we present seven months of monitoring data from a pilot area considered to be the Oligocene Smrekovec volcanic complex outcrops. The first correlation between temperatures and the movement of rock blocks is presented.

**Keywords** rockfalls, monitoring, sensors, temperature, eastern Slovenia

## Introduction

Rockfalls are the result of a long geological process (tectonics, weathering, etc.), but the fall is sudden. The questions most often asked are what causes rockfall to fall (what factors) and how (what mechanisms)? In the case of a meteorological factor, several physical mechanisms may be involved, which may manifest as rockfalls initiated by a slide or a fall (Krautblatter and Dikau 2007; D'Amato et al. 2016; Macciota et al. 2015; Matsuoka 2019). Rock mass is a type of heterogeneous material that contains many nonpersistent joints. When the daytime temperature is high, the water in the joints undergoes periodic freeze-thaw cycles. The periodic freeze-thaw cycles induce the joint cracks to expand continuously, which will lead to the failure of the rock mass. Temperature fluctuations of high magnitude have been shown to cause irreversible displacements leading to cracks in discontinuities. Thermal shock occurs due to rapid temperature change which leads to significant variation of stresses and displacements in brittle rocks. In transient heat flow, rapid

cooling leads to large tensile stresses at the surface, while rapid heating causes large compressive stresses (Kim and Kemeny 2009; Collins and Stock 2016; Notti et al. 2020). The redistribution of stress can lead to the appearance of microcracks, and the development of the microcracks can lead to the failure of the rock face.

Rockfalls are widespread phenomena in mountain ranges, coastal cliffs, volcanos, river banks, and slope cuts (Corominas et al. 2017). Recent studies have shown that losses due to rockfalls are mainly concentrated in populated areas where there is a research deficit and lack of appropriate risk strategies (Petley 2012).

The morphology of slopes, unfavourable geological and tectonic conditions, and climatic diversity contribute significantly to the large rockfall potential in Slovenia (Čarman et al. 2011; Jemec Auflič et al. 2017). According to the information from the rockfall database of DRI Investment Management Ltd (which manages a rockfall database for national roads for the Slovenian Infrastructure Agency), more than 600 km of road links are affected by rockfall events. In Slovenia, major rockfall phenomena, such as large-scale rockfalls with a volume of more than 100,000 m<sup>3</sup>, are not very common. They occur in the seismically active upper Soča valley and even there they are limited to smaller areas (Ribičič and Vidrih 1998; Mikoš et al. 2006). More often we have to deal with rockfalls and blockfalls that endanger residential and commercial buildings, roads and railroads lines. Despite protective nets, falling rock often penetrates the protective net, or the falling rock hits the track after passing the protective net. In some particularly exposed locations, rockfalls severely affect the safety and normal operation of the railroads and cause great economic and material losses. The most problematic are very narrow valleys with very steep slopes above and below the railroads in the eastern part of the country. In the years between 2010 and 2020, about ten large rockfalls with a volume of more than 10,000 m<sup>3</sup> have been observed in the eastern part of Slovenia, causing damage to infrastructure, and claiming two fatalities (URSZR, annual report 2021). Deciding for the installation of an early warning system is an important step towards the protection of railroad users and residents in areas with high risk for a catastrophic event. Because rockfalls occurs suddenly, usually without visible warning signs, they are extremely difficult (or impossible) to

predict and pose a great potential threat to people and infrastructure.

In this paper we will present the monitoring of rockfall-prone area in eastern Slovenia only for a pilot marked with number 2 in Fig. 1. Based on the results, we will show the preliminary correlation between the monitored temperatures and the displacement rates determined by the nearby crackmeters.

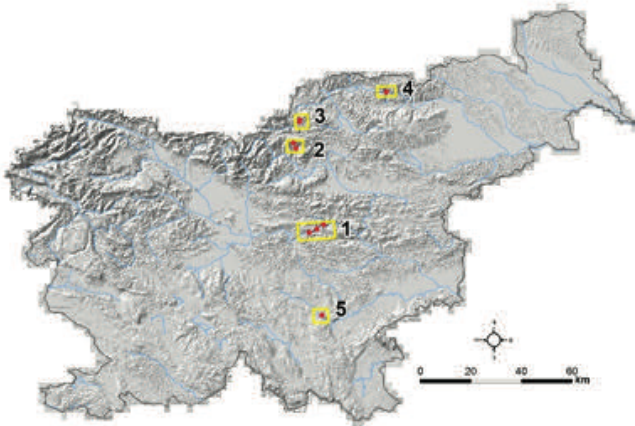


Figure 1 Map with the location of the pilot areas, numbered 1-Zasavje, 2-Smrekovec, 3-Mežica, 4-Brezno, and 5-Žužemberk.

### Methods and material

In the frame of Project »Development of research infrastructure for the international competitiveness of the Slovenian RRI space-RI-SI-EPOS, co-financed by the Republic of Slovenia, Ministry of Education, Science and Sport and the European Union from the European Regional Development Fund, the following measuring equipment have been installed at the selected monitoring areas early in 2021: rain gauges, sensors for air temperature and humidity, tiltmeters, kit for measuring rock stress and deformability, laser distance gauges, crackmeters and near surface rock temperature sensors. The sensors of temperature at the depth of 25, 50 and 75 cm were drilled in homogenous, intact rock with at least 30 cm distance to joints following the design of Gruber et al. (2004). This sampling strategy does not reflect the importance of nonconductive heat transfer through joints, but we avoided complex micro-topography from surrounding bedrock to minimize shadowing or concentration of surface runoff (after snowmelt). Some of the installed sensors can be seen in Fig. 2. Table 1 shows the basic specification of sensors and the number of sensors for each pilot area. The monitoring areas in eastern Slovenia (Fig. 1) were selected according to the following criteria: Frequency of rockfalls, risk to the population and

infrastructure, and diversity of rock composition (carbonate and igneous). Each individual rock type has different engineering properties and predisposing factors that can affect exfoliation, discontinuity formation, and fractures. However, the type of rock, its mineralogical nature, anisotropy or isotropy very often determine the susceptibility to the formation of fractures and their opening.

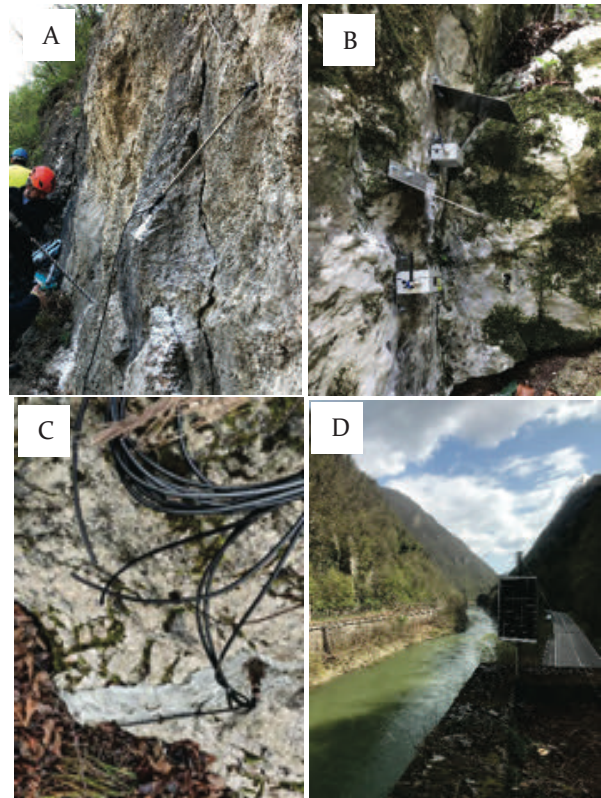


Figure 2 Instalation of the sensors: A-crackmeter, B-tiltmeter and laser distance meter, C-rock temperature sensor, and D-base station with solar panel.

The geotechnical sensors are wired using LoRa communication protocol and LoRa gateway and powered by a base station, which also serves as an in-situ data logger. The Nodes connected to board so that every data coming from the sensor can forward right away using the LoRa network (Long Range Wide Area Network). Thus, the collected data are not transferred right away but going through data processing firsthand. The data also stored in the local storage to minimize the data loss because of a network error. Wide Area Network (WAN) is used in this research based on the LoRa module and makes it possible to send data in an approximately 2 km radius. Due to emerging technologies, battery powered devices using LoRaWAN to communicate can run for many years even without replacement.

Table 1 The basic specification of the sensors and the number of sensors in the pilot areas. The pilot areas are shown in Fig.1 and are marked with numbers from 1 to 5. Abbreviation F.S. characterized Factor Safety.

	Range	Precision	Sampling frequency	Sensor numbers per pilot area (Fig. 1)				
				1	2	3	4	5
Rain gauges	400 cm <sup>2</sup>	0.2 mm/pulse	30 min	1	1	1	1	1
Sensor for air T	-40 to +60 °C	± 0.1 °C	30 min	1	1	1	1	1
Sensor for air humidity	0-100 % Rh	± 1 %	30 min	1	1	1	1	1
Tiltmeter	± 15° biaxial	± 0.01°C	30 min	5	4	2	3	2
Kit for measuring rock stress and deformability	±8.5 MPa	± 0.25 % F.S.	30 min	4	3	3	4	1
Laser distance gauges	0.05 -150 m	0.1 mm	30 min	1	3	1	4	2
Crackmeter	100 mm	± 0.1 % F.S.	30 min	8	8	3	7	3
Rock T sensors	-50 to +150 °C	± 0.2 °C	30 min	4	4	2	4	1

**Smrekovec monitoring area**

The Oligocene Smrekovec Volcanic Complex outcrops along south-easternmost surface extending of the Periadriatic Fault System and forms a part of south-western system of the Pannonian basins (Kralj 2021). It is a remnant of a submarine andesitic stratovolcano composed of complex successions of lavas, autoclastic, pyroclastic, syn-eruptive resedimented volcanoclastic and mixed siliciclastic-volcanoclastic deposits. The stratovolcano hosted hydrothermal system with a deep igneous source and convective-advective flow of hydrothermal fluids that resulted in extensive alteration of volcanic rocks, in particular, the formation of zeolites and clay minerals. Extensive tectonic activity along the Periadriatic Fault System dissected the volcano and displaced the northern sections on a several ten-kilometre-scale toward the south-east, and as a result, only a quarter of the original edifice has been preserved. The present-day rugged morphology of the Smrekovec Volcanic Complex is also a result of extensive glacial erosion that occurred during the last Ice Age (Komac and Zorn 2007).

**Results and discussion**

In this paper, we presented monitoring data from June 2021 to mid-December 2021. To show the temperature differences in the rock face, in the air, and near the ground, we used the box and whisker plots (Fig. 3). Fig. 3 shows the distribution of temperature data in quartiles, with the mean and outliers highlighted. The boxes have vertical lines indicating variability outside the upper and lower quartiles, and any point outside these lines or whiskers is considered an outlier. Fig. 3 shows temperature readings from the temperature sensor measuring temperature at 25, 50, and 75 cm depth (T37157), air temperature, and temperature sensors T12002, T12008, and T12023 attached to the crackmeters and measure temperature 5 cm above the ground. The position of the sensors on the rock face is indicated by red circles in Fig. 4.

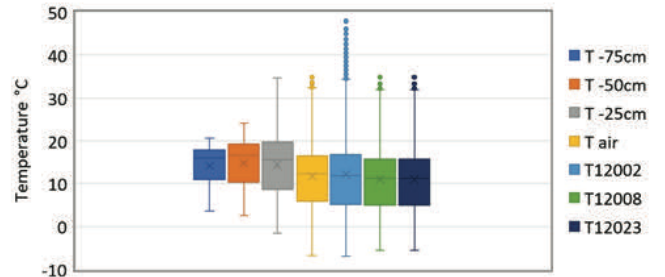


Figure 3 Distribution of temperature data in quartiles, with the mean and outliers highlighted. T air is temperature from the meteorological station (3 km away from the monitoring area). Temperature sensors T37157 which measure the rock temperature at three depths: 25 cm, 50 cm, 75 cm. Sensors T12002, T12008 and T12023 are integrated at the crackmeters and measure temperature 5 cm above the ground.

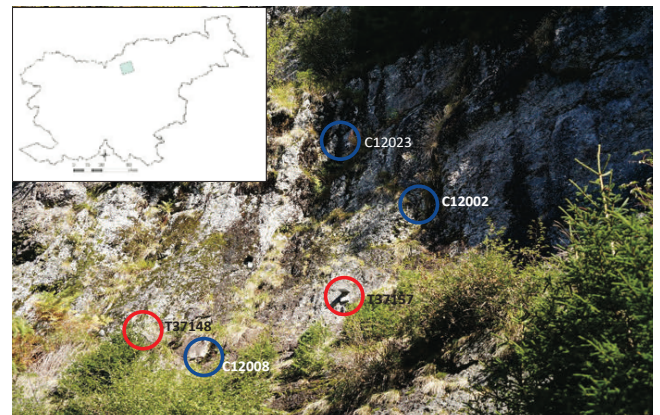


Figure 4 Smrekovec monitoring area. Crackmeters sensors including temperature sensors 5 cm above the ground: CT12002, CT12008, CT12023 (blue circles). Temperature sensors at depths of 25, 50, 75 cm: T37157 and T37148 (red circles).

To show the first observed trends, we plotted the time series of temperatures and measured displacements on the one crackmeter separately for the summer months (June, July, August, September) and for the fall and winter months (October, November, December) (Fig. 5). The time series of the temperature sensors clearly showed that the higher temperatures are measured in the summer months (Fig. 5a), while the air and rock temperatures decrease in the fall and winter (Fig. 5b). The air temperature measured at a height of 5 cm above the ground, and the temperature at a depth of 25 cm in the rock face are very similar during the summer months (Fig. 5a), while the air temperatures fluctuate and remain quite high during the day. Temperatures at 25 cm depth and 5 cm above the ground are rather constant in winter and do not fluctuate significantly (Fig. 5b). Temperatures at depths of 50 and 75 cm are constant and lower in winter (Fig. 5b). From the observed period of seven months, some trends in the movement of the rock block can be seen. Positive crackmeter readings (the values are on the y-axis to the right of the graph) are considered to be expansion

of the rock block and negative ones are considered to be contraction of the rock block. Based on the first finding, we correlate this trend of rock expansion with the drop in temperature at the end of the fall and during the winter months. Although the measured expansion rate is very low, about 0.5 mm, this could be due to a measurement error. The plotted trend line (red colour) tentatively indicates some changes in the motion that could be related to meteorological factors. When  $T_{air}$  and  $T_{12008}$  fall below  $5^{\circ}\text{C}$ , the trend line indicates an expansion of the block. However, more observation periods are needed before this assumption can be confirmed.

To find a significant correlation between the temperatures and the displacements, we made a diagram (Fig. 6) showing two  $T$  readings ( $T_{air}$  and  $T_{12008}$ -temperature sensor at 5 cm above the ground). Over the seven-month period, movements of  $-1\text{ mm}$  to  $0.2\text{ mm}$  can be seen. As temperatures decrease, the rates of movement go from negative to positive values (up to  $0.2\text{ mm}$ ), which could indicate expansion of the rock block during cooling of the air and rock.

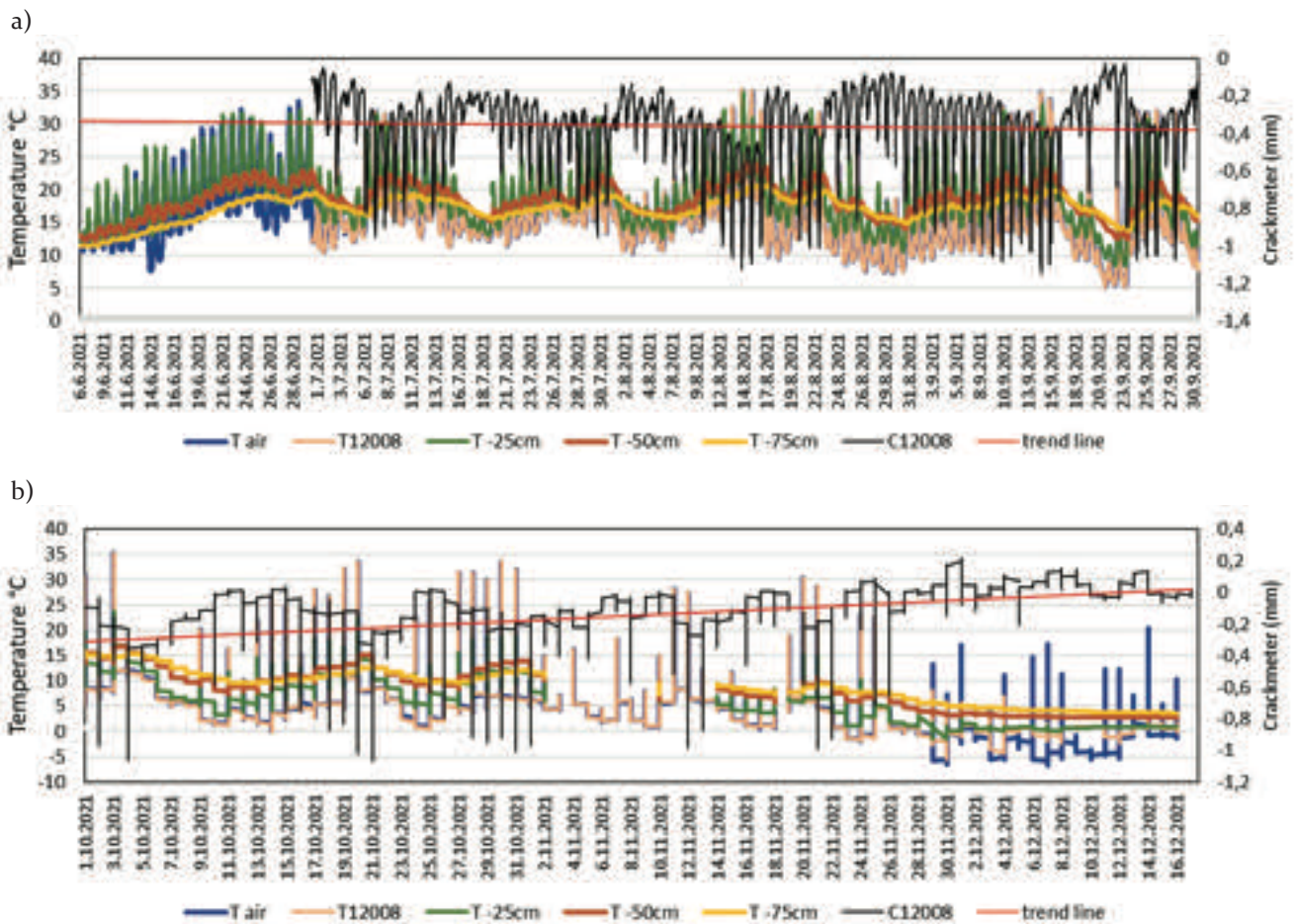


Figure 5 Observed time series of temperature sensor T37157 measuring rock temperature at three depths: 25 cm, 50 cm, 75 cm. T air is the temperature of the meteorological station (3 km from the monitoring area). Crackmeters values are on the y-axis to the right of the graph. Time series of displacements (mm) measured with the C12008 crackmeter (black line), trend line of displacements (red line) and T12008 temperature sensor at 5 cm above the ground. A) The monitoring period is from June to September 2021. B) The monitoring period is from October to mid-December 2021.



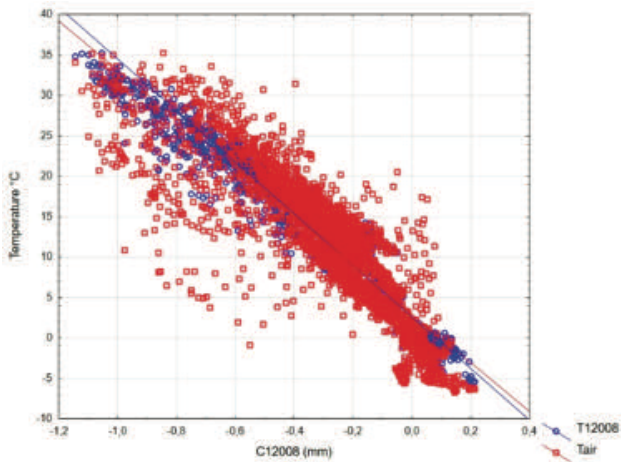


Figure 6 Graph of displacements ( $C_{12008}$ ) and temperatures ( $T_{air}$  - red colour;  $T_{12008}$  - temperature sensor at 5 cm above the ground - blue colour). The monitoring period is from June to mid-December 2021.

## Conclusions

The overall goal of monitoring is to decipher the sensitivity of rock faces to climatic changes and freeze-thaw cycles using a multi-method approach. In this paper, we focused on the outcrops of the Oligocene Smrekovec volcanic complex, which appear in many places in the eastern part of the country and represent rockfall-prone areas. However, the presented observation period is too short to draw relevant conclusions on the correlation of temperatures and displacements. Preliminary results from seven months of observations suggest a correlation between temperature fluctuations and rock block movement, especially in the late autumn and winter months. For next steps, we are aware of the lack of rock surface temperatures, so installation of new sensors is planned (Ibuttons). Rock surface temperature will help us identify freeze-thaw episodes.

## Acknowledgments

The research was funded by the Slovenian Research Agency (Research project J1-3024). The electronic geotechnical sensors were founded by Project »Development of research infrastructure for the international competitiveness of the Slovenian RRI Space – RI-SI-EPOS« The operation is co-financed by the Republic of Slovenia, Ministry of Education, Science and Sport and the European Union from the European Regional Development Fund.

## References

- Collins BD, Stock GM (2016) Rockfall Triggering by Cyclic Thermal Stressing of Exfoliation Fractures. *Nature Geoscience*. 9(5): 395–400. doi: 10.1038/ngeo2686.
- Corominas J, Mavrouli O, Ruiz-Carulla R (2017) Rockfall Occurrence

and Fragmentation BT- Advancing Culture of Living with Landslides. K Sassa, M Mikoš, Y Yin (eds.). Springer International Publishing. pp. 75–97.

- Čarman M, Kumelj Š, Komac M, Ribičič M (2011) Rockfall Susceptibility Map of Slovenia. P. 3 in Workshop on Rock Fall Protection. Innsbruck, Austrian Service for Torrent and Avalanche Control, Geological Service.
- D'Amato J, Hantz D, Guerin A, Jaboyedoff M, Baillet L, Mariscal A (2016) Influence of meteorological factors on rockfall occurrence in a middle mountain limestone cliff. *Natural Hazards and Earth System Sciences*. 16(3): 719–735. <https://doi.org/10.5194/nhess-16-719-2016>.
- Gruber S, Hoelzle M, Haeberli W (2004) Rock-wall temperatures in the Alps: modelling their topographic distribution and regional differences. *Permafrost and Periglacial Processes*. 15(3): 299–307. <https://doi.org/https://doi.org/10.1002/ppp.501>
- Jemec Auflič M, Jež J, Popit T, Košir A, Maček M, Logar J, Petkovšek A, Mikoš M, Calligaris C, Boccali C, Zini L, Reitner J M, Verbovšek T (2017) The variety of landslide forms in Slovenia and its immediate NW surroundings. *Landslides*. 14(4): 1537–1546. <https://doi.org/10.1007/s10346-017-0848-1>
- Kim KM, Kemeny J. (2009) Effect of Thermal Shock And Rapid Unloading On Mechanical Rock Properties. In 43rd U.S. Rock Mechanics Symposium & 4th U.S. - Canada Rock Mechanics Symposium (p. 10). American Rock Mechanics Association.
- Komac B, Zorn M (2007) Slope processes and humans. *Geografija Slovenije* 15. Ljubljana. (in Slovenian)
- Kralj P (2021) Submarine Stratovolcano Peperite Syn-Formational Alteration - A Case Study of the Oligocene Smrekovec Volcanic Complex, Slovenia, Updates in Volcanology - Transdisciplinary Nature of Volcano Science, Károly Németh, IntechOpen. DOI: 10.5772/intechopen.95480. Available from: <https://www.intechopen.com/chapters/74731>
- Krautblatter M, Dikau R (2007) Towards a Uniform Concept for the Comparison and Extrapolation of Rockwall Retreat and Rockfall Supply. *Geografiska Annaler. Series A, Physical Geography*. 89(1): 21–40. <http://www.jstor.org/stable/4621493>
- Macciotta R, Derek Martin C, Edwards T, Cruden DM, Keegan T (2015) Quantifying Weather Conditions for Rock Fall Hazard Management. *Georisk: Assessment and Management of Risk for Engineered Systems and Geohazards*. 9(3): 171–86. doi: 10.1080/17499518.2015.1061673.
- Matsuoka N (2019) A Multi-Method Monitoring of Timing, Magnitude and Origin of Rockfall Activity in the Japanese Alps. *Geomorphology* 336:65–76. doi: <https://doi.org/10.1016/j.geomorph.2019.03.023>.
- Mikoš M, Petje U, Ribičič M (2006) Application of a rockfall simulation program in an alpine valley in Slovenia. In M Hideaki, Mikoš M (eds.). Disaster mitigation of debris flows slope failures and landslides: proceedings of the INTERPRAEVENT international symposium. Universal Academy Press, Tokyo. pp. 199–211.
- Notti D, Cina A, Manzano A, Colombo A, Bendea I H, Mollo P, Giordan D (2020) Low-Cost GNSS Solution for Continuous Monitoring of Slope Instabilities Applied to Madonna Del Sasso Sanctuary (NW Italy). In *Sensors* (Vol. 20, Issue 1). <https://doi.org/10.3390/s20010289>
- Petley D (2012) Landslides and engineered slopes: protecting society through improved understanding. In LS Eberhardt E, Froese C, Turner AK (eds.). *Landslides and engineered slopes*. CRC Press, London. (pp. 3–13)
- Ribičič M, Vidrih R (1998) Earthquake-triggered Landslides and Rockfalls. *Ujma*. 12: 95–105. (in Slovenian).



# Landslide inventory mapping based on LiDAR data: A case study from Hrvatsko Zagorje (Croatia)

Martin Krkač<sup>(1)</sup>, Sanja Bernat Gazibara<sup>(1)</sup>, Marko Sinčić<sup>(1)</sup>, Hrvoje Lukačić<sup>(1)</sup>, Snježana Mihalić Arbanas<sup>(1)</sup>

1) University of Zagreb, Faculty of Mining, Geology and Petroleum Engineering, Zagreb 10000, Pierottijeva 6, Croatia, +385 98 968 21 71 (mkrkac@rgn.hr)

**Abstract** This paper presents a result of landslide inventory mapping at the Bednja Municipality and Lepoglava City study area in Hrvatsko Zagorje region, NW Croatia. The landslides were interpreted from the high resolution (30 cm) digital elevation model (DEM) and its derivatives (slope and contour map, hillshade). The DEM was interpolated from the point cloud obtained by airborne laser scanning undertaken in spring 2020. In the study area of 20.22 km<sup>2</sup>, the total number of interpreted landslides is 912, making the average density of 45.1 ls/km<sup>2</sup>. The average size of the recorded landslides is 448 m<sup>2</sup>. According to the spatial plans, most of the studied area is covered by forests, agricultural areas, pastures, and artificial areas. The highest density of landslides is also in the forest areas, while the lowest is in the artificial areas. Furthermore, almost 64% of the mapped landslides are located within 50 m of the roads, and more than 39% of the mapped landslides are located within 100 m of the buildings and residential houses. Due to the level of detail provided and its completeness, the presented landslide inventory map is an important tool for risk management at the local level because it gives detailed information necessary for risk evaluation as well as to decide about feasible options for risk mitigation, e.g., stabilisation measures vs relocation of the development to a more favourable location.

**Keywords** landslide inventory, LiDAR, high-resolution DEM, land use

## Introduction

A landslide inventory presents a detailed register of the distribution and characteristics of past landslides (Hervás 2013) in some areas. Preparation of a landslide inventory is an essential part of any landslide zoning (AGS 2007). According to the Guzzetti et al. (2012), landslide inventory maps are prepared for: (i) documenting the extent of landslide phenomena in areas ranging from small to large watersheds and from regions to states or nations; (ii) as a preliminary step toward landslide susceptibility, hazard, and risk assessment; (iii) to investigate the distribution, types, and patterns of landslides in relation to morphological and geological characteristics; and (iv) to study the evolution of landscapes dominated by mass-

wasting processes. Landslide maps, including the landslide inventory map, are an essential tool in landslide risk management, supporting authorities, practitioners and decision-makers in the more appropriate and sustainable land planning and risk mitigation strategy development (Roccati et al. 2021).

In recent years, Light Detection and Ranging (LiDAR) data have been commonly used to map landslide morphology and estimate landslide activity in areas that are partly or completely covered by dense vegetation (Razak et al. 2010). LiDAR is a consolidated remote sensing technique used to obtain digital representations of the topographic surface for areas ranging from a few hectares to thousands of square kilometres (Shan and Toth 2009). The technique uses a laser sensor mounted on an aeroplane or helicopter to measure the distance from the instrument and multiple points on the topographic surface. According to Guzzetti et al. (2012), more than 100 points per square meter can be measured. From elevation point clouds obtained by laser scanning, a detailed digital elevation model (DEM) can be produced and different DEM derivatives such as slope, hillshade or contour maps. High resolution DEM (HRDEM), and its derivatives, enables a recognition of landslide morphology and thus interpretation of landslides.

In this paper, a historical inventory map of the study area in NW Croatia, interpreted from LiDAR HRDEM derivatives, is presented and analysed regarding land-use data. In the context of risk assessment, land-use is a useful indicator of elements at risk, because the overlap of landslide inventory with the basic land use categories (forests, agricultural areas, and artificial surfaces) gives us information on landslide impact (e.g., Bernat Gazibara et al. 2019) that is necessary for following up risk assessment.

## Study area

The study area comprises 20.22 km<sup>2</sup> of the hilly terrain, located in the Hrvatsko Zagorje region (Fig. 1). The area belongs to the Varaždin County, i.e., to the Bednja Municipality (14.28 km<sup>2</sup>) and Lepoglava City (5.94 km<sup>2</sup>). According to the land use data from the Bednja Municipality and Lepoglava City, the study area is covered by forests (52%), agricultural areas and pastures (52%) and artificial areas (8%). Approximately 12% of the area have

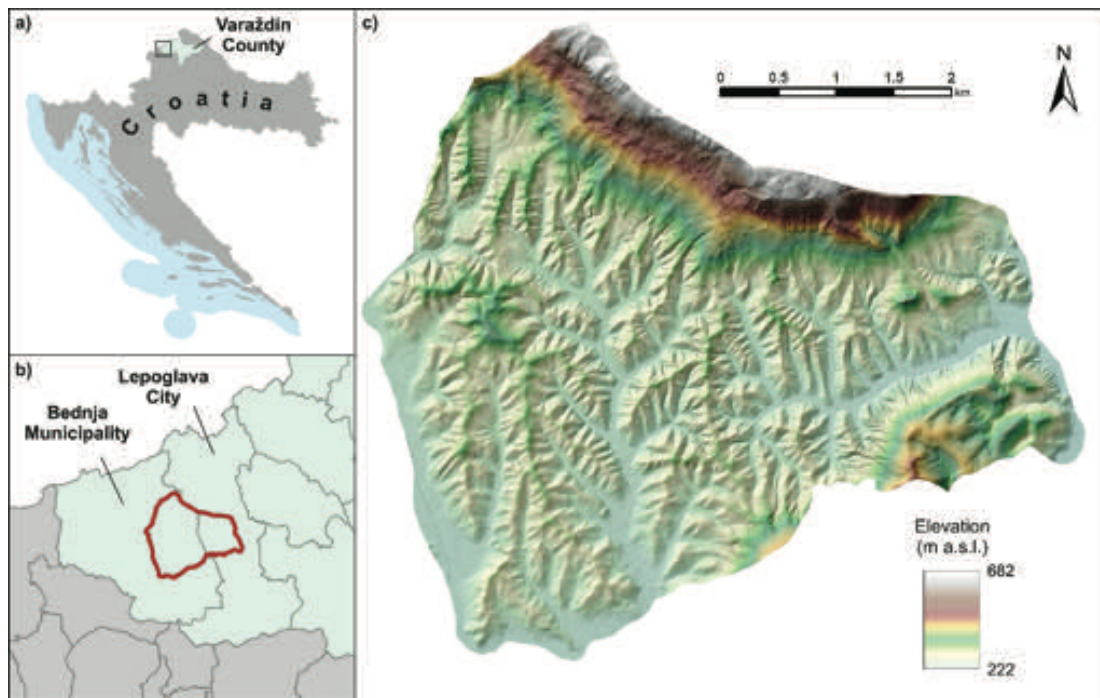


Figure 1 Location of the study area within the administrative units of the Republic of Croatia (a, b) and its relief conditions (c).

slope angles  $<5^\circ$ , 15% of the area  $5^\circ$ – $12^\circ$ , 57% of the area  $12^\circ$ – $32^\circ$  and 14% of the area have slope angles  $>32^\circ$ . The distribution of slope angles makes the study area potentially prone to sliding. The study area is composed of Miocene (78%), Quaternary (14%) and Triassic sediments (7%) according to the Basic Geological Map (Aničić and Juriša 1984; Šimunić et al. 1982). The Triassic sediments, located in the north-eastern part of the study area, are composed of Lower Triassic sandstones, shales, dolomites and limestones and Middle Triassic dolomites, limestones and dolomitised breccias (Šimunić et al., 1982). The Miocene sediments are composed of sandstones, marls, sands and tuffs (Burdigalian), and biogenic, sandy and marly limestones, calcareous marls and sandstones (Tortonian). The Triassic sediments incline mainly towards SW with dip angles  $35^\circ$ – $60^\circ$ . The Miocene sediments are subhorizontal (in W part of the study area) to steeply inclined ( $40^\circ$ – $55^\circ$ ) in NE and E parts of the study area (Aničić and Juriša 1984; Šimunić et al. 1982). The Quaternary sediments, composed of sands, silts and gravels, are located in the valleys around streams and rivers.

Precipitations and human activity are the primary triggers of landslides in NW Croatia (Bernat et al. 2014a). For example, abundant landslide events (Multiple-Occurrence Regional Landslide Events, MORLE) in the hilly areas of NW Croatia occurred in winter 2012/2013 due to the prolonged heavy rainfall periods and the rapid melting of a thick snow cover (Bernat et al. 2014b). Generally, the climate of the study area is continental with a mild maritime influence. The mean annual precipitation for the period of 1949–2020 is 873.7 mm, according to the data from the meteorological station in the City of Varaždin,

located approximately 30 kilometres to the east (DHMZ 2022). The majority of precipitations (approx. 70%) falls mainly from May to November.

## Data and methods

### Lidar data

LiDAR data for the study area was acquired in the framework of the project „Methodology development for landslide susceptibility assessment for land-use planning based on LiDAR technology (LandSlidePlan)“ financed by the Croatian Science Foundation. Airborne laser scanning (ALS) was undertaken in March 2020, which corresponds to the winter leaf-off period in Croatia. The LiDAR system used in this study captured data at a pulse rate of 400 kHz with a surface point horizontal accuracy of 3 cm and vertical accuracy of 4 cm.

The total number of points in the LiDAR point cloud for the area of 20.22 km<sup>2</sup>, was approximately  $6.2 \times 10^8$ . Of all data points, 52.2% were classified as ground (bare earth) points. The average spacing of the ground points was 0.28 m. Those points were used for the creation of the bare-earth digital elevation model (DEM) with a 0.3 m resolution.

### Visual interpretation of landslides on LiDAR DEM

The topographic derivative datasets used to interpret the landslide morphology were hillshade maps, slope maps and contour lines (Fig. 2). In addition, orthophoto images from 2014–2016 were used to check the morphological forms along roads and houses, such as artificial fills and cuts, similar to landslides on DEM derivatives. Derivatives of the LiDAR DEM were computed in ArcGIS 10.8.

Landslide identification on the LiDAR DEM derivatives was manual and GIS-assisted, based on recognising landslide features (e.g., concave main scarps, hummocky landslide bodies and convex landslide toes).

Hillshade maps calculated with different azimuth angles (45°, 135° and 315°) were used to avoid shades covering landslide features hindering the delineation of the landslide boundary (Schulz 2007). A slope map (Fig. 2b) was used to interpret steep areas, which may also indicate scarps, ridges, or landslide toes (Ardizzone et al., 2007). Contour lines with a spacing of 0.5 m were helpful for the identification of concave and convex features such as landslide accumulation and depression zones, respectively. The mapping was performed at a large scale (1:100–1:500) to ensure the correct delineation of the landslide boundaries. Each mapped landslide polygon was assigned with the certainty of landslide identification and precision of mapping.

Anthropogenic landslide conditioning factors analysed in this study were land use data, transport infrastructure network (roads) and buildings (Fig. 3). Land

use data were obtained from the official spatial plans of the Municipality of Bednja (2019) and the City of Lepoglava (2017). Land use classes from both spatial plans were firstly merged using ArcMap 10.8 and then simplified into three categories (artificial areas, agricultural areas and pastures, and forests) as described in Table 1. According to the land use data, 10.5 km<sup>2</sup> (52%) of the study area is covered by forests, 8.07 km<sup>2</sup> (40%) of the area is covered by agricultural areas and pastures and 1.63 km<sup>2</sup> (8%) of the area are artificial surfaces.

Traffic infrastructure was partly obtained from spatial plans and partly by digitising the roads from aerial photos and hillshade maps derived from LiDAR DEM. The total length of the roads covering the study area is 165 km.

The buildings in the study area were obtained from the LiDAR point cloud points classified as buildings according to the ASPRS (2011). The points classified as buildings were converted to polygon shapefiles in ArcMap 10.8 and checked on aerial photos. The total number of mapped buildings in the study area is 1849.

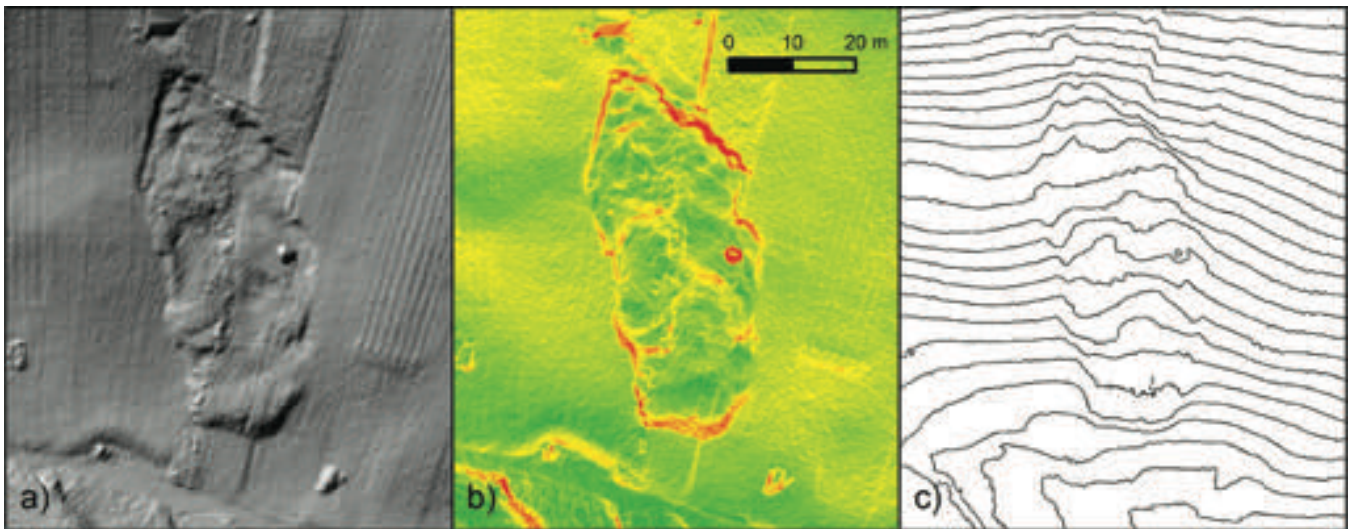


Figure 2 Landslide identified on the three different topographic derivative DTM maps: (a) hillshade map; (b) slope map; and (c) contour map (0.5 m spacing).

Table 1 Land use classes from spatial plans of Municipality of Bednja, City of Lepoglava and merged land use classes of the study area.

Merged classes	Municipality of Bednja	City of Lepoglava
Artificial areas	Settlement area with constructions	Settlement area with constructions
	Construction site	Construction site outside of the settlement area
	Graveyard	Graveyard
Agricultural areas and pastures	Valuable agricultural areas	Valuable agricultural area
	Other agricultural areas	Other agricultural area
	Other agricultural areas and forests	Other agricultural areas and forests
	Settlement area without constructions	Settlement area without constructions
		Areas and buildings related to agricultural activities
Forest areas	Commercial forest	Commercial forest
	Commercial forest under management of the Republic of Croatia	Other forests

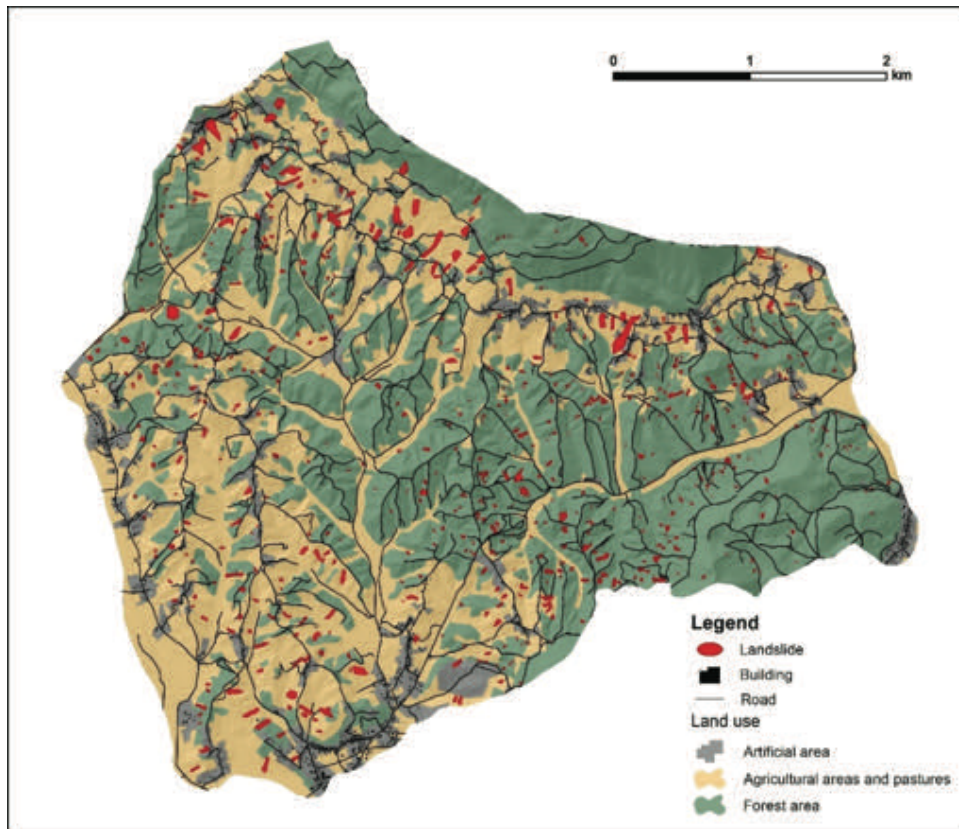


Figure 3 Spatial distribution of the anthropogenic landslide causal factors in the study area and landslide inventory mapped on the LiDAR DEM.

## Results

### Landslide inventory map

Initially, 904 landslides were mapped on the LiDAR DEM derivatives of the study area. 24% (214) of randomly selected landslides were checked on the field. From the 214 checked phenomena, 20 phenomena were rejected as landslides. Additionally, 28 phenomena were mapped in the field and added to the landslide inventory, making the total number of landslides in the inventory 912 (Fig. 3).

The total area of mapped landslides is 0.408 km<sup>2</sup>, or 2.02% of the study area. The mean landslide density is 45.1 slope failures per square kilometre. The size of the recorded landslides ranges from a minimum value of 3.3 m<sup>2</sup> to a maximum of 13,779 m<sup>2</sup>, whereas the average area is 448 m<sup>2</sup> (median = 173 m<sup>2</sup>, std. dev. = 880 m<sup>2</sup>). The most frequent landslides in the inventory have an area of approx. 200 m<sup>2</sup>, and almost 85% of the landslide bodies showed a size between 40 and 2,000 m<sup>2</sup>. The small size of the landslides is probably the result of geological conditions (mainly Miocene marls covered with residual soils) and geomorphological conditions, where the differences between the valley bottoms and the top of the hills are rarely higher than 100 meters.

The frequency-size distribution of all mapped landslides in the pilot area (Fig. 4) shows two scaling regimes: a positive power-law scaling for small landslides and a negative power-law scaling for medium and large

landslides. The transition between the positive and the negative power-law relations can be used to distinguish between small and medium landslides. Based on the rollover at approximately 200 m<sup>2</sup>, 48% of the mapped landslides are small (<200 m<sup>2</sup>) and 52% are medium and large (>200 m<sup>2</sup>) in size. The prevailing dominant types of landslides are probably shallow soil slides.

### The relative relationship between landslides and types of land-use

The analyses of landslide statistics relative to land-use types were performed by using points, which represent landslide polygon centroids. The landslide density per land-use unit (Tab. 2) shows that 73.8% of the mapped landslides appear in forest areas, 23.6% on agricultural areas and pastures, and only 2.6% on artificial surfaces. The mean landslide density in forests is 64 ls/km<sup>2</sup>, more than two times higher than in agricultural areas and pastures (26.7 ls/km<sup>2</sup>) and almost five times higher than in artificial areas (14.7 ls/km<sup>2</sup>). One of the possible explanations is that LiDAR-based landslide inventories can often be incomplete on settlements and arable lands due to frequent anthropogenic influences (Bell et al. 2012; Bernat et al. 2019; Petschko et al. 2015; Steger et al. 2016). Another probable reason is that the higher landslide density in forests is associated with prevailing steep slopes and forest gullies (the average slope angle of the forest class in the study area is 25°).

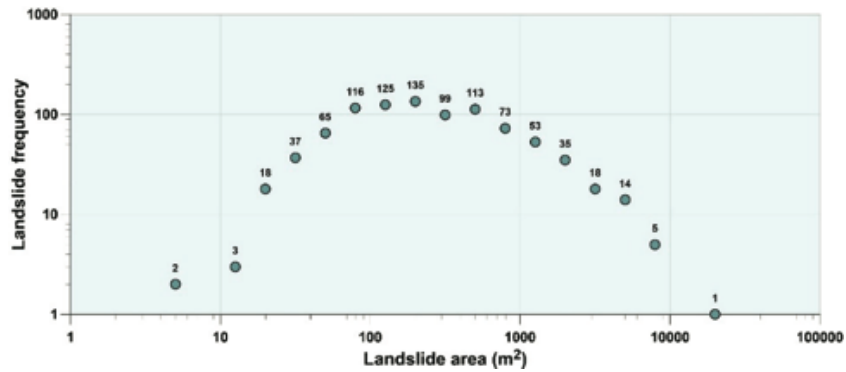


Figure 4 Frequency–size distribution of all mapped landslides in the study area (20.22 km<sup>2</sup>) of the Hrvatsko Zagorje region.

In contrast, the artificial areas and agricultural areas and pastures in the study area are likely to be associated with the less favourable conditions for landslide initiation, i.e. on the surfaces with more gentle slope angles (average slope angle for artificial areas is 14°, and for agricultural areas and pastures 16°).

Analysis of the landslide distribution in the study area shows that more than 56% of the mapped landslides are located within 25 to 75 m from the roads (approx. 45% of the study area). Additionally, more than 39% (314) of the mapped landslides are located within 100 m of the buildings (approx. 34% of the study area).

Table 2 Landslide density per land-use unit in the study area.

Anthropogenic factors	Area (km <sup>2</sup> )	Area (%)	Landslide number (%)
<b>Land use</b>			
Forest areas	10.5	52.1	73.8
Agricultural areas and pastures	8.1	39.9	23.6
Artificial areas	1.6	8.1	2.6
<b>Distance from roads</b>			
0-10 m	3.2	15.7	7.9
10-25 m	4.2	20.8	19.7
25-50 m	5.6	27.5	32.9
50-75 m	3.6	18.0	23.5
75-100 m	2.0	10.0	10.9
>100 m	1.6	8.1	5.2
<b>Distance from buildings</b>			
0-10 m	0.9	4.6	0.8
10-25 m	1.3	6.4	3.3
25-50 m	2.1	10.1	10.0
50-75 m	2.0	9.6	10.6
75-100 m	1.7	8.4	9.8
>100 m	12.3	60.9	65.6

**Conclusions**

LiDAR DEM map and its derivatives were used for detailed landslide mapping of the hilly area in the Hrvatsko Zagorje region, NW Croatia. Visual interpretation of the 20.22 km<sup>2</sup> area resulted in a landslide inventory map with 912 landslides and a mean landslide density of 45.1 ls/km<sup>2</sup>.

LiDAR DEM map with a resolution of 0.3 m, and its derivatives, proved to be a valuable tool for mapping landslides in the Hrvatsko Zagorje region, even for landslides of the small area. The area of the smallest mapped landslide is 3.3 m<sup>2</sup>, and almost 50% of the landslides are smaller than 200 m<sup>2</sup>. The frequency-size distribution shows that the landslide inventory of the study area is substantially complete. Most of the mapped landslides are historical landslides. However, the presence of small landslides and landslides with a significant degree of preserved morphology indicates that the inventory map includes relatively recent seasonal landslides. This seasonal inventory probably represents landslides (re)activated in winter 2012/2013 and in spring 2018.

Most of the mapped landslides are located in forest areas, showing one of the advantages of using LiDAR in the Hrvatsko Zagorje region that enables mapping landslides under dense vegetation cover. Only 26% of landslides are located in artificial areas, agricultural areas and pastures. The difference in landslide density (frequency) between land use classes indicates that landslide inventories in artificial areas, agricultural areas, and pastures are often incomplete due to frequent anthropogenic influences and changes in natural morphology. However, these areas are also less favourable for landslide initiation because of more gentle relief with prevailing smaller slope angles.

Even though the landslide density is two to five times higher in forest areas than in agricultural areas, pastures and artificial areas, the landslides still present a significant threat to transportation infrastructure and buildings. Spatial analyses show that almost 64% of the mapped landslides are located within 50 m from the roads, and more than 39% of the mapped landslides are located within 100 m from the buildings and residential houses.

Due to the level of detail provided and its completeness, presented landslide inventory presents an important tool for the following risk mitigation measures: (i) avoid the risk by measures applied in the process of spatial and urban planning; (ii) reduce the frequency of sliding and its consequences by stabilisation measures; (iii) manage the risk by establishing monitoring and warning systems; and (iv) transfer the risk by, e.g., by the provision of insurance to cover potential property damage.

Because of a variety of possible applications, the presented landslide inventory map is intended for numerous users from spatial and urban planning, construction, and civil protection. In addition, the same map also provides valuable and necessary data for preparing a landslide susceptibility map in the detailed scale for local application, another essential tool for spatial development and land-use planning.

## Acknowledgments

This work has been fully supported by Croatian Science Foundation under the project “Methodology development for landslide susceptibility assessment for land use planning based on LiDAR technology” (LandSlidePlan IP-2019-04-9900).

## References

- AGS (2007) Guideline for Landslide Susceptibility, Hazard and Risk Zoning for Land Use Management. Australian Geomechanics 42(1): 13–36.
- ASPRS (2011) LAS specification (ver. 1.4–R13). American Society for Photogrammetry and Remote Sensing. 27 p.
- Aničić B, Juriša M (1984) Basic geological map, scale 1:100,000, Rogatec, Sheet 33-68 [in Slovenian]. Geological Bureau, Ljubljana, Geological Bureau, Zagreb, Federal Geological Bureau, Beograd. (in Croatian)
- Ardiszone F, Cardinali M, Galli M, Guzzetti F, Reichenbach P (2007) Identification and mapping of recent rainfall-induced landslides using elevation data collected by airborne LiDAR. *Natural Hazards and Earth System Sciences*. 7: 637–650. doi:10.5194/nhess-7-637-2007
- Bell R, Petschko H, Röhrs M, Dix A (2012) Assessment of landslide age, landslide persistence and human impact using airborne laser scanning digital terrain models. *Geografiska Annaler: Series A, Physical Geography*. 94: 135–156. doi:10.1111/j.1468-0459.2012.00454.x
- Bernat S, Mihalić Arbanas S, Krkač M (2014a) Inventory of precipitation triggered landslides in the winter of 2013 in Zagreb (Croatia, Europe). *Landslide science for a safer geoenvironment, volume 2: Methods of landslide studies*. Springer, Cham. pp. 829–836.
- Bernat S, Mihalić Arbanas S, Krkač M (2014b) Landslides triggered in the continental part of Croatia by extreme precipitation in 2013. *Engineering geology for society and territory, volume 2: Landslide processes*. Springer, Heidelberg. pp. 1599–1603.
- Bernat Gazibara S, Krkač M, Mihalić Arbanas S (2019) Landslide inventory mapping using LiDAR data in the City of Zagreb (Croatia). *Journal of maps*. 15(2): 773–779. <https://doi.org/10.1080/17445647.2019.1671906>
- DHMZ (2022) Climatological data, Varaždin. [https://meteo.hr/klima.php?section=klima\\_podaci&param=k1&Grad=varazdin](https://meteo.hr/klima.php?section=klima_podaci&param=k1&Grad=varazdin). (in Croatian)
- Furlani S, Ninfo A (2015) Is the present the key to the future? *Earth-Science Reviews*. 142: 38–46. <https://doi.org/10.1016/j.earscirev.2014.12.005>
- Guzzetti F, Mondini A C, Cardinali M, Fiorucci F, Santangelo M, Chang K-T (2012) Landslide inventory maps: New tools for an old problem. *Earth-Science Reviews*. 112(1-2): 42–66. <https://doi.org/10.1016/j.earscirev.2012.02.001>.
- Hervás J (2013) Encyclopedia of Natural Hazards. *Encyclopedia of Earth Sciences Series*. Bobrowsky P T (ed). Springer, Dordrecht. [https://doi.org/10.1007/978-1-4020-4399-4\\_214](https://doi.org/10.1007/978-1-4020-4399-4_214)
- Petschko H, Bell R, Glade T (2015) Effectiveness of visually analysing LiDAR DTM derivatives for earth and debris slide inventory mapping for statistical susceptibility modeling. *Landslides*. 5: 857–872. doi:10.1007/s10346-015-0622-1.
- Razak K A, Straatsma M, van Westen C J, Malet J P, de Jong S M (2011) Airborne laser scanning of forested landslides characterisation: terrain model quality and visualisation. *Geomorphology*. 126(1-2): 186–200. <https://doi.org/10.1016/j.geomorph.2010.11.003>
- Roccati A, Paliaga G, Luino F, Faccini F, Turconi L (2021) GIS-Based Landslide Susceptibility Mapping for Land Use Planning and Risk Assessment. *Land*. 10(162): 1–28. <https://doi.org/10.3390/land10020162>
- Schulz W H (2007) Landslide susceptibility revealed by LiDAR imagery and historical records, Seattle, Washington. *Engineering Geology*. 89: 67–87. doi:10.1016/j.enggeo.2006.09.019
- Shan J, Toth C K (2009) *Topographic Laser Ranging and Scanning: Principles and Processing*. CRC Press, Taylor and Francis Group. 590 p.
- Steger S, Brenning A, Bell R, Petschko H, Glade T (2016) Exploring discrepancies between quantitative validation results and the geomorphic plausibility of statistical landslide susceptibility maps. *Geomorphology*. 262: 8–23. doi:10.1016/j.geomorph.2016.03.015
- Šimunić A, Pikija M, Hečimović I (1982) Basic geological map, scale 1:100,000, Varaždin, Sheet 33-69. Geological Bureau, Zagreb, Federal Geological Bureau, Beograd. (in Croatian)



# Influence of expert knowledge on completeness and accuracy of landslide inventory maps – Example from Istria, Croatia

Hrvoje Lukačić<sup>(1)</sup>, Sanja Bernat Gazibara<sup>(1)</sup>, Marko Sinčić<sup>(1)</sup>, Martin Krkač<sup>(1)</sup>, Željko Arbanas<sup>(2)</sup>, Petra Jagodnik<sup>(2)</sup>, Vedran Damjanović<sup>(1)</sup>, Snježana Mihalić Arbanas<sup>(1)</sup>

1) University of Zagreb, Faculty of Mining, Geology and Petroleum Engineering, Department of Geology and Geological Engineering, Zagreb, Pierottijeva Street 6, Croatia, +385 1 5535 788 (hrvoje.lukacic@rgn.unizg.hr)

2) University of Rijeka, Faculty of Civil engineering, Department of Geotechnics, Rijeka, Croatia

**Abstract** This paper presents the application of Light Detection and Ranging (LiDAR) data for landslide identification and mapping in the pilot area at the Istria Peninsula (Croatia) and the analyses on the influence of expert knowledge on the quality of landslide inventory. Visual interpretation of landslides was carried out on high-resolution airborne laser scanning (ALS) LiDAR dataset. Scanning was taken in March 2020 for the pilot area in the City of Buzet. Based on the characteristics of the acquired LiDAR Point Cloud, a bare-earth digital elevation model (DEM) with 30 cm resolution was created. Different topographic derivative datasets such as slope, hillshade, contour lines, and roughness maps were created to interpret the LiDAR data. Eight experts with different levels of expert knowledge on LiDAR interpretation were given one week to carry out visual identification and mapping of potential landslides in the pilot area (0.3 km<sup>2</sup>) at a large scale (1:200) to provide detailed landslide mapping. Statistical analyses were performed based on the collected data to determine differences in the mapping accuracy and the number of recognized landslides by the experts. Results show that the experts familiar with the geology of the study area and potential landslide mechanics obtained better results than the experts who mapped landslides based on only ordinary topographic and geomorphological features specific for landslides.

**Keywords** landslides, inventory mapping, remote sensing, LiDAR

## Introduction

Landslide inventory maps present essential input parameters for multiple regional spatial analyses such as landslide susceptibility, hazard, and risk assessment (Guzzetti et al. 2000; van Westen et al. 2006) and to establish a pattern between landslide occurrence and geological and geomorphological conditions. Unfortunately, Croatian local governments do not have reliable data about past landslide locations, so the main problem with the current landslide hazard and risk

management practice in Croatia is insufficient landslide inventory archives (Mihalić Arbanas et al. 2016). However, the traditional methodology for producing landslide inventory maps includes field mapping, which produces a limited amount of data, in case of inaccessible and overgrown areas and, consequently, only a rough estimation of a number of landslides. Therefore, the traditional engineering geological field mapping is time-consuming and ineffective for large study areas.

Remote sensing methods, such as airborne LiDAR, are used for visual landslide interpretation with high accuracy and precision, resulting in substantially complete inventory maps (Đomlija, 2018; Bernat Gazibara, 2019). LiDAR is a fully automated, modern remote sensing technology that uses light beams in a pulsed laser to acquire ground elevation data (Wehr and Lohr, 1999). Based on the characteristics of the acquired LiDAR Point Cloud, primarily due to high point density, it is possible to produce high-resolution Digital Terrain Models (DTM). High-resolution Digital Terrain Models are used in various studies, especially landslide mapping (Schultz, 2007; Bell et al. 2012; Đomlija, 2018; Bernat Gazibara, 2019). However, to use high-resolution LiDAR Point Cloud for such purposes is mandatory to automatically filter vegetation and all other above-earth surface objects, resulting in a bare-earth DEM. Landslides are usually located in forest areas or covered by dense vegetation making LiDAR the only appropriate remote sensing tool in landslide mapping (Gold, 2004). Several different morphometric maps can be derived for the LiDAR dataset, such as slope, hillshade, contour, and roughness map to present specific landslide topography.

This study aims to demonstrate how expert knowledge on LiDAR data interpretation and familiarity with geological and geomorphological conditions of the study area influences the results of landslide identification and mapping. The paper hypothesis is that the joint landslide identification and mapping by several experts with different experiences in LiDAR mapping and knowledge about a research area will result in higher accuracy of landslide inventory maps.

## Study area

The City of Buzet is located in the northern part of the Istria Peninsula in the western part of Croatia. From the geomorphological point of view, it is the part of the mega-geomorphological region of the Dinaric Mountain Belt and macro-geomorphological region of the Istrian Peninsula with the Kvarner Bay coastal region and archipelago (Bognar, 2001). The study area comprises 19,96 km<sup>2</sup> of the hilly area (Fig. 1), southwest of the Čičarija Mountain Range. According to Corine Land Cover (2018) the current land use of the investigated area includes 14.2 km<sup>2</sup> of forests, 5.8 km<sup>2</sup> of agricultural areas, and 0.004 km<sup>2</sup> of water bodies. Therefore, according to the Corine Land Cover classification, there are no artificial surfaces.

Slope angle in the wider study area is steeper than 5° in the 87% of the area, while the prevailing slope angles have a range of 5°–12° (26% of the study area) and 12°–32° (47% of the study area), making this area potentially prone to landslides (Fig. 1a).

The wider study area (Fig. 1b) is dominantly composed of Middle Eocene sediments (86% of the study area) (Pleničar et al. 1969). The Middle Eocene series consists of an alteration of marls and sandstones (flysch deposits), breccia deposits, nummulitic limestone, and limestone deposits. Marls are clayey, greenish to yellowish-grey, sporadically loose due to the weathering, sporadically compact due to higher calcium carbonate content. Sandstones are fine-grained, blue to yellowish and grey. They are very hard due to their higher calcium carbonate content. If there is more lime binder present, they turn into sandy limestone. They appear in layers from 1 cm to 1-2 m thick. The total thickness of this part of the Eocene clastic sediments is about 400 m (Pleničar et al. 1969).

Characteristics of flysch rock mass imply that lithological contact between the highly weathered flysch deposits and fresh Eocene flysch is highly susceptible to landsliding. Landslides in such geological and

geomorphological environments are mainly small to medium-sized landslides.

According to Köppen-Geiger climate classification (Köppen 1936), the climate of the City of Buzet belongs to the "Cfa" climate class, which is temperate with no dry season, hot summer and coldest months averaging above 0°C. Mean annual precipitation (MAP) is 1200 – 1300 mm, and landslides are primarily induced by rainfall (Bernat et al. 2014a).

## Methodology

LiDAR data for the study area were acquired in the framework of the project "Methodology development for landslide susceptibility assessment for land-use planning based on LiDAR technology (LandSlidePlan IP-2019-04-9900) funded by the Croatian Science Foundation". Airborne laser scanning (ALS) was taken in March 2020, using Eurocopter EC 120B equipped with Hasselblad camera and Riegl LMS-Q780 long-range airborne laser scanner. The LiDAR system used in this study captured data at the pulse rate frequency of 400 kHz with the surface point horizontal accuracy of 3 cm and vertical accuracy of 4 cm. Final Point Cloud has approximately 623 million points with a point density of 16,09 pt/m<sup>2</sup>, resulting in an average point spacing of 18 cm. Based on the point density and average point spacing, the final LiDAR dataset was used to create a bare-earth DEM with a 30 cm resolution using the kriging interpolation method.

The hillshade, slope, contour, curvature, and surface roughness maps were derived from the 30 cm resolution digital terrain model (Fig. 2). Derivatives of the LiDAR-based DTM were computed in ArcGIS 10.8 software (2020) from the LiDAR DTM. For calculating curvature and surface roughness, an additional ArcGIS Toolbox Geomorphometry and Gradient Metrics (Evans et al. 2014) were used.

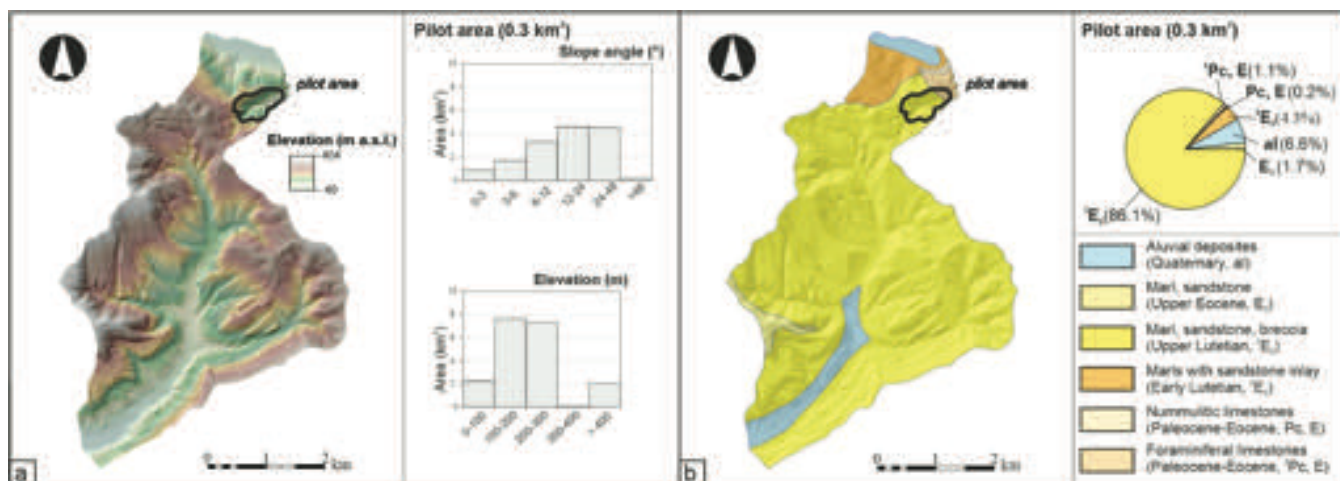


Figure 1 Study area in the City of Buzet with the outline of the pilot area (black line): (a) relief map; (b) geological map (Pleničar et al., 1973).

For this paper, landslide identification was done for the 0.3 km<sup>2</sup> on the topographic derivative maps. Landslide mapping is based on identifying the main landslide features such as main and minor scarps, sudden changes in a slope topography, and landslide foots. Hillshade maps produced with different azimuth angles of the light source (45° and 315°) with the altitude angle of the light source above the horizon set to 45° were used to avoid shades covering landslide features. Along with the hillshade map, the slope map (Fig. 2b) and curvature map (Fig. 2c) were used to interpret changes in the slope topography, such as main landslide scarp and landslide foot (Ardizzone et al. 2007). Terrain roughness map computed by methodology proposed by Riley et al. (1999) was used to visualize elevation or slope angle changes to identify unstable slopes.

Eight experts with different levels of expert knowledge in LiDAR interpretation and different levels of knowledge of the study area were given one week to carry out the visual identification and mapping of potential landslides on the pilot area (0.3 km<sup>2</sup>). Seven experts independently mapped the landslides on the pilot area, while Expert 8 represents the joint mapping procedure of Experts 5 and Expert 6 mentored by an Expert with high LiDAR mapping experience in a similar geomorphological environment. Experience in landslide identification on the topographic derivative maps was expressed as 'high', 'medium', 'low', and 'no experience' for each Expert (Table 1). LiDAR mapping experience was defined as 'high' for experts who are very experienced in landslide mapping, 'medium' for experts familiar with landslide mapping but didn't do it regularly, and 'low' for experts who just recently started working with LiDAR data. 'No experience' category was reserved for the Expert who mapped landslides for the first time using a LiDAR dataset.

On the other hand, research knowledge of the study area was expressed as 'high', 'medium', and 'low' for each Expert (Table 1). Research knowledge of the geological and geomorphological conditions of the study area was defined as 'high' for experts who are familiar with the geological and geomorphological setting and have previous experience with landslide occurrences in similar conditions, and 'medium' for experts who have some experience and basic knowledge about landslide occurrences in similar geological and geomorphological conditions. Finally, research knowledge about geological and geomorphological conditions was expressed as 'low' for experts unfamiliar with the study area.

Landslide mapping was done at a large scale (1:200 - 500) to ensure detailed mapping of landslide boundaries. In addition, the orthophoto map from 2019 was used to check geomorphological forms, which can have a similar appearance to landslides on DTM derivatives.

Landslides identified by experts at the LiDAR dataset were checked during the field survey in January 2022. Boundaries of the checked landslides were eventually modified in the field based on landslide morphology, so

the resulting landslide inventory consisted of correctly identified and mapped landslides.

Statistical analyses were performed based on the collected data using the polygon-based approach to compare different experts inventory maps with valid inventory maps (Van Den Eeckhaut et al. 2005). The analysis included determining the number of mapped landslides and the total area affected by landslides for each Expert. Processed data were then compared with the verified landslides in the inventory. Furthermore, the number of correctly identified landslides were determined for each Expert. Finally, for each Expert, the ratio of correctly identified landslide area and a total area of confirmed landslides was determined, Table 2.

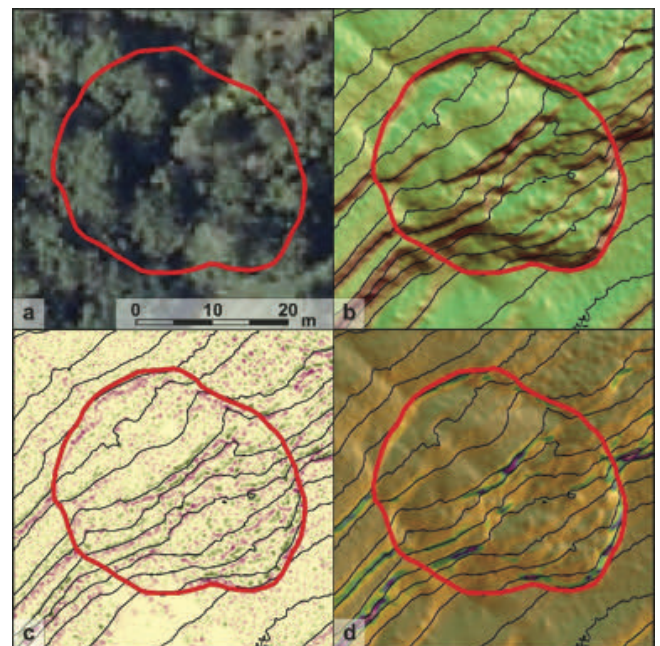


Figure 2 Composite display of the landslide (40 × 40 m) at an orthophoto and three different topographic derivative DTM maps with contour lines (1 m spacing): (a) orthophoto from 2019; (b) transparent slope map on the hillshade map; (c) curvature map; and (d) transparent surface roughness map on the hillshade map.

Table 1 Levels of expert knowledge in LiDAR mapping and research knowledge of study area.

Expert no.	LiDAR mapping experience	Researcher knowledge on study area
Expert 1	Low	High
Expert 2	Medium	Medium
Expert 3	High	Medium
Expert 4	High	Medium
Expert 5	Low	Low
Expert 6	Low	Low
Expert 7	No experience	Low
Expert 8	Medium	High

## Results

The landslide inventory map has been produced on a small part (0.3 km<sup>2</sup>) of the City of Buzet area. The initial landslide inventory map produced by eight experts consisted of 178 landslides, with a total landslide area around 0.037 km<sup>2</sup> which covers approximately 11.96% of the mapping area (0.30 km<sup>2</sup>). Mapped landslides extend from 5.00 m<sup>2</sup> mapped by Expert 2, to 5792.00 m<sup>2</sup> mapped by Expert 1. Fig. 3 shows all 178 initially mapped landslides in the pilot area.

Based on the collected data by seven experts, field verification of the produced landslide inventory was undertaken. Because the field verification was carried out cautiously and systematically, not all the landslides were verified during this paper preparation. The field verification included checking landslide boundaries and modifying them according to landslide morphology in the field. As shown in Fig. 3, approximately 52.2% of landslides were verified. During the field verification of landslides in the central part of the pilot area, it was noticed that a large number of landslides was mapped on slopes with active erosion. Also, it was noticed that the detailed mapping of landslide boundaries at erosion affected slopes is not unambiguously because landslide boundaries are subject to changes during a short period of time. Therefore, it was decided to exclude all previously mapped landslides within the erosion areas and declare that they are a part of multi-hazard areas, including erosion and landslides processes and badland morphology. After the field verification, landslides were divided into four categories: confirmed landslides (19.66% of the total number of mapped landslides), confirmed landslides with modified boundary (5.62%), unconfirmed landslides (9.55%) and abolished landslides within multi-hazard areas (17.42%). The remaining 48.8% of landslides were not verified during the field survey and were excluded from further analysis.

For each Expert, an average of 72% of its mapped landslides were verified. As indicated in Table 2 number of verified landslides ranges from seven, for Expert 7, to 49 for Expert 8. It is important to emphasize that a verified landslide mapped on the field can contain more than one landslide indicated by an expert on LiDAR DTM. That explains the more significant number of verified landslides for some experts than the smaller number of verified landslides for other experts. For example, Expert 1 mapped one landslide of 1687.74 m<sup>2</sup> while Expert 2, within the same boundaries, mapped three smaller landslides with areas ranging from 102.36 m<sup>2</sup> to 532.54 m<sup>2</sup>. Furthermore, the average size of verified landslides ranges from 166.49 m<sup>2</sup>

for Expert 2 up to 1434.77 m<sup>2</sup> for Expert 1, which indicates that Expert 2 mapped primarily small to medium-sized landslides. On the other hand, Expert 1 identified and mapped predominantly large landslides.

The landslide mapping analyses included overlapping individual expert inventories with the inventory that includes only confirmed landslides and confirmed landslides with modified boundaries, i.e. confirmed landslide inventory. The pixel-based approach was applied, and the number of landslide pixels mapped by experts within the limits of confirmed landslides was calculated. As the result, the total calculated area affected by confirmed landslides was 0.007 km<sup>2</sup> or approx. 2.28% of the pilot area. Based on the confirmed landslide inventory, statistical analysis was undertaken. Analysis shows significant discrepancies between eight experts in the landslide mapping accuracy. As shown in Table 2 percentage of correctly mapped landslides varies significantly between experts. The accuracy and precision of landslide mapping depend on LiDAR mapping experience and knowledge about geological settings and geomorphological processes in a study area. Expert 8 has the highest percentage of correctly mapped landslide area (70.04 % of individual landslide inventory). This result can be explained with repeated mapping procedures by two experts, Expert 5 and Expert 6, who were mentored by the Expert with high LiDAR mapping experience in similar geomorphological environments. On the other hand, Expert 7 has the smallest percentage of correctly mapped landslides, only 20.37% of landslide area matched with confirmed landslide inventory, which is expected since Expert 7 has the lowest knowledge on geological and geomorphological characteristics of the study area and experience with LiDAR mapping. Other results range from 25.47% for Expert 1 (low LiDAR mapping experience and high researcher knowledge of study area) to 49.16% for Expert 5 (low LiDAR mapping experience and low researcher knowledge of study area). Expert 2 (medium LiDAR mapping experience and medium researcher knowledge of study area) and Expert 3 (high LiDAR mapping experience and medium researcher knowledge of study area) have a similar percentage of correctly mapped landslides which is 41.40% for Expert 2 and 39.94% for Expert 3. Based on the results presented in Table 2, it can be concluded that the percentage of correctly mapped landslide area directly depends on LiDAR mapping experience and researcher knowledge of the study area. Also, it can be concluded that if more than one expert is involved in landslide mapping in the study area, the result will be a more accurate landslide inventory.

Table 2 Landslide mapping results based on expert knowledge on LiDAR mapping and research knowledge of the study area.

Expert no.	Number of mapped landslides	Number of verified landslides	Minimal area of confirmed landslide (m <sup>2</sup> )	Maximal area of confirmed landslide (m <sup>2</sup> )	Average area of confirmed landslides (m <sup>2</sup> )	Correctly mapped landslide area (m <sup>2</sup> )	Percentage of correctly mapped landslide area (%)
Expert 1	16	13	440.42	5791.88	1434.77	1822.79	25.47
Expert 2	76	38	5.04	681.72	166.49	2962.98	41.40
Expert 3	44	29	11.87	949.78	194.19	2858.13	39.94
Expert 4	21	18	23.00	663.00	223.06	2079.00	29.05
Expert 5	49	36	14.00	1134.00	276.47	3518.37	49.16
Expert 6	26	20	42.00	1208.00	527.75	2348.19	32.81
Expert 7	7	7	120.00	1437.00	724.00	1457.46	20.37
Expert 8	109	49	15.88	1217.40	253.06	5012.19	70.04

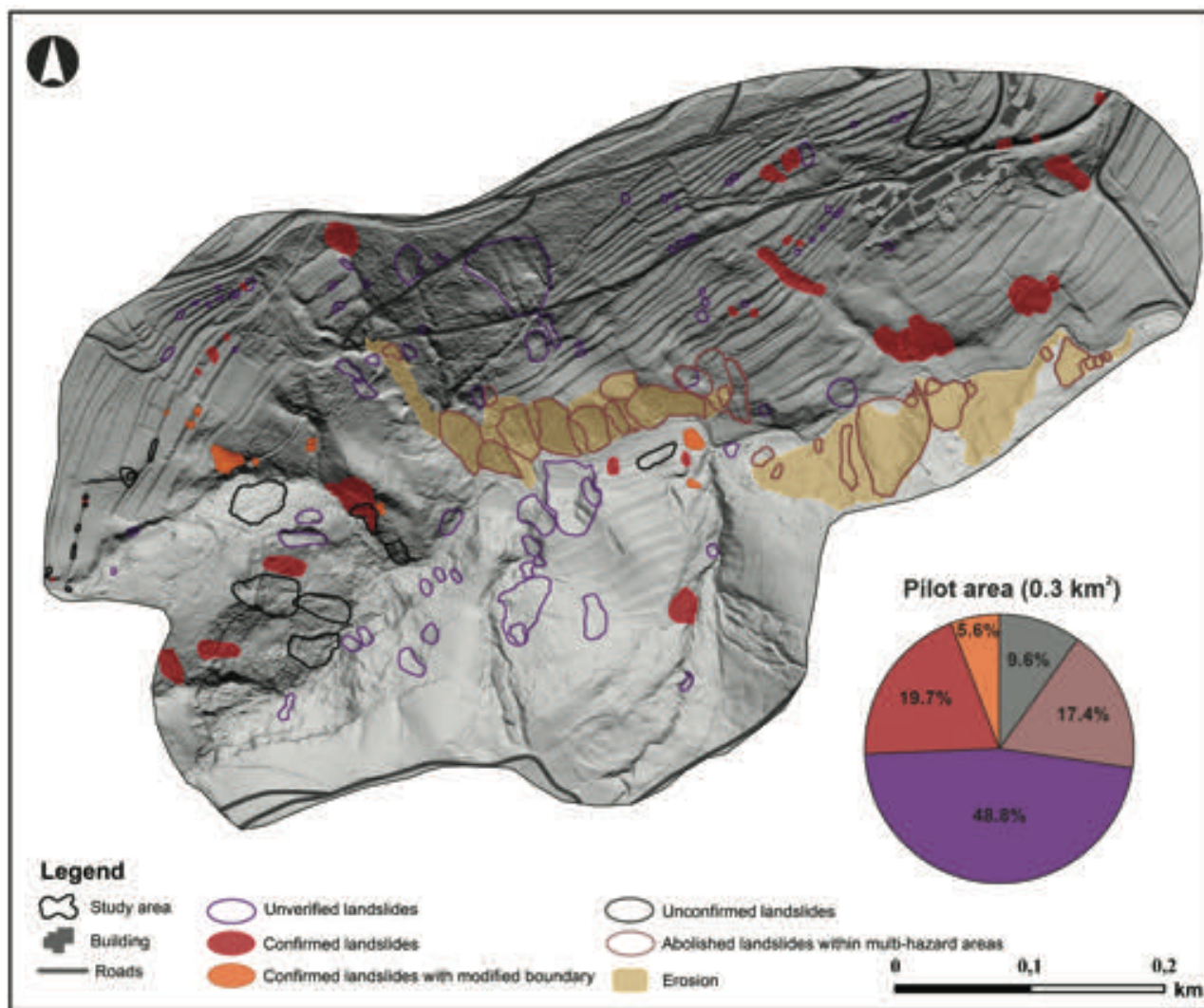


Figure 3 Landslide inventory map produced by the experts with indicated confirmed landslides and erosion.

## Discussion and conclusion

This study demonstrated the efficiency and accuracy of the airborne LiDAR data on landslide identification and mapping and the influence of the expert knowledge on the research results. Landslide interpretation of the pilot area (0.3 km<sup>2</sup>) was done using the 30 cm DTM and its derivatives such as the hillshade, slope and contour maps. Seven experts with different levels of expert knowledge in LiDAR interpretation and study area were given one week to carry out visual identification and mapping of potential landslides to provide detailed landslide mapping at a large scale of DTM maps. The initial landslide inventory map produced by seven experts consists of 178 landslides making up the total landslide area of 0.037 km<sup>2</sup>. In addition, the field verification was conducted on 93 landslides or 51.2 % of the total number of landslides in the inventory. Based on the total number of verified landslides, 37.6 % were confirmed, 10.8% landslides were confirmed with modification of landslides boundaries, 33.3 % of landslides were abolished since a landslide location was inside multi-hazard areas, and 18.3 % of landslides remained unconfirmed. The number of unconfirmed and confirmed landslides with modified landslide boundary during the in situ verification pointed that the common recommendation about verification of 10% of landslides in the final landslide inventory, is not sufficient in the pilot area as well as areas with complex geology settings and multi-hazard processes. Therefore, to ensure the accuracy of the landslide inventory map, it is necessary to increase the ratio of in situ verified and confirmed landslides related to the total number of landslides in an inventory map.

The analysis of landslides mapped by seven experts showed that the experience and knowledge about a research area play a crucial role in landslide recognition in complex geological conditions such as flysch formation in the City of Buzet wider area. Furthermore, obtained results for Expert 8, which represents the joint mapping procedure of three Experts, show that the same pilot area needs to be mapped multiple times to accomplish a high accuracy landslide inventory map.

## Acknowledgements

This work has been fully supported by Croatian Science Foundation under the project Methodology development for landslide susceptibility assessment for land use planning based on LiDAR technology (LandSlidePlan IP-2019-04-9900).

## References

Ardizzone F, Cardinali M, Galli M, Guzzetti F, Reichenbach P (2007) Identification and mapping of recent rainfall-induced landslides using elevation data collected by airborne Lidar. *Natural Hazards and Earth System Sciences*. 7: 637–650.

Bell R, Petschko H, Röhrs M, Dix A (2012) Assessment of landslide age, landslide persistence and human impact using airborne laser

scanning digital terrain models. *Geografiska Annaler: Series A, Physical Geography*. 94(1): 135-156.

Bernat Gazibara S (2019) Methodology for landslide mapping using high resolution digital elevation model in the Podsljeme area (City of Zagreb). PhD thesis, Faculty of Mining, Geology and Petroleum Engineering, Zagreb, Croatia. (in Croatian)

Bernat Gazibara S, Krkač M, Mihalić Arbanas S (2019) Landslide inventory mapping using LiDAR data in the City of Zagreb (Croatia). *Journal of Maps*. 15: 773-779.

Bernat S, Mihalić Arbanas S, Krkač M (2014) Inventory of precipitation triggered landslides in the winter of 2013 in Zagreb (Croatia, Europe). *Landslide Science for a Safer Geoenvironment*, Volume 2: Methods of Landslide Studies, 2-6 June 2014. Beijing, China. 829-836.

Bognar A (2001) Geomorphological regionalisation of Croatia. *Acta Geographica Croatica*. 34: 7-29. (in Croatian).

Đomlija P (2018) Identification and classification of landslides and erosion phenomena using the visual interpretation of the Vinodol Valley digital elevation model. PhD thesis, Faculty of Mining, Geology and Petroleum Engineering, Zagreb, Croatia. (in Croatian)

ESRI 2020. ArcGIS Desktop: Release 10.8 Redlands, CA: Environmental Systems Research Institute.

Evans JS, Oakleaf J, Cushman S A, Theobald D (2014): An ArcGIS toolbox for surface gradient and geomorphometric modelling, version 2.0-0.

Gold RD (2004) A Comparative Study of Aerial Photographs and LIDAR Imagery for Landslide Detection in the Puget Lowland, Washington. Washington Division of Geology and Earth Resources Open file report. 66.

Guzzetti F, Cardinali M, Reichenbach P, Carrara A (2000) Comparing landslide maps: a case study in the Upper Tiber River Basin, Central Italy. *Environmental Management*. 25: 247-263.

Jagodnik P, Jagodnik V, Arbanas Ž, Mihalić Arbanas S (2020a) Landslide types in the Slani Potok gully, Croatia. *Geologia Croatica*. 73(1): 13-28.

Köppen W (1936) The geographic system of climates. Köppen W, Geiger G (eds) *Handbook of Climatology*. Gebruder Borntraeger, Stuttgart. 44.

Mihalić Arbanas S, Krkač M, Bernat Gazibara S (2016) Application of advanced technologies in landslide research in the area of the City of Zagreb (Croatia, Europe). *Geologia Croatica*. 69(2): 179-192.

National Reference Centres Land Cover (NRC/LC). CORINE Land Cover dataset. URL: <https://land.copernicus.eu/pan-european/corine-land-cover> (CLC2018\_CLC2012\_V2018\_20b2.gdb) (accessed 5<sup>th</sup> of January 2022).

Pleničar M, Polšak A, Šikić D (1969) Basic Geological Map of SFRY 1:100.000, Trieste Sheet L33–88. Geološki zavod, Ljubljana; Institut za geološka istraživanja, Zagreb, (1951–1964); Savezni geološki institut, Beograd.

Riley SJ, DeGloria SD, Elliot R (1999) Index that quantifies topographic heterogeneity. *Intermountain*. *Journal of sciences*. 5(1-4): 23-27.

Schulz WH (2007) Landslide susceptibility revealed by LIDAR imagery and historical records, Seattle, Washington. *Engineering Geology*. 89(1-2): 67–87.

Van Den Eeckhaut M, Poesen J, Verstraeten G, Vanacker V, Moeyersons, J, Nyssen J, Van Beek, L P H (2005) The effectiveness of hillshade maps and expert knowledge in mapping old deep – seated landslides.– *Gomorphology*. 67: 351–363.

Van Westen CJ, Asch Th WJ, Soeters R (2006) Landslide hazard and risk zonation-why is it still so difficult?. *Bulletin of Engineering Geology and Environment*. 65: 167-184.

Wehr A, Lohr U (1999). Airborne laser scanning – an introduction and overview. *ISPRS Journal of Photogrammetry and Remote Sensing*. 54(2-3): 68–82.

# Slope gradient anomalies as indicators of potential slope instabilities

Ela Šegina<sup>(1)</sup>, Gorazd Žibret<sup>(1)</sup>

1) Geological Survey of Slovenia, Ljubljana, Dimičeva ulica 14, Slovenia (ela.segina@geo-zs.si)

**Abstract** From a geomorphological point of view, slope mass movements could be considered as natural mechanisms of slope equilibration. Unequilibrated hillslopes could theoretically be indicated with the areas of the ongoing slope processes which will complete with the temporary stabilisation of the hillslope. To determine the areas of potential past occurrences of the slope mass movements, we modified the GLA index which was primarily developed for the identification of river gradient anomalies caused by the recent tectonic uplift or subsidence (Žibret & Žibret 2014, 2017). We present the test whether the modified GLA method named the slope gradient anomaly (SGA) method, can be applied to active slope mass movements, and present preliminary results of the application of this method to hillslopes on several known landslide areas and on several random areas, where we test the wider applicability of the method.

**Keywords** landslide detection, GLA method, SGA method, slope analysis, DEM

## Introduction: the concept

GLA is a newly developed geo-morphometrical index modified to identify the gradient anomalies along the natural river profile as indicators of recently active tectonics (Žibret & Žibret 2014, 2017). It corrects the disadvantages of Hack's SL-index (Hack 1973) and improves its performance. The method is based on the following assumptions: 1) the equilibrated river profile follows an exponential curve with negative exponential form, 2) the adaptation of the river profile to the disturbances is relatively quick and 3) the deviations from the equilibrated profile indicate recent disturbance (uplift or subsidence). The GLA attributes the mathematically defined best-fitting exponential function with a negative exponent to the actual river profile and identifies the deviations of the actual profile from the theoretical one. The guiding process in the evolution of the equilibrated river profiles is fluvial erosion. The concave shape develops due to the downstream increase of the discharge and decrease of the transport capacity when the stream is approaching the base level (Summerfield 2014).

This contribution aims to test, whether the principles of the GLA method can be applied to hillslope mass movement processes, by suggesting the modifications of the GLA method to detect active slope processes. To avoid confusion between the GLA method, which shall be used in the case of fluvial processes, we named this new method

as SGA (slope gradient anomaly) method. The proposed adaptation of the GLA method requires reconsideration of the geomorphological processes involved in slope mass movements and the establishment of new assumptions. Instead of fluvial erosion, the guiding processes of the base rock degradation are chemical (mineral dissolution), mechanical (splattering of raindrops, freezing-thawing, etc.) and biological weathering processes (cracks widening by roots, etc.) (Scheidegger 1970). Essentially, the guiding process of the slope formation is an interplay of the in-situ weathering of the bedrock and the ability of the weathered unconsolidated material to be removed. If considered no transport agent such as fluvial, wind or glacial forces (excluding the gravity), the theoretical equilibrated slope would exhibit the following convex-linear-concave profile (Fig. 1).

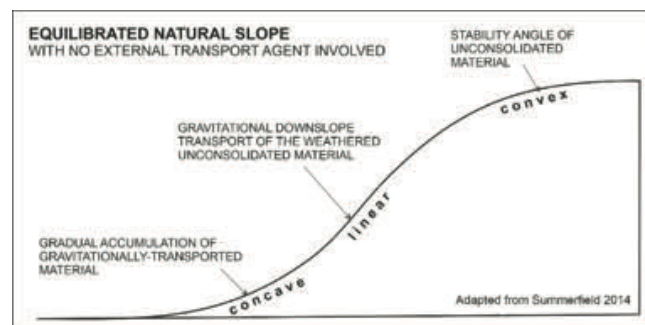


Figure 1 Schematic representation of the theoretical equilibrated hillslope profile

The upper part of the slope profile gains a convex shape depending on the angle of repose of the unconsolidated weathered material. Eventually, the weathered material gravitationally moves downslope and accumulates at the base, forming the concave profile at the lower part of the naturally equilibrated slope profile. Most of the hillslope between those two segments could be satisfactorily defined with the linear function (Summerfield 2014).

In the temperate natural environments as encountered in Slovenia, soil-mantled slopes with linear to linear-convex profiles are most commonly observed (Fig. 2) (assumption 1: the shape of the predicted profile). The lower concave segment of the slope is mostly absent due to a well-developed stream network causing fluvial undercutting at the base of the hillslopes. Slope angles at their linear segments vary with the lithology of the bedrock (Fig. 2). Thus we assume that the SGA method

could be applied only to the lithologically uniform slopes, or the slopes should be segmented based on lithology (assumption 2: the expected impact of lithology). The impact of lithology on reshaping the equilibrated river profile was established to be negligible, presumably due to the high intensity of the fluvial processes and their ability to quickly adapt to the profile anomalies (Žibret and Žibret, 2017). Slope formation processes are considerably less intensive and the equilibrated slopes develop over a considerable amount of time. Slope mass movements are though instantaneous events that cause transportation of a large amount of the material to be transported in a short period of time in a form of landslides. After the landslide occurs, slow cosmopolitan processes (in situ weathering with local gravitational transport of the weathered material) take over to eventually transform the slope profile into the next generation equilibrated slope profile. Based on slow processes occurring on slopes, the GLA method is expected to detect not only recent but the slope mass movements which occurred even in more temporally distant periods (assumption 3: the age of detected anomalies). With time, the slope stability gradually diminishes due to the progressive mechanical, chemical and biological transformation of the material. Decreased cohesion (material available to be transported) mostly

accompanied with transient natural conditions (decreased pore pressure, earthquake, loading of a slope, undercutting etc.) induce the change in the ratio between shear strength of the material and shear stress, triggering the occurrence of a slope failure.

Before the failure, the internal slope stability gradually decreases, but in most cases, the process on the surface remains rather invisible (minor cracks etc.) (assumption 4: the time range of the method's detectability). After the slope failure, the three distinctive morphological elements modify the original profile: steep scarp at the upper point of the failure (recognizable as a sudden increase of the slope angle), followed by the segment where the material has been removed (visible as a deficit in the profile) and finally where the material has been accumulated (landslide's foot) (visible as a surplus in the profile) (assumption 5: the expected morphological elements to be detected) (Fig. 3). As the SGA identifies anomalies of the slope profile from the best-fitting linear function (following the assumption 1), a scarp evidenced as high positive SGA values, displaced material as positive SGA values and accumulated material as negative SGA values in this sequence is expected to indicate the slope mass movement occurred at the specific slope profile.

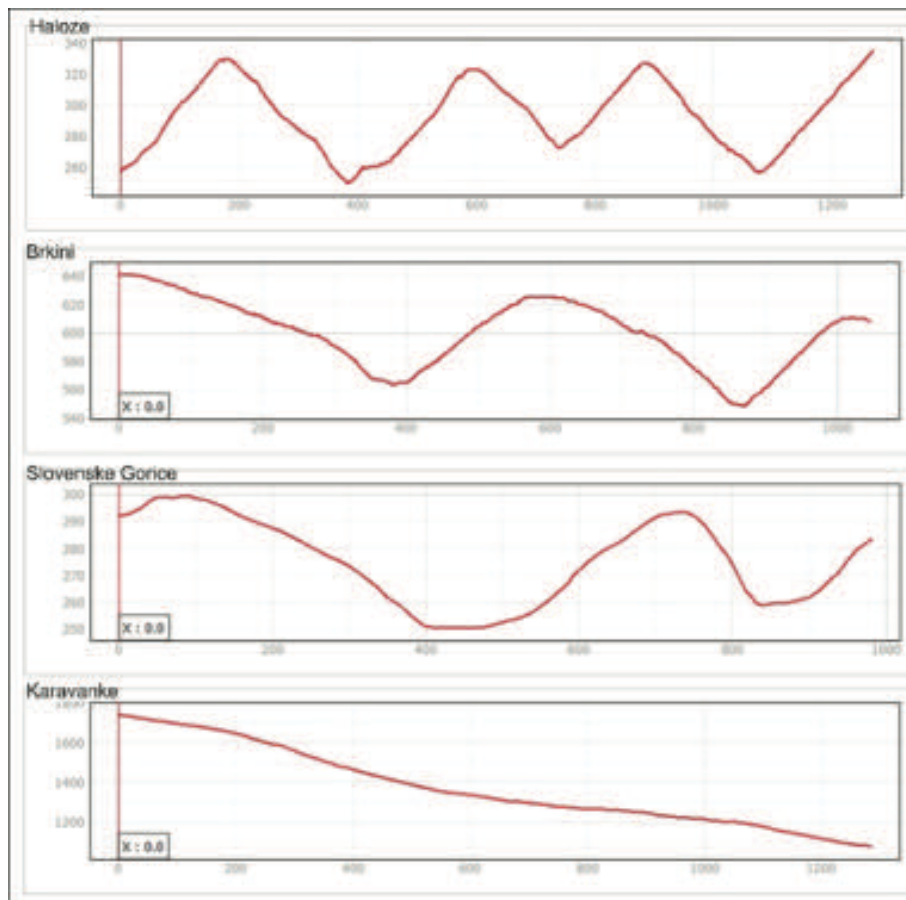


Figure 2 Slope profile shapes in the temperate environment of Slovenia.



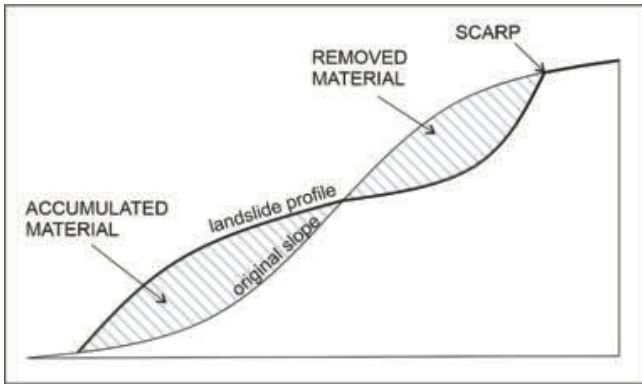


Figure 3 The distinct morphological elements of the slope failure expected to be detected by the SGA method on hillslopes.

Based on the discussed differences between river and slope profiles it is important to carefully select the appropriate profile on the hillslope prior to SGA analysis, to make sure that the profile of interest captures the surface outside the permanent or temporal gullies or other fluviually-developed features, which are commonly dissecting the slopes (assumption 6: the spatial extent of applicability).

Due to discussed differences in the geomorphological processes that shape the slopes in comparison to the river profiles, some modifications were needed to adjust the GLA method for an application to the hillslopes. The modifications are summarized in the following table (Tab. 1).

### Materials and methods

The detailed mathematical background of the GLA method has been presented in Žibret and Žibret (2014) and, with some revisions, in Žibret and Žibret (2017). The adaptation of the GLA method to slopes includes the transformation of the exponential predicted profile to the linear. Other steps remain the same and for the step-by-step explanation of the concept, the reader is referred to the above-listed papers.

The employed digital elevation model (DEM) was based on the publicly available LiDAR data (Slovenian Environmental Agency 2014) with a grid resolution of 1 m. ArcGIS and QGIS software were employed to extract elevation data along slope profiles and to visualize the results. The SGA calculation was carried out with MS Excel software. The performance of the SGA index was tested in several different conditions to evaluate the limitations of the method. The performance was tested on the hillslopes where the slope failures of different dimensions were evidenced before the acquisition of the LiDAR data in 2014. Three size ranges were considered: large, deep-seated landslide covering the area of the app. 360.000 m<sup>2</sup> (Peternel et al., 2017), middle-sized landslide (area = 150 m<sup>2</sup>, depth = 15 m) and shallow landslide (area = 600 m<sup>2</sup>, depth = < 1 m). We analysed profiles on slopes crossed by artificial constructions such as roads and terraces to test if

they are detected as anomalies. The profiles were selected on slopes with uniform and heterogenous lithology to investigate the impact of lithology on the results of the method. We also tested the performance of the SGA on the hillslopes where no slope mass movements have been evidenced up to now. The profiles were delineated manually. To exclude the method's noise resulting from the inaccuracies of DEM, the n-factor which determines the acceptable range of slope gradient anomalies (Žibret & Žibret, 2017, Eqs. 4 and 5) was set to 5 in case of short profiles and 10 in case of the profile across a large deep-seated landslide. To divide both negative and positive, as well as high and low SGA values defining different morphological elements, the SGA values were classified into 5 classes (Tab. 2). Manually, we observed the potential occurrence of the downslope sequence scarp-removed material-accumulated material. In the validation step, the areas of slope anomalies were compared to the lithological conditions and known landslide features.

Table 1 The modifications of the GLA method (Žibret and Žibret 2017) for adaptation to hillslopes.

	GLA on river	SGA on hillslope
<b>The shape of the predicted equilibrated profile</b>	Exponential function	Linear function
<b>Impact of lithology</b>	Negligible	High
<b>Age of detected anomalies</b>	Only recent	Recent and past
<b>Object of detection</b>	Tectonic uplift or subsidence, anthropogenic constructions	Scarp, removed material, accumulated material (landslide's foot)
<b>The spatial extent of applicability</b>	Along the river profile	Along the steepest slope between the mountain ridge and the stream

Table 2 SGA values classification.

	SGA values	Morphological element
<b>Extremely low values</b>	-min - - 5	Extensive material accumulation
<b>Slightly low values</b>	-5 - -1	Material accumulation
<b>Negligible values</b>	-1 - +1	Negligible changes
<b>Slightly high values</b>	+1 - +5	Material removal
<b>Extremely high values</b>	+5 - +max	Scarp and extensive material removal

### Testing and validation of the SGA method

Hillslopes with no known slope failures exhibit no distinct anomalies (Fig. 4 A, B, D). Anthropogenic structures such as terraces and pits occur as rather distinct anomalies (Fig. 4 A, C), while the method does not detect the local roads (Fig.4 B). Results of the SGA method should be manually checked for anthropogenic structures (roads, terraces, pits etc.) as they may give false-positive results.

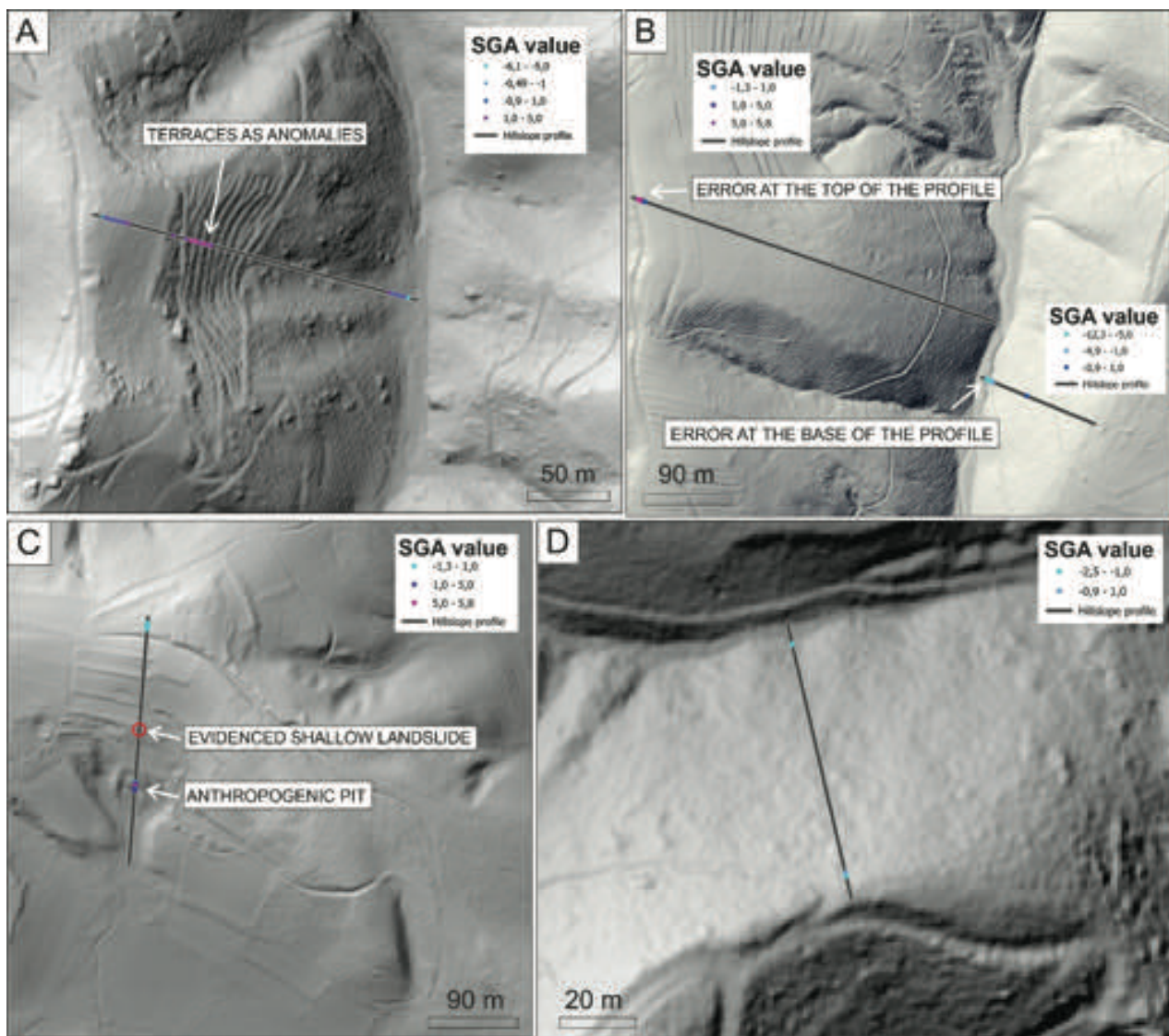


Figure 4 SGA performance on different types of hillslopes.

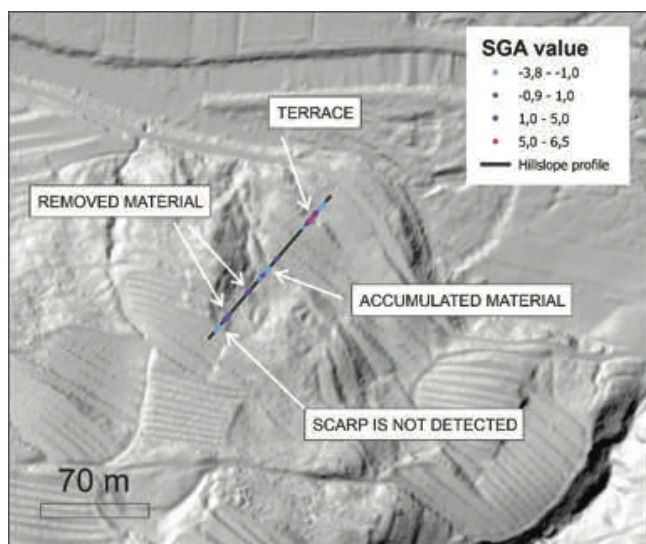


Figure 5 SGA method performance in the case of the middle-sized slope mass movements.

The SGA method was not successful at recognizing very small and shallow slope failures (Fig. 4C), while in the case of the middle-sized landslide both areas of removed and accumulated material were detected (Fig. 5). Scarp was however not expressed as an anomaly. Examples show that the essential characteristic is not the spatial extent of the slope failure, but the depth of the removed or accumulated material.

Analysis of a large deep-seated landslide that crosses several lithological borders gives insight into the detection of large landslide morphological elements and an impact of heterogeneous lithology on results of the SGA method. The method successfully detected scarp, removed material in the landslide's head and accumulation in the sequence (Fig. 6A). Comparison with the results acquired for the particular lithological unit shows additional details which could be acquired when considering only one lithological unit (Fig. 6B).

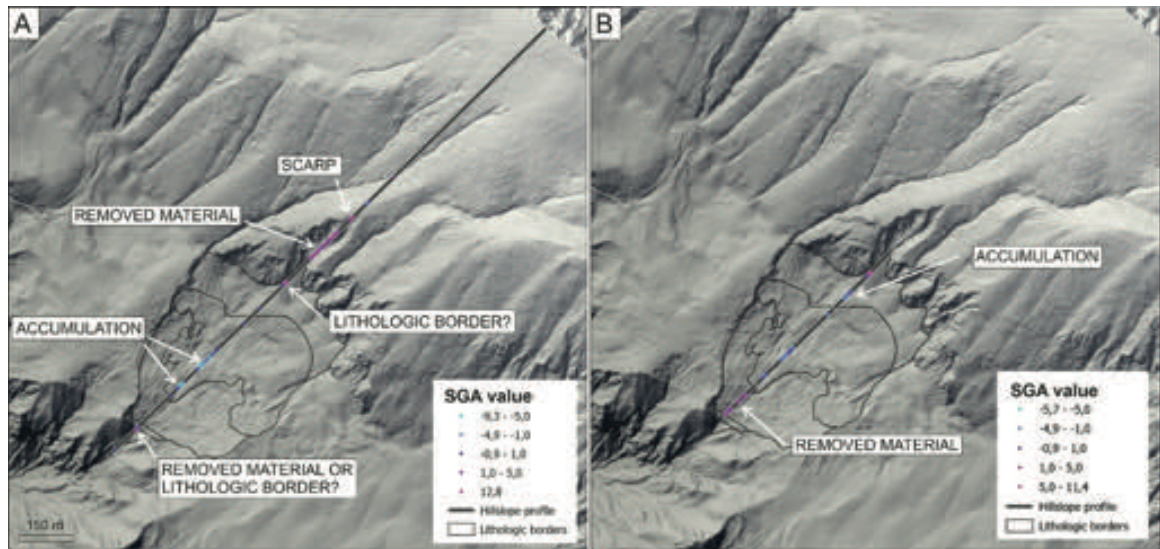


Figure 6 SGA performance in the case of a large deep-seated landslide. A – Single profile across several lithologic units. B – Profile for the separate lithologic unit.

## Discussion

This is the first step to adjust and test the performance of the modified GLA method, named the SGA method, for the detection of slope failures and further work is required to confirm its actual utility value in landslide research. The most promising aspect of this method is in its potential for automated detection of the past landslide events which would allow fast and automatic processing of the large areas of interest and considerably expand the existing landslide databases which presently mostly depend on the probability that the event has been noticed and additionally on the responsibility of individuals or authorities to report the event. Based on the gained understanding of the performance of the SGA method on the hillslopes presented in this paper we will further focus on automatization of the method which will allow us to reach statistically reliable testing results. However, this is only an initial report on how to detect active slope mass movements based on the analysis of DEM. A lot of further tests and modifications are required, including the appropriate selection of correct orientation and position of the profiles, segmentation, correct mathematical slope approximations etc. to develop a reliable new method for the detection of active slope mass movements.

## Conclusion

The adjusted GLA method, named the SGA method, has the potential to evolve into an automated tool for detecting past slope failures from DEM. The method detects scarp, area of slid material and landslide foot or area of slope mass accumulation based on deviations from estimated equilibrated slope profile. Preliminary results of the testing carried out on a limited number of samples indicate a high potential for detecting middle to large-scale events while the method is not able to detect shallow slope mass movements. The testing also exposed some

limitations of the SGA method, such as the importance of precise profile selection and the impact of artificial constructions which may give false-positive results. The method gives better results when considering slopes with uniform lithology. Further work on the automatization of the method, testing of different mathematical slope approximations and their adaptation to different regional topographic characteristics of the slopes, and testing on a larger, statistically reliable set of samples will finally evaluate the reliability and utility of the method in landslide research.

## Acknowledgements

The authors acknowledge the financial support from the Slovenian Research Agency—research core funding no. P1-0419 "Dynamic Earth" and P1-0025 "Mineral resources", and Research Project J1-3024 "Deciphering the sensitivity of rock faces to climatic changes and freeze-thaw cycles in permafrost-free regions".

## References

- Hack JT (1973) Stream-profile analysis and stream-gradient index. *Journal Research of United States Geological Survey*. 1: 421-429.
- Peternel T, Kumelj Š, Oštir K, Komac M (2017) Monitoring the Potoška planina landslide (NW Slovenia) using UAV photogrammetry and tachymetric measurements. *Landslides*. 14(1): 395-406. <https://doi.org/10.1007/s10346-016-0759-6>
- Scheidegger AE (1970) *Theoretical Geomorphology*. Springer. 435p.
- Summerfield MA (2014) *Global geomorphology*. Routledge. 560p.
- Žibret G, Žibret L (2017) River gradient anomalies reveal recent tectonic movements when assuming an exponential gradient decrease along a river course. *Geomorphology*. 281: 43-52. <https://doi.org/10.1016/j.geomorph.2016.12.017>
- Žibret L, Žibret G (2014) Use of geomorphological indicators for the detection of active faults in Southern Part of Ljubljana moor, Slovenia. *Acta geographica Slovenica*. 54(2): 271-291. <https://doi.org/10.3986/AGS54203>



## LandSlidePlan - Scientific research project on landslide susceptibility assessment in large scale

Sanja Bernat Gazibara<sup>(1)</sup>, Snježana Mihalić Arbanas<sup>(1)</sup>, Marko Sinčić<sup>(1)</sup>, Martin Krkač<sup>(1)</sup>, Hrvoje Lukačić<sup>(1)</sup>, Petra Jagodnik<sup>(2)</sup>, Željko Arbanas<sup>(2)</sup>

1) University of Zagreb, Faculty of Mining, Geology and Petroleum Engineering, Zagreb, Pierottijeva 6, Croatia, (sbernat@rgn.hr)

2) University of Rijeka, Faculty of Civil Engineering, Rijeka, Radmile Matječić 3, Croatia

**Abstract** The scientific research project *Methodology development for landslide susceptibility assessment for land-use planning based on LiDAR technology (LandSlidePlan, HRZZ IP-2019-04-9900)*, funded by the Croatian Science Foundation, deals with new and under-investigated subjects in respect of inventory mapping of small and shallow landslides and presents innovative approaches to scientific research of landslide susceptibility assessment using cutting-edge LiDAR technology for collection of input data. The project has three main scientific goals. The first goal is to create the best optimal digital model of the bare-earth terrain that shows realistic landslide footprints and differences between disturbed and undisturbed land that may influence land use. The second goal is to create the most reliable large-scale landslide susceptibility map with the best differentiation of landslide-prone and non-susceptible areas using scientific methods customised to specific engineering geological conditions of Croatian environments with sliding threats. And the third goal is to create maps depicting information about landslides tailored according to the needs of the system of physical planning in Croatia (particularly land-use planning), encompassing local and regional levels under, harmonised at the national level. Due to different natural conditions and land uses in different parts of Croatia, the methodology will be developed for pilot areas in the City of Zagreb, Hrvatsko Zagorje and Istria, selected based on characteristic geological settings and degree of urbanisation.

**Keywords** landslide susceptibility mapping, LiDAR, land use, LandSlidePlan

### Introduction

Sustainable strategic planning and management are impossible without knowing the spatial distribution of geohazards in populated areas, respectively, without the systematic mapping of landslide occurrences (Bell, 2003; Clague and Roberts 2012). Therefore, one of the priorities for an action plan in the Sendai Framework for Disaster Risk Reduction 2015-2030 (UN 2015) is understanding disaster risk in all its dimensions of vulnerability, capacity,

exposure of persons and assets, hazard characteristics and the environment. Based on this data, it is crucially important to disseminate location-based disaster risk information to decision-makers, the general public and communities at risk exposed to disaster, in an appropriate format using geospatial information technology.

In the last fifteen years, a variety of remote sensing techniques and applications have been discussed, considering their usefulness for landslide hazard mapping (Guzzetti et al. 2012; Jaboyedoff et al. 2012; Scaioni et al. 2014). The main advantage of remote sensing techniques is that they enable 3D surface models with high precision and spatial resolution that can be used for large area coverage analysis. The advantage of LiDAR (Light Detection and Ranging) technique and ALS (Airborne Lidar Scanning) data compared to other remote sensing techniques is ground detection in forested terrain and the possibility of creation of high-resolution bare-earth digital elevation models (DEMs), which enables identification and mapping of small and shallow landslides in densely vegetated areas (Chigira et al. 2004; Van den Eeckhaut et al. 2007; Razak et al. 2011; Đomlija 2018; Bernat Gazibara et al. 2019a). Furthermore, the landslide maps obtained through the visual analysis of LiDAR-derived DTMs had better statistics for the landslide size (area) than the inventories obtained through field mapping or the interpretation of aerial photographs (Van den Eeckhaut et al. 2007; Razak et al. 2011; Bernat Gazibara et al. 2019b).

The methodology for landslide susceptibility assessment will be developed for small and shallow landslides in urban, suburban and rural areas in Croatia. Based on the classification system by IPL (2013), landslides in three pilot areas can be classified as shallow landslides (1 - 5 m) to moderate shallow landslides (5 - 20 m), since the depth of the sliding surface of landslides that usually occur is approx. 5 m deep, with a maximum depth of 20 m. Furthermore, the most abundant landslide size in all three pilot areas is approx. 500 m<sup>2</sup> and based on the classification system by van Schalkwayk and Thomas (1991) and landslides can be classified as small (10<sup>1</sup> - 10<sup>3</sup> m<sup>2</sup>).

LiDAR DTM also enables derivation of high-resolution and high-quality landslide-causal factor maps, i.e., elevation, slope gradient, slope aspect, drainage

density maps etc. Namely, for following up analyses of landslide susceptibility, it is important to select the representative factors related to the landslide types and failure mechanisms in each particular environment (Cruden and Varnes 1996). Furthermore, there are multiple sources of uncertainty within statistically-based landslide susceptibility assessment that need to be accounted and monitored, such as: (i) selection of the terrain mapping unit; (ii) selection of the geometric feature type to represent landslides (polygon vs. point); (iii) selection of the ratio of landslides for training and validation; (iv) selection of the validation method; and (vi) selection of the classification method for landslide susceptibility map.

The urgent need of researching the landslide susceptibility assessment for application in land use planning in Croatia arises from national landslide risk assessment (Croatian National Platform for Disaster Risk Reduction, CNPDRR, 2019). The preliminary regional landslide susceptibility analysis showed that approximately 20% of the territory of the Republic of Croatia is potentially prone to landsliding. Furthermore, from the same susceptibility analysis arises that 60% of cities/municipalities (local administrative units) are endangered by Multiple Occurrence of Regional Landslide Events (MORLE) in case of the most probable unfavourable hydrological event experienced in 2013 and 2018 (Bernat Gazibara et al. 2019c). All of the facts mentioned above were the motive for the scientific research project entitled *Methodology development for landslide susceptibility assessment for land use planning based on LiDAR technology (LandSlidePlan IP-2019-04-9900)* funded by Croatian Science Foundation. The research group includes six project members-researchers from two Croatian universities, the University of Zagreb –

Faculty of Mining, Geology and Petroleum Engineering and the University of Rijeka - Faculty of Civil Engineering, and three international project members-researchers from the University of Florence and the University of Ljubljana.

### Study area

Owing to different natural conditions and types of land uses in Croatia, the landslide susceptibility methodology will be developed for three pilot areas (Fig. 1), selected based on characteristic geological settings, geomorphological conditions and degree of urbanisation: (i) pilot area (20 km<sup>2</sup>) in the City of Zagreb; (ii) pilot area (20 km<sup>2</sup>) in Hrvatsko Zagorje; (iii) pilot area (20 km<sup>2</sup>) in Istria. Pilot areas in the City of Zagreb and Hrvatsko Zagorje are located in Pannonian Basin, and the third pilot area is in Istria, which belongs to an undeformed part of the Adriatic Plate (Mihalic Arbanas et al. 2017).

The Podsljeme area of the City of Zagreb includes the southeastern slopes of Medvednica Mt., an area of 180 km<sup>2</sup>. Part of the Podsljeme area of the City of Zagreb was selected as a pilot area because of hilly relief, high degree of urbanisation and Neogene and Quaternary deposits extremely susceptible to landslides. Landslides mainly occur at the boundary between superficial deposits and bedrock, and many known landslides occur at the geological contact between Pleistocene and Upper Pontic deposits. Landslides are predominantly small to medium-sized, with sliding surfaces at depths of several meters to a maximum of 20 m. The preparatory causal factors of slope instabilities in the Podsljeme area depend on geomechanical properties of soils, geomorphological processes and different types of man-made processes (Mihalić Arbanas et al. 2016), and the main triggers are precipitations and human activity.

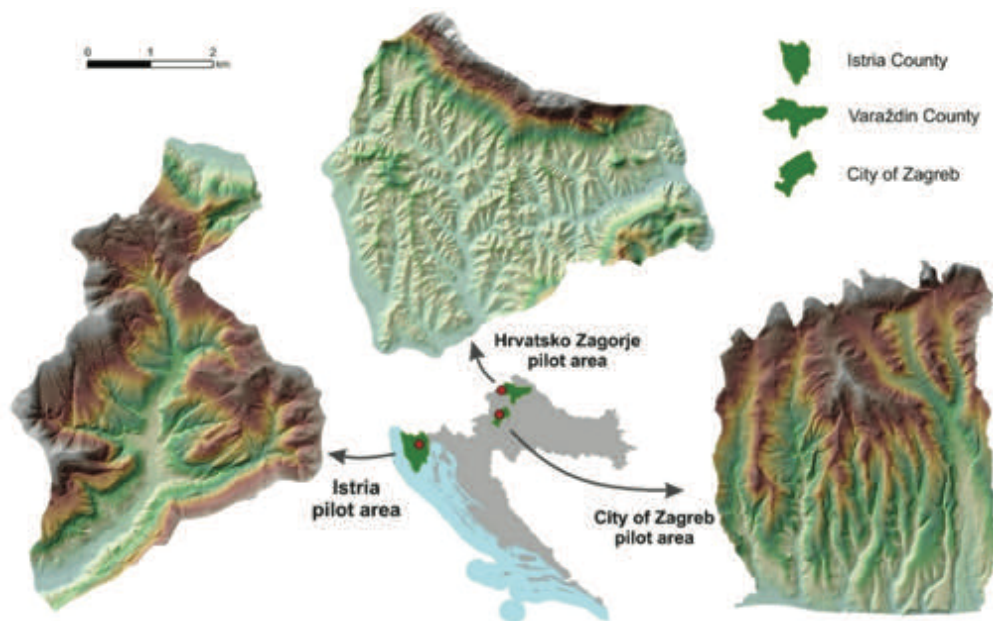


Figure 1 Locations of pilot areas in the scientific research project LandSlidePlan.

Hrvatsko Zagorje is a hilly geographical unit in the northwestern part of Croatia, with a total area of about 2,000 km<sup>2</sup>. The pilot area is located in the northwest part of Hrvatsko Zagorje, in Varaždin County, in the eastern part of the Bednja Municipality and the central part of the City of Lepoglava. The pilot area covers a total of nine settlements, three in the City of Lepoglava and six in the Bednja Municipality. The study area is composed of Miocene, Quaternary and Triassic sediments. Landslides in this area mainly occur in weathered clastic rocks and soils of Miocene age and at the geological contact of the superficial deposits and the bedrock. Landslides are mostly small to medium, with sliding surfaces at depths of several meters to a maximum of 20 m. Precipitations and human activity are the primary triggers of landslides in NW Croatia (Bernat et al. 2014a). For example, abundant landslide events (MORLE) in the hilly areas of NW Croatia occurred in winter 2012/2013 due to the prolonged heavy rainfall periods and the rapid melting of a thick snow cover (Bernat et al. 2014b).

The Istrian peninsula is a geomorphological unit separated from the interior by the limestone mountains of the Čićarija Mt. Istria is geomorphologically composed of a hilly northern edge (White Istria), lower flysch hills (Gray Istria) and low limestone plateaus (Red Istria). The pilot area is located in the northern part of the Istrian County, in Gray Istria, and includes the hilly part of the City of Buzet between the valley of the river Mirna in the north and the accumulation Butoniga in the south. The materials that make up these hills are mainly represented by flysch-like deposits of the Eocene. The pilot area of the City of Buzet includes a total of 15 settlements. In this area, landslides occur in weathered flysch-like deposits of the Eocene and on the geological contact of flysch-like rocks and superficial materials. Block translational landslides are also possible (Arbanas et al. 2010). Landslides are mostly small to medium-sized, with sliding surfaces at depths of several meters to a maximum of 15 m triggered mostly by precipitations and human activity.

## Input data

### LiDAR data

Airborne laser scanning (ALS) was undertaken during the leaf-off period, in March 2020, using Eurocopter EC 120B equipped with Hasselblad camera and Riegl LMS-Q780 long-range airborne laser scanner (ALS). The LiDAR system used in this study captured data at a pulse rate frequency of 400 kHz with a surface point horizontal

accuracy of 3 cm and vertical accuracy of 4 cm. Final Point Cloud for the City of Zagreb has approx. 623 million points with a point density of 16,09 pt./m<sup>2</sup> which results in average point spacing of 0.28 cm. Characteristics of all three LiDAR point clouds in study areas of the City of Zagreb, Bednja Municipality – City of Lepoglava and City of Buzet are listed in Table 1. The resulting point clouds serve for interpolation of bare-earth DTMs.

Preparation of LiDAR DTM was carried out in 6 resolutions (0.15, 0.3, 0.5, 1, 2 and 5 m) using four commonly used interpolation methods, namely Inverse Distance Weighting (IDW), Natural Neighbor, Australian National University DEM (ANUDEM) and Kriging (Razak et al. 2013). In each pilot area, preliminary visual interpretation of DTMs was performed to create a set of landslides for quantitative geomorphological analysis to determine an optimal LiDAR DTM for visual landslide inventory mapping. The quality of DTM for visual landslide identification and mapping was determined based on the topographic signature of landslide morphology using statistical parameters (Chu et al. 2014). The key indirect goal was to statistically determine the most optimal LiDAR DTM for visual landslide inventory mapping of small and shallow landslides in specific environmental/engineering geological conditions related to particular landslide type(s). Based on the point density, average point spacing, and quantitative geomorphological analysis, the bare-earth DTM with a 30 cm resolution using the kriging interpolation method was created for visual landslide identification and mapping in all pilot areas.

### Landslide inventory maps

Landslide data in the form of a landslide inventory map includes visual interpretation of the most optimal LiDAR DTM derivatives, delineation of landslide contours in GIS and field checking of mapped landslides. Based on optimal DTM for interpreting landslide morphology, five topographic derivative datasets were derived: hillshade maps, slope maps, contour lines, curvature and surface roughness maps. Landslide inventory mapping was carried out at a detailed scale (1:100 – 1:500) to ensure a correct delineation of the landslide boundaries (Petschko et al. 2015; Đomlija 2018; Bernat Gazibara 2019a). During visual landslide identification and mapping, Google Earth satellite images were used to check morphological forms along roads and houses, such as artificial landfills and cuts, similar to landslides on DTM derivatives (Đomlija 2018; Bernat Gazibara 2019b).

Table 1 LiDAR point cloud characteristics in three study areas.

Study area	Area (km <sup>2</sup> )	No. of points in point cloud	No. of points in class 2 - terrain	Percentage of points in class 2 - terrain	Point cloud density in class 2 - terrain (pt./m <sup>2</sup> )	Average point spacing in class 2 – terrain (m)
City of Zagreb	20.22	623450816	325409134	52.19 %	16.09	0.28
Bednja-Lepoglava	21.11	577812196	283147378	49.00 %	13.41	0.31
Buzet	19.98	696823831	343826654	49.34 %	17.21	0.27

Visually interpreted landslides on LiDAR DTM derivative maps were additionally field checked, and landslide verification was conducted on 10 - 20% of randomly selected landslides in inventories for each pilot area, which is satisfactory according to Galli et al. (2008). Completed LiDAR-based landslide inventories will be used for further landslide susceptibility analyses, and no additional landslide data, like historical databases or landslide reports, will be used. The key indirect goal is to create sustainably complete landslide inventories for statistical susceptibility modelling in three representative environments in Croatia, e.g., complete landslide inventory for the Hrvatsko Zagorje pilot area (Krkač et al. 2022). The total area of mapped landslides in the Hrvatsko zagorje is 0.408 km<sup>2</sup> or 2.02% of the pilot area, and the mean landslide density is 45.1 ls/km<sup>2</sup>. The average landslide area is 448 m<sup>2</sup> (median = 173 m<sup>2</sup>, std. dev. = 880 m<sup>2</sup>).

#### Landslide causal factors

Collection of landslide causal factors includes morphological factors (elevation, slope, aspect, etc.), geological factors (lithology, distance from faults, etc.), hydrological factors (distance from stream network, drainage density, etc.) and land cover conditions (land-use, land-use changes, distance from roads and buildings, etc.). The selection of landslide controlling factors and processes of its derivation is strongly related to the following up analyses of landslide susceptibility (Soeters and van Westen 1996; Guzzetti et al. 1999; Chacón et al. 2006; Fell et al. 2008a, b).

Preparation of geological and anthropogenic causal factors included the digitalisation of geological units and linear geological structures from the existing geological maps and the digitalisation of buildings, roads and land use from existing digital orthophotos on a scale of 1:5 000. Also, spatial analysis of landslides distribution in relation to different causal factors resulted in a series of causal factor maps classified according to their relative impact on sliding. Causal factor maps derived for all three pilot areas are listed in Table 2. The key indirect goal is to determine which landslide causal factors are necessary and optional for high-quality landslide susceptibility analysis in specific environmental conditions and for specific landslide types, i.e., small and shallow landslides.

#### Landslide susceptibility modelling

##### Methodology

Flow chart of the methodology for landslide susceptibility assessment in the scientific research project LandSlidePlan is shown in Fig. 2. Landslide susceptibility analyses using statistical methods are planned by application of three data-driven approaches: (i) bivariate statistical methods, including Information value method (Yin and Yan 1988) and weights of evidence modelling (Bonham-Carter 1994; van Westen 2002); (ii) multivariate statistical methods, including logistic regression

(Ohlmacher and Davis 2003; Gorsevski et al. 2006) and discriminant analysis (Carrara 1983; Gorsevski et al. 2000); (iii) machine learning methods, including support vector machine (Huang and Zhao 2018) and random forest (Brenning 2005; Stumpf and Kerle 2011). Selected statistical methods represent the most commonly used approaches for landslide susceptibility assessment and show the best prediction modelling rates (Frattini et al. 2010; Reichenbach et al. 2018). Furthermore, susceptibility analysis will be carried out for six different mapping units, including the different sizes of grid-cells (1 m, 2 m, 5 m), terrain units, slope-units (Alvioli et al. 2016) and unique-condition units which are made by overlaying a number of landslide causal factors (Carrara et al. 1995). Susceptibility analyses will be performed using a landslide training group (50% of the inventory randomly selected), while independent validation will be carried out with the other 50% of the landslide inventory (landslide test group). Also, landslide susceptibility models will be computed using the landslide training group represented as visually mapped landslide polygons, the point features at the head scarps of mapped landslides, and the point features corresponding to the centroid of landslides (Petschko et al. 2015).

Table 2 Landslide causal factor maps prepared for three pilot areas.

Group	Landslide casual factor map
Geomorphological factors	Elevation
	Slope gradient
	Slope orientation
	Contour density
	Terrain curvature
	Terrain roughness
	Terrain dissection
	Proximity to gully channel
Geological factors	Lithology (rock type)
	Proximity to geological contact
	Proximity to faults
Hydrological factors	Proximity to drainage network
	Proximity to springs
	Proximity to permanent streams
	Proximity to permanent and temporary streams
Anthropogenic factors	Topographic wetness
	Land use
	Proximity to building
	Proximity to roads
	Proximity to land use contact

Results of landslide susceptibility modelling will be a series of more than 200 landslide susceptibility maps per pilot area, due to variation of three landslide feature geometry, six statistical methods, six mapping units and a few different combinations of landslide causal factor maps. The key indirect goal is to test the possibilities and limitations of applying three statistical techniques for landslide susceptibility assessment on a particular data set representing specific environmental/engineering geological conditions related to small and shallow



landslides. Also, to determine the appropriate resolution of input and resulting maps, mapping units for landslide susceptibility modelling and representation of results and the adequate form of input dependent variable (landslide polygons vs. points representing landslides).

**Verification**

Verification of landslide susceptibility assessments in terms of accuracy of the resulting landslide susceptibility maps will be evaluated using landslide inventory, i.e., landslide training group (50% of the inventory randomly selected) and landslide test group (other 50% of the landslide inventory). All derived landslide susceptibility

maps will be classified in 100 classes of an equal number of terrain units to allow comparison. The prediction skills of susceptibility models will be evaluated using Receiver Operating Characteristic (ROC) analysis expressed by success and prediction rate curves (Gorsevski et al. 2006).

The key indirect goal is to define the best method for landslide susceptibility assessment by its resolution, input parameters of independent variables (landslide casual factor maps) and input parameters in the form of landslide inventory map for specific environmental/engineering geological conditions and small and shallow landslides. In addition, advantages and drawbacks of all applied methods will also be gained, specific for all three pilot areas.

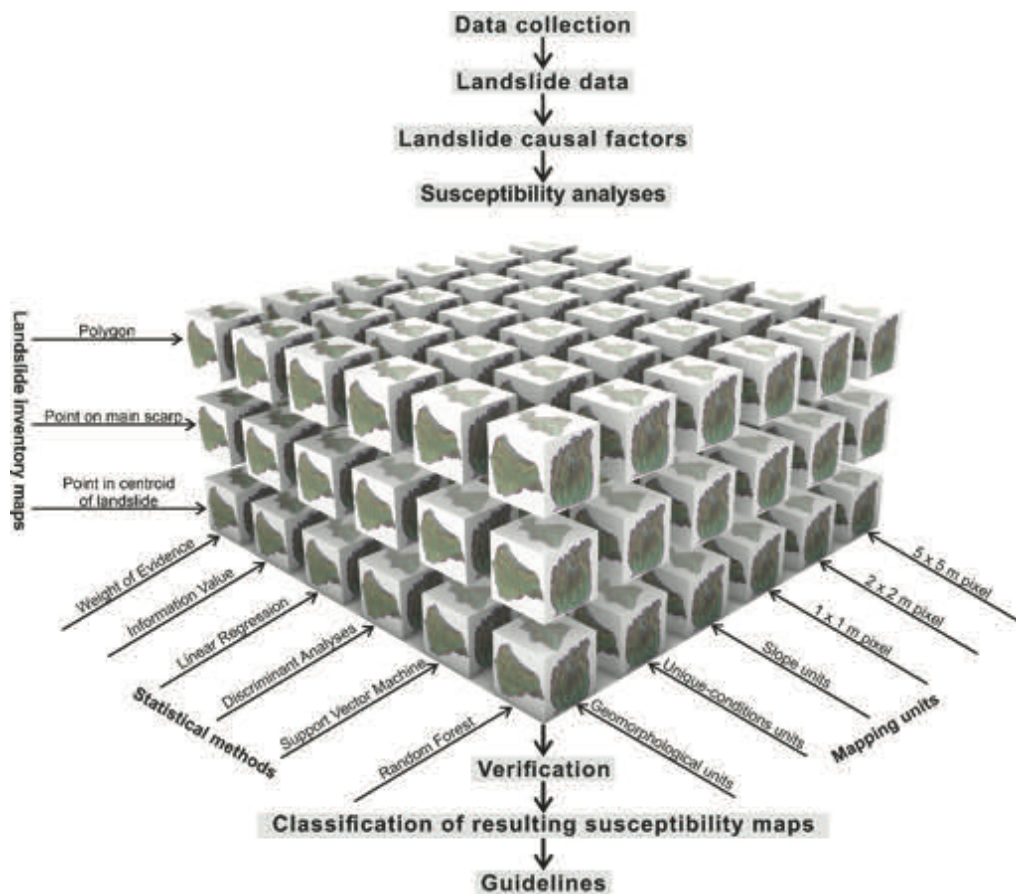


Figure 2 Flow chart of the methodology for landslide susceptibility assessment in the scientific research project LandSlidePlan.

**Application of landslide maps**

Classification of resulting susceptibility maps is crucial for land use spatial planning and management, which influences the possibilities of practical use of maps and the quality of information depicted by the map. An essential issue is the determination of susceptibility thresholds, i.e., the classification of derived landslide susceptibility maps into a limited number of susceptibility classes. Adopting one classification system or another will not only affect the

map’s readability and final appearance, but most importantly, it may affect the decision-making tasks required for effective land management (Chung and Fabbri, 2003). The proposed research will compare and evaluate the reliability of the most commonly used classification methods (Cantarino et al. 2019), including equal intervals, natural breaks, quantiles, head/tail breaks and standard deviation. Also, before applying the best classification method, it is crucial

to define the criteria for discrimination of landslide areas and landslide-prone areas. According to the clearly defined purpose of end-product maps, which the project will derive, criteria and potential uses will be determined by decision-makers, practitioners and experts from the domain of spatial and land use planning. Methodology for deriving expert opinion will include questionnaires, transfer of experience from EU countries (Italy and Slovenia), and one round-table with local and regional government/administration representatives under the Ministry of Physical Planning, Construction and State Assets supervision. The key indirect goal is to develop a derivation model of cartographic information about landslides for sustainable risk management through the land use planning system at the local and regional government (municipalities, cities, and counties).

At the end of the LandSlidePlan project, guidelines about the practical application of the developed methodology in the spatial planning system in Croatia will be written. Based on similar guidelines for landslide susceptibility, hazard and risk zoning for land-use planning (Fell et al. 2008 a, b), LandSlidePlan project guidelines will provide: (i) definitions and landslide terminology; (ii) description of the types and levels of landslide zoning; (iii) suggested scales for zoning maps taking into account the needs and objectives of land use planners and regulators and the purpose of the zoning; (iv) guidance on the information required for different levels of zoning taking account the various environments; (v) guidance on the reliability, validity and limitations of the applied statistical methods, (vi) advice on the required qualifications of the persons carrying out landslide susceptibility zoning.

## Conclusions

The scientific project LandSlidePlan, with the mission to reach new knowledge necessary for practical solutions of landslide susceptibility assessment in all types of Croatian environments prone to sliding, will enhance understanding of the landslide disaster risk due to MORLE (Multiple Occurrence of Regional Landslide Events) in Croatia. The resulting methodology will enable the efficient production of a series of landslide susceptibility maps by exploiting new technologies (i.e., LiDAR and ALS) that enable the mapping of small and shallow landslides. In addition, some goals of the project that are related to the research of the potential of the technological advances for landslide inventory mapping as well as the derivation of landslide causal factor maps on a large scale are also of crucial importance for risk assessment as well as for dissemination of location-based disaster risk information to decision-makers, the general public and communities at risk exposed to disaster. The use of these maps in the project is primarily aimed at the production of landslide susceptibility maps that will be used by the regional and local administration and decision-makers in the processes of land use planning.

The research in the framework of the LandSlidePlan is based on innovative technologies, realistic limitations related to the availability of spatial data in Croatia (limited amount of geological data) and urgent needs for efficient solutions applicable in the Croatian system of physical planning in line with European and global requirements related to sustainable development, human and environmental protection. The scientific and practical objective of the LandSlidePlan project is the development of a methodology for landslide susceptibility assessment using LiDAR technology and the most reliable modelling approaches for characteristic Croatian environments and sliding phenomena. Due to different natural conditions and land uses in different parts of Croatia, the methodology will be developed for three pilot areas, selected based on characteristic geological settings and degree of urbanisation.

LandSlidePlan contributes to developing Croatian scientific research potential by acquiring and applying new knowledge in the project, publishing scientific papers in high-quality journals, and bringing scientific excellence worldwide by developing a new research methodology. Other substantial impacts are:

- OSI<sub>1</sub> - Policy and regulations: LandSlidePlan will help decision-makers better understand tools and methodologies for analysing different landslide hazards and risk elements and their practical use in disaster risk management. Support decision-making with the interaction between policy makers and the scientific community. Improved competencies of policymakers, decision-makers and authorities from local, regional and national governments will improve policies and regulations.
- OSI<sub>2</sub> - Environmental impact: LandSlidePlan will help increase scientific research of landslides for its prevention. This implies new ideas and solutions to environmental threats, like landslides and adaptation measures to climate change.
- OSI<sub>3</sub> - Societal implications: Dissemination, communication and exploitation activities of the LandSlidePlan project will influence awareness and knowledge on landslide risk prevention methods and solutions in society, primarily through the public authorities. Cooperation of governmental authorities with the LandSlidePlan and transferring this information through different media can positively influence trust in public authorities. Furthermore, the practical measures disseminated to the public will also empower citizens in being better informed and community-supported.

## Acknowledgements

This work has been fully supported by Croatian Science Foundation under the project Methodology development for landslide susceptibility assessment for land use planning based on LiDAR technology (LandSlidePlan IP-2019-04-9900).

## References

- Alvioli M, Marchesini I, Reichenbach P, Rossi M, Ardizzone F, Fiorucci F, Guzzetti F (2016) Automatic delineation of geomorphological slope units with r.slopeunits v1.0 and their optimisation for landslide susceptibility modelling. *Geoscientific Model Development*. 9(11): 3975-3991.
- Arbanas Ž, Mihalić S, Grošić M, Dugonjić S, Vivoda M (2010) Brus Landslide, translational block sliding in flysch rock mass. *Proceedings of the European Rock Mechanics Symposium Eurock 2010*, 15-18 June 2010. CRC Press/Balkema, London. pp. 635-638.
- Bell FG (2003) *Geological hazards: their assessment, avoidance and mitigation*. Spon Press, Taylor and Francis Group, London, New York. (ISBN 9780415318518). 656p.
- Bernat S, Mihalić Arbanas S, Krkač M (2014a) Inventory of precipitation triggered landslides in the winter of 2013 in Zagreb (Croatia, Europe). *Landslide science for a safer geoenvironment*, volume 2: Methods of landslide studies. Springer, Cham. pp. 829-836.
- Bernat S, Mihalić Arbanas S, Krkač M (2014b) Landslides triggered in the continental part of Croatia by extreme precipitation in 2013. *Engineering geology for society and territory*, volume 2: Landslide processes. Springer, Heidelberg. pp. 1599-1603.
- Bernat Gazibara S (2019a) Methodology for landslide mapping using high resolution digital elevation model in the Podsljeme area (City of Zagreb). PhD thesis, University of Zagreb, Faculty of Mining, Geology and Petroleum Engineering, Zagreb, Croatia. (in Croatian)
- Bernat Gazibara S, Krkač M, Mihalić Arbanas S (2019b) Verification of historical landslide inventory maps for the Podsljeme area in the City of Zagreb using LiDAR-based landslide inventory. *Rudarsko-geološko-naftnižbornik*. 34(1): 45-58.
- Bernat Gazibara S, Cindrić Kalin K, Erak M, Krkač M, Đomlija P, Arbanas Ž, Mihalić Arbanas S (2019c) Landslide hazard analysis in national-scale for landslide risk assessment in Croatia. In: Uljarević M, Zekan S, Salković S, Ibrahimović Dž (eds.) *Proceedings of the 4th Regional Symposium on Landslides in the Adriatic-Balkan Region*, Sarajevo, Geotechnical Society of Bosnia and Herzegovina, pp. 175-182.
- Bonham-Carter GF (1994) *Geographic information system for geoscientists: modelling with GIS*. Pergamon, Oxford. (ISBN 9781483144948). 398p.
- Brenning A (2005) Spatial prediction models for landslide hazards: review, comparison and evaluation. *Natural Hazards and Earth System Sciences*. 5: 853-862.
- Cantarino I, Carrion MA, Goerlich F, Ibañez VM (2019) A ROC analysis-based classification method for landslide susceptibility maps. *Landslides*. 16(2): 265-282.
- Carrara A (1983) Multivariate models for landslide hazard evolution. *Math Geol*. 15: 403-427.
- Carrara A, Cardinali M, Guzzetti F, Reichenbach P (1995) GIS Technology in Mapping Landslide Hazard. In: *Geographical Information Systems in Assessing Natural Hazards*. Advances in Natural and Technological Hazards Research, vol 5. Carrara A, Guzzetti F (eds). Springer, Dordrecht. (ISBN 9789048145614). pp. 135-175.
- Chacón J, Irigaray C, Fernández T, El Hamdouni R (2006) Engineering geology maps: landslides and geographical information systems. *Bulletin of Engineering Geology and the Environment*. 65: 341-411.
- Chigira M, Duan F, Yagi H, Furuya T (2004) Using an airborne laser scanner for the identification of shallow landslides and susceptibility assessment in an area of ignimbrite overlain by permeable pyroclastics. *Landslides*. 1: 203-209.
- Chu HJ, Wang CK, Huang ML, Lee CC, Liu CY, Lin CC (2014) Effect of point density and interpolation of LiDAR-derived high-resolution DEMs on landscape scarp identification. *GIScience & Remote Sensing*. 51(6): 731-747.
- Chung CJF, Fabbri AG (2003) Validation of spatial prediction models for landslide hazard mapping. *Natural Hazards*. 30: 451-472.
- Clague JJ, Roberts NJ (2012) Landslide hazard and risk. In: *Landslides Types, Mechanisms and Modeling*. Clague J J, Stead D (eds). Cambridge, University Press, United Kingdom. (ISBN 9781107002067). pp. 1-9.
- Croatian National Platform for Disaster Risk Reduction, CNPDRR, (2019) *Disaster risk evaluation for The Republic of Croatia*, Zagreb, pp. 180. (in Croatian)
- Cruden DM, Varnes DJ (1996) *Landslide types and processes*. Special Report – National Research Council, Transportation Research Board, Special Report. 247: 36-75.
- Đomlija P. (2018) Identification and classification of landslides and erosion phenomena using the visual interpretation of the Vinodol Valley digital elevation model. PhD thesis, University of Zagreb, Faculty of Mining, Geology and Petroleum Engineering, Zagreb, Croatia. (in Croatian)
- Fell R, Corominas J, Bonnard C, Cascini L, Leroi E, Savage WZ (on behalf of the JTC-1 Joint Technical Committee on Landslides and Engineered Slopes) (2008a) Guidelines for landslide susceptibility, hazard and risk zoning for land use planning. *Engineering Geology*. 102: 85-98.
- Fell R, Corominas J, Bonnard C, Cascini L, Leroi E, Savage WZ (on behalf of the JTC-1 Joint Technical Committee on Landslides and Engineered Slopes) (2008b) Guidelines for landslide susceptibility, hazard and risk zoning for land-use planning. *Engineering Geology*. 102: 99-111.
- Frattini P, Crosta G, Carrara A (2010) Techniques for evaluating the performance of landslide susceptibility models. *Engineering Geology*. 111(1-4): 62-72.
- Galli M, Ardizzone F, Cardinali M, Guzzetti F, Reichenbach P (2008) Comparing landslide inventory maps. *Geomorphology*. 94: 268-289.
- Gorsevski PV, Gessler P, Foltz RB (2000) Spatial prediction of landslide hazard using discriminant analysis and GIS. *GIS in the Rockies 2000 Conference and Workshop: Applications for the 21st Century*, 25-27 September 2000. Denver, CO, USA. pp. 25-27.
- Gorsevski PV, Gessler PE, Foltz RB, Elliot WJ (2006) Spatial prediction of landslide hazard using logistic regression and ROC analysis. *Transactions in GIS*. 10(3): 395-415.
- Guzzetti F, Carrara A, Cardinali M, Reichenbach P (1999) Landslide hazard evaluation: a review of current techniques and their application in a multi-scale study, Central Italy. *Geomorphology*. 31(1-4): 181-216.
- Guzzetti F, Mondini AC, Cardinali M, Fiorucci F, Santangelo M, Chang KT (2012) Landslide inventory maps: new tools for an old problem. *Earth-Science Reviews*. 112: 42-66.
- Huang Y, Zhao L (2018) Review on landslide susceptibility mapping using support vector machines. *CATENA*. 165: 520-529.
- IPL, International Program on Landslides (2013) World report on landslides URL: <https://iplhq.org/ls-world-report-on-landslide/>
- Jaboyedoff M, Choffet M, Derron MH, Horton P, Loye A, Longchamp C, Mazotti B, Michoud C, Pedrazzini A (2012) Preliminary Slope Mass Movement Susceptibility Mapping Using DEM and LiDAR DEM. In: *Terrigenous Mass Movements*. Pradhan B, Buchroitner M (eds). Springer, Berlin, Heidelberg. (ISBN 9783642254949). pp. 109-170.
- Krkač M, Bernat Gazibara S, Sinčić M, Lukačić H, Mihalić Arbanas (2022) Landslide inventory mapping based on LiDAR data: Case study from Hrvatsko Zagorje (Croatia). *Proceedings of the 5th Regional Symposium on Landslides in the Adriatic-Balkan Region: Landslide Modelling & Application [in Press]*

- Mihalić Arbanas S, Krkač M, Bernat S (2016) Application of advanced technologies in landslide research in the area of the City of Zagreb (Croatia, Europe). *Geologia Croatica*. 69(2): 231–243.
- Mihalić Arbanas S, Sečanj M, Bernat Gazibara S, Krkač M, Begić H, Džindo A, Zekan S, Arbanas Ž (2017) Landslides in the Dinarides and Pannonian Basin—from the largest historical and recent landslides in Croatia to catastrophic landslides caused by Cyclone Tamara (2014) in Bosnia and Herzegovina. *Landslides* 14, 1861–1876. <https://doi.org/10.1007/s10346-017-0880-1>
- Mihalić Arbanas S, Bernat Gazibara S, Sečanj M, Damjanović V, Oršanić D, Penović S, Krkač M, Cindrić Kalin K, Đomlija P, Jagodnik V, Arbanas Ž (2019) Landslide risk management in Croatia: Current state. *Proceedings of the 4th Regional Symposium on Landslides in the Adriatic-Balkan Region, Sarajevo, Geotechnical Society of Bosnia and Herzegovina*, pp. 243-250.
- Ohlmacher GC, Davis J C (2003) Using multiple logistic regression and GIS technology to predict landslide hazard in northeast Kansas. *USA Eng Geol*. 69(33): 331–343.
- Petschko H, Bell R, Glade T (2015) Effectiveness of visually analysing LiDAR DMT derivatives for earth and debris slide inventory mapping for statistical susceptibility modeling. *Landslides*. 13(5): 857–872.
- Razak KA, Straatsma MW, van Westen CJ, Malet J-P, de Jong SM (2011) Airborne laser scanning of forested landslides characterisation: terrain model quality and visualisation. *Geomorphology*. 126: 186–200.
- Razak KA, Santangelo M, Van Westen CJ, Straatsma MW, de Jong SM (2013) Generating an optimal DMT from airborne laser scanning data for landslide mapping in a tropical forest environment. *Geomorphology*. 190: 112-125.
- Reichenbach P, Rossi M, Malamud BD, Mihir M, Guzzetti F (2018) A review of statistically-based landslide susceptibility models. *Earth-Science Reviews*. 180: 60–91.
- Scaioni M, Longoni L, Melillo V, Papini M (2014) Remote Sensing for Landslide Investigations: An Overview of Recent Achievements and Perspectives. *Remote Sensing*. 6: 1-53.
- Soeters R, van Westen CJ (1996) Slope instability recognition, analysis and zonation. In: *Landslides investigation and mitigation*, TRB Special Report 247. Turner AK, Schuster RL (eds). National Academy Press, Washington, DC. (ISBN 030906208X). pp. 129–177.
- Stumpf A, Kerle N (2011) Object-oriented mapping of landslides using random forests. *Remote Sensing of Environment*. 115: 2564–2577.
- UN (2015) Sendai Framework for Disaster Risk Reduction 2015 - 2030. The United Nations Office for Disaster Risk Reduction (eds). UN, Geneva. 37p.
- Van Den Eeckhaut M, Poesen J, Verstraeten G, Vanacker V, Moeyersons J, Nyssen J, van Beek LPH, Vandekerckhove L (2007) Use of LIDAR-derived images for mapping old landslides under forest. *Earth Surface Processes and Landforms*. 32: 754-769.
- Van Den Eeckhaut M, Kerle N, Poesen J, Hervás J (2012) Object-oriented identification of forested landslides with derivatives of single pulse LiDAR data. *Geomorphology*. 173–174: 30-42.
- van Schalkwyk A, Thomas MA (1991) Slope failures associated with the floods of September 1987 and February 1988 in Natal and Kwa-Zulu, Republic of South Africa. *Geotechnics in the African Environment*, pp. 57-63.
- van Westen CJ (2002) Use of weights of evidence modelling for landslide susceptibility mapping. ITC Publication. p21.
- Yin KJ, Yan TZ (1988) Statistical prediction model for slope instability of metamorphosed rocks. *Proceedings of the Fifth International Symposium on Landslides*, vol 2., 10-15 July 1988. Brookfield, VT, USA. pp. 1269–1272.

# Shallow landslide susceptibility assessment for the Polog region (North Macedonia)

Natasha Nedelkovska<sup>(1)</sup>, Igor Peshevski<sup>(2)</sup>, Milorad Jovanovski<sup>(2)</sup>, Jovan Papic<sup>(2)</sup>, Ivan Radevski<sup>(3)</sup>, Svemir Gorin<sup>(3)</sup>

1) Geohydroconsulting Ltd, Skopje, Manapo 7-2/5, North Macedonia, +38978 400 908 ([n\\_nedelkovska@hotmail.com](mailto:n_nedelkovska@hotmail.com))

2) Ss. Cyril and Methodius University, Faculty of Civil Engineering, Skopje, North Macedonia

3) Ss. Cyril and Methodius University, Faculty of Natural Sciences and Mathematics, Skopje, North Macedonia

**Abstract** This paper presents the results of a shallow landslide susceptibility assessment for the Polog region in Macedonia. The geomorphological setting of the Polog study area, the complex geology, and the specific hydro-meteorological conditions make this region one of the most landslide susceptible areas in the country. According to the available landslide inventory for the Polog region, 21% of landslides are classified as shallow landslides. The infinite slope stability method was used for shallow landslide susceptibility assessment over the study area. This is a simple but very useful model for planar sliding, which assumes that landslides are infinitely long but have a shallow sliding surface parallel to the ground surface. Due to the complexity of the analyzed phenomenon, the variability of influential factors, and uncertainty in parameters. Considering that this is a regional-scale analysis, selecting relevant parameters was very challenging. In order to get a sense of the susceptibility to shallow landslides, several possible scenarios were analyzed: with two groundwater levels (0.35 and 0.70 m of soil depth) and minimum and average values of geotechnical parameters of the lithological units. The obtained susceptibility maps indicate that the most prone zones for shallow landslide occurrences match with most landslides from the inventory. However, results are limited regarding the reliability of input data about soil thickness, the relevance of geotechnical parameters of soils, and the groundwater levels. In order to get more advanced analysis on a watershed scale, it is recommended to carry out more detailed geotechnical investigations and tests, monitoring of rainfalls, monitoring of surface water regimes, and groundwater levels.

**Keywords** shallow landslide, assessment, susceptibility map, Polog region

## Introduction

Shallow landslides are typically translational sliding movements of soil material, either earth and/or debris, characterized by a pre-defined, planar sliding surface in a depth of up to 2.0 m (Cruden & Varnes 1996; Hungr et al. 2014). In addition, according to the Swiss

recommendations (BWW, BRP, BUWAL 1997), landslides are classified as “shallow” if they are less than 2.0 m deep.

The shallow landslides are particularly destructive phenomena and lead to considerable loss of human life and property damage (Postance et al. 2017). For example, the catastrophic translational landslides, which occurred at Mt. Umyeon in July 2011, following nearly 49.5 mm/h of heavy rainfall, resulted in 18 deaths and more than 20 injuries in the central Seoul metropolitan area, along with tens of millions of dollars of residential and infrastructural damage (Lee and Park 2015). Another example is the event in October 2011, when the eastern Liguria (Vara Valley and Cinque Terre area) and northwestern Tuscany (Magra Valley) were affected by an extreme rainstorm with almost 600 mm/24 h that caused floods, thousands of shallow landslides, 13 casualties and damage to villages and infrastructure (Bartelletti et al. 2017). During 24–26 October 2010, an intense rainstorm during which the total precipitation in 3 days was around 250 mm affected a part of Tuscany and triggered 50 reported shallow landslides (Tofani et al. 2017). Presented examples lead to rainfall as the major trigger of shallow landslides.

The territory of Macedonia is severely and frequently affected by landslides, which are responsible for direct and indirect impacts on the structures, infrastructure, and population (Peshevski et al. 2017; Haque et al. 2016). A study on landslide distribution in the country has shown that the northwest part of the country, more precisely the Polog region, is the most prone to landslide processes, primarily triggered by heavy rainfalls and favoured by its geological, morphological, and tectonic setting (Peshevski et al. 2019). Therefore, appropriate risk management is urgently needed for this part of the country. Landslide susceptibility hazard and risk assessments are deemed necessary as well. For the Polog study area, preliminary landslide susceptibility studies were performed by Peshevski (2015). Some recent improvements were obtained by Peshevski et al. (2019), who presented a heuristic approach for preliminary regional landslide susceptibility assessment using a limited amount of data.

The main objective of this work was to develop a shallow landslide susceptibility map for the Polog region, considering that according to the landslide inventory, 21%

of the landslides in the region are confirmed in the class of shallow landslides (Nedelkovska et al. 2020).

### Study area

The Polog region is located in the northwest part of Macedonia (Fig. 1). It is characterized by mountainous topography and dense hydrographic network comprising torrential streams and rivers and high population density along the Shar Planina Range and Vardar River. From almost all geological periods, geological formations can be found here: from the Cambrian to the Quaternary period, characterized by different types of igneous, sedimentary,

and metamorphic rocks. The topographic relief of the Polog study area ranges from 265 to 2,700 m above the sea level with a complex morphology that is influenced by the tectonic and geologic conditions.

The Polog region has 3 types of climate:

- Hot continental at altitude of 600–900m a.s.l.
  - Cold continental climate at altitude of 900–1100m a.s.l.
  - Alpine mountainous climate at altitude over 2250m a.s.l.
- Summers are warm and partly humid, winters are cold and snowy, whereas springs and autumns are characterized by rainfall. The study area has the highest annual average amount of rainfall in the country (Ilijovski 2013); it ranges from 600 mm/year to more than 1,250 mm/year.

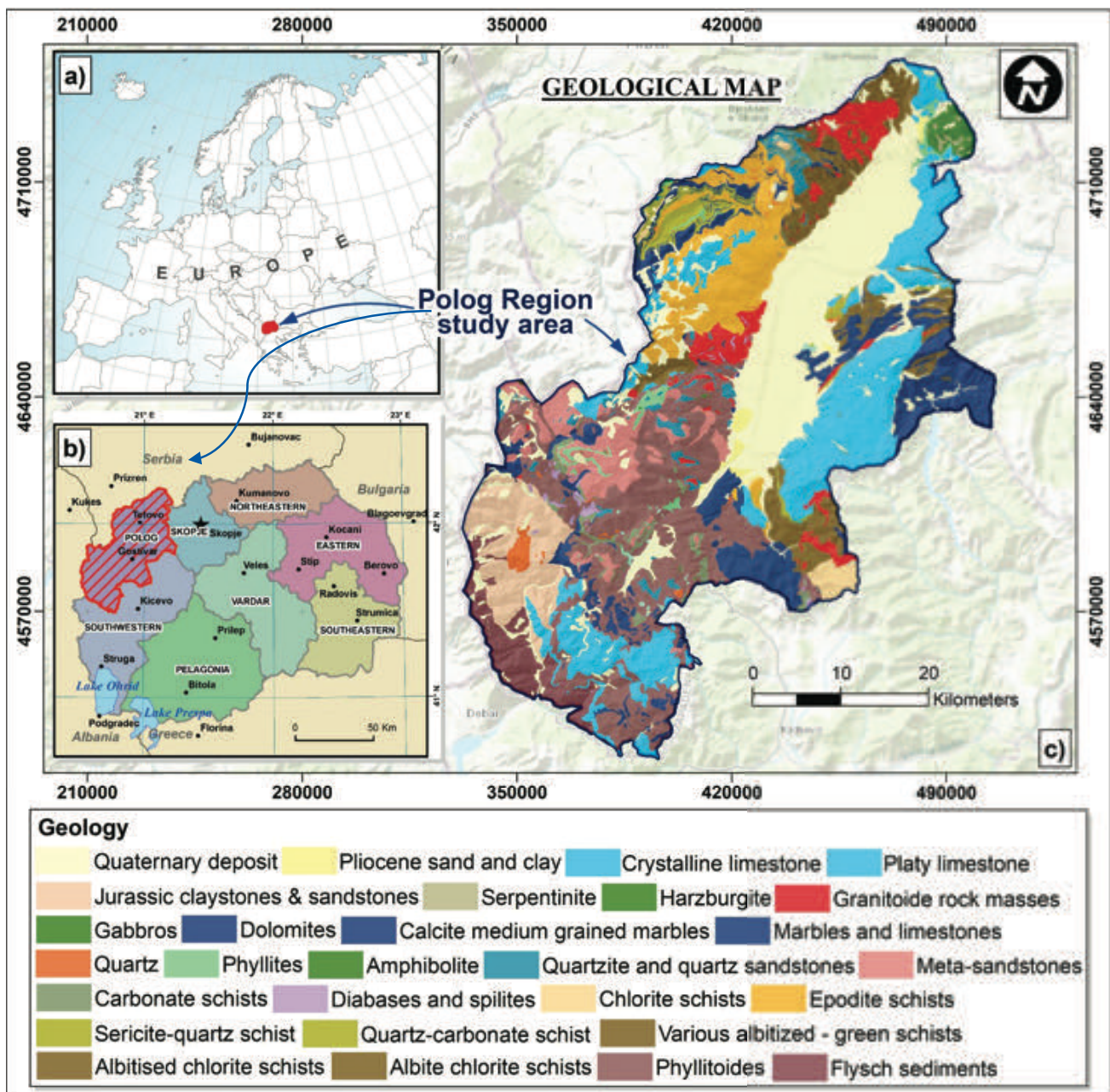


Figure 1 Polog region (North Macedonia) study area: a) location of North Macedonia in Europe; b) location of the Polog region in North Macedonia; c) geological map. (Jovanovski et al. 2021 – in print)

Historically, this region has been exposed to extreme weather conditions and frequent flooding. Numerous of devastating flash floods happened in 2015 and 2016 with huge human and economic losses (Peshevski et al. 2017). The losses were caused by torrential floods and mass flows and inappropriate land-use, such as construction in flood plains, rapid illegal building in hazard zones and constricted river courses, and increased erosion due to logging in forests. All these mentioned artificial changes alter the hydrological processes and regimes, increase the risk of floods and associated effects, such as landslides, rockfalls, mudflows, and generate other unfavorable engineering-geological processes. The effects of such activities are combined with climate changes as well, and related increases in the frequency of hydrological extremes.

### Methodology

A variety of methods have been developed for slope stability analysis on a regional scale (e.g. Montgomery and Dietrich 1994; van Westen and Terlien 1996; Borga et al. 2002; Saha et al. 2002; Ray 2008). The infinite slope method by Skempton and DeLory (1957) is a simple but very useful model for shallow sliding on a slip surface parallel to the slope. The infinite slope model assumes that landslides are infinitely long but have the shallow sliding surface, and therefore, this model is appropriate for the analysis of shallow landslides. The following equation was used for calculation of the safety factor *F* in this study, which has also been used by several other researchers (van Westen and Terlien 1996; Acharya et al. 2006; Ray and Smedt 2008):

$$F = \frac{C_s + C_r}{\gamma_e D \sin \theta} + (1 - m \frac{\gamma_w}{\gamma_e}) \frac{\tan \varphi}{\tan \theta} \quad [1]$$

wherein: *F* is the slope stability factor (adimensional), *C<sub>s</sub>* is the effective soil cohesion (kN/m<sup>2</sup>), *C<sub>r</sub>* is the root cohesion (kN/m<sup>2</sup>), *D* is the depth of the soil above the sliding surface (m),  $\varphi$  is friction angle of the soil (°),  $\theta$  is the slope angle (°),  $\gamma_w$  is the unit weight of water (kN/m<sup>3</sup>),  $\gamma_e$  is the effective unit weight of the soil (kN/m<sup>3</sup>), and *m* is wetness index. The effective unit weight is defined by Van Westen and Terlien (1996), as:

$$\gamma_e = \frac{q \cos \theta}{D} + (1 - m) \gamma_d + m \gamma_s \quad [2]$$

wherein:  $\gamma_d$  is the unit weight of the dry soil (kN/m<sup>3</sup>),  $\gamma_s$  is the unit weight (kN/m<sup>3</sup>) of the saturated soil, and *q* is any additional load on the soil surface (kN/m<sup>2</sup>).

The slope geometry and the different variables in the above equations are shown in Fig. 2, adapted from Skempton and DeLory (1957).

The cohesion, dry and saturated unit weight and the friction angle of the soil (Tab. 1) were adopted from the available 1:200 000 scale engineering-geological map of Macedonia (Geological survey Skopje, 1977).

The slope angle was derived from the digital elevation model of the terrain (DEM), with grid size of 10 x 10 m.

The approach proposed by Saulnier et al. (1997) was used, which expresses the depth of the soil above the sliding surface solely as a function of local elevation and has the form:

$$D = h_{max} - \frac{z_i - z_{min}}{z_{max} - z_{min}} (h_{max} - h_{min}) \quad [3]$$

wherein: *h<sub>i</sub>* is soil depth computed at pixel *i*, *h<sub>max</sub>* and *h<sub>min</sub>* are the maximum and minimum values of the soil depth in the area, *z<sub>i</sub>* is the local value of elevation at pixel *i*, while *z<sub>max</sub>* and *z<sub>min</sub>* are the maximum and minimum values of elevation encountered in the test area.

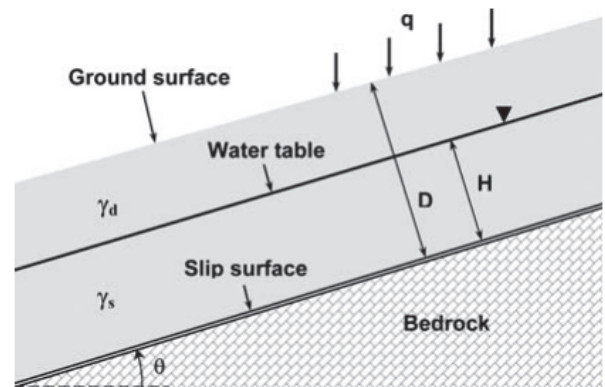


Figure 2 Schematic representation of the infinite slope method depicting the different parameters and variables (adapted from Skempton & DeLory 1957).

Table 1 Geotechnical parameters for the lithological units (Engineering-geological map of Macedonia, Geological survey Skopje, 1977).

Lithological unit	Unit weight of dry soil $\gamma_d$ [kN/m <sup>3</sup> ]		Unit weight of saturated soil $\gamma_s$ [kN/m <sup>3</sup> ]		Cohesion $C_s$ [kN/m <sup>2</sup> ]		Angle of internal friction $\varphi$ [°]	
	min	max	Min	max	min	max	min	max
Alluvial sediments	17.0	18.6	20.0	21.6	0.0	16.0	20.0	36.0
Proluvial sediments	15.5	16.5	18.5	19.5	1.0	22.0	24.0	32.0
Diluvial and eluvial -diluvial sediments	16.0	18.5	19.0	21.5	10.0	30.0	25.0	29.0
Glacial and fluvioglacial sediments	14.0	16.0	17.0	19.0	8.0	20.0	22.0	32.0
Lacustrine sandy-clayey sediments	15.5	18.0	18.5	21.0	13.0	28.0	21.0	34.0

Many researchers have estimated the value of root cohesion for different vegetation species growing in different environments that have been summarized in Chok et al. (2015). Considering the proposed values, as well as the forest cover information and land-use data for the Polog region from Corine Land Cover (CLC 2018) inventory, the representative values of root cohesion are presented in Tab. 2.

The parameter wetness index (m) theoretically expresses the relative position of the water table H/D, where H is the saturated thickness of the soil above the failure plain and D is the total depth of the soil above the failure plain (Ray and Smedt 2008). Since the available data for calculating the wetness index were very limited, two different scenarios were assumed of this value; namely, 0.35 and 0.70.

Since all input parameters were defined, the safety factor was calculated using the equations explained above. Considering that this is a regional scale geospatial analysis, the calculations are performed in GIS environment, using the software. Based on the obtained values for the safety factor, different stability classes (Tab. 3) were adopted according to Ray & Smedt 2008.

Table 2 Root cohesion for land-use types and species in the Polog region (adapted from Chok et al., 2015).

No.	Land-use type	Cr [kN/m <sup>2</sup> ]
1	Discontinuous urban fabric	0.0
2	Industrial or commercial units	0.0
3	Mineral extraction sites	0.0
4	Non-irrigated arable land	0.0
5	Fruit trees and berry plantations	2.0
6	Pastures	2.0
7	Complex cultivation patterns	1.5
8	Land principally occupied by agriculture, with significant areas of natural vegetation	2.0
9	Broad-leaved forest	7.0
10	Coniferous forest	10.0
11	Mixed forest	2.0
12	Natural grasslands	0.0
13	Moors and heathland	2.0
14	Sclerophyllous vegetation	2.0
15	Transitional woodland-shrub	2.0
16	Sparsely vegetated areas	0.0
17	Burnt areas	0.0

Table 3 Adopted slope stability classes (according to Ray and Smedt, 2008).

Safety factor	Slope stability class
$F > 1.5$	Stable
$1.25 < F < 1.5$	Moderately stable
$1 < F < 1.25$	Quasi stable
$F < 1$	Unstable

## Results and discussion

Several scenarios were analyzed for the Polog region, to get landslide hazard/susceptibility assessment in two different groundwater levels (0.35 and 0.70 of soil depth) and by taking into consideration the minimum and average values of the geotechnical strength parameters of the lithological units. Fig. 3 shows the obtained shallow landslide susceptibility maps.

The obtained susceptibility maps show that the most shallow landslide-prone zones match with most landslides from the inventory. In addition, the results suggest that shallow landslides are more likely to occur in the northernmost watersheds than in southern ones. If we consider the hypsometric position of the susceptibility zones in all performed models, it is obvious that most landslides are expected to occur in the transition zone of the mountainous terrain towards the valley. Again, the northernmost part of the region is an exception because, therein, shallow landslides should be expected throughout the entire watersheds.

## Conclusions

The obtained results are limited in regards to the precision of the data related to soil thickness and relatively low number of data (and unevenly distributed sampling points in the region) for the geotechnical parameters of soils, as well as the groundwater levels. All these limitations should be overcome in more advanced studies on sub/watershed scales.

Therefore, it is considered that the proposed approach helps in the preliminary zonation of shallow landslide susceptibility of the region. In order to perform a more detailed analysis on the coarser scale, and with a higher level of confidence in results, much more work should be performed on selected watersheds within the region. The exportation of the same procedure to other regions of Macedonia is envisaged in order to foster the improvement of awareness of authorities for the landslide hazards in the country context.



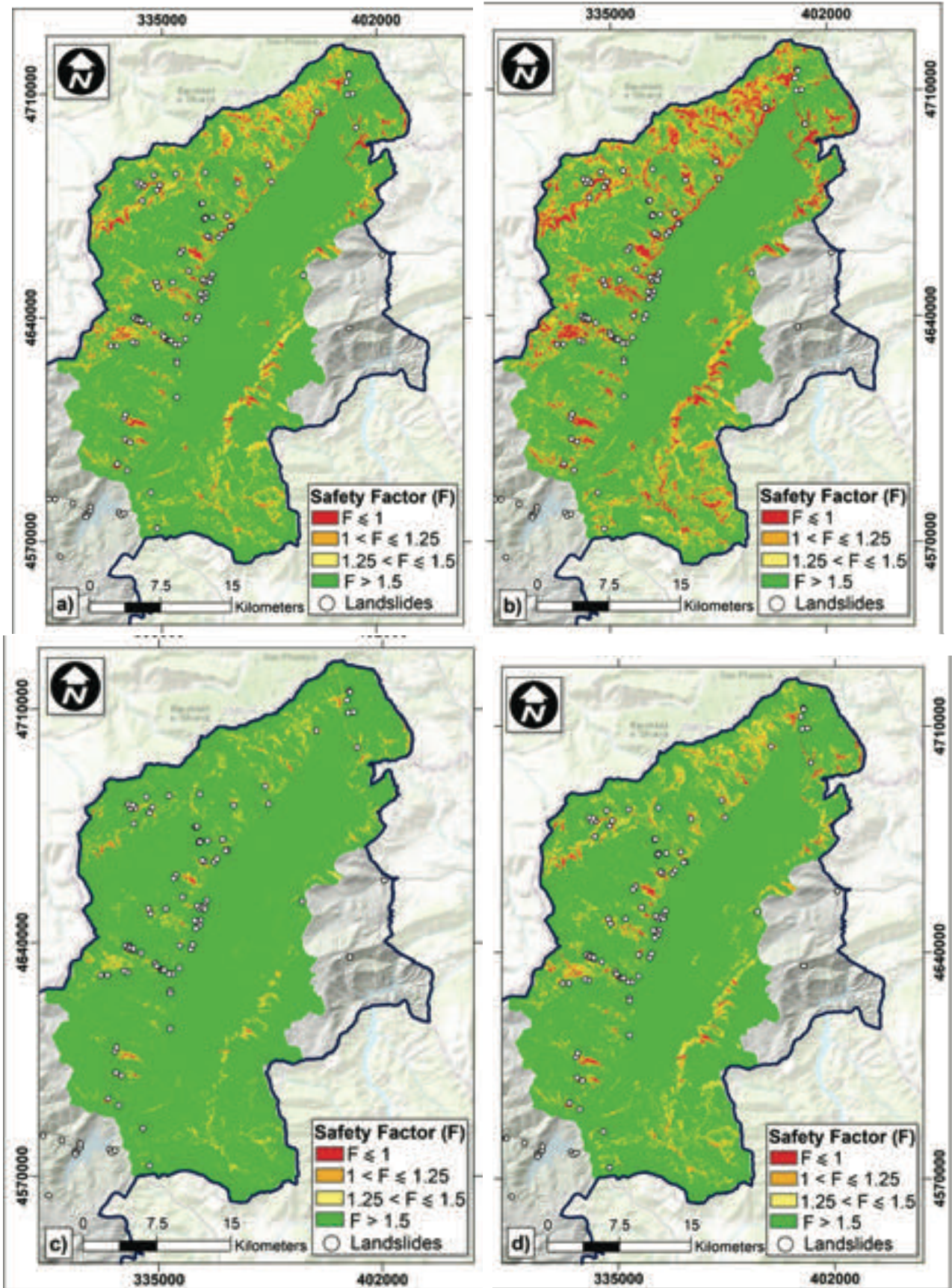


Figure 3 Shallow landslide susceptibility models for Polog Region: minimum values (Tab. 1) of the geotechnical parameters with a)  $m=0.35$  and b)  $m=0.70$ ; average values (Tab. 1) of the geotechnical parameters with c)  $m=0.35$  and d)  $m=0.70$ .

## References

- Acharya G, DE Smedt F, Long NT (2006) Assessing landslide hazard in GIS: a case study from Rasuwa, Nepal. *Bulletin of Engineering Geology and the Environment*. 65(1): 99–107.
- Bartelletti C, Giannecchini R, D'Amato Avanzi G, Galanti Y, Mazzali A (2017) The influence of geological–morphological and land use settings on shallow landslides in the Pogliaschina T. basin (northern Apennines, Italy). *Journal of Maps*. 13(2): 142–152.
- Borga M, Dalla Fontana G, Cazorzi F (2002) Analysis of topographic and climatologic control on rainfall-triggered shallow landsliding–using a quasi-dynamic wetness index. *Journal of Hydrology*. 268: 56–71.
- BWW/BRP/BUWAL (1997) Consideration of Flood Hazards for Activities with Spatial Impact. Recommendations. Bundesamt für Wasserwirtschaft BWW, Bundesamt für Raumplanung BRP, Bundesamt für Umwelt, Wald und Landschaft BUWAL, Berne, Switzerland. (in German, French version also available).
- Chok YH, Jaksa MB, Kaggwa W S, Griffiths D V (2015) Assessing the influence of root reinforcement on slope stability by finite elements. *Geo-Engineering* 6(12): 1–13
- Cruden DM, Varnes DJ (1996) Landslide Types and Processes. In: Turner AK, Schuster RL (eds) *Landslides– investigation and mitigation*. National Research Council, Transportation Research Board, National Academy Press, Washington DC. pp. 36–75.
- Engineering-geological map of Macedonia (1977) Geological survey Skopje. Skopje, Macedonia.
- Haque U, Blum P, Da Silva PF, Andersen P, Pilz J, Chalov RS, Malet JP, Jemec Auflič M, Andres N, Poyiadji E, Lamas CP, Zhang W, Peshevski I, Pétursson GH, Kurt T, Dobrev N, García-Davalillo JC, Halkia M, Ferri S, Gaprindashvili G, Engström J, Keellings D (2016) Fatal landslides in Europe. *Landslides*. 13: 1545–1554.
- Hungr O, Leroueil S, Picarelli L (2014) The Varnes classification of landslide types, an update. *Landslides*. 11: 167–194.
- Ilijovski Z (2013) Methodology for preparation of groundwater vulnerability maps. Doctoral dissertation, Faculty of civil engineering, Skopje, Macedonia.
- Jovanovski M, Peshevski I, Gjorgiev G, Nedelkovska N, Nicodemo G, Reale D, Fornaro G, Peduto D (2021) Landslide characterization in the Polog Region (R.N. Macedonia) by innovative and conventional methods. *Rivista Italiana di Geotecnica*. - in print
- Lee JH, Park HJ (2016) Assessment of shallow landslide susceptibility using the transient infiltration flow model and GIS-based probabilistic approach. *Landslides*. 13: 885–903.
- Montgomery DR, Dietrich WE (1994) A physically based model for the topographic control on shallow landsliding. *Water Resources-Research*. 30(4): 1153–1171
- Nedelkovska N, Peševski I, Jovanovski M, Papić J, Gorin S, Radevski I (2020) Preparation of GIS landslide inventory for the Polog region. *Geologica Macedonica*. 34(2): 137–148.
- Peshevski I (2015) Landslide susceptibility modelling using GIS technology. PhD thesis, Faculty of Civil Engineering, Skopje, Macedonia.
- Peshevski I, Peternel T, Jovanovski M (2017) Urgent need for application of integrated landslide risk management strategies for the Polog region in R. of Macedonia. *Proceedings of 4th World Landslide Forum*, 29 May – 02 June 2017. Ljubljana, Slovenia. pp. 135–145.
- Peshevski I, Jovanovski M, Abolmasov B, Papić J, Marjanović M, Haque U, Nedelkovska N (2019) Preliminary regional landslide susceptibility assessment using limited data. *Geologica Croatica*. 72(1):81–92.
- Postance B, Hillier J, Dijkstra T, Dixon N (2017) Comparing threshold definition techniques for rainfall induced landslides: a national assessment using radar rainfall. *Earth Surface Processes and Landforms*. 43(2): 553–560.
- Ray RL, DE Smedt F (2008) Slope stability analysis on a regional scale using GIS: a case study from Dhading, Nepal. *Environmental Geology*. 57: 1603–1611.
- Saha AK, Gupta RP, Arora MK (2002) GIS-based landslide hazard zonation in the Bhagirathi (Ganga) Valley, Himalayas.- *International Journal of Remote Sensing*. 23(2): 357–369.
- Saulnier GM, Beven KJ, Oblet C (1997) Including spatially variable effective soil depths in TOPMODEL. *Journal of Hydrology*. 202: 158–172.
- Skempton AW, Delory FA (1957) Stability of natural slopes in London clay. *Proceedings of 4th International Conference on Soil Mechanics and Foundation Engineering*, 12–24 August 1957. London, England. pp. 378–381.
- Tofani V, Biondi G, Rossi G et al. (2017) Soil characterization for shallow landslides modeling: a case study in the Northern Apennines (Central Italy). *Landslides*. 14 :755–770.
- Van Westen CJ, Terlien TJ (1996) An approach towards deterministic landslide hazard analysis in GIS: a case study from Manizales (Colombia). *Earth Surface Processes and Landforms*. 21(9): 853–868.

# MASPREM – Slovenian landslide forecasting and warning system

Tina Peternel<sup>(1)</sup>, Jasna Šinigoj<sup>(1)</sup>, Mateja Jemec Auflič<sup>(1)</sup>, Špela Kumelj<sup>(1)</sup>, Matija Krivic<sup>(1)</sup>

1) Geological Survey of Slovenia, Geological Information Centre, Dimičeva ulica 14, Ljubljana, Slovenia. +386 1 2809 813 (tina.peternel@geo-zs.si)

**Abstract** The fact that Slovenia is highly exposed to landslides underlines the need for preventive measures to reduce the hazard associated with landslides in the future. Therefore, in 2011, the Geological Survey of Slovenia (GeoZS) started developing the MASPREM system to predict landslides hazard due to increased rainfall in Slovenia. Today the system is fully automated and based on open source software (PostgreSQL, PostGIS, Java, MapServer, OpenLayers). The system runs every 12 hours and reaches the forecast 24 hours in advance.

The calculation of the forecast model is based on the following input data: national landslide susceptibility map, threshold values for each engineering geological unit and rainfall forecast models ALADIN/SI and INCA (obtained by Slovenian Environment Agency). The results of the calculated landslide forecast models are displayed in the form of maps with a five-level scale on the control panel. In case of a calculated hazard, the system automatically sends an e-warning to registered users. MASPREM is also used by the GeoZS emergency service and by the Administration of the Republic of Slovenia for Civil Protection and Disaster Relief. In addition, the Slovenian landslide forecasting and warning system aims to improve and reduce landslide disaster risk. These goals were also written into the recent Kyoto2020 Commitment for Global Promotion of Understanding and Reducing Landslide Disaster Risk (KS2020), which provides a long-term and global framework for the landslide community to develop ISDR-ICL Sendai Partnerships 2015–2025.

**Keywords** landslide forecast system, rainfall threshold values, Masprem, Slovenia

## Introduction

The morphology of the slopes, unfavourable geological and tectonic conditions and climatic diversity contribute to the high susceptibility to landslides in Slovenia. According to previous studies, one third of Slovenia is highly susceptible to landslides (Komac and Ribičič 2006). Consequently, almost one fifth of the Slovenian population lives in areas that are highly prone to landslides (Komac 2012).

Recently, landslides have been quite frequent and have caused significant damage to infrastructure,

buildings and agricultural land. According to the latest data in Slovenia, the estimated damage caused by landslides is about 100 million for the period from 1994 to 2008 (Komac, 2017). While the Ministry of the Environment and Spatial Planning, reported that landslides have caused damage of about 350 million in the last decade (Intihar, 2020). The damage mainly affected infrastructure, agricultural land and facilities.

The most common phenomenon in Slovenia are shallow landslides, caused mainly by intense short- or long-lasting rain events (Jemec & Komac 2013; Rosi et al. 2016; Jemec et al. 2016; Jemec et al. 2018; Jordanova et al. 2020).

The potential consequences caused by landslides can be mitigated by implementing appropriate hazard management and prevention measures. Regionally, implementation of a landslide early warning system (LEWS) is widely used to assess the probability of occurrence of rainfall-induced landslides in large areas (Piciullo et al. 2017). In general, all LEWS use meteorological forecasts and rainfall threshold values. A comprehensive overview of the different LEWS was given by Piciullo et al. 2017; Pecoraro et al. 2019; Guzzetti et al. 2020. Although landslides are among the major natural hazards causing significant damage to property and infrastructure worldwide, Guzzetti (et al. 2020) noted that many areas with numerous fatal landslides, where landslide risk to the population is high, lack LEWSs.

The aim of this paper is to present the Slovenian landslide forecasting and warning system, from the conceptual to the operational phase.

## Methodology

### Architecture of MASPREM system

The MASPREM system generally consists of 3 separate modules (Fig. 1):

- (1) the module for daily data transmission;
- (2) dynamic forecast modelling module;
- (3) distribution model.

The *module for daily data transmission* ensure that rainfall forecast models (obtained by Slovenian Environment Agency) are transferred to the GeoZS server.

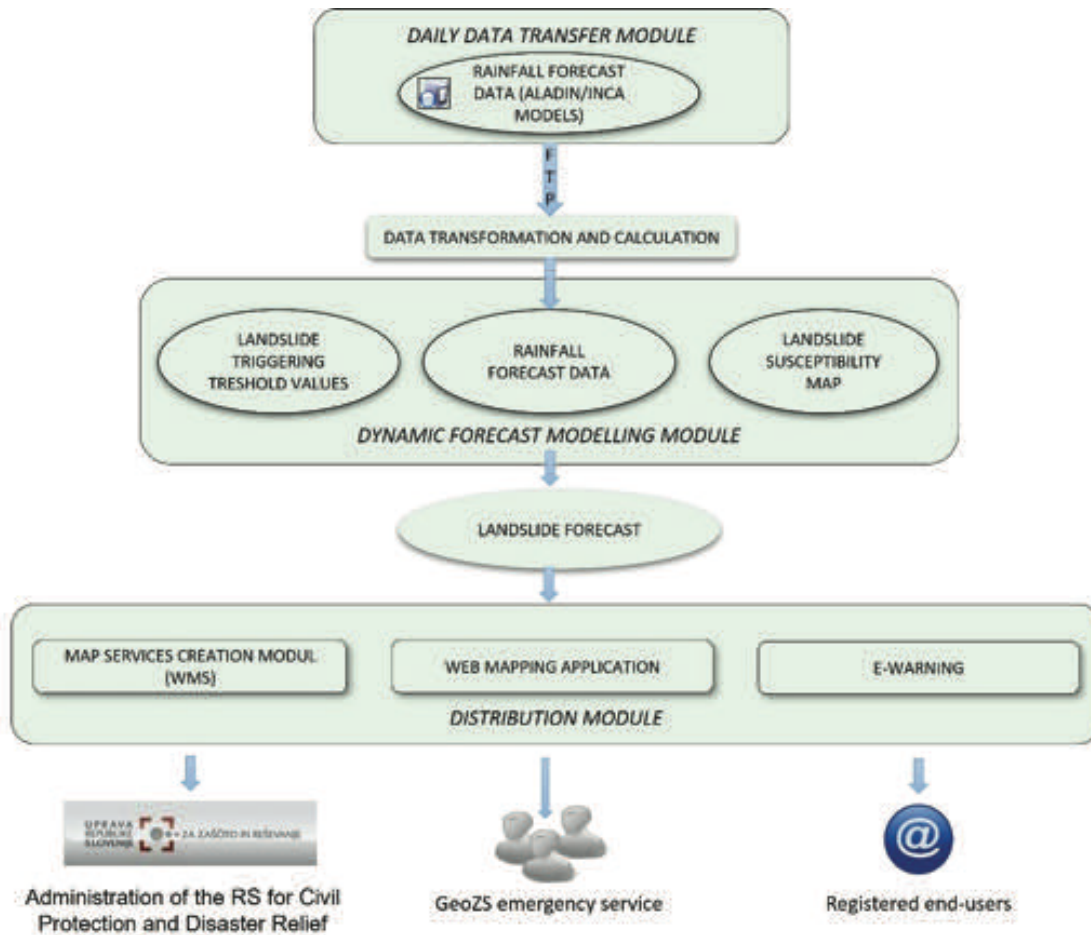


Figure 1 Architecture of MASPREM system.

The core of the landslide forecast system is the *dynamic forecast modelling module*, which is based on an algorithm that enables the calculation of the following input data:

- (1) national landslide susceptibility map at a scale of 1:250,000,
- (2) two types of threshold values determined for each engineering-geologic unit and
- (3) rainfall forecast models ALADIN/SI and INCA.

The *distribution module* provides that the MASPREM system is a fully automated system and runs every 12 hours and reaches the forecast 24 hours in advance. It is based on open-source software (PostgreSQL, PostGIS, Java, MapServer, OpenLayers).

The computed landslide forecast models are calculated in the form of raster maps with a five-level scale with classes from negligible to very high landslide probability. The maps are displayed on the MASPREM web control panel and are intended for use by end users (presented in the Results chapter).

The system has been fully operational since September 2013. Nevertheless, the results should be treated with caution and must be interpreted by experts (GeoZS emergency services).

In the following text we present the *dynamic forecast modelling module* in more detail.

#### Landslide susceptibility map (LSM)

One of the key elements of dynamic forecast modelling module is a Slovenian landslide susceptibility map at scale a 1: 250,000. It represents a static input.

The landslide susceptibility map of Slovenia is based on the extensive landslide database compiled and standardised at the national level and on analyses of spatial occurrence of landslides (Komac and Ribičič 2006). About 3,200 landslides with known location were selected and used for the univariate statistical analyses ( $\chi^2$ ) to predict the occurrence of landslides in relation to the spatiotemporal precondition factors (lithology, slope inclination, slope curvature, slope aspect, distance to geological contacts, distance to structural elements, distance to surface water, flow length, and land cover type) and in relation to the triggering factors (maximum 24-h rainfall, average annual rainfall intensity, and peak ground acceleration). The analyses were performed using GIS in a raster format with a pixel size of 25 x 25 m. Five groups of lithologic units were defined, ranging from low to high susceptibility to landslides. Critical slopes for landslide occurrence, other terrain characteristics and land cover

types more susceptible to landslides were also defined. Critical rainfall amounts and peak ground acceleration were defined as triggering factors. These results were later used as the basis for developing the weighted linear susceptibility model (Komac and Ribičič 2006).

#### Landslide triggering threshold value

Due to the low density of the rainfall gauge network in Slovenia (one rainfall gauge per 460 km<sup>2</sup>) and the associated uncertainty, the rainfall threshold values (RT<sub>1</sub>) are defined using the non-parametric statistical method Chi-square ( $\chi^2$ ) for each lithological unit (Tab. 2). In this order, we separately cross-analysed the occurrence of landslides within each individual class derived from the spatial cross-analysis of the lithologic units and the classes of maximum 24-hour rainfall. Maximum daily rainfall greater than 90 mm was found to be critical for landslide occurrence, particularly in loose soils and in less resistant rocks (e.g., Quaternary, Tertiary, Triassic, and Permo-Carbonian rocks). According to previous analyses (Jemec and Komac, 2013; Jemec et al., 2018; Rosi et al., 2016), the rainfall thresholds have been corrected by experts so that some lithological units have lower rainfall thresholds (RT<sub>2</sub>), as shown by the statistics (Tab. 2). This is due in particular to the large number of landslides in the last 10 years (annual technical reports and bulletins, ACPDR), which are not registered in the landslide database because they could not be precisely located.

#### Rainfall forecast data

Rainfall forecast data is the only dynamic input of the dynamic forecast modelling module. The MASPREM system uses two types of rainfall forecast models provided by the Slovenian Environment Agency.

(1) the regional ALADIN/SI model for Slovenia predicts the state of the atmosphere over the territory of Slovenia up to 72 hours in advance (Pristov et al. 2012). The model simulates precipitation (kg/m<sup>2</sup>), snowfall, water in snowpack, and air temperature data. ALADIN/SI is a grid point model (439×2421×43), where the horizontal distance between grid points is 4.4 km and it runs on a 6-hour cycling mode for the next 54 hours.

(2) The INCA/SI (Integrated Nowcasting through Comprehensive Analysis) model represents very short-term or real-time weather forecasts at high spatial and temporal resolution. The INCA model for approximating atmospheric conditions uses the spatial fields of meteorological variables of a numerical meteorological model (ALADIN) and interpolation methods to compute 3-dimensional high-resolution physical consistency analysis (spatial resolution: 1 km). For that it includes a wide range of different measurements (data from conventional and automatic meteorological stations, radar and satellite data and other available data outside the national meteorological network) (Šajn Slak et al. 2012).

Table 1 Landslide triggering rainfall threshold values for lithostratigraphic units (RT<sub>1</sub>-statistical defined; RT<sub>2</sub>-corrected in accordance to annual landslide reports). Critical 24-h rainfall intensities are presented only for lithostratigraphic units for which the number of observed landslides were statistically higher than the number of expected landslides.

Lithostratigraphic unit	RT <sub>1</sub> (mm)	RT <sub>2</sub> (mm)
predominantly clay soils	-	-
marsh and lake sediments (clay, silt, peat)	-	-
alluvium, fluvial loose sediments in terraces	-	-
clayey – diluvial, proluvial	90 - 120	70 - 90
gravely with a clayey component	150 - 180	150 - 180
gravely (predominantly thick fraction), moraines	210 - 240	210 - 240
clayey	90 - 120	70 - 90
alternation of fine and coarse grain soils	90 - 120	70 - 90
pebbly	90 - 120	70 - 90
mine tailings – gangues	120 - 150	120 - 150
clayey, marly rocks	90 - 120	70 - 90
clayey, marly and limestone	90 - 120	90 - 120
alternation of different materials (marl, sand, sandstone, conglomerate pebble, clay)	90 - 120	70 - 90
conglomerate	90 - 120	90 - 120
(slaty) claystones with inclusion of other rocks	120 - 150	120 - 150
marl and sandstone (flysch) with inclusions of other rocks	210 - 240	150 - 180
sandstones and conglomerates with inclusions of other rocks	120 - 150	120 - 150
stratified and cliff limestones	-	-
flat limestones	-	-
limestones and dolomites	-	-
dolomites	-	-
limestones with marls	90 - 120	90 - 120
limestones with inclusions of other rocks	210 - 240	210 - 240
limestone conglomerates and breccia	120 - 150	120 - 150
phyllites, schists and slate	180 - 210	180 - 210
amphibolite and gneiss	120 - 150	120 - 150
diabase and other magmatic rocks with tuff	120 - 150	120 - 150
amphibolites, serpentinites, diaphthorites	120 - 150	120 - 150
tonalite, dacite, granodiorite	-	-

## Results

#### Landslide forecast models

Currently, the MASPREM system calculates five different landslide models in parallel. They differ in the combination of LSM, forecast models (ALADIN, INCA) and threshold values (RT<sub>1</sub>, RT<sub>2</sub>), as follows:

- Model 1: LSM + ALADIN forecast + RT<sub>1</sub>
- Model 2: LSM + 2-day ALADIN antecedent rainfall + ALADIN forecast + RT<sub>1</sub>

- Model 3: LSM + 2-day ALADIN antecedent rainfall + ALADIN forecast + RT<sub>2</sub>
- Model 4: LSM + 2-day INCA antecedent rainfall + ALADIN forecast + RT<sub>1</sub>
- Model 5: LSM + 2-day INCA antecedent rainfall + ALADIN forecast + RT<sub>2</sub>.

In order to achieve the higher reliability of the models, we regularly perform an evaluation and validation of the results. The validation of the results is based on a visual comparison of the landslide database (provided by e-Plaz) and the system's calculations of the probability of landslide occurrence for each day (Jordanova et al. 2019).

However, we must take into account that there are also limitations related to the input data that should not be neglected: the spatial resolution of the ALADIN model, the incomplete landslide inventory that is important for the validation, the definition of how many days of antecedent rainfall significantly affect the occurrence of landslides, the characteristics of the lithological units by water contents (Jemec Auflič et al. 2016; Jemec Auflič et al. 2017).

#### **Web-application e-Plaz**

Since 1998, GeoZS has been developing a landslide database that contains data from various archives and inventories. With the development of new methods for landslide, debris flow and rockfall susceptibility, the need for faster and more accurate updating of the database has increased. In order to ensure uniform (and standardized) collection of new data on landslide occurrence for the entire Slovenian territory, GeoZS created the Landslide and Erosion Inventory Sheet in 2015. The selection of data contained in it corresponds directly to the scheme used in the e-Plaz web application.

The main functions of the e-Plaz web application are to view, add and edit events, and attach additional documentation. These functions are defined by different views and controllers using the MVC model (Kumelj & Šinigoj 2017). The data model of the e-Plaz application combines several sets of objects of the same type: (a) basic information about the event - location, type; b) damaged and/or endangered parcels and objects; c) mitigation measures taken; d) additional documentation - reports, photos) describing the landslide based on its individual properties (attributes). Wherever possible, spatial data can be captured using a map and attributes can be described using predefined or categorized values, such as the categorisation of land use prescribed by the Ministry of Environment and Spatial Planning, and the Surveying and Mapping Agency of the Republic of Slovenia.

Standardized recording of landslide phenomena can make an important contribution to the quality and reliability of data on such events. At the same time, it enables spatial and temporal tracking of landslides, has a significant impact on verifying the reliability of the methodology for their assessment, and generally contributes to their understanding.

e-Plaz is available to stakeholders at national, regional (ACPDR branches), and municipal levels. GeoZS monitor the data input and use of the application itself and, together with ACPDR and the Ministry of Environment and Spatial Planning, ensures its long-term continuity.

The printout of the e-Plaz web application does not reflect the actual status of the occurrence of slope mass movements in Slovenia, but only the status of the collected events until the end of October 2021. Therefore, the printouts show only the data entered by registered users. By the end of October 2021, a total of 477 landslides for the period 1996-2021, covering 56 Slovenian municipalities, were entered into the e-Plaz web application (Fig. 2). A total of 225 users were registered, including 180 users from 132 out of 212 municipalities, 17 users from 11 out of 13 branches of the Protection and Rescue Administration of the Republic of Slovenia, and 28 users from 5 national organizations.

#### **First local early warning system**

In addition to the national landslide forecast system, we have developed the first local early warning system (EWS) specifically for landslide-prone area in the hinterland of the settlement of Koroška Bela (Karavanke mountain, NW Slovenia) (Peternel et al., 2022). The EWS is based on threshold values determined from analyses of real-time monitoring data (geotechnical, hydrometeorological and geodetic sensors) and reconstruction of past events.

For the GeoZS emergency service and stakeholders (civil protection, municipality, etc.), we have set up customised web dashboard that allow access to all real-time monitoring sensors (Zupan et al. 2022). In the future, we plan to upgrade the local warning system with emails notifications sent to registered users when determined threshold values will be exceeded.

#### **End-users**

The end users of the MASPREM system are:

- GeoZS Emergency Services provides early warnings in the case of increased hazard of landslides;
- Administration of the Republic of Slovenia for Civil Protection and Disaster Relief which carries out the management, preparation and operation of the system for protection against natural and other disasters in Slovenia;
- Ministry of the Environment and Spatial Planning which provides funding for the research and expert bases for the identification of landslide hazard areas.

End users also include municipalities and civil protection, which are actively involved in landslide data acquisition and collection using of landslide central landslide database e-Plaz, as well as experts dealing with landslides and landslide-related issues, such as contractors, foresters, etc. For the future, we plan to strengthen cooperation also with national infrastructure authorities.

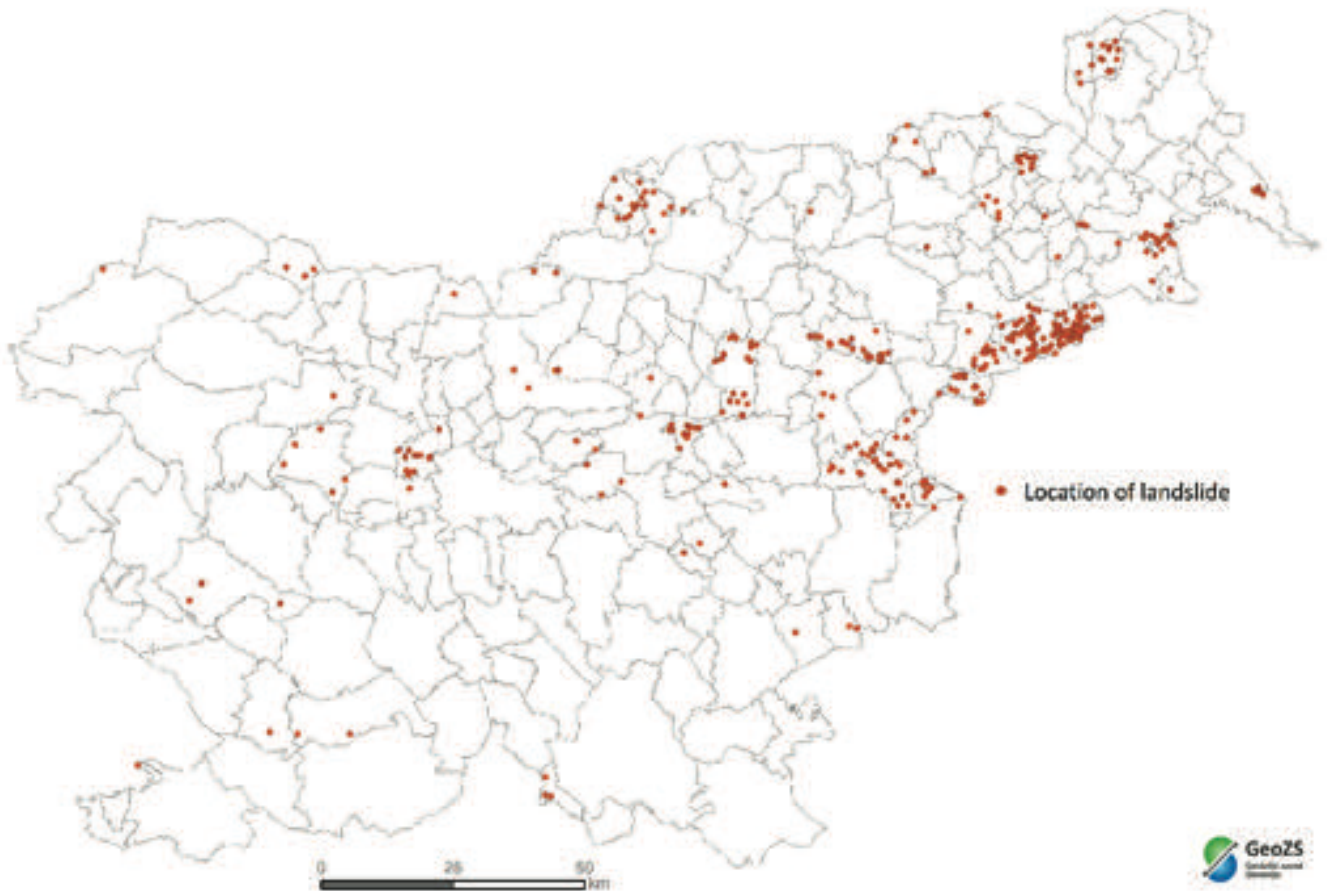


Figure 2 Locations of landslides collected in the e-Plaz web application till end of October 2021.

## Conclusions

According to the landslide database of Geological Surveys of Europa, 7,273 landslides have been recorded in Slovenia. Thus, the calculated landslide density is 0.4 landslides/km<sup>2</sup> or 1 landslide per 2,5 km<sup>2</sup> (Herrera et al., 2018). The triggering mechanisms for landslide occurrence in Slovenia are mainly related to intense precipitation. Due to climate change, the frequency and intensity of precipitation events is expected to increase, and thus the occurrence of landslides in Slovenia (Jemec Auflič et al., 2021).

Therefore, an operational landslide forecasting system is essential to reduce the impact of landslide activity. In Slovenia, the MASPREM system and its web-application e-Plaz have proven valuable and the GeoZS service regularly uses it to inform the relevant authorities of an increased probability of landslide occurrences due to exceeding the rainfall thresholds values. Despite the fact that the system is operational, it is still being constantly validated and improved.

In 2021, the system MASPREM received the Bronze Award for Regional Innovation from the Chamber of Commerce and Industry of Slovenia.

## Acknowledgments

The development of Slovenian landslide forecasting and warning system was conducted in the frame of MASPREM project, funded by the Administration of the Republic of Slovenia for Civil Protection and Disaster Relief (Ministry of Defence).

The research was also supported by the Slovenian Research Agency (Research Program P1-0419, project Z1-2638, Infrastructure programme I0-0007), the Ministry of Environment and Spatial Planning, and the Municipality of Jesenice.

## References

- Guzzetti F, Gariano SL, Peruccacci S, Brunetti MT, Marchesini I, Rossi M, Melillo M (2020) Geographical landslide early warning systems. *Earth-Science Reviews* 200: 102973.
- Herrera G, Mateos RM, García-Davalillo JC et al (2018) Landslide databases in the Geological Surveys of Europe. *Landslides* 15: 359-379.
- Intihar A (2020). S plazovi se moramo naučiti živeti. *Delo* 16. 11. 2020. URL: <https://www.delo.si/lokalno/primorska-in-notranjska/nauciti-se-moramo-sobivati-s-plazovi/> (17. 1. 2021)
- Jemec M, Komac M (2013) Rainfall patterns for shallow landsliding in perialpine Slovenia. *Nat Hazards*. 67: 1011–1023.

- Jemec Auflič M, Šinigoj J, Krivic M, Podboj M, Peternel T., Komac M (2016) Landslide prediction system for rainfall induced landslides in Slovenia (Masprem). *Geologija*. 59(2): 259-271.
- Jemec Auflič M, Šinigoj J, Krivic M (2017) Challenges for operational forecasting of rainfall-induced landslides in Slovenia. *Proceedings of the 3rd Regional Symposium on Landslides in the Adriatic Balkan Region*, 11-13 October 2017. Ljubljana, Slovenia. pp. 71-76.
- Jemec Auflič M, Šinigoj J, Peternel T, Podboj M, Krivic M, Komac M (2018) TXT-tool 2.386-2.1 A System to Forecast Rainfall-Induced Landslides in Slovenia. *Landslide Dynamics: ISDR-ICL Landslide Interactive Teaching Tools*. Sassa K et al (eds). Springer, Cham. (978-3-319-57774-6). 391p.
- Jemec Auflič M, Bokal G, Kumelj Š, Medved A, Dolinar M, Jež J (2021) Impact of climate change on landslides in Slovenia in the mid-21st century. *Geologija*. 64(2): 159-171.
- Jordanova G, Gariano SL, Melillo M, Peruccacci S, Brunetti MT, Jemec Auflič M (2020) Determination of Empirical Rainfall Thresholds for Shallow Landslides in Slovenia Using an Automatic Tool. *Water*. 12: 1449.
- Jordanova G, Verbovšek T, Jemec Auflič M (2019) Validation and proposal of new rainfall thresholds for shallow landslide prediction in Posavsko hills, Eastern Slovenia. *Proceedings of the 4th Regional Symposium on Landslides in the Adriatic-Balkan Region*, 23–25 October 2019. Sarajevo, BIH. pp. 37–42.
- Komac M, Ribičič M (2006) Landslide susceptibility map of Slovenia at scale 1:250,000. *Geologija* 49(2):295–309.
- Komac M (2012) Regional landslide susceptibility model using the Monte Carlo approach - the case of Slovenia. *Geol Q*. 56(1): 41-54.
- Komac M (2017) Preučevanje zemeljskih plazov v Sloveniji v preteklih dveh desetletjih z vidika geologije in sorodnih ved ter predstavitev primera metodologije prostorske analize pojavljanja zemeljskih plazov. *Ujma*. 31: 161-170.
- Kumelj Š, Šinigoj J (2017) e-Plaz – spletna aplikacija za popis in pregledovanje plazov in erozije. *Trajnostni razvoj mest in naravne nesreče*. Zorn M et al (eds) GIAM ZRC SAZU, Ljubljana. (ISBN 978-254-993-0). 117 p.
- Pecoraro G, Calvello M, Picoulo L (2019) Monitoring strategies for local landslide early warning systems. *Landslides*. 16: 213-231.
- Peternel et al (2022) Mountainous slopes above Koroška Bela (NW Slovenia) – a potential source area of debris flows. *Abstract proceedings of the 5th Regional Symposium on Landslides in the Adriatic-Balkan Region (In press)*, 23-26 March 2022. Rijeka, Croatia.
- Piciullo L, Gariano SL, Melillo M, Brunetti MT, Peruccacci S, Guzzetti F, Calvello M (2017) Definition and performance of a threshold-based regional early warning model for rainfall-induced landslides. *Landslides*. 14: 995 – 1008.
- Pristov N, Cedilnik J, Jerman J, Strajnar B (2012) Priprava numerične meteorološke napovedi ALADIN-SI. *Vetrnica*, pp 17–23
- Rosi A, Peternel T, Jemec Auflič M, Komac M, Segoni S, Casagli N (2016) Rainfall thresholds for rainfall-induced landslides in Slovenia. *Landslides*. 13(6):1571–1577
- Zupan M, Bavdek A, Vihtelič A, Šinigoj J (2022) Utilisation of central datahub and web application for collecting and disseminating landslide monitoring data. *Abstract proceedings of the 5th Regional Symposium on Landslides in the Adriatic-Balkan Region (In press)*, 23-26 March 2022. Rijeka, Croatia.



# Harmonized approach for mapping the earthquake-induced landslide hazard at the cross-border region between North Macedonia, Greece and Albania

Julijana Bojadjieva<sup>(1)</sup>, Vlatko Sheshov<sup>(1)</sup>, Kemal Edip<sup>(1)</sup>, Radmila Shalic<sup>(1)</sup>, Marta Stojmanovska<sup>(1)</sup>, Roberta Apostolska<sup>(1)</sup>, Stavroula Fotopoulou<sup>(2)</sup>, Dimitris Pitilakis<sup>(2)</sup>, Neritan Shkodrani<sup>(3)</sup>, Markel Babaleku<sup>(3)</sup>, Francesca Bozzoni<sup>(4)</sup>, Antonella di Meo<sup>(4)</sup>

1) University Ss Cyril and Methodius, Institute of earthquake engineering and engineering seismology -IZIS, Skopje, N. Macedonia

2) Aristotle University of Thessaloniki - AUTH, Thessaloniki, Greece

3) Polytechnic University of Tirana, Albania, Faculty of Civil Engineering

4) European Centre for Training and Research in Earthquake Engineering, Eucentre, Pavia, Italy

**Abstract** This paper presents the harmonized approach for landslide susceptibility and hazard assessment at the cross-border region between North Macedonia, Albania, and Greece. The European ELsusv2 initiative is selected as a harmonized approach for regional landslide susceptibility mapping for the area study. An analytical relationship is used to assess the permanent slope displacement for different earthquake scenarios. The final product of the landslide hazard zonation is presented by GIS maps showing the expected permanent displacements for pre-defined earthquake scenarios. The presented approach for the cross-border region is a simple tool used to recognize the hazardous areas, where only limited geomorphological, geological and seismological datasets exist. The presented research was performed in the framework of the project named CRISIS (“Comprehensive RISk assessment of basic services and transport InfraStructure”) supported by the Union Civil Protection Mechanism. The landslide hazard maps will contribute to the definition of the risk for critical infrastructure at regional scale due to landslide triggering in the project. Overall, the CRISIS project and the landslide hazard zonation provided for the cross-border region will contribute towards better long-term risk mitigation strategies in each of the countries involved in the study.

**Keywords** landslide hazard assessment, earthquake, permanent displacements, cross-border region, civil protection.

## Introduction

The primary requirement in predicting future landslides is a well-documented landslide inventory of the studied area including the mapping of past and recent slope movements, together with the identification and mapping of the predisposing factors of slope instability (Corominas et al., 2014, Van Westen et al. 2008). For the

purpose of mapping the landslide hazard in a certain cross border region, unified harmonized approach needs to be adopted which will characterize the hazard in equivalent approach. This paper is summarizing at first the current level of landslide research in the three object countries, North Macedonia, Albania and Greece and second the selected harmonized approach for mapping of the earthquake-induced landslide hazard in the cross-border region. The research is performed in the project CRISIS project which aims at improving the disaster and emergency management through building a harmonized and efficient system for risk assessment of basic services and transport infrastructure in the cross-border region between North Macedonia, Albania and Greece (<http://www.crisis-project.org/>).

The main project activities include:

1. Cross-border multi hazard assessment (earthquakes and landslides)
2. Needs assessment
3. Crossborder multi-risk assessment
4. Development of cross-border web base platform for risk assessment and management

## National perspective of landslide hazard in the three object countries

### North Macedonia

Republic of N. Macedonia (25,713 km<sup>2</sup>) is a mountainous country where 2% of the territory is covered by water (lakes), 19% are plains and valleys, and the greatest part of 79% are hills and mountains. Because of frequent changes of mountains and deep valleys, mean slope of the terrain in the country is very high, 15.2°, with 39.5% of the area steeper than 15° (Milevski, 2018).

Landslides are one of such threats which very often occur in North Macedonia, especially during the rainfall, fast snowmelt or earthquake shaking. For instance, several landslides were activated recently with road and canal construction in susceptible terrain, or by building major structures on steep terrain.

In N. Macedonia no official landslide hazard map at national level is currently available. Only landslide inventories provided by the Crisis management Center and several research efforts for selected locations across the country are available. Tab. 1 summarize the available references regarding landslide hazard and risk definition in N. Macedonia.

### Albania

Republic of Albania (28,748 km<sup>2</sup>) is mostly a mountainous country, where around 75% of its territory are hills and mountains. Because of the diversity of the terrain, the slope of the high terrain varies from 15°-40° (GSA, 2015).

Geodynamic phenomena of slope instability, especially landslides, are largely encountered in the Albanian territory (GSA, 2015). The study and mapping of this phenomenon began in 1950, due to the need for works relating to the construction of roads, hydroelectric plants, etc. The studies, before the 90s, were conducted by the Geology and Geodesy Body and by the Albanian Geological Survey (GSA) in the following period. In 2010 GSA undertook a project aimed at compiling the Landslide Inventory and Landslide Susceptibility Map at 1:50 000 for each of the 12 main administrative units (Qark) of Albania (GSA, 2015). The results were collected for the entire Albanian territory in a global GIS based Map at 1: 200,000 scale.

### Greece

Sabatakakis et al. (2013) presented a preliminary national-scale assessment of the landslide susceptibility in Greece using a landslide inventory derived from historical archives. More specifically, a large number of technical reports and studies including landslide occurrences, mainly obtained from KEDE (Central Union Of Municipalities Of Greece) and IGME (The Institute of Geology and Mineral Exploration), were analyzed, and after the appropriate modifications, mainly to standardize the terminology, 1635 well-documented landslide cases covering a long time period (up to 2010) were collected, recorded and digitally stored. The inventory mainly included earth slides (rotational and translational) having consequences on the reliability of susceptibility assessments.

In national-scale planning, according to Sabatakakis et al. (2013) the geological formations of Greece were grouped into seven engineering geological units based mainly on their origin and relevant age. The presence of the tectonically highly sheared and weathered geological formations of the alpine basement as well as of the neogene sediments contributed to the periodically induced instability phenomena mainly triggered by heavy rainfalls and human activity (e.g., high cut slopes etc.).

A few research efforts were carried out for landslide susceptibility zonation at selected locations across the Greece cross-border region, such as Kalantzi et al. (2010), Ambas et al. (2016) and Kyriou & Nikolakopoulos (2020).

However, no official landslide hazard map at national level is currently available in Greece.

Table 1 Available studies in N. Macedonia dealing landslides.

Reference	Type of data	Availability in GIS	Level
CMC database 2015-2020	Landslide inventory	GIS	National level
Peshevski, I. (2015).	Landslide inventory	GIS	National level
Milevski, I., & Dragičević, S. (2019).	Landslide susceptibility	GIS	National level
Bojadjieva et al., (2018)	Earthquake-induced landslide, hazard and risk	GIS	Suburban part of Skopje, local level
Sheshov, Talaganov (1998)	Susceptibility to landslide and liquefaction	Scan, TIFF	National level
Peshevski et al. (2019)	Landslide susceptibility	GIS	Polog region, regional level
<a href="https://interreg.eu/programme/interreg-ipa-cbc-bulgaria-former-yugoslav-republic-of-macedonia/">https://interreg.eu/programme/interreg-ipa-cbc-bulgaria-former-yugoslav-republic-of-macedonia/</a>	Landslide susceptibility	GIS	Pehcevo (N. Macedonia), Simitli (Bulgaria), regional level

### Mapping the landslide susceptibility at the Cross-Border region

The main prerequisite for any kind of landslide susceptibility assessment is information on spatial occurrence of landslide events, even if incomplete. Although many European countries regional or national landslide inventories or maps have available with different degrees of completeness, the attempt has been overtaken to gather basic spatial information on landslides over European territory and the project is known as ELSUS1000 (Günther et al. 2014) and ELSUSv2 (Wilde et al. 2018). It is important to note that ELSUS is known for its small scale (is to be viewed at scales up to 1:200,000), landslide susceptibility assessment project over a large area (i.e. at continental scale) which mainly suffers from high generalization, low resolution of spatial input data and incomplete inventory of landslides.

Despite the mentioned limitations, the map shows a harmonized overview of European landslide susceptibility even if at 1: 5 Mil. scale. It therefore provides a synoptic zoning of the susceptibility to landslides by the cell size of 200x200 m. This map shows harmonized digital information on the distribution of consolidated, partially consolidated and unconsolidated geological materials on the European territory. The database for the ELSUSv2 susceptibility maps is free access and can be easily download by request on the following website: <https://esdac.jrc.ec.europa.eu/content/european-landslide-susceptibility-map-elsus-v2>

Based on thorough review on national perspective and available data in the three countries from the Cross Border Region, N. Macedonia, Albania and Greece as well as available European research projects regarding landslide hazards, it can be concluded that the ELSUS approach is the most suitable methodology for harmonized landslide susceptibility and hazard assessment in the cross-border region.

The landslide susceptibility map of the cross-border region of Greece, North Macedonia and Albania is presented based on the Pan-European Landslide Susceptibility Map version 2 (ELSUS v2, Wilde et al. 2018) (Fig. 1). The methodological approach for the elaboration, validation and classification of ELSUSv2 is the same as the previous version called ELSUS 1000 reported in Günther et al. (2014). More specifically, a semi-quantitative method is used, combining landslide frequency ratios information with a spatial multi-criteria evaluation model of three thematic predictors: slope angle, shallow subsurface lithology and land cover. The terrain gradient was calculated using the slope algorithm of Horn (1981) and classified into eight classes. The IHME 1500 lithology information was grouped into 19 classes considering landslide density information, class sizes and distributions, and semantic compatibility. The land cover information derived from the global GlobCover data set (ESA, 2010).

Fig. 2, and 3 illustrate the adopted terrain gradient and lithology maps for the cross-border region of Greece, North Macedonia and Albania according to ELSUS v2 methodology. Fig. 4 shows confidence (or reliability) levels of the classified landslide susceptibility according to ELSUS v2 for the cross-border region calculated either statistically or by expert evaluation. A moderate confidence level is considered for the whole Albania cross-border region and the larger part of Greece cross-border region while no information is provided for the N. Macedonia cross-border region.

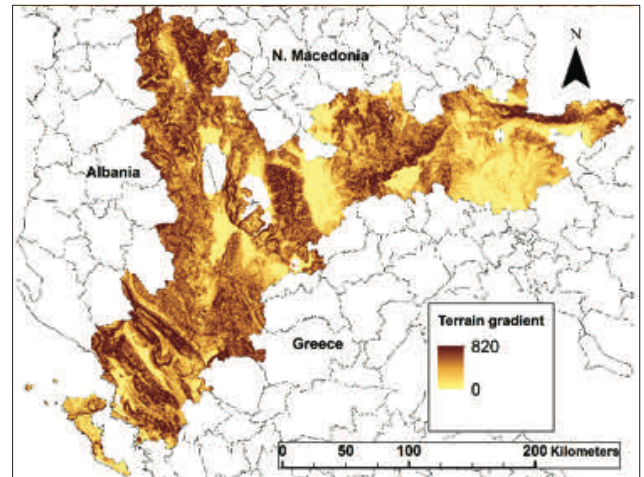


Figure 2 Terrain gradient of the cross-border region of Greece, North Macedonia and Albania according to ELSUS v2 (Wilde et al. 2018).

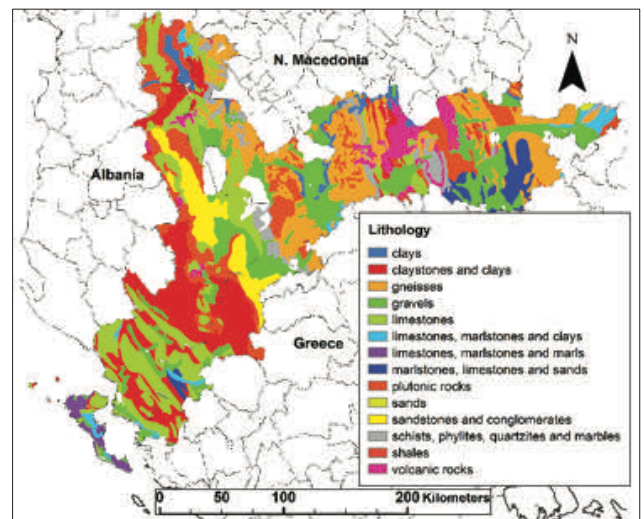


Figure 3 Lithology of the cross-border region of Greece, North Macedonia and Albania according to ELSUS v2 (Wilde et al. 2018).

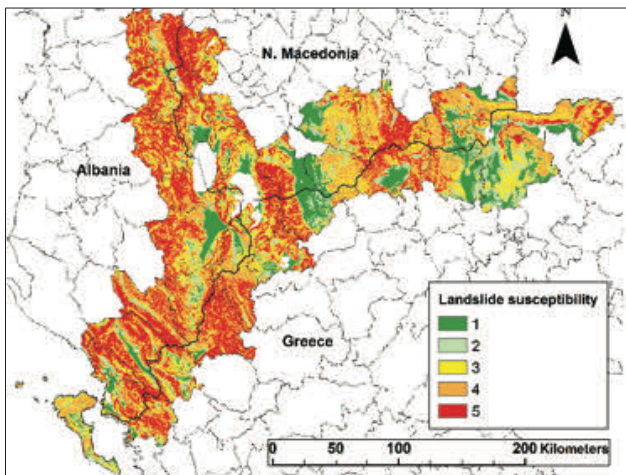


Figure 1 Landslide susceptibility map of the cross-border region of Greece, North Macedonia and Albania (where landslide susceptibility 1 = very low; 2 = low; 3 = moderate; 4 = high; 5 = very high) adopted from ELSUS v2 (Wilde et al. 2018).

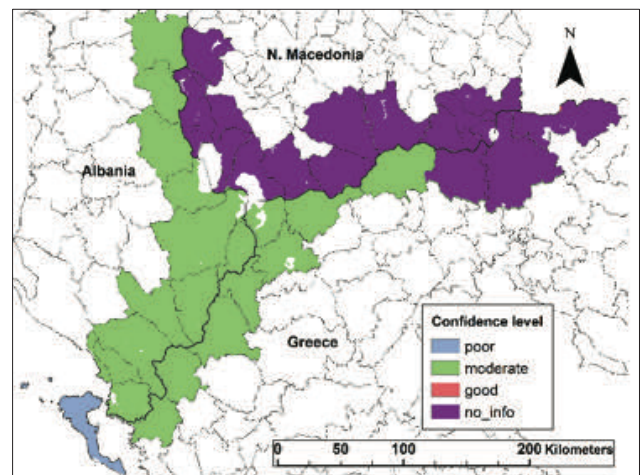


Figure 4 Confidence level of the cross-border region of Greece, North Macedonia and Albania according to ELSUS v2 (Wilde et al. 2018).

### Earthquake-induced landslide hazard assessment for the cross-border region

For the purpose of the CRISIS project, based on its scope and objectives, the seismic events as a triggering to cause landslides are taken into consideration. Indeed, landslide hazard maps are computed in terms of permanent displacements caused by different earthquake scenarios. The ground shaking caused by earthquakes can induce landslides either through the application of horizontal and vertical accelerations to the sliding mass along a hillside slope. The value of the peak ground acceleration within the slide mass required to just cause the factor of safety to drop to 1.0 is denoted by the critical or yield acceleration  $a_c$ . This value of acceleration is commonly determined based on pseudo-static slope stability analyses and/or empirically based on observations of slope behaviour during past earthquakes. Starting from the pioneer study of Newmark (Newmark, 1965), several empirical models are currently available to predict seismically induced displacements of sliding masses, such as the ones of Jibson (2007), Rathje and Antonakos (2011) and Bray and Travararou (2007). Downslope deformations occur during the time periods when the induced peak ground acceleration within the slide mass exceeds the critical acceleration  $a_c$ . Such methods are based on the sliding rigid block assumption providing an index of the dynamic slope performance. Fotopoulou and Pitilakis (2015), on the other hand, proposed analytical predictive relationships for seismically induced slope displacements based on advanced numerical simulations and statistical analysis.

Tab. 2 presents the assigned critical acceleration values as a function of landslide susceptibility based on ELSUS2. The adopted  $a_c$  values, based on engineering judgement, are in line with the ones proposed in Hazus methodology for landslide hazard evaluation (NIBS, 2004; Pitilakis et al. 2009). Fig. 5 presents the critical acceleration map for the cross-border region (CBR).

Table 2 Critical acceleration values as a function of landslide susceptibility based on ELSUSv2.

Susceptibility (ELUSV2)	Critical acc. $a_c$ [g]
Very low (1)	0.40
Low (2)	0.30
Medium (3)	0.20
High (4)	0.15
Very high (5)	0.10

To assess the permanent slope displacement for the different earthquake scenarios, the following analytical relationship proposed by Fotopoulou & Pitilakis (2015) is used:

$$\ln(D) = -2.965 + 20127 * \ln(PGA) - 6.583 * ky + 0.535 * M \pm \varepsilon * 0.72$$

where:

- PGA is the peak ground acceleration at the ground surface in g.
- $ky$  is the yield or critical acceleration ratio in g.
- $M$  is the magnitude of the earthquake.
- $\varepsilon$  is the standard normal variant with zero mean and unit standard deviation

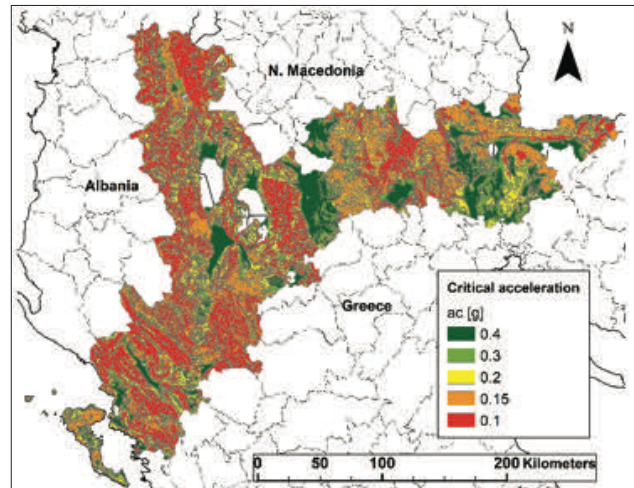


Figure 5 Critical acceleration map as a function of landslide susceptibility for CBR.

As previously mentioned, two seismic scenarios are defined with return periods equal to 475 years and 975 years based on the available European seismic hazard model, named ESHM13 (Giardini et al., 2014). Tab. 3 presents the earthquake magnitudes assumed for each considered seismic scenario.

Table 3 Selected magnitude value for the predefined earthquake scenarios.

Earthquake Scenario	Selected magnitude value $M$
Return period 475 years (ESHM13)	6
Return period 975 years (ESHM13)	7

In order to account for litho-stratigraphic amplification, a simplified approach based on the use of the global  $V_{30}$  map proposed by USGS (<https://earthquake.usgs.gov/data/vs30/>) is used in order to categorize the ground type based on Eurocode (2003; hereinafter EC8). (Fig. 6 and Tab. 4). Based on the ESHM13 hazard maps for 475 and 975 years and the soil amplification factors, the PGA surface maps for both return periods are created.

Table 4 Definition of surface PGA based on Ec8 Spectrum type 1

Ground type	Soil amplification factor (EC8)
A ( $V_{s30} > 800$ )	1
B ( $360 < V_{s30} < 800$ )	1.2
C ( $180 < V_{s30} < 360$ )	1.15

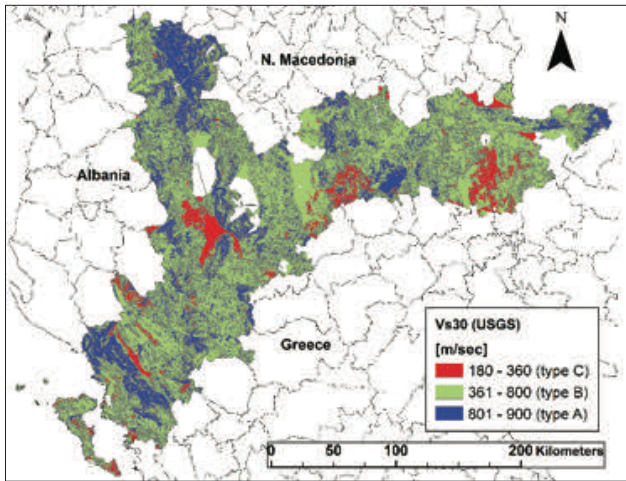


Figure 6 Vs30 map based on USGS for the CBR.

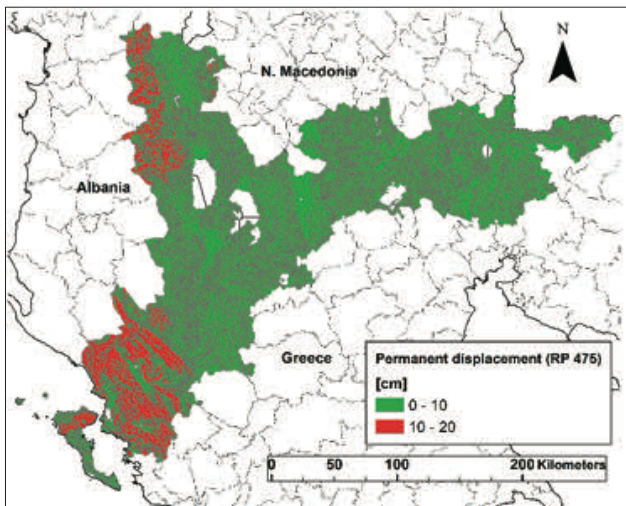


Figure 7 Spatial distribution of permanent ground displacement due to landslide (PGD) at the free surface for the CBR region for the seismic scenario of 475 years.

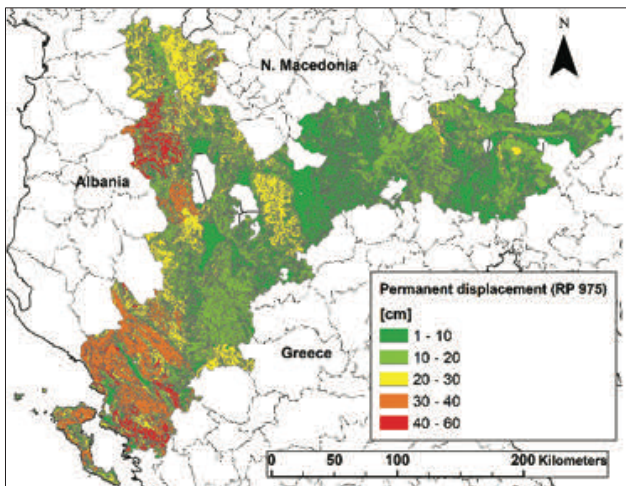


Figure 8 Spatial distribution of permanent ground displacement due to landslide (PGD) at the free surface of the terrain for the CBR region for the seismic scenario of 975 years.

The final product of the landslide hazard zonation is presented by digital maps of expected permanent displacements for the pre-defined earthquake scenarios (Fig. 7 and Fig. 8). The values represent displacements expected at the free surface of the terrain. The presented maps for the cross-border region represent a simple map which can be used to identify the hazardous areas. It should be pointed out that the outcome from this study can be a good starting point for fostering in-depth analysis based on more detailed input datasets, which are progressively developed in the communities dealing with landslide hazard.

### Conclusions

In order to assess the landslide hazard at the cross-border region between N. Macedonia, Albania and Greece, a thorough review of the current national perspective in the three countries and a review of the available European initiatives dealing landslides hazard assessment were undertaken.

Based on the findings of the review, the ELSUSv2 was selected as harmonized approach for regional landslide susceptibility mapping at the cross-border region under investigation in this study. Based on the susceptibility map, the following observations can be made:

- Up to 65% of the territory of the cross-border region falls within high and very high susceptibility to landslides, which is due to the fact that the larger portion of the territory is mountainous region.
- A moderate confidence (or reliability) level is considered for the whole Albanian part of the cross-border region and the larger part of Greece cross-border region while no information are available for the N. Macedonia cross-border region.

To produce earthquake-induced landslide hazard zonation for the cross-border region, critical acceleration values are assigned to each category of landslide identified in the susceptibility maps. The suggested values based on engineering judgement are in line with the ones proposed in Hazus methodology for landslide hazard evaluation (NIBS, 2004; Pitilakis et al. 2009). Further on, to assess the permanent slope displacement for the different earthquake scenarios, analytical relationship proposed by Fotopoulou & Pitilakis (2015) is used.

The final product of the landslide hazard zonation is presented by digital maps of expected permanent displacements for the pre-defined earthquake scenarios for 475 and 975 return period, respectively. Based on the created maps for 475 years return period permanent displacements are expected to be in the range up to 20 cm for some parts in eastern Albania and the southern part of cross border region between Albania and Greece. On the other hand, for 975 years return period, expected permanent displacements reach 60 cm with variation of

the values across the whole territory of the cross-border region.

The presented approach for the cross-border region is a simple tool which can be adopted to identify the hazardous areas, where only limited geomorphological, geological and seismological datasets are available. The computed maps will be used in the CRISIS project as standalone product and also as input for risk assessment of critical infrastructures at regional scale. It is worth remarking that such maps can be adopted as starting point for fostering in-depth analysis based on more detailed input datasets, which are progressively under development in the communities dealing with landslide hazard.

## Acknowledgments

The presented research was done in the framework of the project CRISIS “Comprehensive RISK assessment of basic services and transport InfraStructure” supported by the Union Civil Protection Mechanism (101004830 - CRISIS - UCPM-2020-PP-AG).

## References

- Ambas V, Katsaros E, Alexoudi M, Olasoglou E, Tsapanos T, Koravos G, Drakatos G, Tzamos E (2016) Landslides in Vitsi (Florina) territory. *Bulletin of the Geological Society of Greece*. 50(2): 577-585. doi: <https://doi.org/10.12681/bgsg.11762>.
- Bojadjieva J, Sheshov V, Bonnard C (2018) Hazard and risk assessment of earthquake-induced landslides—case study. *Landslides*. 15(1): 161-171.
- Bray JD, Travasarou T (2007) Simplified procedure for estimating earthquake-induced deviatoric slope displacements. *Journal of geotechnical and geoenvironmental engineering*, 133(4): 381-392.
- CMC Landslide inventory database from 2015-2020. Crisis Management Center, North Macedonia.
- Corominas J, van Westen C, Frattini P, Cascini L, Malet J P, Fotopoulou S, Smith J T (2014) Recommendations for the quantitative analysis of landslide risk. *Bulletin of engineering geology and the environment*, 73(2): 209-263.
- ESA (2010) Globcover 2009. Paris: European Space Agency.
- Eurocode 8 (2003). Design of structures for earthquake resistance, Part 1: General rules, seismic actions and rules for buildings, Pr-EN1998-1, European Committee for Standardization (CEN), Brussels.
- Fotopoulou SD, Pitilakis KD (2015) Predictive relationships for seismically induced slope displacements using numerical analysis results. *Bulletin of Earthquake Engineering*, 13(11): 3207-3238.
- Geological Society of Albania (2015). Landslide inventory and susceptibility map of Albania, Albania.
- Giardini D, Woessner J, Danciu L, (2014) Mapping Europe’s Seismic Hazard. *EOS*, 95(29): 261-262.
- Günther A, Van Den Eeckhaut M, Malet J-P, Reichenbach P, Hervás J (2014) Climate-physiographically differentiated Pan-European landslide susceptibility assessment using spatial multi-criteria evaluation and transnational landslide information. *Geomorphology*. 224: 69-85.
- Horn BKP (1981) Hill shading and the reflectance map. *Proceedings of the IEEE*. 69: 14–47.
- IPA cross-border programme: Joint Applicable Research for Natural Recourses Preservation and Environmental Protection in the Cross-border Region within the municipalities of Pehchevo and Simitli, 2007CB16IPO007-2012-2-106.
- Jibson RW (2007) Regression models for estimating coseismic landslide displacement. *Engineering geology*, 91(2-4): 209-218.
- Kalantzi F, Doutsou I, Koukouvelas I (2010) Historical landslides in the prefecture of Ioannina- Collection and analysis of data. *Bulletin of the Geological Society of Greece*. 43: 1350-1360.
- Kyriou A, Nikolakopoulos K (2020) Landslide mapping using optical and radar data: a case study from Aminteo, Western Macedonia Greece. *European Journal of Remote Sensing*. 53(sup2): 17-27.
- Milevski I, Dragicevic S. (2018) GIS-Based Landslide Susceptibility Modelling of the Territory of the Republic of Macedonia. In 7th International Conference on Cartography and GIS. pp. 82-91.
- Milevski, I, Dragičević S (2019). Landslides susceptibility zonation of the territory of north macedonia using analytical hierarchy process approach. *Contributions, Section of Natural, Mathematical and Biotechnical Sciences*. 40(1): 115-126.
- National Institute of Building Sciences (NIBS), Earthquake Loss Estimation Methodology HAZUS 2004, Technical Manual, FEMA, Washington DC, <http://www.fema.gov/hazus>, 2004.
- Newmark, N. M. (1965). Effects of earthquakes on dams and embankments. *Geotechnique*, 15(2): 139-160.
- Peshevski I. (2015) Landslide susceptibility modelling using GIS technology. Extended abstract of candidate’s thesis, 181. North Macedonia
- Peshevski, I, Jovanovski M, Abolmasov B, Papić J, Đurić U, Marjanović M, Nedelkovska N (2019) Preliminary regional landslide susceptibility assessment using limited data. *Geologia Croatica*. 72(1): 81-92.
- Pitilakis et al. (2009). D8: Microzonation study of Grevena. Work Package 3-1: Detailed Microzonation study (site effect analysis for outcrop conditions, evaluation of the dynamic response of soil profiles in 1D and 2D conditions) for Grevena. Synthesis of available inventories and classification of elements at risk in GIS format. Inventories and classification of elements at risk in GIS.SRM-DGC A.1.010 Development and Proposition for Implementation of an Efficient Methodology and Appropriate Local Instruments for the Management, Prevention and Reduction of Seismic Risk in Düzce-Turkey, Grevena-Greece and Catania-Italy
- Rathje EM, Antonakos G (2011) A unified model for predicting earthquake-induced sliding displacements of rigid and flexible slopes. *Engineering Geology*. 122(1-2): 51-60.
- Sabatidakis N, Koukis G, Vassiliades E, Lainas S (2013) Landslide susceptibility zonation in Greece, *Natural Hazards*. 65: 523–543 doi: 10.1007/s11069-012-0381-4.
- Sheshov V, Talaganov K (1998) Zonation of earthquake geotechnical hazards, landslides and liquefaction in R. of Macedonia
- Van Westen CJ, Castellanos E, Kuriakose SL (2008). Spatial data for landslide susceptibility, hazard, and vulnerability assessment: An overview. *Engineering geology*, 102(3-4): 112-131.
- Wilde M, Günther A, Reichenbach P, Malet J P, Hervás J (2018). Pan-European landslide susceptibility mapping: ELSUS Version 2. *Journal of maps*. 14(2): 97-104.

# A proposal for the landslide damage questionnaire in suburban areas

Uroš Đurić<sup>(1)</sup>, Biljana Abolmasov<sup>(2)</sup>, Miloš S. Marjanović<sup>(1)</sup>, Sanja Jocković<sup>(1)</sup>, Miloš D. Marjanović<sup>(2)</sup>

1) University of Belgrade, Faculty of Civil Engineering, Belgrade, Bulevar Kralja Aleksandra 73, Serbia, +381 11 3218587 (udjuric@grf.bg.ac.rs)

2) University of Belgrade, Faculty of Mining and Geology, Belgrade, Serbia

**Abstract** Landslides are one of the most often natural disasters that have an extensive impact on society including loss of life, destruction of infrastructure and properties, damage to land and loss of natural resources. Landslide losses can significantly vary and they depend on a variety of different criteria such as the size and type of landslide, lithological setting of terrain, the terrain slope gradient, the quality of materials used for construction, and the construction typology. Damage from landslides is usually characterized as either direct or indirect and in most questionnaires only the data referring to the direct damage is collected. In this paper, a landslide damage questionnaire that can be used for landslide damage characterization and determination of landslide hazard and risk in urban areas is proposed. The questionnaire contains 11 groups of questions that include all necessary fields for gathering the data which is essential for both landslide hazard and risk estimation. It was used as an inventory landslide damage form in suburban housings which usually occupy larger land plots, while objects built on such plots are mostly houses for an individual living or ancillary type.

**Keywords** survey, property, landslide, risk, assessment

## Introduction

A landslide damage questionnaire is a crucial tool for landslide risk management. Cooper (2008) provided an overview of various distinct methodologies for mapping facilities damaged by landslides and subsidence, as well as a recommendation for a new hybrid version of the methodology. Corominas et al. (2014) suggest general guidelines for designing a landslide damage questionnaire based on the size area of the research. In contrast, Palmisano et al. (2016) provide a more extensive description of the methodology for landslide damage assessment using the survey approach (2016). Finally, in Uzielli et al. (2008) and Peduto et al. (2017) successful examples of landslide damage assessment are provided.

There is no official form (census sheet or questionnaire) for the Republic of Serbia that can be used to quickly and precisely identify landslide-damaged objects (with damage classification and assessment). This

issue is relevant in Serbia and in international practice, in contrast to the earthquake damage assessment (EMS98), which is very well established and recognized internationally (Cooper, 2008).

For example, after the extreme precipitation, which was followed by catastrophic floods that occurred in Serbia in May 2014, the Unique Methodology for the Assessment of Losses from Natural Disasters (Official Gazette of SFRY no. 27 of 10 April 1987) was used by the official expert teams for the flood damage assessment. According to this methodology, all buildings and facilities, regardless of their purpose, are classified into five categories of damage, which are the consequences of earthquakes. Therefore, amendments to the same methodology were made for the 2014 flood damage assessment, while landslide damage was not defined, although a large number of objects and facilities were affected by the landslide processes that occurred during and after the flood events (Marjanović et al. 2017).

## Materials and Methods

### Case study

Umka landslide area is selected for testing the landslide damage questionnaire, as a typical example of landslide in suburban areas. Umka landslide is the most systematically investigated and largest populated landslide in Serbia. Umka landslide mechanism was defined by Abolmasov et al. (2012), Abolmasov et al. (2015), while most details about the Umka landslide were described in Đurić et al. (2018) and Đurić (2020).

Although the landslide is well-known and occasionally mentioned in public and mass media, certain population migration in that area is still evident. Besides constant landslide movement, some new objects with permanent residents are still being built, even within the most active and most affected part of the landslide. This is probably caused by significantly lower market prices of households and plots in this area. The last inventorying and damage classification on objects was performed during 1990, when a map and a brief report of the damaged objects (with the type of foundation, walls, and category of an object) was created (Vujanić et al. 1992, 1995). During that investigation, the local water system was mapped and the population was evaluated using the most recent census

data. Even though the last inventorying was performed 30 years ago, the vulnerability of the population is present, as a consequence of unplanned and illegal construction works during and after 2005, when all construction works have been officially forbidden (for the most active parts of the landslide). Furthermore, previous inventorying didn't include the information about households, working population and life habits which are necessary data for the risk estimation. Given the foregoing, there was a need for a proposal of the new questionnaire and survey methods that should result with the updated inventory of all objects within the landslide area.

### Questionnaire

According to Palmisano et al. (2016), the main objectives and guidelines for landslide damage assessment are to quickly acquire the relevant information that can be used for landslide hazard assessment, especially if they are collected in combination with the geotechnical monitoring data and according to geodynamical and morphological settings of the terrain; to form the database that will be used for the landslide risk assessment. The guidelines mentioned above were essential for forming the questionnaire proposal and included a survey research method and data about constructions and their damage assessments collected directly on the field.

The proposal of a new questionnaire was based on the fact that most objects will be inspected visually by noticing the damage that has occurred on small individual houses, cottages, ancillary objects etc. The data collected for the Umka landslide had to be sufficient for the level of advanced landslide risk assessment proposed by Fell et al. (2008), and for both direct and indirect losses The Highway Institute - Belgrade's questionnaire from 1990 (Vujanić et al. 1992, 1995) served as a basis for the development of the questionnaire proposal that consists of 11 main question groups. Tables 1 & 2 show an example of a blank questionnaire proposal, while brief description of each question group is described in the following lines.

The groups of questions were as follows:

1. General information about the object / facility
2. Information about the construction
3. Damage to the construction
4. Information about the foundation
5. Information about household members
6. Damage assessment (brief estimation)
7. Emergency and temporary interventions
8. Possibility of damage repair
9. Information about water supply, sewage, surface and groundwater at location
10. Object or facility damage sketch
11. Other observations

### General information about the object / facility

This group of questions contains the basic information about the surveyed object like owner or tenant, address of the object, cadastral parcel, year of the construction, estimated lifespan, object coordinates, etc. If the object was extended or modified, here it should be noted.

According to our practice, owners usually report a smaller useful surface than it is in reality if the object is illegally constructed or extended. Considering that fact, the approximate useful surface should be estimated by the surveyor. For estimating the value of the property, the last known tax record for the property can be noted here (if it is shared with the surveyor by the owner). It is very important for the surveyor to adequately categorize the object by its main purpose which can be of various typological types (Fig. 1). Information about storeys and number of vehicles that are used by the household should be noticed as well. The questionnaire design proposal for this group of question is shown in section 1 of Table 1.



Fig. 1 Typology of most common types of objects by the purpose: residential house or cottage, garage, commercial, greenhouse and barn

### Information about construction

Questions and predefined answers about the object construction (above ground) are shown in section 2 of Table 1. If the object was built using the different types of materials or construction types, the most dominant should be used as primary selection. Besides construction typology, it was important to include questions about roof geometry and dominant wall material. Some examples of typological selections that are proposed within this group of questions are shown in Fig. 2.



Most common typology of object construction: load bearing walls; masonry; timber framing; steel framing; RC



Most common typology of object roof type: flat; inclined; curved; unfinished/plate; without roof



Most common typology of dominant wall material: masonry brick; hollow clay block; wood; masonry stone; cane/mud

Fig. 2 Typology of most common types of object construction, roof type and dominant wall material

### Damage to the construction

For the objects damage classification purposes, it is generally recommended to use the EMS-98 earthquake damage classification and descriptions as the basis for the



landslide damage assessment (Grünthal 1998). The scale can be modified for the landslide damage assessment (Palmisano et al. 2016). If historical damage assessment databases or records of finished surveys exist for the research area, it is very important to provide local classification within the questionnaire and to classify all objects by damage again during the new survey (for the comparison). Some examples of typological selections within this group of questions are shown in Table 1 - Section 3a & 3b and Fig. 3.



Fig. 3 Typology of most common object damage classification: negligible; negligible to slight; moderate; prone to collapse; destroyed

**Information about the foundation**

Information about the object foundations can be divided into two sections - the one defining the type of foundation and the other defining the foundation material. In the case of mixed types of foundation or materials, the most dominant should be evidenced. Questions about foundation depths and foot width can be included here, but this is very hard to estimate precisely in most cases. The foundations material is mostly the same or similar to the one for dominant wall material. Some examples of proposed typological selections within this group of questions are shown in Table 1 - Section 4 and Fig. 4.

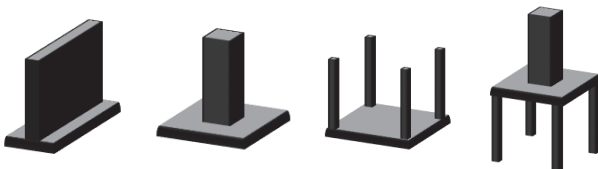


Fig. 4 Typology of the most common types of foundations: strip footing; spread footing; mat (raft); piles

**Information about household members**

This group of questions represents the most basic population census data. For the possibility of basic landslide risk assessment, it is necessary to collect the data about the number of household members, employment rate, number of minors or incapable of work etc. All collected data should be anonymous. Question examples within this group of questions are shown in Table 1 - Section 5.

**Damage assessment (brief estimation)**

Within this section, several questions about brief damage assessment are proposed. It is important to distinguish whether the damage assessment is documented by the official authorities' documentation or is it estimated relatively by the surveyor. Estimated direct damage should be the damage to the object caused by the landslide movement. Indirect damage should be expressed as the

value amount that the owner or household members should spend annually to fix the damage so the object remains functional. Question examples proposed within this group of questions are shown in Table 1 - Section 6.

**Emergency and temporary interventions**

The surveyor recommendation and expenses needed for emergency or temporary interventions on the object or its surroundings to reduce the risk to the household members or neighbours should be noted. Question examples proposed within this group of questions are shown in Table 1 - Section 7.

**Possibility of damage repair**

The surveyor estimation of the possibility to repair the damage, for example, can range from "not needed" to "not possible". Question examples proposed within this group of questions are shown in Table 1 - Section 8.

**Information about water supply, sewage, surface and groundwater at location**

This question group should collect information about the object water supply or sewage disposal systems at the location and information about the surface waters and well conditions. Since the ground and surface waters are usually one of the dominant triggering factors for the landslide (re)activation, the surveyor should mandatorily fill this group of questions. Question examples proposed within this group of questions are shown in Table 2 - Section 9.

**Object or facility damage sketch**

The schemes for sketching the sides of the objects and damage that is observed on the field and some typological questions about objects and surrounding terrain conditions are shown in Table 2 - Section 10. It is recommended that "A" side of the object (Fig. 5) should be the side that mostly "looks" toward the possible vector of landslide movement and all other sides should be labelled in a clockwise direction, starting from the "A" side. If the object is of irregular shape (has more than four side walls), those sides should be sketched from the surveyor point of view and considered as one single side with indicating the wall break lines (Fig. 5, right). Within this section, data about the total object damage should be noted, same as subsidence and surrounding terrain deformation if occurs. An example of labelling convention and sketched side from point of surveyor view of an object is shown in Fig. 5.

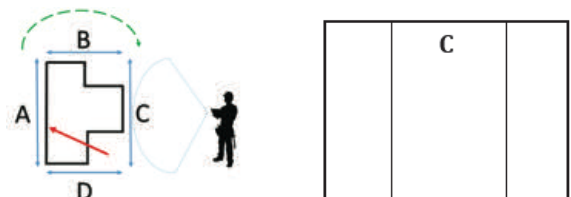
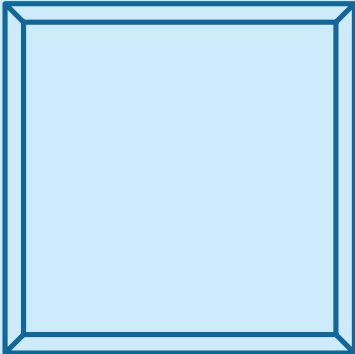
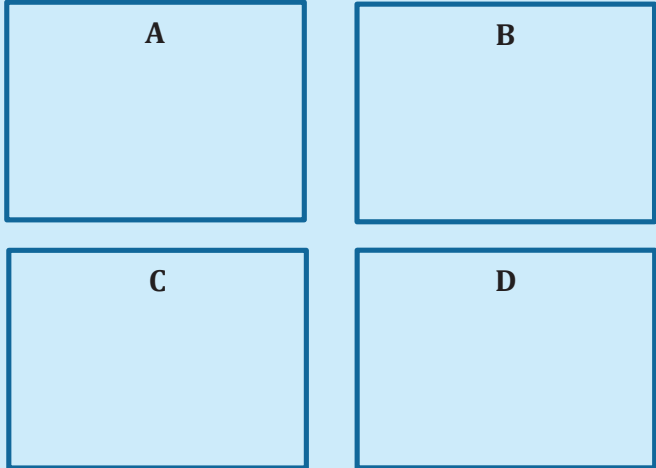


Table 1. Front page of the proposed landslide damage questionnaire

UNIQUE OBJECT ID:									
<b>1. GENERAL INFORMATION ABOUT THE OBJECT / FACILITY</b>									
Owner's name & surname				Purpose of the object / facility					
Address				Residential	<input type="checkbox"/>	Greenhouse	<input type="checkbox"/>		
				Cottage	<input type="checkbox"/>	Barn	<input type="checkbox"/>		
				Garage	<input type="checkbox"/>	Shed	<input type="checkbox"/>		
Cadastral parcel				Canopy	<input type="checkbox"/>	Summer kitchen	<input type="checkbox"/>		
Year of construct.	Lifespan est.				Commercial	<input type="checkbox"/>	Temporary	<input type="checkbox"/>	
Building permit		Yes <input type="checkbox"/>	No <input type="checkbox"/>		Religious	<input type="checkbox"/>	Ancillary / Other	<input type="checkbox"/>	
X coordinate			Useful surface			m <sup>2</sup>	Last know prop. tax (€)		
Y coordinate			Storeys						
Extension		Yes <input type="checkbox"/>	No <input type="checkbox"/>		No. of vehicles				
<b>2. INFORMATION ABOUT CONSTRUCTION</b>					<b>3A DAMAGE TO THE CONSTRUCTION</b> <small>CLASSIFIED BY THE HIGHWAY INSTITUTE - BELGRADE</small>				
Load bearing walls	<input type="checkbox"/>	Roof		Dominant wall material		Demolished		<input type="checkbox"/>	
Masonry	<input type="checkbox"/>	Flat	<input type="checkbox"/>	Masonry Brick	<input type="checkbox"/>	Prone to collapse		<input type="checkbox"/>	
Timber framing	<input type="checkbox"/>	Inclined	<input type="checkbox"/>	Hollow clay block	<input type="checkbox"/>	Moderate		<input type="checkbox"/>	
Steel construction	<input type="checkbox"/>	Curved	<input type="checkbox"/>	Wood	<input type="checkbox"/>	Negligible to slight		<input type="checkbox"/>	
Prefabricated	<input type="checkbox"/>	Concrete plate	<input type="checkbox"/>	Masonry stone	<input type="checkbox"/>	Negligible		<input type="checkbox"/>	
Reinforced (RCC)	<input type="checkbox"/>	Without	<input type="checkbox"/>	Cane / Mud	<input type="checkbox"/>				
<b>4. INFORMATION ABOUT THE FOUNDATION</b>					<b>3B DAMAGE TO THE CONSTRUCTION</b> <small>CLASSIFIED BY UNIQUE METHODOLOGY (SFRY)</small>				
Type of foundation		Foundation material		<b>V</b>	With destruction of construction		<input type="checkbox"/>		
Strip footing	<input type="checkbox"/>	Stone	<input type="checkbox"/>	<b>IV</b>	Very heavy damage		<input type="checkbox"/>		
Spread footing	<input type="checkbox"/>	Brick	<input type="checkbox"/>	<b>III</b>	Substantial to heavy damage		<input type="checkbox"/>		
Mat (Raft)	<input type="checkbox"/>	Concrete	<input type="checkbox"/>	<b>II</b>	Moderate damage		<input type="checkbox"/>		
Piles	<input type="checkbox"/>	Wood	<input type="checkbox"/>	<b>I</b>	Negligible to slight		<input type="checkbox"/>		
Unknown	<input type="checkbox"/>	Unknown	<input type="checkbox"/>		Negligible		<input type="checkbox"/>		
<b>5. INFORMATION ABOUT HOUSEHOLD MEMBERS</b>					<b>6. DAMAGE ASSESSMENT (BRIEF ESTIMATION)</b>				
Household members		Employment rate (1/3 ...)		Assessment meth.	Relative <input type="checkbox"/>	Document.		<input type="checkbox"/>	
0	<input type="checkbox"/>			Estimated direct damage (€)					
1	<input type="checkbox"/>	Number of minors		Estimated indirect damage (€/yr.)					
2	<input type="checkbox"/>			<b>7. EMERGENCY AND TEMPORARY INTERVENTIONS</b>					
3	<input type="checkbox"/>	No. of work incapable		Population displacement and demolition		<input type="checkbox"/>			
	<input type="checkbox"/>			Major construction and earthworks		<input type="checkbox"/>			
Years, dates or periods of significant landslide activity:				Additional geotechnical and geological invest.		<input type="checkbox"/>			
				Estimated value of interventions (€)					
<b>CONTACT PERSON</b>					<b>8. POSSIBILITY OF DAMAGE REPAIR</b>				
Surname & Name				Not possible	<input type="checkbox"/>	Minor civil works		<input type="checkbox"/>	
Telephone number				Major civil works	<input type="checkbox"/>	Ordinary maintenance		<input type="checkbox"/>	
e-mail address				Moderate civil works	<input type="checkbox"/>	Repair is not needed		<input type="checkbox"/>	
Survey copy		Yes <input type="checkbox"/>	No <input type="checkbox"/>		Estimated value of damage repair measurements (€)				
Data Processing Agreement (signature):									

Table 2. Back page of the proposed landslide damage questionnaire

9. INFORMATION ABOUT WATER SUPPLY, SEWAGE, SURFACE AND GROUNDWATER AT LOCATION						
Water supply		Local well condition				
<input type="checkbox"/>	Municipality water system	<input type="checkbox"/>	Active			
<input type="checkbox"/>	From the local well	<input type="checkbox"/>	Collapsed			
<input type="checkbox"/>	Do not have water supply	<input type="checkbox"/>	Damaged at _____ m of depth from the surface			
Disposal of household waste and technical water		X coordinate of well				
		Y coordinate of well				
<input type="checkbox"/>	Municipality sewage system	Water level from the surface at survey day _____ m				
<input type="checkbox"/>	Septic tank	Surface waters	regulated <input type="checkbox"/>	not regulated <input type="checkbox"/>		
<input type="checkbox"/>	Leaching cesspool or direct infiltration into a ground	Other observations:				
10. OBJECT OR FACILITY DAMAGE SKETCH						
<p><b>Plan view of the object</b></p> <p>Using the arrow, indicate the possible sliding direction. This arrow also indicate the A side of the object. Other sides should be lettered by the clockwise order labelling (B,C,D)</p> 		<p><b>Side views of the object</b></p> <p>Approximately sketch the observed damage on main walls or object sides. If there is more than four walls, break lines should be sketched too.</p> 				
Total damage estimate		%				
Inclined toward	A B C D	Subsidence	No <input type="checkbox"/>	Yes <input type="checkbox"/>	Subs. est. _____ m	
Terrain deformation	No <input type="checkbox"/>	Scars <input type="checkbox"/>	Ridges <input type="checkbox"/>	Inclined trees <input type="checkbox"/>	Soil cracks <input type="checkbox"/>	
11. OTHER OBSERVATIONS						
Photo (image) file names or numbers:						
Observation date:			Surveyor:			

### Other observations

This section represents the blank textual field where surveyor should enter all other observations considered as important for the specific object. Some of the previous selections or entries can be explained here in detail.

### Discussion and Conclusion

The main advantage of field surveying is the fact that all details about the object condition and damage can be noted and evidenced. This is not always possible with the other survey methods such as remote sensing for example. Another advantage is that the surveyor can discuss with the object owner and ask him about some details that cannot be assessed only from the side looking at the object. For example, an owner can let the surveyor in the basement to inspect the condition of beams, footings etc. Also, the owner can probably provide the surveyor the project documentation (if exists) where other important information regarding the material type, foundations depths and geometry can be checked and entered into a questionnaire.

The survey should be performed only by qualified staff and our general recommendation is that it should be done by engineers with a geotechnical background (civil + geological). Not all fields need to be filled by the surveyor, but some of them that are essential for the landslide hazard and risk estimation should be mandatory, such as information about the construction, damage estimation, and purpose of the object, household members, water & sewage and deformation sketch.

We have proposed a landslide damage questionnaire that is calibrated for the large and slow-moving landslides that are affecting the suburban areas. On such landslides, there is great dispersion of damage intensity across the landslide body (from negligible to destruct), while objects are mostly for individual living, smaller cottages or ancillary type and they are still occupied despite the fact the landslide activity. The questionnaire presented in this paper is adjusted for the most common typology choices that are expected for the mechanism and dynamics of the slow moving landslide as a presented case study. For other types of landslides (with different velocity, magnitude, mechanism and dynamics) and type of objects, modifications of the questionnaire is highly encouraged. During the preparation of the questionnaire, it was important to format it in such manner it can be filled quickly and easily, but still comprehensive. Our experience from the Umka landslide damage assessment showed us that time for filling the questionnaire vary from 1 - 2 hours per object.

### References

- Abolmasov B, Milenković S, Jelisavac B, Vujanić V, Pejić M, Pejović M (2012) Using GNSS sensors in real time monitoring of slow moving landslides - a case study. Proceedings of the 11th International and 2nd American Symposium on Landslides and Engineered Slopes, Banff, Canada, 3-8 June, 2012. Taylor&Francis Group, London, 1381-1385.
- Abolmasov B, Milenković S, Marjanović M, Đurić U, Jelisavac B, (2015) A geotechnical model of the Umka landslide with reference to landslides in weathered Neogene marls in Serbia. *Landslides*, 12(4): 689–702.
- Cooper A H (2008) The classification, recording, databasing and use of information about building damage caused by subsidence and landslides. *Quart. J. of Eng. Geol. and Hydrogeology*. 41: 409–424.
- Corominas J, Van Westen C, Frattini P, Cascini L, Malet JP, Fotopoulou S, Catani F, Van Den Eeckhaut M, Mavrouli O, Agliardi F, Pitilakis K, Winter M G, Pastor M, Ferlisi S, Tofani V, Hervás J, Smith JT, (2014) Recommendations for the quantitative analysis of landslide risk. *Bulletin of Eng. Geology and the Environment*. 73: 209–263.
- Đurić U, Abolmasov B, Marjanović M, Samardžić Petrović M, Pejić M, Brodić N, Popović J (2018) IPL Project 181 – Study of slow moving landslide Umka near Belgrade, Serbia – progress report for 2017 & 2018. Proceeding of IPL Symposium on Landslides 2018, Organized by International Consortium on Landslides (ICL), 03 December 2018, Kyoto, Japan. pp 41-45.
- Đurić U (2020) Quantitative risk assessment of “Umka” landslide near Belgrade. PhD thesis, University of Belgrade, Faculty of Mining and Geology, Belgrade, Serbia [Serbian only]
- Fell R, Corominas J, Bonnard C, Cascini L, Leroy E, Savage W Z, (2008) Guidelines for landslide susceptibility, hazard and risk zoning for land use planning. *Engineering Geology*. 102: 85–98.
- Grünthal G (1998) European Macroseismic Scale 1998 (EMS-98) European Seismological Commission, sub commission on Engineering Seismology, Working Group Macroseismic Scales, Vol. 15, Luxembourg.
- Marjanović M, Abolmasov B, Đurić U, Bogdanović S, Krautblatter M. (2015) Landslide events in Serbia in May 2014: An Overview. Proceedings of the 2nd Regional Symposium on Landslides in the Adria-Balkan Region ReSyLAB, 14-16 May 2015. University of Belgrade – Faculty of Mining and Geology, Serbia. pp 239-243.
- Palmisano F, Vitone C, Cotecchia F, (2016) Methodology for Landslide Damage Assessment. *Procedia Engineering*. 161: 511-515.
- Peduto D, Nicodemo G, Maccabiani J, Ferlisi S, (2017) Multi-scale analysis of settlement-induced building damage using damage surveys and DInSAR data: A case study in The Netherlands. *Engineering Geology*. 218: 117–133.
- Uzielli M, Nadim F, Lacasse S, Kaynia A M, (2008) A conceptual framework for quantitative estimation of physical vulnerability to landslides. *Engineering Geology*. 102: 51–256.
- Vujanić V, Jotić M, Jelisavac B (1992). Geotechnical investigation of the terrain in the area of landslides Umka and Duboko, Vol. I-V, Highway institute, Belgrade (study in Serbian).
- Vujanić V, Jotić M, Jelisavac B, Božinović D, Čorić S (1995) Sinteza rezultata geotehničkih istraživanja klizišta na Savi: Umka i Duboko. Istraživanje i sanacija, Drugi simpozijum, D. Milanovac, Srbija, 335-351 (in Serbian).

# Slopes of higher protection priority rating using modified Colorado Rockfall Hazard Rating System - Case study

Valentina Kocijan<sup>(1)</sup>, Mirko Grošić<sup>(1)</sup>, Lovro Blažok<sup>(1)</sup>

1) Geotech d.o.o., Rijeka, Ciottina 21, Croatia, +385914294090 (valentina.kocijan@geotech.hr)

**Abstract** Rockfall is the fastest and the most frequent type of landslide affecting the Croatian coastal area, and as such represents the threat to infrastructure positioned under rock slopes. On the large-scale roadcut sections, it is necessary to determine zones that pose a greater risk to the infrastructure, i.e., higher protection priority zones. The studied road section is located on the south-eastern coast of Istrian Peninsula, connecting villages Brsec on the south-west and Moscenicka Draga on the north-east. The existing road is approximately 8,0 km in length, executed mostly by cutting into the existing terrain, with the sub-vertical slopes up to 16,0 m high. Rock mass of the roadcuts is built out of sedimentary carbonate rocks - limestones and dolomites. The wide area belongs to the Ucka-Cicarija Onlay, a tectonically very active area in geological history, causing many discontinuity systems and fault zones resulting in different structural problems within roadcuts. To determine the zones of higher protection priority, a modified Colorado Rockfall Hazard Rating System (CRHRS) was used. Within the project, 66 zones of the studied road section were distinguished. Different slope protection measures were carried out according to the recommended priority levels.

**Keywords** rockfall, roadcut, slope protection, traffic accidents, CRHRS classification

## Introduction

Intensive tectonics of the wide-area of studied road section connecting villages Brsec and Moscenicka Draga, cause many different discontinuity systems and fault zones that are, along with unfavourable roadcuts, the main cause for rockfall. After several rockfall events on the studied road section, implementation of the slope protection measures was necessary. As rockfall events occurred on separate road sections, it was required to determine the zones of higher protection priority, which was carried out using the modified Colorado Rockfall Hazard Rating System (CRHRS).

The development of Rockfall Hazard Rating Systems (RHRS) by state of Oregon in 1984. has enabled us to categorize rock slopes with a proactive and logical way to set rockfall project priorities and allocate limited repair funds (Pierson 1991) according to the degree of hazard present. Traffic infrastructure development and busier

roads over the years required modification of the original classification. Modification of RHRS, developed by Russel et al. in 2008 (CRHRS), recognizes several different factors that contribute to rockfall: slope profile factor, geological factor, climate, and presence of water on the slope, rockfall history, and a number of traffic accidents attributed to rockfall.

The sum of the given points from categories for slope, climate, and geological conditions summarizes the actual rockfall hazard that a slope presents gives the Total Hazard Score. Traffic parameters rate the overall risk of a vehicle having an accident due to rockfall occurrence. The sum of the scores from these parameters gives the Total Risk Score. Total Hazard Score and Total Risk Score are rated separately, and according to a comparison of overall risk to overall hazard, higher priority sections are singled out when choosing which slopes to remediate first.

## Methodology

### Modified Colorado Rockfall Hazard Rating System - CRHRS

To address the immediate issue of determination of high protection priority zones, a modified Colorado Rockfall Hazard Rating System (CRHRS) was used. CRHRS was developed for three types of rocks - sedimentary rock (undercutting and differential erosion tend to control rockfall), crystalline rock (the rock mass inhomogeneity and fractures tend to control rockfall), block-in-matrix materials (colluvium, glacial till, debris flow deposits, etc. - an erosion of the matrix material and subsequent ravelling of the larger blocks tends to control rockfall).

CRHRS recognizes several different factors that contribute to rockfall (Russel et al. 2008) which are described in further subsections.

### Slope profile factor

- slope height - total slope height is measured from the road to the highest point of the potential rockfall source. If only the cut slope is being rated, the maximum height of the cut is considered.
- slope inclination - the slope angle is divided into four categories, ranging from 35° to > 65°. If no rockfall hazard is present above the cut face (natural terrain), the slope angle is taken from the cut. The measurement that poses the higher hazard to the roadway, is used to score the slope angle.

- slope continuity (launching features) - to determine the criteria for launching features is subjective, and engineering judgment is needed. Rating is divided into four categories: none (relatively smooth slope, with little or no topographic variation along the slope profile), minor, many, and major (highly irregular slope profile with large rock outcrops, or the presence of large ridges or benches extending more than 1.8 m from the slope surface (Fig. 1)).
- ditch catchment - ditch shape effectiveness is rated based on the slope profile - the more irregular slope profile is - the greater chance that the rockfall is activated. Ditch catchment is divided into four categories: type I (presence of barriers - hexagonal mesh with steel ropes, rod and self-drilling anchors, or Jersey bumpers), type II (effective hexagonal mesh), type III (barriers are local and/or ineffective), and type IV (no barriers present). If the irregularity of the slope relief extends 1.8 m, the ditch catchment is scored type IV.
- segment length - segments are divided according to similar slope characteristics.

#### Geological factor

The following described factors apply to sedimentary rock masses.

- degree of undercutting generally dominated by differential erosion and weathering in various lithologies with resulting undercutting and failure (Vandewater et al., 2005; Shakoor, 2005).
- jar slake - undercutting in sedimentary units (Fig. 2) that involve a weaker shale unit interbedded with a more competent sandstone or limestone (flysh) and is divided into categories according to a number of weaker units.
- weathering degree of rock mass - describes weathering grades within four categories.
- block size/ volume of material expected to fail - larger blocks have more kinetic energy when they fall and are more likely to roll further and end up in the roadway. They will also cause more damage during a collision with a vehicle. Larger blocks falling down a rock face are more likely to dislodge other blocks and result in additional rockfall.
- number of discontinuity sets (Fig. 3)- the more discontinuities a rock slope has, the more avenues exist for physical and chemical weathering to occur (Vandewater et al., 2005; Senior, 1999; Maerz et al., 2005; Romana, 1988; Nichol & Watters, 1983; Mazzoccola & Hudson, 1996).
- persistence and orientation of discontinuities - this factor takes into consideration both persistence and orientation in one category. E.g. highly persistent discontinuity with favourable dip direction with respect to roadway falls into the first category, while highly persistent discontinuity with an adverse dip direction with respect to roadway falls into the last category.



Figure 1 Example of the slope with major launching features present (segment from km 19+300 to km 19+490)



Figure 2 Example of the slope with a high degree of undercutting (segment from km 18+950 to km 19+150)

- aperture of discontinuities - higher the aperture, higher the possibility of water infiltration, frost wedging, and associated ravelling (Senior, 1999; Maerz et al., 2005; Romana, 1988; Mazzoccola & Hudson, 1996)
- weathering condition of discontinuities - the strength of discontinuity surfaces has a major influence on rockfall potential; chemical weathering and hydrothermal alteration reduce mechanical

properties of the entire rock mass (Patton & Deere, 1970; Romana, 1988). Along with weathering, the classification incorporates discontinuity infill in the same category.

- friction of discontinuities - this category observes smoothness and roughness respectively.

**Climate and presence of water on the slope**

- annual precipitation - amounts of rainfall and snowfall during the year. It is divided into four categories ranging from <250 mm to >1000 mm.
- occurrence of freeze and thaw periods - freeze/thaw index defined by the product of the monthly percentage of days with precipitation exceeding 25 mm and the number of freezing cycle days. Freezing cycle days are defined as the annual average number of days when the daily temperature fluctuates above and below freezing (Lienhart, 1988). It is divided into four categories ranging from 1 to ≥16 cycles.
- seepage/water - the presence of water on the slope is also considered within four categories ranging from dry to running water on the slope.
- slope aspect - based on evidence that south-facing slopes experience far more freeze/thaw cycles annually than north-facing slopes. North-facing slopes are in the shade most of the day, so they will experience the least amount of temperature variation throughout a given day and are rated the lowest. East, west, northeast, and northwest will experience some sunshine through the day and are rated second to lowest. Southeast and southwest-facing slopes will experience more sunshine and are rated second highest. Directly south-facing slopes will experience the most temperature variations over 24 hours and are rated the highest.

**Rockfall history**

- frequency of rockfall occurrence - occurrence of rockfalls per specific time, such as seasonal rockfall occurrence, or rockfall every 1-2 years

**Traffic conditions**

- sight distance - the percent decision sight distance is defined by the following equation:

$$\frac{\text{Actual Decision Sight Distance}}{\text{Required Decision Sight Distance}} \times 100\% \quad [1]$$

where actual decision sight distance is defined as the distance on a roadway that a 15 cm object placed on the edge of the road is visible to a driver, and required sight distance is based on speed limits according to the following table (Pierson and Van Vickle, 1993), where speed and distance units were adapted to the metric system.



Figure 3 Example of the slope with three discontinuity sets plus random discontinuities (segment from km 16+530 to km 16+640)

Table 1 Required decision sight distance based on posted speed limits (modified after Pierson and Van Vickle, 1993).

Posted speed limit (km/h)	Decision Sight Distance (m)
40	120
50	150
60	180
70	210
80	240

- average vehicle risk (AVR) - the amount of time a vehicle is within the segment length of a rockfall prone area. It takes into account the Average Daily Traffic (ADT), speed limit, and the length of the cut i.e., the length of the slope. It is defined by the following equation:

$$AVR = 100 \times \frac{[ADT \text{ (cars per day)} \times \text{Slope Length (km)}] / 24 \text{ (h/day)}}{\text{Posted Speed Limit}} \quad [2]$$

- number of accidents - information on accidents caused by rockfall, obtained from Traffic Safety Office.

**Categorization of higher priority sections**

According to conducted engineering-geological mapping along the studied road section, CRHRS recognizes three overall hazard categories and two overall risk categories.

- Overall hazard categories
  - Low - sections with 0-549 given points for sedimentary and crystalline rock masses, and 0-449 given points for rock-in matrix. Low hazard category can also be achieved with effective mitigation, low slope height, a favourable distance of the slope from the road, etc. which is mostly subjective, and has to be further explained in the comments.
  - Medium - sections with 550-699 given points for sedimentary and crystalline rock masses, and 450-599 given points for rock-in matrix.

- High - sections with  $\geq 700$  given points for sedimentary and crystalline rock masses, and  $\geq 600$  given points for rock-in matrix. High hazard category can be also present due to unfavourable local or global effects, and has to be further explained in the comments.
- Overall risk categories
- Low - sections with 0-75 given points represent low risk traffic condition
- High - sections with  $\geq 75$  given points represent low risk traffic condition

Comparison of overall risk to overall hazard, sections are further categorized into three groups, according to higher priority protection measures:

- Group A - sections with low to medium overall hazard category and low overall risk category
- Group B - sections with low to medium overall hazard category and high overall risk category or sections with high overall hazard category and low overall risk category
- Group C - sections with high overall hazard category and high overall risk category

### Geological features of the studied area

The researched area is part of the Istrian Peninsula known as the “White Istria”, karstified rock outcrops characterized by overthrust structures. Ucka-Cicarija Onlay is composed of Upper Cretaceous and Eocene carbonates, and Eocene flysch deposits (Fig. 4). According to Vlahovic et al. (2003), deformation of the Istrian Peninsula is divided into four deformation stages with similar characteristics, dated from Middle Jurassic epoch (D<sub>1</sub>), Cretaceous (D<sub>2</sub>), Eocene (D<sub>3</sub>) to Neotectonic deformation (D<sub>4</sub>) that takes place to this day.

The effects of deformation D<sub>1</sub> (Upper Bathonian) were local emersion and intensified relief of the subtidal area, as a consequence of mild compression. According to the orientation of gentle folds, they were accompanied by small faults, the greatest principal stress ( $\sigma_1$ ) being in the direction of 40–220°. Tectonic activity during the Cretaceous (D<sub>2</sub>) is seen as periodic synsedimentary movements occurring throughout the period. The greatest regional stress was acting along the direction 125–305°. In the third deformation (D<sub>3</sub>), taking place in Eocene, the main role has transgression. D<sub>3</sub> deformation is a decisive factor in the tectogenesis of the Dinarides. In Istria marks the beginning of subduction of the NE part of the Western Istrian Anticlinorium beneath the future structures of Cicarija. The question of the upper boundary of D<sub>3</sub> deformation is not definitively denoted. Neotectonic deformation (D<sub>4</sub>) activity comprised either the formation of new, neotectonic structures, reactivation of inherited old brittle structures into the regional transcurrent faults, or rotation of already existing structures towards the new stress orientation.

According to Sikic et al. (1963) Ucka-Cicarija Onlay extends from Plomin bay on the south to Preluka cove on

the north. Karstic Ucka massif gradually rises above the sea, building a sharp ridge in the west, which falls steeply towards Cepicko polje and Plomin Bay. Strata of the eastern part of Ucka mountain are inclined mainly to the east, in the southeast-northeast range.



Figure 4 Segment of the basic geological map, sheet Labin (Sikic et al., 1963) with studied road section.

According to conducted research works (detailed engineering-geological mapping) and the correlation with the existing data of previous research, it is determined that the investigated area is built of Upper Cretaceous carbonate deposits (limestone and dolomite) of the Cenomanian-Turonian age.

### Results

After detailed engineering-geological mapping was conducted, 66 different zones on the studied road section were singled out, according to the CRHRS classification. In the classification, imperial units were adapted to the metric system. The studied road section is approximately 8,0 km in length, and the length of singled zones ranges from 20,0 m to 300,0 m. Zones were defined during engineering-geological mapping, according to similar slope characteristics: slope geometry, number of discontinuity sets, condition and orientation of discontinuities, rock mass weathering grade, block sizes, and applied mitigation, but also sight distance, as studied road section is windy. Along with conducted CRHRS rock mass classification of each section, main discontinuity orientations were measured, and possible structural failures defined. Moreover, if present, unstable individual rock blocks were highlighted.



After compiling the results, a number of given points for overall hazard in individual zones ranges from 0 to 1068, and from 0 to 165 for overall risk, where higher number represents higher priority slope protection zone. Following table shows zone distribution of each of the three groups (A, B and C).

Table 2 Number of higher priority protection zones distributed in groups with their total lengths.

Priority protection groups	Number of zones on studied road	Total lengths of zones (m)
Group A	13	670
Group B	16	1305
Group C	37	4940

The largest number of zones (37 of them) is categorized to the group C, with a total length of 4940 m, 16 of them are categorized to the group B, with a total length of 1305 m, and only 13 are categorized to the group A, with a total length of 670 m (Fig. 5). Parts of the road section that contains no roadcuts are not included in the categorization. According to this result, most of the studied road sections required immediate slope protection measures.

According to the recommendation, different slope protection measures were carried out (underpinning with stone blocks, installation of galvanized double-twisted hexagonal wire mesh with or without steel ropes, installation of rod and self-drilling anchors, installation of shotcrete, profiling of rock slopes, installation of New Jersey bumpers, and removal of potentially unstable rock blocks).



Figure 5 Distribution of the priority protection groups from km 21+240 to km 22+160; Group C (red line), Group B (yellow line) and Group A (green line).

**Discussion**

Modification of RHRS developed by Russel et al. (2008) (CRHRS) is designed for three types of rock masses - crystalline, block-in-matrix, and sedimentary. However, the modification was designed for Colorado Front Range and included 51 crystalline, 35 block-in-matrix, and only 8 sedimentary slopes. As there were not enough sedimentary slopes, categorization was partly adapted to crystalline rock mass. Further development of sedimentary rock mass categorization of CRHRS, which would also include flysch rock mass as a separate type, would highly benefit better high priority protection measures planning in the area such as the coastal part of Croatia, where many rockfall events occur during the year. Furthermore, CRHRS classification can be also applied to proluvial and delluvial poorly lithified breccia roadcuts, present along the coastal area, as part of the block-in-matrix classification. Different rock mass classifications used to determine slope stability, SMR, developed by

Romana (1985), and Q-Slope method (Bar and Barton, 2015) in correlation to CRHRS, include more parameters to determine slope stability, while CRHRS is simplified, created to address the immediate issue of determination of high protection priority zones, taking into account traffic and rockfall history.

At this point, no systematic mapping for high priority slope protection classification is underway. Slope protection design is usually underway when rockfall occurs, and funding becomes available. From the obtained results of this project, we can conclude that the geological complexity of a wide area poses significant rockfall hazards on many busy roads, and this approach would give us an overview of potential hazardous sections over the country. To achieve standard classification that can be systematically applied to Croatian coastal area, it needs to be adapted both to European standards and to the area planned to be applied for (adaptation of measurement units to the metric system, type of rock mass, climate features of the area, seasonal traffic frequency, etc.).

## Acknowledgments

This study case was made to determine high priority protection road sections on the state road D66, section 003, from km 15+000 to km 23+000, for the Investor Hrvatske ceste d.o.o., Vončinina 3, Hr-10000 Zagreb. The geotechnical report and slope protection design was carried out by Geotech d.o.o., Ciottina 21, Hr-51000 Rijeka.

## References

- Barton N, Bar N (2015) Introducing the Q-slope method and its intended use within civil and mining engineering projects. Proceedings of the ISRM regional symposium, Eurock 2015 and 64th geomechanics colloquium, Salzburg, 7–10 October 2015, pp 157–162.
- Bieniawski ZT (1976) Rock mass classification in rock engineering. In: Bieniawski ZT (ed) Exploration for rock engineering; Proceedings of the symposium, Cape Town, Balkema, pp 97–106
- Bieniawski ZT (1989) Engineering rock mass classifications: a complete manual for engineers and geologists in mining, civil, and petroleum engineering. Wiley, New York, p 272p
- Lienhart, DA (1988) The geographic distribution of intensity and frequency of freeze-thaw cycles: Bulletin of the Association of Engineering Geologists, Vol. XXV, no. 5, pp. 465-469.
- Maerz, NH, Youssef A, Fennessey TW (2005) New risk-consequence rockfall hazard rating system for Missouri highways using digital image analysis: Environmental & Engineering Geoscience, 9(3): 229-249.
- Mazzoccola, DF., Hudson, JA (1996) A comprehensive method of rock mass characterization for indicating natural slope instability: Quarterly Journal of Engineering Geology, Vol. 29, pp. 37-56.
- Nichol MR, Waters RJ (1983) Comparison and effectiveness of rockfall mitigation techniques applied by states in the U.S.A. and Canada. Proceedings of the 20th Annual Engineering Geology and Soils Engineering Symposium, Boise, Idaho.
- Patton FD, Deere DU (1970) Significant geologic factors in rock slope stability. Proceedings of the Symposium on the Theoretical Background to the Planning of Open Pit Mines with Special Reference to Slope Stability, A.A. Balkema, Cape Town, Amsterdam, pp. 265-274.
- Pierson LA (1991) The Rockfall Hazard Rating System, Oregon Department of Transportation
- Pierson LA., Van Vickle R (1993) Rockfall Hazard Rating System Participant's Manual. Federal Highway Administration Publication SA-93-057, 104 p.
- Romana M (1985) New adjustment ratings for application of Bieniawski classification to slopes. Proceedings of the ISRM international symposium on role of rock mechanics in excavations for mining and civil works, Zacatecas, pp 49–53
- Romana M (1988) Practice of Slope Mass Rating (SMR) classification for slope appraisal: Glissements de Terrain, pp. 1227-1229.
- Russell CP, Santi P, Higgins JD (2008) Modification and Statistical Analysis of the Colorado Rockfall Hazard Rating System. Colorado School of Mines, Report No. CDOT-2008-7
- Shakoor A (2005) Development of a rockfall hazard rating matrix for the state of Ohio: The Ohio Department of Transportation Office of Research & Development Executive Summary Report.
- Senior SA (1999) Rockfall hazard remediation along Ontario highways: 50th Annual Highway Geology Symposium, Proceedings and Field Trip Guide, pp. 276-286.
- Sikic D, Polsak A, Magas N, Grimani I, Susnjar M, Simunic A (1969) Basic geological map scale 1:100.000, with legend, sheet Labin L 33-101, Institute for geological research works Zagreb, Federal Geological Association, Belgrade.
- Vandewater CJ, Dunne WM, Mauldon M, Drumm EC, Batemann V (2005) Classifying and assessing the geologic contribution to rockfall hazard: Environmental & Engineering Geoscience, 9(2): 141-154.
- Vlahovic I, Tisljar J, Velic I, Maticec D, Skelton PW, Korbar T, Fucek L (2003) Main Events Recorded in the Sedimentary Succession of the Adriatic Carbonate Platform from the Oxfordian to the Upper Santonian in Istria (Croatia). Field trip guidebook: evolution of depositional environments from the palaeozoic to the quaternary in the Karst Dinarides and the Pannonian Basin / 22nd IAS Meeting of Sedimentology

# Rock Frost Weathering and Rockfall Activity Assessment in Slovenia

Matjaž Mikoš<sup>(1)</sup>, Mateja Jemec Auflič<sup>(2)</sup>, Jernej Jež<sup>(2)</sup>, Nejc Bezak<sup>(1)</sup>

1) University of Ljubljana, Faculty of Civil and Geodetic Engineering, Ljubljana, Jamova cesta 2, Slovenia, +386 4768 590 (matjaz.mikos@fgg.uni-lj.si)

2) Geological Survey of Slovenia, Ljubljana, Slovenia

**Abstract** Rockfalls as mass movements occur more frequently in areas with high energy potential of the terrain (steep slopes, rock faces), which is enhanced by the weathering of the rocks on site. For physical weathering, hydrometeorological factors are important (air humidity & temperatures, wind direction & intensity, precipitation types & amounts). The weathering rate depends on the rock type and the discontinuities present.

In order to study rock frost weathering and potential rockfall activity in Slovenia, an analysis of land surface temperatures and air temperatures was performed. For the former, the ERA5-Land reanalysis data provided by Copernicus were used, and for the latter the measurement data from the precipitation monitoring network of Slovenia (Slovenian Environment Agency-ARSO) were used. The grid for LST was 9x9 km, and the number of meteorological stations in Slovenia used was more than 150 (period 2016-2020). We used hourly data to better assess frost weathering potential. Station-based air temperatures were compared to land surface temperatures and their diurnal, monthly, and seasonal differences were discussed. Using reanalysis ERA5-Land data, analysis of the annual number of daily freeze-thaw cycles was conducted and a freeze-thaw map of Slovenia was prepared. Additionally, multiple simple rockfall susceptibility models were tested. Several impact factors were used as input data such as slope, lithology, aspect, mean annual precipitation, 5-minute rainfall with the 100-year return period, seismic-hazard map and freeze-thaw map were selected. It was confirmed that slope and lithology are the two factors that have the most significant effect on the model performance. Consideration of the newly developed freeze-thaw map of Slovenia did not significantly improve the performance of the simple rockfall susceptibility model. The same can be said for the consideration of the seismic-hazard map. This especially applies to the rockfalls that occur in coastal flysch cliffs. In this area (Mediterranean coastal area) the number of freeze-thaw cycles are the smallest, the seismic-hazard map is characterized by lower acceleration values, and total precipitation amount is not very high, though rockfalls are abundant.

**Keywords** rockfalls, hazard assessment, frost weathering, Slovenia

## Introduction

In Slovenia, rockfalls, landslides, torrential erosion in headwaters, and riverbank erosion are one of the most hazardous phenomena (Mikoš et al., 2004). In Slovenia, there are a variety of landslide forms (Jemec Auflič et al., 2017). Rockfalls and rock slides are common in northern and north-western Slovenia, in steep gorges or canyons and in overthrust areas where carbonate rocks overthrust the softer rocks (mostly flysch) (Mikoš et al., 2013). For a long, rockfall susceptibility was relatively poorly investigated in Slovenia (Komac, 2017a). After the devastation in Log pod Mangartom in 2000, caused by a debris flow, the development of landslide research in Slovenia was obvious (Komac, 2017a; Mikoš, 2020).

Rockfalls were more often studied at a local scale rather than regional or national scale: developing a deterministic model for rockfall hazard assessment (Zorn and Komac, 2004), rockfall computer simulations (Petje et al., 2005b), dynamics of rockfall motion on slopes (Petje et al., 2006), rockfalls as a hazard for traffic infrastructure (Turković et al, 2005; Petje et al., 2005a) or rockfalls causing rockwall retreat on badlands (Zorn and Mikoš, 2008).

At larger scales, the first modern susceptibility map of Slovenia was produced in 1995/6 by the Geological Survey of Slovenia (Ribičič, 2002) on the basis of the Engineering-Geological Map of Slovenia in scale 1:400,000 from 1994, introducing a 4-classes susceptibility map, originally called Stability Map of Slovenia – Rockfalls (GeoZS, 2021) in a gridded 242 x 242 m raster form (Fig. 1).

In 2011, a new Rockfall Susceptibility map of Slovenia in scale 1:250,000 was prepared by the Geological Survey of Slovenia (Čarman et al., 2011). The map was produced in the GIS environment based on slope, lithology and distance to tectonics features (Fig. 2). The most important factors considered were: lithology (lithological map of Slovenia in scale 1:250,000), slope angle and distance to tectonic-structural elements (Komac, 2017b). Susceptibility was divided into 6 classes from high susceptibility to no susceptibility (Fig. 2).

The main problem in any work on rockfall susceptibility in Slovenia is a lack of a consistent cadastre and a lack of abundant historical data to validate a statistical model. The first validated rockfall susceptibility map was prepared at the municipal scale of 1:25,000 for Bovec Municipality in NW Slovenia (Čarman et al. 2015)

(Fig. 3). The map was developed, based on the probabilistic model of slope mass movement susceptibility proposed for Bovec municipality by Komac (2005). This study has a

research question: can the analysis of rock frost weathering improve/change the assessment of rockfall susceptibility in Slovenia?

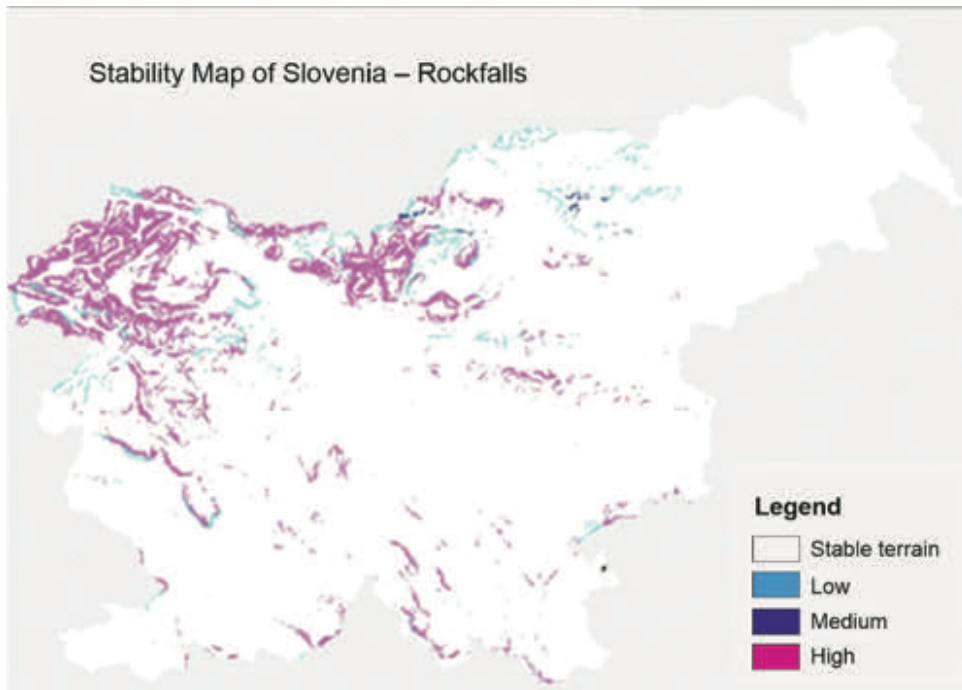


Figure 1 Stability Map of Slovenia – Rockfalls in the scale 1:400,000 from 1995/6.

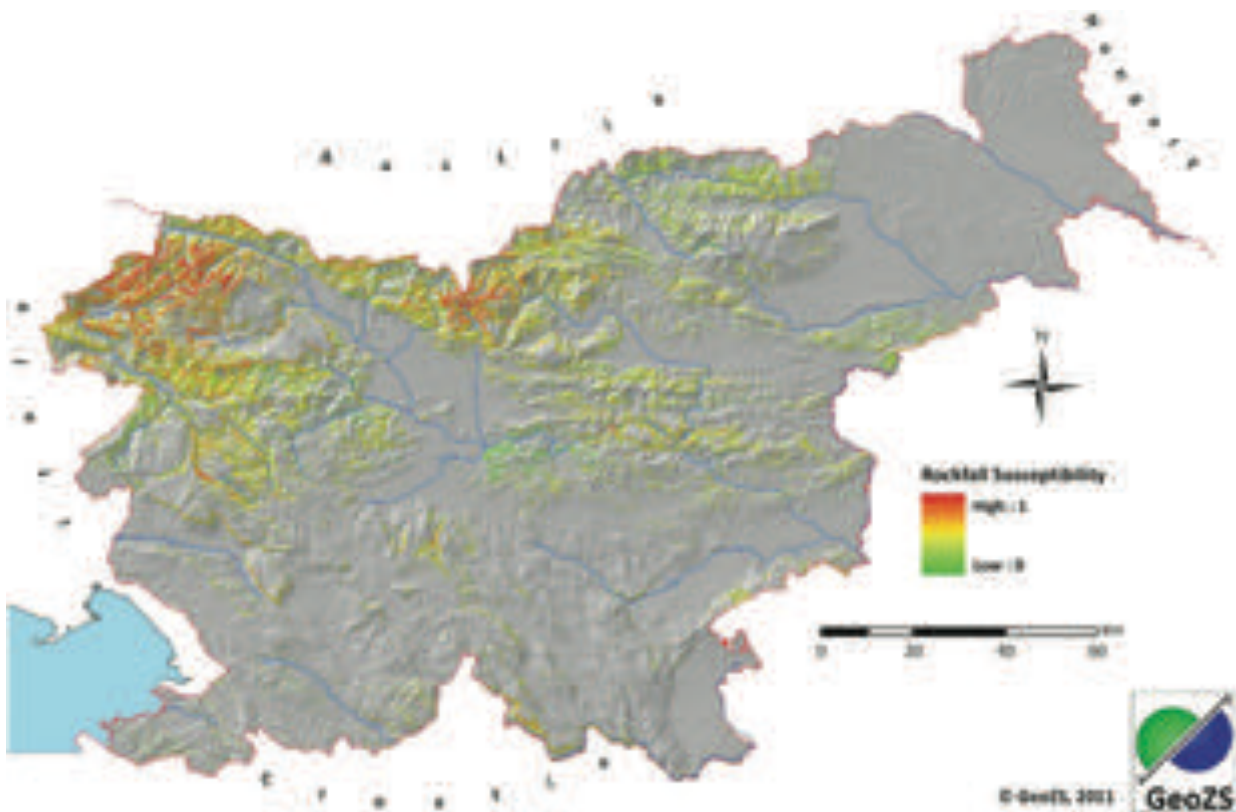


Figure 2 Rockfall Susceptibility Map of Slovenia at scale 1:250,000 (Čarman et al., 2011)

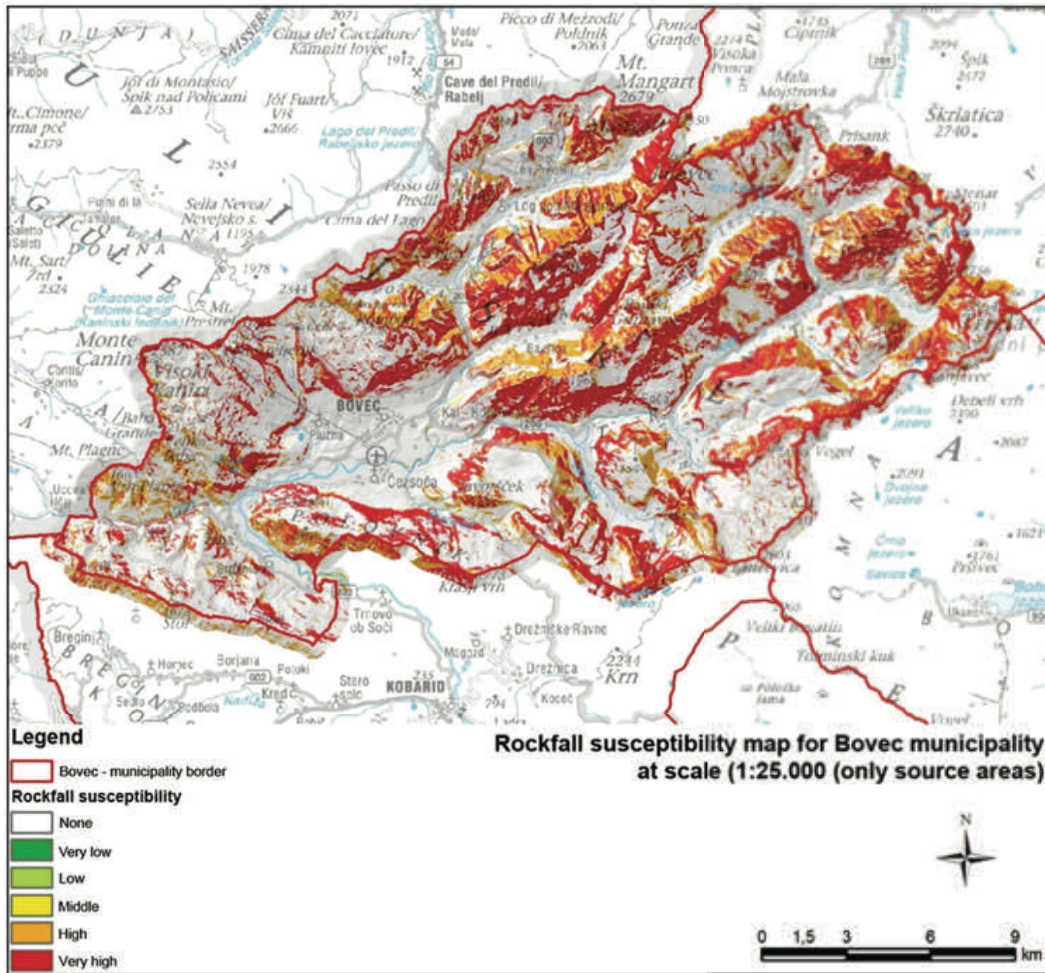


Figure 3 Rockfall Susceptibility Map of Bovec Municipality at scale 1:250,000 (Čarman et al., 2015).

## Materials and Methods

### Frost weathering

Frost weathering of rocks is defined as a collective term for several mechanical weathering processes induced by stresses created by the freezing of water in rocks discontinuities.

### Rockfall causal factors

Rockfalls can be triggered by earthquakes, strong storms or thunderstorms, by strong winds and heavy rainfall, not to mention human activities, such as slope undercutting or blasting. The study was focused on the question “Where it can happen?” and not to the question “When it can happen? Since the result in the form of a regional/national rockfall susceptibility map was envisaged, the following rockfall causal factors were considered:

- Lithology – the Lithological map of Slovenia in scale 1:250,00 was used in its digital form (shape files for each lithological unit on the map). All in all, 28 engineering-geology units were classified into 6 classes with regard to the susceptibility of lithology to weathering and crack initiations due to frost and

thermal weathering and susceptibility to seismic activity.

- New Seismic Hazard (SH) map of Slovenia (ARSO, 2021) showing peak ground accelerations (PGA), determined for the 475-year return period (Fig. 4).
- These accelerations are valid for bedrock or other geological formations with at least an elastic wave velocity of 800 m/s and less than 5 m of weak soil cover. For the new seismic hazard map, for the first time is Slovenia, active faults and fault sources were considered that might be of importance also for rockfall susceptibility modelling.
- Slope gradient as an indicator for available terrain energy available to release rockfalls.
- Slope aspect as an indicator of thermal stress due to solar insulation.
- Mean annual precipitation (P), and 5-minute precipitation with the 100-year return period ( $P_{100}$ ) (from the Crossrisk project, <https://www.crossrisk.eu/en/>) as an indicator for weathering rates, rock moisture, and snow cover.
- Freeze-thaw cycles as an indicator for crack initiations in rocks – cycles were estimated using diurnal fluctuations of air temperatures and land surface temperatures.

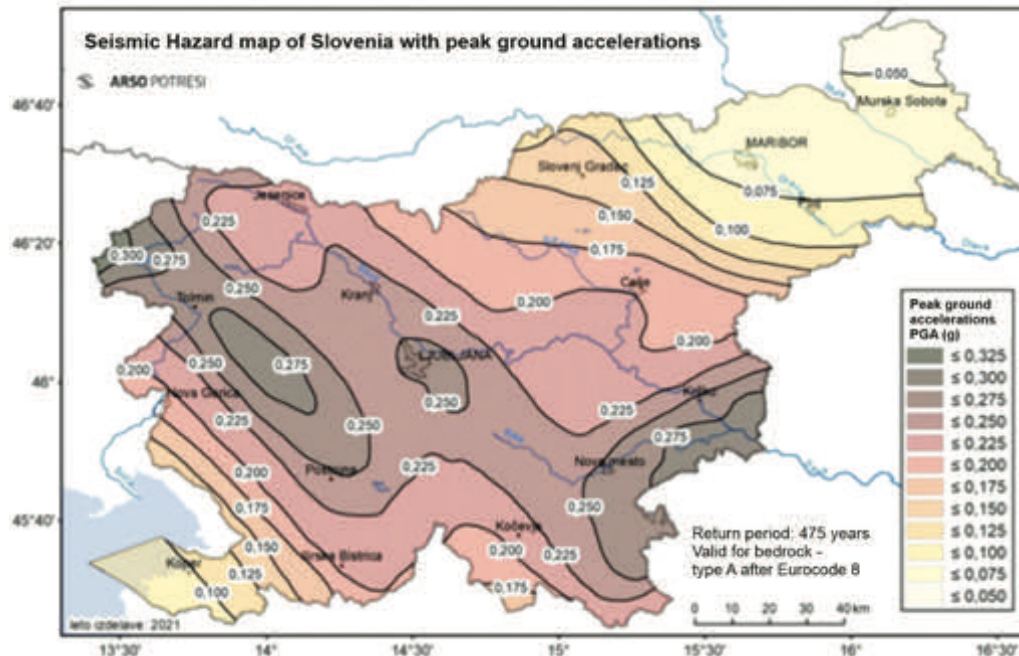


Figure 4 Seismic Hazard map of Slovenia with peak ground accelerations (PGA in g), return period 475 years and valid for bedrock – type A after Eurocode 8 (ARSO, 2021).

#### Reanalysis data and meteorological data

The relevant reanalysis data was used, i.e. the ERA5-Land reanalysis hourly data for the period 2016-2020 provided by the Copernicus (2021). We applied the following data: “2 m temperature”, “Soil temperature level 1”, and “Snow depth”. “2m temperature” represents the air temperature at 2m above the surface of land, sea or in-land waters (Copernicus, 2021). It is obtained by the interpolation of the Earth’s surface and lowest model level (Copernicus, 2021).

The “Soil temperature level 1” represents temperature of the soil level (0-7 cm) that comes from the ECMWF Integrated Forecasting System (Copernicus, 2021). While the “Snow depth” variable represents the grib-box mean of the snow thickness on the ground while excluding snow on the canopy (Copernicus, 2021). An example of the reanalysis data is shown in Fig. 5.

Additionally, the 2-m air temperature at hourly scale was obtained for the same periods 2016-2020 from over 150 meteorological stations from the state monitoring system operated by ARSO (Slovenian Environmental Agency, 2021). Fig. 6 shows the location of stations that had air temperature data available in the 2016-2020 period.

#### GIS environment and tools

Investigations related to the extraction of the reanalysis data were carried out using program R (2021) and available packages such as *raster*, *rgdal*, *sp*, and *gstat*. R software was also used for pre-processing the hourly station-based data and for the interpolation. Analyses related to susceptibility models were performed in the SAGA GIS environment that is a free open access software for geoscientific analyses (SAGA, 2021) – we used version 8.

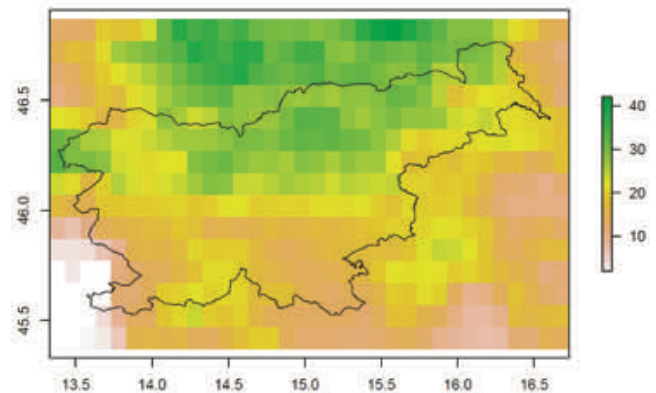


Figure 5 Era5-Land reanalysis data for the area of Slovenia, the legend shows average number of days when soil temperature at level 1 is below and above 0°.

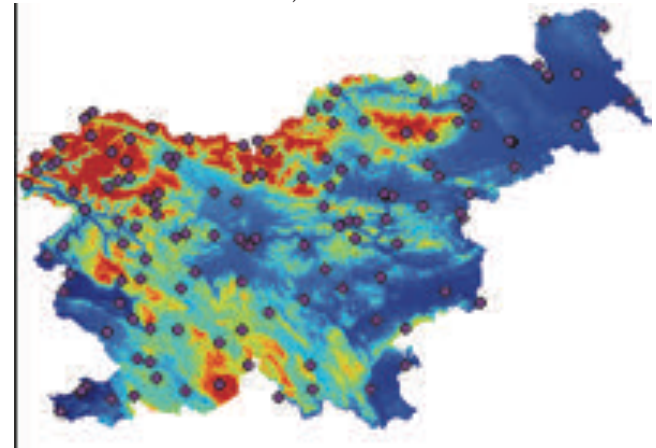


Figure 6 Location of meteorological and climatological stations with the hourly 2m air temperature data availability in the period 2016-2020. Digital elevation model is shown as background.

**Rockfall cadastre data**

A rockfall cadastre was compiled based on data from various sources (GH50 project, Civil Administration database, and personal collections). A total of 164 rockfalls from GH50 project were used in this study.

**Results and Discussion**

**Reanalysis data and station-based data investigations**

For the investigations related to the freeze-thaw cycles we used both reanalysed and station-based data. Fig. 7 shows the average number of days when the air temperature is below and above 0°. It can be seen that these maps are to some extent different as the one shown in Fig. 5.

Thus, the further comparison was made between air temperature and soil temperature data (Fig. 8). It was found that differences to some extent depend on the station location since for high altitude stations differences were more explicit than for low-altitude stations (Fig. 8).

This was further confirmed by conducting a similar analysis for all the locations shown in Fig. 6. The results are presented in Fig. 9. It can be seen that the difference in the number of freeze-thaw cycles depends on the station altitude. The main reason for these differences is the snow cover depth that varies from station to station. Moreover, we additionally compared air temperature data obtained from ERA5-Land and station-based data (ARSO). It was again found that agreement between two datasets depended on the station location (Fig. 11) and was estimated as acceptable.

**Freeze-thaw map of Slovenia based on the soil temperature**

Based on the conducted investigations, we decided to use the soil temperature data from the ERA5-Land to estimate the average annual number of freeze-thaw cycles for entire Slovenia. This variable was assumed to be the most relevant for the description of the actual number of freeze-thaw cycles. Based on the location of stations (Fig. 6) we extracted the ERA5-Land data and performed interpolation using the ordinary kriging. The final map is shown in Fig. 11. This map was used in the further steps of this study.

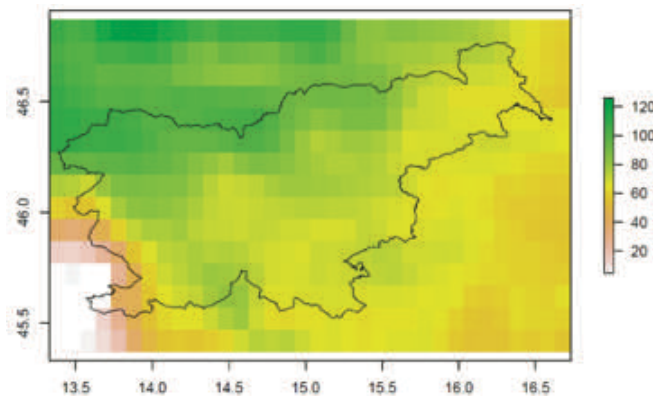


Figure 7: Average number of days when air temperature data is below and above 0°.

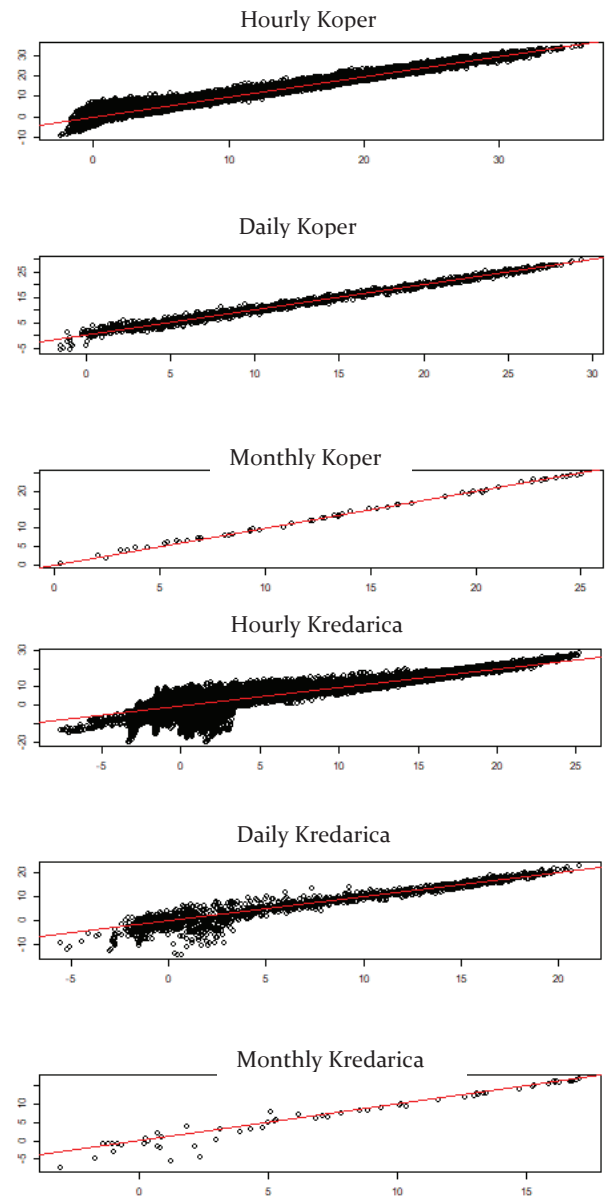


Figure 8: Comparison between 2 m air temperature (y-axis) and soil temperature level 1 (x-axis) at hourly, daily and monthly time step for Kredarica (high-altitude Alpine station) and Koper (low-altitude Mediterranean station) stations.

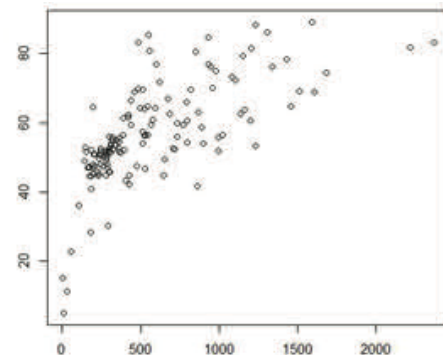


Figure 9: Relationship between station altitude (x-axis) and number of cycles calculated using air temperature and soil temperature data (y-axis). The grid locations for all stations shown in Fig. 6 are shown (one point-one station).

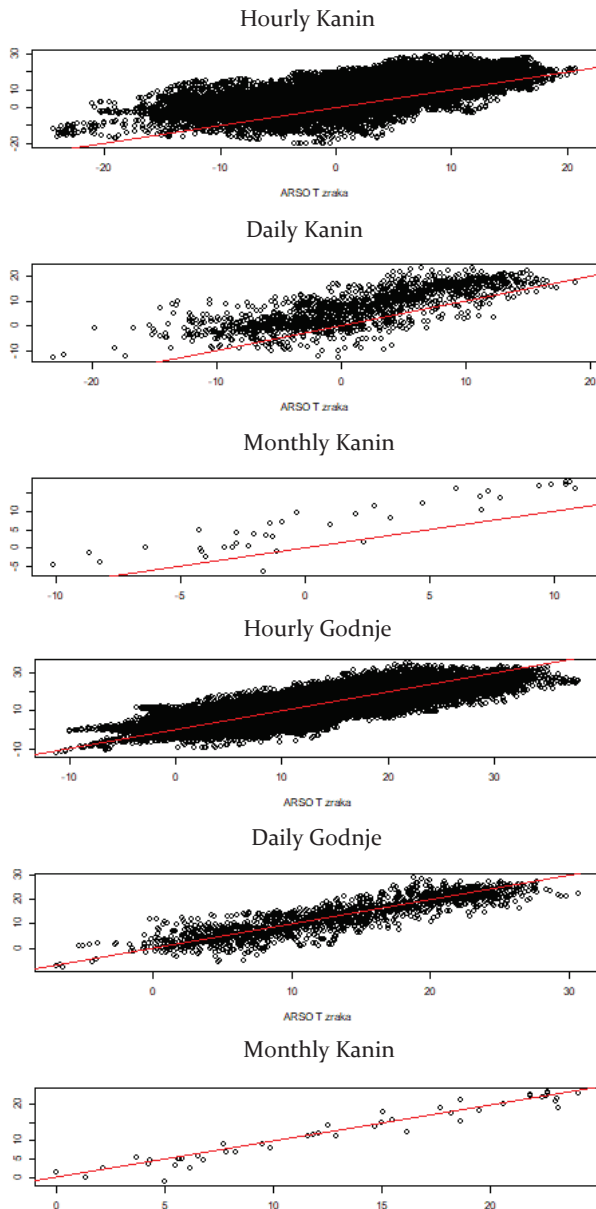


Figure 10: Comparison between 2 m air temperature from the ERA5-Land (y-axis) and station-based air temperature (x-axis) at hourly, daily and monthly time step for Kanin (high-altitude Alpine station) and Godnje (low-altitude Mediterranean station) stations.

### Rockfall Susceptibility Models

Multiple simple models were tested to evaluate if the developed freeze-thaw map can improve the performance of simple rockfall susceptibility models (Tab. 1). In addition, simple evaluation of model performance was performed (Tab. 1). Some examples of the tested models are shown in Fig. 12, Fig. 13, Fig. 14 and Fig. 15.

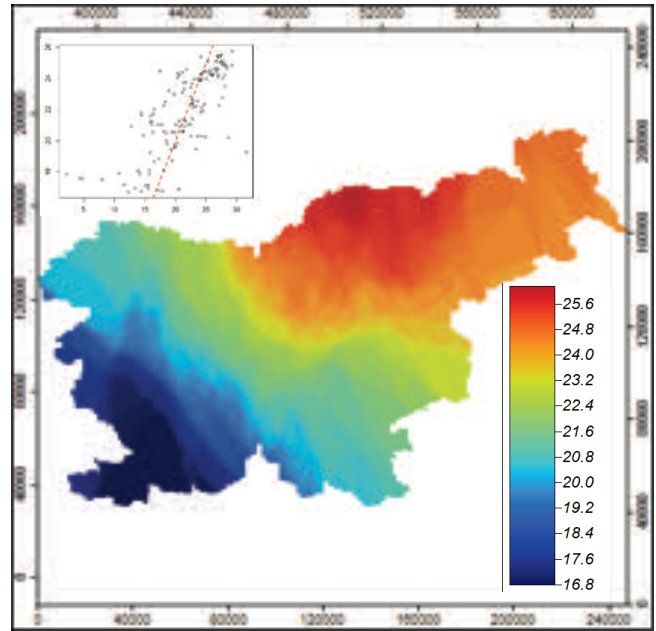


Figure 11: Freeze-thaw map of Slovenia (average annual daily free-thaw cycles) based on the ERA5-Land soil temperature data and results of the leave-one-out cross validation (scatter plot) for ordinary kriging (elevation was used for the interpolation).

Table 1. List of tested rockfall susceptibility models (legend: S-Slope; LI-Lithology; FT-Freeze-Thaw, A-Aspect, P-Total annual precipitation; P<sub>100</sub>-5-minute rainfall with 100-year return period; SH-Seismic-Hazard). For all models, mean values are given for the entire Slovenia (MVS) and for the cells with rockfalls (MVR).

ID	Model	MVS	MVR (Min-Max values)
1	$0.2*S+0.2*LI+0.2*P+0.2*FT+0.2*A$	0.46	0.55 (0.15-0.87)
2	$0.3*S+0.3*LI+0.1*P+0.2*FT+0.1*A$	0.47	0.59 (0.12-0.90)
3	$0.3*S^{1/2}+0.3*LI+0.1*P+0.2*FT+0.1*A$	0.51	0.63 (0.19-0.89)
4	$0.3*S^{1/2}+0.3*LI^{1/2}+0.1*P+0.2*FT+0.1*A$	0.55	0.67 (0.19-0.91)
5	$0.5*S^{1/2}+0.5*LI^{1/2}$	0.51	0.68 (0.18-0.94)
6	$0.7*S^{1/2}+0.3*LI^{1/2}$	0.45	0.63 (0.24-0.93)
7	$0.7*S^{1/2}+0.3*LI$	0.42	0.60 (0.24-0.92)
8	$0.3*S^{1/2}+0.3*LI^{1/2}+0.1*P_{100}+0.2*FT+0.1*A$	0.56	0.68 (0.22-0.88)
9	$0.3*S^{1/2}+0.3*LI^{1/2}+0.1*P_{100}+0.1*FT+0.1*A+0.1*SH$	0.50	0.64 (0.22-0.91)



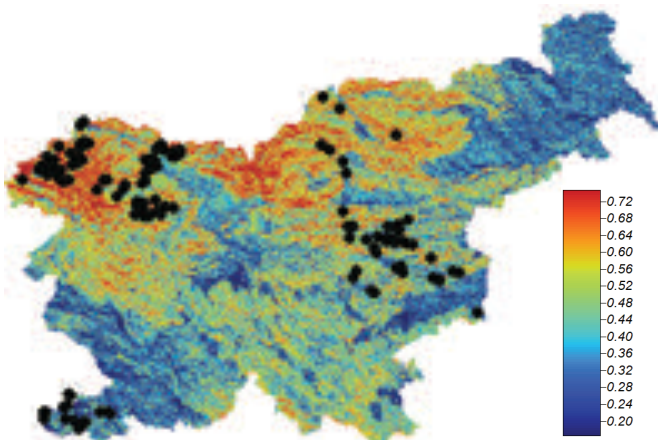


Figure 12: Tested rockfall susceptibility model number 1 with the location of 164 rockfalls used in this study.

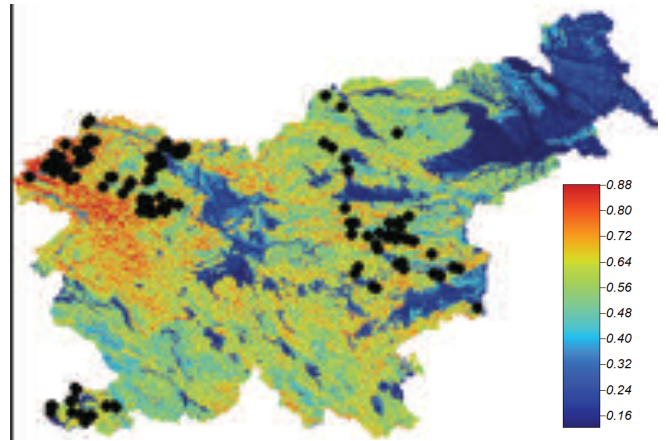


Figure 15: Tested rockfall susceptibility model number 9 with the location of 164 rockfalls used in this study.

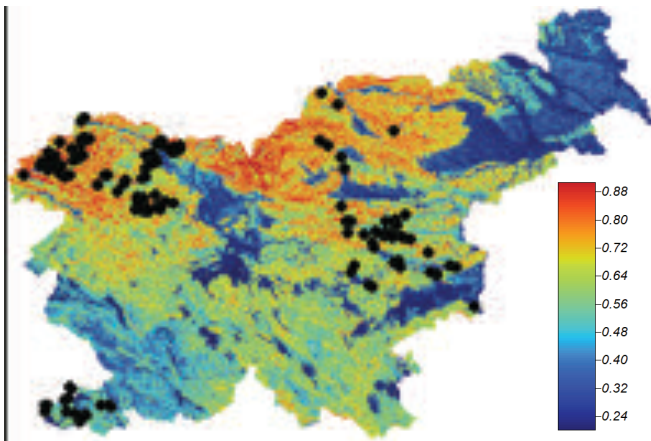


Figure 13: Tested rockfall susceptibility model number 4 with the location of 164 rockfalls used in this study.

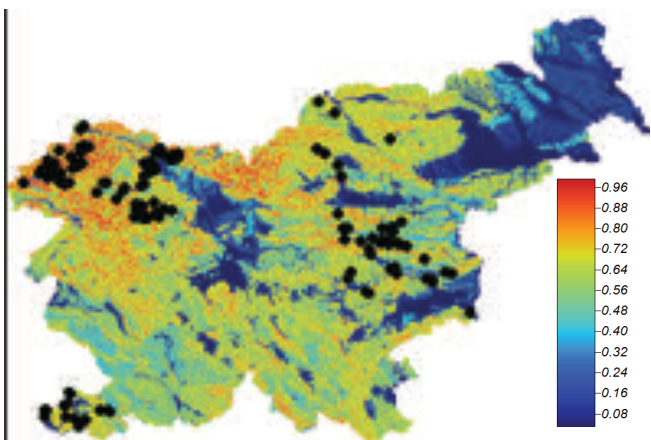


Figure 14: Tested rockfall susceptibility model number 5 with the location of 164 rockfalls used in this study.

## Conclusions

Based on the presented results it can be concluded that the consideration of the newly developed freeze-thaw map of Slovenia does not significantly improve the performance of the simple rockfall susceptibility model. The same can be said for the consideration of the seismic-hazard map.

Based on the results, slope and lithology are considered as the main preconditioning factors that impact the performance of such simple rockfall susceptibility models. This especially applies for the rockfalls that occur in coastal flysch cliffs. In this area (Mediterranean coastal area) the number of freeze-thaw cycles is the smallest, the seismic-hazard map is characterized by lower peak ground acceleration (PGA) values and the total precipitation amount is not very high. A variable that could be used in this part of the Slovenia is the  $P_{100}$ . Moreover, additional investigations are needed to improve the performance of the larger-scale regional rockfall susceptibility model.

## Acknowledgments

The authors would like to thank Slovenian Research Agency (ARRS) for financial support through core financing P2-0180 and P1-0011, and two research projects J1-2477 and J1-3024, respectively.

## References

- ARSO (2021) Nova karta potresne nevarnosti (New Seismic Hazard Map). URL: <https://www.gov.si/novice/2021-03-02-nova-karta-potresne-nevarnosti/> [Last accessed: 2 December 2021].
- COPERNICUS (2021) ERA5-Land hourly data from 1950 to present. URL: <https://cds.climate.copernicus.eu/cdsapp#!/dataset/reanalysis-era5-land?tab=overview> [Last accessed: 2 December 2021].
- Čarman M, Kumelj Š, Komac M, Ribičič M (2011) Pregledna karta verjetnosti pojavljanja podorov v merilu 1:250.000 (General rockfall probability map in scale 1:250,000). Geološki zbornik 21. Ljubljana.

- Čarman M, Bavec M, Komac M, Krivic M (2015) Rockfall Susceptibility Assessment at the Municipal Scale (Bovec Municipality, Slovenia). In: Engineering Geology for Society and Territory – Volume 2: Landslide Processes. Lollino G, Giordan D, Crosta G B, Corominas J, Azzam R, Wasowski J, Sciarra N (eds). Chapter 358. Springer, Cham. (ISBN 978-3-319-09057-3). 2177 p.
- Đurović B, Ribičič M, Mikoš M (2005) RHDM procedure for analysis of the potential specific risk due to a rockfall hazard. *Geologija*. 48(1): 33–51.
- GeoZS (2021). Stabilitetna karta Slovenije – podori (Stability Map of Slovenia – Rockfalls). URL: [https://www.geo-zs.si/PDF/Podatki/Stabilitetna\\_karta\\_slo\\_podori.pdf](https://www.geo-zs.si/PDF/Podatki/Stabilitetna_karta_slo_podori.pdf) [Last accessed: 2 December 2021].
- Jemec Auflič M, Jež J, Popit T, Košir A, Maček M, Logar J, Petkovšek A, Mikoš M, Calligaris C, Boccali C, Zini L, Reitner J M, Verbovšek T (2017) The variety of landslide forms in Slovenia and its immediate NW surroundings. *Landslides*. 14: 1537–1546.
- Komac M (2005) Verjetnostni model napovedi nevarnih območij glede na premike pobočnih mas – primer občine Bovec (Probabilistic model of slope mass movement susceptibility – a case study of the Bovec municipality, Slovenia). *Geologija*. 48(2): 311–340.
- Komac M (2017a) The geological and geology-related study of landslides in Slovenia in the past two decades and the presentation of methodology of spatial analysis of the landslide occurrence. *UJMA*. 31:161–170.
- Komac M (2017b) A Joint Regional Slope Mass Movement Susceptibility Map. In: GIS Landslide. Yamagishi H, Bhandary NP (eds). Chapter 7. Springer, Tokyo. (ISBN 978-4-431-54391-6). 230 p.
- Mikoš M (2020) After 2000 Stože Landslide: Part I – Development in landslide research in Slovenia. *Acta hydrotechnica*. 33(59): 129–153.
- Mikoš M, Brilly M, Ribičič M (2004) Poplave in zemeljski plazovi v Sloveniji = Floods and Landslides in Slovenia. *Acta hydrotechnica*. 22(37): 113–133.
- Mikoš M, Jemec Auflič M, Ribičič M, Čarman M, Komac M (2013) Earthquake-Induced Landslides in Slovenia: Historical Evidence and Present Analyses. In: Earthquake-Induced Landslides. Ugai K, Yagi H, Wakai A (eds). Chapter 23. Springer Verlag, Berlin. (ISBN 978-3-642-32238-9). 996 p.
- Petje U, Mikoš M, Ribičič M (2005a) Hazard assessment due to falling stones on a reach of the regional road in the Trenta valley, Slovenia. *Geologija*. 48/2: 341–354.
- Petje U, Ribičič M, Mikoš M (2005b) Computer simulation of stone falls and rockfalls. *Acta geographica Slovenica*. 45(2):93–120.
- Petje U, Mikoš M, Majes B (2006) Motion of rock masses on slopes. *Geologija*. 49(2): 393–408.
- Program R (2021) The R Project for Statistical Computing. URL: <https://www.r-project.org/> [Last accessed: 2 December 2021].
- Ribičič M (2002) Zemeljski plazovi, usadi in podori (Landslides, slumps, and rockfalls). In: Nesreče in varstvo pred njimi. Ušeničnik B (ed.). Uprava za zaščito in reševanje, Ministrstvo za obrambo, Ljubljana. 569 p.
- SAGA (2021) System for Automated Geoscientific Analyses. URL: <http://www.saga-gis.org/en/index.html> [Last accessed: 2 December 2021].
- Zorn M, Komac B (2004) Deterministic modeling of landslide and rockfall risk = Deterministično modeliranje ogroženosti zaradi zemeljskih plazov in skalnih podorov. *Acta geographica Slovenica*. 44(2): 53–100.
- Zorn M, Mikoš M (2008) Rockwall retreat on badlands in Slovene Istria. *Geologija*. 51(1): 107–118.
- Zorn M, Komac B, Kumelj Š (2012) Mass movement susceptibility maps in Slovenia: the current state. *Geografski vestnik*. 84(1):99–112.

# Regional rockfall exposure assessment, experiences from Serbia

Miloš Marjanović<sup>1</sup>, Biljana Abolmasov<sup>1</sup>, Uroš Đurić<sup>2</sup>, Jelka Krušić<sup>1</sup>, Snežana Bogdanović<sup>1</sup>

1) University of Belgrade, Faculty of Mining and Geology, Djušina 7, 11000 Belgrade, Serbia, +381 11 3219 224, (milos.marjanovic@rgf.bg.ac.rs)

2) University of Belgrade, Faculty of Civil Engineering, Belgrade, Serbia

**Abstract** Rockfalls are common in hilly and mountainous areas, especially along roads with engineered slopes and cuts. Such is the case for most of the state and local road routes in Central, Serbia, which was the subject in this case study. A road network of 276 km covering roughly 1700 km<sup>2</sup> between the cities of Kraljevo, Čačak and Ivanjica is presented. Assessing of such wide areas needs to be conducted from large to site-specific scale, i.e., using GIS spatial tools and 2D-3D stability models, respectively. The regional scale of assessment using GIS tools was in focus. The primary input was the Digital Terrain Model, obtained from open data ALOS mission at 12.5 m resolution, as well as appropriate sheets of geological maps at 1:100,000 scale. The first step was to delineate areas that can host unstable blocks by inspecting planar sliding kinematic condition against available data. These included raster data (slope angle and azimuth) but also, point-based data (discontinuities' strike, dip and friction angle) which had to be estimated or interpolated across the area by various GIS operations. In total, there were nearly 5000 potential detachments delineated. Further step was to run the rockfall simulation by using these detachment zones as initiation sources in a simple kinetic model CONEFALL, standalone software. The output model simulated several thousands of rockfalls, with various runout distance (<650 m), velocity (<46.5 m/s) and energy (<540 kJ). When overlapped with the road network, this model revealed the road exposure to rockfall. Locations with runouts that reached the road lines make about 6.7 % of the total network length. Zones of estimated energies higher than serviceable threshold (300 kJ) occupy 0.9 % of the total and require additional remediation design. Presented analysis is a promising tool for supporting planning and decision making in the road management sector.

**Keywords** CONEFALL, exposure, GIS, rockfall, Serbia

## Introduction

Rockfalls are common in hilly and mountainous areas, especially along roads with engineered slopes and cuts. Such is the case for most of the road routes in Central, Eastern, Western and Southern Serbia, especially on low-category state and local roads. Rockfalls can induce hazard of high magnitude (frequency, velocity, energy etc.), causing temporary or long-term effects. They impose constant problems to the road management enterprises,

requiring frequent maintenance or mitigative activities. In addition, population growth and entailed urbanization, as well as climate change impacts (extreme weather conditions) all imply further emphasis on this type of hazard, together with all other climate-affected slope processes (Gariano and Guzzetti, 2016). Therefore, strategies that are including rockfall hazard assessment (as well as other road-threatening processes) are increasingly important in road management, but also in planning, engineering design and research (Davies et al., 2014), and such practice is in its beginnings in Serbia and throughout the region (Abolmasov, 2017; Marjanović et al., 2018; Marjanović et al., 2019, Marjanović et al., 2020).

## State-of-the-art

Although the rockfall mechanism is precisely defined in the conventional landslide and mass movement classifications (Hung et al., 2014, Dikau et al., 1996), it is rather common to assess mixed types of mechanisms, i.e. falling in combination with sliding and toppling, as well as bouncing, fragmenting etc., instead of solely free-falling rock. This is justified due to the actual, realistic events, which are always complex in this and many other aspects, but rock avalanches and large rockslides, as well as DSGSD (deep-seated gravitational slope deformation) are to be differentiated from rockfall mechanism, as perceived herein. Regardless of the scale and due to their different mechanism in comparison to other landslide types (high mobility and velocity), the assessment practice of rockfall hazard commonly includes (i) delineation of the release or detachment or source zones, (ii) characterization of the source material (block shape, size, strength, etc.) and the background (roughness, vegetation, deformability), and (iii) rockfall simulation with trajectory runout modelled per several parameters (reach distance, jump height, velocity, energy, etc.) (Dorren et al., 2011). The scale of assessment dictates the level of detail of input data, and complexity of the model. Obviously, regional scale models cannot be provided with site-specific level of input data, which is why they are usually confined to steps (i) and simplified step (iii) (Jaboyedoff and Labiouse, 2011).

Many authors have reported rockfall hazard case studies ranging from large to local scales, endangering roads, rails or hiking tracks. A full overview of the state-of-the-art would be beyond the topic and purpose of this paper, which is why only most relevant works, regarding

regional scales and road network exposure context, will be addressed hereinafter. As step (i) requires delineation of sources, it is worth mentioning that such procedure for larger scales is commonly automated and GIS-based. Alternatively, there are procedures that integrate field and operative data for mapping of slopes and their classification specifically for the roads (Budetta, 2003). Inconveniently, they overlap procedures from (i), (ii) and (iii) in a single classification procedure, commonly subjective. Loye et al. (2009) reported a procedure based on high-resolution (airborne LiDAR) Digital Elevation Model (DEM) analysis. They have decomposed slope angle distribution to map cliffs and steep slopes as predominant rockfall sources in alpine regions and argue that such global criterion can be easily applied to any other mountainous area with slight adjustments. Since they have offered global criterion, they have not considered geological or kinematic conditions. Even though inspiring, their approach was not directly implemented in this research, as the principal intention herein was to include other important conditions. Similarly, Aksoy and Ercanoglu (2006) used rule-based fuzzy analysis over a set of morphological, but also structural (field) data for the city-wide assessment of rockfall source areas. Fanos and Pradhan (2019) performed comprehensive rockfall hazard assessment at city-wide scale but demonstrated how machine learning algorithms can extract potential source areas from high-resolution DEMs, which might be direction of our future research. Copons and Vilaplana (2008) have introduced a case of rockfall risk assessment at scales 1:5,000-25,000 for land use planning purposes, by calculating and statistically processing the exposure distribution at the foot of the designated large-scale slope of known dynamics, which has inspired our approach, too. Road and rail networks at regional scales were the subject of several researchers (Lato et al. 2009; Michoud et al., 2012; van Veen et al., 2018), wherein it is typical to adopt realistic scenarios using confirmed source areas, based on historical remote sensing and LiDAR monitoring data (static or mobile). These were further using various tools, usually simplified, for solving step (iii) and calculating the exposure of the target infrastructure.

Common for most of these studies is the use of high-resolution DEM from airborne LiDAR campaigns, which is not widely available in Serbia. Another conformity, with some exceptions, is the preference of morphological rather than integrated (geological and structural) criteria for delineating source zones. It is also apparent that the level of detail of the terrain surface model severely affects both, detection of potential source areas and propagation of the rockfall trajectories. Higher level of detail (1x1 m or less) commonly implies greater rockfall hazard than the coarse DEMs (10x10 m or more) over the same area, so optimization of inputs is also indicative suggestion in described works. It is also indicative that shifting from small-scaled and detailed to large-scaled and general rockfall assessment implies application of less complex simulation models at step (iii).



Figure 1 The area of interest with its categorized road network.

#### Area of interest

In this article, experience from a case study in Central Serbia, covering a road network 276 km long within an area of roughly 1700 km<sup>2</sup> will be presented (Fig. 1). It is situated between cities of Čačak, Kraljevo and Ivanjica within a mixed terrain configuration, from flat river valleys to the north, to hilly-mountainous terrain to the south. The wider investigation concept is defined in the World Bank project: Mainstreaming climate resilience in road transport management in Serbia, conducted in 2020-2021 for Public Enterprise Roads of Serbia. The presented analysis of rockfall exposure is just a fraction of all performed spatial and traffic modelling, which was targeted at developing and testing methodology for quantitative risk assessment in respect to relevant natural hazards including the current and future climates.

In brief, the project framework included several key tasks. Firstly, the area of interest was scoped for examples of instabilities, resulting with a database, used as input and validation data for hazard models, i.e., hazard maps. This subproject was named ClirTheRoads and contains digital repository (<http://clirtheroads.rgf.rs/>). The exposure of the network was analysed by overlapping road network over these maps while introducing quantified vulnerability parameters of the road assets. The next task was to detect critical locations and develop scenarios in respect to traffic and population distress. For each scenario a cost-benefit analysis was conducted to test the balance between the importance of the scenario and risk mitigation costs. Finally, this information was used to prioritize road sections which will be future investment candidates.

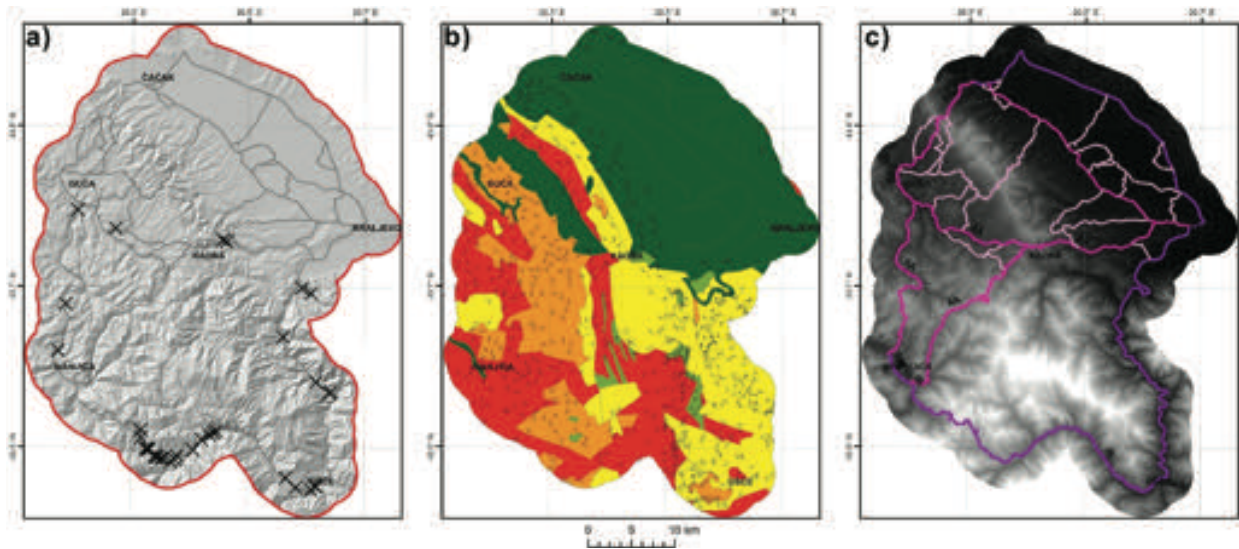


Figure 2 Raw inputs: a) field mapped rockfall examples; b) simplified engineering geological map in respect to rockfall susceptibility (more prone to rockfall from green to red) overlaid by planar discontinuity measurements (dip and dip direction); c) DEM (ranging from 231 to 1620 m a.s.l.) overlain by categorized road network (road category increases from light pink to violet).

## Materials and Methods

As indicated before, the approach in this study is split into: step (i) source delineation, by using both morphologic and geologic/structural features, validated by field data, therein including free-fall but also block sliding mechanisms of detachment; and step (iii) which includes simplified kinetic trajectory simulation tool. Given that it represents a subtask in a larger project framework, only respective (rockfall assessment-related) data acquisition and methodology will be presented hereinafter.

### Input data

The following base maps and resources were used for both task (i) and (iii) implementation (Fig. 2):

- Field locations database (subproject ClirTheRoads, <http://clirtheroads.rgf.rs/>)
- Engineering-geological and geological map 1:300,000 (Geological Survey of Serbia, <https://geoliss.mre.gov.rs/karte/igk300.html>)
- Digital Elevation Model (DEM) 12.5 m resolution (ALOS PALSAR mission open products, <https://earthdata.nasa.gov/>)
- Pilot road network (Public Enterprise Roads of Serbia, excerpt from the national road network vector, <https://www.putevi-srbije.rs/index.php/>)

These were used directly or for derivation of intermediate raster inputs such as:

- Aspect (derived from DEM at 12.5 m resolution using standard D8 GIS algorithm)
- Slope (derived from DEM at 12.5 m resolution using standard D8 GIS algorithm)
- Dip angle (nearest-neighbour-interpolated from planar features on geological map 1:300,000)
- Dip direction (nearest-neighbour-interpolated from planar features on geological map 1:300,000)

- Friction angle (assigned using experience-based values for formations defined on engineering geological map 1:300,000 and encountered during the field survey)

### Modelling

Task (i) requires a delineation of potential rockfall sources, marking areas where blocks are easily detachable. Foremost, it was needed to mask all areas that do not consist of solid rocks, which was done by masking appropriate units, i.e. assigning zero values in the digitized engineering geological map (dark green in Fig. 2). Secondly, the remaining areas covered by solid rocks were scored according to their susceptibility to rockfall occurrence. The scoring factor  $F$  value was set arbitrarily, within the 0-1 interval, and relied on experience from the field surveys conducted in 2020. In general, loose, jointed, weak, tabular and schistose rocks had higher scores than fresh igneous or compact isometric sedimentary rocks. Subsequently, the block sliding conditions along planar discontinuities (Eq. 1-2) as defined by conventional Markland's kinematic criteria (Hoek and Bray, 1981), were tested against the intermediate raster layers: Aspect ( $\psi$ ); Slope ( $\beta$ ); Dip angle ( $\alpha$ ); Dip direction ( $\nu$ ) and Friction angle ( $\varphi$ ) in a GIS environment.

$$\nu = \psi \pm 20^\circ \quad [1]$$

$$\varphi < \alpha < \beta \quad [2]$$

Directional tolerance of  $\pm 20^\circ$  corresponds to maximal probability which (1). The tolerance was successively enlarged while failure probability  $P$  of instances that meet such condition was proportionally reduced. The failure probability was subsequently normalized against all pixels that meet Markland's condition to 0-1 range. These were finally multiplied with scoring factor (0-1)  $F$ .

Next modeling step required solving of rockfall trajectory runout, velocity and energy. A standalone software CONEFALL was used (Jaboyedoff and Labiouse 2011), as it relies on a simple “dry friction” triangle (cross-section along the block’s trajectory) between the source area, its vertical base and its horizontal reach, or the shadow angle (Fig. 3). In 3D setting the triangle is promoted to cone, and in both cases the shadow angle limit is arbitrary, but empirical evidence suggests using a range between 27-38°. It further relies on potential  $E_p$  to kinetic  $E_k$  energy proportion (energy conservation law), and suggests that at any point along the propagation axis  $X$ , the velocity  $v$  is proportional to the difference of topographic and cone surface  $dH$  by the power of 2 (Eq. 3). Knowing the gravitational constant  $g$  and assuming unit volume  $V$ , velocity and kinetic energy can be easily calculated along each trajectory.

$$E_p = E_k \Rightarrow g \frac{m}{v_{\rightarrow 1}} dH = \frac{mv^2}{2} \Rightarrow dH = \frac{v^2}{2g} \quad [3]$$

The hazard map was generated by the adopting the distribution of the energy value, although velocity value or their combination are available as an output form. Since most of the protective measures refer to impact velocity thresholds (<https://www.geobrugg.com/>), the hazard map was kept in said values, split according to intervals that are more or less manageable by protective measures (0-100 kJ low; 100-300 kJ moderate; >300 kJ high).



Figure 3 Cone model (red rectangle is source, black line is topographic surface, blue line is cone surface, shade angle ~ 32°, green area is a trajectory domain) of 2020 event in the background (photo M. Marjanović).

The last step involves superimposing the spatially distributed rockfall hazard to a linear object, i.e., the road network vector. This has been completed by segmenting the entire road network into 500 m intervals and averaging the overlapping pixels (12.5 m resolution) per each segment of the hazard map using the zonal statistics tool in the GIS environment. Thereby, highly exposed segments of the road network are emphasized in contrast to low exposed ones visually, but also quantitatively.

## Results and discussion

The results of the task (i) are indicating relatively low susceptibility to host rockfall, while the rockfall hazard in general seems to be limited to narrow sections of the road isolated in the southernmost regions of the area of interest (Fig. 4-5). Hereinafter, a more detailed review of these outcomes follows.

### Source areas

Kinematic analysis rectified by an experience-based lithological criterion and with lateral limits expanded to  $\pm 45^\circ$  suggests that there are few cases that comply with sliding block failure. In total, 34.5 km<sup>2</sup> or only about 2 % of the area is prone to such failure mode, while lateral tolerance is expanded to great extents (Fig. 4). However, evidence from the field suggests higher slope activity, but mainly along road cuts, which could not be represented with the current low-resolution DEM. In fact, its derived slope model shows that majority of the slope faces lie below 30° inclination, while the overall average is about 13°. Only 0.2 km<sup>2</sup> of the total is steeper than 50°, which reduces to isolated cases/pixels. Rough, steep faces, especially along the road cuts are presumably smoothed by 12.5 m resolution of the DEM, which is insufficient to capture greater level of detail.

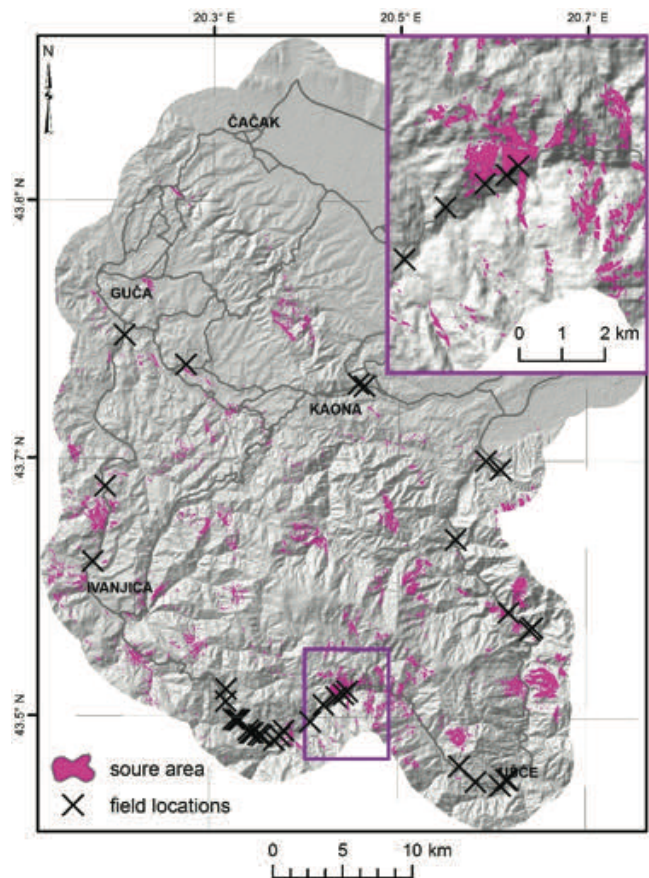


Figure 4 Source area distribution (representative detail of the southern rockfall hot-spot given in the top right).

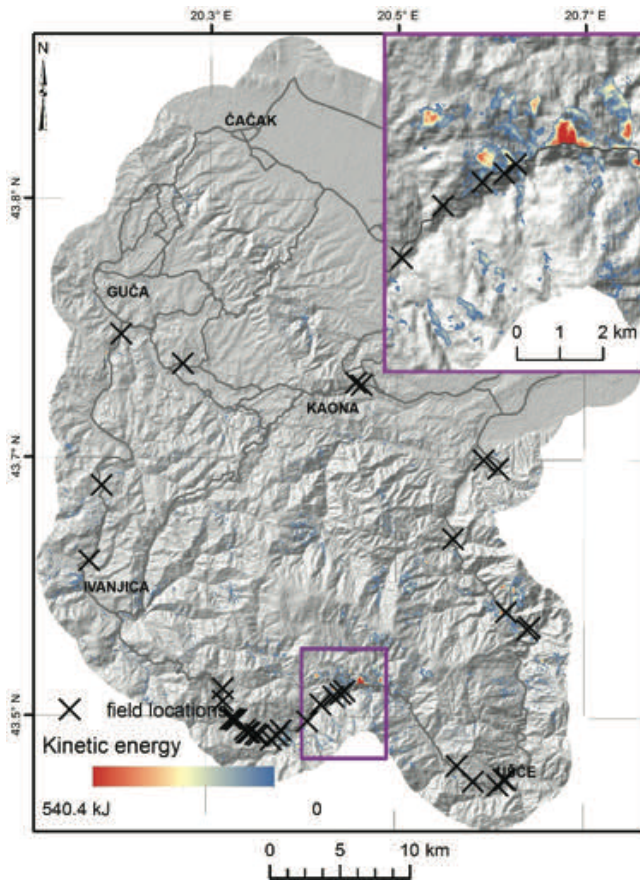


Figure 5 Rockfall kinetic energy distribution (representative detail of the southern rockfall hot-spot given in the top right).

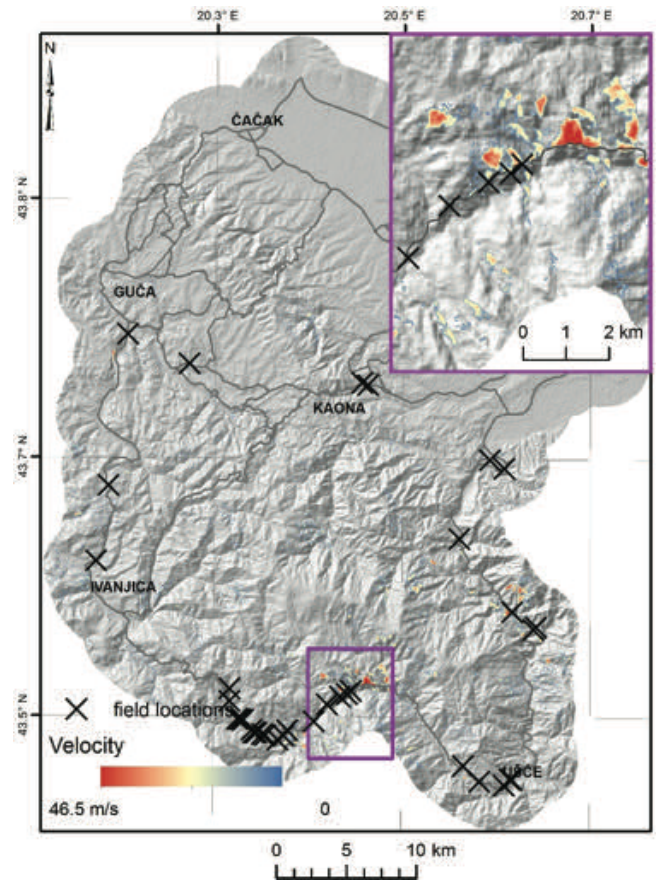


Figure 6 Rockfall velocity distribution (representative detail of the southern rockfall hot-spot given in the top right).

### Rockfall hazard and road exposure

Cone model “trajectories”, which are but per pixel calculations of Eq. 3, suggest rather a moderate rockfall hazard in both aspects, spatial and intensity-wise (energy and velocity). Reach distances were simulated by using the cone shadow angle of 32° which has been confirmed as the most realistic value during the field investigations in 2020 (ClirTheRoads subproject), blocks were assumed as cubical, while their average dimension was set to 0.5-0.7 m, meaning that average block mass was about 500 kg (assuming bulk density around 20 kN/m<sup>3</sup>). By converting the raster output as a vector, the runouts were approximated, and their axial dimension was estimated to range between 50 and 650 m, wherein only 1 % is longer than 500 m.

Rockfall energy distribution (Fig. 5) can be divided into low hazard 0-100 kJ which occupies 88 % of the total area, moderate hazard 100-300 kJ which covers 11 % of the area, while the remaining 1 % is a high hazard with energies >300 kJ. This is a generally adopted threshold in respect to the serviceability limits of common road meshes and drapes used in practice. In addition, velocities are calculated, and their distribution seems more uniform (Fig. 6).

Overlapping road segmented (500 m) network over kinetic energy raster and using the same criteria for classifying low-high hazard and translating it to the exposure to rockfall, the following distributions are obtained (Fig. 7). Zero hazard is occupying most of the area, as well as most of the road length, i.e., 93.3 %, which is even more optimistic than 88 % for the areal distribution. Thus, 6.7 % is non-zero exposure, i.e., 18.6 km of 276 total network length. Moderate exposure covers 5.8 % of the total length of 16 km, which means that the remaining 0.9 % or 2.6 km is covered in high exposure to rockfall. It is located in the southernmost part of the area of interest, along the Ivanjica-Ušće route, as well as along the Ibar river valley to the east (Kraljevo-Ušće route), with some seldom occurrences in other parts of the network.

Clearly, the models do not comply with field data particularly well (35 wide-spread rockfall occurrences, few of which were indicated as critical for potential road closure and detouring), which means that the approach is more general than desired. The principal reason is the level of DEM detail available. LiDAR-based DEM (airborne) of a meter or sub-meter resolution would allow mapping of much steeper local cliffs, as well as shoulders, breaks etc. giving a more realistic source area delineation as well as better background for running simulations.

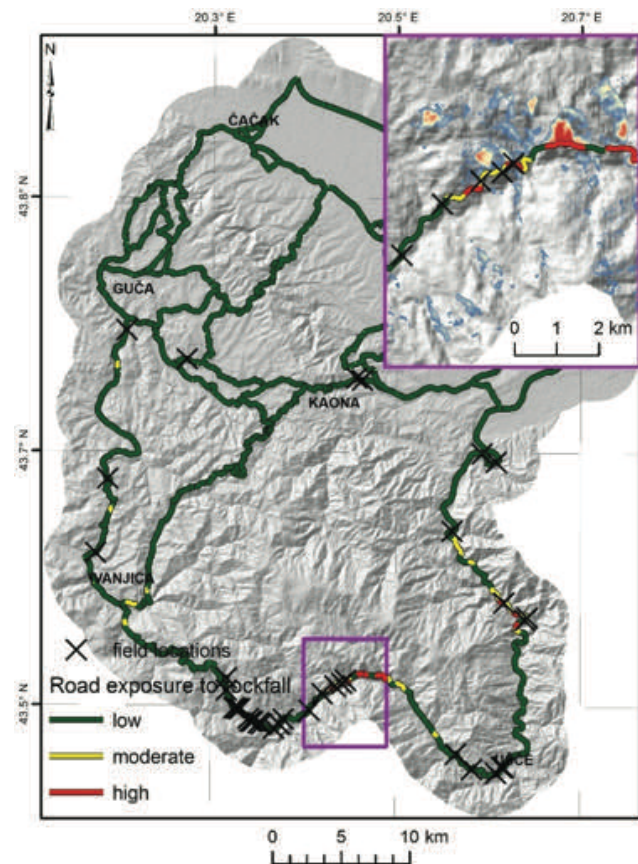


Figure 7 Road exposure to rockfall underlain by kinetic energy model (representative detail of the southern rockfall hot-spot given in the top right).

## Conclusions

This work presents a quantitative approach for determining road exposure to rockfall hazards in a medium-sized area located in central Serbia. The terrain configuration is susceptible to rockfalls in the southern and eastern parts, which has been confirmed by a thorough field survey, conducted in 2020. Expert-driven and physical modelling are herein coupled to perform task (i) - rockfall source zones delineation, and (iii) - simulation of rockfall trajectories and their features. The results are considered appropriate for a general assessment level of planning and prioritizing but require some improvements. A major drawback is the lack of high-resolution DEM which would resolve most of the modelling issues in both tasks (i and iii). Further improvements are possible by including more realistic surfaces, but also, land use features (forests, and other surface fabric) which can be used as a correction factor in the postprocessing of energy and velocity calculations, as a task (ii). Even though mismatching in some aspects, the field validation and models are statistically speaking comparable (a relatively low level of hazard is present in both). The simplicity of the simulation model is also a source of error. However, one “hot-spot” area in the southern part is a very representative example where the model meets a realistic scenario.

## References

- Abolmasov B (2017) Uticaj promena klime na procenu hazarda od klizišta na putnoj mreži Srbije. *Put i saobraćaj* 63(3): 21-34. ISSN 0478-9733 (in Serbian)
- Aksoy H, Ercanoglu M (2006) Determination of the rockfall source in an urban settlement area by using a rule-based fuzzy evaluation. *Nat. Hazards Earth Syst. Sci.* 6: 941-954.
- Budetta P (2003) The modified "Rockfall Hazard Rating System": a new tool for roads risk assessment. *Natural Hazards and Earth System Sciences.* 4: 71-81.
- Copons R, Vilaplana JM (2008) Rockfall susceptibility zoning at a large scale: from geomorphological inventory to preliminary land use planning. *Engineering Geology.* 102: 142-151.
- Dikau R, Brunsden D, Schrott L, Ibsen ML (1996) *Landslide recognition.* John Wiley and Sons, Chichester. (ISBN: 0-471-96477-8). 251p.
- Dorren L, Domaas U, Kronholm K, Labiouse V (2011) Methods for Predicting Rockfall Trajectories and Run-out Zones. In: Lambert and Nicot (eds.) *Rockfall Engineering.* John Wiley & Sons, London, UK (ISBN: 978-1-84821-256-5). pp.143-173.
- Fanos AM, Pradhan B (2019) A novel rockfall hazard assessment using laser scanning data and 3D modelling in GIS. *Catena.* 172: 435-450.
- Gariano SL, Guzzetti F (2016) Landslides in a changing climate. *Earth-Science Reviews* 162: 227-252.
- Hoek E, Bray JW (1981) *Rock Slope Engineering.* The Institute of Mining and Metallurgy. London, UK. 358 p.
- Hungro O, Leroueil S, Picarelli L (2014) The Varnes classification of landslide types, an update. *Landslides.* 11(2): 167-194.
- Jaboyedoff M, Labiouse V (2011) Preliminary estimation of rockfall runout zones. *Nat. Hazards Earth Syst. Sci.* 11: 819-828.
- Lato M, Hutchinson J, Diederichs M, Ball D, Harrap R (2009) Engineering monitoring of rockfall hazards along transportation corridors: using mobile terrestrial LiDAR. *Nat. Hazards Earth Syst. Sci.* 9: 935-946.
- Loye A, Jaboyedoff M, Pedrazzini A (2009) Identification of potential rockfall source areas at a regional scale using a DEM-based geomorphometric analysis. *Nat. Hazards Earth Syst. Sci.* 9: 1643-1653.
- Marjanović M, Abolmasov B, Đurić U, Krušić J (2018) Assessment of landslide-related hazard and risk on the road network of the Valjevo city, Serbia. *Proceedings of the 16th Danube - European Conference on Geotechnical Engineering* 7-9 June 2018, Skopje, North Macedonia. pp. 365-370.
- Marjanović M, Abolmasov B, Milenković S, Đurić U, Krušić J, Samardžić-Petrović M (2019) Multihazard Exposure Assessment on the Valjevo City Road Network. In: *Spatial Modeling in GIS and R for Earth and Environmental Sciences.* Pourghasemi and Gokceoglu (eds.) Elsevier, Amsterdam, Netherlands, (ISBN 978-0-12-815226-3) pp. 671-688.
- Marjanović M, Abolmasov B, Peshevski I, Reeves J, Georgievska I (2020) Regional Slope Stability Analysis in Landslide Hazard Assessment Context, North Macedonia Example. *Proceedings of the 5th World Landslide Forum, 2-6 November 2021, Kyoto, Japan.* pp. 267-273.
- Michoud C, Derron MH, Horton P, Jaboyedoff M, Baillifard FJ, Loye A, Nicolet P, Pedrazzini A, Queyrel A (2012) Rockfall hazard and risk assessments along roads at a regional scale: example in Swiss Alps. *Nat. Hazards Earth Syst. Sci.* 12: 615-629.
- van Veen M, Hutchinson DJ, Bonneau DA, Sala Z, Ondercin M, Lato, M (2018) Combining temporal 3-D remote sensing data with spatial rockfall simulations for improved understanding of hazardous slopes within rail corridors. *Nat. Hazards Earth Syst. Sci.* 18: 2295-2308.



# Numerical simulations of landslide physical model results

**Sabatino Cuomo**

University of Salerno, Department of Civil Engineering, Fisciano (SA), Via Giovanni Paolo II 132, Italy, +39089964231 (scuomo@unisa.it)

**Abstract** Physical models are widely used in landslide research. They allow direct and accurate measurement of the main driving forces and features of the fundamental processes regulating a landslide. Physical modelling is principally used to: i) investigate specific or general landslide mechanisms, ii) validate mathematical formulations or numerical codes, iii) infer how a real in-situ slope and landslide scenario may evolve. This paper will provide some remarks on the first two issues. The FEM (Finite Element Method) and MPM (Material Point Method) analyses of a reduced-scale slope model that is gradually saturated by water table raising, is used as a benchmark. In this case, the experiment shows that the slope fails by shear and then liquefaction occurs, and numerical simulations can capture such slope instability sequence. On the other hand, flume tests of saturated granular flows are simulated via SPH (Smooth Particle Hydrodynamics) to interpret the spatio-temporal evolution of the pore water pressure within the rapid flow. An example of test regarding Landslide-Structure-Interaction is also proposed. The paper discusses the extent to which physical models and numerical simulations are complementary. The limitations of both types of approaches are also highlighted, such as scale-effects or computational costs.

**Keywords** mechanisms, experimental, numerical

## Introduction

There are several reasons that make the analysis of landslides a complex task. These include, for instance, multiple combined mechanisms, the strain-dependent behaviour of the involved soils, and the transient groundwater regime, especially in partially saturated soils and in fast-moving landslides.

It is generally accepted that landslide recognition and diagnosis are the first two fundamental steps to be taken.

Landslide recognition includes the assessment of site boundary conditions and the evolution of the slope over time. Landslide diagnosis involves relating the causes (factors) and the effects. These relationships are usually named mechanisms. The individuation of landslide mechanisms can be pursued at different scales, from regional/territorial to local/micro scales. Qualitative or quantitative, empirical or physically based interpretations are applicable depending on the general scope of the

activities, for instance, land-use planning or design of protection structures.

In the most complex cases, landslide physical modelling is a powerful tool for direct observation of landslide mechanisms. An undoubtable advantage is the high accuracy of the measurements it allows. Nevertheless, a simplification of the site stratigraphy and geometrical conditions is always required. Another important limitation concerns the reduced dimensions of the landslide model compared to the site problem. In this sense, scale effects can be opportunely managed, and even much reduced if a centrifuge device is used. Independent on the type of physical model, its combination with geomechanical numerical simulations has proven to be efficient for an advanced landslide diagnosis. This paper reports 4 emblematic cases, where complex scientific questions could be answered thanks to the combined use of physical and numerical landslide models.

## Failure first, then liquefaction: a lesson learnt

### Experimental results

The scientific question was: Is static liquefaction of soil the only cause of flow-like landslides? In other words, is liquefaction the cause or the effect of a slope instability when a flow-like landslide occurs?

Eckersley (1990) and several later slope model results (including Lourenco et al., 2006) have demonstrated that a slope model of loose material subjected to a rise in the groundwater table (eventually in conjunction with water inflow from the ground surface) first fails, then liquefaction occurs, and finally a retrogressive slope instability is initiated (Fig. 1). Images of slope instabilities observed through transparent side walls and measurements of pore water pressure at different points inside the slope were supported this explanation. The interested readers may refer to the references given.

### Small-deformation FEM modelling

How to confirm these experimental results via numerical modelling? Analyses based on no-deformation or small-deformation approaches could be used. Definitions and examples are reported in Cuomo et al. (2021a). For instance, while it is not possible to simulate the slope multiple retrogression failures observed by Eckersley (1990), static liquefaction is capturable if an advanced soil constitutive model is used.

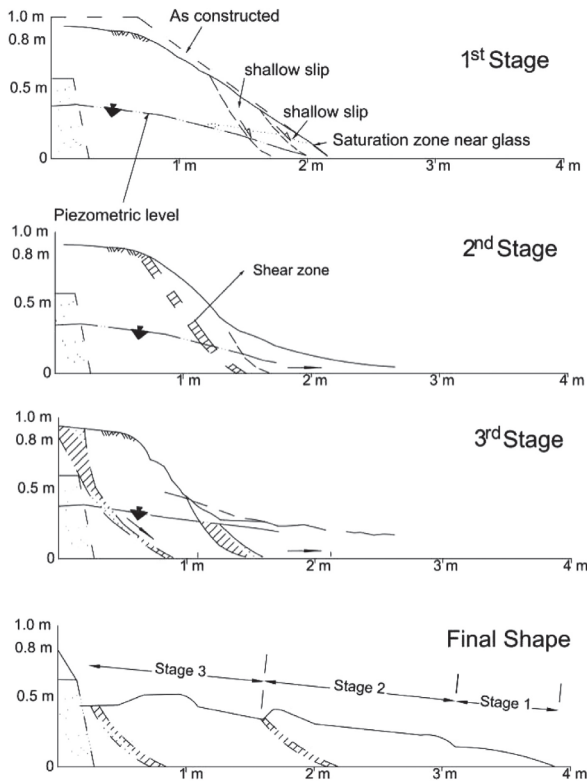


Figure 1 Experimental results of one flume test of Eckersley (1990): failure and post-failure stages.

First, a simplified limit equilibrium analysis pointed out a slope safety factor close to one for a groundwater table equal to that observed at the occurrence of slope failure. This means that soil shear failure plays a role.

Then, the liquefiable behaviour of the soil measured in undrained compression triaxial tests for different values of porosity was simulated by an advanced constitutive model based on Generalised Plasticity (Pastor et al., 1990). Some of these results are reported in Cascini et al. (2013).

Finally, FEM analyses, based on a hydro-mechanical fully coupled approach, were performed. A series of numerical simulations carried out with the GHM (GeHoMadrid) code (Pastor et al., 2004) outlined that the failure of the toe of the slope can be simulated consistently to the flume test results. In conclusion, numerical modelling corroborated the experimental evidence in a physically based framework, which has been appropriately implemented in the numerical code.

#### Large-deformation MPM modelling

The same experiments have been simulated again some years later by Cuomo et al. (2019).

As in the previous case, the geomechanical framework relied on full hydro-mechanical coupling and advanced constitutive modelling. The latter was based on the hypoplasticity theory (Von Wolffersdorff, 1996). However, this time the problem this time was casted in terms of large soil deformations and the numerical technique of the Material Point Method (MPM) was used by the Anura3D code.

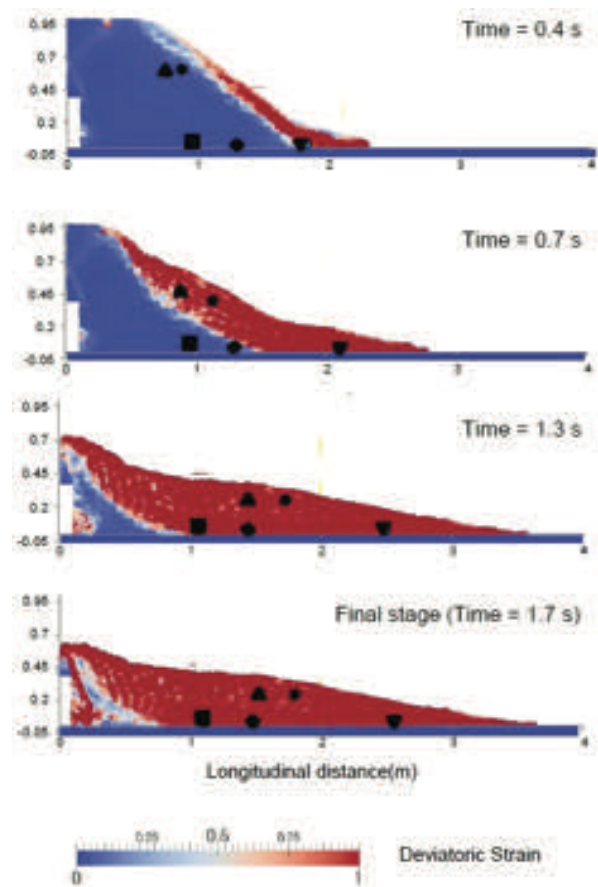


Figure 2 Displacements and deviatoric shear strains computed at different times by Cuomo et al. (2019).

MPM is an enhancement of the classical FEM. The use of MPM in this context implies that both shear failure and subsequent liquefaction at the base of the slope could be captured. In addition, the spatio-temporal evolution of soil liquefaction on the slope was tracked, and the retrogressive type of the slope instability (Fig. 2) was captured (Cuomo et al., 2019). It was demonstrated that static liquefaction is attained at the toe of the slope, which then largely deforms. Hence, a retrogressive landslide is triggered, which causes a lateral decompression and an increase in shear stress in the rear of the slope. Static liquefaction propagates backwards, thus triggering other multiple retrogressive failures. As the failed material propagates and finally comes to rest, global instability brings to the final flat deposit. What is the lesson learnt? The failure stage depends on the hydraulic boundary conditions. The post-failure stage, i.e., the transition of a slide into a flow, is regulated by soil static liquefaction. The later slope evolution until it stops is controlled by large deformations of the soil and the change in geometry.

#### Loose and dense sands both prone to flow landslides?

##### Experimental results

A fundamental scientific question is that: soil behaviour or site condition, what is the most important factor?

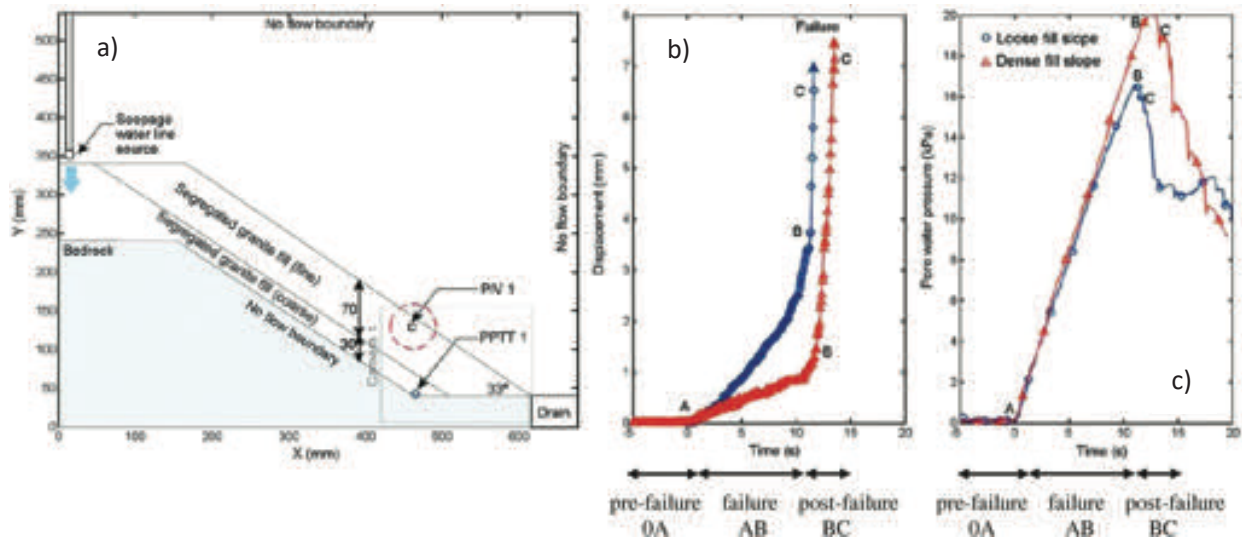


Figure 3 Centrifuge slope model for loose and dense soils: (a) centrifuge model scheme, (b) displacement measured at PIV<sub>1</sub>, and (c) pore-water pressures measured at PPTT<sub>1</sub> (modified from Take et al. 2004).

This issue is especially relevant for flow-like landslides, sometime called runaway landslides. It is agreed that loose, saturated sands may undergo static liquefaction and generate flowslides.

However, from field observations, there are also known cases where the soils were not so loose but still suffered from slope instabilities that later evolved into flow-like landslides. Take et al. (2004) provided convincing experimental evidence for the first time by using an unsaturated slope model in a centrifuge. A two-layer slope model was prepared, with coarser material at the top and finer material at the contact with the impervious bedrock. Displacements were measured with a high-speed camera and image processing, and pore water pressures with transducers embedded in the slope. A transient seepage was induced in the upper layer, leading to the formation of a perched water table at the top of slope (Fig. 3).

The most-important evidence was that a flow-like landslide was triggered in the coarser material, regardless of soil density, either in the loose or dense case. This experimental evidence has important practical implications. It means that the chance for flow-like landslides in the field cannot be absolutely limited to the case of loose materials. Dense materials also deserve attention. However, how to explain such evidence from a geomechanical viewpoint?

**FEM modelling**

Both soil constitutive response (static liquefaction) and transient seepage (constrained in the layered slope stratigraphy) are the two key factors.

This was the working idea of Cascini et al. (2013). The authors set up a numerical model corresponding to the prototype of the centrifuge tests of Take et al. (2004).

The GHM (GeHoMadrid) code was used also in this case in combination with a Generalized Plasticity soil

constitutive model (Pastor et al., 1990), which can reproduce static liquefaction for loose sand.

The main numerical outcomes can be summarized as follows: slope instability is simulated in both loose and dense slope models; the failed soil volumes are similar in the two cases; transient constrained seepage plays a role in both cases; however, in the dense slope model, localized failure occurs (a shear band starts at the toe of the slope and propagates backwards); in the loose slope model, diffuse failure due to static liquefaction occurs; failure is brittle for dense slopes and more delayed in time for loose ones.

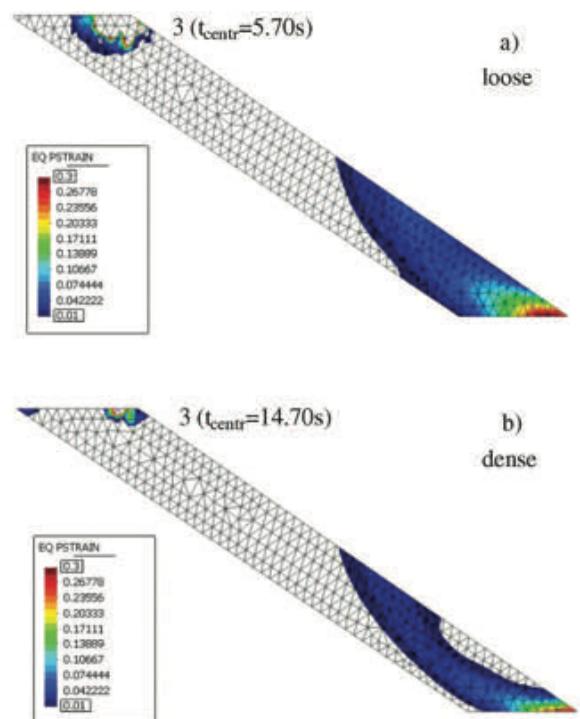


Figure 4 Time trend of the equivalent plastic strains computed for (a) loose and (b) dense soils by Cascini et al. (2013).

## Pore water pressure during propagation: new insights

### Experimental results

Excess pore water pressures in fast-moving landslides are recognized as responsible for long runout distances travelled even along gentle piedmont areas. Small and (more recent) large flume tests have helped to understand how much interstitial fluid is important. When flow thickness, total weight and basal pore water pressures are measured at specific locations, information about a liquefied state (or not) of the flowing material can be obtained.

In the experiments of Iverson et al. (2010), such measurements were performed at the terminal part of an 80 m long flume (Fig. 5). Pore water pressures close or equal to the total stress values were measured. It entails that the material is completely liquefied while propagating downslope. However, such high pore water pressures are dissipated during flow deposition.

### SPH modelling

In this case, a large deformation framework is absolutely needed to reproduce the movement of the initial soil mass along the slider. However, the hydro-mechanical coupling of the soil is also fundamental.

Among a series of approaches potentially applicable to this case, Cascini et al. (2016) selected a compromise solution approach based on the following: hydro-mechanical coupled propagation approach; depth-integrated formulation instead of a 3D model; Smooth Particle Hydrodynamics (SPH) numerical tool to ensure fast computation with good numerical accuracy. Details



Figure 5 Photo of a 10 m<sup>3</sup> debris flow tested in the USGS flume (from Iverson et al., 2010).

about the used SPH formulation are given in Pastor et al. (2009). However, a SPH-FDM formulation (Pastor et al., 2015) was also employed, which combines the SPH model with a 1D vertical FDM (Finite Difference Method) model for a more accurate evaluation of pore water pressures along the height of the flowing mass. Both formulations are available in the GeoFlowSPH code developed by Prof. Pastor and coworkers. In both models, a frictional rheological behaviour of soil was assumed with the pore water pressure computed separately. Fig. 6 shows the accurate reproduction of the measurements obtained along the slope at two different distances from the gate. Both the SPH and the SPH-FDM formulations were adequate to reproduce the observed behaviors.

## Landslide structure interaction: challenges for flows

### Experimental results

Complementary to the previous debris flow flume experiments are those investigating the interaction of flows (dry or saturated) against walls, obstacles or structures, reproduced at reduced scale in flume or centrifuge tests.

Song et al. (2017) performed a series of centrifuge tests with saturated granular materials initially stored into a tank and then released through a bottom gate. The material flows downwards very rapidly and impacts against a fixed, rigid wall. In some cases, the material stops behind the wall; in other conditions, the flow overcomes the wall; even combined modes are observed. In all tests, the time-trend of lateral pressure exerted against the wall is measured at five locations along the wall.

This provides complete experimental evidence is for the so-called Landslide-Structure-Interaction (LSI).

### MPM modelling

Modelling such complex behavior is not an easy task. It requires a formulation of large-deformations, a fully coupled hydro-mechanical approach, and efficient numerical algorithms to accurately reproduce such a dynamic problem (rapid propagation) and an impulsive action (impact against the wall).

MPM modelling of these tests was proposed by Cuomo et al. (2021b) using a version of the Anura3D MPM code developed by Deltares (Delft, Netherlands), and a simple non-associative elasto-plastic constitutive model. Fig. 8 shows a time lapse where the material is extremely elongated, with the front part impacting the wall at about 20 m/s and the rear part of the flow not yet having moved from away from the bottom of the tank. Such numerical result is consistent with the experimental measurements. Interested readers can find details about the calibration and validation of the modelling approach in Cuomo et al. (2021b). This demonstrates the capability of the numerical model to reproduce the complex geometrical configurations of the flow during the flow.

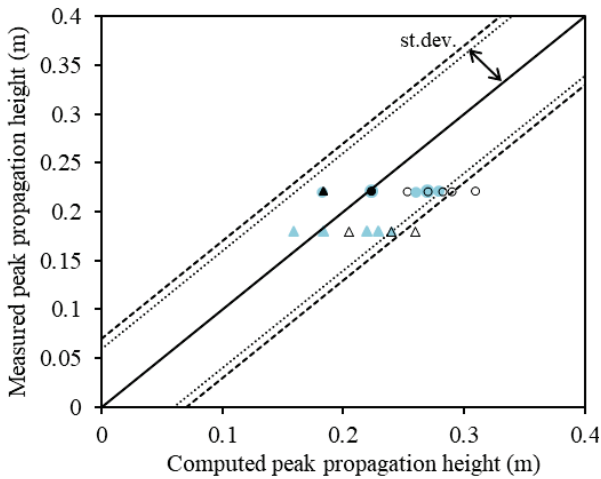


Figure 6 Experimental results versus numerical simulations. Measurements taken at 32 m (circles) and 66 m (triangles) from the gates. The mean values and standard deviation ( $\sigma$ ) of the two set of measurements. Empty symbols: SPH model. Solid symbols: SPH-FDM model (modified from Cascini et al., 2016).

On the other hand, it is worth noting that the experimental centrifuge facility can reproduce such high (realistic) velocities well for the flow-structure impact scenarios.

The dynamic behaviour of landslides is well simulated by the numerical modelling and, interestingly, the time-trends of the LSI are also well captured. For instance, Fig. 9 shows the experimental values of the impact pressure over time at the base of the wall compared to the numerical results. In this case, three different hypotheses for the Ergun coefficient (Ergun, 1952), which regulates the non-linear contribution of the seepage velocity on the solid-liquid interaction forces (relevant in high porosity mixtures) are reported; and a negligible role of this factor is highlighted. In general, either the peak pressure or the subsequent drop over time is well captured by the modelling.

### Concluding remarks

The paper has presented 4 selected cases of landslide physical models: 2 flume tests (one with a length of 2 m for triggering, and another 80 m long used for propagation); and 2 centrifuge tests (one with a length of 0.6 m for triggering at  $N=30$  times the gravity acceleration, and another 1.2 m long used for landslide-structure-interaction at  $N=22$ ).

In all cases, the size of the model (although amplified by  $N$  in the centrifuge tests) is smaller than the real site conditions. Thus, some scale effects are expected in comparison to the real landslide behaviour.

Another important issue is the high complexity of the (i) landslide model and (ii) numerical model. The former strongly depends on the quality (accuracy and readiness) of the sensors, and an adequate slope geometry simplification is relevant as well. The latter relies on an

appropriate geomechanical framework (equations to be solved), a robust numerical technique and a sound constitutive or rheological soil model.

Based on the experience achieved so far, two combined analyses seem particularly well suited. i) Detailed field investigations combined with traditional geomechanical analyses of groundwater seepage and slope limit equilibrium conditions are especially useful to establish landslide diagnosis and recognition. ii) A physical model combined with numerical analysis is the next step to corroborate the landslide mechanisms identified by the field evidence and the analyses from stage i).

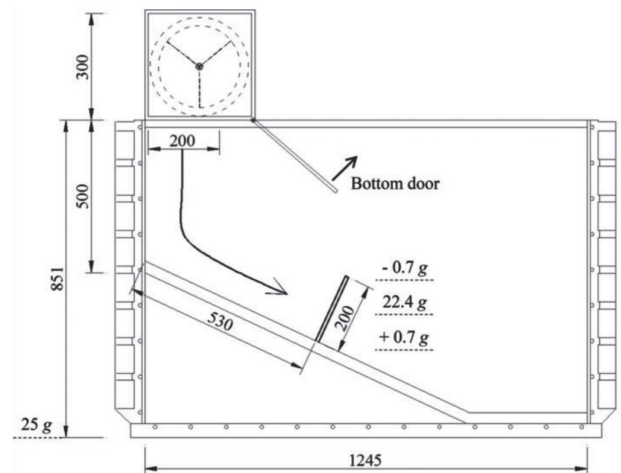


Figure 7 Centrifuge device used in the experiment of Song et al. (2017). All dimensions in millimetres.

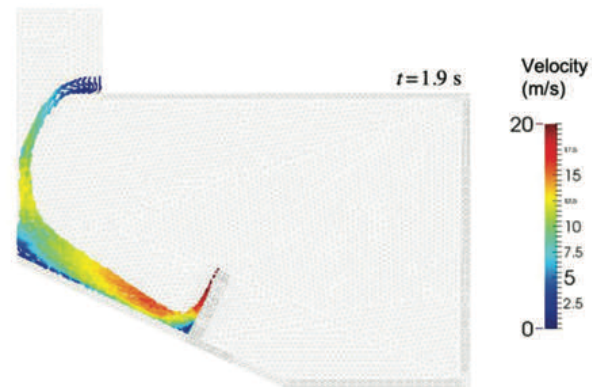


Figure 8 Example of velocity distribution for SL50 test run by Song et al. (2017). (Image modified from Cuomo et al., 2021b)

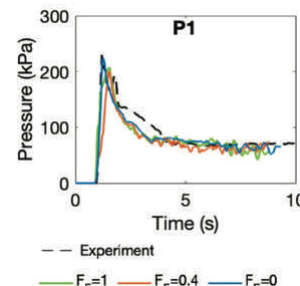


Figure 9 Experimental measurements and simulated values of the pressure at the impact zone for the SL50 test run by Song et al. (2017) (modified from Cuomo et al., 2021b).

## Acknowledgments

Prof. Manuel Pastor and colleagues of the UPM (Universidad Politecnica de Madrid, Spain) are deeply acknowledged for the scientific support and for the permission to use the GeHoMadrid FEM code and different versions of the GeoFlow SPH code. The author is grateful to Dr. Mario Martinelli for the support in the MPM simulations, which were performed through the Anura3D code (<http://www.mpm-dredge.eu/>) and using also a version of Anura3D developed by Deltares (Delft, Netherlands). Colleagues from the University of Salerno (Italy) are much acknowledged for the support in modelling and for several scientific discussions: Prof. Leonardo Cascini, Dr. Angela Di Perna, Dr. Pooyan Ghasemi, Dr. Ilaria Rendina and Dr. Claudia Sacco.

## References

- Cascini L, Cuomo S, Pastor M, Rendina I (2016) SPH-FDM propagation and pore water pressure modelling for debris flows in flume tests. *Engineering Geology*. 213: 74-83.
- Cascini L, Cuomo S, Pastor M, Sacco C (2013) Modelling the post-failure stage of rainfall-induced landslides of the flow type. *Canadian Geotechnical Journal*. 50(9): 924-934.
- Cuomo S, Di Perna A, Martinelli M (2021a) Modelling the spatio-temporal evolution of a rainfall-induced retrogressive landslide in an unsaturated slope. *Engineering Geology*. 294: 106371.
- Cuomo S, Di Perna A, Martinelli M (2021b) MPM hydro-mechanical modelling of flows impacting rigid walls. *Canadian Geotechnical Journal*. 58(11): 1730-1743.
- Cuomo S, Ghasemi P, Martinelli M, Calvello M (2019) Simulation of liquefaction and retrogressive slope failure in loose coarse-grained material. *International Journal of Geomechanics*. 19(10): 04019116.
- Eckersley D (1990) Instrumented laboratory flowslides. *Geotechnique*. 40(3): 489-502.
- Ergun S (1952) Fluid flow through packed columns. *Chemical Engineering Progress*. 48: 89-94.
- Iverson R M, Logan M, LaHusen R G, Berti M (2010). The perfect debris flow? Aggregated results from 28 large-scale experiments. *Journal of Geophysical Research: Earth Surface*. 115: 1-29.
- Lourenco S D N, Sassa K, Fukuoka H (2006) Failure process and hydrologic response of a two-layer physical model: implications for rainfall-induced landslides. *Geomorphology*. 73(1-2):115-130.
- Moriguchi S, Borja R I, Yashima A, Sawada K (2009) Estimating the impact force generated by granular flow on a rigid obstruction. *Acta Geotechnica*. 4(1): 57-71.
- Pastor M, Fernandez-Merodo J A, Gonzalez E, Mira P, Li T, Liu X (2004) Modelling of landslides: (I) Failure mechanisms. *Degradations and Instabilities in Geomaterials*. Springer. 287-317.
- Pastor M, Haddad B, Sorbino G, Cuomo S, Drempetic V (2009) A depth-integrated, coupled SPH model for flow-like landslides and related phenomena. *International Journal for numerical and analytical methods in geomechanics*. 33(2): 143-172.
- Pastor M, Martin Stickle P, Dutto P, Mira P, Fernandez Merodo J A, Blanc T, Sancho S, Benitez A S (2015a) A viscoplastic approach to the behaviour of fluidized geomaterials with application to fast landslides. *Continuum Mechanics and Thermodynamics*. 27(1): 21-47.
- Pastor M, Zienkiewicz O C, Chan A (1990) Generalized plasticity and the modelling of soil behaviour. *International Journal for numerical and analytical methods in geomechanics*. 14(3): 151-190.
- Song D, Ng C W W, Choi C E, Zhou G G, Kwan J S, Koo R C H (2017) Influence of debris flow solid fraction on rigid barrier impact. *Canadian Geotechnical Journal*. 54(10): 1421-1434.
- Take W A, Bolton M D, Wong P C P, Yeung F J (2004) Evaluation of landslide triggering mechanisms in model fill slopes. *Landslides*. 1(3): 173-184.
- Von Wolffersdorff P A (1996) A hypoplastic relation for granular materials with a predefined limit state surface. *Mechanics of Cohesive-frictional Materials: An International Journal on Experiments, Modelling and Computation of Materials and Structures*. 1(3): 251-271.

# Physical modelling investigation and integrated analysis of landslides for defining risk scenarios

Giovanna Capparelli<sup>(1)</sup>, Gennaro Spolverino<sup>(1)</sup>, Irasema Alcántara-Ayala<sup>(2)</sup>, Noemi Sharon Ruiz-Cortés<sup>(2)</sup>

1) University of Calabria, Department of Informatics, Modelling, Electronics and System Engineering, Arcavacata di Rende (CS), Via P. Bucci 42C, Italy, +39 3475446857 (giovanna.capparelli@unical.it)

2) National Autonomous University of Mexico (UNAM), Institute of Geography, Av. Universidad 3000, Mexico City, Mexico.

**Abstract** Predicting natural processes, such as rainfall-induced landslides, is a problem of great importance. Every year, meteorological events trigger both superficial and deep landslides on many slopes, causing damage and victims. The study presented here focuses on the hydraulic and hydrologic issues that take place in an unstable slope under the rainfall infiltration. The mentioned studies are dealt through a physical modelling, a numerical simulation techniques, and through in situ experimental measurements. Our research is based on an integrated approach which, starting from the observation of the real phenomenon, reproduces the observed phenomenon in the laboratory and models it using an appropriate mathematical scheme. The in situ data refer to a monitoring station installed near the site where a large mudflow occurred. The physical model consists of 2 connected, independently tilting flume branches (respectively designed to study landslide triggering and propagation), each 1m wide and 3m long. The flume is equipped with tensiometers for measuring soil water potential inside the slope, a Time Domain Reflectometry (TDR) system and probes for measuring soil volumetric water content, and laser transducers for measuring soil surface displacements in the direction orthogonal to the sliding plane. The analysed landslide-prone area is located in Campania (southern Italy), where disastrous mudflows occurred in May 1998, with many human casualties. The applications allow a better understanding of the role of the rainfall infiltration and pore water pressure changes in the triggering mechanism, and suggests how the porosity of the soils involved can affect the kinematic behaviour. The author believes that these changes must be carefully considered when assessing hazard levels, planning mitigation interventions regarding slope stability and designing future mitigation strategies for risk reduction.

**Keywords** Laboratory flume tests, triggering model, hazard assessment

## Experimental Site

Catastrophic mudflows often occur in mountains covered with volcanic soils. Some examples of these landslides are

those that occurred in southern Italy, near the volcano Vesuvius and those that occurred in Mexico.

In fact, significant rainfall-induced landslides have taken place in Mexico. In particular, in the Sierra Norte de Puebla, a mountain system in the state of Puebla within the transition of the physiographic provinces the Sierra Madre Oriental and the Trans-Mexican Volcanic Belt, these phenomena are recurrent (Flores and Alcántara-Ayala 2002; Alcántara-Ayala 2004). Such recurrence derives from the physical characteristics of the territory, characterized by its exposure to hydro-meteorological events including tropical storms and hurricanes, but also due to the presence of mountain ranges with steep slopes and complex geology composed by sedimentary and metamorphic rocks overlaid by volcanic material such as ignimbrite and ash-pumice flow deposits (Alcántara-Ayala 2004; Murillo-García and Alcántara-Ayala 2017) resulted from the activity of the Los Humeros caldera (Ferriz and Mahmood 1984). Owing to the vulnerability conditions of people living in these areas, disasters triggered by rainfall-induced landslides are frequent in this region (Alcántara-Ayala et al. 2017). The worst and latest episode took place in October 1999 in the municipality of Teziutlán. This municipality is located on a large plateau extent of a non-welded pyroclastic deposit of ignimbrite type, characterized by a sandy texture and the presence of pumice fragments. In 1999, extraordinarily heavy rains associated with Tropical Depression N°11 in the Gulf of Mexico triggered a large number of landslides leading to the largest disaster in decades, with significant human and economic losses, including 263 fatalities (Bitrán 2000; Alcántara-Ayala 2004; Alcántara-Ayala et al. 2017).

The instability of pyroclastic soils is one of the most topical and catastrophic problems involving also the Campania region (southern Italy). In this area, several volcanic eruptions of large complexes, i.e. Somma-Vesuvius, Campi Flegrei and Roccamonfina, have occurred over the last 40,000 years (Rolandi et al. 2003; Di Crescenzo and Santo 2005). The resulting materials are spread over a large area around the City of Naples and the slope coverings are frequently affected by to rain-induced landslides. (e.g. Cascini et al. 2008; Revellino et al. 2008; Di Martire et al. 2012). In recent years, the scientific

community has been urged to study and investigate the instability of soils of pyroclastic origin covering the slopes around the Vesuvius area (Naples, Italy). In particular the Pizzo d'Alvano ridge has been analyzed, especially following the tragic landslide events of 5-6 May 1998 which killed 152 people. In this area the deposits are incoherent, varying in grain size from sands, silty sands and silts (ashes) to gravels and sands with gravels (pumices). In particular, the ashes show a rather variable degree of compaction, with porosity ranging from 0.5 to 0.75 (Sorbino and Nicotera 2013). Along the slopes, the hydrogeological characteristics of the pyroclastic deposits are mainly related to the continuity of the ash and pumice layers, which affect the rainfall infiltration process.

In the area described, the decision was made to install a monitoring station to study the infiltration processes responsible for triggering landslides. The station was installed in particular geological-stratigraphic and geomorphologic conditions. Specifically, the monitored site is located in the upper part of the slope of Pizzo d'Alvano, near the relief known as "Torre Savaio" and close to some of the landslides that occurred in Sarno in May 1998. This site is of particular interest because it represents an area that was not affected by the landslide events of May 1998 at Sarno and it represents, with good approximation, the pre-event hydrogeological conditions.

### Monitoring Station

The monitoring station consists of 7 tensiometers and 8 Time Domain Reflectometry (TDR) probes at different depths to measure suction ( $\psi$ ) and volumetric water content ( $\theta$ ), respectively. The sensors continuously record the state of the soil, taking systematic measurements every minute. The data is sent to a data logger at 10-minute intervals and can be downloaded directly on site or from a

remote server. In addition to the sensors monitoring the ground conditions, a tipping rain gauge was installed to record rainfall events at the site. The station uses electricity from a battery which is recharged by a solar panel. The installation of the station was preceded by the construction of a hand-dug trench, approximately 2m wide and 2m deep. The TDR probes were pushed horizontally into the walls of the trench at various depths (depths indicated in Fig. 2). At the points where they emerged from the ground, the sensors were protected by concrete manholes.

The cables were routed through a spiral pipe, which in turn was protected by a double-walled cable duct. The schematic of the monitoring station is shown in Fig. 1. Direct investigations carried out on site (exploratory pits and trenches) delineated the stratigraphy and thickness of the pyroclastic blanket, revealing the alternation of sandy-gravelly pumices interspersed with silt-sandy-clay cineritic palaeosols. The stratigraphy and the levels affected by the installation of the sensors are shown schematically in Fig. 2.

The data recorded by the monitoring station for the hydrological year from 01.10.2015. to 30.09.2016. were analysed and an initial screening was performed, eliminating all "no-data" readings and all unreliable figures. Pairs of suction and water content measurements recorded at the same time at the same depths were correlated in order to construct the soil water retention curve. These values were interpolated with the mathematical formulation of the van Genuchten model curve (Van Genuchten 1980). Fig. 3 shows the pairs of suction and saturation degree values and the curve identified by their interpolation. The graph also shows the main imbibition and drying curves obtained from a laboratory test (Capparelli and Spolverino 2020).

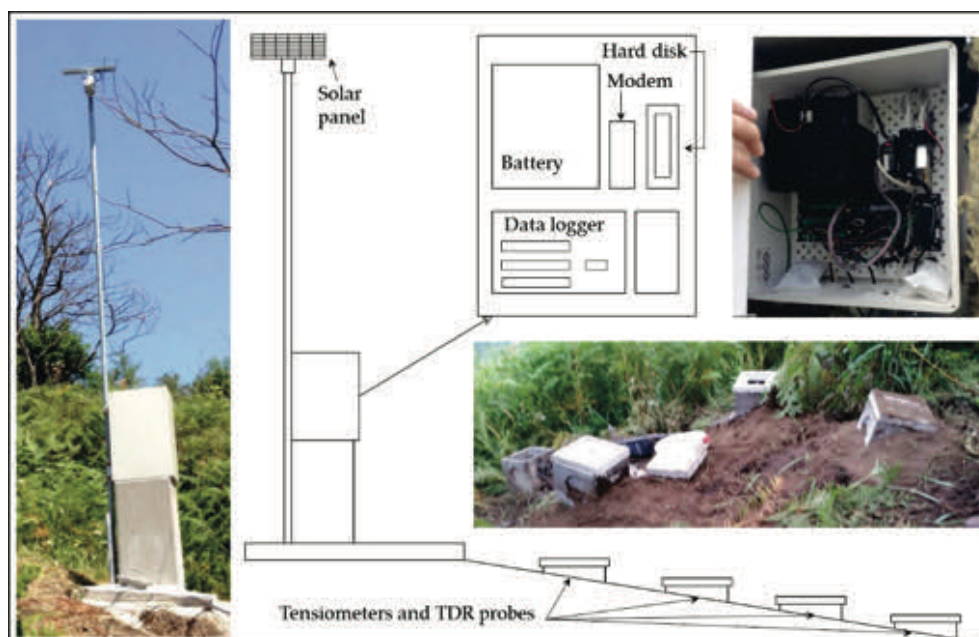


Figure 1 Monitoring station diagram.



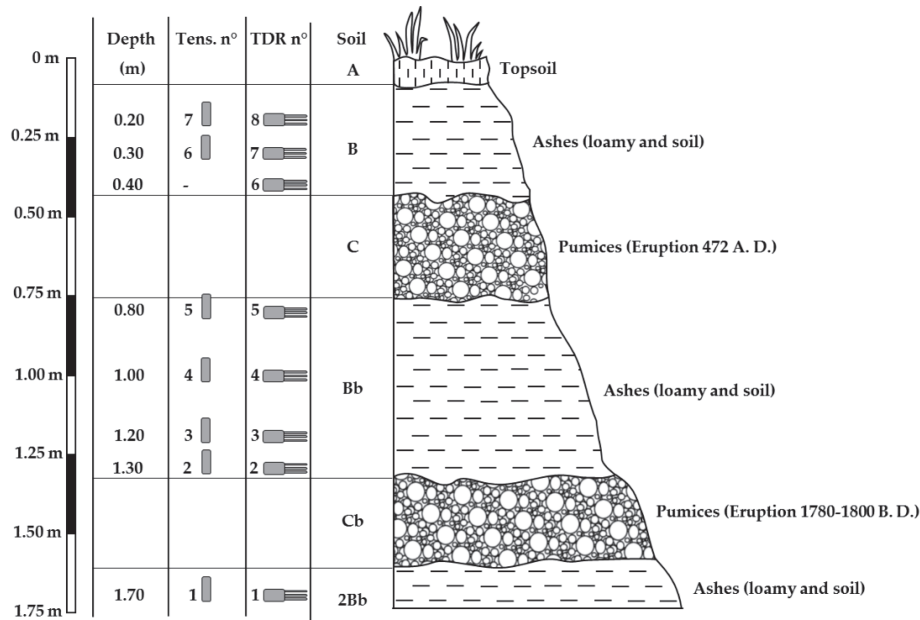


Figure 2 Stratigraphy and the levels affected by the installation of the sensors.

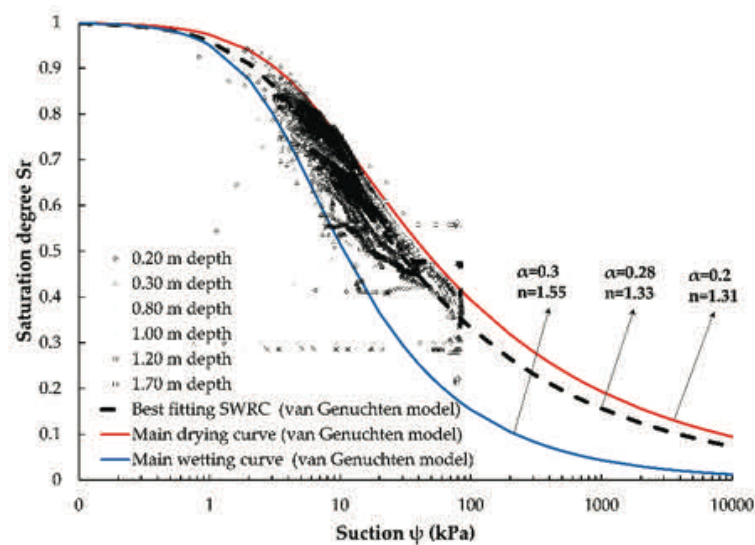


Figure 3 Pairs of suction and saturation degree values, the curve identified by their interpolation, and the main imbibition and drying curves obtained from a laboratory test.

The curve obtained by interpolating the on-site data lies within the hysteresis formed by the two main curves. This was to be expected, since the data used to construct the curve refer to both periods of infiltration and drying. The result is therefore, an average water retention curve that takes into account both imbibition and drying processes.

### Physical model

The physical model is a channel with a rectangular cross-section that is homogeneous and constant along its entire length (Spolverino et al. 2019). The structure, supported by metal pipes, is 1 m high, 6 m long in total, divided into 3 m

for the triggering and 3 m for the propagation, and 1 m wide. Fig. 4 shows the side and front views of the channel. Both the side walls and the bottom wall are made of transparent plexiglass panels to ensure that the movement can be both viewed and filmed during the landslide. On the flume bed it is possible to reproduce both an impermeable and permeable bottom-base. In the former case, an impermeable rough bed is laid, which acts as an interface with the test soil, consisting of a plastic sheet on which gravel grains are glued; in the latter case, a permeable geotextile or geonet is used. To hold the deposit, a draining grid is laid at the foot of the reconstructed slope.



Figure 4 Physical model: (a) side view; and (b) frontal view.

Grids of different heights can be inserted according to the thickness of the reconstructed deposit. The grid is formed by a perforated metal sheet, on which a permeable geotextile is placed which permits drainage. Moreover, on the front part of the grid, transversal to the slope, small water collection channels can be mounted to measure both surface runoff and runoff from the individual soil layers.

Artificial rainfall was applied with a 24-nozzle water particle sprinkler system, fed by a main 1000-liter tank and four 200-liter auxiliary tanks. The rainfall system integrates four pressure sensors and three auxiliary rain gauges. The arrangement of the nozzles was optimized so as to ensure rainfall uniformity, and minimize surface erosion and interference with the video system. The pressure range varies between 0.1 and 7 bar with an intensity that can vary according to the nozzles used. The maximum variation, for each nozzle, ranges from 0.28 to 6.13 mm/h.

In addition to the artificial rainfall system, further acquisition systems are installed which permit data collection with a series of sensors for a total of 48 channels from tensiometers, pressure transducer, laser sensors to detect the soil level, auxiliary sensors (inclination and pressure) and rain gauges. The individual sensors are placed in various positions and each may be positioned to operate on various measurement configurations and simulations. Finally, a series of motorized activation and control systems were installed, including pneumatic and hydraulic controls. The instrumentation in the artificial channel is able to measure the main parameters that control the physical phenomenon, thanks to the installation of the following equipment:

- Tensiometers (used to measure soil suction);
- Pressure transducers (used to measure pore water pressure);
- TDR device (used to measure soil water content);
- Rainfall system (used to simulate rainfall);

- Laser sensors (used to measure the soil profile and  $uz$  displacements );
- High-resolution video cameras (used to measure displacements along  $ux$  and  $uy$ ).

This sensor system is essential for measuring and monitoring the main parameters that control and regulate the phenomenon of landslides triggered by rainfall infiltration.

#### First test with homogeneous soil

The pyroclastic soil used for the experimental tests was collected in the area of Sarno in southern Italy, about 15 km from the volcano Vesuvius. In May 1998, in this area, large and rapid landslides devastated the town, causing an enormous number of victims. At these sites, the stratigraphy consists of limestones covered by layers of pyroclastic deposits.

These soils are the product of different eruptions of more volcanoes like Somma-Vesuvius, Flegrei fields and other volcanoes present in the region that are no longer active. The ashes, coming out after the eruption and carried by the wind, travel for kilometres from the eruption zone, resulting in a non-uniform stratigraphy throughout the region (Del Prete et al. 1998; De Vita and Nappi, 2013; Cascini et al. 2008). Generally, they are incoherent deposits with variable granulometry, ranging from sands, silty sands and silts (ashes) to sands with gravel (pumice) and gravels. Inside the flume test, a homogeneous deposit of pyroclastic ash has been reconstructed, which can be attributed to the Plinian eruption of "Pollena" of 472 B.C.

The slope was formed by a layer of volcanic ash 20 cm thick, occupied the entire width of the flume (100 cm) and was 150 cm long. This geometry allows the deposit to be assimilated to an indefinite slope. At the base of the model there was an impervious rough bed to simulate conditions similar to those of a natural slope. At the foot of the slope a geotextile-coated drainage grid was placed.

The ash in question was sieved with a 0.4 cm mesh to remove coarse contamination occurring during the sampling phase. The artificial slope was re-constituted inside the flume by layers with the moist-tamping technique, with volcanic ash porosity of between 68% and 76%. The volumetric water content of the ash ( $\theta$ ) was about 20%. Inside the artificial slope, 12 tensiometers were installed to measure suction and six TDR probes to measure volumetric water content. The sensors were installed at depths of 5 cm, 11 cm and 17 cm below the ground surface, both in the upslope and downslope zones of the deposit. Three neutral pressure transducers were arranged on the flume bed, while four laser displacement transducers were installed to measure displacements perpendicular to the slope surface. Fig. 5 shows schematically the location of the sensors installed inside the deposit. Rainfall was generated by a sprinkler system placed about 100 cm above the sliding surface. The nozzles were arranged so as to ensure rainfall uniformity and avoid surface erosion. Several test stages were carried out:

1. The first test was conducted with the deposit in a horizontal position. A constant rainfall of considerable intensity was simulated (about 220 mm/h) for about 50 minutes. The test was performed to activate infiltration phenomena so as to stabilize the slope before tilting.
2. The deposit was then left under natural evaporation for about 14 days, acquiring the values recorded by the various sensors.
3. The slope was then inclined at 38° and exposed to evaporation for about 8 days to redistribute the suction values and water content in the new configuration.
4. Finally, a new infiltration phase was simulated with constant rainfall at an intensity of about 220 mm/h, which lasted until slope failure (about 40 minutes).

**Test results**

During the various tests, values of suction and volumetric water content were acquired both in the upslope and downslope zones at different depths. Displacements perpendicular to the slope surface were also measured, produced by the variation in the tension state, and the water pressure on the flume bed. The final infiltration phase was initiated with inclined deposit, with a high-intensity artificial rainfall (about 220 mm/h) to reach conditions that trigger a landslide along the artificial slope.

The suction pattern during the last infiltration phase (Fig. 6) clearly shows that saturation conditions at many of the tensiometers are swiftly reached. It is also possible to note the moment in which the curves for tensiometers placed downslope at 5 cm and 11 cm of depth have a rapid variation in slope, that is when part of the slope is detached and a small surface landslide is triggered. Trends in soil volumetric water content are reported in Fig. 7. It appears evident, also in this phase of infiltration in a sloping channel, the progressive advancement of a wetting

front from the top, although some differences are observed between the upslope and downslope zones where, perhaps due to the imperfect homogeneity of the spatial distribution of the artificial rainfall, but especially due to the subsurface flow parallel to the slope, the increase in water content appears anticipated. It should also be pointed out that all the TDR probes, despite there being absolute evidence that much of the deposit reaches complete saturation conditions, detected water content values between 50% and 55%. This is doubtless to be attributed to compaction experienced by the deposit during the previous test phases, which had led to a reduction in height from the initial 20 cm to around 18 cm, corresponding to an estimated reduction in porosity of around 10%. This graph also shows the moment in which a small landslide is detached, producing an abrupt change in the steepness of the curve for the TDR positioned in the most superficial part downslope. In this case the landslide

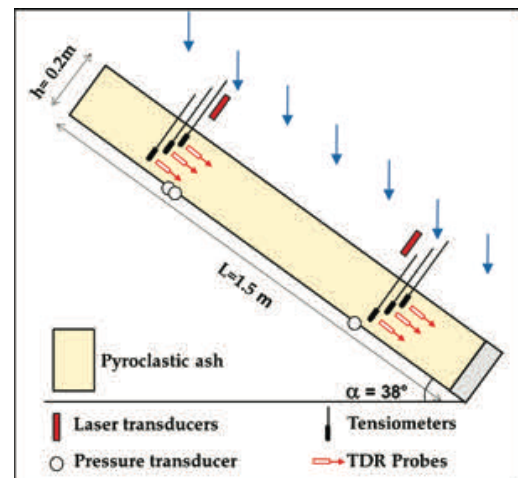


Figure 5 Position of the sensors in section in test n.1.

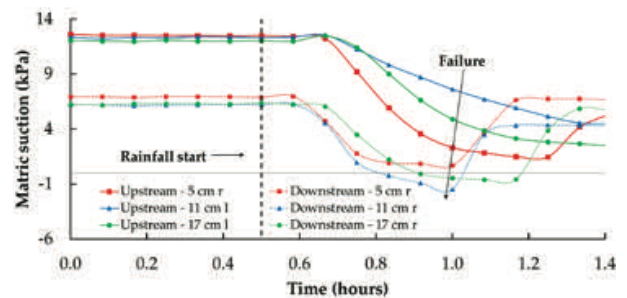


Figure 6 Time course of suction.

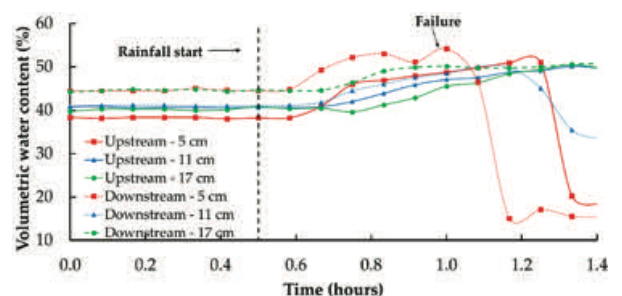


Figure 7 Volumetric water content vs. time.

brought the TDR to the surface and from this point on, the values measured by the sensor are no longer representative of the actual water content.

Slope failure, consistent with the compacted configuration assumed by the deposit during the previous test phases, did not trigger a mud-flow. The instability took the form of a progressive erosion of the more superficial soil layers, initially and chiefly concentrated in the downslope zone, where the intense sub-surface flow resulted in conditions of greater moisture being reached and, at the same time, encouraged soil mobilization. The first local failures began to occur about 20 minutes after the beginning of artificial rainfall, and only after that did they extend so far as to affect the points in which some of the tensiometers and TDR probes had been installed.

### Second test with homogeneous soil

A homogeneous deposit of volcanic ash was reconstructed, similar to that of the previous test: 20 cm thick, 60 cm wide and 270 cm long (Fig. 8). Also in this case, an impervious rough bed was placed, while a geotextile-coated drainage was placed at the foot of the slope. The porosity was between 68% and 76% and the volumetric water content of the ashes was about 20%. Inside the deposit, 12 tensiometers were installed to measure the suction, and 7 TDR probes to measure the volumetric water content. At the bottom of the flume, 6 pressure transducers were arranged, while 6 laser technology displacement transducers were installed to measure the displacements orthogonal to its surface of the slope. Fig. 8 shows the position of the sensors in section. Rainfall was generated by a sprinkler system placed about 100 cm above the sliding surface. The nozzles were arranged so as to ensure rainfall uniformity and avoid surface erosion. Various test stages were carried out:

1. The first phase was performed with the deposit in a horizontal position simulating a constant rain of 50 mm/h intensity for about 20 minutes, to activate infiltration phenomena so as to stabilize the slope before tilting it.
2. Subsequently, the slope was inclined at  $38^\circ$  and left to evaporate for about 20 days, in order to redistribute the suction and water content values in the new configuration.
3. Finally, an infiltration phase was carried out, simulating a rainfall with a constant intensity of 50 mm/h, which lasted about 4 hours, until the slope failure.

### Test results

The last infiltration phase with the inclined deposit was characterized by artificial rainfall with an intensity of 50 mm/h. The evolution of suction during this phase until the slope failure is represented in Fig. 9. This shows that all the values recorded by the tensiometers tend to converge to a suction value equal to zero, which indicates the achievement of the saturation condition in the entire deposit. The values of the volumetric water content were

measured with 7 TDR probes. The trends are shown in Fig. 10 from which note the progressive advancement of the wet front from top to bottom. Differences can be observed between the upstream and downstream areas, presumably due to an imperfect homogeneity of the spatial distribution of rainfall, but above all due to the sub-surface flow parallel to the slope.

From the graph it can be seen that failure phenomena occurred about 120-130 minutes from the start of the test. There was a detachment of a large area of the soil which caused the triggering of an evident mudflow (Fig. 11). In this test, in contrast to the first, there was a sudden detachment of the soil and the formation of a mudslide. This difference in behaviour is due to the greater porosity of the soil in the second test.

This avoided the formation of volumetric collapse and therefore of soil compaction. We can therefore deduce

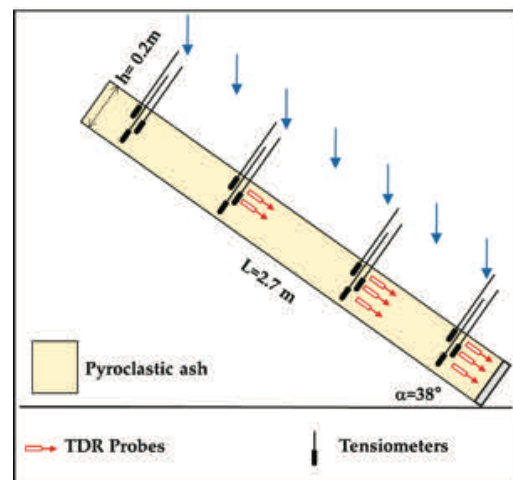


Figure 8 Position of the sensors in section in test n.2.

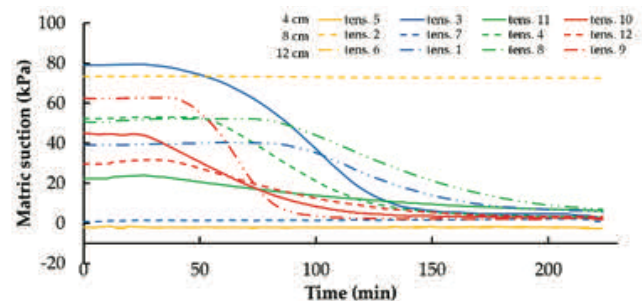


Figure 9 Time course of suction.

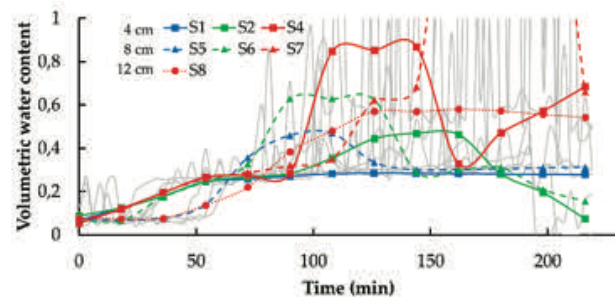


Figure 10 Volumetric water content vs. time.

that these soils lead to the formation of mudslides only if they maintain a high porosity, otherwise the detachments will be minor and retrogressive in nature.

## Conclusions

In this work, experimental data on site were presented, measured by a monitoring station installed in Sarno, in southern Italy. This area was affected by several mudflows in May 1998, causing a lot of damage and deaths. The suction values and saturation degrees recorded at different depths for an entire hydrological year were analyzed. Pairs of values of these quantities made it possible to define the water retention curves. It has been shown that the SWRC of these soils show a strong hysteresis between the wetting and drying phases. This aspect must be taken into consideration when performing numerical simulations aimed at defining the mechanical response of the slope.

Two experimental tests performed with a physical laboratory slope model were also presented. In both cases, the deposits were homogeneous and composed of pyroclastic ashes. Tests were developed in different test stages: phases of rainfall infiltration and evaporation with horizontal deposit, and rainfall phases with the deposit inclined. The mechanical response of the deposits in the two tests was decidedly different. In the first test, the instability occurred in a form of small detachments of a retrogressive nature. In the second, however, there was a mudflow. This difference is due to the different porosity of the soil. In fact, in the second test, the rainfall and evaporation phases with the horizontal deposit lasted much shorter than in the first test. This avoided the phenomenon of volumetric collapse and thus the compaction of the soil.

This experimentation is grounds for the study of pyroclastic soil samples from other areas such as Sierra Norte de Puebla in Mexico, with the aim of highlighting any similarities in behavior and response to rainfall infiltration.



Figure 11 Detachment niche of the mudflow.

## Acknowledgments

The authors gratefully acknowledge the financial support provided by the framework of the SILA—PONa3\_00341 project An Integrated System of Laboratories for the Environment.

## References

- Alcántara-Ayala I (2004) Hazard assessment of rainfall-induced landsliding in Mexico. *Geomorphology*. 61:19–40.
- Alcántara-Ayala I, Garnica-Peña RJ, Coll-Hurtado A, Gutiérrez de MacGregor MT (Coords.) (2017) Inestabilidad de laderas en Teziutlán, Puebla. Factores inductores del riesgo de desastres, Instituto de Geografía, Universidad Nacional Autónoma de México, pp 130.
- Bitrán D (2000) Evaluación del impacto socioeconómico de los principales desastres naturales ocurridos en la República Mexicana durante 1999 (Evaluation of the socioeconomic impact of the main natural disasters that occurred in the Mexican Republic during 1999), Cuadernos de Investigación, 50, Centro Nacional de Prevención de Desastres, México. (In Spanish).
- Capparelli G, Spolverino G (2020) An empirical approach for modeling hysteresis behavior of pyroclastic soils. *Hydrology*. 7(1): 14.
- Cascini L, Cuomo S, Guida D (2008) Typical source areas of May 1998 flow-like mass movements in the Campania region, Southern Italy. *Engineering Geology*. 96: 107-125.
- Del Prete M, Guadagno F M, Hawkins A B (1998) Preliminary report on the landslides of 5 May 1998, Campania, southern Italy. *Bull. Engineering Geology and the Environment*. 57: 113-129.
- De Vita P, Nappi M (2013) Regional distribution of ash-fall pyroclastic soils for landslide susceptibility assessment. In *Landslide Science and Practice*; Margottini, C., Canuti, P., Sassa, K., Eds.; Springer: Berlin/Heidelberg, Germany. pp. 103–109.
- Di Crescenzo G, Santo A (2005) Debris slides—rapid earth flows in the carbonate massifs of the Campania region (Southern Italy): morphological and morphometric data for evaluating triggering susceptibility. *Geomorphology*. 66: 255-276.
- Di Martire D, De Rosa M, Pesce V, Santangelo M A, Calcaterra D (2012) Landslide hazard and land management in high-density urban areas of Campania region, Italy. *Nat. Hazards Earth Syst. Sci*. 12: 905–926.
- Ferriz H, Mahood G (1984) Eruption rates and compositional trends at Los Hornos volcanic center, Puebla, Mexico. *J. Geophys. Res.-Earth*. 89: 8511-8524.
- Flores L P, Alcántara- Ayala I (2002) Cartografía morfogenética e identificación de procesos de ladera en Teziutlán, Puebla. *Investigaciones geográficas*. 49: 7-26. (In Spanish).
- Murillo-García F, Alcántara-Ayala I (2017) Landslide inventory, Teziutlán municipality, Puebla, México (1942–2015). *Journal of Maps*. 13(2): 767-776.
- Revellino P, Guadagno F M, Hungr O (2008) Morphological methods and dynamic modelling in landslide hazard assessment of the Campania Apennine carbonate slope. *Landslides*. 5(1): 59-70.
- Rolandi G, Bellucci F, Heizler M T, Belkin H E, De Vivo B (2003) Tectonic controls on the genesis of ignimbrites from the Campanian volcanic zone, southern Italy. *Miner. Petrol*. 79: 3-31.
- Sorbino G, Nicotera M V (2013) Unsaturated soil mechanics in rainfall-induced flow landslides. *Eng. Geol*. 165: 105-135.
- Spolverino G, Capparelli G, Versace P (2019) An instrumented flume for infiltration process modeling, landslide triggering and propagation. *Geosciences*. 9(3): 108.
- Van Genuchten M.T, (1980). A closed form equation for predicting the hydraulic conductivity of unsaturated soils. *Soil Sci. Soc. Am. J*. 44, pp. 892-898.



# Role of stratigraphy for rainfall-induced shallow instabilities in volcanic soils: a case study

Luca Crescenzo<sup>(1)</sup>, Michele Calvello<sup>(1)</sup>

1) University of Salerno, Department of Civil Engineering, Fisciano (SA), Via Giovanni Paolo II 132, Italy, +39089962223 (lcrescenzo@unisa.it)

**Abstract** A large area close to the Somma-Vesuvio volcanic complex (Campania region, Italy) is covered by thin layered pyroclastic soils produced by successive explosive eruptions of the volcano, wind transportation and air-fall deposition. These soil layers can be found on very inclined slopes, their stability being ensured by the soils' unsaturated conditions and related matrix suction (Cascini et al., 2014). Therefore, it is not surprising that the most superficial layers are often affected by rainfall-induced slope instabilities that later originate high mobility debris flows or debris avalanches. Numerical modelling of the triggering phase of these phenomena is particularly complex due to the mechanical and hydraulic characteristics of the materials involved (Cascini et al., 2013). This study examines the transient groundwater regime and the associated stability conditions within a relatively small but very steep slope (height difference 24 m, average slope angle  $38^\circ$ ) for which the stratigraphical and geotechnical characteristics of the soils are well characterized. The slope was affected by a debris flow that initiated in the topmost 2 m of soil at the end of a 4-day long rainfall event. Rainfall data recorded at a nearby rain gauge were used to impose the transient hydraulic boundary conditions at the ground surface, for a period of 1 month prior to the instability. Given the role played by the partial saturation conditions of the soil layers, a series of coupled hydro-mechanical finite element analyses has been conducted, considering different schematizations of the stratigraphical settings in the topmost portion of the slope, to assess the role played by the soil water characteristic curves and the permeability functions adopted in the model for the different soil layers. The time-dependent stability conditions in the slope were assessed adopting the c-phi strength reduction technique, considering daily steps of the transient model. The results of the analyses provide indications on the level of stratigraphic detail needed to properly model the observed instability in the considered slope, as well as on the hydraulic properties that must be considered for the most superficial soil layers to effectively simulate the response of the slope to the rainfall conditions applied at the ground surface.

**Keywords** shallow landslides, unsaturated soils, transient groundwater flow, numerical modelling

## Introduction

Rainfall-induced landslides are common phenomena caused by intense and prolonged rainfall. Infiltration of rainfall water in the soil causes various complex mechanisms that may lead to the triggering of landslides such as: decrease of matrix suction; increase in water content and consequent increase in the unit weight of the soil; increase of porewater pressure and groundwater level, which in turn affect the shear strength of the soil. This study reports and discusses the results of a series of numerical analyses of the transient groundwater regime, and of the associated stability conditions, conducted for a steep slope covered by thin layered pyroclastic soils.

## Case study

In this study a debris flow triggered by intense rainfall event has been analysed. The landslide phenomenon involved an approximately square area, about 30 m on each side, with 24 m vertical height difference between the landslide crown and a secant pile wall delimiting the natural slope (Fig. 1). The total volume mobilized is about 1700 m<sup>3</sup>, with a slip surface about 2 m below the ground surface. After the triggering phase, a high velocity propagation stage developed and the landslide mass deposited downstream of the retaining wall, also hitting a residential building placed at the toe of the slope, breaking parts of its outer wall and completely filling its second floor.

Fig. 2 presents rainfall data coming from a rain gauge located near the study site, part of the monitoring network of the regional civil protection. The figure shows the cumulative precipitation for the 19 hydrologic years (from September 1 to August 31) preceding the landslide, and for the year of the event. As it can be seen, the landslide occurs after a few days of significant rainfall, during a wet season that has been particularly rainy.

## Numerical model

A series of fully coupled analyses have been carried out, using a commercial finite element software (Plaxis 2D), to investigate the seepage regime within the slope in response to rainfall, applied as a transient hydraulic

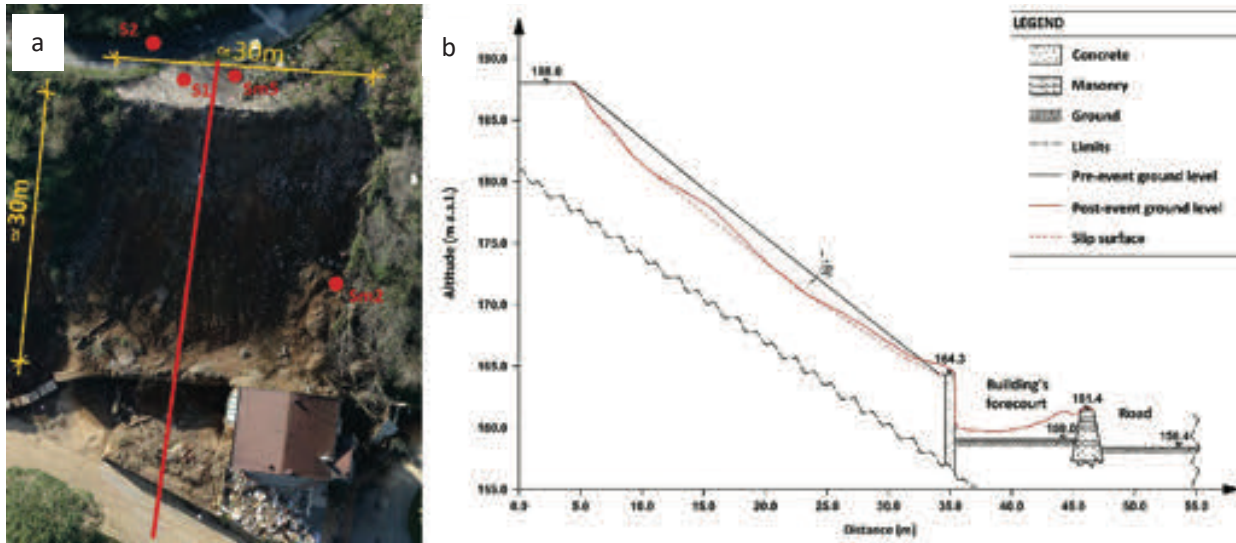


Figure 1 Landslide geometry: orthophoto with dimensions and track of cross section (a); cross section (b)

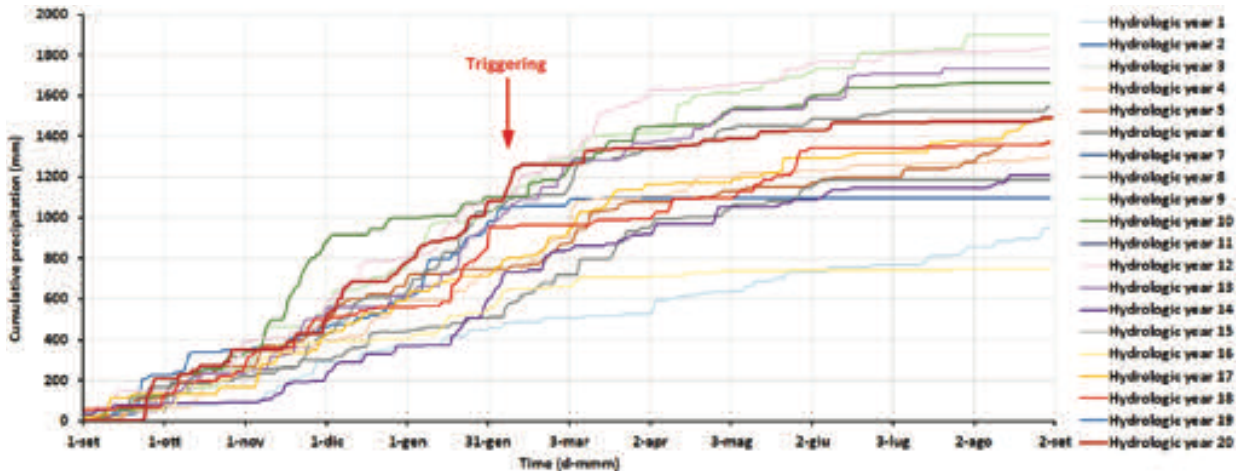


Figure 2 Cumulative precipitation recorded for 20 hydrologic years preceding the landslide event.

boundary condition at the ground surface, and to consequently evaluate the factor of safety of the slope.

The numerical model consists of 4,754 elements of 15-nodes and 38,713 nodes. Fig. 3 shows the main characteristics of the numerical model. In particular: i) the upstream and the downstream contours are assumed impervious, since the secant pile wall does not have drains, and the horizontal displacements are constrained; ii) the lowest contour has been considered permeable; iii) a porewater pressure linearly increasing with depth has been assumed as initial condition at the bottom boundary; iv) the rainfall has been applied at the ground surface without considering any evapotranspiration effect.

The transient seepage regime in unsaturated soils has been calculated solving numerically the Richard's partial differential equation, that can be written as:

$$\frac{\partial}{\partial x} \left( k(h) \frac{\partial h}{\partial x} \right) + \frac{\partial}{\partial y} \left( k(h) \frac{\partial h}{\partial y} \right) = - \frac{\partial nS(h)}{\partial t} \quad [1]$$

where:  $k(h)$  is the unsaturated hydraulic conductivity,  $h$  is the water head,  $n$  is the porosity of the soil, and  $S$  is the degree of saturation.

The hydraulic conductivity is function of the water content, which in turn depends on matrix suction. In the literature, numerous contributions have been proposed to assess the relationship between the water content and the matrix suction, known as Soil Water Characteristic Curve, hereinafter SWCC. In this study the van Genuchten SWCC and permeability function (1980) have been adopted:

$$S(h) = S_r + \frac{(S_s - S_r)}{[1 + (g_a h)^{g_m}]^{g_m}} \quad [2]$$

$$k_{rel}(S) = (S_{eff})^{g_l} \left\{ 1 - \left[ 1 - S_{eff} \left( \frac{g_n}{g_n - 1} \right) \right]^2 \right\} \quad [3]$$

with

$$S_{eff} = \frac{S - S_r}{S_s - S_r} \quad [4]$$



and

$$\sigma' = \sigma' - S_{eff} u \quad [5]$$

where:  $S_r$  is the residual saturation,  $S_s$  is the degree of saturation at saturated conditions,  $S_{eff}$  is the effective degree of saturation,  $k_{rel}$  is the relative hydraulic permeability coefficient (the ratio between the current hydraulic permeability and the saturated hydraulic permeability),  $g_a$ ,  $g_n$ ,  $g_l$ , and  $g_m$  are the fitting curve parameters with  $g_m=1-1/g_n$ ,  $\sigma'$  is the effective stress,  $\sigma$  is the total stress,  $u$  is the porewater pressure.

The geotechnical parameters of the soil involved have been obtained from laboratory tests, whereas the van

Genuchten parameters have been obtained from the granulometric characteristics of the soils (Tab. 1).

To quantify the contribution of the shallow layer in terms of both seepage regime and slope stability conditions, three stratigraphical settings have been considered (Fig. 4). In particular, the Case 0 considers the extremely detailed stratigraphy of the in-situ findings. The second scheme (Case 1) refers to a simplified stratigraphy where all the shallow layers are merged into a unique cluster of homogeneous geotechnical characteristics. In Case 2 the topmost layer is explicitly modelled, yet a simplified stratigraphy below this layer is considered.

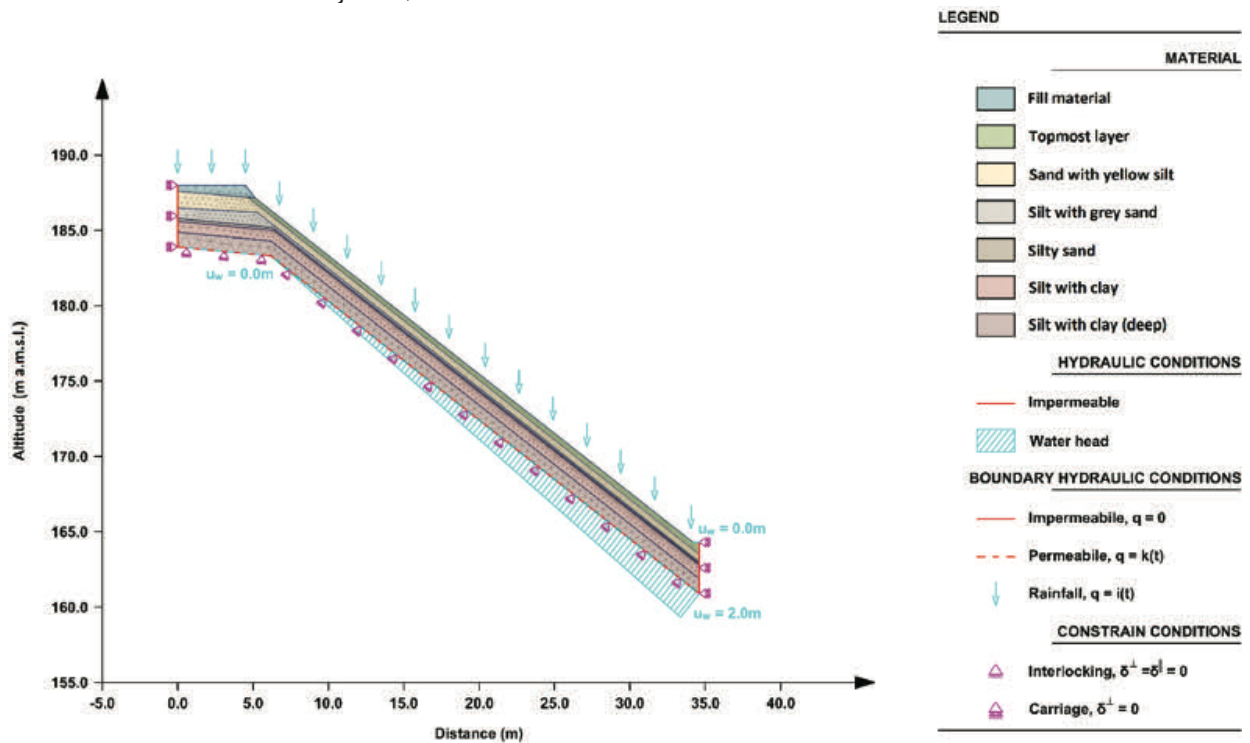


Figure 3 Numerical domain with initial and boundary conditions, and calculation mesh.

Table 1. Geotechnical properties of the involved soils. Legend:  $\gamma_{unsat}$  is the weight per unit of volume above the groundwater level;  $\gamma_{sat}$  is the weight per unit of volume below the groundwater level,  $e_{initial}$  is the initial void ratio,  $c'$  is the effective cohesion,  $\phi'$  is the friction angle,  $S_{res}$  is the residual degree of saturation,  $S_{sat}$  is the saturated degree of saturation,  $g_n$ ,  $g_a$ ,  $g_l$  are the van Genuchten parameters,  $k_{sat}$  is the saturated hydraulic conductivity.

Parameter		Silt with clay (deep)	Silt with clay	Silty sand	Silt with grey sand	Sand with yellow silt	Topmost layer	Fill material
$\gamma_{unsat}$	(kN/m <sup>3</sup> )	14.1	14.1	14.1	12.6	12.8	12.8	16.5
$\gamma_{sat}$	(kN/m <sup>3</sup> )	15.4	15.4	15.4	14.0	14.3	14.3	17.6
$e_{initial}$	(-)	1.9	1.9	1.9	3.0	2.7	2.7	1.3
$c'$	(kN/m <sup>2</sup> )	12.0	4.0	10.0	10.0	10.0	20.0	5.0
$\phi'$	(°)	31.3	34.5	35.0	28.0	28.0	28.0	37.4
$S_{res}$	(-)	0.1	0.1	0.1	0.1	0.1	0.1	0.1
$S_{sat}$	(-)	1.0	1.0	1.0	1.0	1.0	1.0	1.0
$g_n$	(-)	2.8	2.8	2.9	3.0	2.9	1.3	2.7
$g_a$	(1/m)	0.2	0.2	0.4	0.6	0.45	1.0	0.35
$g_l$	(-)	0.0	0.0	0.0	0.0	0.0	0.0	0.0
$k_{sat}$	(m/d)	1.0E-03	1.0E-03	4.0E-01	3.0E-02	2.0E-01	3.5E+00	3.0E-01

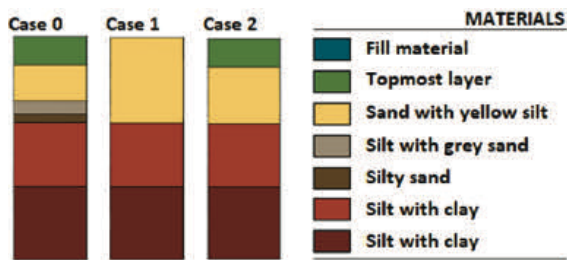


Figure 4 Stratigraphical settings considered.

## Results

The effects of the rainfall on the slope have been analysed monitoring the variation over time of the factor of safety of the slope, as well as the porewater pressures at certain points inside the domain.

The factor of safety has been evaluated adopting the c-phi reduction technique, thus the positions of the critical slip surface is automatically detected within the domain at each time step. Concerning to the porewater pressures, data from several points have been recorded, yet for the purposes of this study only the following two points, along a vertical at 24.6m on the x-axis, will be considered: A, at the base of the topmost layer, and B, at the base of the silt with grey sand layer. Fig. 5 shows the variation of both the factor of safety and of the porewater pressures over time, in response to the rainfall applied at the ground surface, in all the three cases considered. The safety conditions worsen in three moments of the considered period, due to the presence of three peaks on the porewater pressure curves, which are in turn a consequence of three intense rainfall periods.

Comparing the results of three stratigraphical settings examined, one can notice that Case 0 and the Case 2 are very similar in terms of factor of safety. They reach the critical conditions on the 31<sup>st</sup> day of analysis, for which the porewater pressures in the monitored points coincide. Differently, Case 1 is extremely sensitive to the rainfall applied. In fact, the slope in this case is already unstable on the 21<sup>st</sup> day of the analysis, when the porewater pressures reach the maximum possible value in both monitored points.

The results show that considering a simplified stratigraphy in the intermediate depth does not influence the results significantly, whereas the presence in the model of a shallow layer is fundamental for correctly predicting the triggering of the slope.

From Case 2, another series of three simulations has been carried out changing the hydraulic parameters of the topmost layer only (Fig. 6). In these cases, the response of the system is extremely different from the previous ones and is function of the value adopted for the SWCC. In particular, in Case 2b and Case 2c the changes of the factor of safety are negligible, despite the application of the rainfall boundary conditions, in contrast with the evidence of the slope becoming unstable at the end of the considered period. This is due to the value assumed for the air-entry value of the SWCC (governed by parameter  $g_a=0.45/m$ ), approximately double the base case ( $g_a=1.0/m$ ). For Case 2a, only the  $g_n$  parameter has been changed compared to Case 2, reducing it of about 30% (from 2.9 to 2.1). In this case the results show, as expected, a certain sensitivity of the factor of safety to the imposed rainfall even, although the slope appears still stable at the end of the analysis (the factor of safety is about 1.3).

It is worth noting that Case 1 and Case 2c are different only for the value assumed by the saturated hydraulic conductivity of the topmost layer, yet the porewater pressure regime is completely different in the two cases (see Figures 5 and 7). This is due to the higher capability of the shallow layer to drain the water flow coming from the rainfall in Case 2c, combined with a lower capability for the water to seep towards deeper layers considering the value assumed by  $g_a$ . In other words, the topmost layer behaves as a “drain interface” between the atmosphere and the deeper layers, thus significantly reducing the flow rate that is able to reach the deeper strata. Therefore if, as in this case, the topmost layer is also characterized by higher strength parameters, the factor of safety of the slope becomes essentially insensitive to the rainfall conditions.

## Conclusion

In this study, the triggering phase of a debris flow in pyroclastic soil has been numerically modelled employing

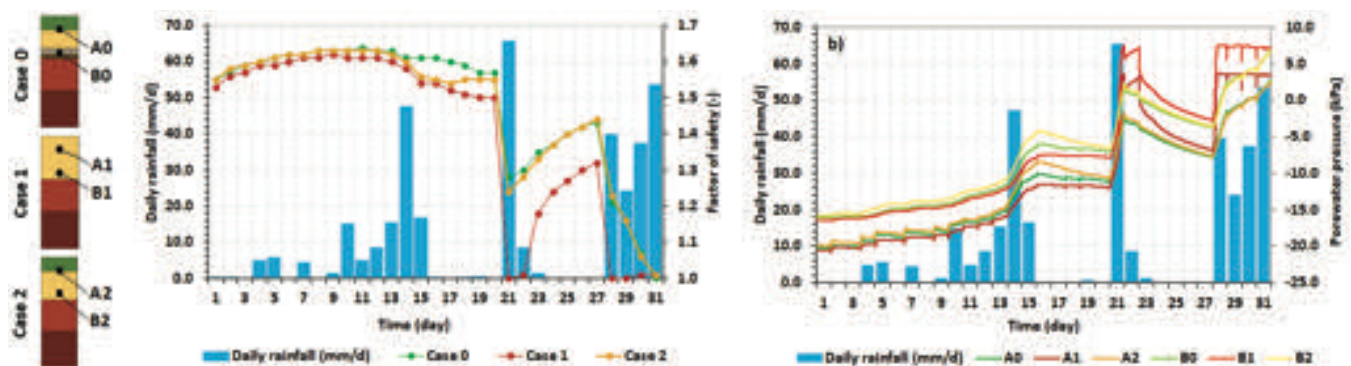


Figure 5 Trend over time of the factor of safety (a) and the porewater pressure (b) for the three cases considered.

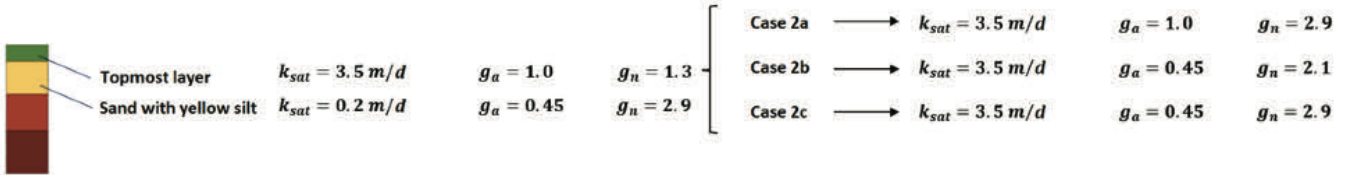


Figure 6 Parametric analysis from Case 2 considering different hydraulic parameters of the topmost layer: increasing parameter  $g_n$  (Case 2a); decreasing parameter  $g_a$  (Case 2b); combination of both changes (Case 2c).

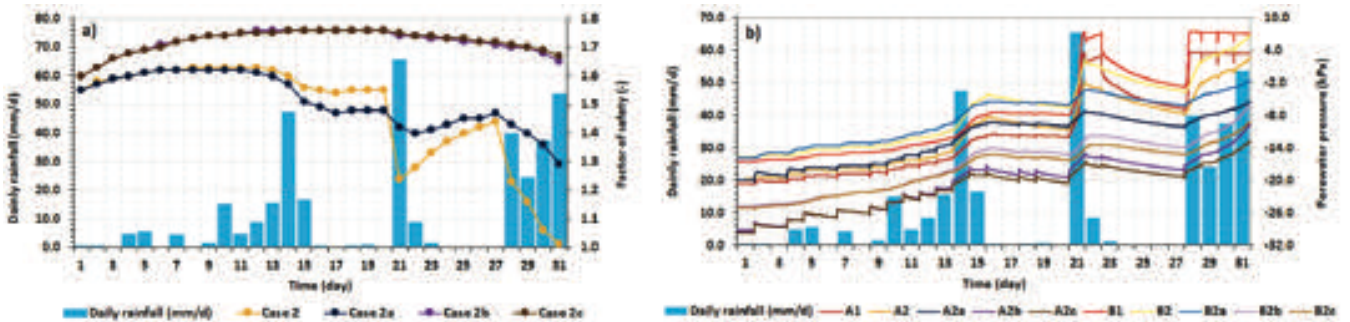


Figure 7 Results of parametric analysis from Case 2: factor of safety (a) and porewater pressures (b).

fully coupled finite element analyses. The soils involved lied on a very steep slope and mobilised at the end of a significant rainfall period. The parametric analyses conducted, starting from a “base case” analysis in line with the in-situ evidence, highlight the importance of an adequate hydraulic characterization of the shallow soil layers. Indeed, the partial saturation conditions of these soils affect considerably the transient porewater pressure regime in response to rainfall applied as a boundary condition at the ground surface. It is important to stress that the soil-atmosphere interaction has not been taken into account in this study, although the authors are well aware that it can play a fundamental role for rainfall-induced landslides, especially for long term analyses (Tagarelli and Cotecchia, 2020).

### References

Cascini L, Cuomo S, Pastor M (2013) Inception of debris avalanches: remarks on geomechanical modelling. *Landslides*. 10(6): 701-711.

Cascini L, Sorbino G., Cuomo S, Ferlisi S (2014) Seasonal effects of rainfall on the shallow pyroclastic deposits of the Campania region (southern Italy). *Landslides*. 11(5): 779-792.

Tagarelli V, Cotecchia F, (2020) The effects of slope initialization on the numerical model predictions of the slope vegetation atmosphere interaction. *Geosciences*. 10(2): 85.

Van Genuchten M T, (1980) A closed-form equation for predicting the hydraulic conductivity of unsaturated soils. *Soil science society of America journal*. 44(5): 892-898.



# Small-scale physical landslide models under 1g infiltration conditions and the role of hydrological monitoring

Josip Peranić<sup>(1)</sup>, Vedran Jagodnik<sup>(1)</sup>, Nina Čeh<sup>(1)</sup>, Martina Vivoda Prodan<sup>(1)</sup>, Sara Pajalić<sup>(1)</sup>, Željko Arbanas<sup>(1)</sup>

1) University of Rijeka, Faculty of Civil Engineering, Rijeka, Radmile Matejčić 3, Croatia, +38551265943 (josip.peranic@gradri.uniri.hr)

**Abstract** Despite the considerable progress made in recent decades, there is still a need for a deeper understanding of the physical processes, mechanisms and crucial factors that lead to rainfall-induced landslides. With ongoing climate change affecting the frequency and intensity of meteorological extremes, and the imperatives of continuous urban expansion undoubtedly influencing the frequency and magnitude of landslides, it is no coincidence that the issue of rainfall-induced landslides has received increasing attention from both the scientific community and landslide practitioners in recent decades. Close observation of the hydromechanical response of slopes exposed to different rainfall loads plays a crucial role in understanding the driving mechanisms and factors affecting rainfall-induced landslides. In combination with appropriate monitoring techniques, small-scale physical landslide models can provide accurate insight into the relevant variables under precisely controlled initial and boundary conditions. This paper presents a model platform for physical modelling of scaled slopes under 1g rainfall infiltration conditions, developed at the Faculty of Civil Engineering, University of Rijeka, Croatia, within the four-year research project "Physical modelling of landslide remediation constructions' behaviour under static and seismic actions". Some of the main features of the model platform and the materials used for testing are described. Special attention is given to the sensor network that allows precise monitoring of soil moisture and pore water pressure in a scaled slope during rainfall simulation. Finally, two interesting examples of monitoring data are singled out and analysed with working frameworks relevant to the study of scaled slope models exposed to rainfall.

**Keywords** physical modelling, scaled slopes, landslides, rainfall, hydraulic monitoring, sensors

## Introduction

Landslides are one of the most common geological hazards, usually caused by intense and/or prolonged rainfall. With the ongoing climate change, the continuous expansion of urban areas and the development of infrastructure, the increasing interaction between humans

and landslides seems inevitable. It is therefore no coincidence that the issue of rainfall-induced landslides has received increasing attention from both the scientific community and landslide practitioners in recent decades.

Despite considerable efforts and progress in understanding the physical processes and mechanisms responsible for triggering rainfall-induced landslides, the issue remains an important topic for the landslide scientific community. Complex physical processes controlling the hydro-mechanical response of slopes during transient infiltration of rainfall, highly non-linear material properties and spatial variations of the soils involved, quantification of time-dependent boundary conditions, associated hysteresis effects exhibited by the soil as a function of flow direction, and strong spatial and temporal variations in rainfall characteristics are just some of the aspects contributing to the complexity of the problem.

Various approaches have been successfully used to study the hydraulic response and failure mechanisms of landslides triggered by a rainfall. For example, numerical models have been used to investigate how different factors affect the stability of both shallow and deep-seated landslides (e.g., Casagli et al. 2006; Rahimi et al. 2011; Comegna et al. 2013; Leung and Ng 2013; Cascini et al. 2014; Lollino et al. 2016; Hinds et al. 2019; Kang et al. 2020; Marino et al. 2021; Peranić et al. 2021) Field monitoring has been successfully used to observe the hydraulic and mechanical response of slopes in different geological and climatic contexts (e.g. Greco et al. 2013; Springman et al. 2013; Bordoni et al. 2015; Leung and Ng 2016; Chen et al. 2018; Kim et al. 2021; Sattler et al. 2021). Particularly valuable data have been obtained from field experiments on instrumented slopes exposed to artificial rainfall or soil moisture increase conditions (e.g. Krzeminska et al., 2014; Rahardjo et al., 2005; Sitarenios et al., 2021; Springman et al., 2013; Sun et al., 2021; Zhang et al., 2019). Various laboratory devices have provided useful information on the hydromechanical behaviour of soil samples tested under conditions similar to those found on field slopes during rainfall infiltration (e.g. Casini et al. 2013; Cuomo et al. 2017; Peranić and Arbanas 2020).

While size effects, problems associated with taking and testing intact soil samples, and stress conditions and loading paths that cannot fully replicate field conditions

are often highlighted as major shortcomings of laboratory sample-size experiments, the interpretation of data from large-scale field experiments can also be complicated by complex soil profile conditions, difficulties in installing monitoring equipment, introducing preferential water flow paths into the slope, etc. Testing small- or large-scale physical landslide models is an additional useful approach that allows accurate observation of the hydraulic and mechanical responses of a slope under precisely controlled initial and boundary conditions. In combination with advanced monitoring techniques and appropriate sensor networks, they have been successfully used, for example, to study the infiltration process, landslide initiation and the propagation phase of landslides triggered by artificial rainfall under 1g conditions (e.g., Moriwaki et al. 2004; Take et al. 2004; Tohari et al. 2007; Damiano et al. 2017; Spolverino et al. 2019; Pajalić et al. 2021; Yang et al. 2021).

This paper presents a model platform for physical modelling of small-scale slopes under 1g rainfall conditions developed at the Faculty of Civil Engineering, University of Rijeka, Croatia. The main features and capabilities of the model platform are described, with particular emphasis on the advanced sensor network that enables precise monitoring of the hydraulic response of scaled slopes under simulated rainfall conditions. Two examples of monitoring data are presented and analysed with working frameworks relevant to the study of scaled slope models initiated by rainfall.

### Physical model

One of the main objectives of the four-year research project "Physical modelling of landslide remediation constructions' behavior under static and seismic actions", which started in October 2018 at the Faculty of Civil Engineering, University of Rijeka, Croatia, was to develop platforms that enable the study of small-scale physical landslide models under static (rainfall) and seismic (earthquake) conditions. The main idea of the Project is to compare the responses of scaled slope models that are built of different soil types and geometric conditions, with and without remediation measures, exposed to different loading conditions. It was expected that the results obtained would provide useful data that could be used to predict the behaviour of real-scale slopes and to improve design procedures and the selection of appropriate landslide remediation measures.

The physical model for testing small-scale soil slopes under 1g rainfall infiltration conditions considered in this paper was developed to enable the triggering of landslides by an artificial rainfall. A sensor network consisting of miniature pore water pressure (pwp) and soil moisture sensors allows observation of the hydraulic response of the scaled models, while suitable photogrammetric equipment and accelerometers allow measurement of displacements during a test. The model consists of several main parts, which are briefly described in the following

text. A detailed description can be found in Arbanas et al. (2020), Jagodnik et al. (2021), and Pajalić et al. (2021).

The model platform itself consists of steel elements and plates with transparent plexiglass side walls that allow the advancement of the wetting front and the onset of displacement to be observed during the experiment. Three basic steel segments, 1 m wide and 0.3 m, 1.4 m and 0.8 m long, form the upper, middle and lower parts of the platform respectively. The joint connections and adjustable height of the upper part allow the models to be built with different inclinations from 20 to 45 degrees. The geogrid attached to the bottom of the platform prevents the soil from sliding along the impermeable steel plates during the test. Liquid rubber and silicone are used to seal small gaps between plexiglass walls and perforations in the structure to ensure that the model is watertight during a test. Drainage pipes inserted through the plexiglass in the lower part of the model allow the water level to be controlled during the test and the water to be drained after the test. The empty platform before the installation phase is shown in Fig. 1a.

### Model construction and soil properties

The platform is suitable for any soil type and installation at any predefined conditions in terms of initial density and moisture content. Any of the appropriate standard laboratory methods commonly used to install soil samples in conventional soil testing laboratory equipment can be used to create the model at the desired density or moisture content.

The results presented in this study were obtained on two different soil materials, which are described in the following text. A fine-grained sand was used as the base

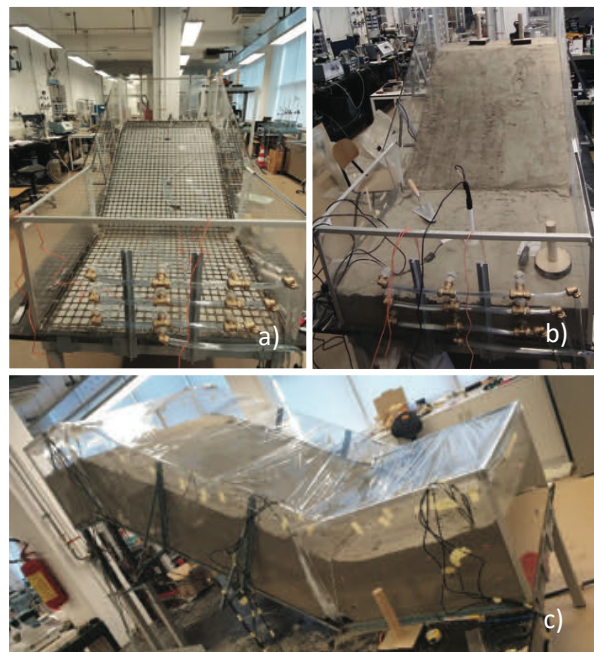


Figure 1 Details from the model construction phase: a) The empty model platform; b) Compaction of the soil material and installation of the measuring instruments; c) Scaled slope model with installed measuring instruments before the start of the test.

soil and the simplest soil material. Another soil type was obtained by adding 15% by weight of kaolin clay to a clean sand (hereafter referred to as SK15). The clean sand was installed at 50% of the relative density ( $Dr_i$ ) and at 2% of the initial moisture content ( $w_i$ ), while the  $Dr_i$  and  $w_i$  were 75% and 8.1% for the SK15, respectively. For both soil materials, Ladd's method of under-compaction (Ladd 1974) was used to construct 30 cm deep slope models. This involved compaction of 5 layers of soil, each 6 cm high, and attempting to achieve as homogeneous conditions as possible in terms of density and soil moisture distribution (Fig. 1b). After the model was built, the entire model was covered with nylon to prevent excessive drying due to evaporation until the start of the test (Fig. 1c). Tab. 1 shows the basic soil properties of the previously described soils.

### Rainfall simulator

In addition to the hydraulic properties of the soil, the rainfall characteristics play a decisive role when it comes to rainfall-induced landslides. The development of the rainfall simulator that meets the specific requirements of the Project was an important step in the early stages of developing a small-scale physical landslide model. In particular, the ability to apply a wide range of rainfall intensities depending on the soil material tested and the specific objectives of the experiment, sufficient spatial uniformity of the simulated rainfall and the ability to modify rainfall patterns and characteristics, preventing excessive erosion due to raindrop impact forces (which are closely related to the diameter of simulated raindrops, impact velocity and/or water pressure), the portability of the rainfall simulator due to its possible use not only with the platform for testing under static conditions but also under dynamic conditions, and the limited budget available for the construction of the simulator were the main considerations in the design and construction of the rainfall simulator.

The rainfall simulator developed consists of three independent branches that deliver water from the main control block to the spray nozzles. The main control

Table 1 Basic soil properties of sand and sand with 15 % kaolin by mass (SK15) with the target initial conditions.

Parameter (unit)	Material	
	Sand	SK15
Specific gravity, $G_s$	2.70	2.67
Effective particle size		
$D_{10}$ (mm)	0.19	0.056
$D_{60}$ (mm)	0.37	0.207
Uniformity coefficient, $c_u$	1.95	54.11
Minimum void ratio, $e_{min}$	0.64	0.54
Maximum void ratio, $e_{max}$	0.91	1.43
Hydraulic conductivity, $k_s$ (m/s)	1.0E-05	3.5E-06
Friction angle, $\phi$ (°)	34.9	31.8
Cohesion, $c$ (kPa)	0	4.4
Initial porosity, $n_i$	0.44	0.43
Initial relative density, $Dr_i$	0.50	0.75
Initial water content, $w_i$ (%)	2.0	8.1

block is connected to a water supply and consists of the control units that regulate the intensity and work of the rainfall simulator, such as pressure regulators, manometers, flow meters, filters, etc. High-density polyethylene pipes convey the pressurised water from the control block to three sprinkler branches, which are adjustable in height and equipped with various spray nozzles (Fig. 2). At the reference pressure of 2 bar, the axial-flow full-cone nozzles (Tab. 2) can produce intensities ranging from less than 30 mm/h to more than 150 mm/h. The setup can be easily modified to achieve any other desired rainfall intensity or pattern.

### Monitoring equipment

The monitoring equipment can be divided into two main parts: i) geodetic monitoring system based on innovative photogrammetric equipment based on multitemporal landslide analysis (Zanutta et al. 2009). of image sequences obtained from a pair of high-speed stereo cameras (Feng et al. 2016) and terrestrial laser scanning and structure-from-motion (SfM) photogrammetry surveys that allow the determination of the surface model of the slope in the pre- and post-failure phase (Bitelli et al. 2003); ii) geotechnical monitoring system consisting of a network of miniature sensors to measure changes in soil moisture, pwp, soil temperature and electrical conductivity, displacements, etc.

The ARAMIS is an optical, non-contact 3D measurement system (GOM GmbH) that provides the entire workflow from taking measurements to analysing the data and displaying the results. A set of two 4-megapixel and two 12-megapixel high-speed cameras is used for multitemporal analysis of landslides from captured stereo image sequences. The system allows continuous monitoring of the 3D coordinates of reference points through all stages of the activity of scaled landslide models. The terrestrial laser scanner FARO Focus 3D X 130 (FARO Technologies Inc.) is used to capture the high-resolution 3D model surface before the start and at the end of the test. The scanner uses phase shift technology to accurately determine the relative 3D position of the

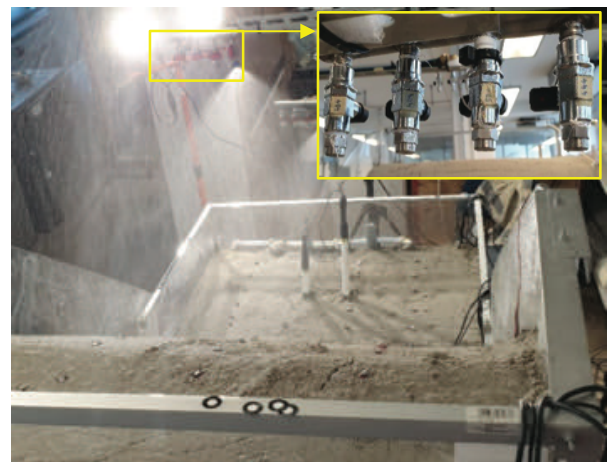


Figure 2 Simulated rainfall with an intensity of 23 mm/h with a detail of the sprinkler branch with axial flow full-cone nozzles.

Table 2 Technical characteristics of full-cone nozzles used to simulate rainfall: spray angle and flow rates ( $v$ ) for different working pressures ( $p$ ) (lechler.com).

Spray angle	Type	$v$ (l/min)			
		$p$ (bar)			
		1.0	2.0	3.0	5.0
60°	490.404	0.76	1.00	1.18	1.44
60°	490.444	0.95	1.25	1.47	1.80
60°	490.484	1.21	1.60	1.88	2.31
60°	490.524	1.52	2.00	2.35	2.89
90°	460.524	0.30	0.40	0.47	0.58

scanned points, while reference points are used to overlap the scanned areas and define the relative coordinate system. A Nikon D500 camera with an ultra-wide angle Tokina AT-X 11-20 lens is used for the SfM photogrammetry survey of the physical models. This technique allows the creation of 3D models from multiple overlay images taken at different triangulation angles. Fig. 3 shows the mentioned equipment, a detailed technical description can be found in Pajalić et al. (2021).

The geotechnical monitoring system consists of a complex network of miniature sensors equivalent to the equipment used for field monitoring. All sensors are connected to data loggers that allow continuous data collection of soil moisture, positive pwp and soil suction, displacement, etc. As the focus of this presentation is on the role of hydraulic monitoring of scaled slopes, the measuring devices are described in more detail in the following section.

### Equipment for monitoring the hydraulic response

Accurate monitoring of the hydromechanical response of scaled slopes under controlled initial and boundary conditions provides valuable information on the variables controlling the instability phenomena of rainfall-induced landslides. The development of a suitable sensor network for the test conditions and the selection of appropriate measurement techniques are therefore crucial steps in the development of small-scale physical landslide models.

The following part describes the main components that make up the hydrological monitoring system of the physical model. There were several requirements that were considered in the selection of the measurement equipment. Firstly, information on soil moisture and changes in pwp had to be available at appropriate time intervals, which necessitated the use of digitised sensors in combination with suitable data loggers. Secondly, the Project envisaged testing a wide range of soils, from sand to clay. Therefore, the selected measurement equipment had to be able to cover a wide measurement range occurring in different soil textures, while ensuring sufficient precision, resolution, and responsiveness.

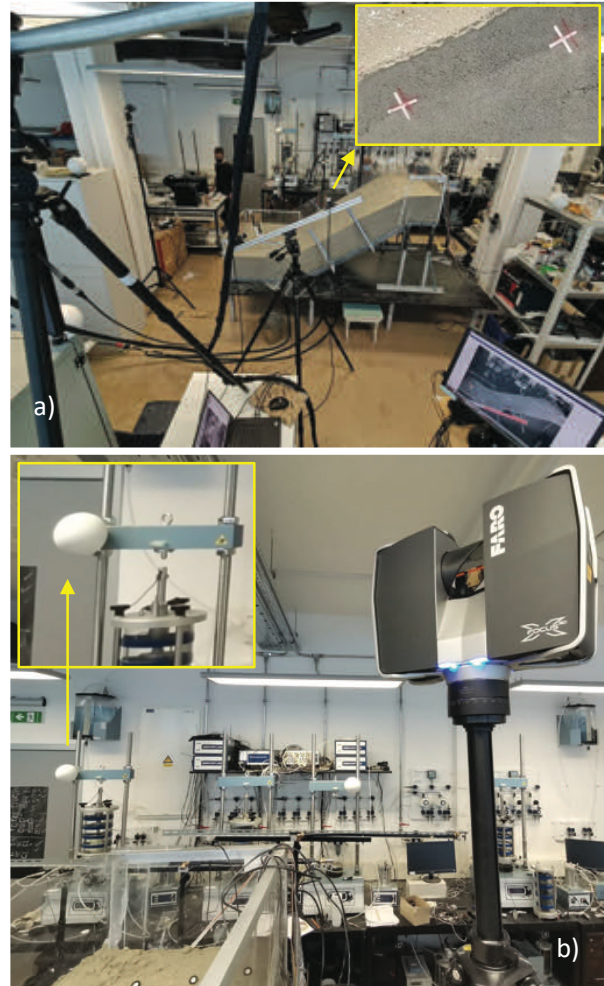


Figure 3 Geodetic monitoring equipment: a) A view of the model from the ARAMIS measuring system (GOM GmbH) and a detail of the (front) 12 megapixel camera monitoring displacements through the plexiglass wall; b) The FARO Focus 3D X 130 (FARO Technologies Inc.) terrestrial laser scanner and a detail of the position of the reference sphere.

The solution was found in the capacitance-based soil water content sensors, which provide rapid detection of changes in soil volumetric water content (VWC) for a wide range of soil textures and conditions, and in the simultaneous use of mini tensiometers for rapid measurement of pwp and matric suction values within the measurement range of standard tensiometers. The soil water potential sensors based on the dielectric constant measurement method were intended for measurements in soils where high soil suction values are expected. Another consideration concerns data redundancy: data had to be collected simultaneously at several depths and along different profiles in order to obtain a complete picture of the temporal-spatial evolution of the different variables during the experiment. Finally, the chosen monitoring equipment should be used in both the small-scale physical landslide models for testing under static (rainfall) and seismic (earthquake) conditions.



**Sensors for measuring the water content of the soil**

The TEROS 10 and TEROS 12 are soil moisture sensors from METER Group (Inc.) for indirect measurement of the VWC of porous materials. Both sensors are based on the capacitance method for predicting the amount of water in the soil based on the electrical properties of the soil and the calibration procedure proposed by Topp et al. (1980). An electromagnetic field (70 MHz oscillating wave) is used to measure the apparent dielectric permittivity ( $\epsilon_a$ ) of the soil. The sensor delivers an oscillating wave to sensor needles that charge according to the dielectricity of the material. The charging time is proportional to the dielectricity of the substrate and the VWC of the substrate (TEROS 10 manual). Depending on the measured charging time, a microprocessor outputs a raw sensor value (RAW) based on the substrate  $\epsilon_a$ . Finally, a calibration equation specific to the substrate is used to convert RAW values to VWC values. The high measurement frequency ensures insensitivity to variations in soil texture and electromagnetic conductivity (TEROS 10 manual). In all tests, a generic calibration equation from the manufacturer for mineral soils was used to predict VWC, based on the RAW output of the METER data logger ZL6:

$$\theta = 4.824 \cdot 10^{-10} \cdot RAW^3 - 1.222 \cdot 10^{-6} \cdot RAW^2 + 2.855 \cdot 10^{-3} \cdot RAW - 2.154 \quad [1]$$

For RAW outputs from the METER data logger, the apparent dielectric permittivity can be used to determine VWC, e.g., with the Topp’s equation (1980):

$$\epsilon = 1.054 \cdot 10^{-4} \cdot e^{2.071 \cdot 10^{-3} \cdot RAW} \quad [2]$$

TEROS 10 has a VWC range for mineral soils of 0.00-0.64 m<sup>3</sup>/m<sup>3</sup> with a resolution of 0.001 m<sup>3</sup>/m<sup>3</sup> and an accuracy of  $\pm 0.03$  m<sup>3</sup>/m<sup>3</sup> in mineral soils with a solution EC<8 dS/m (TEROS 10 manual). On the other hand, TEROS 12 has a slightly larger VWC measurement range (0.00-0.70 m<sup>3</sup>/m<sup>3</sup>) with the same resolution and accuracy as TEROS 10. The temperature range for TEROS 12 is -40 to 60 °C, with a resolution of 0.1°C and a measurement accuracy of  $\pm 1$ °C. The measuring range of the TEROS 12 for total electrical conductivity is 0-20 dS/m with a resolution of 0.001 dS/m and a measuring accuracy of  $\pm 3\%$  (TEROS 12 manual). The volume of the measuring sensitivity of the TEROS 12 with 1010 mL is significantly larger than the measuring volume of the TEROS 10 with 430 mL (Fig. 4). Fig. 5 shows some details on the installation and calibration of the sensors.

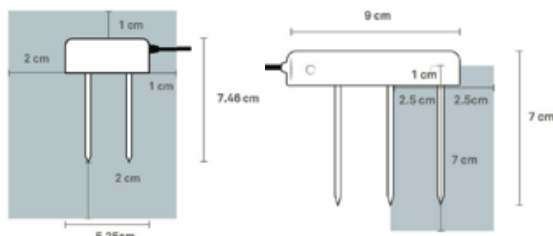


Figure 4 Influence volume for VWC measurements with TEROS 10 (left) and TEROS 12 (right) sensors (TEROS manual).

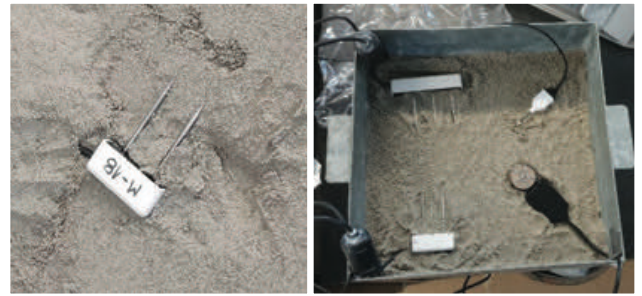


Figure 5 Installation of TEROS 10 during model build-up (left) and calibration for clean sand.

**Sensors for measuring the water potential of the soil**

At some point in the development of the Project, standard tensiometers with vacuum gauges (IR -45 and T1) and digital (TEROS 32) tensiometers, mini tensiometers (TEROS 31) and TEROS 21 soil water potential sensors were purchased to measure soil water potential, depending on project needs and available funds. The non-digitised standard tensiometers IR -45 (Irrometer Company, Inc.) and T1 (MMM Tech Support GmbH & Co. KG) were already purchased in the initial phase of the Project and used for the first test on clean sand (Fig. 6a). The TEROS 32 (Fig. 6b) and TEROS 31 (Fig. 6c) digitised tensiometers (METER Group, Inc.) were procured in the later stages of the Project and used with ZL6 data loggers from METER to continuously record measurements at time intervals of up to 1 minute in other soil materials. The TEROS 21 (METER Group, Inc.) sensors were intended to be used in a measurement range beyond that of standard (mini) tensiometers. In addition to good hydraulic contact of the ceramic with the surrounding soil, which is necessary for accurate measurement of all the above sensors, the tensiometers must be appropriately conditioned before insertion into the soil to achieve the full measuring range and a fast response during the equilibration phases.

TEROS 21 is a maintenance-free matric potential sensor designed for long-term, continuous field measurements (TEROS 21 manual). It uses a similar approach as the VWC sensors TEROS 10 and TEROS 12: The sensor measures the  $\epsilon_a$  of a solid matrix (porous ceramic discs) to determine its water content. Since the  $\epsilon_a$  of porous ceramic discs strongly depends on the amount of water present in the pore spaces and the porous ceramic discs tend to reach a hydraulic equilibrium with the surrounding soil, the measured water content of the solid matrix is used to determine the water potential of the soil based on a known soil water retention curve (SWRC) of porous stones.

The measuring range for the water potential of the TEROS 31 mini-tensiometer is -85 to +50 kPa with a resolution of  $\pm 0.0012$  kPa and an accuracy of  $\pm 0.15$  kPa. It also provides temperature measurements in the range of -30 to +60°C with a resolution of  $\pm 0.01$  °C and an accuracy of  $\pm 0.5$  °C. The TEROS 21 has a measuring range of -9 to -100 000 kPa for water potential and -40 to 60 °C for soil temperature.

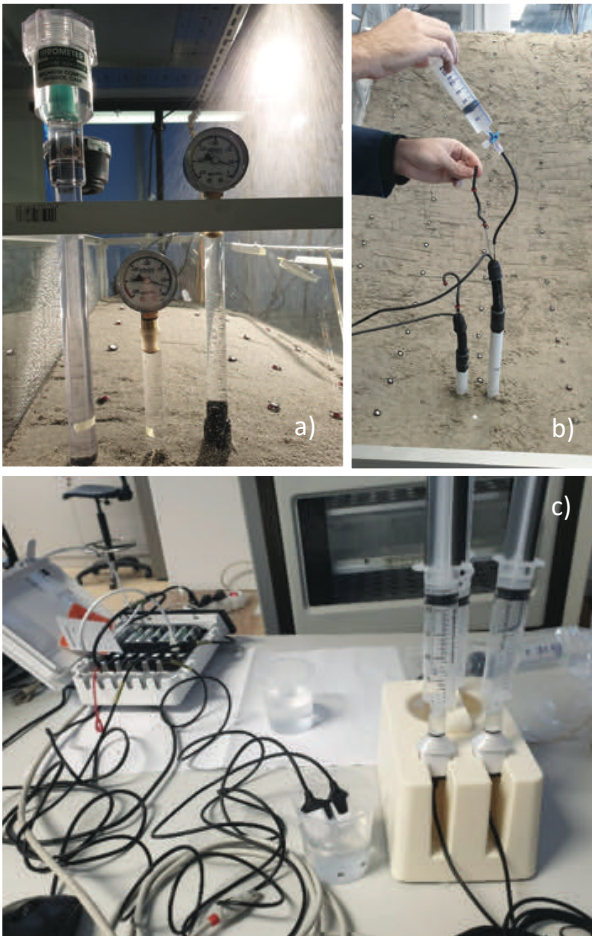


Figure 6 a) Standard, non-digitised IR and T1 tensiometers; b) preconditioning of TERSO 32; and c) TERSO 31 tensiometers.

### Examples of measurement and data analysis

This section presents some examples of hydraulic monitoring results for different soil materials, geometric, initial and boundary conditions. The results are interpreted in the context relevant to the study of the mechanisms and factors driving the instability of rainfall-induced landslides. For two different soil materials and tests, particular details were singled out and discussed in detail.

#### Example 1: Initiation of a sandy slope due to the rise of the groundwater level (GWL)

The first example considers the case of the initiation of a scaled slope built of clean sand with a slope of  $35^\circ$ , subjected to a constant rainfall intensity of 72.6 mm/h until the occurrence of the first instability in the form of a small rotational landslide at the toe of the slope. After the first slide, further instabilities developed in the form of retrogressive slides up to the top of the slope. Fig. 7 shows images taken by the Aramis system at the beginning of the test, together with measurement profiles in the upper (H), middle (M) and lower (L) parts of the model (a); 49 minutes after the start of the rainfall, when the first traces

of GWL reaching the surface in the central part of the base are visible (yellow square in Fig. 7a) (b); 51 minutes after the start of the rainfall, when the entire base is submerged (c); and 56 minutes after the start of the rainfall simulation (d), when the first small rotational landslide occurs at the toe of the slope (bottom right in (d)).

For the same test, the VWC values measured with TERSO 10 and TERSO 12 sensors at the base of the model (L) are shown in Fig. 8. The measurement results indicate that the GWL reaches the sensors installed at 24, 18 and 12 cm after about 23, 39 and 41 minutes, respectively. The readings become constant (indicating saturated conditions) and the maximum value is reached after about 48 minutes at a depth of 6 cm, which is exactly in line with the observations during the experiment and timing reported in Fig. 7. This indicates that, despite certain deviations in the absolute reading values, which could be due to various reasons such as requirements on the calibration procedure of each sensor, different readings of the TERSO 10 and TERSO 12 sensors or different soil densities achieved around the moisture probes, or unequal conditions in terms of contact and presence of gaps between the surrounding soil and the needles of the sensor, can provide useful data on the trend of soil moisture increase in general, providing information on the saturation state during the infiltration process.

#### Example 2: Hydraulic pathways and a reduction in the shear strength of the soil due to infiltration

The second example deals with the hydraulic paths and stress states experienced by the scaled  $40^\circ$  slope of SK15 material under simulated rainfall conditions. In this test, the continuous rainfall intensity of 20.5 mm/h was interrupted by 10-minute breaks to observe the hydraulic response of the soil (Fig. 9).

The numerical markers in Figs. 9 to 12 serve as reference points to follow the course of the experiment and the simulated rainfall conditions when the data are presented in different forms and planes. The number "1" marks the beginning of the experiment, i.e. the start of the rainfall simulation for the first 30 minutes. The numbers "2" and "3" mean that all three nozzles are closed and that the rainfall is stopped for 10 minutes. After that, the rainfall simulation continues for the next 30 minutes with the same intensity as in the previous phase of the test. The number "4" represents the start of another 10-minute rainfall break. Finally, the number "5" indicates the point in the test where the end has been declared and the rainfall simulation has ended.

For the sake of brevity, the hydraulic path in Figs. 10 and 11 is shown only for one monitoring point (M-6) located at 6 cm depth in the middle section of the model (M-profile - the same analogy as in Example 1 is used, i.e., see Fig. 7a). As the monitoring point was equipped with a pair of TERSO 10 and TERSO 31 sensors, both the changes in pwp (or matric suction) and VWC are available throughout the test.

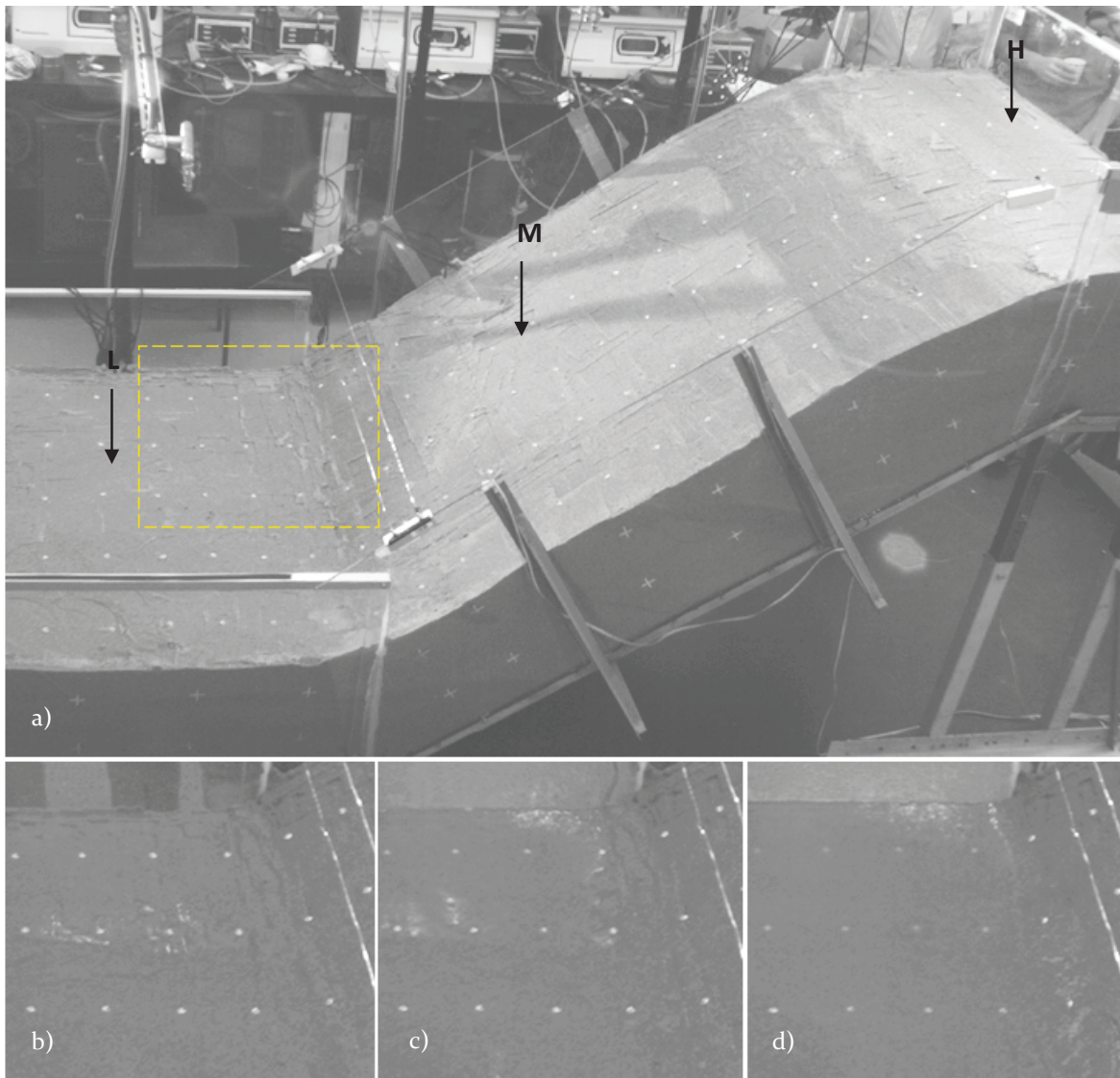


Figure 7 Test with clean sand inclined at 35°, taken with the Aramis system: At the beginning of the test with measurement profiles in the upper (H), middle (M) and lower (L) sections of the slope, respectively (a); 49 minutes after the start of the rainfall: the first traces of GWL reaching the surface in the middle part of the base (b); 51 minutes after the start of the rainfall: the entire base is submerged (c); The first small rotational landslide at the foot of the slope (bottom right), 56 minutes after the start of the rainfall simulation.

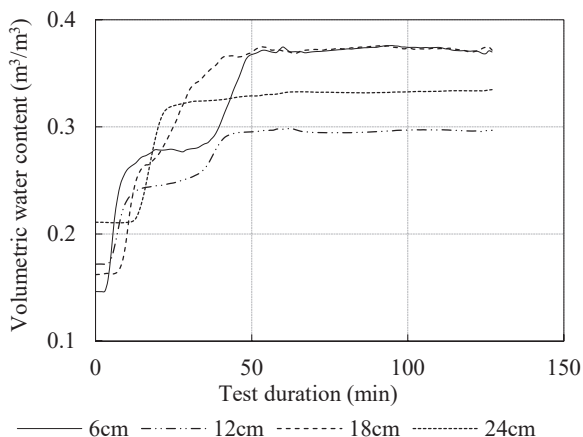


Figure 8 VWC values measured with TEROS10 and TEROS12 sensors at the base (L) section of the model at 6, 12, 18 and 24 cm depth in Example 1.

Fig. 12 shows how infiltration of rainfall affects the shear strength of the soil by reducing the effective stresses at measurement point M-6. The initial stress state and corresponding shear strength, located on the right-hand side of the path, reflect the soil moisture conditions at the start of the test, most of which are reached during model construction and kept constant until the start of the test. With the onset of rainfall infiltration, the VWC increase and dissipation of the matric suction take place in the form of a transient process (Fig. 10; "1"-2"). If a simplified assumption is made that capillarity is the only retention mechanism, a reduction in effective stress during rainfall infiltration can be quantified from the VWC and pwp values observed during the experiment, using, for example, the equation for effective stress by Bishop (1959):

$$\sigma' = \sigma - u_a + \chi(u_a - u_w) \quad [3]$$

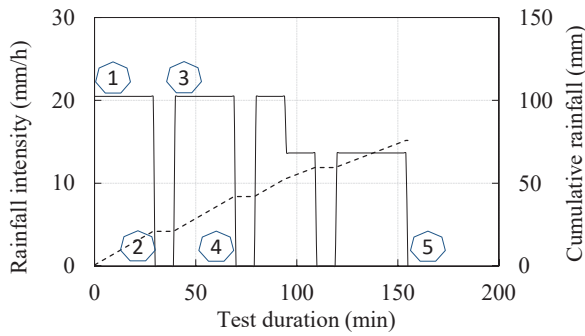


Figure 9 Simulated rainfall in Example 2.

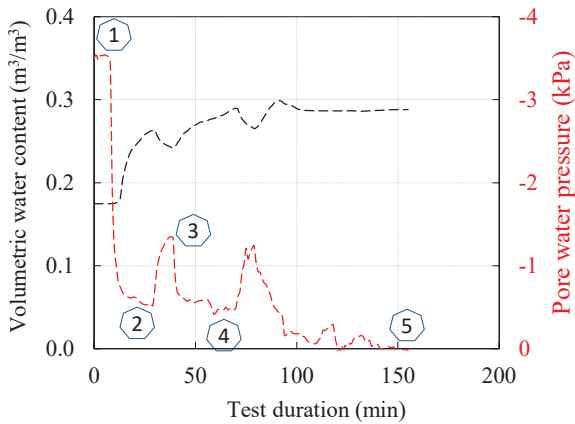


Figure 10 Pwp (matric suction) and VWC values measured at 6 cm depth in the middle (M) section during the test in Example 2.

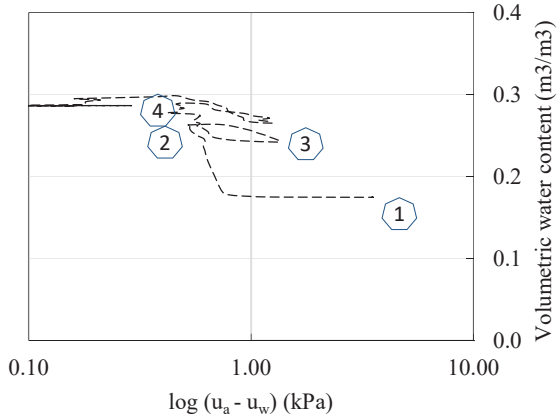


Figure 11 Hydraulic response in  $\log(u_a - u_w)$  vs. VWC plane for measuring point M-6 during the test in Example 2.

where the effective stress parameter  $\chi$  is set equal to the effective degree of saturation. For the residual VWC set to  $\theta_r = 0.05 \text{ m}^3/\text{m}^3$  (an assumption based on observations from other tests on SK15 soil material) and the saturated VWC is set to  $\theta_s = 0.3 \text{ m}^3/\text{m}^3$  (according to the VWC measurements in Fig. 10), the monitored values result in a stress path shown in Fig. 12. Movement from right to left indicates that the matric suction is dissipating, and saturation is increasing. The cross on the left side of the path indicates the effective stress at the observed point at the beginning of the test, without taking into account the correction of the effective stress for unsaturated soil conditions, i.e., as defined in Terzaghi's effective stress equation.

## Discussion and concluding remarks

This paper presented a newly developed platform for physical modelling of small-scale slopes under 1g rainfall conditions, developed at the Faculty of Civil Engineering, University of Rijeka, Croatia, as part of a four-year research project "Physical modelling of landslide remediation constructions' behaviour under static and seismic actions". The main features of the platform and its main components, namely the monitoring equipment and the rainfall simulator, as well as the characteristics of the soil materials used for the construction of the scaled slopes are presented. Since the focus of the paper was on monitoring the hydraulic response of scaled slope models, special attention was given to the sensor network that allows monitoring soil moisture and pore water pressure changes during rainfall simulation. Among the many results obtained through the various research activities of the Project, two interesting examples were singled out to analyse hydrological monitoring data in the context of instability mechanisms of scaled slopes exposed to simulated rainfall.

The first example showed how monitoring changes in soil moisture can provide accurate (apparently also instantaneous) insights into the different stages of moisture content increase during the different phases of transient infiltration as well as the subsequent GWL rise. These results are placed in the context of the initiation of a scaled sandy slope due to the GWL rise. The data on the observed hydraulic response, known initial and boundary conditions can be used as valuable tools for establishing relationships in a scaled slope model, an investigation of the conditions and mechanisms leading to slope failure.

In the second example, the hydraulic paths exhibited by the scaled slope of a sand mixture with 15% kaolin content during a simulated rainfall were investigated. The results show how simultaneous observation of VWC and pore water pressure, when embedded in appropriate working concepts, can provide valuable insights into the hydraulic paths and effective stress states experienced by the model during tightly controlled infiltration conditions during rainfall. Results interpreted in the  $\log(u_a - u_w)$  vs. VWC plane for the monitored point indicate that the soil exhibits hysteresis effects as it undergoes multiple drying-wetting cycles (e.g., points 2-3-4 in Fig. 11). This suggests

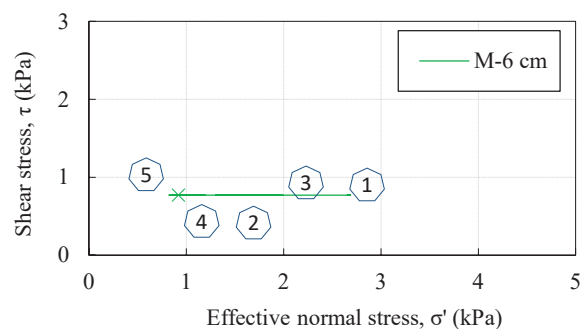


Figure 12 Stress path calculated with Eq. (3) that the monitored point M-6 undergoes during the rainfall infiltration from the Example 2.

the possibility of using small-scale physical slope models to investigate the role of hydraulic hysteresis effects on the behaviour of slopes under different rainfall patterns, in general.

## Acknowledgments

The research presented in this paper was supported by Croatian Science Foundation under the Project IP-2018-01-1503 “Physical modelling of landslide remediation constructions behaviour under static and seismic actions (ModLandRemSS)”. This work has been supported in part by Ministry of Science, Education and Sports of the Republic of Croatia under the project Research Infrastructure for Campus-based Laboratories at the University of Rijeka, number RC.2.2.06-0001. The project has been co-funded from the European Fund for Regional Development (ERDF). These supports are gratefully acknowledged. The authors would like to thank laboratory technician Juraj Stella for his help in conducting the tests.

## References

- Arbanas Ž, Jagodnik V, Peranić J, et al (2020) Physical Model of Rainfall Induced Landslide in Flume Test: Preliminary Results. Proceedings of 4th European Conference on Physical Modelling in Geotechnics - ECPMG 2020, 15-17 March 2020. Luleå, Sweden. pp. 115-122.
- Bitelli G, Dubbini M, Zanutta A, et al (2003) Terrestrial Laser Scanning and Digital Photogrammetry Techniques to Monitor Landslide Bodies. *Interiors*. 1-6.
- Bordoni M, Meisina C, Valentino R, et al (2015) Hydrological factors affecting rainfall-induced shallow landslides: From the field monitoring to a simplified slope stability analysis. *Eng. Geol.* 193: 19-37. <https://doi.org/10.1016/j.enggeo.2015.04.006>
- Casagli N, Dapporto S, Ibsen ML, et al (2006) Analysis of the landslide triggering mechanism during the storm of 20th-21st November 2000, in Northern Tuscany. *Landslides*. 3(1): 13-21. <https://doi.org/10.1007/s10346-005-0007-y>
- Cascini L, Sorbino G, Cuomo S, Ferlisi S (2014) Seasonal effects of rainfall on the shallow pyroclastic deposits of the Campania region (southern Italy). *Landslides*. 11(5): 779-792. <https://doi.org/10.1007/s10346-013-0395-3>
- Casini F, Serri V, Springman SM (2013) Hydromechanical behaviour of a silty sand from a steep slope triggered by artificial rainfall: From unsaturated to saturated conditions. *Canadian Geotechnical Journal*. 50(1): 28-40. <https://doi.org/10.1139/cgj-2012-0095>
- Chen P, Lu N, Formetta G, et al (2018) Tropical storm-induced landslide potential using combined field monitoring and numerical modeling. *J. Geotech. Geoenviron.* 144(11): 05018002. [https://doi.org/10.1061/\(ASCE\)GT.1943-5606.0001969](https://doi.org/10.1061/(ASCE)GT.1943-5606.0001969)
- Comegna L, Picarelli L, Bucchignani E, Mercogliano P (2013) Potential effects of incoming climate changes on the behaviour of slow active landslides in clay. *Landslides*. 10(4): 373-391. <https://doi.org/10.1007/s10346-012-0339-3>
- Cuomo S, Moscariello M, Foresta V (2017) Wetting tests of partially saturated soils under simple shear conditions. *Geotechnique Letters*. 7(2): 197-203. <https://doi.org/10.1680/jgele.17.00019>
- Damiano E, Greco R, Guida A, et al (2017) Investigation on rainwater infiltration into layered shallow covers in pyroclastic soils and its effect on slope stability. *Engineering Geology*. 220: 208-218. <https://doi.org/10.1016/j.enggeo.2017.02.006>
- Feng T, Mi H, Scaioni M, et al (2016) Measurement of surface changes in a scaled-down landslide model using high-speed stereo image sequences. *Photogrammetric Engineering and Remote Sensing*. 82(7): 547-557. <https://doi.org/10.14358/PERS.82.7.547>
- Greco R, Comegna L, Damiano E, et al (2013) Hydrological modelling of a slope covered with shallow pyroclastic deposits from field monitoring data. *Hydrology and Earth System Sciences*. 17(10): 4001-4013. <https://doi.org/10.5194/hess-17-4001-2013>
- Hinds E, Lu N, Mirus B, Wayllace A (2019) Effects of Infiltration Characteristics on Spatial-Temporal Evolution of Stability of an Interstate Highway Embankment. *Journal of Geotechnical and Geoenvironmental Engineering*. 145(9): 02019008. [https://doi.org/10.1061/\(ASCE\)GT.1943-5606.0002127](https://doi.org/10.1061/(ASCE)GT.1943-5606.0002127)
- Jagodnik V, Peranić J, Arbanas Ž (2021) Mechanism of Landslide Initiation in Small-Scale Sandy Slope Triggered by an Artificial Rain. *Understanding and Reducing Landslide Disaster Risk*. Arbanas Ž, Bobrowsky P T, Konagai K, Sassa K, Takara K (eds). Springer, Cham. (978-3-030-60712-8). pp. 177-184.
- Kang S, Cho SE, Kim B, Go GH (2020) Effects of two-phase flow of water and air on shallow slope failures induced by rainfall: Insights from slope stability assessment at a regional scale. *Water (Switzerland)*. 12(3). <https://doi.org/10.3390/w12030812>
- Kim KS, Jeong SW, Song YS, et al (2021) Four-year monitoring study of shallow landslide hazards based on hydrological measurements in a weathered granite soil slope in South Korea. *Water (Switzerland)* 13(17). <https://doi.org/10.3390/w13172330>
- Krzeminska DM, Bogaard TA, Debieche TH, et al (2014) Field investigation of preferential fissure flow paths with hydrochemical analysis of small-scale sprinkling experiments. *Earth Surface Dynamics*. 2(1): 181-195. <https://doi.org/10.5194/esurf-2-181-2014>
- Ladd RS (1974) Specimen Preparation and Liquefaction of Sands. *Journal of the Geotechnical Engineering Division*. 100(10): 1180-1184. <https://doi.org/10.1061/aigeb6.0000117>
- Leung AK, Ng CWW (2013) Analyses of groundwater flow and plant evapotranspiration in a vegetated soil slope. *Can. Geotech.* 50(12): 1204-1218. <https://doi.org/10.1139/cgj-2013-0148>
- Leung AK, Ng CWW (2016) Field investigation of deformation characteristics and stress mobilisation of a soil slope. *Landslides*. 13(2): 229-240. <https://doi.org/10.1007/s10346-015-0561-x>
- Lollino P, Cotecchia F, Elia G, et al (2016) Interpretation of landslide mechanisms based on numerical modelling: two case-histories. *European Journal of Environmental and Civil Engineering*. 20(9): 1032-1053. <https://doi.org/10.1080/19648189.2014.985851>
- Marino P, Santonastaso GF, Fan X, Greco R (2021) Prediction of shallow landslides in pyroclastic-covered slopes by coupled modeling of unsaturated and saturated groundwater flow. *Landslides*. 18(1): 31-41. <https://doi.org/10.1007/s10346-020-01484-6>
- Moriwaki H, Inokuchi T, Hattanji T, et al (2004) Failure processes in a full-scale landslide experiment using a rainfall simulator. *Landslides*. 1(4): 277-288. <https://doi.org/10.1007/s10346-004-0034-0>
- Pajalić S, Peranić J, Maksimović S, et al (2021) Monitoring and data analysis in small-scale landslide physical model. *Applied Sciences (Switzerland)*. 11(11). <https://doi.org/10.3390/app11115040>
- Peranić J, Arbanas Ž (2020) Impact of the wetting process on the hydro-mechanical behavior of unsaturated residual soil from flysch rock mass: preliminary results. *Bulletin of Engineering Geology and the Environment* 79:985-998. <https://doi.org/10.1007/s10064-019-01604-0>
- Peranić J, Mihalić Arbanas S, Arbanas Ž (2021) Importance of the unsaturated zone in landslide reactivation on flysch slopes: observations from Valići Landslide, Croatia. *Landslides*. 18(12): 3737-3751. <https://doi.org/10.1007/s10346-021-01757-8>

- Rahardjo H, Lee TT, Leong EC, Rezaur RB (2005) Response of a residual soil slope to rainfall. *Canadian Geotechnical Journal*. 42(2): 340-351. <https://doi.org/10.1139/t04-101>
- Rahimi A, Rahardjo H, Leong EC (2011) Effect of antecedent rainfall patterns on rainfall-induced slope failure. *Journal of Geotechnical and Geoenvironmental Engineering*. 137(5): 483-491. [https://doi.org/10.1061/\(ASCE\)GT.1943-5606.0000451](https://doi.org/10.1061/(ASCE)GT.1943-5606.0000451)
- Sattler K, Elwood D, Hendry MT, et al (2021) Quantifying the contribution of matric suction on changes in stability and displacement rate of a translational landslide in glaciolacustrine clay. *Landslides*. 18(5): 1675-1689. <https://doi.org/10.1007/s10346-020-01611-3>
- Sitarenios P, Casini F, Askarinejad A, Springman S (2021) Hydro-mechanical analysis of a surficial landslide triggered by artificial rainfall: The Ruedlingen field experiment. *Geotechnique*. 71(2): 96-109. <https://doi.org/10.1680/jgeot.18.P.188>
- Spolverino G, Capparelli G, Versace P (2019) An instrumented flume for infiltration process modeling, landslide triggering and propagation. *Geosciences (Switzerland)*. 9(3). <https://doi.org/10.3390/geosciences9030108>
- Springman SM, Thielen A, Kienzler P, Friedel S (2013) A long-term field study for the investigation of rainfall-induced landslides. *Geotechnique*. 63(14): 1177-1193. <https://doi.org/10.1680/geot.11.P.142>
- Sun P, Wang H, Wang G, et al (2021) Field model experiments and numerical analysis of rainfall-induced shallow loess landslides. *Engineering Geology*. 295. <https://doi.org/10.1016/j.enggeo.2021.106411>
- Take WA, Bolton MD, Wong PCP, Yeung FJ (2004) Evaluation of landslide triggering mechanisms in model fill slopes. *Landslides*. 1(3): 173-184. <https://doi.org/10.1007/s10346-004-0025-1>
- Tohari A, Nishigaki M, Komatsu M (2007) Laboratory Rainfall-Induced Slope Failure with Moisture Content Measurement. *Journal of Geotechnical and Geoenvironmental Engineering*. 133(5): 575-587. [https://doi.org/10.1061/\(asce\)1090-0241\(2007\)133:5\(575\)](https://doi.org/10.1061/(asce)1090-0241(2007)133:5(575))
- Topp GC, Davis JL, Annan AP (1980) Electromagnetic determination of soil water content: Measurements in coaxial transmission lines. *Water Resources Research*. 16(3): 574-582. <https://doi.org/10.1029/WR016i003p00574>
- Yang KH, Nguyen TS, Rahardjo H, Lin DG (2021) Deformation characteristics of unstable shallow slopes triggered by rainfall infiltration. *Bulletin of Engineering Geology and the Environment*. 80(1): 317-344. <https://doi.org/10.1007/s10064-020-01942-4>
- Zanutta A, Baldi P, Bitelli G, et al (2009) Qualitative and quantitative photogrammetric techniques for multi-temporal landslide analysis. *Annals of Geophysics*. 49(4-5). <https://doi.org/10.4401/ag-3117>
- Zhang M, Yang L, Ren X, et al (2019) Field model experiments to determine mechanisms of rainstorm-induced shallow landslides in the Feiyunjiang River basin, China. *Engineering Geology*. 262. <https://doi.org/10.1016/j.enggeo.2019.105348>
- [http://publications.metergroup.com/Manuals/20788\\_TEROS10\\_Manual\\_Web.pdf](http://publications.metergroup.com/Manuals/20788_TEROS10_Manual_Web.pdf) [Last accessed: 13 January 2022].
- [http://publications.metergroup.com/Manuals/20587\\_TEROS11-12\\_Manual\\_Web.pdf](http://publications.metergroup.com/Manuals/20587_TEROS11-12_Manual_Web.pdf) [Last accessed: 13 January 2022].
- <http://library.metergroup.com/Integrator%20Guide/18204%20TEROS%2021%20Gen1%20Integrator%20Guide.pdf> [Last accessed: 12 January 2022].
- [http://library.metergroup.com/Manuals/20799\\_TEROS%2031\\_Manual\\_Web.pdf](http://library.metergroup.com/Manuals/20799_TEROS%2031_Manual_Web.pdf) [Last accessed: 16 January 2022].
- <https://tms-lab.com/product/soil-water-potential-sensor-meter-teros-21/> [Last accessed: 13 January 2022].

# Digital image correlation and the use of high-speed cameras for 3D displacement monitoring in 1g small-scale landslide models

Nina Čeh<sup>(1)</sup>, Josip Peranić<sup>(1)</sup>, Vedran Jagodnik<sup>(1)</sup>, Sara Pajalić<sup>(1)</sup>, Martina Vivoda Prodan<sup>(1)</sup>, Željko Arbanas<sup>(1)</sup>

1) University of Rijeka, Faculty of Civil Engineering, Rijeka, Radmile Matejčić 3, Croatia, +38551265956 (nina.ceh@uniri.hr)

**Abstract** Small-scale physical models of landslides triggered by rainfall and seismic conditions provide a good insight into the initiation and progression of full-scale landslides in nature. In order to track and document the displacements on the surface of the small-scale model, a digital image correlation-based optical measuring system with high-speed cameras is used here. Each model is prepared for the optical measurements by adding specially chosen marker points (pins) that are monitored by a pair of high-speed cameras during each experiment. An additional set of non-high-speed cameras with higher resolution is used to monitor the deformation field on a selected smaller part of the model. This enables to obtain the 3D displacements and velocities of each marker point in order to detect any movement or crack opening on the surface both visually and accurately from the optical measurement results. The described system and established measurement procedure are advantageous as they provide the 3D displacement and velocity data for a large number of points on the surface with less equipment than conventional contact measurement methods. The collected data, in combination with other monitoring sensors, allow the observation of landslide initiation and the analysis of landslide evolution in all parts of the model slope during the sliding process. In this paper we present the measurement procedure and the results obtained optically in selected small-scale experiments.

**Keywords:** landslides, 1g small-scale models, digital image correlation, optical measurement, surface displacements.

## Introduction

Landslides are one of world's major hazards with serious consequences for both infrastructure and human lives. Heavy and prolonged rainfall alone and in combination with dynamic events such as earthquakes increase landslide risk (Petley 2012). Monitored and well-documented laboratory experiments conducted on small-scale landslide models allow a better understanding of the conditions that influence and trigger landslide initiation, as well as the investigation of possible landslide mitigation measures.

Motivated by this, a research project with an extensive experimental programme on small-scale

landslide models was initiated (Arbanas et al 2019; 2020), with an aim to investigate the behaviour of structures used for mitigation of landslides triggered in static or dynamic conditions. Static conditions imply rainfall, whereas dynamic conditions imply earthquake excitation (in combination with significant saturation of the soil in a slope) (Pajalić et al. 2021).

In order to monitor the displacement field at the slope surface in a small-scale landslide model, it is necessary to use an approach that does not interfere with the model's geometry and the mass distribution on the slope. Non-contact optical measurement systems are chosen here, which can replace most of the conventional measurement devices for displacement and strain, as shown in Hunger and Morgenstern (1984), Okura et al. (2002), Moriwaki et al. (2004), Orense et al. (2004), Suits et al. (2009), Scaioni et al. (2013), Ooi et al. (2014), Lu et al. (2015) or Feng et al. (2016).

## Digital image correlation (DIC) and optical measuring system

A 3D optical measuring system comprises a set of two cameras connected to a control unit and a suitable software used to conduct the measurement as well as post-process the data (Dobrilla et al. 2018; Čeh et al. 2018). Here we use two optical measuring systems: GOM Aramis 4M and GOM Aramis 12M. Their characteristics are given in Tab. 1.

The optical measuring procedure consists of calibration (with respect to the measuring volume or size of the monitored surface), surface preparation (which includes dyeing the whole surface or attaching marker points at discrete positions of interest, as shown in Fig. 1), measurement (obtaining pairs of snapshots at a given

Table 1 Characteristics of the two Aramis optical measuring systems.

System	Frame rate	Resolution (pixels)
Aramis 4M	168 fps 1300 fps	2400 × 1728 2400 × 168
Aramis 12M	25 fps 75 fps 100 fps	4096 × 3000 pixels (full resolution) 4096 × 1000 pixels (1/3 of image) Reduced resolution (binning)



Figure 1 Pins with attached markers on the surface of the model.

frequency throughout the experiment) and post-processing of the raw data. The results in the form of displacements of the surface points are obtained based on digital image correlation procedure in the post-processing, whereas the strains, velocities and any other values need to be derived from the displacements.

#### Experimental set-up (experiment on 14 February 2022)

The analysed experiment was conducted on a sandy slope with an angle of  $35^\circ$  exposed to a constant rainfall intensity of  $73 \text{ mm/min}$  (Arbanas et al. 2020; Pajalić et al. 2021b). The optical measuring equipment is positioned as shown in Fig. 2 for all experiments with static conditions: the high-speed Aramis 4M system positioned to capture the entire surface of the model, and the high-resolution 12M system focused on a small part on the side of the model.

The view from the left and right cameras of the 4M system is shown in Fig. 3, with the detected points marked in green. With a grid of 5 by 24 points, a total of 120 points were monitored. The experiment was optically monitored for 2 hours and 11 minutes, with a lower measurement frequency at the beginning, which was increased when surficial movements were detected (Tab. 2).

#### Results

The results are presented for the longitudinal profile shown in Fig. 4, which begins with point 2,1 in the lower part of the slope and ends with point 2,24 in the upper part of the slope. The position data of some markers are lost during the experiment due to water droplets accumulating on the markers and physical obstacles such as the elements of the sprinkler system or the reinforcements of the plexiglass side walls. Longitudinal profile 2 is chosen here for analysis, as all points (except point 2,1) were visible to both cameras. In addition to the profile considered, Fig. 4 shows the location of 2 points that are

analysed in more detail due to their particular location in relation to the development of the landslide: points 2,19 and 2,21 near the upper part of the slope.

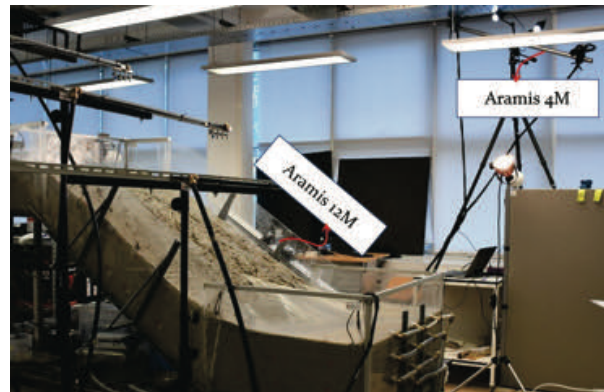


Figure 2 Setup of the optical measuring system in models subjected to static loading conditions (simulated rainfall).

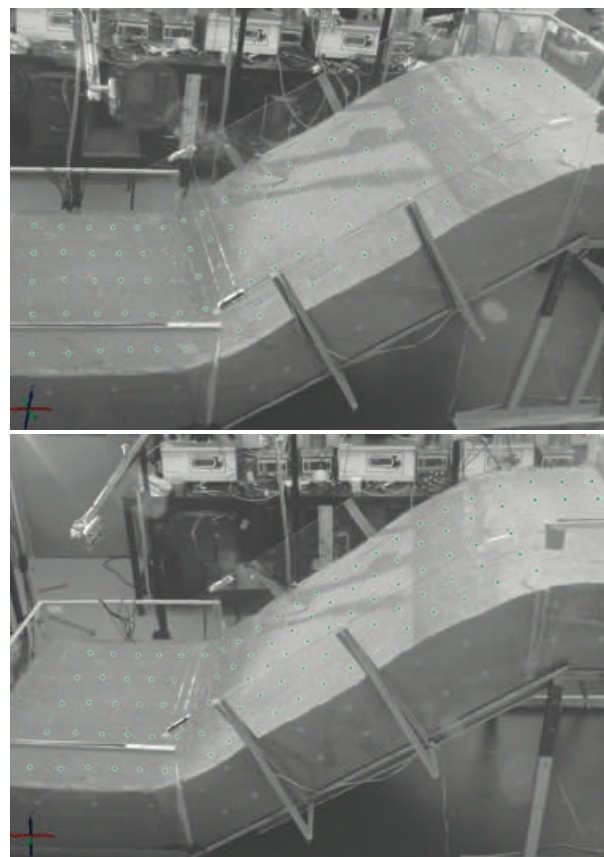


Figure 3 Left-camera (top) and right-camera (bottom) view of the model with monitored points (green dots) (from Maksimović (2020), Pajalić et al. (2021)).

Table 2 The measuring frequency and duration of the optical measuring system.

Part	Measuring frequency	dt	Duration
1	1/300 fps	300 s	52 min 59 s
2	1/10 fps	10 s	1 h 18 min 11 s



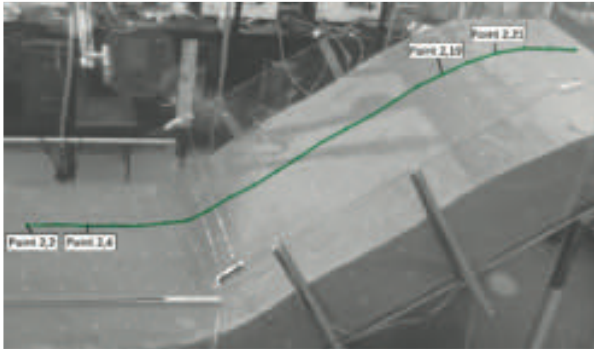


Figure 4 Longitudinal profile no. 2 in the reference stage and the location of the points used for the detailed analysis of the displacement evolution.

The orientation of the coordinate system used with the corresponding signs is given in Fig. 5. The shape of the profile throughout the experiment is shown in Fig. 6 (top). There is clear evidence of the development of larger displacements in the top of the slope between stages 300 and 434, specifically between stages 390 and 434. These stages correspond to a test time of 121 and 128 minutes (or 7262 and 7702 seconds) after the start of the test, i.e. the rainfall simulation (see Fig. 6, bottom). Snapshots of stages 390 and 434 from the left camera are also shown in Fig. 13.

The behaviour of the points in the upper part of the slope in profile 2 is analysed in detail. The points at the top were not covered by water at any time during the rainfall simulation, so, the both cameras were able to take clear photos of them until the end of the experiment. The time courses of the vertical displacements for the two chosen points (2,19 and 2,21) (marked in Fig. 4) are shown in Fig. 7.

Fig. 7 shows that the vertical displacements of the monitored points in the upper part of the slope are close to zero until about 3700 seconds (which roughly corresponds to the time when the first instability at the very bottom of the slope is noticed), which is followed by a slow linear increase until the last part of the experiment, when a rapid non-linear increase occurs, announcing a failure of the slope. This can also be seen in Fig. 8, where the stage (i.e. time) corresponding to the significant increase in displacements and cracking at the top of the slope can be accurately identified.

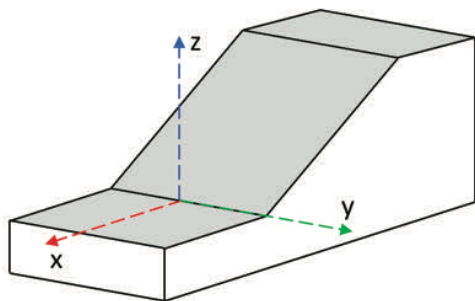


Figure 5 Coordinate system orientation used in the optical measurement and post-processing.

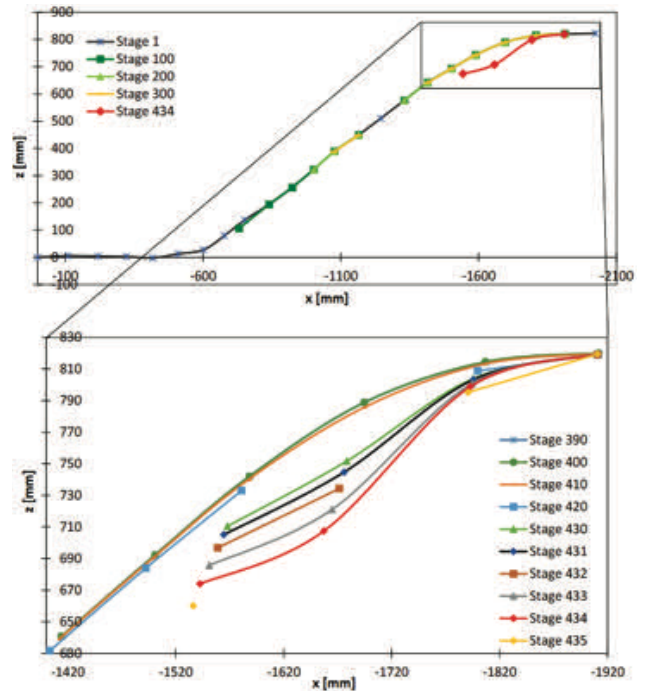


Figure 6 Longitudinal profile no. 2 shown in the x-y plane throughout the experiment (top) and the upper part of the profile between stage 390 and 435 (bottom) (Maksimović 2020; Pajalić et al. 2021).

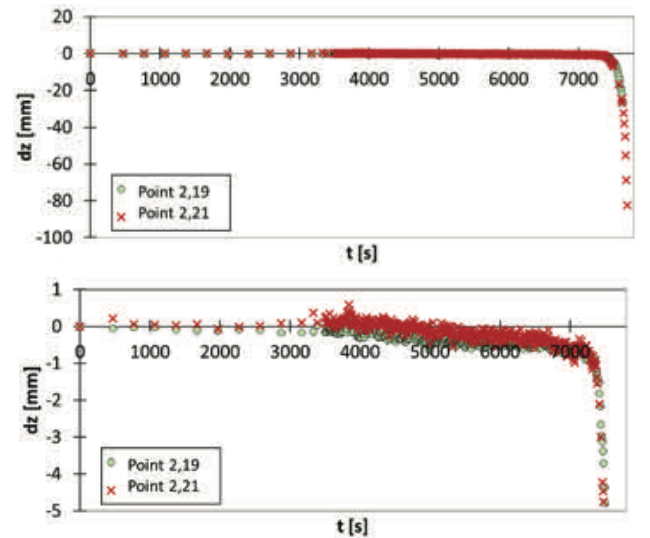


Figure 7 Time course of the displacements along the z-axis of points 2,19 and 2,21 in the upper part of the scaled slope: displacements on a scale up to -100 mm (top) and up to -5 mm (bottom).

A similar behaviour can be observed for the time courses of the horizontal displacements (Figs. 9 and 10). The two horizontal directions are defined so that the x-direction is longitudinal and the y-direction is transverse (see Fig. 5). Positive and negative values in the y-direction mean a movement down and up the slope, respectively, while positive and negative values in the x-direction mean a movement to the right and to the left, respectively, as seen from the crown.

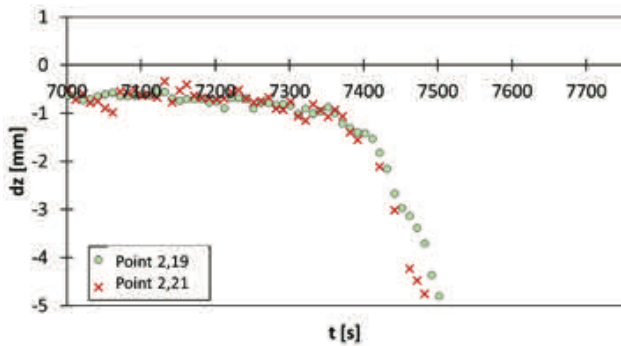


Figure 8 Time course of the displacements along the z-axis of points 2,19 and 2,21 between 116 and 130 minutes in the experiment (7000 and 7800 seconds, respectively).

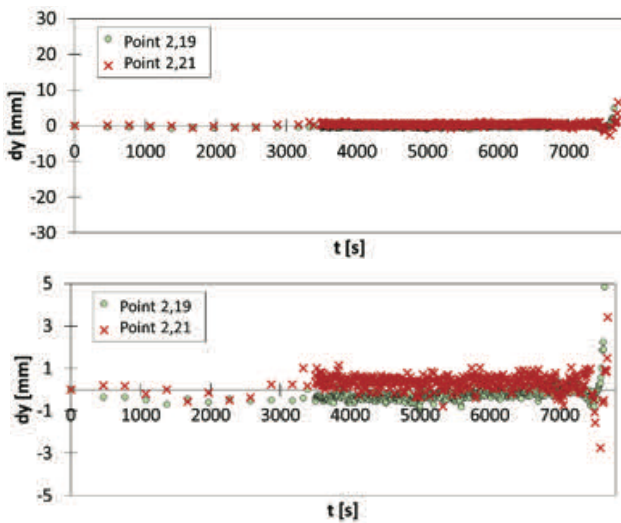


Figure 9 Time course of the displacements along the y-axis of points 2,19 and 2,21 in the upper part of the scaled slope: displacements on a scale up to -30 mm (top) and up to -5 mm (bottom).

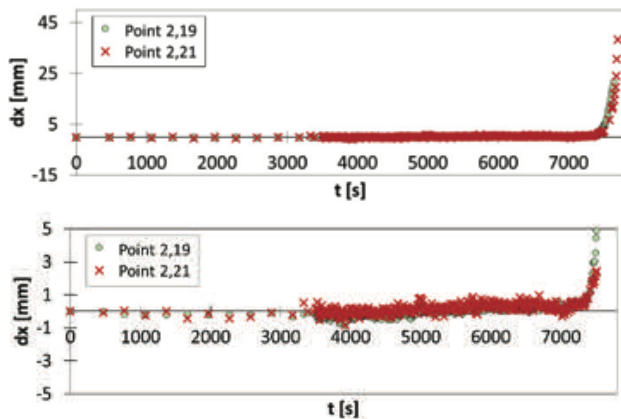


Figure 10 Time course of the displacements along the x-axis of points 2,19 and 2,21 in the upper part of the scaled slope: displacements on a scale from -15 to 45 mm (top) and from -5 to 5 mm (bottom).

We can again notice a slow linear increase between 3700 and 7500 seconds and a significant non-linear

increase after that in x direction displacements, while y direction displacements increase as well, but the displacements are lower. Both directions are better analysed in Figs. 11 and 12, where the time when the displacements start to increase in a non-linear manner can be determined more precisely. A series of nine snapshots taken by the left camera during the last part of the experiment is shown in Fig. 13.

An increase in the vertical displacements of points 2,19 and 2,21 in Figs. 6-11 is presented after  $t=7400$  s. However, as can be seen from stage 420 ( $t=7562$  s) in Fig. 12, it is difficult to see only by visual inspection of the scaled slope model, that the points experience significant movements in the period before they are affected by the retrogressive sliding, as can be clearly seen for stage 430 ( $t=7662$  s) in the same figure. The rapid increase in vertical displacements in Fig. 7 corresponds to the progression of instability in the form of the retrogressive sliding towards the top of the slope. As given in Tab. 2 the optical measurements are obtained from snapshots taken every 10 seconds in this part of the experiment, which results in 10 snapshots between the two stages of interest: stage 420 and 430. The used optical system, however, is able to monitor the model with frequency up to 168 fps, but limited to less than 60 seconds of continuous monitoring due to RAM capacity of the system. It is important to note that the time from the first instability in the model, which took a form of small rotational slide at the foot of the slope due to groundwater level rise, to when the retrogressive slide reached the analysed points at the top

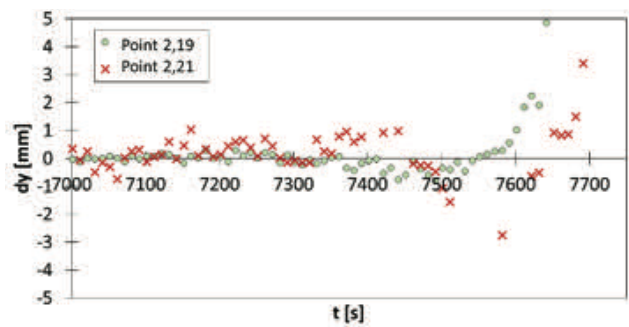


Figure 11 Time course of the displacements along the y-axis of points 2,19 and 2,21 in the upper part of the scaled slope.

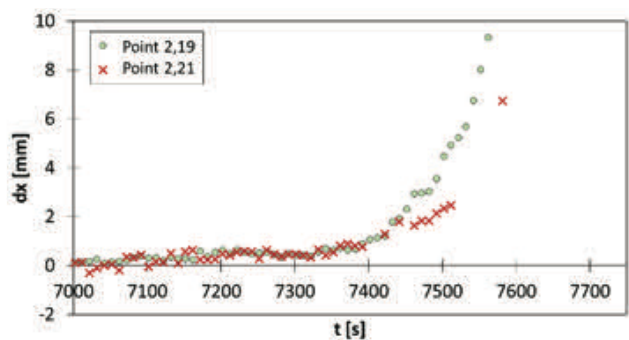


Figure 12 Time course of the displacements along the x-axis of points 2,19 and 2,21 in the upper part of the scaled slope. .

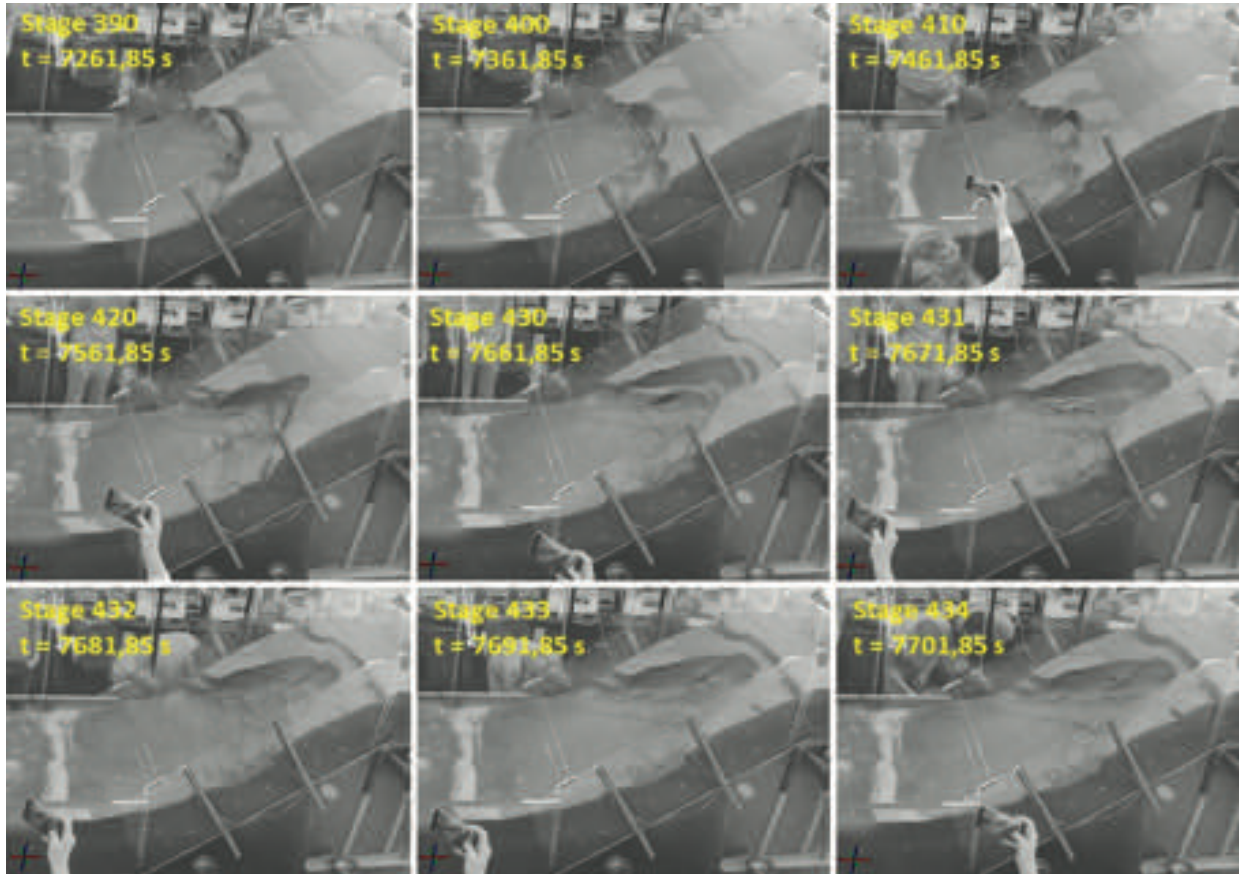


Figure 13 Left camera snapshots on the stages shown in Fig. 4 (corresponding to time between 7261.85 s in stage 390 and 7261.85 s in stage 434).

of the slope was about 60 minutes. Thus, monitoring the entire instability evolution with high frequency is not possible. These observations suggest that in a case where high frequency data of surface displacements are needed, i.e. in the analysis of processes that develop relatively quickly after a long period of inactivity, as is the case with fast moving flow-like landslides, rockfalls and tracking of the rockfall trajectories and/or the impact forces and interaction of fast moving slope material with the landslide remediation structures in scaled slope models etc., the usefulness of the non-contact measurement system, as the one presented in this study, becomes limited due to the requirement of postprocessing of the measurement data. However, the data obtained concurrently with some of the conventional landslide monitoring techniques (geodetic and geotechnical) that allow real-time monitoring of displacements or other quantities that can be used as indications that the scaled slope is approaching conditions of instability could be used to adjust the frequency of data collection and optimise the monitoring process of such non-contact systems during all phases of instability development, i.e. from stable conditions through the phase of initiation of movement, development and to deposition at the end. This could be the approach that would provide adequate

data for a detailed analysis of the instability process and the mechanisms involved.

### Discussion and Conclusions

Displacement data of the slope surface obtained with an optical measurement technique from the experiment conducted on a small-scale sandy slope initiated by simulated rainfall are presented. Two non-contact optical measurement systems, a high-speed camera system and a slower system with higher resolution, are used to monitor the 3D displacements of the surface of the model. Based on sets of snapshots from two precisely tuned cameras, the displacements of the marker points on the slope are obtained, post-processed and analysed.

One of longitudinal profiles of interest is presented here, where it is easy to keep a track of the profile shape throughout an experiment. Furthermore, the displacement data of two selected points at the top of the slope, combined with a series of snapshots, show how a significant increase in displacement can be detected and used to accurately detect any instability or cracking. Such an optical measurement method using high-speed camera systems in combination with other monitoring sensors installed in the model can provide much important and

well-documented data describing the behaviour of the surface in a small-scale landslide test.

This paper presented the results of a single test conducted to present the basic data that can be provided by this type of monitoring. The possibilities that the digital image correlation offers and the use of high-speed cameras for 3D displacement monitoring in small-scale landslide models are far greater and will be used in further analyses of landslide initiation and evolution in subsequent steps of the Project. The precision offered by this monitoring system will enable the following data that cannot be registered by the human eye: measurements of the deformation caused by the change in the unit weight of the soil and the stress changes during the infiltration of the rain; 3D displacements of the marker points on the slope surface, taking into account all the components of the displacement vectors; identification of the displacement rate in different parts of the slope and cross-relationships with data obtained from other monitoring sensors (tensiometers, accelerometers, MEMS, etc.). Analyses of these data will ensure significantly better insight into landslide initiation and evolution of landslides in small-scale landslide models as well as in real landslides on slopes made of similar soil materials.

## Acknowledgments

This work is supported by Croatian Science Foundation under the Project IP-2018-01-1503 Physical modelling of landslide remediation constructions behaviour under static and seismic actions (ModLandRemSS).

## References

- Arbanas Ž, Jagodnik V, Peranić J, et al (2020) Physical Model of Rainfall Induced Landslide in Flume Test: Preliminary Results. Proceedings of 4th European Conference on Physical Modelling in Geotechnics - ECPMG 2020, 15-17 March 2020. Luleå, Sweden. pp. 115-122.
- Arbanas Ž, Pajalić S, Jagodnik V, et al (2019) Development of physical model of landslide remedial constructions' behaviour. Proceedings of the 4th Regional Symposium on Landslides in the Adriatic - Balkan Region, 23-25 October 2019. Sarajevo, Bosnia and Herzegovina. pp 103-108
- Čeh N, Jelenić G, Bićanić N (2018) Analysis of restitution in rocking of single rigid blocks. *Acta Mechanica*. 229:4623-4642. <https://doi.org/10.1007/s00707-018-2246-8>
- Dobrilla S, Čeh N, Tuhtan M, Jelenić G (2018) Eksperimentalna analiza odziva grednog nosača na nejednoliku pobudu oslonaca Experimental Analysis of Structure Response to Non-uniform Support Excitation. *Zbornik radova*. 20:175-188. <https://doi.org/10.32762/zr.20.1.11>
- Feng T, Mi H, Scaioni M, et al (2016) Measurement of Surface Changes in a Scaled-Down Landslide Model Using High-Speed Stereo Image Sequences. *Photogrammetric Engineering & Remote Sensing*. 82:547-557. <https://doi.org/10.14358/PERS.82.7.547>
- Hunger O, Morgenstern NR (1984) Experiments on the flow behaviour of granular materials at high velocity in an open channel. *Géotechnique*. 34:405-413. <https://doi.org/10.1680/geot.1984.34.3.405>
- Lu P, Wu H, Qiao G, et al (2015) Model test study on monitoring dynamic process of slope failure through spatial sensor network. *Environmental Earth Sciences*. 74:3315-3332. <https://doi.org/10.1007/s12665-015-4369-8>
- Maksimović S (2020) Analiza površinskih pomaka na modelu klizišta. University of Rijeka, Faculty of Civil Engineering, Rijeka, Croatia. (in Croatian).
- Moriwaki H, Inokuchi T, Hattanji T, et al (2004) Failure processes in a full-scale landslide experiment using a rainfall simulator. *Landslides*. 4:277-288. <https://doi.org/10.1007/s10346-004-0034-0>
- Okura Y, Kitahara H, Ochiai H, et al (2002) Landslide fluidization process by flume experiments. *Engineering Geology*. 66:65-78. [https://doi.org/10.1016/S0013-7952\(02\)00032-7](https://doi.org/10.1016/S0013-7952(02)00032-7)
- Ooi GL, Wang YH, Tan PS, et al (2014) An instrumented flume to characterize the initiation features of flow landslides. *Geotechnical Testing Journal*. 37(5). <https://doi.org/10.1520/GTJ20130158>
- Orense R, Shimoma S, Maeda K, Towhata I (2004) Instrumented Model Slope Failure due to Water Seepage. *Journal of Natural Disaster Science*. 26:15-26. <https://doi.org/10.2328/jnds.26.15>
- Pajalić S, Peranić J, Maksimović S, et al (2021) Monitoring and Data Analysis in Small-Scale Landslide Physical Model. *Applied Sciences*. 11:5040. <https://doi.org/10.3390/app11115040>
- Petley D (2012) Global patterns of loss of life from landslides. *Geology*. 40:927-930. <https://doi.org/10.1130/G33217.1>
- Scaioni M, Lu P, Feng T, et al (2013) Analysis of spatial sensor network observations during landslide simulation experiments. *European Journal of Environmental and Civil Engineering*. 17:802-825. <https://doi.org/10.1080/19648189.2013.822427>
- Suits LD, Sheahan TC, Olivares L, et al (2009) An Instrumented Flume to Investigate the Mechanics of Rainfall-Induced Landslides in Unsaturated Granular Soils. *Geotechnical Testing Journal*. 32:101366. <https://doi.org/10.1520/gtj101366>

# Mechanism of rainfall induced landslides in small-scale models built of different materials

Martina Vivoda Prodan<sup>(1)</sup>, Josip Peranić<sup>(1)</sup>, Sara Pajalić<sup>(1)</sup>, Vedran Jagodnik<sup>(1)</sup>, Nina Čeh<sup>(1)</sup>, Željko Arbanas<sup>(1)</sup>

1) University of Rijeka, Faculty of Civil Engineering, Rijeka, Radmile Matejčić 3, Croatia, +3851265938 (martina.vivoda@gradri.uniri.hr)

**Abstract** Physical modelling of landslides by analysing the behaviour of small-scale landslide models subjected to artificial rainfall can be divided into modelling under 1g conditions and under increased acceleration (n times gravity) in a centrifuge. In this paper, the landslide initiation, progression, and deposition caused by artificial rainfall in three small-scale models built with sand or sand-kaolin mixtures at the same slope angle will be described. The evolution of landslides is monitored by observation of volumetric water content, matric suction, and pore water pressure, as well as by monitoring slope deformations and failure development. Analysis of the factors affecting the landslide initiation, propagation and their relationship to the slope material, the infiltration process, and the overall resistance of the soil in a slope in terms of soil strength, effective pressure and the contribution of matric suction in the unsaturated part of the slope will be discussed. The main observations from the results of the tests carried out in relation to the initiation and development of the observed instabilities of sandy and clayey slopes are given.

**Keywords** landslide, small-scale model, artificial rainfall, sandy and clayey slopes

## Introduction

Landslides are hazardous motions of a mass of rock, earth or debris down the slope (Cruden 1991) that threaten vulnerable human settlements in different environments all around the world. For a long time, modelling of landslide initiation was based only on numerical modelling results using soil strength parameters obtained from soil laboratory testing in conventional laboratory apparatus. Physical modelling of landslide behaviour using small-scale models was introduced as a solution in different landslide researches in 1970s and 1980s in Japan (Oka 1972; Kutara and Ishizuka 1982) on natural slopes exposed to artificial rainfall. Laboratory experiments on landslide behaviour in a scaled physical models (known as flume or flume test) began in the 1980s in Canada (Hungry and Morgenstern, 1984), Japan (Yagi et al. 1985) and Australia (Eckersley 1990) under 1g conditions. Small-scale landslide modelling under increased acceleration in a

geotechnical centrifuge has also been successfully adopted (e.g. Kimura 1991; Take et al. 2004), but under circumstances of centrifuge limitations.

This paper discusses small-scale landslide modelling under 1g loading conditions. The main task of landslide physical modelling was research of initiation, propagation and accumulation of fast flow-like slides caused by the infiltration of rainfall in a slope and fluidification. This research was conducted within the Project “Physical modelling of landslide remediation constructions’ behaviour under static and seismic actions” at the University of Rijeka, Croatia (Arbanas et al. 2019). The main objective of the Project is modelling and analysing behaviour of landslide remedial measures in physical models of scaled landslides under static (Arbanas et al. 2020) and seismic conditions. This paper presents the results of landslide initiation tests in sandy and clayey scaled slopes subjected to artificial rainfall. Landslide development was monitored by observing surface displacements using structure-from-motion (SfM) photogrammetry, terrestrial laser scanner (TLS) and a pair of high-speed cameras, and by observing landslide movements within the displaced mass using accelerometers. Pore water pressure and soil moisture sensors were used to observe the hydraulic response of a slope.

## Materials and methods

The physical model of a scaled slope was designed to enable the initiation of a landslide by controlled artificial rainfall and equipped with adequate photogrammetric equipment and a complex sensor network with ability to measure displacements, soil moisture and pore water pressures within a slope, Fig. 1 (Arbanas et al. 2020; Jagodnik et al. 2021). The dimensions of the slope model are 1.0 m (width) x 2.3 m (length) x 0.5 m (height). The maximum depth of the soil material in the slope was adopted to be 30 cm. Slope inclination is adjustable from 20° to 45°. The series of tests described in this paper were carried out on slope inclination of 35° with three different soil types as a slope material. To prevent possible sliding of the soil mass at the contact with the model base, the geogrid mesh is fixed to the flume base to increase friction.

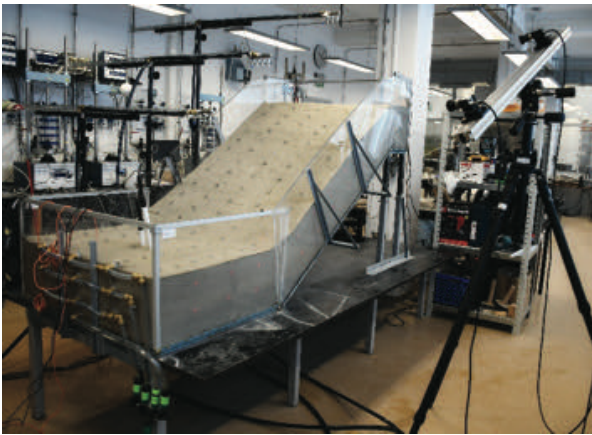


Figure 1 Photo of the small-scale landslide model at 35°.

### Soil material properties

Three different and simple materials are selected to build in the small-scale physical model: sand and sand-kaolin mixture with 10% and 15% of mass of kaolin. The fine-grained (0 – 1 mm) Drava River sand was chosen as the base material to represent cohesionless slopes. Another material is a mixture of the base material with 10% and 15% by mass of industrial kaolin and represents the behaviour of fine-grained, cohesive materials with stable cohesion. Kaolin is chosen as clay with low plasticity and a relatively well graded grain size distribution curve and is not too sensitive to changes in water content. The Mohr-Coulomb strength parameters-friction angle and cohesion were determined in a direct shear apparatus at low normal stresses similar to those in the slope model, while hydraulic conductivity was determined using the falling head test method. The grain size distribution curves of the described materials are presented in Fig. 2, while the basic physical – mechanical properties of the described materials and the initial conditions at the start of the tests are given in Tab. 1.

### Testing procedure

The three materials previously described were built in slopes with an inclination of 35°, by compaction of 5 layers, each 6 cm thick, until a 30 cm high slope was completed. The prepared sandy material with a water content of  $w=2\%$  and the sand-kaolin mixture with 10% and 15% by mass of kaolin with a water content of  $w=5\%$  and  $w=8.1\%$ , respectively, were installed using the under-compaction method (Ladd 1978). The installation of the material at the targeted initial water contents ensured the same initial densities. The higher initial water content for the sand-kaolin mixture was necessary for effective compaction, as previously determined by the Proctor test. The initial water content could not be maintained during model construction; model construction extends over several days and evaporation and internal redistribution of water content are the reasons for the non-uniform water content distribution in a model at the start of the tests. Each layer was compacted using the manual compactor to the medium dense conditions of relative density  $Dr=50\%$  for

sandy slopes and sand-kaolin mixture with 10% of mass of kaolin, and  $Dr=75\%$  for sand-kaolin mixture with 15% of mass of kaolin. Before placing the next layer, the surface of the previous layer was raked and sprayed with a small amount of water to maintain the initial moisture content and achieve good contact between the particles of the two layers. In order to achieve homogeneity of the material in the slope and relatively uniform conditions in the build-up material, the model was built up in three segments – lower (L), middle (M) and upper (H) parts, building up the material from the foot to the top of the slope.

The monitoring system established in a physical model follows the principles used in the observation of real landslides and consists of a geotechnical and a geodetic monitoring systems. The geotechnical monitoring system comprises of a complex network of miniature sensors equivalent to the geotechnical monitoring devices used in the field (Wieczorek and Snyder, 2009). Thus, accelerometers, soil water content sensors, mini-

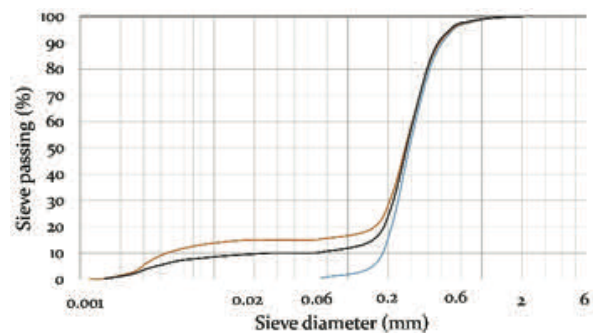


Figure 2 Grain size distribution curves of the sand (blue), sand-kaolin mixture with 10% kaolin by mass (black) and 15% kaolin by mass (brown).

Table 1 Basic physical – mechanical properties of the sand and sand-kaolin mixture with 10% and 15% of mass of kaolin built in the small-scale model and the initial conditions at the start of a test.

Parameter	Sand	Sand-kaolin mixture	
		10% of mass of kaolin	15% of mass of kaolin
Specific gravity, $G_s$	2.70	2.69	2.67
Dry density, $\rho_d$ (g/cm <sup>3</sup> )	1.52	1.43	1.51
Total density, $\rho_t$ (g/cm <sup>3</sup> )	1.55	1.50	1.63
Effective particle size			
$D_{10}$ (mm)	0.19	0.038	0.056
$D_{60}$ (mm)	0.37	0.31	0.207
Uniformity coefficient, $c_u$	1.947	8.16	54.107
Minimum void ratio, $e_{min}$	0.641	0.647	0.544
Maximum void ratio, $e_{max}$	0.911	1.121	1.430
Hydraulic conductivity, $k_s$ (m/s)	1E-05	6.78E-06	3.5E-06
Friction angle, $\phi$ (°)	34.9	31.3	31.75
Cohesion, $c$ (kPa)	0	3.9	4.4
Initial porosity, $n_i$	0.44	0.469	0.434
Initial void ration, $e_i$	0.78	0.884	0.766
Initial relative density, $Dr_i$	0.5	0.5	0.75
Initial water content, $w_i$ (%)	2	5	8.1

tensiometers and pore-pressure transducers were installed to measure soil moisture, pore pressure, displacement, suction, etc. All sensors used in the tests are constantly connected to data loggers for continuous data collection during the time of the test.

The water-related sensors, which are the focus of this paper, are positioned along the central line of the slope to avoid the possible influence of the plexiglass sides of the model on the measured values. Similar types of sensors to monitor volumetric water content and soil potential as our monitoring of the small-scale model were used by Huang and Lo (2013) and Wu et al. (2017). The locations of the sensors are chosen as critical points in the slope model for observation of slope movements and changes in moisture content. The sensors are installed on different depths of 6, 12, 18 and 24 cm along the same profile to provide data at the same cross-section that enables validation and numerical analysis of the observed landslide initiation.

The geodetic monitoring system is based on an innovative photogrammetric equipment for multi-temporal landslide analysis (Zanutta et al., 2006) of image sequences obtained by a pair of high-speed stereo cameras. Terrestrial laser scanning and Structure-from-Motion (SfM) photogrammetry surveys enable the surface of the slope model to be determined in the pre- and post-slide phases. A detailed description of the equipment used in the geotechnical monitoring system is described in Pajalić et al. (2021).

The landslide initiation and motion caused by rainfall infiltration in the small-scale model is fully controlled by the rainfall simulator that was constructed as part of the Project. The rainfall simulator consists of three sprinkler branches, each equipped with four different axial-flow full-cone nozzles with a spray angle of 45° or 60°. Each branch has been placed at such a height that the water can reach the edges of the plexiglass sides without creating too much water on the edges or water coming out of the model. A wide range of rainfall intensities and the possibility to change the location of the rainfall by opening or closing valves on each of the branches allows the modelling of different rainfall patterns and different rainfall intensities applied to the slope model (Arbanas et al. 2020).

After installing the soil in the slope model and the monitoring equipment within the slope, the slope models were exposed to artificial rainfall from three nozzles, one nozzle in each part of the slope – upper (H), middle (M) and lower (L) parts. The slopes were exposed to different rainfall intensities (Fig. 3): rainfall on the sandy slopes had an intensity of 73 mm/h, while the slopes built of sand-kaolin mixture with 10% and 15% mass of kaolin had intensities of 22 mm/h. The selection of rainfall intensities was based on infiltration conditions and the main requirement was that all water at the point of contact on the model surface is infiltrated without forming surface runoff. The applied intensities were at the upper precipitation values that can be infiltrated in a soil.

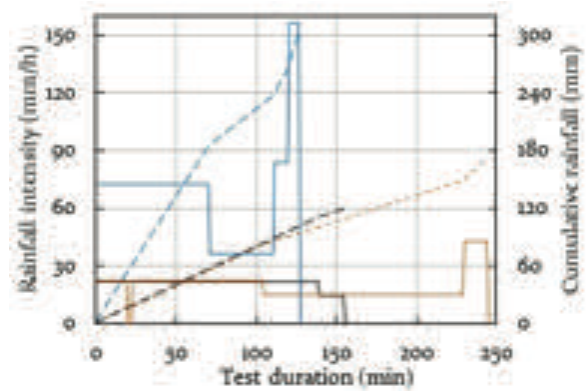


Figure 3 Simulated rainfall in a small-scale model built in sand (blue), a sand-kaolin mixture with 10% by mass of kaolin (black) and 15% by mass of kaolin (brown).

### Testing results

The basic data of the three performed tests are given in Tab. 2, and the results of the tests are presented in the following text: clean sand was used in Test 1, while the mixture of sand with 10% of mass of kaolin was used in Tests 2 and mixture of sand with 15% of mass of kaolin in Tests 3.

After the initial establishment of a constant rainfall intensity and a stable infiltration process, the models were exposed to constant intensity rainfall until the slope failed or until the end of the test. The end of the test was declared when further retrogressive sliding was no longer possible: after 126 min for the sandy slope (Fig. 4d), and after 155 and 245 minutes for the slopes built of sand-kaolin mixture with 10% and 15% kaolin by mass, respectively (Figs 4e and 4f).

In the test conducted on sandy slope, the slope remained stable until the ground water level reached the slope surface in the foot of the slope and consequently caused a decrease in the soil shear strength, sliding and further retrogressive landslide development towards the top of the slope. Test was continued until the retrogressive slides reached the top of the slope. The time from the rainfall start to the first signs of instability in the slope foot was relatively long - 62 minutes (Fig. 4a), while the retrogressive development to the top of the slope occurred in the following 30 minutes.

Table 2 Basic information on the performed tests.

Test no.	Test 1	Test 2	Test 3
Slope angle	35°		
Material	sand	sand + 10% kaolin	sand + 15% kaolin
Rainfall intensity (mm/h)	73/55	22	22
Time to initiation (min)	62	24	35
Test duration (min)	126	155	245

In the tests conducted on slopes with sand-kaolin mixture, the failure mechanism was completely different from that observed for sandy slope. Although the rainfall intensities were significantly lower than the intensities on sandy slope, the first signs (cracks) of sliding in test on slopes with sand-kaolin mixture appeared relatively quickly after the rainfall began - 24 and 35 minutes for the sand-kaolin mixture with 10% and 15% by mass of kaolin, respectively (Figs. 4b and 4c). After appearance of the first cracks, the further retrogressive landslide development occurred to the top of the slope. This development took place without significant movements in the slope; just new tension cracks were opening. The new stage occurred at the moment when the ground water level reached the slope surface in the middle part of the slope, forming small springs and surface flows. At this moment, the joint mechanism of sliding and surface erosion started with a relatively fast retrogressive instability development up to the top of the slope.

The described superficial signs of sliding initiations as well as the causes of their occurrences can be explained from the results of the continuous volumetric water content (VWC) monitoring presented in Fig. 5, as well as the measurement of matric suction and temperature, presented in Fig. 6. The results at part H are not presented as the least important. The changes in VWC in the different parts of the slope indicate the progress of the infiltration process until the saturation of a soil and formation of a ground water level; knowledge of this

process allows better understanding of the sliding initiation.

After analysis of the measured results, the landslide processes could be explained as follows. (i) There is no homogeneous moisture distribution in the sand model due to retention characteristics of the sandy material. All sensor measurements showed slightly higher initial values of VWC from the start of the test, starting from an initial moisture content of 2% that corresponds to VWC of  $0.03 \text{ m}^3/\text{m}^3$  at the moment of sand material preparation. The highest difference can be seen at the sensor at 24 cm depth, Fig. 5d, and this non-uniform water content distribution in the model at the start of the test can be explained due to hydraulic properties of the sand and the time of model construction that extends over several days with evaporation and internal redistribution of water content taking place simultaneously. (ii) In the lowest part of the slope, at the deepest sensors (M—24 cm), in Test 1 (Fig. 5d), the initial value of VWC increases sharply and is then constant caused by soil full saturation. However, in the M part, the water level increases but does not reach the maximum value for some time, and from 20 to 45 min there is a steady-state flow. When the ground water level reaches the soil surface in the slope foot, the water level in the M part rises and the material saturation begins in the upper part of the model. (iii) Rising of the ground water level in the middle part of the slope is noticeable at the deepest sensors (M—24 cm), in Test 1 after 15 min of rainfall, in Test 2 after 51 min of rainfall, and in Test 3 after 32 min of rainfall.

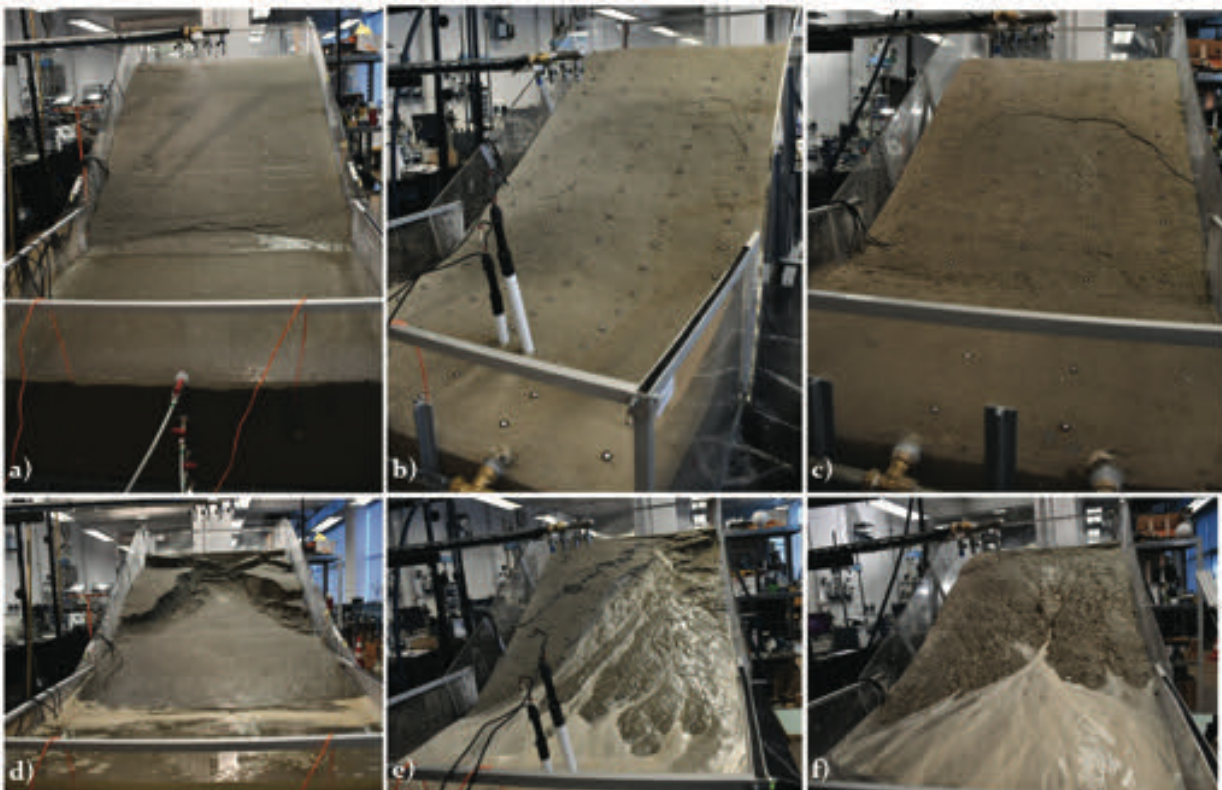


Figure 4 Photos of, a),b), c) initiation of instabilities and d), e), f) end of the test in the small-scale model at  $35^\circ$  built of clean sand-Test 1, sand-kaolin mixture with 10% by mass of kaolin-Test 2 and 15% by mass of kaolin-Test 3, respectively.



The rising of the ground water level continued until the water level reached the surface of the slope foot, firstly for the sandy slope, then for the slope built in sand +15% kaolin mixture, and finally for the slope built in sand+10% kaolin mixture (Fig. 5d). (iv) Faster increase in VWC was observed in shallow layers in both parts of the slope for both the sandy and clayey slopes except in the L part of the slope built from sand+10% kaolin mixture. (v) Seepage through the slope was established with suction decreasing (Fig. 6), the slope was saturated from the bottom layers to the slope surface, leading to the loss of the soil strength in the foot of the slope.

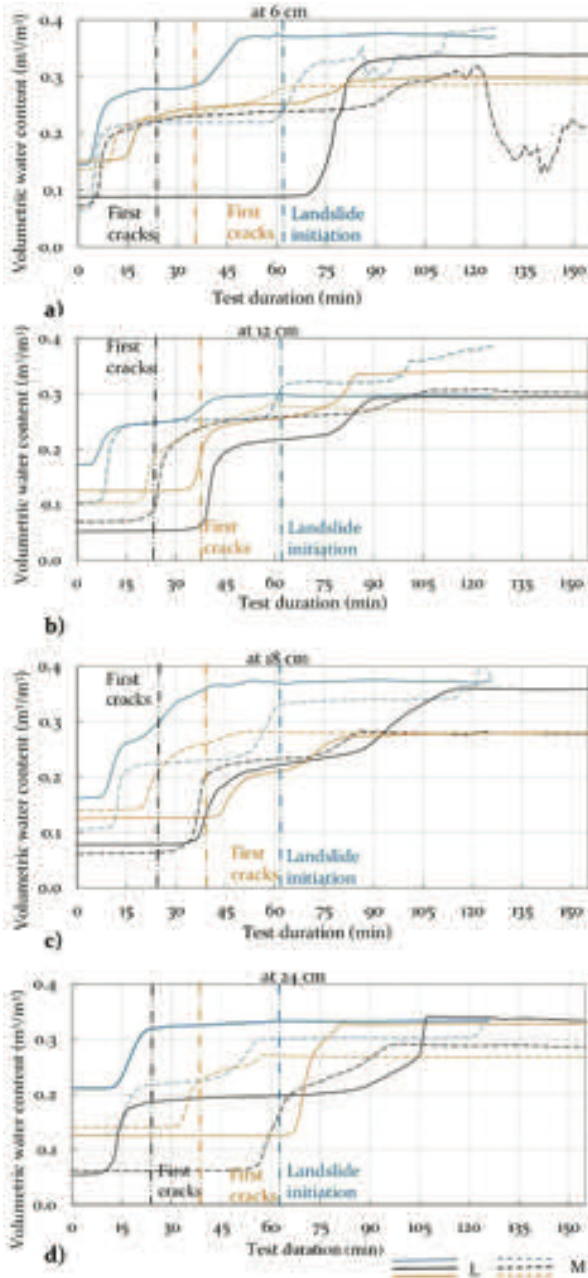


Figure 5 Volumetric water content (VWC) in tests on clean sand (blue)-Test 1, sand-kaolin mixture with 10% by mass of kaolin (black)-Test 2 and 15% by mass of kaolin (brown)-Test 3 in the middle (M), and lower (L) part of the slope at a) 6 cm, b) 12 cm, c) 18 cm, d) 24 cm from the slope surface.

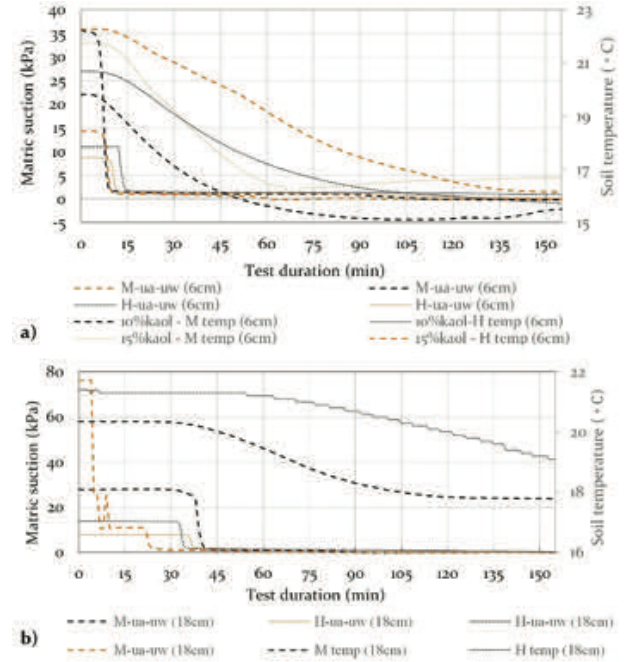


Figure 6 Matric suction and temperature measurements in tests on sand-kaolin mixture with 10% by mass of kaolin (black)-Test 2 and 15% by mass of kaolin (brown)-Test 3, in upper (H) and middle (M) parts at a) 6 cm and b) 18 cm from the slope surface.

(vi) Fig. 6 shows that the soil temperatures at depths of 6 and 18 cm decreases proportionally to the increase in VWC as the water level reached certain layers of the slope, which served as a confirmation of establishing of the ground water level in the slope. (vii) In the sandy slope with a relatively high hydraulic conductivity, the VWC increases due to infiltration until the full saturation in the deepest part of the slope, forming the water table. As it is established, a flow down the slope started causing a rapid rise in the groundwater level in the lower part of the slope. This led to a decrease in the soil shear strength with complete loss of matric suction, failure and further retrogressive landslide development to the top of the slope. (viii) For slopes made of sand-kaolin mixture with lower hydraulic conductivity and relatively higher retention capability, the process of saturation firstly took place in the surface layer, leading to an increasing in weight of the surface layer and causing cracks and shallow instabilities in the middle part of the slope without significant movements. The cracks opening allowed water to penetrate in deeper layers and form separated saturated zones in the slope, but with a matric suction maintained in the most parts of the slope. In some isolated local zones, near the existing cracks, the ground water level rises to the surface, causing springs and surface flows.

### Conclusions

This paper presents the results on landslide initiation in small-scale slopes exposed to artificial rainfall. The results of the conducted tests on slopes built of three different

types of soil materials at the slope angle of  $35^\circ$  are presented. The observed failure mechanisms are described and explained, as well as the infiltration process based on the results of the volumetric water content measurements. The results presented form the basis for the numerical analyses and a better understanding of the processes and initiation of landslides in small-scale slope models.

Besides the monitoring results presented in this paper, several additional measurements have been carried out and are still being analysed. The results obtained by geodetic monitoring and the observations of surface movements should complete the analyses carried out, while the analyses of changes in matric suction, which are only briefly described in this paper, will play an important role in fully explaining the process of landslide initiation.

## Acknowledgments

This research was funded by Croatian Science Foundation under the Project IP-2018-1503 Physical modelling of landslide remediation constructions behaviour under static and seismic actions (ModLandRemSS). The part of the laboratory equipment used for laboratory testing was provided in the frame of the Project Research Infrastructure for Campus-based Laboratories at the University of Rijeka, co-funded in a part by the Ministry of Science, Education, and Sports of the Republic of Croatia and the European Regional Development Fund (ERDF). These supports are gratefully acknowledged.

## References

- Arbanas Ž, Pajalić S, Jagodnik V, Peranić J, Vivoda Prodan M, Jagodnik P, Dugonjić Jovančević S (2019). Development of Physical Model of Landslide Remedial Constructions' Behaviour; In Proceedings of the 4th Regional Symposium on Landslides in the Adriatic – Balkan Region, Sarajevo, Bosnia and Herzegovina, 23–25 October 2019. Sarajevo, Bosnia and Herzegovina. pp. 103–108.
- Arbanas Ž, Jagodnik V, Peranić J, et al (2020) Physical Model of Rainfall Induced Landslide in Flume Test: Preliminary Results. Proceedings of 4th European Conference on Physical Modelling in Geotechnics - ECPMG 2020, 15-17 March 2020. Luleå, Sweden. pp. 115-122.
- Cruden D M (1991). A simple definition of a landslide. *Bulletin of the International Association of Engineering Geology*. 43(1): 27-29.
- Eckersley D (1990). Instrumented laboratory flowslides. *Géotechnique*. 40 (3): 489-502.
- Huang C C, Lo C L (2013) Simulation of Subsurface Flows Associated with Rainfall-Induced Shallow Slope Failures. *Journal of GeoEngineering*. 8: 101–111
- Hungr O and Morgenstern N R (1984). Experiments on the flow behaviour of granular materials at high velocity in an open channel. *Geotechnique*. 34(3): 9.
- Jagodnik V, Peranić J, Arbanas Ž (2021). Mechanism of Landslide Initiation in Small Scale Sandy Slope Triggered by an Artificial Rain, in: Arbanas, Ž., Bobrowsky, P.T., Konagai, K., Sassa, K., Takara, K. (Eds.), *Understanding and Reducing Landslide Disaster Risk: Volume 6 Specific Topics in Landslide Science and Applications*, Springer International Publishing, Cham, pp. 177-184. [https://doi.org/10.1007/978-3-030-60713-5\\_19](https://doi.org/10.1007/978-3-030-60713-5_19)
- Kimura T (1991). Failure of fills due to rain fall. *Centrifuge, Balkema*, pp. 509-516.
- Kutara K and Ishizuka H (1982). Seepage flow in the embankment and stability of slope during rain (in Japanese). *Tsuchi to kiso*, Paper No 1330.
- Ladd R S (1978). Preparing Test Specimens Using Undercompaction. *Geotechnical Testing Journal*. 1: 16-23. <https://doi.org/10.1520/GTJ10364J>
- Oka H (1972). Impacts by the “artificial landslide”: re examine the rage of nature (in Japanese). *Kagaku Asahi* 32 (1): 152-153.
- Pajalić S, Peranić J, Maksimović S, Čeh N, Jagodnik V, Arbanas Ž (2021) Monitoring and Data Analysis in Small Scale Landslide Physical Model. *Applied Sciences*. 11(11): 5040. <https://doi.org/10.3390/app11115040>
- Take W A, Bolton M D, Wong P C P, Yeung F J (2004). Evaluation of landslide triggering mechanisms in model fill slopes. *Landslides*. 1(3): 173-184.
- Wieczorek G F, Snyder J B (2009) Monitoring slope movements, in: *Geological Monitoring*. Geological Society of America. [https://doi.org/10.1130/2009.monitoring\(11\)](https://doi.org/10.1130/2009.monitoring(11))
- Wu L Z, Zhou Y, Sun P, Shi J S, Liu G G, Bai L Y (2017) Laboratory Characterization of Rainfall-Induced Loess Slope Failure. *CATENA*. 150: 1–8. <https://doi:10.1016/j.catena.2016.11.002>
- Yagi N, Yatabe R, Enoki M (1985). Laboratory and Field Experiments on Prediction Method of Occurring Time of Slope Failure due to Rainfall. *Journal of Japan Landslide Society*. 22, 1 7\_1. [https://doi.org/10.3313/jls1964.22.2\\_1](https://doi.org/10.3313/jls1964.22.2_1)
- Zanutta A, Baldi P, Bitelli G, Cardinali M, V A (2006) Qualitative and quantitative photogrammetric techniques for multi temporal landslide analysis. *Annals of Geophysics* 49 (4-5). <https://doi.org/10.4401/ag3117>

# Impact of gravity retaining wall on the stability of a sandy slope in small-scale physical model

Željko Arbanas<sup>(1)</sup>, Josip Peranić<sup>(1)</sup>, Vedran Jagodnik<sup>(1)</sup>, Martina Vivoda Prodan<sup>(1)</sup>, Nina Čeh<sup>(1)</sup>, Sara Pajalić<sup>(1)</sup>, Davor Plazonić<sup>(1)</sup>

1) University of Rijeka, Faculty of Civil Engineering, Rijeka, Radmile Matejčić 3, Croatia, +385 51 265 936 (zeljko.arbanas@gradri.uniri.hr)

**Abstract** Physical modelling of landslides by analysing the behaviour of small-scale landslide models subjected to artificial rainfall can be divided into modelling under 1g conditions and under increased acceleration (n times gravity) in a centrifuge. Physical modelling of landslide initiation began in Japan in the 1970s on scaled natural slope models. After initial experiences with field and laboratory researches, small-scale landslide modelling has found wide application around the world in various aspects of landslide investigations, analysing different types of landslides, different types of slope materials and landslide movements. The main task of landslide physical modelling has been to study the initiation, motion and accumulation of fast flow-like slides caused by infiltration of surface water. Studies that have included landslide mitigation measures in the small-scale physical model are rare and have not established correlations with the behaviour of on-site mitigation structures. This paper discusses the behaviour of a small-scale sandy slope supported by a gravity retaining wall in the foot of the slope, during artificial rainfall in 1g loading conditions. Two models of sandy slopes, with and without retaining wall applied, were exposed to identical intensities of artificial rainfall. The results of the simulations indicated that the slope supported by the gravity retaining wall at the toe remained stable under the same conditions under which the sandy slope collapsed. The supported slope also remained stable under much longer rainfall. At the end of the simulation, the supported slope was subjected to much higher rainfall intensities, well above the infiltration capacity of the sandy material, and surface runout was affected. The combination of surface erosion and saturation of the superficial layer of the slope led to the initiation of a debris flow, while the complete saturation of the slope at the moment when the ground water level reached the surface of the slope caused the soil strength to be exceeded and the formation of a surface of rupture and consequently movements of the formed landslide body. Although the landslide movement caused displacement and longitudinal deformation of the gravity wall at the slope foot after local shear failure in front of the wall foundation, in general the gravity wall significantly improved the stability of the slope. The results of the measurements carried out with the installed geodetic and geotechnical monitoring system allowed a comprehensive

understanding of the whole process of infiltration of precipitation and reduction of soil strength until the development of the fracture surface in the slope, as well as the process of incremental load development on the retaining structure until the limit resistance of the structure.

**Keywords** landslide, physical modelling, sandy slope, remedial measures, monitoring

## Introduction

Landslides as motions of a mass of rock, earth or debris down the slope (Cruden 1991) that threaten vulnerable human settlements in mountains, cities, riverbanks, coasts and islands. Changing climate influences on an increase in the frequency and/or intensity of heavy rainfall, and that consequently increase the risk of landslides in landslide-prone areas. Developments in mountainous and coastal areas, including the construction of infrastructure, expansion of urban areas due to population growth and migration, and deforestation and land use changes increase exposure to the landslide hazard. Strong earthquakes have the potential to trigger rapid landslides with long runout distances and in combination with heavy rainfall can lead to catastrophic landslides such as debris flows, rock falls and mega slides.

Landslide modelling was, for a long time, mostly based on numerical modelling techniques using soil strength parameters determined by laboratory testing in direct shear, triaxial or ring shear apparatus but with obstacles and limitations related to the soil sample size, sample disturbance, shear strain values before the failure, unsaturated soil conditions, effective stress and suction measurements, drop in strength to the residual values, etc. Physical modelling in small-scale slope models was introduced as a natural solution for better simulation of overall condition in a slope before, during the initiation and motion and post-motion of a landslide.

Physical modelling of landslide by analysing small scale landslide models behaviour started in early 1970s and 1980s in Japan (Oka 1972; Kutara and Ishizuka 1982) on natural slopes exposed to artificial rainfall. The laboratory experiments of landslide behaviour in a scaled physical

model (also called flume or flume test) started in 1980s and 1990s in Canada (Hungar and Morgenstern 1984), Japan (Yagi et al. 1985) and Australia (Eckersley 1990) under 1g conditions as well as in geotechnical centrifuge under increased acceleration ( $ng$ ) in 1990s (Kimura 1991).

The small-scale landslide modelling after initial experiences has found a wide application around the world in different aspects of landslide investigations, analysing different types of landslides as well as different types of soil and rock materials and landslide movements. The main task of landslide physical modelling was research of initiation, motion and accumulation of fast flow-like slides caused by infiltration of surface water in a slope and fluidification (Peranić et al. 2022).

Although the modern monitoring techniques and different monitoring equipment enable good insight into initiation and development of landslides in the small-scale landslide physical models (Pajalić et al. 2021), the crucial issue is to establish relationship between small-scale, brief, idealized and by artificial boundary restricted model with the complex natural landslide process (Iverson, 2015). This relationship is known as scaling or scaling law, and plays a crucial role in small-scale model designing and interpretation of results. Successful scaling (of material parameters, model dimensions, boundary conditions, rainfall intensity and shaking parameters as triggering factors, measured movements, velocities and accelerations etc.) is a necessary precondition for successful small-scale landslide modelling. Since a landslide is a complex geomorphological process, considering all the factors that should be taken into account when modelling a real landslide, it is clear that a landslide process is too complex for all elements to be covered by the similarity laws to fully describe the mechanism, initiation and run off process of a landslide. The simulation of a real landslide in a small-scale landslide model must be limited to the application of the most important elements affecting a landslide process, while all other elements are adjusted to imitate a real process of sliding.

At the Faculty of Civil Engineering, University of Rijeka, Croatia, the research Project “Physical modelling of landslide remediation constructions’ behaviour under static and seismic actions”, funded by Croatian Science Foundation, started in October 2018. The main objective of the Project is modelling and analysing behaviour of landslide remedial measures in physical models of scaled landslides under static and seismic conditions (Arbanas et al., 2019). In this paper, the behaviour of small-scale sandy slope supported by gravity retaining wall in the foot of the slope under artificial rain in 1g loading conditions will be discussed. Two models of sandy slope, with and without of applied gravity retaining wall, were exposed to identical intensities of artificial rainfall. The results of simulations indicated that the slope supported by the gravity retaining wall in the toe retained stability of the slope in the same conditions in which the sandy slope collapsed. Landslide development was monitored by observing surface displacements using terrestrial laser scanner (TLS) and a

pair of high-speed cameras, and by observing landslide movements within the modelled displaced mass using accelerometers (Pajalić et al. 2021). Pore water pressure and soil moisture sensors were used to observe the hydraulic response of a slope (Peranić et al. 2022). While the observed landslide movements are still being analysed, this paper presents the observations of the landslide impact on the gravity retaining wall due to the pore water pressures and water content development within the slope.

## Materials and methods

The physical model of a scaled slope was designed to enable initiation of a landslide caused by controlled artificial rainfall and equipped with adequate photogrammetric equipment and complex sensor network (Arbanas et al. 2020; Jagodnik et al., 2021). Dimensions of the slope model are 1.0 m (width) x 2.3 m (length) x 0.5 m (height). The maximum depth of a soil material in the slope was adopted to be 30 cm. Flume slope inclination can be adjusted from 20° to 45°. To prevent possible sliding of the soil mass at the contact with the flume base, the geogrid mesh is fixed to the flume base to increase friction.

This paper describes results of the tests carried out on slope inclinations of 35° degrees built of fine grained Drava River sand that was chosen as the base material for all tests within research. The first test was carried out at the sandy slope while in the second test the gravity retaining wall was built-in as adopted remedial measure and then the slope was exposed to identical intensities of artificial rainfall as the slope in the first test. The gravity retaining wall was chosen as an appropriate remedial measure (Mihalić Arbanas and Arbanas 2015, Popescu 2001) against instability that was occurred at the slope in the first test (Arbanas et al. 2020)

### Slope material properties

For the first test in the constructed flume, the fine sandy material was chosen to be built-in in the flume slope at an inclination of 30° (Fig 1). Fine graded 0-1.0 mm (Fig. 2) the Drava River Sand ( $D_{60} = 0.37$  mm,  $D_{10} = 0.19$  mm,  $C_u = 1.947$ ) was built-in in the flume in 6 cm height 5 layers, 30 cm in total, at relative density  $D_r = 0.5$  and reached void ratio of  $e = 0.78$ . Each layer was compacted by a manual compactor at the water content of  $w = 2\%$ . The specific gravity of sand is  $G_s = 2.7$  (Arbanas et al. 2020). The strength properties of the slope material was determined in direct shear apparatus at the same relative density as it is in the model of  $D_r = 0.5$  and low normal stresses appropriate to the stresses present in the flume model. The average friction angle of the Drava River Sand is  $\phi = 34.9^\circ$  while the hydraulic conductivity at the same relative density as it is in the model of  $D_r = 0.5$  determined in oedometer at low normal stresses appropriate to the stresses present in the model is  $k = 5 \times 10^{-5}$  m/s. Measured matric suction at the

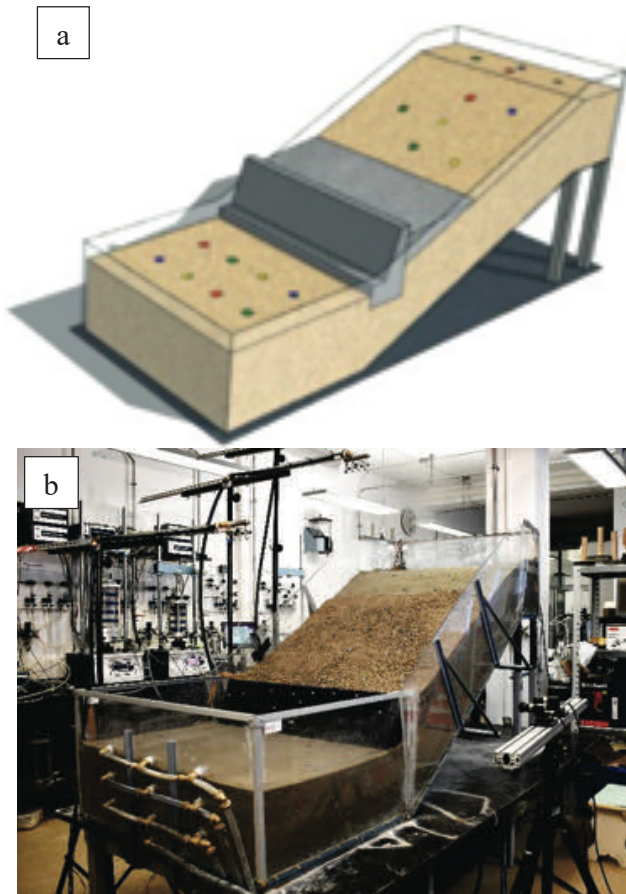


Figure 1 Small-scale model built in sandy material with installed retaining gravity wall: a) schematic views at the model; b) prepared model with installed retaining gravity wall ready for testing.

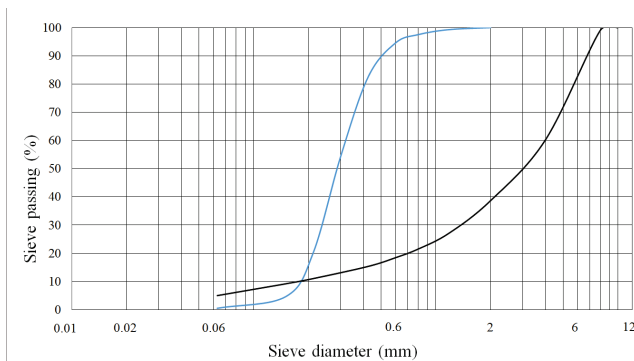


Figure 2 Grain size distribution curves of the Drava River Sand (blue) and gravel material used as the backfill behind the retaining wall (black).

water content of  $w = 2\%$  varies from 6 to 8 kPa. Previously described material was installed in the model in 5 layers, each 6 cm thick, up to a total height of 30 cm. Prepared sandy material with a water content of  $w=2\%$  was installed using the under-compaction method (Ladd 1978). Each layer was compacted using the manual compactor to the medium dense conditions of relative density  $D_r = 50\%$ . In order to achieve homogeneity of the material in the slope and relatively uniform conditions in the built-up material, the model was built up in three segments – lower (L),

middle (M) and upper (H) parts, building up the material from the foot to the top of the slope.

### Gravity retaining wall installation

In the second test after construction of the sand slope in same conditions as in the first test without remedial measures, installation of gravity retaining wall was completed using following the order of works that it is performing in a real slope. The gravity retaining wall was installed of five  $h = 30$  cm elements printed by 3D printer interconnected by an articular connection. The height of the wall was determine based on geometrical similarity of 1:20. Material used for the backfill of the wall was gravel which grain size distribution (Fig. 2) was determined from geometrical similarity with coarse crushed stone fill material 1:20. According to the position in the slope, the strength parameters of this material have no importance, while the hydraulic conductivity is significantly higher than for sand in the slope and has no influence on infiltration process.

When the model slope of sandy material was built, the foundation pit in the foot of the slope were excavated and additionally compacted, the retaining gravity wall was lined (Fig. 3a, b) and after installation of sensors, filling with gravel material was continued. Surface of the slope was stepwise excavated to ensure adequate contact between sandy slope and gravel buttressing embankment. Gravel material was divided from sandy material by geotextile and compacted by a manual compactor (Fig. 3c, d).

### Rainfall simulator

One of the most demanding challenges in physical models of landslide initiation and motion caused by rainfall infiltration is possibility to control and adjust intensities of

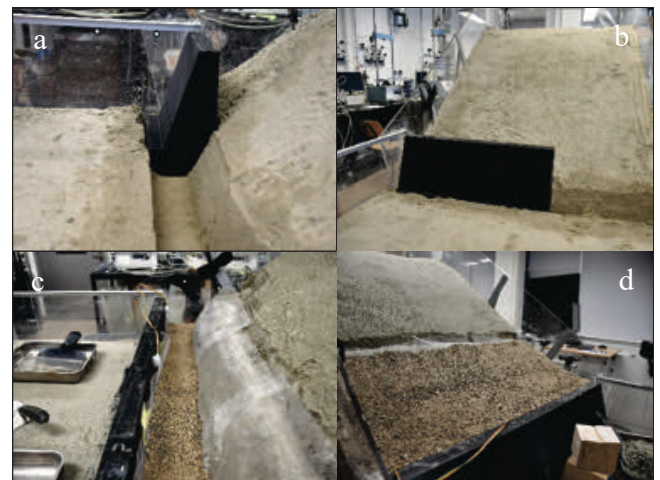


Figure 3 Installation of gravity wall and buttressing embankment behind the wall in prepared sandy slope: a) excavated foundation pit and installed element of the gravity wall, b) a view at the partially installed wall in the foot of the slope, c) filling the gravel material behind the wall with installed sensors; geotextile is laid to the steps in the sandy slope; d) filled buttressing embankment behind the gravity wall along the slope.

artificial rainfall applied to small-scale models. Rainfall simulators are widely used tools to study hydrological processes such as interaction of rainfall with soil (Lora et al. 2016). The rainfall simulator, constructed within the Project, consists of three sprinkler branches, each equipped with four different axial-flow full-cone nozzles with a spray angle of 45° or 60°. Each branch has been placed at such a height that the water can reach the edges of the plexiglass sides. This solution covers a wide range of rainfall intensities, from less than 30 l/h/m<sup>2</sup> to more than 140 l/h/m<sup>2</sup> at a reference pressure of 2 bar (Arbanas et al., 2020).

### Monitoring equipment

An active landslide is defined by existing movements down a slope (Cruden 1991), and observation of the movement distribution along a slope in relationship with observation of changes in soil condition (soil moisture, water content, pore pressures etc.) during the sliding process is one of the most important data for landslide analysis (Mihalić Arbanas and Arbanas 2015). The monitoring system established in a physical model follows the principles used in the observation of real landslides and consists of a geodetic monitoring system and a geotechnical monitoring system. The geodetic monitoring system is based on innovative photogrammetric equipment for multi-temporal landslide analysis (Bitelli et al. 2004) of image sequences obtained by a pair of high-speed stereo cameras (Feng et al. 2016). Terrestrial laser scanning and *Structure-from-Motion (SfM)* photogrammetry surveys enable the surface of the slope model to be determined in pre- and post-slide phases (Bitelli et al. 2004). The geotechnical monitoring system comprises of a complex network of miniature sensors equivalent to the geotechnical monitoring devices used in the field (Wieczorek and Snyder 2009). All sensors used in the tests are constantly connected to data loggers for continuous data collection during the time of the test. A detailed description of the equipment used in the geotechnical monitoring system is described in Pajalić et al. (2021).

### Testing results

After installing the soil in the slope model and installing monitoring equipment within the slope, the slope models were exposed to artificial rainfall from three nozzles, one nozzle in each part of the slope – upper, middle and lower part. In this paper results of two tests are presented: two models of sandy slope, with and without of applied gravity retaining wall, were exposed to identical intensities of artificial rainfall. The course of the test developments is shown in Fig. 4.

In both test the slopes were exposed to initial rainfall intensity: rainfall of 72.6 mm/h. The selection of rainfall intensity was based on the infiltration conditions in and the main requirement was that all the rainfall water at the

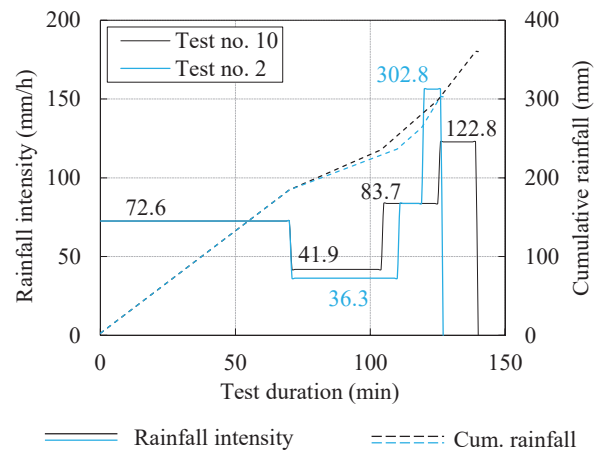


Figure 4 Simulated rainfall in: a) test on the sandy slope without applied gravity wall (blue) and tests on the sandy slope with applied gravity wall in the foot of the slope (black).

point of contact on the model surface is infiltrated without forming surface runoff. The applied intensities were at the upper precipitation values that can be infiltrated in a soil.

After the initial establishment of a constant rainfall intensity and a stable infiltration process, the models were exposed to rainfall at the constant intensities for both slope to enable similar rainfall conditions in a slope with and without of applied gravity retaining wall. Intensity of 72.6 mm/h was maintained till the 70 min, immediately after the first crack occurrence in the slope model without applied gravity retaining wall and after the ground water level reached soil surface in the lower part of the model. The groundwater level in this part of the model was maintained to the end of the model and the nozzle over the lower part of the model was closed. The intensities then were reduced to 36.3 and 41.9 mm/h and maintained additional 45 minutes. In this period landslide in the slope without applied gravity wall was retrogressively developed to the top of the slope, while in the slope the slope with applied gravity wall in all this period were no evidences of landslide initiation in a form of cracks development.

When the retrogressive development of landslide in the slope without gravity wall reached the top of the slope, the rainfall intensity was increased to 83.7 mm/h in next 10 minutes, and finally increase to 302.8 mm/h to the final failure of the slope after 128 minutes from the start of the test. Similar succession of rainfall was applied to the slope without gravity wall, but there was no initiation of a landslide in the similar time period and similar rainfall intensities (Fig. 4).

During the both tests, except that almost the same conditions of exposure to fall have been achieved, the monitoring equipment was installed at the same positions in the slope to enable measuring of changes in volumetric water content. Sensors measuring volumetric water content were installed at four different depths (6, 12, 18 and 24 cm below the slope surface) in the lower (L), middle (M) and upper (H) parts of the slope (Fig. 5).

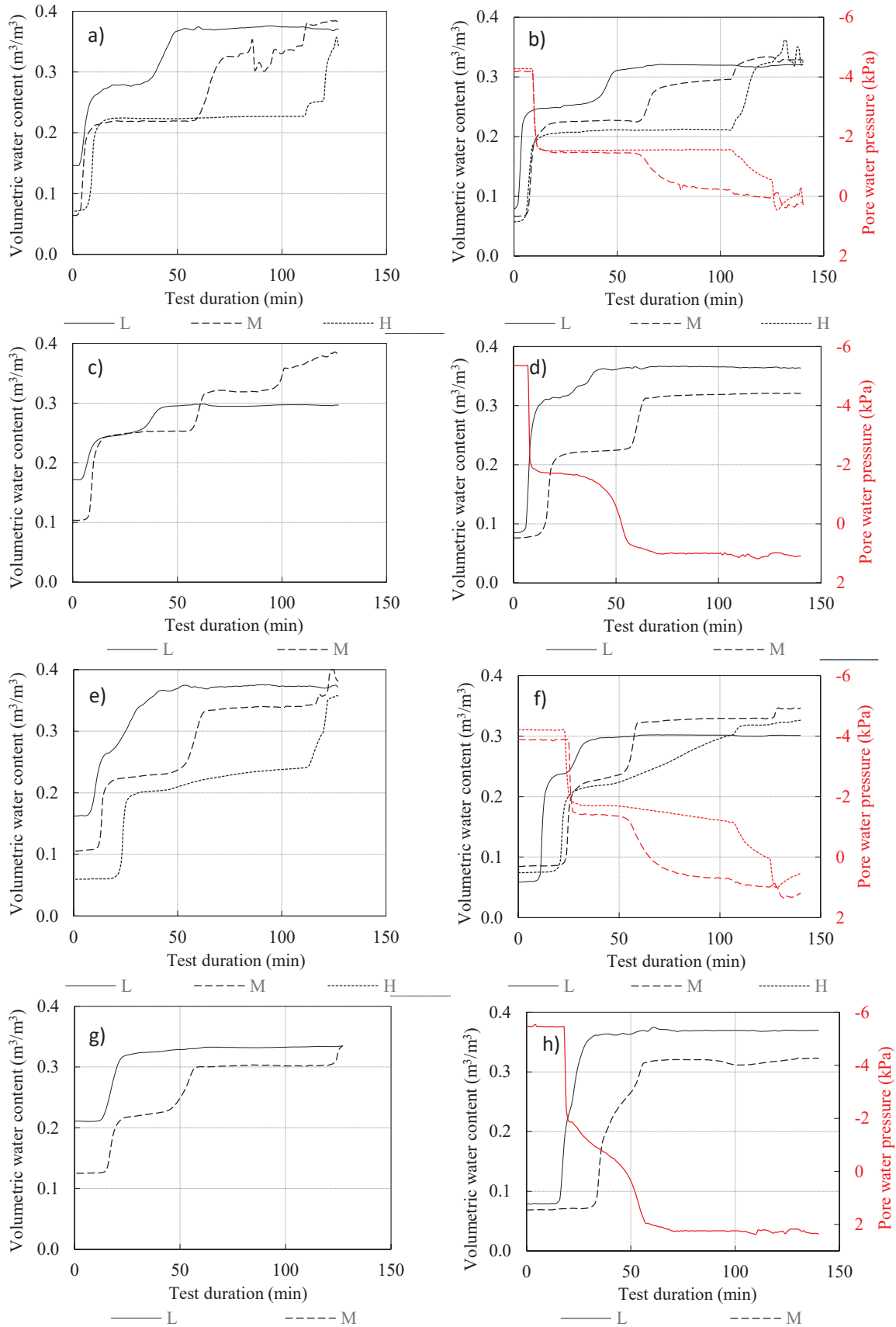


Figure 5 Volumetric water content and pore water pressure measurements in tests without applied gravity retaining wall a) at 6 cm below the surface; c) 12 cm below the surface; e) 18 cm below the surface; g) 24 cm below the surface and in the test with applied gravity retaining wall; b) at 6 cm below the surface, d) 12 cm below the surface; f) 18 cm below the surface; h) 24 cm below the surface in upper (H), middle (M), and lower (L) part of the slope.

Test at the slope with applied gravity wall was completed after 128<sup>th</sup> minute (end of test without applied retaining wall) with opening of nozzles at the upper part of the slope with the intensity of 122.8 mm/h that was higher than infiltration capacity of sandy material.

The occurred superficial signs of sliding initiations and the causes for their occurrence in the case of slope without applied gravity wall can be explained by results of the continuous volumetric water content monitoring (Fig. 5a,c,d,g). The process of landslide initiation and development was described by the volumetric water content increasing due to infiltration until saturation in the deepest part of the slope, forming the water table. As it becomes established, a flow down the slope begins, causing a rapid rise in the groundwater level in the lower part of the slope. This leads to a decrease in the soil shear strength with complete loss of matric suction, failure and further retrogressive landslide development to the top of the slope (Peranić et al. 2022), Fig. 6a.

As it noted before, in the same time under the same rainfall conditions, no sliding process in the slope with applied retaining gravity wall was occurred that indicate that the applied remedial measures with gravity wall and coarser backfill material behind the wall confirmed the intended role to retain sandy slope stability, Fig. 6b.



Figure 6 a) retrogressive slide in the test on the sandy slope without applied gravity wall after 120 min of rainfall; b) a view at the sandy slope with applied gravity wall after 120 min of rainfall.

Analysing the development of rainfall infiltration and forming a ground water level along the slope in both models with and without applied gravity retaining wall, it wasn't identify significant deviations in measuring results (Fig. 5). Neglecting the differences in initial and trough the tests water contents caused by initial differences and heterogeneity of soil density (primarily) and water content (that is related to density too), the graphs that representing the development of volumetric water content in the model within the tests have similar trends in similar time period of applied rainfall. That pointed on the conclusion that the main role of applied gravity wall and coarser backfill material behind the wall is in a raising of soil strength in the slope foot and associated erosion prevention in slopes without applied remedial measures.

After applying of the high rainfall intensity at the upper part of the slope (122.8 mm/h) that is higher than infiltration capacity of sandy material, sudden development of erosion process of sandy material and global instability of slope occurred, causing the exceeding of the bearing capacity of the soil below the retaining wall foundation, Fig. 7. Although the retaining wall was not completely collapsed and overturned, horizontal

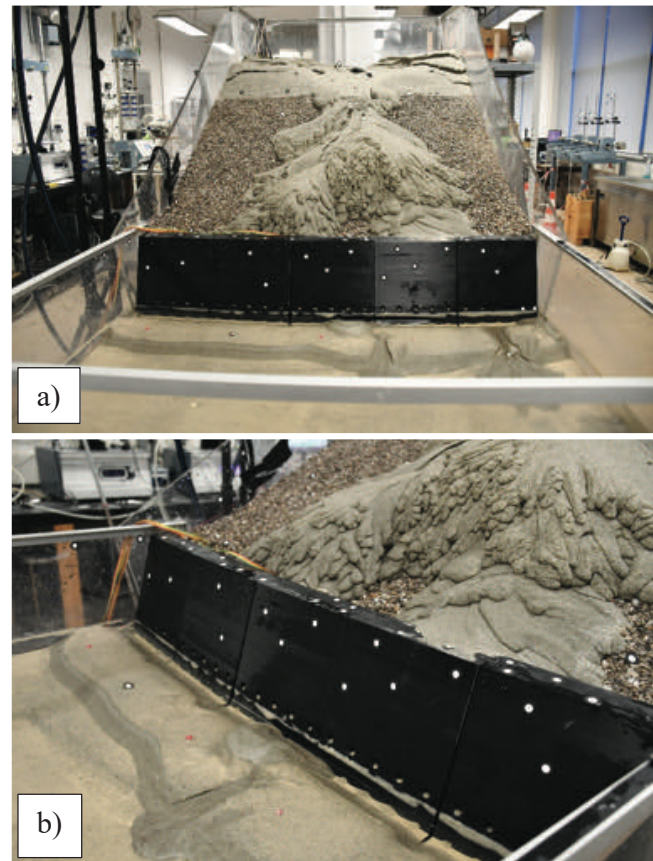


Figure 7 a) a global collapse of the slope in the test on the sandy slope without applied gravity wall with opening of nozzles at the upper part of the slope with the intensity of 122.8 mm/h after 138 min of rainfall; b) a view at the applied gravity wall at the end of the test; there are visible movements along the gravity wall and zone of uplifted Rankine passive zone in a front of gravity wall foundations.



displacement enabled by the local failure of below the retaining wall foundation and horizontal soil compaction in the foot of the slope enabled global collapse of the slope. The applied rainfall intensities that caused this global collapse are significantly high, and, taking into account scaling relative to real slope sizes, represent rare extreme rainfall events.

## Discussion and conclusions

In the previous chapter, the results of two tests carried out on slope inclinations of 35° degrees built of fine grained Drava River Sand with and without applied remedial measures were presented. The first test was carried out at the sandy slope while in the second test the gravity retaining wall was built-in as adopted remedial measure and then the slope was exposed to identical intensities of artificial rainfall as the slope in the first test. The gravity retaining wall was chosen as an appropriate remedial measure against instability that was occurred at the slope in the first test (Arbanas et al. 2020). The models, material and procedures that were applied during the model installation were presented in detail. Both models with and without applied gravity retaining wall were exposed to almost completely identical rainfall scenarios to enable comparison of achieved results of slope behaviours and effects of applied remediation measures to slope stability.

As it was described in previous chapter, in the same time exposed to the same rainfall scenarios, no sliding process in the slope with applied retaining gravity wall was occurred that indicate that the applied remedial measures with gravity wall and coarser backfill material behind the wall confirmed the intended role to retain sandy slope stability. Analyses of the rainfall infiltration and forming a ground water level along the slope in both models with and without applied gravity retaining wall, doesn't identify significant deviations in measuring results neglecting the differences in initial and trough the tests water contents caused by initial differences and heterogeneity of soil density and water content. The graphs that representing the development of volumetric water content in the model within the tests have similar trends in similar time period of applied rainfall in both tests, that pointed on the conclusion that the main role of applied gravity wall and coarser backfill material behind the wall is in a raising of soil strength in the slope foot and associated erosion prevention in slopes without applied remedial measures.

After applying of the rainfall intensity at the upper part of the slope (122.8 mm/h) higher than infiltration capacity of sandy material, sudden development of erosion process of sandy material and occurrence of global instability of slope have been appeared, causing the exceeding of the bearing capacity of the soil below the retaining wall foundation. The retaining wall was not completely collapsed and overturned but horizontal displacement enabled global collapse of the slope. The

applied rainfall intensities that caused this global collapse are significantly high, and, taking into account scaling relative to real slope sizes, represent rare extreme rainfall events, but despite this fact, in the following tests the applied remedial measures should be improved to avoid this kind of collapse even in extreme circumstances.

During the tests, some other equipment was used within the slope monitoring, e.g. photogrammetric equipment for multi-temporal landslide analysis of image sequences obtained by a pair of high-speed stereo cameras, terrestrial laser scanning and SfM photogrammetry surveys, that results were not included in this paper analyses. These data were recorded and collected during the conducted tests, and these results will enable kinematic analyses of the points at the surface of the slope model determined in pre- and post-slide phases (Pajalić et al. 2021).

For the purpose to identify surface deformation at the start and the end of the test, terrestrial laser scanning survey were conducted enabling creation 3D high resolution point cloud (3D HRPC) of the model slope surface, Fig. 8. Terrestrial laser scanner (TLS) used to capture model surface is the FARO Focus 3D X 130 (FARO Technologies Inc., Lake Mary, FL, USA) (Pajalić et al. 2021). Analysing the 3D HRPCs of the model surfaces before and at the end of the test, georeferenced to the same position in the laboratory, it was possible to precisely compare model slope surfaces and detect of 3D movements at the comparable part of the surface. This comparison was very important in detecting displacements in the zone of applied gravity retaining wall, to identify values of the horizontal displacements of the gravity wall crown, longitudinal deformations of the wall as well as reconstruction of uplift in a front of gravity wall foundation, Fig 8b,d.

Although the currently analysed results already give a detailed insight into the impact of the gravity retaining wall in increasing of overall slope stability in the model, comprehensive analysis of all collected data will enable more detailed and precise description of any part of the model and especially of remediation structure behavior.

## Acknowledgments

This research was funded by Croatian Science Foundation under the Project IP-2018-1503 Physical modelling of landslide remediation constructions behaviour under static and seismic actions (ModLandRemSS). The part of the laboratory equipment used for laboratory testing was provided in the frame of the Project Research Infrastructure for Campus-based Laboratories at the University of Rijeka, co-funded in a part by the Ministry of Science, Education, and Sports of the Republic of Croatia and the European Regional Development Fund (ERDF). These supports are gratefully acknowledged.

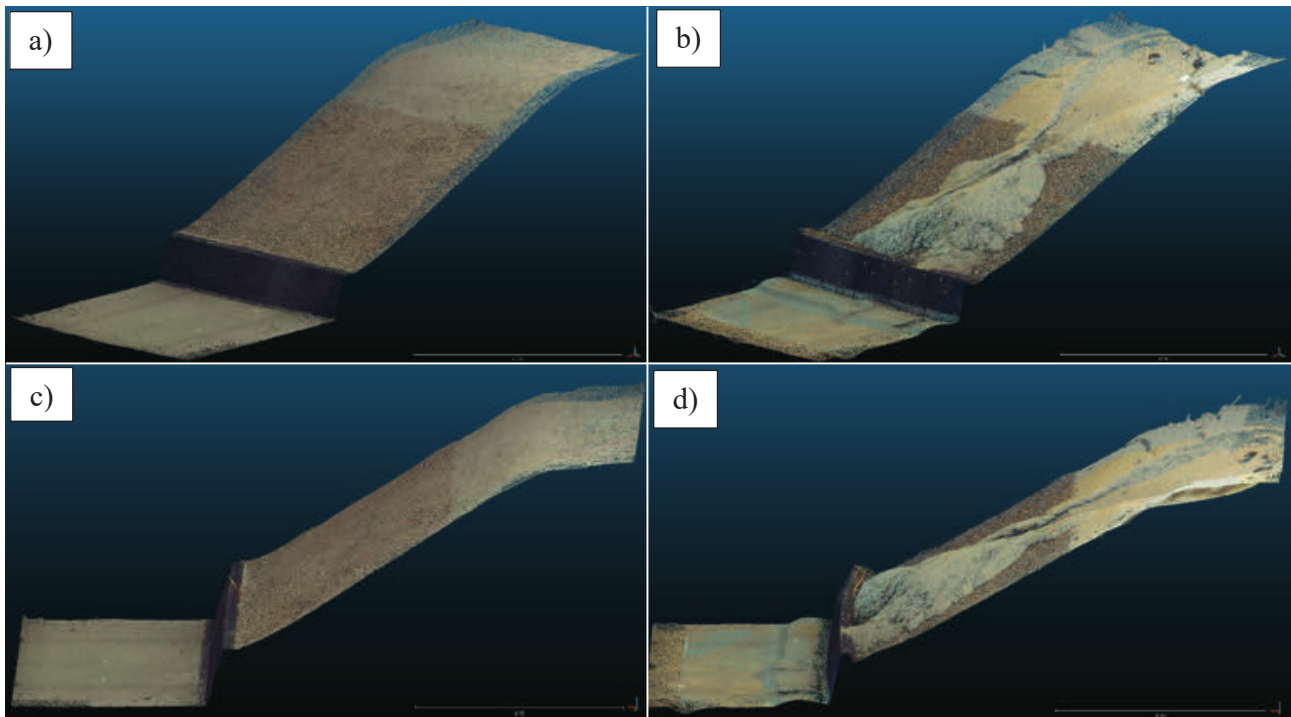


Figure 8 3D high resolution point clouds (3D HRPC) of the model captured by terrestrial laser scanner (TLS): a) a view at the slope before testing; b) a view at the slope at the end of the test; c) side view at the slope before testing; d) side view at the slope at the end of the test.

## References

- Arbanas Ž, Jagodnik V, Peranić J, et al (2020) Physical Model of Rainfall Induced Landslide in Flume Test: Preliminary Results. In: Proceedings of European Conference of Physical Modeling in Geotechnics. p 8.
- Arbanas Ž, Pajalić S, Jagodnik V, et al (2019) Development of physical model of landslide remedial constructions' behaviour. In: Proceedings of the 4th Regional Symposium on Landslides in the Adriatic - Balkan Region. Bosna and Herzegovina Geotechnical Society, pp 103–108.
- Bitelli G, Dubbini M, Zanutta A (2004) Terrestrial laser scanning and digital photogrammetry techniques to monitor landslide bodies. In: International Archives of Photogrammetry, Remote Sensing and Spatial Information Sciences. Istanbul, Turkey, pp 246–251
- Cruden DM (1991) A simple definition of a landslide. *Bulletin of the International Association of Engineering Geology*. 43:27–29. <https://doi.org/10.1007/BF02590167>
- Eckersley D (1990) Instrumented laboratory flowslides. *Géotechnique*. 40:489–502. <https://doi.org/10.1680/geot.1990.40.3.489>
- Feng T, Mi H, Scaioni M, et al (2016) Measurement of Surface Changes in a Scaled-Down Landslide Model Using High-Speed Stereo Image Sequences. *Photogrammetric Engineering & Remote Sensing*. 82:547–557. [https://doi.org/10.1016/S0099-1112\(16\)82061-3](https://doi.org/10.1016/S0099-1112(16)82061-3).
- Hung O, Morgenstern NR (1984) Experiments on the flow behaviour of granular materials at high velocity in an open channel. *Géotechnique*. 34:9.
- Jagodnik V, Peranić J, Arbanas Ž (2021) Mechanism of Landslide Initiation in Small-Scale Sandy Slope Triggered by an Artificial Rain. In: Arbanas Ž, Bobrowsky PT, Konagai K, et al. (eds) *Understanding and Reducing Landslide Disaster Risk: Volume 6 Specific Topics in Landslide Science and Applications*. Springer International Publishing, Cham, pp 177–184.
- Kimura T (1991) Failure of fills due to rain fall. *Centrifuge*. Balkema, pp. 509–516.
- Kutara K, Ishizuka H (1982) Seepage flow in the embankment and stability of slope during rain (in Japanese). *Tsuchi-to-kiso*, Paper No 1330.
- Ladd RS (1978) Preparing Test Specimens Using Undercompaction. *GTJ*. 1:16–23. <https://doi.org/10.1520/GTJ10364J>
- Lora M, Camporese M, Salandin P (2016) Design and performance of a nozzle-type rainfall simulator for landslide triggering experiments. *CATENA*. 140:77–89. <https://doi.org/10.1016/j.catena.2016.01.018>
- Mihalić Arbanas S, Arbanas Ž (2015) Landslides: A Guide to Researching Landslide Phenomena and Processes. *Handbook of Research on Advancements in Environmental Engineering* 474–510. <https://doi.org/10.4018/978-1-4666-7336-6.ch017>
- Oka H (1972) Impacts by the “artificial landslide”: re-examine the rage of nature (in Japanese). *Kagaku Asahi* 32:152–153
- Pajalić S, Peranić J, Maksimović S, et al (2021) Monitoring and Data Analysis in Small-Scale Landslide Physical Model. *Applied Sciences*. 28.
- Popescu M E (2001) A suggested method for reporting landslide remedial measures. *Bulletin of Engineering Geology and the Environment*. 60(1): 69–74. doi:10.1007/s100640000084
- Peranić J, Jagodnik V, Čeh N, et al (2022) Landslide initiation in small-scale sandy and clayey slopes exposed to artificial rain. *Proceedings of the 20th International Conference on Soil Mechanics and Geotechnical Engineering Sydney 2020 6 (In Press)*.
- Wieczorek GF, Snyder JB (2009) Monitoring slope movements. In: *Geological Monitoring*. Geological Society of America
- Yagi N, Yatabe R, Enoki M (1985) Laboratory and Field Experiments on Prediction Method of Occuring Time of Slope Failure due to Rainfall. *Journal of Japan Landslide Society*. 22:1-7\_1. [https://doi.org/10.3313/jls1964.22.2\\_1](https://doi.org/10.3313/jls1964.22.2_1)

# Preliminary results on the undrained cyclic behavior of uniform sand at low confining stress

Vedran Jagodnik<sup>(1)</sup>, Martina Turković<sup>(1)</sup>, Željko Arbanas<sup>(1)</sup>

1) University of Rijeka, Faculty of Civil Engineering, Rijeka, Radmile Matejčić 3, Croatia, +385 51 265 941 (vedran.jagodnik@gradri.uniri.hr)

**Abstract** Earthquakes are one of the main landslide triggering factors. Earthquake induced cyclic shear strain and stress generate the rise in the pore water pressure and soil strength degradation which tends toward soil failure. Slopes in which shallow landslide can be formed due to geological conditions are most susceptible to such kind of loading mainly because of soil low confining stress. Confining effective stress has a significant role on the soil response during static and cyclic load. Tests performed on soil samples under monotonic shear indicate that the shear strength properties increase with decreasing effective stress due to dilatancy. This paper presents preliminary results of an undrained cyclic triaxial test on sand material used for modelling small scale shallow landslides under *lg* conditions. Based on the scaling rules for *lg* conditions, frequencies of straining amplitudes for undrained strain-controlled cyclic triaxial tests were defined. Undrained cyclic triaxial tests on the type of sand used in a small-scale landslide model were performed. Samples were consolidated on low confining stress which corresponds to an assumption of a shallow landslide used as prototype. All tests were conducted in the Laboratory for geotechnics at the Faculty of Civil Engineering in Rijeka, Croatia. The influence of loading frequency and low confining stress was investigated and a simple model for pore pressure build-up was proposed which can be used to estimate the increase in pore water pressure due to cyclic loading at low confining stress for frequencies of loading less than 1 Hz.

Keywords: uniform sand, low confining stress, strain controlled, cyclic triaxial test

## Introduction

One of the main landslides triggering factor is considered to be an earthquakes (i.e. Popescu 2002; Highland and Bobrowsky 2008; Wu et al. 2015; Kumar et al. 2017). Cyclic shear stress and strain which are the result of an earthquake induced shear wave propagation, degrades the soil strength, and generates the build-up of pore pressure which in turn leads to soil failure. Such behaviour is critical for slopes which are prone to shallow landslides. Shallow landslides are considered to have a depth up to around 5m (ICL 2016) and are greatly affected by earthquake and/or rainfall (i.e. Gabet and Mudd 2006; Yang et al. 2015). This is largely due to a low confining stress of soil (White 2020).

Low confining stress has a significant influence on soil strength since the soil is considered to be pressure dependent material.

White (2020) performed experiments in a triaxial cyclic device at low effective stresses (less than 50 kPa). All undrained cyclic tests were performed after isotropic consolidation until initial liquefaction has been reached. Such stresses would correspond to a stress level at a depth of less than 10 m from the soil surface. Higher values lead to faster accumulation of pore pressures. The secant shear modulus,  $G_s$ , was found to decrease with increasing number of cycles and with decreasing effective stress,  $\sigma'_{c,0}$ .

Test results of an equivalent viscous ratio show significant noise in the data, especially for lower cyclic load values, which in some experiments makes it difficult to reliably estimate damping ratio (White 2020). The results show that when the shear cyclic strain  $\gamma_{cyclic}$  is less than approximately  $10^{-4}$ , the damping of soil does not increase so much and remains relatively the same with the number of cycles. This coincides with the literature (Dobry et al. 1982; Vucetic 1994; Tabata and Vucetic 2010; Vucetic and Mortezaie 2015) where the cyclic volumetric shear stress threshold,  $\gamma_{tv}$  is equal to  $10^{-4}$ , regardless of the effective stress, compaction, and sample structure. Once this threshold is exceeded, the damping of soil changes with the change in shear cyclic deformation and the number of cycles.

Kumar et al. (2017) found that the sample tested at lower effective stresses (50 kPa) shows a higher damping quotient compared to higher effective stresses (100 and 150 kPa) which is attributed to relatively higher stiffness due to sample constraints.

Chakraborty and Salgado (2010) conducted triaxial compression in drained conditions, and in-plane compression experiments (*plane-strain*). The sand was tested at low effective stresses to determine the dependence of dilatation and friction angle with relative compaction and effective stress. The authors concluded that sand dilatation decreases with decreasing compaction and increasing effective stress. Also, it was observed that for less effective stress (less than 50 kPa) there is a larger scatter in results, compared to higher values of effective stress (greater than 100 kPa).

Shaoli et al. (2003) in their study emphasized that clean sand has a more significant dilating behaviour at lower effective stresses. Therefore, clean sand is more stable

at low effective stresses compared to behaviour at high effective stresses. This is usually not the case with fine sand because such sand is subjected to static liquefaction at low effective stresses and thus complete loss of strength occurs. The amplitude of the cyclic load has a significant effect on the generated pore pressure, while porosity plays a dominant role in sand behaviour.

Sture et al. (2004) performed cyclic triaxial tests with a deformation control method in drained and undrained conditions. It should be emphasized that the experiments were performed in a microgravity. Microgravity is a weightless state in which people or objects are not seemingly affected by gravity (NASA 2012). This is done because many soil properties such as stability, strength, stiffness, deformation, etc. are greatly influenced by interparticle forces (Sture et al. 2004). Therefore, it can be concluded that the behaviour of the soil at low effective stresses depends on the gravitational force. High friction angles and dilatation were observed in drained tests on medium-compacted samples. In undrained tests with weakly compacted samples, the transition from the stable solid to the viscous liquid state (liquefaction) was observed in several undrained tests.

This paper presents preliminary results of the undrained cyclic triaxial test on sandy material used for modelling of small scale shallow landslide caused by artificial rainfall under  $1g$  conditions. Frequencies of straining amplitudes for strain controlled cyclic triaxial tests were defined based on the scaling rules for  $1g$  conditions and a small-scale landslide model dimension. Sand samples were tested at low confining stress which corresponds to the assumption of shallow landslide forming in a prototype landslide.

## Methods and materials

### Small scale dynamic landslide testing

For the purposes of an ongoing research project focused on the behaviour of small-scale landslide under  $1g$  conditions subjected to cyclic excitation, it was necessary to examine the cyclic behaviour of the used material. The material used was uniform sand which will be thoroughly defined later in the text. The small-scaled landslide is subjected to a cyclic excitation representing an earthquake load. Earthquake load was simulated using the Quanser STI-III seismic platform, located in the Laboratory for structures at the Faculty of Civil Engineering, University of Rijeka, Croatia (i.e. (Bićanić et al. 2016; Dobrilla et al. 2018)). The platform is driven by an electromagnetic motor controlled via LabView-based software. Scaling factor in this research was 40 and it was used to determine the corresponding values of similitude rules which are summarised in Tab. 1. For the purpose of this research, scaling factor type II, according to lai et al. (2005) were used.

Quanser STI-III seismic platform is limited with the weight capacity so it was necessary to check what is the maximum frequency that the platform can achieve with

Table 1 Similitude rules used for this research.

Quantity	Scaling factors, Type II*	Value
Length	$\mu$	40
Time	$\mu^{0.75}$	15.91
Frequency	$\mu^{-0.75}$	0.063
Strain	$\mu^{0.5}$	6.32
Displacement	$\mu^{1.5}$	252.98
Acceleration	1	1

\* -  $\mu_\epsilon = \mu^{0.5}$  and  $\mu_\rho = 1$

respect to amplitude. Several trial tests were performed to determine the maximum frequency which was roughly around 8 Hz for an amplitude of 2 mm. This maximum frequency fortunately coincides with the prototype frequency of 0.5 Hz for scaling factor 40. Tab. 2 shows the comparison of frequencies calculated according to the scaling law and the one achieved by trial tests. Based on Tab. 2 frequencies of 0.1, 0.2 and 0.5 Hz were used to test soil samples in cyclic triaxial apparatus.

### Cyclic triaxial equipment

Cyclic tests were performed on Dynatriax triaxial system manufactured by Controls Group Ltd (2017). The Dynatriax system (Fig. 1) is a closed loop triaxial system with the capability of performing dynamic cyclic triaxial test in both drained and undrained conditions. The maximum cell pressure that can be applied to the soil samples is 1 MPa. Actuator (Fig. 1 (b)) has a frequency of 10 Hz and maximum dynamic capacity of 15 kN and it is controlled through the control unit with a pneumatic air control (Fig. 1(g)). The system has two linear variable differential transformers (LVDT's) that are used for measuring vertical displacement, one outside triaxial cell and another within the actuator.

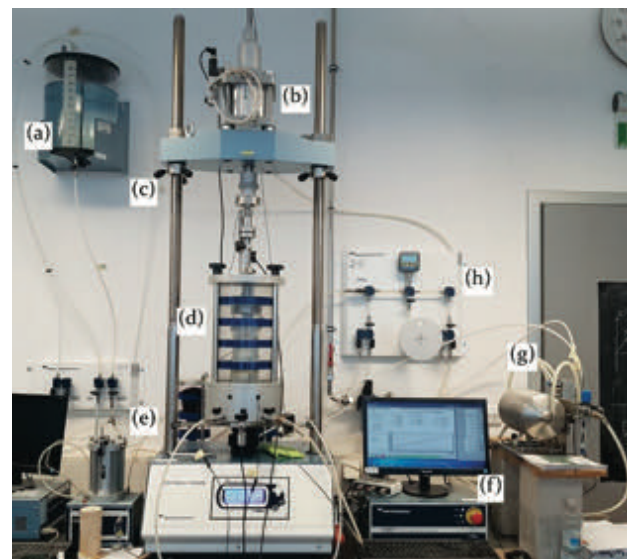


Figure 1 Cyclic triaxial system: (a) water tank, (b) pneumatic actuator, (c) triaxial loading frame, (d) triaxial cell, (e) volume controller, (f) PC with data acquisition system, (g) pneumatic control system for pressures and actuator and (h) water distribution panel.

Table 2 Relation of frequencies: prototype – model.

Frequency of prototype, $f_p$ (Hz)	Frequency of model according to scaling law, $f_{m,law}$ (Hz)	Frequency of model tested in seismic platform, $f_{m,pl}$ (Hz)
0.1	1.59	1.7
0.2	3.17	3.2
0.5	7.93	8.1

The submerged load cell (Fig. 1 (d)) with the capacity of 25 kN is used to measure a load on the sample. Cell, back and pore pressures are measured using pressure transducers connected on the lower part of triaxial cell.

### Soil type and specimen preparation

Soil used in this research was classified as uniform sand, locally known as Drava sand (Pajalić et al. 2021). Basic classification tests, which consisted of sieve analysis, index density tests and specific gravity tests, were performed by Pajalić et al. 2021, according to the ISO standards (EN/ISO 14688-2 2017). Basic parameters are summarised in Tab. 3.

Specimens for triaxial testing were prepared using moist compaction method, also known as undercompaction method, developed by Ladd (1978). As mentioned in the previous section, selected relative density for small scale landslide tests under dynamic loading was 50%. Corresponding void ratio  $e_0$  was calculated based on the minimum and maximum void ratio which is 0.78 for this type of material and relative density of 50%. Fig. 2 shows stages of sample preparation.

Prior to consolidation stage, samples were saturated using CO<sub>2</sub> and water percolation together with back pressurising. Percolation with CO<sub>2</sub> and water ensured that air was significantly removed from sample and voids were filled with water, which in turn, ensured large value of Skempton's B coefficient ( $B \approx 0.98$ ) with back pressure values less than 90 kPa. Such small values of back pressures had a negligible volume deformation during saturation stage.

### Testing methodology

Cyclic strain-controlled tests were performed on 9 samples. Samples were tested under three different low confining stress and three different frequencies. Values of confining stress were determined based on the scaling rules in Tab. 1 and the assumption that the landslide depth is approximately 6m. List and characteristic of performed

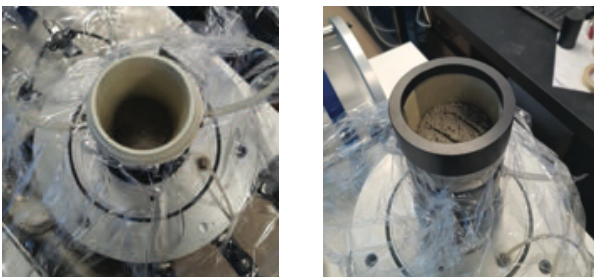


Figure 2 Sample preparation using undercompaction method.

tests are presented with Tab. 4. All tests were performed in undrained condition. Strain controlled tests were performed as a multistage test with different cyclic axial strain,  $\epsilon_{a,c}$ . Since the tests were undrained the cyclic shear strain can easily be calculated from axial strain using the equation [1]. The values of cyclic axial strain,  $\epsilon_{a,c}$ , are summarised with Tab. 5.

$$\gamma = 1.5 \cdot \epsilon_{a,c} \quad [1]$$

### Degradation and pore pressure build-up

Special focus was given to soil damping and pore pressure build-up during cyclic shearing. Since the tests were performed using the cyclic triaxial apparatus, cyclic loop is not symmetrical (i.e., Kumar et al. 2017) as in dynamic simple shear apparatus (i.e., Silver et al. 1980; Vucetic and Mortezaie 2015; Thian and Lee 2017). Hence, in the calculation of soil degradation during cyclic test, the one must consider both the compression branch and the extension branch of the cyclic loop. Example of a nonsymmetric loop is presented with Fig. 3.

Secant shear modulus for the samples subjected to triaxial shearing can be calculated using the equation [2], while the average secant shear modulus is calculated using the equation [3].

$$G_{s,\blacksquare} = \frac{q_{\blacksquare}}{3 \cdot \epsilon_{a,cyc}} \quad [2]$$

where  $q_{\blacksquare}$  is the deviatoric stress in compression and  $\blacksquare$  stands for either compression or extension.

$$G_{s,av} = \frac{G_{s,comp} + G_{s,extension}}{2} \quad [3]$$

The equivalent viscous damping ratio,  $\lambda$ , was calculated based on a Fig. 3 and equation [4]:

$$\lambda = \frac{1}{\pi} \cdot \frac{\text{Area of loop}}{\frac{1}{2}(|q_{comp}| + 3 \cdot |q_{ext}|) \cdot |\epsilon_{q,cyc}|} \quad [4]$$

where  $|q_{comp}|$  is the absolute value of deviatoric stress in compression,  $|q_{ext}|$  is the absolute value of deviatoric stress in extension and  $|\epsilon_{q,cyc}|$  is the absolute value of deviatoric strain of the cycle.

Table 3 Basic physical properties of tested sand according to Pajalić et al. (2021).

Physical property	Symbol	Value	Unit
Specific gravity	$G_s$	2.70	(-)
Effective grain size	$D_{10}$	0.19	(mm)
Coefficient of uniformity	$C_u$	1.947	(-)
Coefficient of curvature	$C_c$	1.092	(-)
Minimum void ratio	$e_{min}$	0.641	(-)
Maximum void ratio	$e_{max}$	0.911	(-)
Hydraulic conductivity	$k_s$	$10^{-5}$	(cm/s)

Table 4 Characteristics and list of performed strain controlled cyclic triaxial test.

Test ID	h/d* (mm/mm)	Effective confining stress $\sigma'_c$ (kPa)	Frequency f (Hz)
MDL_002_50_50_UND	100 / 50	50	0.1
MDL_003_50_25_UND	100 / 50	25	
MDL_006_50_10_UND	100 / 50	10	
MDL_009_50_50_UND	140 / 70	50	0.2
MDL_010_50_25_UND	140 / 70	25	
MDL_011_50_10_UND	140 / 70	10	
MDL_013_50_50_UND	140 / 70	50	0.5
MDL_014_50_25_UND	140 / 70	25	
MDL_015_50_10_UND	140 / 70	10	

\*h/d - sample height to diameter ratio

Table 5 Stages of strain controlled cyclic triaxial test.

Stage ID	Cyclic axial strain $\epsilon_{a,c}$ (%)	Cyclic shear strain $\gamma_c$ (%)
1	0.0033	0.005
2	0.005	0.0075
3	0.0067	0.01
4	0.013	0.02
5	0.033	0.05
6	0.05	0.075
7	0.067	0.1
8	0.133	0.2
9	0.333	0.5
10	0.667	1

Pore pressure build-up was calculated based on the excess pore water pressure and is expressed as:

$$r_u = \frac{\Delta u}{\sigma'_c} \quad [5]$$

where  $\Delta u$  is the excess water pressure in kPa and  $\sigma'_c$  is the confining stress.

## Results

The results of cyclic undrained triaxial tests on uniform sand are presented in the following section. The results of an equivalent viscous ratio are presented in Fig. 4. Datapoints present the results of an ongoing research while solid and dashed line present the research on similar sand but under somewhat larger confining stress.

Pore pressure was measured in every stage and pore pressure ratio,  $r_u$ , was calculated. The values of pore pressure ratio at different cycles shear strain for cycle N=2 is plotted in the Fig. 5 as data points. The authors examined the influence of frequency on the values obtained from cyclic triaxial test and proposed a simple analytic model that considers the frequency and number of cycles. Nonlinear least square method was used to obtain the best fit parameters (Chavent 2009; Virtanen et al. 2020). Due to limitation in paper length, the authors are presenting the model for N = 2, given with the equation [6].

$$r_u(f, \gamma_c) = 0.623 \cdot f^{0.276} \cdot \log_2(\gamma_c + 0.132 \cdot f^{-0.036}) + 1.791 \cdot f^{0.284} \quad [6]$$

where  $f$  is the frequency and  $\gamma_c$  is the cyclic shear strain.

## Discussion and conclusions

Low confining stress has a great impact in the analysis of slope stability, especially if they are in seismically active areas. An ongoing research project focused on the behaviour of small-scaled landslide at  $1g$  conditions subjected to cyclic loading indicated that drainage conditions and frequency also plays a significant role in slope behaviour. Scaling laws for  $1g$  conditions were used to examine the frequency of cyclic triaxial tests on sand samples which are equivalent to prototype.

The preliminary results of equivalent viscous damping,  $\lambda$ , and normalised pore water pressure ratio,  $r_u$ , are presented. The tests were performed under undrained condition with cyclic triaxial test on uniform sand subjected to strain-controlled loading at low confining effective stresses. The results of equivalent viscous damping fit very well with the results from literature (Seed and Idriss 1970; Darendeli 2001). From the obtained results it can easily be noticed that low confining stress has significant role on soil damping at low cyclic shear strain, Fig.4, as mentioned by Chakraborty and Salgado (2010). This scatter is also due to type of available equipment used in this research. Dynatriax system used here is a pneumatic based system and is highly sensitive on the system control parameters, adjusted via Proportional-Integrate-Derivative parameter (PID), (Panda 2012). Scatter is reduced when the soil passes the cyclic shear strain threshold,  $\gamma_{t,u}$ , after which soil degradation takes place.

The values of normalised pore pressure show a significant rise after the cyclic shear strain of 0.01% is passed, which corresponds to the literature. Proposed analytical model for pore pressure rise (blue line in Fig. 5) which is in function with cyclic shear strain and frequency fits well with the data obtained by laboratory tests.

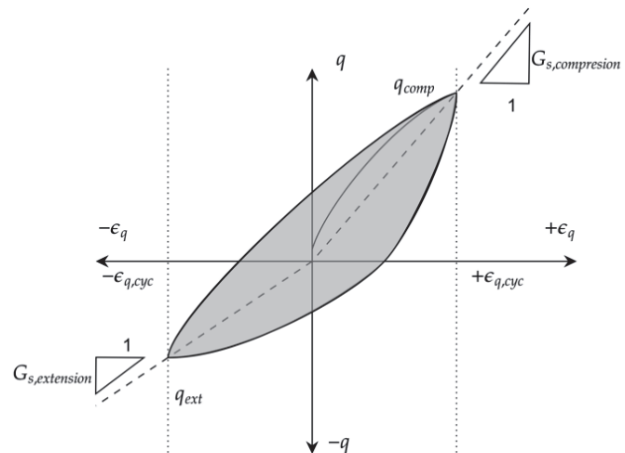


Figure 3 Nonsymmetry in triaxial cyclic loop.

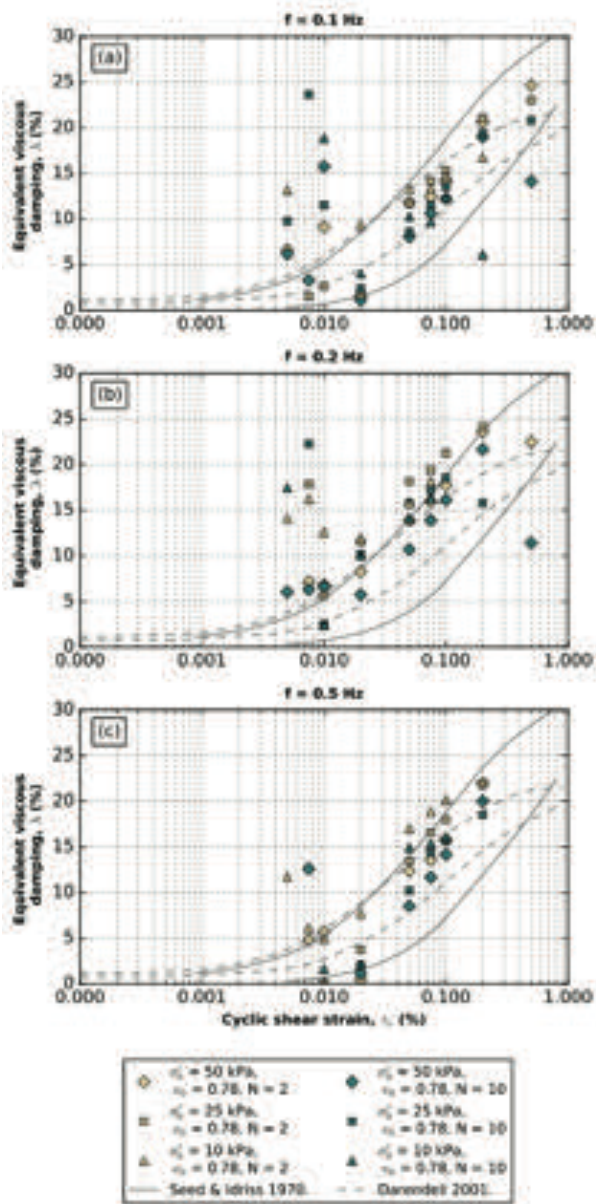


Figure 4 Influence of frequency and cyclic shear strain on equivalent viscous damping,  $\lambda$ : (a) Frequency of 0.1 Hz, (b) Frequency of 0.2 Hz and (c) Frequency of 0.5 Hz.

From the presented results it can be concluded that the confining stress plays significant role in soil damping. Despite that, the data for soil damping are in good comparison with the one from literature, which are based for higher values of confining stress. From Fig. 5 it can be concluded that the higher the frequency the higher soil damping is observed. Also, soil damping for frequencies lower than 0.3 Hz show some minor discrepancies for the shear strain smaller than threshold value of 0.01%.

The values of residual pore pressure are consistent with the theory as well. The higher the frequency the higher is the  $r_u$  ratio. This means that the critical value of  $r_u = 1$  is reached in only few cycles of cyclic shearing for frequency

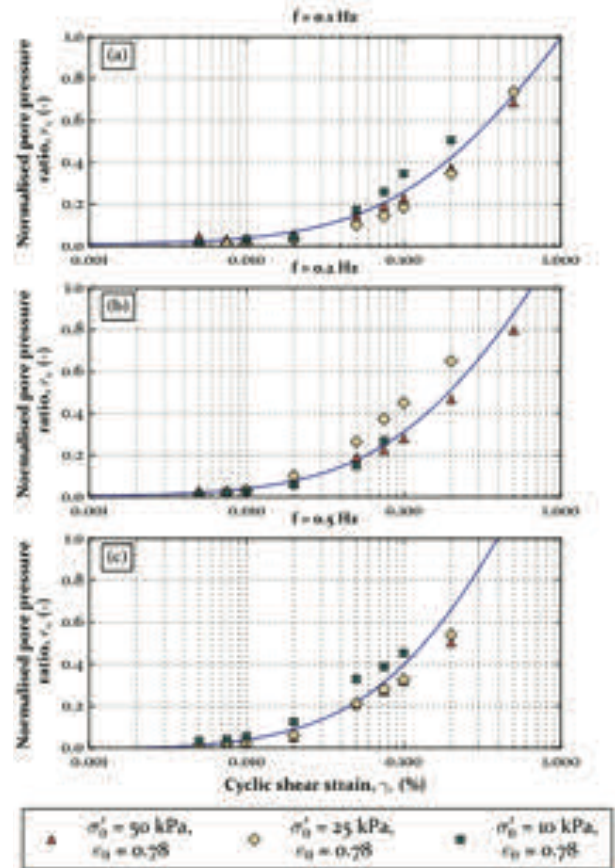


Figure 5 Analytical model for pore pressure build-up [6]: (a) Frequency of 0.1 Hz, (b) Frequency of 0.2 Hz and (c) Frequency of 0.5 Hz.

higher than 0.2 Hz. Proposed analytical model for second cycle of dynamic loading fits very well to measured data and can be used for a quick calculation of pore pressure build up.

### Acknowledgments

The research presented in this paper was partially supported by the following projects:

- University of Rijeka uniri-tehnic-18-113 Laboratory research of static and cyclic behaviour at landslide activation;
- Ministry of Science, Education and Sports of the Republic of Croatia under the project Research Infrastructure for Campus-based Laboratories at the University of Rijeka, number RC.2.2.06-0001. Project has been co-funded from the European Fund for Regional Development (ERDF);
- Croatian Science Foundation under the Project IP-2018-01-1503 Physical modelling of landslide remediation constructions behaviour under static and seismic actions (ModLandRemSS).

Their support is gratefully acknowledged.

## References

- Bićanić N, Camenen JF, Čeh N, Koziara T (2016) Characterisation of pattern formation in constrained multiblock assembly subjected to horizontal harmonic excitation. *International Journal of Masonry Research and Innovation*. 1(4): 375 - 397. <https://doi.org/10.1504/IJMRI.2016.081271>
- Chakraborty T, Salgado R (2010) Dilatancy and Shear Strength of Sand at Low Confining Pressures. *Journal of Geotechnical and Geoenvironmental Engineering*. 136(6): 527 - 532. [https://doi.org/10.1061/\(asce\)gt.1943-5606.0000237](https://doi.org/10.1061/(asce)gt.1943-5606.0000237)
- Chavent G (2009) *Nonlinear least squares for inverse problems: theoretical foundations and step-by-step guide for applications*. Springer Verlag, Dordrecht; New York. 9789048127849. 366p.
- Controls Group Ltd. (2017) Dynamic electromechanical triaxial systems, Controls. <https://www.controls-group.com/usa/dynamic-testing-systems/dynamic-triaxial-system-dynatriax-ems.php> [Last accessed: 15.11.2021.]
- Darendeli MB (2001) A new family of normalized modulus reduction and material damping curves. PhD Dissertation, University of Texas at Austin. 362p.
- Dobrilla S, Čeh N, Tuhtan M, Jelenić G (2018) Experimental Analysis of Structure Response to Non-uniform Support Excitation. *Zbornik radova*. 20:175–188. <https://doi.org/10.32762/zr.20.1.11>
- Dobry R, Ladd RS, Yokel FY, et al (1982) Prediction of Pore Water Pressure Buildup and Liquefaction of Sands During Earthquakes by the Cyclic Strain Method. 150p.
- EN/ISO 14688-2 (2017) Geotechnical investigation and testing — Identification and classification of soil — Part 2: Principles for a classification. Geneva, CH. 1 – 11.
- Gabet EJ, Mudd SM (2006) The mobilization of debris flows from shallow landslides. *Geomorphology*. 74(1-4):207–218. <https://doi.org/10.1016/j.geomorph.2005.08.013>
- Highland LM, Bobrowsky P (2008) *The landslide handbook—A guide to understanding landslides*. U.S. Geological Survey Circular 1325, Reston, Virginia. 147p.
- Iai S, Tobita T, Nakahara T (2005) Generalised scaling relations for dynamic centrifuge tests. *Geotechnique*. 55(5):355–362. <https://doi.org/10.1680/geot.2005.55.5.355>
- ICL (2016) *Instruction for World Reports on Landslides*. URL: <http://www.iplhq.org/> [Last accessed: 15.01.2022.].
- Kumar SS, Krishna AM, Dey A (2017) Evaluation of dynamic properties of sandy soil at high cyclic strains. *Soil Dynamics and Earthquake Engineering*. 99:157–167. <https://doi.org/https://doi.org/10.1016/j.soildyn.2017.05.016>
- Ladd R (1978) Preparing Test Specimens Using Undercompaction. *Geotechnical Testing Journal*. 1(1):16–23. <https://doi.org/10.1520/GTJ10364J>
- NASA (2012) What Is Microgravity?. URL: <https://www.nasa.gov/audience/forstudents/5-8/features/nasa-knows/what-is-microgravity-58.html> [Last accessed: 15.11.2021.]
- Pajalić S, Peranić J, Maksimović S, et al (2021) Monitoring and data analysis in small-scale landslide physical model. *Applied Sciences (Switzerland)*. 11(11): 1 - 26. <https://doi.org/10.3390/app11115040>
- Panda RC (2012) Introduction to PID controllers: theory, tuning and application to frontier areas. InTech, Rijeka, Croatia. 9789533079271. 272p.
- Popescu ME (2002) Landslide causal factors and landslide remedial options. In: 3rd International Conference on Landslides, Slope Stability and Safety of Infra-Structures. pp 61–81.
- Seed HB, Idriss IM (1970) Soil Moduli and Damping Factors for Dynamic Response Analyses. 48p.
- Shaoli Y, Sandven R, Grande L (2003) Liquefaction of sand under low confining pressure. *Journal of Ocean University of Qingdao*. 2(2): 207 - 210. <https://doi.org/10.1007/s11802-003-0053-9>
- Silver ML, Tatsuoka F, Phukunhaphan A, Avramidis AS (1980) Cyclic undrained strength of sand by triaxial test and simple shear test. In: Proceedings of the 7th world conference on earthquake engineering. pp 281 – 288.
- Sture S, Batiste SN, Lankton M, Parisi J (2004) Properties of Sand under Low Effective Stresses. *Eng Constr Oper Challenging Environ Earth Sp 2004 Proc Ninth Bienn ASCE Aerosp Div Int Conf*. pp 78 – 84. [https://doi.org/10.1061/40722\(153\)12](https://doi.org/10.1061/40722(153)12)
- Tabata K, Vucetic M (2010) Threshold Shear Strain for Cyclic Degradation of Three Clays. *International Conferences on Recent Advances in Geotechnical Earthquake Engineering and Soil Dynamics*. 1.15a. pp 1 – 12.
- Thian SY, Lee CY (2017) Cyclic stress-controlled tests on offshore clay. *Journal of Rock Mechanics and Geotechnical Engineering*. 9(2): 376 – 381. <https://doi.org/10.1016/J.JRMGE.2016.06.013>
- Virtanen P, Gommers R, Oliphant TE, et al (2020) {SciPy} 1.0: Fundamental Algorithms for Scientific Computing in Python. *Nature Methods*. 17(3): 261 – 272. <https://doi.org/10.1038/s41592-019-0686-2>
- Vucetic M (1994) Cyclic threshold shear strains in soils. *Journal of Geotechnical Engineering*. 120(2): 2208 - 2228. [https://doi.org/10.1061/\(ASCE\)0733-9410\(1994\)120:12\(2208\)](https://doi.org/10.1061/(ASCE)0733-9410(1994)120:12(2208))
- Vucetic M, Mortezaie A (2015) Cyclic secant shear modulus versus pore water pressure in sands at small cyclic strains. *Soil Dynamics and Earthquake Engineering*. 70: 60 – 72. <https://doi.org/10.1016/j.soildyn.2014.12.001>
- White JRF (2020) *A Laboratory Investigation Into the Behaviour of Sand at Low Confining Stresses*. PhD Dissertation. University of Oxford, United Kingdom. 281p.
- Wu LZ, Huang RQ, Xu Q, et al (2015) Analysis of physical testing of rainfall-induced soil slope failures. *Environmental Earth Sciences*. 73(12): 8519 – 8531. <https://doi.org/10.1007/s12665-014-4009-8>
- Yang H, Wang F, Miyajima M (2015) Investigation of shallow landslides triggered by heavy rainfall during typhoon Wipha (2013), Izu Oshima Island, Japan. *Geoenvironmental Disasters*. 2(1): 1 - 15. <https://doi.org/10.1186/s40677-015-0023-8>



# Laboratory rheology measurements of natural debris material

Timotej Jurček<sup>(1)</sup>, Matjaž Mikoš<sup>(1)</sup>, Matej Maček<sup>(1)</sup>

1) University of Ljubljana, Faculty of Civil and Geodetic Engineering, Ljubljana, Jamova cesta 2, Slovenia, +386 31 219 166 (timotej.jurcek@fgg.uni-lj.si)

**Abstract** Debris flows are fast-moving masses of debris material that often occur in mountainous regions. Due to high velocity, they endanger the local population. To predict the time of arrival and the extent of hazard zones, the rheological properties of debris flow material, among others, are needed. This study presents the rheological investigation of debris flow materials in Slovenia. The rheological parameters were measured at different sediment concentrations using two shear-rate controlled coaxial cylinder rheometers (Brookfield DV3T HB and ConTec Viscometer 5) and standard tests for determining the workability and flowability of construction materials (e.g., funnels, V-funnel, flow channel, flow table, L-box). The measured data were evaluated by using the Bingham rheological model. The study was conducted in two separate stages. Firstly, the rheological parameters were measured only on fines (0-0.063 mm). These tests were used to determine the correctness of the rheological parameters measured in the rheometer by predicting their behaviour in standard tests. Afterwards, an attempt to predict rheological properties from these tests was made. In the second stage of this study, debris materials up to 16 mm were tested. A comparison of the rheological parameters obtained from the two coaxial cylinder rheometers was made. The study shows that the rheological parameters measured with the coaxial cylinder rheometers give reasonably good predictions of standard tests results, while the vice versa, i.e., from these standard tests estimation of rheological parameters is not possible. Although fines predominate the behaviour of a debris flow, the rheological properties are not only defined by fines, and thus should be tested in large rheometers with a wide grain-size distribution.

**Keywords** BING model, debris flow, debris material, laboratory test, rheology, rheometers

## Introductions

Debris flows are natural disasters that pose a great threat to life and infrastructures around the world. Numerical simulation of debris flow is very important element of potential hazard zones determinations. An important part of numerical models is estimation rheological parameters. The rheological behaviour of debris flow is depended on grain size distributions, fines and sediment concentration. In the past decades considerable work has been carried out

to provide rheological parameters for debris material using different types of viscometers and rheometers (e.g., Contreras and Davies 2000, Schatzmann et al. 2009, Bisantino et al. 2010, Maček et al. 2017). Many authors have pointed out, that there is a need to determine the rheological behaviour of debris flow with as large particle size as possible (Jeong 2006).

This study presents rheological measurements of debris flow materials from four Slovenia landslides – Stože, Stogovci, Čikla and Urbas. Measurements were executed using two coaxial cylinder rheometers and standard tests for determination workability and flowability of construction materials. Two coaxial cylinder rheometers were used to evaluate influence of geometry and maximum grain size of specimens. The low-cost standard test for determination workability and flowability of construction materials were used to investigate the determination possibility of rheological parameters from these tests.

## Development of debris flow research in Slovenia

Practically one-third of Slovenian's territory is highly susceptible to landslides. Furthermore, susceptibility model reveals that about 15% of Slovenia is highly susceptible to debris flows events (Komac et al. 2009). Interest on debris-flow hazard has increased in Slovenia after the catastrophic debris-flow event from the Stože landslide in November 2000. Various studies have been performed in order to better understand this type of natural hazard (Mikoš, 2020).

Majes et al. (2002) reported first rheological parameters of three Slovenian landslides – Stože, Slano blato and Strug, measured on fines. These parameters were than used by Četina et al. (2006) for back analysis of the Stože debris flow. They found that a different set of rheological parameters is needed.

Later Maček et. al. (2017) analysed influence of rheometer size and grain distribution on rheological parameters of debris flow using larger rheometer. A new back analyse was made by Sodnik (2017) using these rheological parameters. Again, there were differences between material parameters and model prediction.

Bezák et. al. (2021) also used rheological parameters obtained from large rheometer to calibrate a debris flow model for the Koroška Bela landslides.

## Rheological behaviour of debris material

Debris materials display non-Newtonian flow behaviour, which could be described by the Bingham model. The Bingham model is one of the simplest and most popular rheological models for pseudoplastic materials. This model preserves linear relationship between shear stress ( $\tau$ ) and shear rate ( $\dot{\gamma}$ ) including yield stress ( $\tau_y$ ) and plastic viscosity ( $\eta_p$ ).

$$\tau = \tau_y + \eta_p \dot{\gamma} \quad [1]$$

The rheological parameters of debris material are usually expressed depending on sediment concentration (O'Brien and Julien 1988). The sediment concentration ( $C_v$ ) in this study was calculated from the measured water content assuming full saturation of specimen.

$$C_v = \frac{V_s}{V} = \frac{1}{1 + \frac{w \rho_s}{S_r \rho_w}} \quad [2]$$

where  $V_s$  is the volume of particles,  $V$  is the volume of soil,  $w$  is the water content,  $S_r$  is the degree of saturation (1 for fully saturated soil),  $\rho_s$  is the density of particles, and  $\rho_w$  is the density of water.

### Rheometers

Physical problem of soil deformation in rheometers is very complex (Schramm, 2000). The mathematical solution is acceptable with some basic assumptions – laminar flow, steady state flow, no slip at the cylinder surface, no end effect, homogeneity of soil and no chemical or physical changes during testing (Jeong, 2006).

From the measurements by coaxial cylinder rheometers, the properties of the Bingham model were determined considering the possibility of plug flow (Feys et al. 2013, Smolar et al. 2016). In the plug flow regime not all material flows, and the boundary between the sheared “fluid” and the un-sheared “solid” is called the plug radius ( $R_p$ ).

$$R_p = \sqrt{\frac{T}{\tau_y 2 \pi h}} \leq R_0 \quad [3]$$

where  $T$  is torque,  $h$  is height of the inner cylinder and  $R_0$  is radius of container.

Rheological parameters were determined by using proper mathematical equation (Eq. 1) considering boundary conditions (Eq. 3). The Eq. 4 is obtained by integrating shear rates between inner and outer cylinders.

$$T = \frac{4 \pi h \ln\left(\frac{R_s}{R_i}\right)}{\left(\frac{1}{R_i^2} - \frac{1}{R_s^2}\right)} \tau_y + \frac{8 \pi^2 h}{\left(\frac{1}{R_i^2} - \frac{1}{R_s^2}\right)} \eta_p N \quad [4]$$

where  $R_s = \min(R_p, R_0)$  defined after Fig. 1 and  $R_i$  is inner cylinder radius. From the measured sets of rotational velocity ( $N$ ) and corresponding torque ( $T$ ), the Bingham

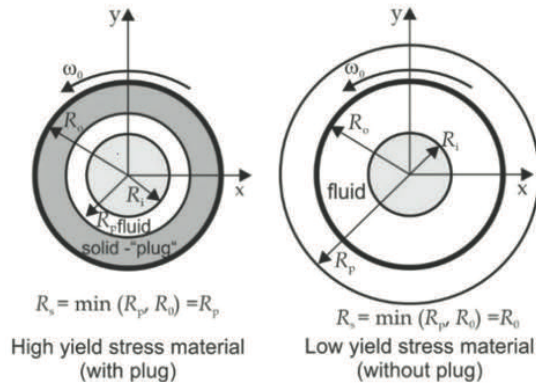


Figure 1 Top view of coaxial cylinder left – with plug flow, right – without plug flow (Feys et al. 2013).

rheological parameters can be calculated by using least-squares method.

### Standard laboratory tests

There are numerous standard tests for determination workability and flowability of construction materials. Furthermore, such determination of rheological properties frequently enables only measurements of material response to test (e.g., material spreading, time needed to flow) without determinations of rheological parameters. However, in this study the possibility of determination Bingham rheological parameters by using standard tests (funnels, V-funnel, and flow channel) were also carried out.

### Funnels

The Bingham rheological parameters were determined according to outflow time from funnels using semi-analytical approach introducing by Nguyen et al. (2006). The outflow times were calculated by numerical integration. Rheological parameters were obtained by comparing measured data with calculated ones.

### V-funnel and flow channel

The possibility of rheological parameters determination from V-funnel and flow channel measurements was performed by using parametric analysis. However, after initial measurements on fines were concluded that V-funnel is not suitable for rheological investigation of debris material. Debris material at low volume concentrations flowed from the V-funnel rapidly (about in 1 second), while material at higher volume concentration did not flow (dripping). Due to this only flow channel was used afterwards.

### Materials investigated

Investigated materials are from 4 different Slovenian landslides – Stože, Stogovci, Urbas and Čikla landslides. Grain size distribution curves of debris materials are shown in Fig. 2 and index properties of fines are shown in Tab. 1.

## Testing equipment and methods

### Rheometers

Two types of shear rate controlled coaxial cylinder rheometers were used in this study – Brookfield DV<sub>3</sub>T HB (DV<sub>3</sub>T HB) and ConTec Viscometer 5 (CTK 5). The main differences between these rheometers are the volume and maximal grain size of the specimen.

#### DV<sub>3</sub>T HB Rheometer

Smaller DV<sub>3</sub>T HB rheometer is suitable for measurements on fine-grained debris material (0-0.063 mm) at different sediment concentrations (Fig. 3). Tests in this rheometer were conducted by using different size of vane and smooth spindles. However, spindle was found not suitable for rheological investigation of debris material due to problems with slippage at the contact of material and spindle. Same problem is reported by Smolar et al. (2016) on marine clays.

Measurements were performed by decreasing shear rate from 250 to 10 RPM (revolutions/ minute) in stages of 10 RPM. Each step lasted until the vane had rotated at least one revolution (360°). During the investigation the outer cylinder was fixed, while vane was rotating. The resulting torque was calculated for each step as the average of measured values after equilibrium was reached.

#### ConTec Viscometer 5

Larger ConTec Viscometer 5 is primary designed for rheological testing fresh mortars and concrete (Fig. 4). It enables measurements on material with maximum grain size of 22.4 mm.

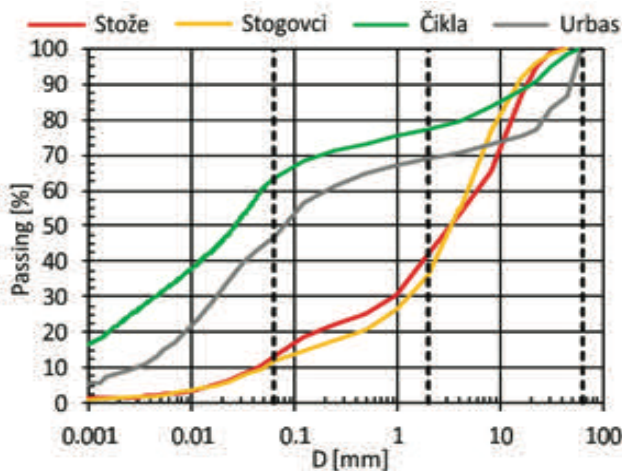


Figure 2 Grain size distribution of tested samples.

Table 1: Index properties of fines.

Material	w <sub>L</sub> [%]	I <sub>p</sub> [°]
Stože landslide	16.2	11.6
Stogovci landslide	20.4	9.1
Čikla landslide	20.0	39.3
Urbas landslide	31.7	23.3



Figure 3 DV<sub>3</sub>T HB rheometer.



Figure 4 ConTec Viscometer 5.

In this study grain size of debris material was reduced to 16 mm as elongated particles could jam the gap between the inner and outer radius (Maček, 2017). After the initial pre-shear period of around 6 seconds the measurements were performed by decreasing shear rate from 1.1 RPS (revolutions/ second) to 0.1 RPS in steps of 0.1 RPS. The last stage of the test was shearing at rotational velocity of 0.7 RPS to check segregation of the material. The resulting torque for each step was calculated from the 10 lowest measured values in 15 seconds of measurement, after an equilibration time of 1 second.

### Standard laboratory tests

#### Funnels

Rheological measurements using funnels were performed on fine-grained debris material at different sediment concentration (Fig. 5). The time of specimen flow through different nozzle diameter (4.75, 8, 9, 10, 11, 13 mm) in step by 200 ml was measured. Measurements were performed while flow was continuous. In case of segregation or dripping specimens out of nozzle, the measurements were terminated.

#### Flow channel

By using the flow channel, the impact of rheological properties on the time and length of spreading 1 L fine-grained debris material at different sediment concentration were investigated. The test started by opening valve and the material started to spread along the channel. After 30 second the spread was measured.

The entire measurement was enhanced by recordings with GoPro Hero 4 camera with an accuracy of 25 images

per second. The recordings were afterwards equipped with image counter (Fig. 6). The rate of spreading was determined from these images.

### Test results

#### Fine-grained debris material

##### Rheometer and funnels

Measured data from DV<sub>3</sub>T HB rheometer was analysed by using Eq. 4. Furthermore, the rheological parameters were estimated from funnel measurements by using semi-analytical equations by Nguyen et al. (2006). It was found that one rheological parameter was close to rheometer measurements while the other exhibit significant uncertainties. Best results were obtained if rheological parameters from funnel measurements were fitted using initial approximation of yield stress as remoulded undrained shear stress ( $c_{ur}$ ). Additionally, analysis could be improved by considering relationship between rheological parameters and volume concentration (O'Brien and Julien, 1988) as presented in Fig. 7.

Remoulded undrained shear stress of fine-grained debris material was measured separately with laboratory vane at 0.25 RPM.

##### Flow channel

The results of flow channel measurements are presented in Fig. 8.



Figure 5 Funnel with different nozzle diameter.



Figure 6 Flow channel.

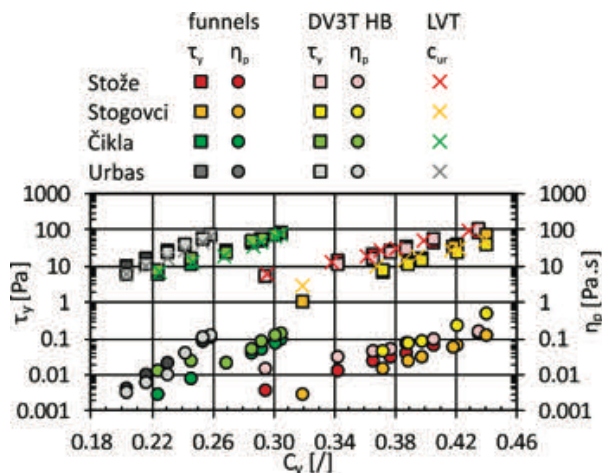


Figure 7 Rheological parameters and remoulded undrained shear stress of fine-grained debris material.

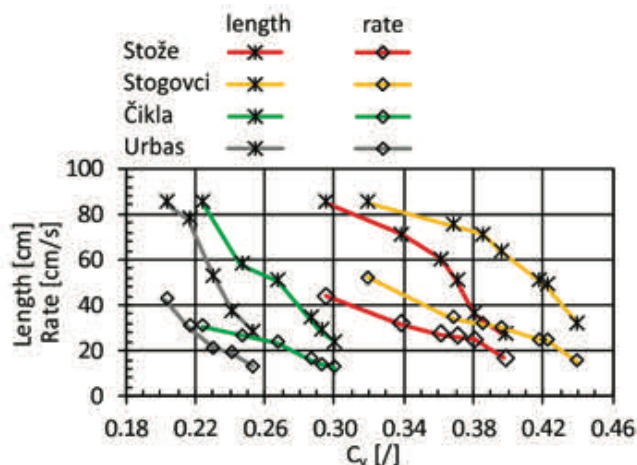


Figure 8 Length and rate of spreading fine-grained debris material in flow channel.

#### Coarse-grained debris material

##### Rheometer

Measured data from CVT 5 rheometer was analysed by using Eq. 4 (Fig. 9). Rheological measurements on coarse-grained debris material from the Čikla landslide were performed in twice within the interval of 3 months. Yield stresses were close while plastic viscosity were approximately two times different.

### Analysis of results and discussion

#### Rheometers

Rheological parameters obtained by rheometers were compared considering grain composition and relationship between shear stress and plastic viscosity. In case that rheological properties would be predominately defined by nature and consistency of fines, then rheological parameters would be only consistency of fines dependent. In Fig. 10 sediment concentration of fines was calculated by assuming that water is only bonded on fines (i.e., coarse grains floats in fine-grained matrix). However, the results

show significant differences between tests on fine-grained fractions or on material 0-16 mm, thus measurement only on fine-grained fractions cannot describe the flow behaviour of debris material.

**Flow channel**

A parametric analysis was performed to investigate a relationship between rheological parameters of fine-grained debris material and length/speed of spreading material over the channel. Fig. 11 compares the measured and estimated length and rate (Eq. 8 and 9). The accuracy of prediction is  $\pm 5$  cm for length or  $\pm 5$  cm/s for rate. By inverting the problem, it was found that only yield stress could be reasonably estimated by measuring length and rate of spread, but not plastic viscosity.

A better prediction was trying to obtain by using one-dimensional BING model for simulating the flow of debris flows in subaqueous or subaerial environment. The input parameters of the model are the longitudinal profile of the bed, the initial shape of debris source (parabolic), the density of debris material and rheological parameters. The output produced by BING includes runout distance and frontal velocity of material.

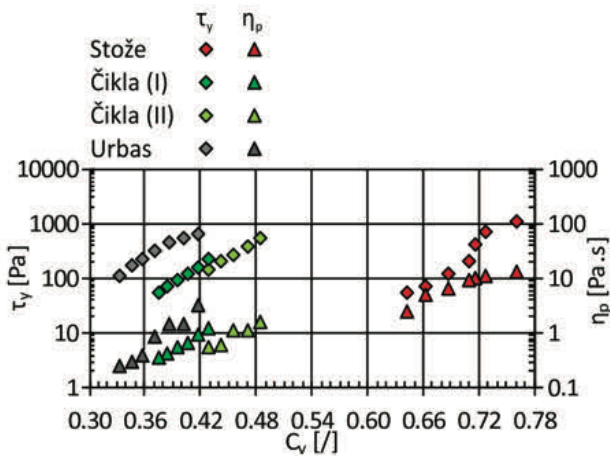


Figure 9 Rheological parameters of coarse-grained debris material.

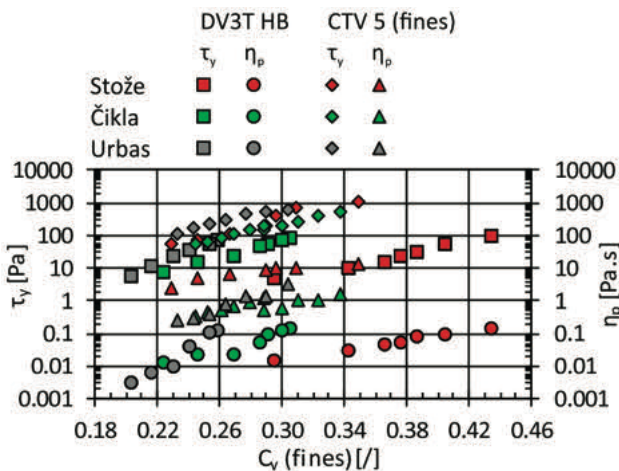


Figure 10 Yield stress, plastic viscosity and sediment concentration (for fines) from DV<sub>3</sub>T HB and CTV<sub>5</sub> rheological measurement.

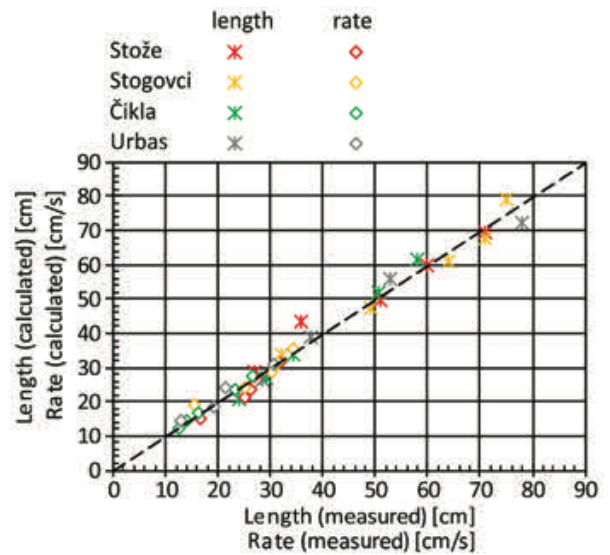


Figure 11: Measured and calculated (parametric analysis) length and rate of spreading.

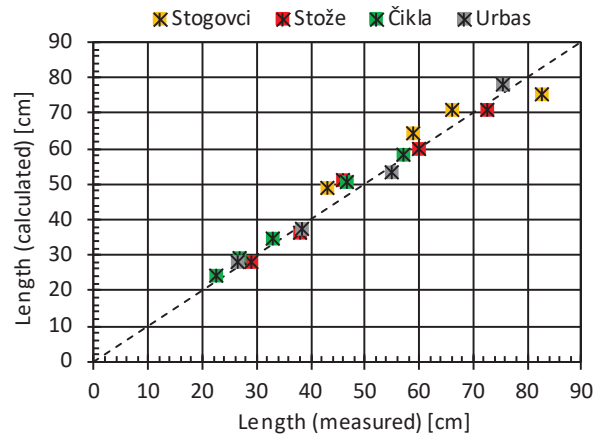


Figure 12 Measured and calculated (BING model) length and rate of spreading.

The funnel flow measurements were calculated based on rheological parameters from DV<sub>3</sub>T HB rheometer. The initial material shape (parabola) was such that potential energy was approximately the same. The model describes well the influence of each type of fine-grained debris material on the behaviour (runout distance) of the flow (Fig. 12), although the velocities were significantly overestimated. The same is also reported by Rémire et al. (2005) and Jeon (2014).

**Conclusions**

The main conclusions based on this study are:

- The debris materials behave as Bingham viscoplastic fluid.
- The rheological parameters depend on sediment concentration and grain size distribution. The increase of sediment concentration or maximal grain size increases both yield stress and plastic viscosity.

- The rheological properties of debris flows are not defined only by fines.
- The rheological parameters measured in coaxial cylinder rheometers give reasonably good predictions of standard test results, while from these standard tests estimations of rheological parameters are not possible. Standard tests are suitable for quality assessment of rheological measurements.
- For real field cases, rheological properties of debris materials should be tested in large rheometers with as wide grain-size distribution as possible.

## Acknowledgment

The study was financed by the Division for Rehabilitation after Natural and Other Disasters of the Ministry of the Environment and Spatial Planning of the Republic of Slovenia. Additional financial support was provided by the Slovenian Research Agency through research grant J1-8153. The study was also a part of the project IPL 216 – Diversity and hydrogeology of mass movements in the Vipava Valley, SW Slovenia.

## References

- Bezák N, Sodnik J, Maček M, Jurček T, Jež J, Peternel T, Mikoš M (2021) Investigation of potential debris flows above the Koroška Bela settlement, NW Slovenia, from hydro-technical and conceptual design perspectives. *Landslides*. 18(10): 3891-3906. <http://dx.doi.org/10.1007/s10346-021-01774-7>
- Bisantino T, Fischer P, Gentile F (2010) Rheological Characteristics of Debris-Flow Material in South-Gargano Watersheds. *Natural Hazards*. 54(2): 209-223. <http://dx.doi.org/10.1007/s11069-009-9462-4>
- Contreras S M, Davies T R H (2000) Hysteresis and time-dependent rheology of debris flow material. *Journal of Hydraulic Engineering*. 126(12): 938-941. [http://dx.doi.org/10.1061/\(ASCE\)0733-9429\(2000\)126:12\(938\)](http://dx.doi.org/10.1061/(ASCE)0733-9429(2000)126:12(938))
- Četina M, Rajar R, Hojnik T, Zakrajšek M, Krzyk M, Mikoš M (2006) Case Study: Numerical Simulations of Debris Flow below Stože, Slovenia. *Journal of Hydraulic Engineering*. 132(2): 121-130. [http://dx.doi.org/10.1061/\(asce\)0733-9429\(2006\)132:2\(121\)](http://dx.doi.org/10.1061/(asce)0733-9429(2006)132:2(121))
- Feys D, Wallevik D E, Yahia A, Khayat K H, Wallevik O H (2013) Extension of the Reiner–Riwlin equation to determine modified Bingham parameters measured in coaxial cylinders rheometers. *Materials and Structures*. 46(1-2): 289-311. <https://doi.org/10.1617/s11527-012-9902-6>
- Jeong S W (2006) Influence of physic-chemical characteristics of fine-grained sediments on their rheological behaviour. PhD Thesis, Faculte de Sciences et Genie, University Laval, Quebec, Canada. <https://corpus.ulaval.ca/jspui/bitstream/20.500.11794/18566/1/24116.pdf> [Last accessed: 15 February 2022].
- Komac M, Kumelj Š, Ribičič M (2006) Debris-flow susceptibility model of Slovenia at scale 1:250,000. *Geologija*. 52(1): 87-104. <https://doi.org/10.5474/geologija.2009.010>
- Maček M, Smolar J, Petkovšek A (2017) Influences of rheometer size and the grain size on rheological parameters of debris flow. WLF 2017: Advancing Culture of Living with Landslides, Vol. 2, June 2017. Ljubljana, Slovenia. pp. 399-406. [http://dx.doi.org/10.1007/978-3-319-53498-5\\_46](http://dx.doi.org/10.1007/978-3-319-53498-5_46)
- Majes B, Petkovšek A, Logar J (2002) The Comparison of Material Properties of Debris Flows from Stože, Slano Blato and Strug Landslide. *Geologija*. 45(2): 457-463. <http://dx.doi.org/10.5474/geologija.2002.048>
- Mikoš M (2020) After 2000 Stože Landslide: Part I – Development in landslide research in Slovenia – Po zemeljskem plazu Stože leta 2000: Del I – Razvoj raziskovanja zemeljskih plazov v Sloveniji. *Acta Hydrotechnica*. 33(59): 129-153. (in Slovenian) <https://doi.org/10.15292/acta.hydro.2020.09>
- Nguyen V H, Remond S, Gallias JL, Bias J P, Muller P (2006) Flow of Herschel-Bulkley fluids through the Marsh cone. *Journal of Non-Newtonian Fluid Mechanics*. 139(1-2): 128-134. <https://doi.org/10.1016/J.JNNFM.2006.07.009>
- O'Brien J S, Julien P Y (1988) Laboratory analysis of mudflow properties. *Journal of Hydraulic Engineering*. 114(8): 877-887. [https://doi.org/10.1061/\(ASCE\)0733-9429\(1988\)114:8\(877\)](https://doi.org/10.1061/(ASCE)0733-9429(1988)114:8(877))
- Remaitre A, Malet JP, Maquaire O, Ancey C, Locat J (2005) Flow behavior and runout modelling of a complex debris flow in a clay-shale basin. *Earth Surface Processes and Landforms*. 30: 479–488. <https://doi.org/10.1002/esp.1162>
- Schatzmann M, Bezzola G R, Minor H-E, Windhab E J, Fischer P (2009) Rheometry for Large-Particulated Fluids: Analysis of the Ball Measuring System and Comparison to Debris Flow Rheometry. *Rheologica Acta*. 48(7): 715-733. <http://dx.doi.org/10.1007/s00397-009-0364-x>
- Schramm G, (2000) A practical approach to Rheology and Rheometry, 2nd Edition. Karlsruhe, Germany, Gebrüder HAAKE GmbH.
- Smolar J, Maček M, Petkovšek A (2016) Rheological properties of marine sediments from the port of Koper. *Acta Geotechnica Slovenica*. 13(2): 57-65.
- Sodnik, J (2017) Ocenjevanje nevarnosti zaradi delovanja drobirskih tokov na hudourniških vršajih. PhD thesis, Faculty of Civil and Geodetic Engineering, University of Ljubljana, Slovenia. Available at: <https://repozitorij.uni-lj.si/Dokument.php?id=108683> (in Slovenian). [Last accessed: 15 February 2022]

# A use of similarity laws in landslide physical modelling: preliminary considerations

Sara Pajalić<sup>(1)</sup>, Josip Peranić<sup>(1)</sup>, Vedran Jagodnik<sup>(1)</sup>, Martina Vivoda Prodan<sup>(1)</sup>, Željko Arbanas<sup>(1)</sup>

1) University of Rijeka, Faculty of Civil Engineering, Rijeka, Radmile Matejčić 3, Croatia, +38551265943 (spajalic@uniri.hr)

**Abstract** Physical modelling of landslides has started in the 1970s in Japan on natural slopes exposed to artificial rain. Subsequently, small-scale laboratory models' development began in the 1980s with the aim of studying landslide behaviour such as triggering, movement, and accumulation. The research presented here is part of the Project funded by the Croatian Science Foundation entitled "Physical modelling of landslide remediation constructions' behaviour under static and seismic actions". When remediation constructions become part of a small-scale model, the determination of a scale ratio and the need to establish, at least partially, similarity laws with regard to a real slope is inevitable. Although many studies use a small-scale model to research landslide behaviour of a real slope, there are only few studies that consider the scale ratio and similarity laws. In this paper, a summary of some of these studies is provided, along with an overview of all similarity laws and the characteristics that make them up in relation to landslides. Since the most important problem with small-scale models at 1g are low values of the overburden stresses in a model, laboratory tests are performed in an attempt to determine the relationship between the constitutive behaviour of the material in a small-scale model and a real slope. An example of geometric similarity is given here using the grain-size distribution curve and its influence on other similarities and their characteristics like infiltration rate, weight, and strength of soil, etc. Some preliminary results of laboratory tests are presented together with a discussion about possibilities and limitations in achieving better similarity of small-scale models to real slopes.

**Keywords** physical modelling, landslide, scale ratio, similarity laws

## Introduction

As one of the major geohazards, landslides are vastly investigated all over the world in a variety of fields, including landslide modelling and landslide remediation. Initially, landslide modelling was based solely on numerical methods. The development of landslide physical modelling began in the early 1970s in Japan on natural slopes subjected to artificial rainfall (Oka 1972; Yagi et al. 1985) Laboratory experiments on scaled physical models started in 1980s and 1990s, designed to study

landslide initiation and behaviour under 1g conditions (Hung and Morgenstern 1984; Eckersley 1990). The greatest advantage of using physical models in research is their wide range of applications. So, in the years that followed noticed researches, studies using landslide physical models, covered a wide range of topics, from landslide initiation and motion (Wang and Sassa 2001; Okura et al. 2002; Moriwaki et al. 2004), rainfall infiltration and permeability (Damiano and Olivares 2010) to modelling partially saturated conditions and the effects of suction on slope stability (Greco et al. 2010; Yang et al. 2021).

Although there are numerous studies and literature on landslide physical models and their behaviour, most of the studies present only the results of the experiments, completely or partially neglecting the theory and laws of similarity. In 1957, Rocha (1957) was the first to systematically describe the problems of scaling models of shallow foundations and retaining walls in soil mechanics. He proposed scaling the constitutive behaviour of soil models and assumed a linear stress-strain relationship between a model and a soil "prototype". Roscoe (1968) conducted model experiments on walls, monitoring stresses at the wall-sand contact and deformations in the sand. He emphasized the ability of the model to fully replicate the behaviour of the soil whose response depends on its own unit weight. The deformation behaviour will be the same when two soil elements are subjected to similar stress paths, which is the case when their initial state is equidistant from the critical state line. Iai and others (1989; 2005) determined the similarity for experiments with a saturated soil-structure-fluid model conducted under 1g conditions on a shaking table. This similarity was determined based on the basic equations for equilibrium of soil mass and pore fluid pressure. An assumption was made that the stress-strain relationship is independent of overburden stresses when scaling factors are introduced for both stress and strain. The results showed that this assumption is only applicable in the range of small deformations, i.e., the deformation before a failure occurrence. Altaee and Fellenius (1994) continued the path of Roscoe and emphasized the need to determine the critical state line, since the behaviour of a cohesionless soil is a function of its position in the  $e - \ln p'$  plane and its vertical distance from the critical state line, as it was mentioned by Roscoe. Some researchers (e.g. Gibson 1996; Meymand 1998) used an approach of the distance of soil

element state from the critical state line to achieve a normalized constitutive behaviour of a material when using scaled models.

The research presented here is funded by the Croatian Science Foundation as a part of the Project “Physical modelling of landslide remediation constructions’ behaviour under static and seismic actions”, whose main objective is to model and study the behaviour of remediation constructions. The results could provide a basis for improving the standard design of remediation constructions in engineering practice. While results from small-scale landslide physical models are undoubtedly very useful in researching certain problems (e.g., debris flow initiation, propagation), even without considering scaling laws, the law of similarity becomes necessary and unavoidable when considering remediation constructions. The focus of this research is to analyse the different similarity laws and to determine the mutual influences/relations between the different types of similarity. In this paper, an overview of the similarity laws and their mutual influences will be given, along with simple examples of their application.

### Similarity laws in small-scale landslide physical models

There is a wide field of engineering problems, including both fluid, solid mechanics, and their interaction, in which various types of physical models are used to predict a behaviour of particular physical systems, also known as prototypes (Buckingham 1914; Baker et al. 1991). The three main laws of similarity are: geometric similarity, kinematic similarity, and dynamic similarity (Baker et al. 1991). Geometric similarity means that the corresponding linear dimensions are in the same proportion, i.e., the model has the same or similar dimensions as the prototype; in our case, this would be a real slope. Kinematic similarity means that displacements, velocities, and accelerations change uniformly on both the model and the real slope. Finally, dynamic similarity means that the ratios of all forces acting on both the model and the real slope are constant. Geometric similarity is the easiest to achieve, and even models that are not completely similar geometrically can behave similarly. It will be shown later that even a change in such a simple law of similarity as geometric similarity can have a major effect on all other similarity laws.

When considering the similarity between a small-scale landslide model and a real slope, the main challenge is to achieve constitutive behaviour similar to that of a real slope, whose response is closely related to the overburden stresses present in the soil due to its own weight. In small-scale models, the height of the soil layer is much lower than in real slopes, and consequently the overburden stresses in the model are much smaller that have significant impact to soil resistance.

A complete similarity implies that all three similarity laws are satisfied, which is very difficult to achieve in

practice regardless of which engineering problem is observed. Depending on the problem considered, each similarity law includes different characteristics. Tab. 1. gives an overview of the characteristics that are included in each of similarity laws.

The process of determining similarity is significantly complex and requires linking several similarity characteristics, each of that affects several other characteristics in different ways. Often, due to the complexity of a model, satisfying the conditions for just one or two similarity laws are adopted. Complete similarity between the real slope and a model that accurately predicts the behaviour of the real slope is probably impossible to be achieved.

As an example, a geometric similarity characteristic, grain-size distribution, can be taken and its influence on other characteristics and similarity laws considered. Grain-size distribution affects dynamic similarity by changing of soil strength parameters – cohesion and internal friction. Also, a change in grain-size distribution affects kinematic similarity by change in the shearing velocity, infiltration rate, flow velocity, etc. The mutual influence of similarities and individual characteristics in landslide similarity is very extensive and hard to encompass all at once.

### Materials and Methods

A small-scale physical model was designed to enable landslide initiation under the influence of rainfall and equipped with a complex monitoring system. Since the focus of this research is on the similarity of small-scale and real landslides and the possibility of achieving it as much as possible, the focus of this paper is on laboratory tests on the materials used in the model. More on the experiments performed on the physical model can be found in Jagodnik et al. (2021) and Peranić et al. (2022).

Table 1 Similarity laws and their characteristics in relation to landslides modelling.

Geometric similarity	Kinematic similarity	Dynamic similarity	
Model dimensions	Particle displacements	Soil unit weight	
Slope angle inclination	Particle velocities	Strength parameters	Friction angle
			Cohesion
Grain-size distribution	Particle accelerations		
Moisture content	Water flow velocity		
Soil volumetric characteristics	Rainfall intensity		
	Infiltration		



**Material**

Because of relatively simple behaviour in terms of infiltration and landslide initiation, sand was chosen as the basic material in initial small-scale experiments and for determination of similarity laws in this study. A further simplification is that the influence of suction on hydraulic and mechanical response of sand is completely neglected, considering very small values of suction that may exist in such a soil. This makes the characteristics of the similarity laws much less complicated.

The used sandy material is the Drava River fine graded sand with a maximum grain size of 2.0mm. The grain-size distribution curve is shown in Fig. 1, while Tab. 2. presents the basic physical properties of the soil and the initial conditions at the beginning of the experiments.

**Methodology**

Laboratory testing includes direct shear tests, large shear tests, and triaxial tests on the sandy material, but the last will not be discussed in detail here. The main objective of conducting laboratory tests is to determine relationships between soil material behaviour in a small-scale model and a prototype, i.e., a real slope in nature. The geometric scale ratio selected for this study is 1:20, i.e.,  $\lambda = 20$ . The 1:20 scale ratio was chosen in view of the depth of the shallow sliding surfaces of several meters. This is consistent with the depth of the sliding surfaces in the model of 15 to 20cm in the total slope layer height of 30cm. As mentioned in the previous section, the biggest problem in small-scale models is the influence of the soil stresses magnitude in a model to the shear strength of the slope material caused by small overburden (self-weight)

Table 2 Basic physical properties of the Drava River sand and the initial conditions at the beginning of the experiments.

Soil properties	Values
Specific gravity $G_s$ (/)	2.70
Dry density $\rho_D$ ( $g/cm^3$ )	1.52
Total density $\rho_T$ ( $g/cm^3$ )	1.55
Effective particle size $D_{10}$ (mm)	0.183
Effective particle size $D_{30}$ (mm)	0.237
Effective particle size $D_{60}$ (mm)	0.320
Uniformity coefficient $C_u$ (/)	1.749
Curvature coefficient $C_c$ (/)	0.959
Minimum void ratio $e_{min}$ (/)	0.641
Maximum void ratio $e_{max}$ (/)	0.911
Hydraulic conductivity $k_s$ (m/s)	1E-05
Peak/residual friction angle $\varphi$ (°)	35 / 33
Cohesion $c$ (kPa)	0
Initial porosity $n_i$ (/)	0.437
Initial void ratio $e_i$ (/)	0.776
Initial relative density $Dr_i$ (%)	50
Initial water content $w_i$ (%)	2

stresses. The differences in the magnitude of the soil stresses in the small-scale model and a real slope (factor of 1:20) can be seen in Fig. 2. Stress-strain analysis was performed in Rocscience software, program package RS2, version 2020 11.003 (2020).

To illustrate the complexity of using similarity laws in landslide modelling, an example is given here. A geometric similarity, i.e., grain-size distribution, is chosen here as one of the characteristics to show how much the characteristics of similarity are intertwined. If the grain-size distribution as a geometric characteristic and a scale ratio of 1:20 is taken as, the grain-size distribution curve is determined that is 20 times larger, as it can be seen in Fig. 3. In reality, this is a much coarser material (i.e., gravel) than the sand used in the model. It has a much larger permeability and water flow, which affects the kinematic similarity, and different strength parameters (friction angle and cohesion), which affect the dynamic similarity.

Both the sand and this 20 times larger material (i.e., gravel) were tested in direct shear and large shear tests, respectively, to determine shear strength parameters.

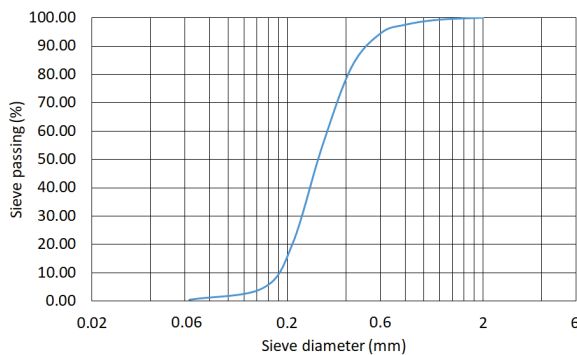


Figure 1 Grain-size distribution curve of the Drava River sand.

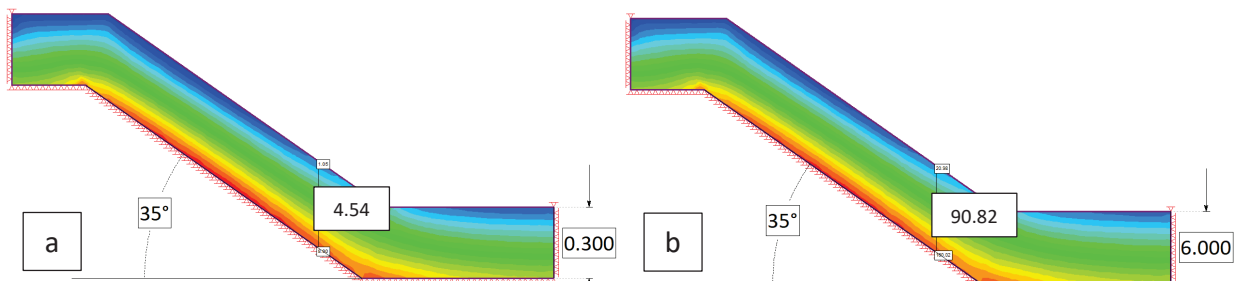


Figure 2 Magnitude of effective vertical soil stress in: a) small-scale model, b) real slope (factor 1:20).

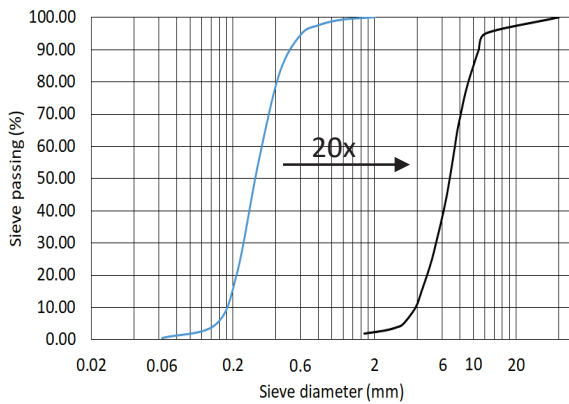


Figure 3 Grain-size distribution curve of the Drava River sand and scaled material 20 times larger.

Tests on sand in direct shear apparatus were performed at small normal stresses (4, 8, 15kPa) and at larger normal stresses, similar to the standard tests (25, 50, 100kPa). Large shear tests on the scaled material were performed at stresses 20 times larger than those present in the small-scale slope model. The results are presented in the next section.

## Preliminary results

### Laboratory tests

In this section, the preliminary results of the soil testing are presented. In Fig. 4a, shear strength envelopes are presented, obtained from the direct shear tests under very small normal stresses, similar to those of the small-scale model, and at larger normal stresses, similar to those of a real slope or model slope scaled by a factor of 20. The difference between the friction angle of the soil at small normal stresses ( $\varphi = 39^\circ$ ) and at large normal stresses ( $\varphi = 35^\circ$ ) can be noticed. Since the results suggest that the relationship is not linear over the entire stress range, more detailed tests should be performed under the stress conditions that exist in the small-scale model. In Fig. 4b, the results from the large shear tests performed on the larger, scaled material can be seen. The friction angle of the scaled material is much larger ( $\varphi = 51^\circ$ ) than those of the original material.

### Slope stability analysis

Fig. 5 shows a stability analysis performed in the software Rocscience, program package Slide2, version 2020 9.008 (2020), in which the factor of safety (FoS) is compared for the following simple examples: small-scale sandy slope, real slope with sandy material, and real slope with gravelly material. The stability analysis performed is the simplest possible, with the aim of showing and comparing these few examples of similarities in landslides. All three analyses are performed at a slope inclination of  $35^\circ$  for the same initial conditions and at a water level rise to the toe of the slope. It can be observed that the small-scale model with sand (Fig. 5a) has a higher FoS (1.211) with respect to the real

slope model with sand (Fig. 5b), while the real slope model with gravel (Fig. 5c) has a significantly higher FoS (1.846) than both sand models.

These examples of stability analysis give two directions in observing the similarity laws - one from the aspect of changing the dimensions of the geometric model and the other from the aspect of changing the grain-size distribution curve. Both characteristics are aspects of geometric similarity, which is the easiest law to achieve. To even begin to compare the results of the stability analysis in Fig. 5, you must consider the overburden stresses present in both slopes, as shown in Fig. 2. While the small-scale slope has effective stresses of about 4kPa in the middle of the slope layer (Fig. 2a), the real slope has effective stresses of about 90kPa in the same profile area (Fig. 2b). Although the increased stress level in the laboratory tests reduces the friction angle, there are some aspects that need to be considered when comparing FoS in Fig. 5a and Fig. 5b. Here, a unit weight of the material in a real slope is much larger, which consequently means greater compaction of the material and greater overburden stresses in the slope, which in turn contributes to greater shear resistance of the soil. Thus, the stability analysis and the FoS cannot be unambiguously considered.

The stability analysis shows a similar position of the sliding surface in all three models. Of course, the conditions in these models are different, with the exception of the water level at the toe of the slope, but it is likely that the mechanism of slope failure is very similar to that which occurred in the experiments on the physical model. Because of the nature of the material in Fig. 5c and the initial conditions of the material in Fig. 5b (i.e., infiltration to a larger soil layer height, required rainfall intensities, rainfall duration, etc.), the conditions leading to failure of the slope will be different from those in the small-scale slope model in Fig. 5c.

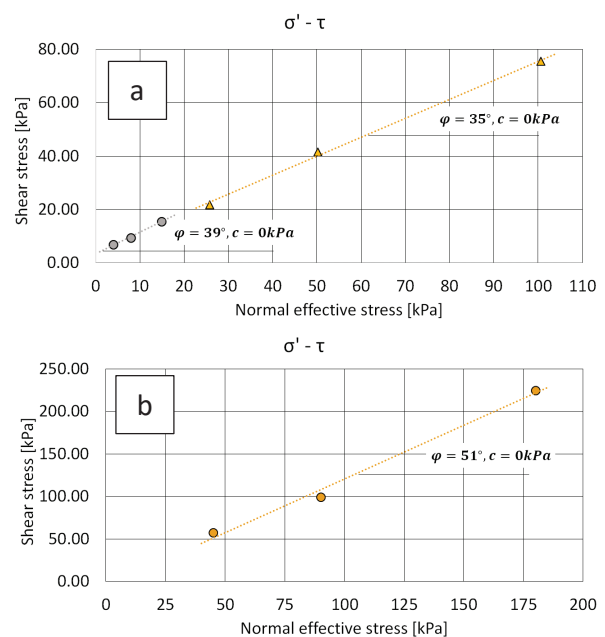


Figure 4 Soil strength parameter results from: a) direct shear tests, b) large shear tests.

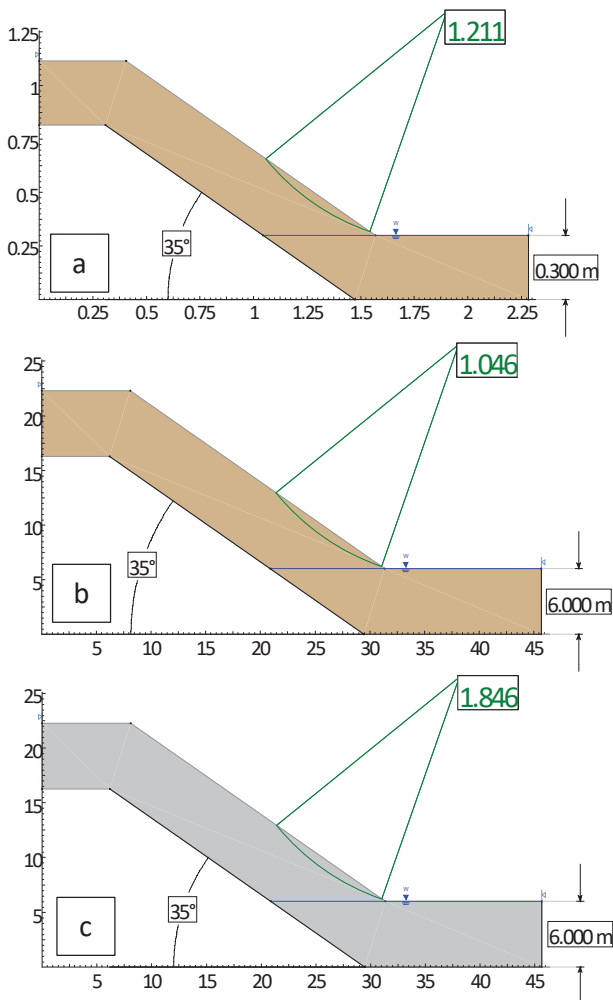


Figure 5 Stability analysis for slope at 35°: a) small-scale model, b) real slope with sandy material (factor 1:20), c) real slope with gravelly material (1:20).

## Discussion and conclusions

An application of the similarity laws to the physical modelling of landslides is presented here. Two characteristics of geometric similarity are presented here as the simplest examples - geometric similarity of model dimensions and similarity of the grain-size distribution curve. It is necessary to highlight other characteristics and influences of different similarity laws in relation to landslide physical models, which are listed in Tab. 1.

This paper analyses the geometric similarity of the model dimensions for the sandy material used in the small-scale model and for the real slope using a slope stability analysis. The original material was tested in direct shear under a range of stresses corresponding to the overburden stresses in the small-scale model (Fig. 2a) and the real slope with dimensions 20 times larger (Fig. 2b). The preliminary results of the tests indicate that the shear strength envelope depends on the magnitude of the effective stresses and that increasing the stress level decreases the friction angle (Fig. 4a). The geometric

similarity of grain-size distribution curve is analysed by scaling the grain-size distribution curve to a material 20 times larger (i.e., gravel). Due to the size of the particles, this material was tested in the large shear under stresses similar to those in the real slope to determine the soil strength parameters. The results of the scaled material give a much greater friction angle compared to the original material (Fig. 4b).

The change in the grain-size distribution curve affects a variety of other similarity characteristics. Both materials (i.e., sand and gravel) have relatively simple behaviour - they are cohesionless soils with high permeability and infiltration rates, while the values of suction that can occur in sand are very low, so suction can be completely neglected. However, if the similarity of the grain-size distribution curve is used to obtain a different type of material, the same aspects and their influence can be observed. For example, if this material is a clayey soil, the conditions and processes in the model would be very different. Behaviour of clay is completely different than sand or gravel because of existence of cohesion, much lower permeability, and higher soil suction values. When these physical properties are combined with a change in model dimensions to those of a real slope, several other problems arise, and the effects on a variety of similarity characteristics should be considered. In a real slope model with a much larger soil layer height and a much lower infiltration rate, the conditions that lead to failure would take much longer to develop. In addition, an appropriate amount of rain must fall on a such slope in a given period of time. Unlike sandy and gravelly material, the time to failure here could be measured in days or months, not just a few hours. Since it is unlikely that this type of material will absorb all of the rainfall, runoff must also be considered in the slope model.

Two simple changes in geometric similarity (i.e., model dimensions and grain-size distribution) would cause a change in dynamic similarity by changing the soil weight, which depends on model dimensions and corresponding overburden stresses, and a change in soil strength parameters, which depends on a material obtained by scaling the grain-size distribution curve. The above-mentioned effects are the result of considering only two simple characteristics, the dimensions, and the grain-size distribution curve, although there are more characteristics that could be taken into account. It is obvious that the process of obtaining similarity is very complex.

The best results in achieving similarity can be obtained with the simplest similarity characteristics presented in this paper - the model dimensions and the grain-size distribution curve, since they represent the geometric similarity. Achieving similarity becomes more complicated when dealing with more complex soil materials with a higher percentage of fine particles. In this case, other characteristics must be also considered - cohesion, suction, infiltration rate, rainfall intensities, etc. In these small-scale models under 1g conditions caused by

rainfall, kinematic behaviour in terms of particle velocity and acceleration is not so much significant. In this type of experiment, where the mechanism of sliding (but not flowing) is observed, the displacement velocity is not so important as a results. Here, the mechanism of the sliding and failure along with all the conditions that lead to failure are of the most important interest. These conditions are rainfall and its associated intensity, the rate of infiltration into the slope, the amount of runoff, the rainfall duration necessary for a given intensity to cause sliding, etc.

In the literature, a very few results obtained in small-scale models were back-analysed to examine what actually happened in real slopes. Although the results are undoubtedly useful to investigate certain problems in landslide research, when combining a physical model with a scaled construction such as retaining walls or pile walls, the similarity law must be considered, at least to some degree of acceptance. Only then the models and the real-size mitigating solutions can be comparable and thus provide more realistic results. Establishing the similarity between the various characteristics presented in this paper is a necessary prerequisite for further research and detailed development of similarity aspects as well as small-scale remediation designs.

## Acknowledgments

The research presented in this paper was supported by Croatian Science Foundation under the Project IP-2018-01-1503 Physical modelling of landslide remediation constructions' behaviour under static and seismic actions (ModLandRemSS). The part of the laboratory equipment used for laboratory testing was provided in the frame of the Project Research Infrastructure for Campus-based Laboratories at the University of Rijeka, co-funded in a part by the Ministry of Science, Education, and Sports of the Republic of Croatia and the European Regional Development Fund (ERDF). This support is gratefully acknowledged.

## References

- Altaee A, Fellenius BH (1994) Physical modeling in sand. *Can Geotech J.* 31:420–431. <https://doi.org/10.1139/t94-049>
- Baker WE, Westine PS, Dodge FT (1991) Similarity methods in engineering dynamics: Theory and practice of scale modeling Revised edition. Elsevier Science Publishing Company Inc., New York, USA. (978-0444881564). 384p.
- Buckingham E (1914) On physically similar systems; Illustrations of the use of dimensional equations. *Phys Rev.* 4:345–376. <https://doi.org/10.1103/PhysRev.4.345>
- Damiano E, Olivares L (2010) The role of infiltration processes in steep slope stability of pyroclastic granular soils: laboratory and numerical investigation. *Natural Hazards.* 52:329–350. <https://doi.org/10.1007/s11069-009-9374-3>
- Eckersley JD (1990) Instrumented laboratory flowslides. *Géotechnique.* 40:489–502. <https://doi.org/10.1680/geot.1990.40.3.489>
- Gibson AD (1996) Physical scale modeling of geotechnical structures at one-G. Dissertation, California Institute of Technology, California, USA
- Greco R, Guida A, Damiano E, Olivares L (2010) Soil water content and suction monitoring in model slopes for shallow flowslides early warning applications. *Physics and Chemistry of the Earth.* 35:127–136. <https://doi.org/10.1016/j.pce.2009.12.003>
- Hungr O, Morgenstern NR (1984) Experiments on the flow behaviour of granular materials at high velocity in an open channel. *Géotechnique.* 34:405–413. <https://doi.org/10.1680/geot.1984.34.3.405>
- lai S (1989) Similitude for shaking table tests on soil-structure-fluid model in 1g gravitational field. *Soils and Foundations.* 29:105–118. <https://doi.org/10.3208/sandf1972.29.105>
- lai S, Tobita T, Nakahara T (2005) Generalised scaling relations for dynamic centrifuge tests. *Géotechnique.* 55:355–362. <https://doi.org/10.1680/geot.2005.55.5.355>
- Jagodnik V, Peranić J, Arbanas Ž (2021) Mechanism of landslide initiation in small-scale sandy slope triggered by an artificial rain. In: Arbanas Ž, Bobrowsky PT, Konagai K, et al. (eds) *Understanding and Reducing Landslide Disaster Risk: Volume 6 Specific Topics in Landslide Science and Applications.* Springer International Publishing, Cham, pp 177–184. [https://doi.org/10.1007/978-3-030-60713-5\\_19](https://doi.org/10.1007/978-3-030-60713-5_19)
- Meymand P (1998) Shaking table scale model tests of nonlinear soil-pile-superstructure interaction in soft clay. Dissertation, University of California, California, USA
- Moriwaki H, Inokuchi T, Hattanji T, et al (2004) Failure processes in a full-scale landslide experiment using a rainfall simulator. *Landslides.* 1:277–288. <https://doi.org/10.1007/s10346-004-0034-0>
- Oka H (1972) Impacts by the “artificial landslide”: re-examine the rage of nature (in Japanese). *Kagaku Asahi.* 32:152–153.
- Okura Y, Kitahara H, Ochiai H, et al (2002) Landslide fluidization process by flume experiments. *Engineering Geology.* 66:65–78. [https://doi.org/10.1016/s0013-7952\(02\)00032-7](https://doi.org/10.1016/s0013-7952(02)00032-7)
- Peranić J, Jagodnik V, Čeh N, et al (2022) Landslide initiation in small-scale sandy and clayey slopes exposed to artificial rain. *Proceedings of the 20th International Conference on Soil Mechanics and Geotechnical Engineering Sydney 2020 6 (In Press)*
- Rocha M (1957) The possibility of solving soil mechanics problems by the use of models. *Proceedings of the 4th International Conference on Soil Mechanics and Foundation Engineering, 12-24 August 1957.* London, UK. pp. 183-188.
- Rocscience (2020) RS2 Tutorial. URL: <https://www.rocscience.com/help/rs2/tutorials/tutorials-overview>. [Last accessed 31 January 2022].
- Rocscience (2020) Slide2 Tutorial. URL: <https://www.rocscience.com/help/slide2/tutorials>. [Last accessed 31 January 2022].
- Roscoe KH (1968) Soils and model tests. *Journal of Strain Analysis.* 3:57–64. <https://doi.org/10.1243/03093247V03I057>
- Wang G, Sassa K (2001) Factors affecting rainfall-induced flowslides in laboratory flume tests. *Géotechnique.* 51:587–599. <https://doi.org/10.1680/geot.2001.51.7.587>
- Yagi N, Yatabe R, Enoki M (1985) Laboratory and field experiments on prediction method of occurring time of slope failure due to rainfall. *Journal of Japan Landslide Society.* 22:1-7\_1. [https://doi.org/10.3313/jls1964.22.2\\_1](https://doi.org/10.3313/jls1964.22.2_1)
- Yang K-H, Nguyen TS, Rahardjo H, Lin D-G (2021) Deformation characteristics of unstable shallow slopes triggered by rainfall infiltration. *Bull Eng Geol Environ.* 80:317–344. <https://doi.org/10.1007/s10064-020-01942-4>

# The Krvavec bottom cabin lift station protection against torrential hazards by a new slit check dam and a series of flexible net barriers

Jošt Sodnik<sup>(1,2)</sup>, Matjaž Mikoš<sup>(2)</sup>

1) Tempos, environmental civil engineering Ltd, Ljubljana, Slovenia. + 386 41 288 442 (jost.sodnik@gmail.com)

2) University of Ljubljana, Faculty of Civil and Geodetical Engineering, Ljubljana, Slovenia

**Abstract** In May 2018, during a heavy local rainfall, a debris flood transported some 20000 m<sup>3</sup> debris and destroyed torrential structures and damaged the bottom station of the Krvavec ski resort cabin lift. The return period of the local rainfall event was estimated to be above 50 years. After immediate mitigation measures in 2018 to remove deposited debris and clean the station, a technical documentation was prepared in 2019–2021 for a more detailed mitigation in order to protect the area from future debris floods and potential debris flows. After reconstruction of destroyed torrential control structures in the lower section, a large reinforced concrete slit check dam was planned at the confluence of the two main tributaries: Lukenjski and Brezovški graben. Its retention volume is 14000 m<sup>3</sup> and its capacity to stop the inflowing debris will be supported by a series of flexible net barriers in the two tributaries, 12 barriers in total. Their height ranges from 3 to 6 m and their span from 9 to 25 m. This paper presents a good example of the holistic approach how to control erosion processes that results in small landslides and granular/hyperconcentrated flows.

**Keywords** debris floods, mitigation measures, RAMMS, ring nets, Slovenia, flexible barriers

## Introduction

Substantial parts of Slovenia are subjected annually to landsliding (Mikoš et al. 2004). Different forms of mass movements (e.g. Jemec Auflič et al. 2017) are triggered mainly during strong local storms with heavy precipitation, after prolonged rainfalls, or during and after strong earthquakes. Such events are focus of numerous research activities (Mikoš 2020), but also require for engineering mitigation works in hazard areas. In Slovenia, various torrential hazards are threatening also infrastructure, among others also touristic infrastructure. Since tourism is an important economic sector in Slovenia, safe operation of any infrastructure in touristic destinations is of paramount importance for sustainable tourism and individual safety of tourists during leisure and holidays, including indoor and outdoor sport activities and recreation. This paper describes a torrential event in May 2018, when a strong local thunderstorm damaged the bottom cabin lift to the Krvavec ski area in N Slovenia, and

its mitigation to secure its safe operation during and after strong local thunderstorms triggering debris floods and debris flows (Sodnik et al. 2021).

## Materials and Methods

### The Krvavec ski area in N Slovenia

Krvavec Mountain is a ski resort in the Kamnik-Savinja Alps (northern Slovenia) and stretches from 1450 to 1971 m a.s.l. It is a high Alpine ski resort having its own artificial snow producing system, being therefore potentially resilient also for incoming climate changes. The first ski lift was constructed in 1958. With 29 km of ski slopes, it is one of the largest ski resorts in Slovenia. The main approach for the resort is the cabin lift, that was completely reconstructed in late 90's. Due to its high altitude, the Krvavec ski resort is very popular and the operational and safe cabin lift is crucial for its operating and further development.

### Rainfall and debris flood event in May 2018

On May 30, 2018, an intense rainfall event occurred in the Krvavec area. Approximately 50 mm of rain in 30 minutes was recorded at the Krvavec weather station at 1740 m a.s.l. The rainfall intensity for 30min duration was estimated as 50 to 100-year return period event. Numerous small landslides occurred and resulted in mass flows that travelled downstream in the Brezovški and Lukenjski graben. Around 10000 m<sup>3</sup> of the debris from the Brezovški graben was deposited around the bottom station of the Krvavec cabin lift, which was partially damaged (Fig. 1).



Figure 1 The Krvavec bottom station of the cabin lift after May 2018 event.

Fortunately, the debris material from the Lukenjski graben was deposited on the flatter part of the channel, upstream from the confluence with the Brezovški graben. Shortly after the May 2018 event, Slovenian Water Agency approached to the mitigation works. After first field interventions (i.e. cleaning of deposits), geological survey was carried out and a conceptual design was prepared. After a formal acceptance of the proposed technical solutions, final technical design for the proposed mitigation works was prepared.

## Results

### Geological investigations

After the first field interventions, geological survey of the area was carried out, focusing on the estimation of amount of debris material that could mobilize in future events. Geological map with critical sediment sources areas was prepared. General characteristics of the May 2018 event source area, transport of the material and lithological characteristics of accumulated material indicated that event characteristics were more typical for a hyperconcentrated flow (i.e. debris flood) rather than for a debris flow. The source area of deposited material was not an individual landslide, but rather a longer torrent section where erosion and small side slumps occurred. Based on the field survey, it was estimated that events with similar magnitudes could occur in the future. More detailed results are presented in the literature (Bezak et al. 2020).

### Hydrological investigations and debris flood modelling

Hydrological model, using HEC-HMS was prepared to simulate runoff conditions in the Brezovški and Lukenjski graben. The peak discharge  $Q_{100}$  was estimated for further use in the design process of mitigation works. The numerical simulation model RAMMS-DF was applied to simulate May 2018 event. The main aim of modelling was to obtain debris flow pressure on structures and flow velocities. The model was calibrated based on the position and volume data about deposited debris material. More detailed results are presented in literature (Bezak et al. 2020).

### Proposed mitigation measures

Conceptual design suggested three main mitigation measures: i) restoration of regulation of the Reka torrent downstream from Brezovški and Lukenjski graben confluence; ii) a new large check dam (barrier) with large sediment trap; iii) erosion control measures on the Brezovški and Lukenjski graben to prevent large sediment and erosion outbursts in the future.

Final execution designs were prepared for all three stages. Restoration of the Reka regulation (check dams, rip rap bank protection) was carried out in 2021. New large slit dam with 14000 m<sup>3</sup> sediment deposit capacity with associated measures presented in Fig. 2 is in the phase of building permit and land acquisition and is planned for construction in 2<sup>nd</sup> half of 2022 or in 2023.

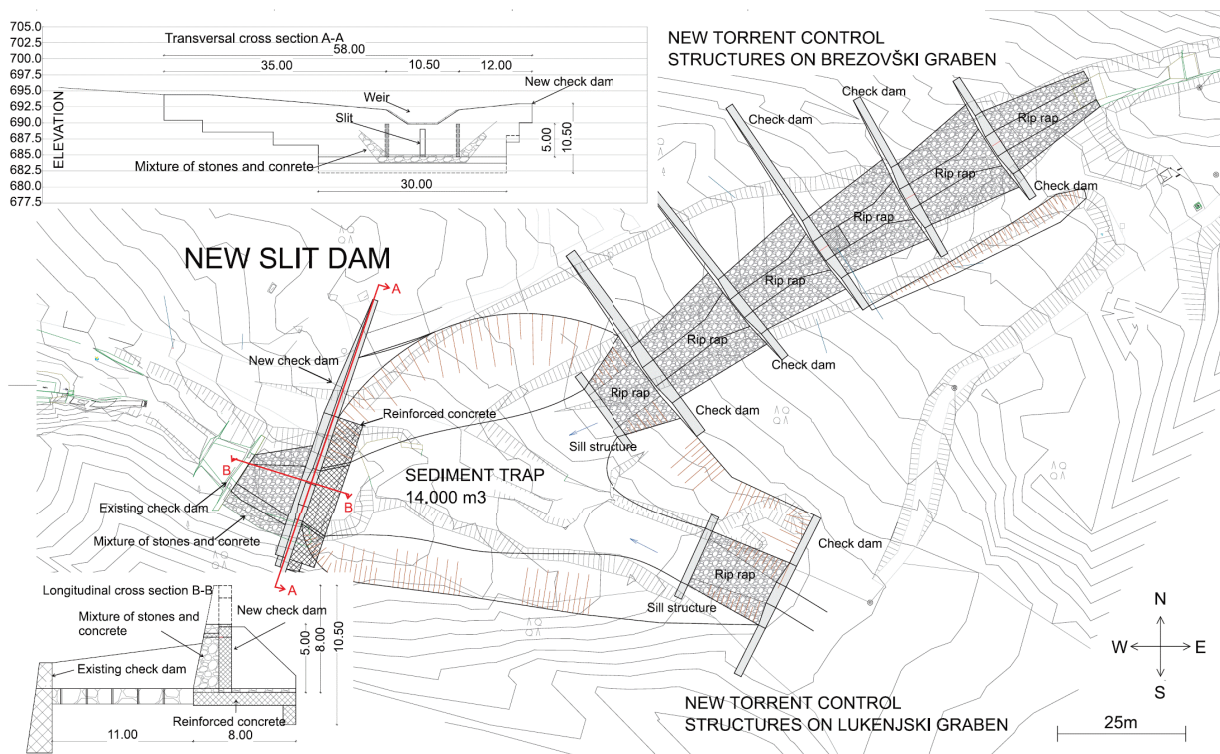


Figure 2 The slit check dam location and its main characteristics with its the transversal and longitudinal cross section. Spacing among contour lines is 2 m. Additional structures that are to be built are also shown in the figure (e.g. several sill structures).

Flexible net ring barriers proved to be a successful countermeasure for shallow landslides and debris flows (Geobruigg 2022a). Based on these experiences, a series of flexible net barriers is planned in the channels of the Brezovški and Lukenjski graben (Fig. 3), to prevent side erosion (bank collapses, slumps) and thus to limit sediment supply from sediment sources. Eight flexible barriers are planned on the Brezovški graben (Fig. 4) and four on the Lukenjski graben. Height of the barriers varies between 2,5 and 6 m and the sediment trap capacity between 100 and 800 m<sup>3</sup>. Top width of the barriers varies between 9 and 25 m.

All the barriers were designed and dimensioned using DEBFLOW online tool, developed by Geobruigg (Berger et al. 2021). The design of the barriers was modified because the deposits are not intended to be removed after the events, but the main purpose of the barriers is to reduce channel slope, reduce velocities and support unstable channel banks. Because of this specific design, not all barriers are designed for debris flow impact, but all of them are designed for overflowing forces. The upstream barriers and the barriers with larger distance to next

upstream barriers are designed for debris flow impact, which is one of the possible scenarios in the phase where barriers will be filling up with sediments. The final state of the barriers will be, when all of them are filled up, torrential bed slope reduced and bank erosion mostly mitigated. Based on the topographic characteristics, VX type of barriers (Fig. 5) are chosen. Some of them were customized with additional ropes and anchors, since there was no need to use stronger, more resistant nets, but only to add some ropes to fulfil all the design requirements (stability, resistance).

The downstream section of the Lukenjski graben is accessible by road, but the upstream part is not. Therefore, special equipment will be used for the construction of the 4 barriers in the Lukenjski graben. The Brezovški graben, on the other hand, is accessible only on foot. Therefore, an old forest road will be reconstructed to get close to the channel. Several logging lifts will be installed to transport the construction material to the construction sites, and most of the work will be done manually, because it will not be possible to get the excavator to the exact locations of the most of the barriers in the Brezovški graben.

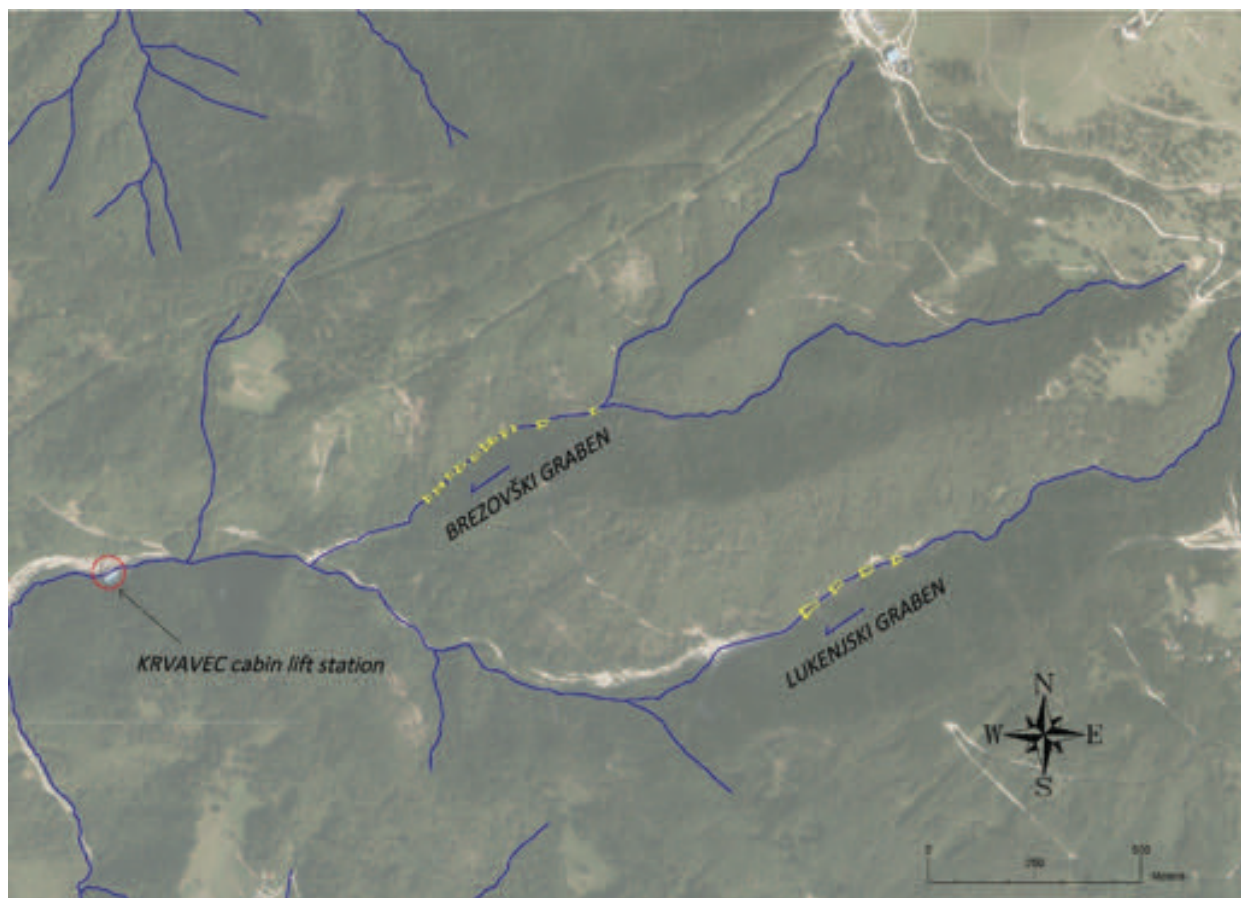


Figure 3 Digital orthophoto with Brezovski graben, Lukenjski graben and planned flexible barriers (yellow marks).



Figure 4 A longitudinal profile of the Brezovški graben with the locations of the 8 flexible net barriers.

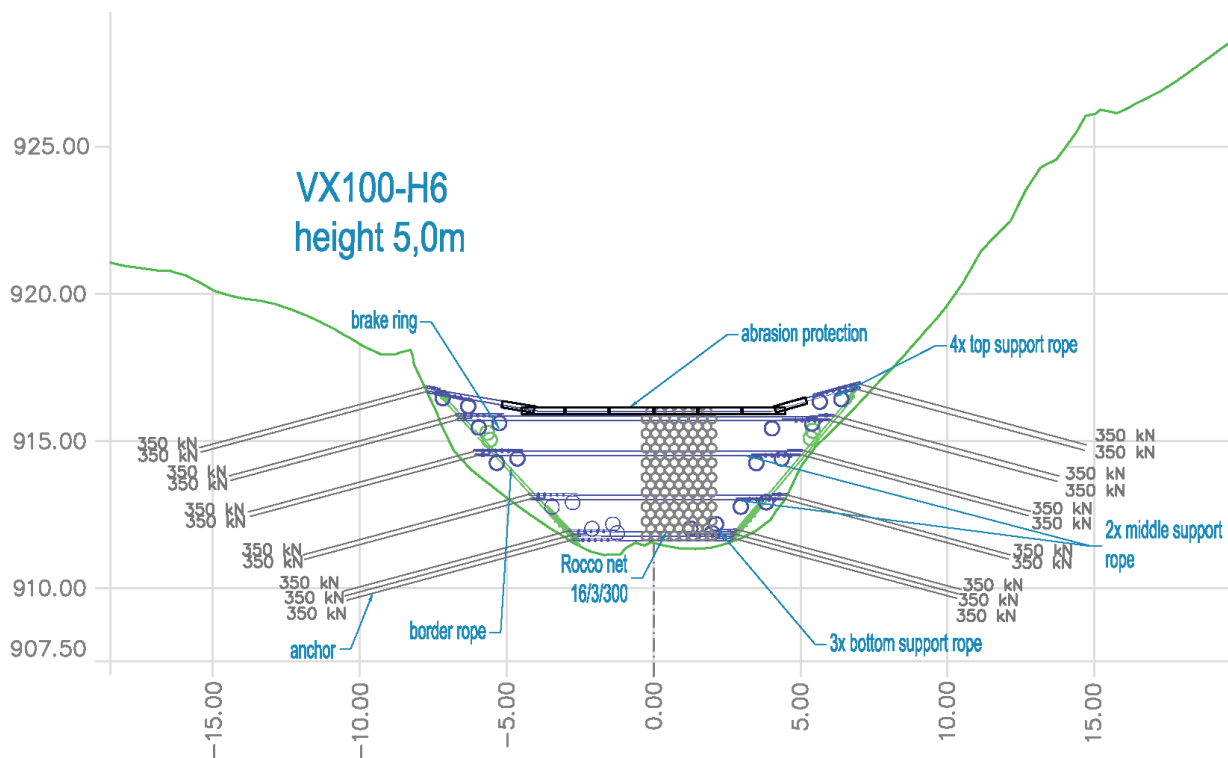


Figure 5 Example of a designed VX barrier.

### Debris flow monitoring

The proposed mitigation works were soon also seen as a good opportunity to put research into practice by jointly developing a field debris flow observatory for a better understanding of debris flow dynamics and its interaction with protection structures.

### GeobruGG GUARD and debris flow dynamics

The GUARD is a waterproof small device (2.6 kg), simply installed on the suspension rope of every protection barrier (GeobruGG 2022b; Fig. 6). Since it is packed with a selection of sensors which transmits environmental and physical data over a mobile network (GSM / UMTS / LTE) for decades, rockfall or debris flow events are clearly logged. One needs to correlate the locally measured weather data (wind, air temperature, precipitation, ...) with the logged data in the Guard.





Figure 6 Example of the Geobrug Guard installation (Geobrugg 2022b).

For the purpose of this project, several Guards will be installed on protection barriers in the Brezovški graben to:

- estimate corrosion of the nets,
- detect single debris flow events (including single surges) by measuring impacts on the barriers up to 200 g and forces in the barrier ropes up to approximately 300 kN, knowing orientation of the Guard.

The field site of a protection barrier will be supported by video monitoring using simple hunting trail cameras used for wildlife photography. Such cameras can be triggered by movement of a debris flow just before it hits the protection barrier. Video surveillance will enhance the understanding of debris flow dynamics in the retention area above each net barrier.

Several occasional field measuring campaigns are planned to estimate the volume of retained debris after each debris flood respectively debris flow. Different techniques may be applied for this purpose, such as small drones (UAV), stereo photogrammetry or terrestrial laser scanning.

#### Concrete mixtures abrasion monitoring

The durability of torrential protection structures against torrential hazards is a function of environmental factors (such as air temperature, insulation, snow and rain, frost and chemical weathering, impacts of rocks or debris, etc....) as well as the materials used for their production (such as concrete durability, steel corrosion, wood decay).

Positive experiences with regard to abrasion durability of concrete mixtures used for hydraulic structures were gathered in the past (Kryžanowski et al. 2009; 2012). Therefore, their upgrade is planned by an investigation in the harsher torrential environment governed by debris floods and debris flows rather than by suspended loads, as it was the case in the past in the Lower Sava River. For such a concrete durability tests, one needs to know exact mechanical loads that are causing abrasion. Such field tests correspond well with the standardised laboratory test for underwater abrasion of concrete (ASTM 2006).

Within the framework of this project, in-situ measurements of concrete abrasion resistance will be performed. The following steps will be executed:

- casting of concrete plates in a laboratory, using different recipes. The foreseen size is 50 x 50 cm due to transport reasons. Up to four different recipes are to be prepared, using expertise from on-site measurements on the Lower Sava River (Kryžanowski et al. 2009). Two replicates will be prepared for each concrete type, using also a typical concrete mixture to be normally applied in torrent control works in

Slovenia, as well as some advanced concrete mixtures with enhanced abrasion resistance using micro silica and steel fibers.

- placement of the concrete plates in a steel frame on the torrential bed in the Brezovški graben upstream of the upstream-most located net barrier.
- occasional measurements of the abrasion of plates will be performed in-situ, using precise techniques to differentiate changes on the order of 0.1 mm.
- plates will be finally removed and weighted in a laboratory to determine the exact weight changes due to abrasion.
- using data on debris deposited upstream of the net barrier, estimated sediment transport rates will be gathered and correlated with the abrasion rates of different concrete mixture types subjected to real debris flows and hyperconcentrated flows in the Brezovški graben.

#### Conclusions

The Krvavec May 2018 case study has shown the true vulnerability of existing touristic infrastructure in Slovenia due to natural hazards. The proposed mitigation measures will decrease the rest risk and potential damages for future torrential events triggering fast flowing phenomena such as debris flows or debris floods. Under different climate change scenarios, it is our aim to adapt to more extreme weather events and to recognise existing risks in order to minimise risk gaps.

The Sendai Framework for Disaster Risk Reduction 2015-2030 asked to apply science, technology and research in the field of disaster risk reduction. A small contribution to these world-wide efforts should be our planned field observatory that will transfer remotely gathered data to us via mobile network for maintenance and inspection planning and early warning purposes. We hope to be able to report on its successful installation and initial results at the next ReSyLAB Symposium.

#### Acknowledgments

This study resulted from two research projects: J7-8273 "Recognition of Potentially Hazardous Torrential Fans Using Geomorphometric Methods and Simulating Fan Formation" and J1-8153 "Studying Landslide Movements from Source Areas to Zone of Deposition using a Deterministic Approach" that were financed by the Slovenian Research Agency (ARRS).

Both projects were also approved by the International Programme on Landslides (IPL) as the IPL-225 and IPL-226 Project, respectively (<http://iplhq.org/category/iplhq/ipl-ongoing-project/>).

We would like to thank the Slovenian Environment Agency (ARSO) for data provision. The check dam design and design of other mitigation measures were financed by the Slovenian Water Agency.

## References

- ASTM C 1138M-05 (2006) Standard Test Method for Abrasion Resistance of Concrete (Underwater Method). Annual Book of ASTM Standards, vol. 04.02. American Society for Testing and Materials, West Conshohocken. pp. 621-624.
- Berger C, Denk M, Graf C, Stieglitz L, Wendeler C (2021) Practical guide for debris flow and hillslope debris flow protection nets. WSL Berichte. 113: pp. 79  
[https://www.wsl.ch/fileadmin/user\\_upload/WSL/Publikationen/WSL\\_Berichte/WSL-Berichte/pdf/Ber-113\\_2021-Practical\\_guide\\_for\\_debris\\_flow- published\\_version .pdf](https://www.wsl.ch/fileadmin/user_upload/WSL/Publikationen/WSL_Berichte/WSL-Berichte/pdf/Ber-113_2021-Practical_guide_for_debris_flow- published_version .pdf)
- Bezak N, Jež J, Sodnik J, Jemec Auflič M, Mikoš M (2020) An extreme May 2018 debris flood case study in northern Slovenia: analysis, modelling, and mitigation. Landslides. 17(10): 2373–2383.  
<https://doi.org/10.1007/s10346-019-01325-1>
- Geobruigg (2022a) Debris Flow & Shallow Landslide Protection - project overview. <https://www.geobruigg.com/en/Debris-Flow-Shallow-Landslide-Protection-77515,7860.html> [Last accessed: 19 January 2022].
- Geobruigg (2022b) Geobruigg GUARD: Remote Status Monitoring. <https://www.geobruigg.com/en/Geobruigg-GUARD-157047,7859.html> [Last accessed: 19 January 2022].
- Jemec Auflič M, Jež J, Popit T, Košir A, Maček M, Logar J, Petkovšek A, Mikoš M, Calligaris C, Boccali C, Zini L, Reitner JM, Verboveš T (2017) The variety of landslide forms in Slovenia and its immediate NW surroundings. Landslides. 14(4): 1537-1546.  
<https://doi.org/10.1007/s10346-017-0848-1>
- Kryžanowski A, Mikoš M, Šušteršič J, Planinc I (2009) Abrasion Resistance of Concrete in Hydraulic Structures. American Concrete Institute (ACI) Material Journal. 106(4): 349-356.
- Kryžanowski A, Mikoš M, Šušteršič J, Ukrainczyk V, Planinc I (2012) Testing of Concrete Abrasion Resistance in Hydraulic Structures on the Lower Sava River. Strojniški vestnik – Journal of Mechanical Engineering. 58: 245-254. DOI:10.5545/sv-jme.2010.217
- Mikoš M (2020) After Stože Landslide: Part I – Development in Landslide Research in Slovenia. Acta hydrotechnica. 33(59): 129-153. <https://actahydrotechnica.fgg.uni-lj.si/paper/a33mm1.pdf>
- Mikoš M, Brilly M, Ribičič M (2004) Poplave in zemeljski plazovi v Sloveniji = Floods and Landslides in Slovenia. Acta hydrotechnica. 22/37: 113-133. <https://actahydrotechnica.fgg.uni-lj.si/paper/a37mm.pdf>
- Sodnik J, Bezak N, Jež J, Jemec Auflič M, Mikoš M (2021) Mitigation measures in the Kravec ski-resort area (N Slovenia, Europe) against debris floods and debris flows. Extended Abstracts of the 14<sup>th</sup> Congress INTERPRAEVENT 2021, 31 May – 2 June 2021. Bergen, Norway. pp. 344-346.  
[http://www.interpraevent.at/palm-cms/upload\\_files/Publikationen/Proceedings/IP\\_2021\\_EA.pdf](http://www.interpraevent.at/palm-cms/upload_files/Publikationen/Proceedings/IP_2021_EA.pdf)

# Design of the rockfall protection at the Špičunak location, Gorski kotar, Croatia

Maroje Sušac<sup>(1)</sup>, Mirjana Vugrinski<sup>(1)</sup>, Dalibor Udovič<sup>(1)</sup>, Davor Marušić<sup>(2)</sup>, Željko Arbanas<sup>(3)</sup>

1) Geolog savjetovanje Ltd, Samobor, Pod borom 3, Croatia, +385 91 4294 008 (maroje.susac@geolog.hr)

2) Terraforming Ltd., Rijeka, Croatia

3) University of Rijeka, Faculty of Civil Engineering, Rijeka, Croatia

**Abstract** The Špičunak location at the state road D3, near the Lokve settlement in the Gorski kotar region, Croatia, is well – known by numerous traffic interruptions caused by slide and rockfall occurrences. The rockfalls at the Špičunak location are mostly predisposed due to geological setting and heavy jointed rock mass in the road cut of approximately 180.0 m length and 23.0 m height. Structural and kinematic analysis of possible future rockfall were carried out following the modern approaches and recent techniques in rockfall hazard analysis. These approaches include application of remote-sensing techniques enabled to ensure digital terrain models (DTM) from three-dimensional high-resolution point cloud (3D HRPC) of the rock cut surface; engineering geological mapping using combination of remote-sensing techniques and field mapping. The three-dimensional high-resolution point cloud (3D HRPC) were established based on terrestrial laser scanning (TLS) and photogrammetry survey employing unmanned aerial vehicle (UAV) using *Structure from Motion* (SfM) technique. Based on established 3D models, the cut was analysed to identify the main characteristics of the rock mass structure as well as to detect and map the discontinuities and discontinuity sets, orientation and dip of discontinuities, spacing of discontinuities, persistence of discontinuities and roughness of discontinuities. Traditional geotechnical survey was conducted to determine the characteristics of the main discontinuity sets at the cliff, as well as to carry out a rock mass classification using Rock Mass Rating (RMR) system and Geological Strength Index (GSI). Detailed analyses of field survey and remote sensing data pointed to three different zones, based on their properties and rock block standings according to the general orientation and dip of the cut face. To identify possibility of failures associated with the present joint sets and their orientations, the kinematic analyses of plane, wedge and toppling failure mechanisms were carried out based on joint sets discontinuity features data collected by both traditional geological and geotechnical field survey and remote sensing survey and data analysis. Based on the kinematic analyses results, adequate protection measures to prevent further brock block detachments and rockfalls were selected and designed. In this paper we will describe field investigation,

establishing of the rock cut model based on remote sensing and traditional geotechnical investigations, stability analysis, as well as design element necessary for ensuring of stability of the rock mass in the cut and safety of the traffic along the road.

**Keywords** rockfall, rockfall protection, remote sensing, 3D modelling, kinematic analysis

## Introduction

Rockfall, as type of landslide, is one of the most frequent and dangerous instability type that can cause fatalities and high economic and social damage. Rockfall process includes detachment from an almost vertical rock slope, fall, rolling and bouncing of rock block along a slope (Dorren 2003; Volkwein et al. 2011), singly or in clusters, and can be defragmented during impacts (Hungar et al. 2014). A rockfall occurrence can vary from small rocky fragments to massive blocks of different volumes and shapes. The high speed, mobility and energy of falling blocks disable getting a necessary time for fast response through evacuation or protection (Ritchie 1963; Siddique et al. 2019; Volkwein et al. 2011).

The Špičunak rock slope is located at the route of the State road DC3 (Rijeka – Zagreb), about 5 km south from the Lokve settlement, Fig. 1. The rock slope extends in the northeast-southwest direction and it was formed by cut excavation during the road construction in 1950's. The length of the investigated part of the cut is approx. 180.0 m, while its height at the highest part is up to 23.0 m, Fig. 2. The existing surrounding terrain has a general elevation of approx. 865.0 m a.s.l.

Problems due to sliding and rockfalls at the Špičunak location existed more than 50 years and caused numerous traffic interruptions. The road construction was repaired several times while the slide remediation was completed in 2021. Rockfall protection measures were applied to the rock cut several times, last time in 2005, according to then available techniques (Arbanas et al. 2012) and only to one part of the cut. Due to further rock mass weathering as well as freezing and thawing process, numerous rockfalls were triggered during winters followed by fallen blocks at

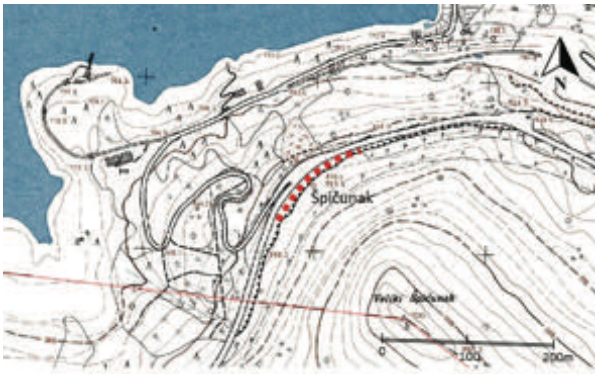


Figure 1 The map of the Špičunak location.



Figure 2 A view at the rock cut at the Špičunak location.

the road, indicating the need of new rockfall protection design and implementation which started in 2021.

### Geological settings

The Špičunak rock slope is situated in the Gorski kotar region, south of the Lokve settlement, and the wider area of the investigated slope belongs to the structure of the Lokve Lake Dome, within the Gorski Kotar Structural Unit (Savić and Dozet 1989). The Lokve Lake Dome is built of Upper Cretaceous and Lower to Middle Permian clayey and sandy-conglomerate deposits, while the flanks are built of Upper Triassic dolomite and clastic deposits.

The slope at the location is composed of well-layered Upper Triassic dolomites of general north-south to northwest-southeast orientation, with a continuous dip of layers of 15-30 (40) ° to the west-southwest. Dominant joint systems are steep to subvertical, oriented N-S, NW-SE and W-E. One 30 m wide subvertical (108/87) shear fault zone (108/87) without pronounced vertical displacement was determined in the middle part of the slope. In the south-western part of the slope, a local steep fault (52/73) with approx. 0.5-2.0 m wide fault zone is registered.

### Field investigation

In determination of the detailed geological structure of the rock cut at the Špičunak location, several campaigns of field investigations were carried out during the last

decades. The last one carried out for the remedial measures and rockfall protection design was conducted using traditional methods of engineering geological survey and mapping combined with the remote sensing techniques based on Unmanned Aerial Vehicle (UAV) photogrammetry data (Froideval et al. 2019; Giordan et al. 2020; Antoine et al. 2020) and terrestrial laser scanning (Jaboyedoff et al. 2012) in combination with data collected by traditional survey (Francioni et al. 2019).

Traditional geological and geotechnical field survey consisted of field mapping of cliff face; direct measuring of discontinuity orientations and dip direction, persistence, spacing, aperture, and roughness; as well as determination of discontinuity wall weathering grades and discontinuity infilling limited to the accessible zone at the foot of the rock cut. Field investigations were combined with the study at the orthophoto (in scale 1:500) and 3D HRPC of about 35.6 million of points (Fig. 3) for better understanding of geological and geomorphological features at the study area. Traditional geotechnical survey was conducted to determine the characteristics of the main discontinuity sets at the rock cut, as well as to carry out a rock mass classification using Rock Mass Rating system (RMR) (Bieniawski 1989) and Geological Strength Index (GSI) (Marinos and Hoek 2000). In this study a combination of traditional geological and geotechnical field survey (Bolla and Paronuzzi, 2020) and remote sensing techniques are employed to geotechnical model of the Špičunak rock cut including the discontinuities and discontinuity sets, orientation and dip of discontinuities, as well as other discontinuity features necessary for analyses of rockfall occurrences and their consequences as well as representative block volumes for each of discontinuity sets (Palmstrom 2001).

Detailed analyses of field survey and remote sensing data pointed to three different zones, based on their properties and rock block standings according to the general orientation and dip of the rock cut face. These zones (Zone I to III) are presented at the 3D HRPC (Fig. 3) while the borders that separate zones were determined analysing changes in orientation and dips of the main joint sets as well as changes in rock block volumes. The *Cloud Compare* software (CloudCompare 2015) was employed to identify discontinuity sets. The rock cut face was divided in three zones (Fig. 3), and for each segmented zone an extraction of joint planes using the *Cloud Compare Facet* and *Compass* plugins (Dewez et al. 2016; Nagendran et al. 2019) (*Fast Marching* procedure) were employed to identify their orientations (dip directions and dips). The spacing between the joints for each joint set necessary to determine block volumes was determined using the *Cloud Compare Distances* tool, while the persistence of joints in accessible rock cut face zones were measured *in situ*. The other discontinuity features (separation, infilling, discontinuity wall roughness and weathering grade) were obtained by *in situ* traditional geological and geotechnical surveys.

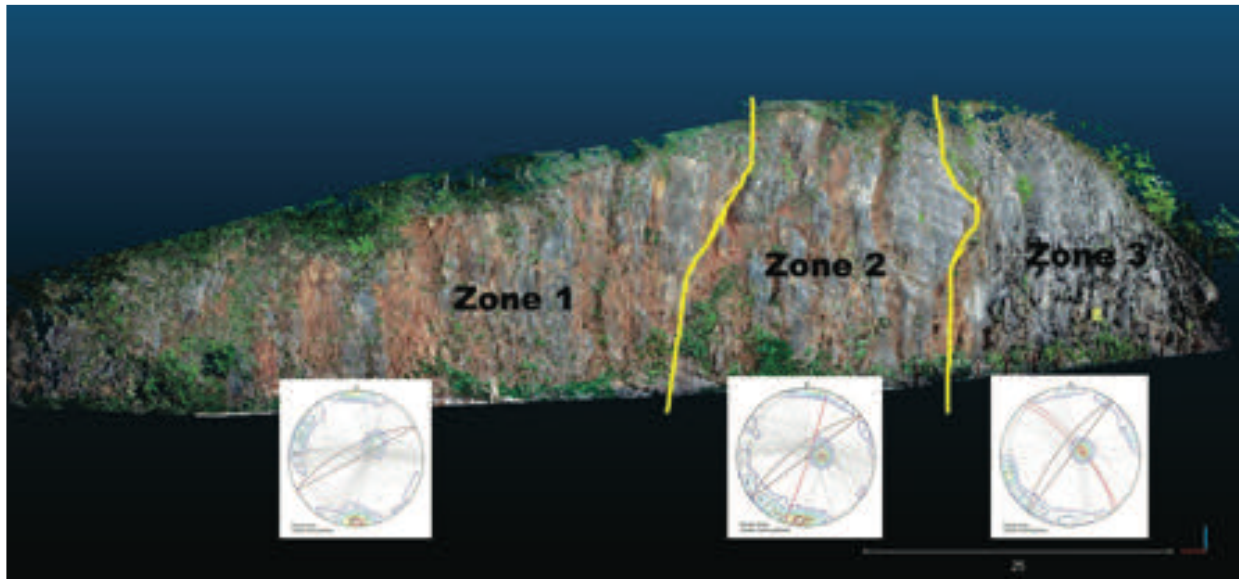


Figure 1 The three-dimensional high-resolution point cloud (3D HRPC) of the Špičunak rock cut with different zones and stereonet plots for each zone.

### Geotechnical model

Based on previously described field and remote sensing investigations and analyses, a geotechnical model for each of determined geotechnical zones was established in order to conduct the necessary kinematic and slope stability analyses. In all of determined three geotechnical zones, three different geotechnical units (GU) were identified and presented in Tab. 1.

Talus deposits (GU 1) are present at the foot of the part of the rock cut, as a result of weathering of the dolomite rock mass. Significant accumulations of talus, which cover the toe of the investigated part of the cut, are up to 2.0 m, and are represented below the fault zones with pronounced shedding of highly weathered rock mass.

Highly to moderately weathered (HW/MW) dolomites (GU 2) are present along the slope within the fault zones, and extend from the bottom to the top of the cut due to subvertical faults extension. Within highly to moderately weathered (HW/MW) dolomites, the distance between discontinuities is usually small; from 6 to 20 cm. The roughness of the discontinuity walls is

smooth. The discontinuity separation is open to medium wide (0.5-10.0 mm), in places wide (up to 10 cm), mostly filled with clay filling, while the interlayer separations are narrow (<0.25 mm) to partially open (0.25-0.50 mm). Persistence of discontinuities is long, >20m. The discontinuity systems represented mainly form polyhedral, rarely and equidimensional blocks, mostly small to medium in size (0.1-0.5 m<sup>3</sup>). The rock structure of highly to moderately weathered (HW/MW) dolomites is disintegrated (D) to blocky/disturbed (B/D) (Marinos and Hoek 2000). The RQD value as an indicator of the rock mass quality is estimated as 0-25% (very poor to poor). Laboratory tests determined a wide range of uniaxial compressive strength of intact rock mass; the interval of 45.0-53.0 MPa was adopted as representative value.

Slightly weathered (SW) dolomites (GU 3) are present along the slope at the initial (Zone 1) and final part (Zone 3) of the investigated rock cut and are locally interrupted by fault zones with highly to medium weathered (HW/MW) dolomites. Within the slightly weathered (SW) dolomites, the distance between discontinuities is usually small to medium, 6-60 cm. The roughness of the rock discontinuity walls is predominantly smooth. The discontinuity separation is mostly partially open to medium wide (0.5-10.0 mm), predominantly fulfilled with clay filling and partially without infilling, while the interlayer separations are narrow (<0.25 mm). Persistence of discontinuities is long, >20m. The discontinuity systems represented mainly form polyhedral to equidimensional blocks; small to large in size (0.2-1.0 m<sup>3</sup>). The rock structure of weakly dilapidated dolomite is blocky/disturbed (B/D) to very blocky (B)(Marinos and Hoek 2000). The RQD value as an indicator of the rock mass quality is estimated as 25-50% (poor). The uniaxial compressive strength of intact rock mass is identical for

Table 1 Description of geotechnical units (GU).

Geotechnical unit	Geotechnical description
GU 1	Talus, gravelly clay and poorly graduated clayey gravel with pebbles and blocks.
GU 2	Highly to medium weathered (HW/MW) dolomites, medium to high compressive strength, layered, disintegrated to a blocky/disturbed structure.
GU 3	Slightly weathered (SW) dolomites, medium to high compressive strength, layered, blocky/disturbed to very block-like structure.

GU 2 and GU 3; interval of 45.0-53.0 MPa was adopted as representative value.

Based on the results of the traditional geological and geotechnical field surveys, as well as the remote sensing survey and data analysis, the geotechnical model of the Špičunak rock cut was established, which presented the main recognized joint sets, their orientations, and all other discontinuity features that are important for conducting stability analyses and identification of the causes of rockfall occurrences. For each of the identified zones, the mean values of joint set orientations and dip directions, as well as other discontinuity features were determined. According to the identified discontinuity features, the Geotechnical rock mass classification (Rock Mass Rating, RMR) (Bieniawski 1989) was determined and the mean RMR values were calculated for each cut zone. The mean descriptions and values of weathering grade, block volumes and RMR for each cut zone are presented in Tab. 2.

### Stability analyses

After establishing of the geotechnical model of the Špičunak rock cut, as well as determination of geotechnical parameters necessary for slope stability analyses (RMR and uniaxial compressive strength), slope stability and kinematic analyses were conducted for each zone of the cut. Stability analyses of the cut in all three zones conducted using *RocScience Slide2* software (Rocscience 2021) pointed on acceptable values of factors of safety (FoS) in all three zones of the cut (FoS > 1.7) that is confirmed with the fact that the Špičunak rock cut has been globally stable during the last 70 years, while the instabilities mostly occurred as local detachments of individual rock blocks or several blocks from the cut caused by local planar, wedge or topple failures. This fact implied on necessary kinematic analyses to identify present rockfall susceptibility.

### Kinematic analysis

Once the geotechnical model of the Špičunak rock cut was established based on the traditional geological and geotechnical field surveys and remote sensing analysis, it was possible to analyze the causes of instability and detachment of rock blocks from the cut face and the initiation of rockfall occurrences. To identify possibility of failure associated with the existing joint sets and their orientations, kinematic analyses of plane, wedge and toppling failure mechanisms (Wyllie and Mah 2004) were performed based on the data of the joint set discontinuity features collected along the rock cut. Kinematic analyses were performed for each rock cut zone employing the *RocScience Dips* software (Rocscience 2021). For each cliff zone, the exported discontinuity plane (facets), orientation (dip and dip directions) data extracted using the *Cloud Compare Facet* plugin (CloudCompare 2015)

Table 2 Description of zones of the Špičunak rock cut with descriptions and values of weathering grade, block volumes and RMR.

Rock Cut Zone	Weathering Grade	Block Volume	RMR
Zone 1	SW/MW	0.2-1.0 m <sup>3</sup>	41
Zone 2	HW/MW	0.1-0.5 m <sup>3</sup>	37
Zone 3	SW/MW	0.2-1.0 m <sup>3</sup>	40

were imported into the *RocScience Dips* software, and kinematic analyses were performed for each type of failure mechanism. The results of kinematic analyses are presented in Fig. 4.

The analyses were conducted for each cut zone as it follows:

In Zone 1, analyses were conducted for 296 discontinuities that daylighting in the rock face analyses at dip and dip orientation of 76/330°. The results pointed on probability of 45.27% for planar failure, 51.16% for wedge failure and 53.38% for toppling.

In Zone 2, analyses were conducted for 515 discontinuities that daylighting in the rock face analyses at dip and dip orientation of 82/315°. The results pointed on probability of 31.65% for planar failure, 47.66% for wedge failure and 41.94% for toppling.

In Zone 3, analyses were conducted for 364 discontinuities that daylighting in the rock face analyses at dip and dip orientation of 88/275°. The results pointed on probability of 16.15% for planar failure, 33.41% for wedge failure and 33.33% for toppling.

The results of kinematic analyses are expressed as probability occurrence for any of possible failure mechanisms (planar sliding, direct toppling and flexural toppling; wedge failure was excluded because of very low probability of occurrence). Probability is expressed as the ratio of number of planes (or combination of planes) meeting the conditions for a failure related to the number of all planes (or combination of planes). An expression of probability of failure occurrence was presented as kinematic hazard index (KTI) by Casagli and Pini (1993), as a number of failures meeting kinematic conditions of failure relative to total number of possible failures. Here is applied the same approach, but the probability is related to each failure mechanism separately. As the temporal component of rockfall occurrences is not included, the calculated probabilities indicate on rockfall susceptibility rather than rockfall hazard.

The results of the analyses indicated a nearly high probability of all three failure mechanisms, that it was expected according to hard jointed rock mass and relatively small volumes of rock blocks at the cut face. The results and rock mass structure in all three zones of the cut, indicate on an approach that will include protection of the entire rock cut face and does not consider measures to support individual blocks at the slope, except in Zone 3, where bigger rock blocks are present.

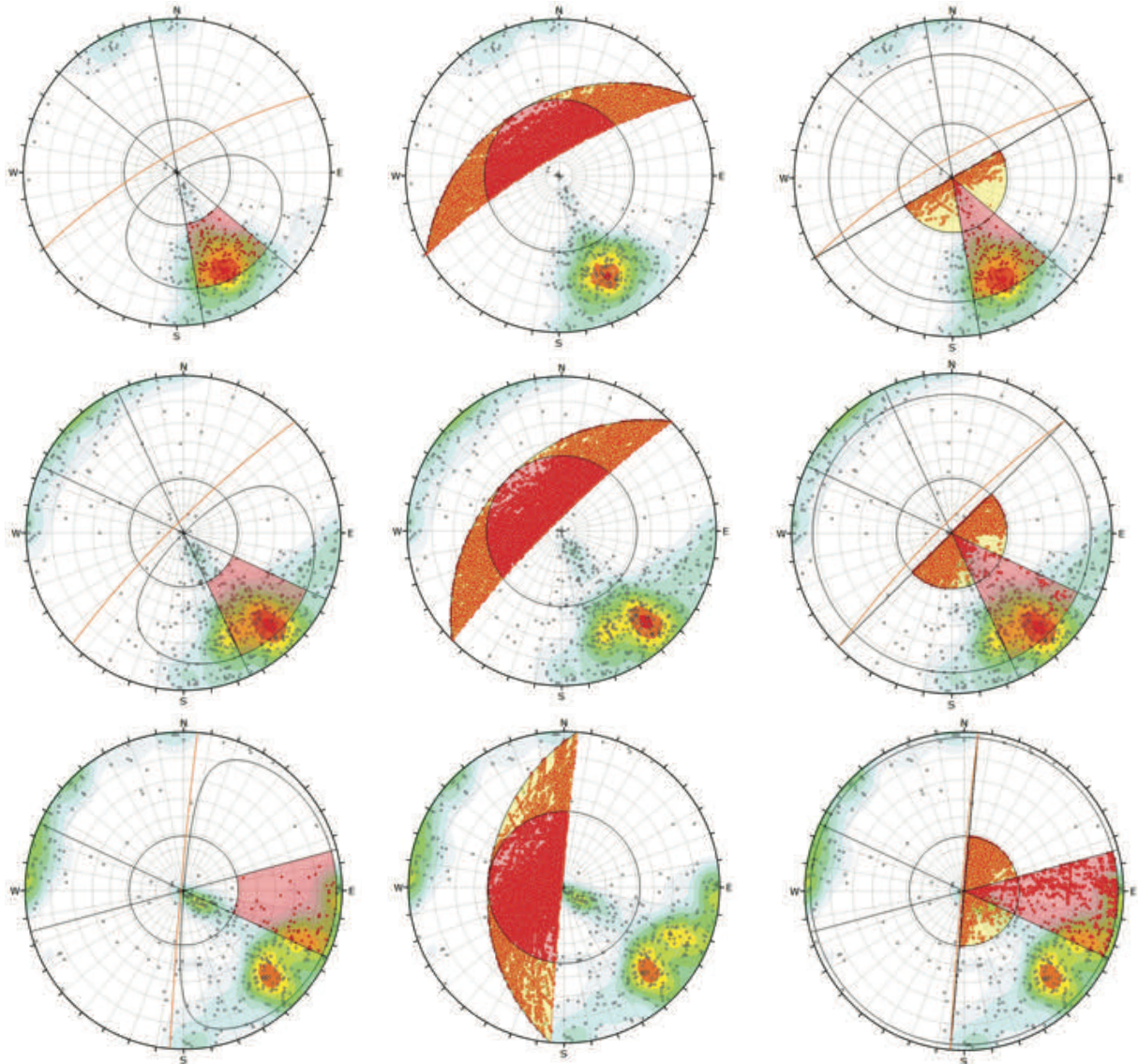


Figure 4 Kinematic analyses of the Špičunak rock cut by cut zones according to planar sliding, wedge and direct toppling, conducted using *Rocscience Dips* software. The results are presented in rows for each zone (e.g., Zone Z1 is in the first row). The results of planar sliding are in the first column, wedge failure in the second column, and direct toppling in the third column.

### Slope protection systems

According to the results of slope stability and kinematic analyses, as well as rock mass structure in the cut, rockfall protection measures were designed. Two design approaches were considered (Arbanas et al 2012): (i) the prevention of rockfalls by removing potentially unstable rock mass or by installing rock mass support systems and (ii) the reduction of rockfall mass energy and suspension of running rockfall mass using rockfall protection ditches, walls or barriers (Volkwein et al 2011). After analyses of technical and economic aspects of possible remedial and protection measures, application of rock mass support system in combination with rockfall protection walls in the foot of the cut was selected.

In Zone 1, with the lowest cut heights and relatively distant from the road, the rock cut protection is designed using rockfall protection fences that enable detachment of small blocks and their fall to the slope toe, but without reaching the road. In Zone 2, where the rockfall hazard and a possibility that detached running blocks reach the road and endanger vehicles, the support system consisted of rockbolts and multi-layered reinforced shotcrete that will cover overall cut face was designed. Rockbolts designed on a raster of 3.0 x 3.0 m, lengths of 6.0 and 9.0 m, and bearing capacity of 240 kN in combination with two-layered shotcrete lining will have significant impact on complete prevention of further rockfall occurrences as well as an increasing of global slope stability, Fig. 5.

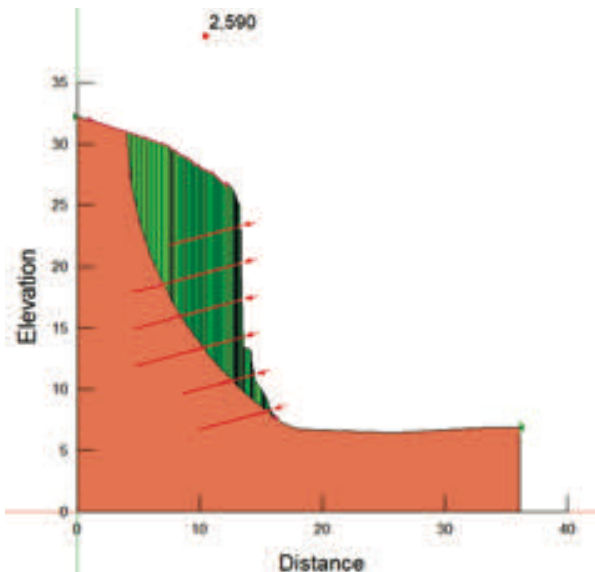


Figure 5 Results of global rock cut stability analysis with applied slope protection measures in Zone 2, conducted using RocSlide software.

In Zone 3, where the kinematic analyses indicate the lowest probability of rockfall occurrences, but with the biggest rock blocks in the cut and closest to the road, a combination of individual rock blocks support by rockbolts, support system consisted of rockbolts and multi-layered reinforced shotcrete and protective gabion wall along the road edge was designed.

Application of these rockfall measures at the Špičunak rock cut will practically completely eliminate further rockfall hazard in Zone 2 and 3, while the further rockfall processes associated with rock mass weathering process, rinsing of the discontinuity infilling related to freezing and thawing processes as well as temperature effects on rock mass, will take place in Zone 1. Anyhow, engineering judgment and analyses indicated on acceptable rockfall risk and rockfall protection using protection fences was adopted as an adequate and economically justified protection measure.

## Acknowledgments

The part of this research is carried out in the frame of the UNIRi Project uniri-tehnic-18-276-1448 Research of Rockfall Processes and Rockfall Hazard Assessment supported by University of Rijeka, Croatia. This support is gratefully acknowledged.

## References

Antoine R, Lopez T, Tanguy M, et al (2020) Geoscientists in the Sky: Unmanned Aerial Vehicles Responding to Geohazards. *Surv Geophys* 41:1285–1321. <https://doi.org/10.1007/s10712-020-09611-7>

Arbanas Ž, Grošić M, Udovič D, Mihalić S (2012) Rockfall Hazard Analyses and Rockfall Protection along the Adriatic Coast of

Croatia. *JCEA* 6:344–355. <https://doi.org/10.17265/1934-7359/2012.03.008>

Bieniawski ZT (1989) *Engineering Rock Mass Classifications A Complete Manual for Engineers and Geologists in Mining, Civil, and Petroleum Engineering*. Wiley-Interscience, New York

Casagli N; Pini G (1993) Analisi cinematica della stabilità di versanti naturali e fronti di scavo in roccia. *Geologia Applicata e Idrogeologia*. 1993, 28 223–232 (in Italian).

CloudCompare (2015) User manual. (<http://www.cloudcompare.org>) (last accessed 30 January 2022)

Dewez TJB, Girardeau-Montaut D, Allanic C, Rohmer J (2016) Facets: A CloudCompare plugin to extract geological planes from unstructured 3D point clouds. *Int Arch Photogramm Remote Sens Spatial Inf Sci XLI-B5:799–804*. <https://doi.org/10.5194/isprs-archives-XLI-B5-799-2016>

Dorren LKA (2003) A review of rockfall mechanics and modelling approaches. *Progress in Physical Geography: Earth and Environment* 27:69–87. <https://doi.org/10.1191/0309133303pp359ra>

Francioni M, Calamita F, Coggan J, et al (2019) A Multi-Disciplinary Approach to the Study of Large Rock Avalanches Combining Remote Sensing, GIS and Field Surveys: The Case of the Scanno Landslide, Italy. *Remote Sensing* 11:1570. <https://doi.org/10.3390/rs11131570>

Froideval L, Padoja K, Garestier F, et al (2019) A low-cost open-source workflow to generate georeferenced 3D SfM photogrammetric models of rocky outcrops. *Photogram Rec* 34:365–384. <https://doi.org/10.1111/phor.12297>

Giordan D, Adams MS, Aicardi I, et al (2020) The use of unmanned aerial vehicles (UAVs) for engineering geology applications. *Bull Eng Geol Environ* 79:3437–3481. <https://doi.org/10.1007/s10064-020-01766-2>

Hungr O, Leroueil S, Picarelli L (2014) The Varnes classification of landslide types, an update. *Landslides* 11:167–194. <https://doi.org/10.1007/s10346-013-0436-y>

Jaboyedoff M, Oppikofer T, Abellán A, et al (2012) Use of LIDAR in landslide investigations: a review. *Nat Hazards* 61:5–28. <https://doi.org/10.1007/s11069-010-9634-2>

Marinos P, Hoek E (2000) GSI: A Geologically Friendly Tool For Rock Mass Strength Estimation. *ISRM International Symposium, Melbourne, Australia, November 2000* 19

Nagendran SK, Mohamad Ismail MA, Wen YT (2019) Photogrammetry approach on geological plane extraction using CloudCompare FACET plugin and scanline survey. *BGSM* 68:151–158. <https://doi.org/10.7186/bgsm68201916>

Palmstrom A (2001) Measurement and Characterization of Rock Mass Jointing. In: Sharma, V.M. and Saxena, K.R., Eds., *In-Situ Characterization of Rocks*, A.A. Balkema Publishers, London, 97

Ritchie AM (1963) Evaluation of Rockfall and Its Control. *Highway Research Record* 17:13–28

Rocscience (2021) (<http://www.rocscience.com/software>) (last accessed 30 January 2022)

Savić D, Dozet S (1989) Basic geological map scale 1:100 000, (Sheet Delnice). Institute for geological research, Zagreb.

Siddique T, Pradhan SP, Vishal V (2019) Rockfall: A Specific Case of Landslide. In: Pradhan SP, Vishal V, Singh TN (eds) *Landslides: Theory, Practice and Modelling*. Springer International Publishing, Cham, pp 61–81

Volkwein A, Schellenberg K, Labiouse V, et al (2011) Rockfall characterisation and structural protection – a review. *Nat Hazards Earth Syst Sci* 11:2617–2651. <https://doi.org/10.5194/nhess-11-2617-2011>

Wyllie DC, Mah CW (2004) *Rock Slope Engineering: Civil and Mining*, 4th Edition. Spon Press 456



# The Ladiser Landslide mitigation project with a flexible high tensile steel mesh protection system

Vjekoslav Budimir<sup>(1)</sup>, Helene Lanter<sup>(2)</sup>, Armin Roduner<sup>(2)</sup>, Ronald Steinlechner<sup>(3)</sup>

1) Geobrugg AG, Zagreb, Croatia (vjekoslav.budimir@geobrugg.com)

2) Geobrugg AG, Romanshorn, Switzerland

3) Geobrugg Austria, Salzburg, Austria

**Abstract** Slope stabilization systems with meshes made of high-tensile steel wire have been in use for 20 years and have proven to be reliable systems on loose rock and soil slopes. Design can be carried out for any specific geotechnical setting of a slope using a freely available software called RUVOLUM®. The flexible, high tensile steel mesh can also be used to stabilise landslide areas in combination with a previously dimensioned anchor grid using global stability analysis software. This paper presents a landslide case study in Austria where TECCO®, flexible, high tensile steel wire meshes for slope stabilization were successfully applied while previously installed concrete rib works failed. Several rockfalls and slides led to road closures in Tyrol during the winter of 2018. Focus will be on an event in the Oberinn Valley, southwest of Innsbruck. The Ladiserroad (L286), a state road in Tyrol, was affected twice within a short period of time. The cause of the rockfall and the landslide is most certainly due to the particularly unfavourable combination of weather conditions at the time, with heavy rain, heavy snowfall, thaw, and then freeze-thaw cycles. Part of the slope, from the Bündnerschiefer formation, was previously secured with concrete ribs that were carried away. A larger section of the slope than previously identified failed and subsequent protection measures were planned and executed in the summer of 2018. The chosen solution became an anchored solution using TECCO®, a high tensile flexible steel mesh cover. Approximately 10000 m<sup>2</sup> were stabilised with an optimised nail grid of 2.5x 2.5 m, while the nail length ranged from 3 to 15 m. The landslide and its mitigation, design and installation will be presented in detail, as well as the state of the project four years later.

**Keywords** landslide mitigation, high-tensile steel mesh, flexible protection system, TECCO®

## Introduction

For more than 20 years, steel wire meshes made of high-tensile steel has been used for slope stabilization. This type of protection measure represents an ecological solution compared to classic slope stabilisation works, as much less material is used on site. For example, light steel mesh is

used instead of concrete and an optimised nail pattern can be implemented that requires fewer anchor bars and less drilling. The flexible, high tensile steel mesh can also be used for landslide site stabilisation in combination with a previously dimensioned anchor grid by global stability analysis software.

This paper presents a landslide case study, in Austria, where flexible, high tensile steel wire meshes for slope stabilization were successfully applied while previously installed concrete rib works failed. Two sites, Ladiserstrasse and Serfauserstrasse, which are geographically close to each other and were affected by an exceptional series of events in the Tyrol region during the same period of time. After a brief description of the geology and the triggering factors of the events, the mitigation solution will be presented in detail. Finally, an outlook on the state of the measures four years later will be given with regards to the slope stability and revegetation of the slope.

## Overview of the region

### Geographical setting

The two sites are situated in the Oberinnvalley, south of Landeck, in the Tyrol region of Austria. The site further north is referred to Ladiserstrasse and the site further south corresponds to the Serfauserstrasse (red rings in Fig. 1).



Figure 1 The two sites Ladiserstrasse (red ring further North) and the Sefauserstrasse (red ring further South) in the Oberinn Valley (tirisMaps 2018).

## Geology

The geology of the Oberinn Valley, and in particular of the two sites in question, is dominated by the greyish calcareous Bündnerschiefer formation (Hammer 1914) from the Mesozoic, surrounded by the older Silvretagneiss formation. The greyish Bündnerschiefer consists of more or less metamorphosed calcareous formations and clayey schists as well as breccias and conglomerates.

The digital terrain model (Fig. 2), from 2014, when studied in detail, shows disturbances at both sites that could indicate past movement on the slope. This would also explain the presence of mitigation systems at both sites, such as concrete ribs holding the slope in place.

## The landslide events in 2018: Ladiserstrasse and Serfauserstrasse

### Weather and circumstances

An exceptional series of natural hazard events marked the Tyrol region at end of January 2018, affecting sites such as the Pillerstrasse, the Vals landslide, the old Reschenstrasse, etc. This series of events was due to a particular set of weather patterns that occurred at the end of January and beginning of February. This included a heavy rainfall at first, followed by heavy snowfall. This was followed by a rise in temperature that led to snow melting and finally a freeze-thaw cycle (ORF 2018a). A rockfall had already occurred on the Ladiserstrasse between Ried im Oberinntal and Ladis in the last week of January. The road was then buried several meters high by a second event, this time a major landslide, and was closed for several weeks. The rockslide was triggered by extensive creep movements on the slope, which were underway and concerned a large forested steep slope above and below the state road. Experts agree that the cause of the rockfall and the slide most certainly lies in these particularly unfavourable combination of weather conditions at the time (ORF 2018b).

### Ladiserstrasse

The digital terrain model highlights the Ladiserstrasse landslide (Fig. 3) and Figs. 4 and 5 show the extent of the damage.

Part of the slope, from the Bündnerschiefer formation, was secured with concrete ribs that were spectacularly carried away during the sliding and captured on video. A larger part of the slope than previously identified failed, leading to road closures and the need to prepare immediate mitigation measures.

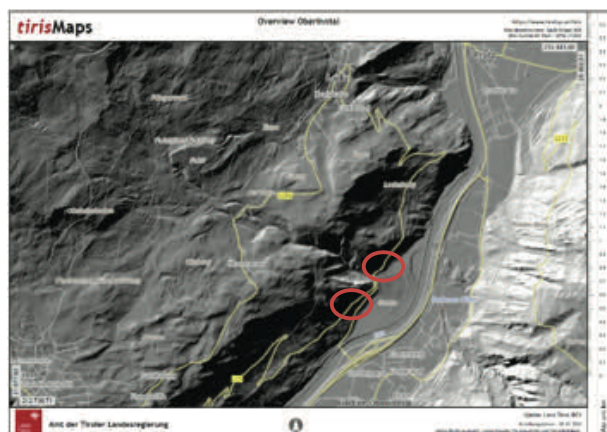


Figure 2 Digital Terrain Model of the Oberinn Valley, 1 m resolution (tirisiMaps 2014).

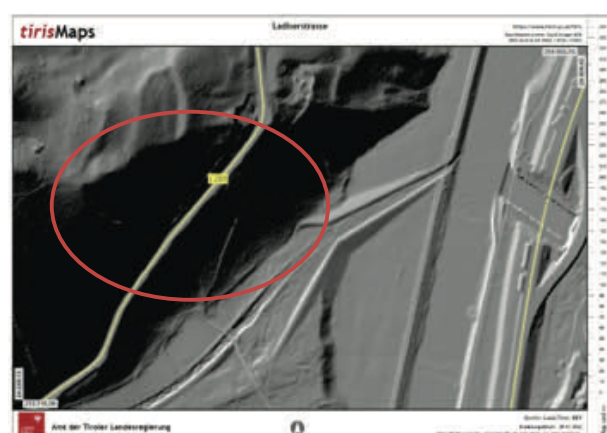


Figure 3 Close up of the digital terrain model, where the red ring indicates the Ladiserstrasse landslide area in 2018 (tirisiMaps 2014).



Figure 4 View from the blocked Ladiserstrasse, where a large part of the slope failed after the extreme weather conditions in January 2018.



Figure 5 View from the top of the landslide along the Ladiserstrasse.

### Serfauserstrasse

The Serfauserstrasse landslide presents a slope failure similar to that at the Ladiserstrasse. The digital terrain model highlights the Serfauserstrasse landslide (Fig. 6) and Figs. 7 and 8 show the extent of the damage. The concrete ribs were applied before the landslide event to stabilise the slope.



Figure 6 Detail of the digital terrain map showing unstable slope features, with the ring indicating the slope failure of the Serfauserstrasse in winter 2018 (tirisMaps 2014).



Figure 7 View from top of the landslide along the Serfauserstrasse, approximately one month after the event.



Figure 8 View of the beginning of works to clear the road from the landslide mass.

### Mitigation solutions

Slope failures occur when the shear stress along a plane exceeds the shear strength of the substrate, which is quite a similar process to a fault rupture (Clague and Stead 2012). Increase of the shear stress in the ground depends on multiple factors starting with the type of rock, type of underlying rock, stratigraphy, weathering state, and surrounding hydrogeology. Variations in temperature and precipitation, especially the alternation between extremes can act as a trigger for ground motion (Clague and Stead 2012).

#### Landslide mitigation with high tensile steel facing and nailing

According to the European Norm EN 14490 there are three different types of facings for slope stabilisation purposes: hard, soft and flexible.

Hard facing generally corresponds to shotcrete or concrete structures. These systems are more vulnerable to an earthquake because the stiffer a structure is, the more it is accelerated and risks damage. Once the protection measure is damaged, it loses its retention capacity.

Soft facings for slope stabilization consist of different geogrids, geomembranes or geotextiles. This type is generally applied for temporary slope stabilisation or as erosion control mats.

Flexible facings, also defined as active slope stabilization systems are a combination of steel wire mesh and soil nailing. As the following case studies will show, one type of flexible facing, the TECCO system (high tensile steel wire mesh transmitting the forces of the slope acting on the mesh back into the ground via soil nails), is suitable for this type of site.

#### Dimensioning of high-tensile steel mesh

Slope stabilisation always begins with the design of the slope through classical geotechnical calculations. This allows getting a nail grid spacing. Subsequently, the flexible facing can be dimensioned using RUVOLUM®, a freely available software, to verify stability of the shallow

slope ( $\leq 2\text{m}$ ) and the stability between the nail grid. Both load cases are termed “sliding off parallel to the slope” and “local wedge-shaped rupture bodies”. Detailed explanations of the RUVOLUM® dimensioning concept can be found in Cala et al. 2020.

### Works on landslide stabilization

The necessary protection measures were planned and executed shortly after the events and were completed in the summer 2018. First, scaling and profiling of the slope was carried out with walking excavators and a 2200 m<sup>2</sup> concrete anchor wall of was constructed at the bottom of both slopes. Up to 3 walking excavators and two drilling trucks with a reach of 32 m each, and up to 15 people were used throughout the construction period (Berger + Brunner Construction Company 2018).

The chosen landslide stabilisation solution became an anchored solution with a high tensile flexible steel mesh cover. An area of approximately 10000 m<sup>2</sup> was stabilised with an optimised nail grid of 2.5 x 2.5 m. 15000 meters of IBO anchors with diameters of 32, 38 and 51 mm were drilled, with the length of each anchor ranging from 3 to 15 m (Berger + Brunner Construction Company 2018).

Additionally, 35 m<sup>3</sup> of in-situ concrete anchor beams were installed in the rock face, partly to secure the concrete ribs still in place. Finally, in Serfauserstrasse a rockfall protection fence was installed on top of the slope covered with mesh. The fence was 4 m high and 75 m long with a capacity of 2000 kJ.

The following Figs 9 to 12 highlight the details of the works on Ladiserstrasse and Figs 13 to 15 on Serfauserstrasse landslide stabilization (Berger + Brunner Construction Company 2018).



Figure 9 View of the unstable slope at Ladiserstrasse, where the first part of anchoring and mesh deployment is completed, allowing secure works underneath to be completed.



Figure 10 A walking excavator in action, drilling the next row of anchors, while being already protected from the top, as the high-tensile steel mesh is already installed.



Figure 11 Rope access work while installing the high-tensile steel mesh.



Figure 12 Stabilisation of the concrete ribs that were undamaged during the slope failure, with a concrete anchor beam and high-tensile steel mesh cover. Note the larger spike plates in this section, belonging to the TECCO system, which can support higher loads.



Figure 13 View of the unstable slopes along Serfauserstrasse.



Figure 14 Drilling truck starting on the stabilisation works at the bottom part of the Serfauserstrasse instability.



Figure 15 Final works underway at the Serfauserstrasse, with a highlight on the greening mat along the bottom part of the road.



Figure 16 Orthophoto of the stabilised slope along the Ladiserstrasse (tirisMaps, 2018).



Figure 17 Ladiserstrasse as seen from the road (Google Earth Pro, 2018).



Figure 18 Orthophoto close-up for the stabilised slope along the Serfauserstrasse (tirisMaps, 2018).

The works on landslide stabilization were completed in June 2018 and the Figs 16 to 20 illustrate the results.



Figure 19 Serfauserstrasse as seen from the road (Google Earth Pro, 2018).



Figure 20 Serfauserstrasse stabilised slope, with a rockfall barrier at the top, anchored high-tensile steel mesh in the middle and greening mats in the bottom part of the slope.

### Revegetation of the slopes

In general, there is a danger of erosion on steep soil slopes (Cala et al., 2020) for example by rainwater falling directly on the protected slope. In case of high intensity and long duration of rain, this can lead to major erosion problems. The problem can be solved with a full-surface vegetation face. The roots stabilize the surface layer and considerable amount of water is stored in the vegetation layer before it runs off. However, it takes time for effective vegetation to form. Vegetation cannot develop on a slope subjected to movements and erosion. Therefore, it is often necessary to provide erosion protection together with the mesh to prevent erosion and washing-out for the time being and to create conditions for successful greening later on.

At the site along the Ladiserstrasse a one-season solution for erosion control with a coconut cover was chosen. In Serfaus, a multi-season solution for erosion control was chosen, combined with a high-tensile steel mesh. This gives the vegetation an opportunity to come back over the course of several seasons, instead of one or two seasons.

### Conclusion and Outlook

This case study with Ladiserstrasse and Serfauserstrasse sites highlights how well stabilisation of an area prone to landslide can be carried out with flexible facing and anchors. The design of the facing is possible and allows to choose the appropriate mesh for the present load cases. When greening is considered at the very beginning of a stabilisation project, successful revegetation can be achieved. In the spring 2022 the state of the solution at both sites will be assessed again and presented.

### References

- Berger + Brunner Construction Company (2018) Land Tirol - Sofortmaßnahme L286 Ladiser Straße und L219 Serfauserstraße. URL: <https://www.bb-bau.at/de/land-tirol-sofortmassnahme-l286-ladiser-strasse-und-l219-serfauserstrasse.html>, [last accessed: 03.01.2022].
- Cala M, Flum D, Roduner A, Rügger R, Wartmann, S (2020) TECCO® Slope Stabilization System and RUVOLUM® Dimensioning Method (2020th ed.). E-book. AGH UNIVERSITY OF SCIENCE AND TECHNOLOGY, Faculty of Mining & Geoen지니어ing. ISBN 978-3-033-03296-5. 267 p.
- Clague J J, Stead D (2012) Landslides: Types, Mechanisms and Modeling. Cambridge University Press. ISBN 1107002060, 420 p.
- DIN EN 14490:2010-11 Execution of special geotechnical works - Soil nailing
- Google Earth Pro (2021) Street View [Photograph]. Google Earth Pro.
- Hammer W (1914) Das Gebiet der Bündnerschiefer im tirolischen Oberinntal. Jahrbuch d. k. k. geol. Reichsanstalt, 54. Band, 3. Heft. (in German)
- ORF: Felssturz und Hangrutsch durch Schmelzwasser. (2018a) ORF. URL: <https://tirol.orf.at/v2/news/stories/2891423/>, [last accessed: 03.01.2022]
- ORF: Neuerlich folgenschwere Felsstürze im Oberland. (2018b) ORF. URL: <https://tirol.orf.at/v2/news/stories/2893155/>, [last accessed: 03.01.2022]
- tirisMaps. (2018) Orthophoto map from the Ladis area [Map]. Region of Tyrol. URL: [https://maps.tirol.gv.at/synserver?user=guest&project=tmap\\_m\\_aster](https://maps.tirol.gv.at/synserver?user=guest&project=tmap_m_aster), [last accessed: 03.01.2022]
- tirisMaps. (2014) Digital terrain model of the Ladis area [Map]. Region of Tyrol. URL: [https://maps.tirol.gv.at/synserver?user=guest&project=tmap\\_m\\_aster](https://maps.tirol.gv.at/synserver?user=guest&project=tmap_m_aster), [last accessed: 03.01.2022]

# Highway construction in fossil landslides zones – lessons learned from the Grdelica Gorge, Serbia

Biljana Abolmasov<sup>(1)</sup>, Marinos Skempas<sup>(2)</sup>, Svetozar Milenković<sup>(3)</sup>, Janko Radovanović<sup>(4)</sup>, Miloš Marjanović<sup>(1)</sup>

1) University of Belgrade, Faculty of Mining and Geology, Belgrade, Đušina 7, Serbia, +381 69 1710 708 (biljana.abolmasov@rgf.bg.ac.rs)

2) The World Bank

3) GeoMonitoring Team Co., Belgrade, Serbia

4) Beoexpert Design Co., Belgrade, Serbia

**Abstract** During the E75 Highway construction in the Grdelica Gorge in Serbia (Corridor X), complex fossil landslides were reactivated in two cuts. The geotechnical investigations were performed in several phases from the Preliminary through the Main Design, but comprehensive remedial measures were developed after additional geotechnical monitoring and re-design in the final stage of highway construction. Both fossil landslides were formed in complex geological settings, i.e. extremely anisotropic albite-chlorite-muscovite schists from early Paleozoic. Engineering geological conditions were determined by lithological composition, presence of highly weathered and tectonized zones, as well as presence of local torrential streams and surface erosion. In this paper two case studies of fossil landslides reactivated during highway construction in complex geological conditions and lessons learned after several phases of investigation and design will be presented.

**Keywords** fossil landslides, highway construction, geotechnical investigations, design

## Introduction

Construction-induced landslides usually occur in slopes/cuts mostly due to excavation, which can cause many problems and delays in transport infrastructure projects realization. It is not unusual that large volume excavations for highway construction lead to massive instabilities in particular when complex morphological and geological settings prevail. Zhang et al. (2012) discussed a case of repeated failures on a high cut due to multi-excavation for G212 highway in China. The analysis shows that the excavation-induced repeated failures was related to the exposure of the weak bedding plane and the toe unloading of the slope cut. Solberg et al. (2008) reported reactivation of large, prehistoric clay slides due to the construction of a new highway (E39) in Buvika, mid-Norway. Unexpected instabilities in the flysch and molassic formation caused by Egnatia Odos highway construction in the Greece were explained in Christaras

(1997). Skempas (2017) describes some case histories with slope instability problems at various sections of the Egnatia Odos Highway Project in Greece and the methods that have been applied for overcoming these events and constructing the highway. In recent years, China's road infrastructure projects expansion causes many landslides triggered by engineering activities because of complicated and misinterpreted geological features (Zhang et al. 2021; Yu et al. 2020).

During the Corridor X highway construction through the Republic of Serbia many instabilities were caused by excavation frequently in combination with unforeseen or poorly investigated ground conditions on both the Corridor X sections (E75 and E80). Georgalas et al. (2017) explains geological and geotechnical conditions during construction of E80 highway from Niš to Bulgarian border, and noticed that out of 20 excavated cuts, 18 have faced sliding failures, resulting in suspension of the works, awaiting remedial geotechnical designs. The implications of the insufficient geotechnical investigations that caused delays and a significant increase in the project costs and schedule overruns on E75 section of Corridor X were presented in Berisavljević et al. (2016) and Berisavljević (2018). The most demanding section along the E75 highway was the one through the Grdelica Gorge, where Cut 3 and Cut 5 were found to be crossing two fossil landslides which were reactivated during highway excavations. In this paper we will present lessons learned after several phases of investigation, design and highway construction in complex geotechnical conditions.

## General data

### Corridor X Project

The integration of the Serbian transport network into the regional and Trans-European Network (TEN-T) remains critical for Serbia's economic and social development. Corridor X is the longest and busiest road transport corridor in the Western Balkans. It passes through Serbia and the Republic of North Macedonia, connecting Croatia

and Hungary with Bulgaria and Greece. The total length of the Corridor is 726 km, 531 km of which are in Serbia. As the most important transport route for Serbia, Corridor X enhances regional connectivity through linkages to the TEN-T Orient/East-Med Corridor and represents the shortest link to Europe (through Croatia and Hungary), and to the Middle East, Asia, and Africa (through Greece and Bulgaria). In 2008 the Government of the Republic of Serbia (GoRS) committed to completion of the core road infrastructure on Corridor X.

Construction activities started in 2012, but both sections (E75 and E80) were opened for traffic in 2019 after almost two years delay. Geographical position of E75 section and position of critical cuts (CUT3 and CUT5) are presented in Fig. 1.

### Study area

The Grdelica Gorge is a part of the South Morava River basin, located in the southeastern part of Serbia. In the mid-1950s, the Grdelica Gorge was identified to belong to the areas most endangered by soil erosion in Europe. Namely, there are 137 torrential streams, direct tributaries of the South Morava river, registered on the small area, along 26.6 km of the Grdelica Gorge length (Kostadinov et al. 2018). After the Second World War numerous erosion control works had been performed in the Grdelica Gorge, as well as the entire South Morava river basin, which resulted in significant reduction of soil erosion by the end of the 1980s. The bedrock predominantly belongs to Paleozoic Serbo-Macedonian Massif (SMM). SMM in Serbia and North Macedonia represents an entirely metamorphic belt comprising a structurally lower unit (the Lower Complex) and an upper unit (the Vlasina Unit), as originally proposed by Dimitrijević (1997). These units are commonly differentiated on the basis of their metamorphic grade, with the Lower Complex predominantly metamorphosed at medium to lower amphibolite facies, and the Vlasina Unit at greenschist facies (low-grade crystalline). The Vlasina Unit consists of the pre-Ordovician greenschist facies represented by chlorite, biotite, muscovite, sericite and epidote schists (Antić et al. 2016).

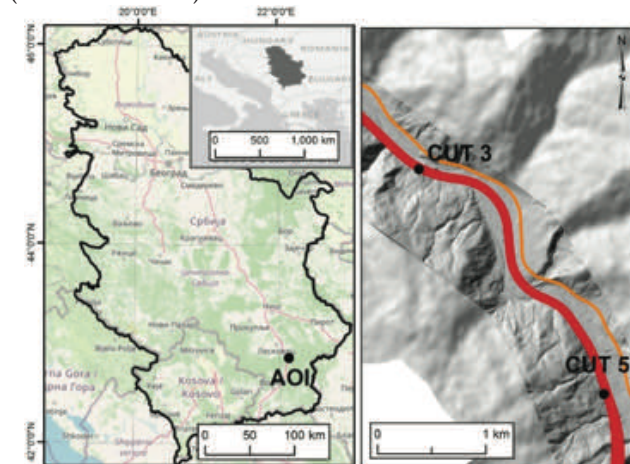


Figure 1 Geographical position of Grdelica Gorge (Area of Interest - AOI) and position of CUT3 and CUT5 within AOI.

Both fossil landslides are formed in highly weathered and tectonized albite, chlorite, muscovite, and sericite schists from the Vlasina Unit on the left bank of the South Morava river.

### Evolution of landslides

The highway construction on E75 section Grabovnica-Srpska Kuća started in 2012 according to the FIDIC Conditions of Contract for Construction, the Red Book form, which meant that technical documentation was provided by the Investor (the Republic of Serbia). The Main Design assumptions were based on very limited knowledge from site investigation together with the prepared engineering geological mapping and laboratory testing. The lack of access roads to the location of cuts was one of the main reasons for the limited scope of site investigations, as well as the very short time available for preparing technical documentation for the final design and tendering of the project (Berisavljević, 2018).

Initial instabilities in both fossil landslides (CUT3 and CUT5) started in 2014 during excavations for the highway construction according to the Main Design. Shallow landslides occurred at that time and additional geotechnical investigations were performed in 2015. Re-design of a frame supporting structure and micropile walls as remedial measure were suggested by Contractor and accepted by Investor in 2016. Implementation of the proposed measures started in mid 2016, but displacements progressed and escalated in both cuts during late winter of 2017 and early spring of 2018. More geotechnical investigations were performed again – including LiDAR survey, numerous boreholes, laboratory testings and geotechnical monitoring, which started in 2017. Table 1 shows geotechnical investigation works conducted for the Main Design and during highway construction on the CUT3 and CUT5 from 2014 to 2019.

### Landslides features

#### CUT3

The first shallow instabilities on CUT3 began in 2014, but the large fossil landslide was not recognized after additional geotechnical investigations performed in 2015, as well as in the Main Design (2010). According to the new design from 2016, construction of micropile wall was executed, but micropile wall monitoring showed uniform cumulative displacement of 45 cm from December 2017 to March 2018. High-resolution LiDAR scanning from 2018 had detected indicators of earlier occurrences flow-like landslide on high-resolution terrain surface model, as well as displacement of the South Morava river because of deep-seated landslide which probably blocked the river in the past (landslide dam). All installed inclinometers (2017–2018) showed displacement depth between 8 m and 43 m, i.e., up to 15 m below the highway platform. Landslide was approximately 600 m long and 200 m wide, and average slope angle was 15°.



Table 1 List of geotechnical investigation conducted from 2010-2019.

Name of CUT and chainage	Geotechnical investigation for Main Design (2010)	Additional geotechnical investigations 2014-2016	Additional geotechnical investigations 2017-2019
CUT3 km 876+510 to km 876+740	5 trial pits	(2015) 7 boreholes in total length 134 m; laboratory, geophysics, piezometer (1) and inclinometer (1) installation	(2017) 12 boreholes in total length 433 m, only piezometers and inclinometers installation (2017) 3 available boreholes logs in total length 140.3 m, geophysics (2018) 3 boreholes in total length 150 m, laboratory, and inclinometers installation (3)
CUT5 km 879+350 to km 879+775	12 boreholes (max depth 17 m) in the zone of retaining structure at toe of the slope, laboratory (mainly index tests)	(2015) 10 boreholes in total length 116 m; laboratory, piezometer (1) and inclinometer (1) installation	(2017) 21 boreholes in total length 284 m, only piezometers and inclinometers installation; (2018) 30 boreholes in total length 708 m, geophysics, laboratory, inclinometers installation (8); (2019) 11 boreholes in total length 260 m, laboratory, inclinometers (7) and piezometers (4) installation

Type of landslide material is predominantly sandy/silty clay (completely disintegrated schists-S<sup>\*\*\*</sup>) in the upper part of landslide body and highly weathered schists (debris and boulders in fine-grained silty/clay matrix - S<sup>\*\*</sup>- S<sup>\*</sup>) in the lower part of landslide body. Basic material properties of landslide body and stable ground are presented in Table 2. The residual strength parameters from direct shear tests proximal to the zone of sliding surface were  $\phi_r' = 13-16^\circ$  and  $c_r' = 3-6$  kPa. Failure mechanism was a combination of sliding (in the lower parts), and flowing in the upper parts of the slope.

Simplified map of the landslide is shown on Fig. 2, while representative cross-section is shown on Fig. 3a. In general, the entire slope has a high groundwater table. Saturation on the ground surface was recognized during all field campaigns and it was caused by inflow from two gullies located on the upper part of slope, but fluctuation of piezometric groundwater levels were not significant, except in December 2017-February 2018 period (Fig. 3b).

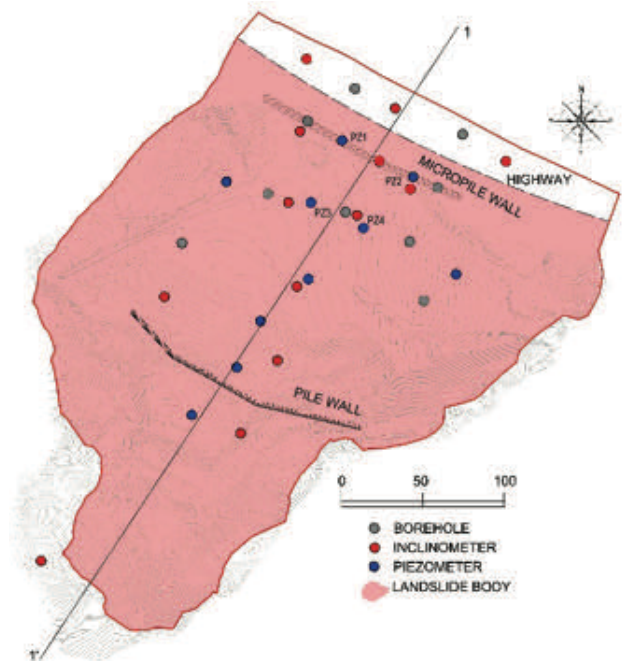


Figure 2 Simplified map of landslide area (CUT3).

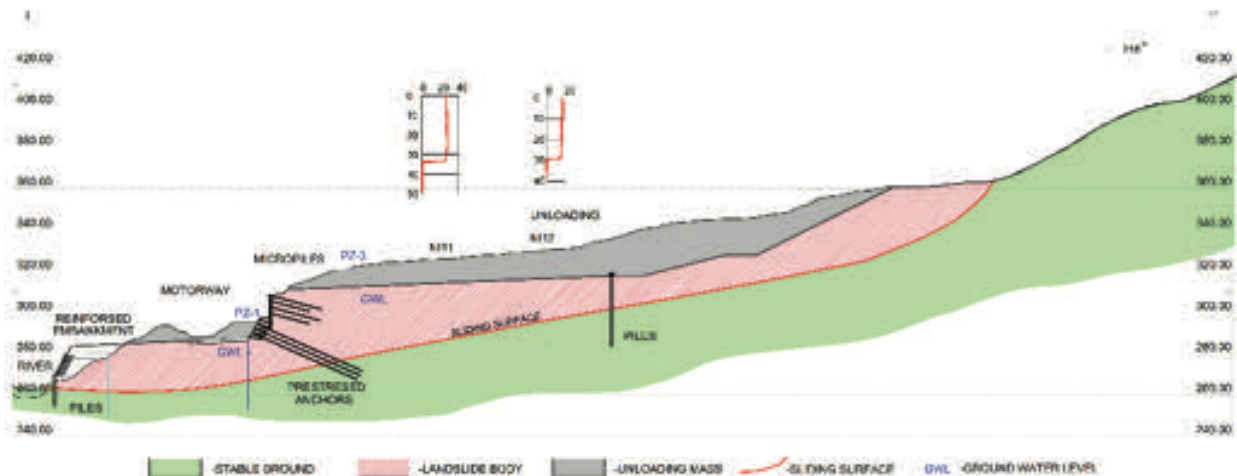


Figure 3 Simplified cross section of landslide and proposed remedial measures on CUT3.

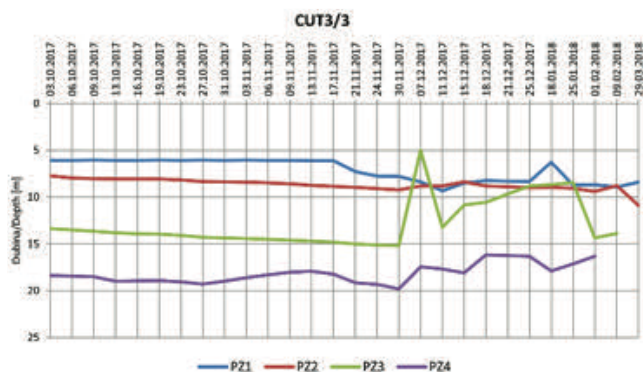


Figure 4 Ground water level on CUT3 from October 2017-March 2018.

**CUT5**

Potential instabilities on CUT5 were recognized within technical documentation for the Main Design and area was marked as “marginally stable slope”. The first displacements started in October 2014 during excavations in the slope toe area, and construction of micropilles was implemented according to the re-design of initial remediation measures available from the Main Design. During 2016 the landslide was widening and was retrogressing upslope and beyond the expropriation line.

Landslide width was 200 m in the zone of main scarp and 400 m in the zone of the landslide toe, while landslide length was 350 m in January 2018. Landslide material predominantly consists of Quaternary elluvial-dilluvial silty clays and completely disintegrated and highly weathered schists (S\*\*\*- S\*\*). Average slope angle was about 25°, but many local morphological indications of previous movements and steeper parts of the landslide surface were indicated.

Engineering geological mapping, analysis of borehole logs, and morphological analysis of high-resolution LiDAR image had confirmed the presence of a complex fossil landslide in reactivation stage. Inclinator readings showed several sliding surfaces (9-15 m), with the deepest

sliding surface at 22 m, indicating a translation mechanism of sliding and “blocky” movements.

A simplified engineering geological map is presented in Fig. 5, while a representative cross-section is given in Fig. 6. Basic material properties of landslide body and stable ground are presented in Table 2, while residual values of shear strength parameters from direct shear tests in the zone of sliding surface were  $\phi_r' = 20-23^\circ$  and  $c_r' = 3$  kPa.

The diagram of piezometric ground water level fluctuation showed slight influence of seasonal inflow from precipitation (from June 2017-March 2019), except the period from December 2017-March 2018 when snow and snow melting caused rising of ground water level in several piezometers (Fig. 7).

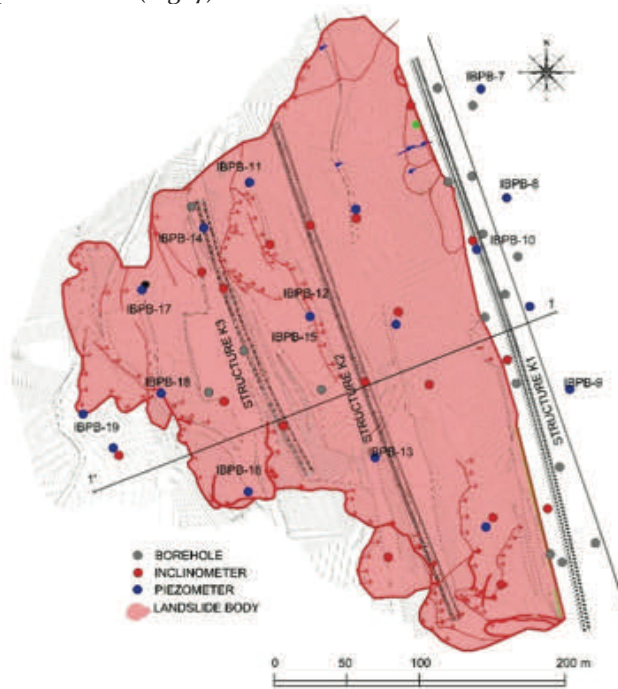


Figure 5 Simplified map of landslide on CUT5.

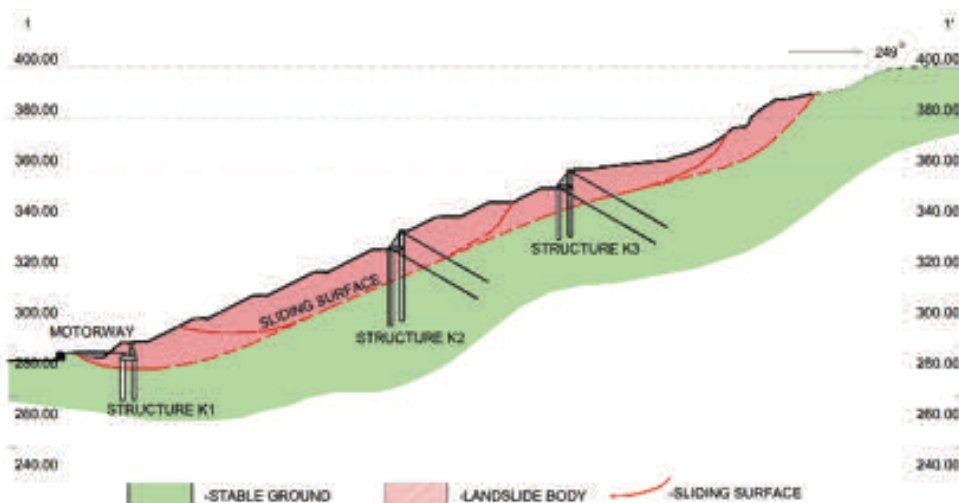






Figure 6 Simplified cross section of landslide 1-1' and proposed remedial measures on CUT5.

Table 2 Material properties of engineering geological units identified on CUT3 and CUT5.

Description of Engineering geological units on CUT3 and CUT5	RQD	Laboratory results			Photos of borehole logs
		$\gamma$ (kN/m <sup>3</sup> )	c (kPa)	$\phi$ (°)	
S*** Completely weathered and disintegrated shists – mainly surface parts of the slope and a part of landslides bodies		18-22	3-14	13-23	
S** Highly jointed and weathered schists – mainly below S*** and part of landslides bodies	< 20	20-23	5-20	20-23	
S* Medium jointed shists – partially weathered along joints, structure is preserved and part of landslides bodies	20-50	25-27	17-40	29-37	
S Jointed non-weathered shists – grey to green albite-muscovite-chlorite schists, structure and texture are preserved – stable ground	>50	27-28	>250	45-55	

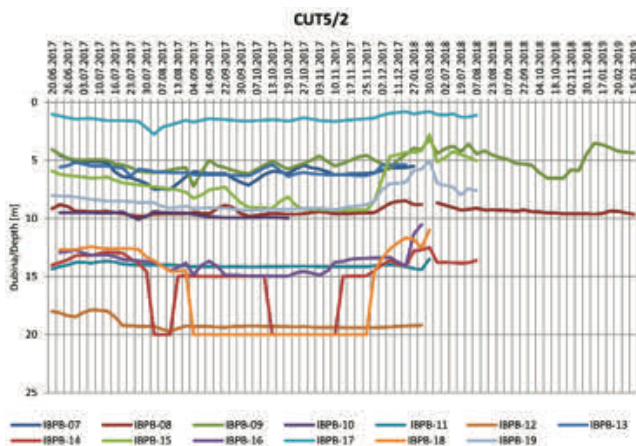


Figure 7 Ground water level on CUT 5 from June 2017-March 2019.

**Final remedial measures design**

**CUT3**

The remedial measures from the original Design from 2015 consisted of a combination of micro pile wall and shotcrete supported by pre-stressed and self drilling anchors. The protective structure was in the final stage of the construction works in August 2017 when excessive movement of the supporting structure had been reported after excavation of the last stage and the starting of construction works on road and pavement. As mentioned earlier, additional geotechnical investigations and airborne LiDAR scanning were performed in the next few months.

The new remedial measures proposed consisted of various works planned in three phases of construction. The first phase (as the most important), had consisted of 200.000 m<sup>3</sup> landslide material unloading behind existing retaining structure of micro-pilles and construction of drainage trenches for surface drainage. The second stage

consisted of large diameter pile wall (Ø 1200 mm) next to the South Morava river side in the toe of landslide with a reinforced embankment. In the third phase the construction of vertical reinforced concrete beams along the micropile wall had been involved. The beams were supposed to be anchored with long (55 m) pre-stressed anchors in stable rock layer behind sliding surface. On the platform of the berm a 6 m gabion wall is designed in order to stabilize the existing support structure with micro piles. During implementation on the third phase of remedial measures and after continuous monitoring by inclinometers and geodetic bench marks additional large diameter pile wall (Ø 1500 mm) is designed in the upper part of landslide. Simplified cross-section with remedial measures is presented in Fig. 5, while panoramic view of remedial works on CUT3 is presented in Fig. 8.

**CUT5**

According to the Main Design in the zone of CUT5 a simple 7 m high concrete wall was originally designed. The total length of the cut was approximately 500 m and around 7 m high. During excavation and construction of the wall, in the last 100 m of the cut a small landslide was activated in 2014. After two years of investigations and monitoring it was concluded that the entire cut area was a pre-existing landslide.

New remediation design was prepared by the Institute for traffic and transportation (CIP) in November 2017. Remedial measures included construction of three stiff structures (K1, K2 and K3) consisted of two rows of large diameter piles (Ø 1500 mm), long pre-stressed anchors (40 m) and additional excavation in between. Simplified cross-section with remedial measure is presented in Fig. 6, while a panoramic view of remedial measures on CUT5 is presented in Fig. 9.



Figure 8 Google Earth Pro view on CUT<sub>3</sub> from August 2021 (access January 2022).



Figure 9 Google Earth Pro view on CUT<sub>5</sub> from August 2021 (access January 2022).

## Conclusions

In this paper two case studies of fossil landslides reactivated during E75 highway construction in Serbia under complex geological conditions are presented. Both fossil landslides on CUT<sub>3</sub> and CUT<sub>5</sub> are formed in highly weathered and tectonized albite, chlorite, muscovite, and sericite schists from the early Paleozoic Vlasina Unit on the left South Morava river bank. After several phases of investigation and design some conclusions can be summarized as follows:

- Lack of understanding of the prevailing complex geological settings in the Feasibility study resulted to the wrong selection of the highway corridor alignment; it is recommended that advanced remote sensing techniques should be introduced for the future planning of infrastructure corridors
- Insufficient geotechnical investigations during the early phases of highway design (Preliminary and Main design) resulted to cut slopes instability problems during excavations, which subsequently necessitated additional geotechnical investigations
- Additional geotechnical investigations should had been extended beyond the expropriation line by the Investor and fine-tuned according to complexity of ground conditions
- Advanced geodetic survey, like LiDAR scanning should had been performed before construction excavations and combined with detailed morphological

analysis, especially in the zones of fossil or dormant landslides

- A geotechnical monitoring system should had been recognized by the Investor and Contractor and installed early enough and systematically, for the accurate detection of the sliding surface(s) and the mechanism of movement
- Design solutions should be climate resilient and conservative when applied in complex geotechnical conditions; insufficient measures always lead to re-design and significant increases of project costs and schedule overruns.

## References

- Antić M, Peytcheva I, Quadt A, Kounov A, Trivić B, Serafimovski T, Tasev G, Gerdjikov I, Wetzel A (2016) Pre-Alpine evolution of a segment of the North-Gondwanan margin: Geochronological and geochemical evidence from the central Serbo-Macedonian Massif. *Gondwana Research* 36: 523-544.
- Berislavljević Z, Radić Z, Đurić U (2016) High cuts on the critical path of the construction of Corridor 10 through Grdelica Gorge: contractual arrangements and site investigations. *Zbornik sedmega posvetovanja slovenskih geotehnikov, Podčetrtek 2016, Podčetrtek, 16-18 junija 2016, Jovičić V (ed). Slovensko geotehniško društvo. pp. 57-63.*
- Berislavljević Z (2018) Construction of high cuttings as a part of Corridor X highway project – geotechnical investigations, design and construction. *Conference Proceedings - Contemporary civil engineering practice, Andrevlje, 31. maj i 1. jun 2018. Department of Civil Engineering and Geodesy, Faculty of Technical Sciences Novi Sad and Society of Civil Engineers of Novi Sad. pp. 7-26.*
- Christaras B (1997) Landslides in iliolitic and marly formations. Examples from north-western Greece. *Engineering Geology* 47: 57-69.
- Dimitrijević MD (1997) *Geology of Yugoslavia. Geological Institute GEMINI, Special Publication, Belgrade. 187p.*
- Georgalas A, Vakiris D, Papacharalambous G (2017) Slope sliding failures in the construction of Highway E80, Bancarevo - Crvena Reka (LOT2). *Proceedings of the 2<sup>nd</sup> Regional Symposium on Landslides, Belgrade, 2015, Abolmasov B, Marjanović M, Đurić U (eds). pp. 181-186.*
- Kostadinov S, Braunović S, Dragičević S, Zlatić M, Dragović N, Rakonjac N (2018) Effects of Erosion Control Works: Case Study—Grdelica Gorge, the South Morava River (Serbia). *Water* 10, 1094; 1-19. doi:10.3390/w10081094
- Skempas M (2017) Egnatia Odos Highway-Variouse case histories of slope instabilities. *Proceedings of the 2<sup>nd</sup> Regional Symposium on Landslides, 14-16 May 2015, Belgrade. Abolmasov B, Marjanović M, Đurić U (eds). pp. 221-226.*
- Solberg IL, Hansen L, Rokoengen K (2008) Large, prehistoric clay slides revealed in road excavations in Buvika, mid-Norway. *Landslides* 5:291–304. DOI 10.1007/s10346-008-0122-7
- Yu H, Li C, Zhou J, Chen W, Long J, Wang X, Peng T (2020) Recent rainfall- and excavation induced bedding rockslide occurring on 22 October 2018 along the Jian-en expressway, Hubei, China. *Landslides* 17:2619–2629. <https://doi.org/10.1007/s10346-020-01468-6>
- Zhang F, Liu G, Chen W, Liang S, Chen R, Han W (2012) Human-induced landslide on a high cut slope: a case of repeated failures due to multi-excavation. *Journal of Rock Mechanics and Geotechnical Engineering* 4 (4): 367–374.

# Remediation measures of landslides on State roads in the Republic of Croatia – Presentation of case studies

Mirko Grošić<sup>(1)</sup>, Ivan Volf<sup>(1)</sup>, Ivana Blagdan<sup>(1)</sup>

1) Geotech d.o.o., Rijeka, Ciottina 21, Croatia, +385 99 40589 998 (mirko.grosic@geotech.hr)

**Abstract** Landslides are common on roads, which directly affect the flow of traffic and the connection and functioning of the population in surrounding area. Therefore, it is necessary to investigate them in the shortest possible time and to determine and carry out the remediation solution. Functionality of the state roads is immensely important so it is necessary to ensure that the traffic is maintained during remediation activities. Therefore, design solutions and remediation execution technology should be adapted to these requirements. Landslides are frequently formed in the road embankments and cover materials on the top of the bedrock due to exceeded soil strength parameters as a result of groundwater flow.

The paper presents experiences from practice on landslides remediation in the Republic of Croatia: landslide Laz 18 on state road D29 in section 38+254, landslide Dedin on state road DC3, section 015 in section 2+060, landslide Vranja on state road DC500, section 001 in section 2+400, landslide Dubravci on state road DC3, section 012 in section 4+400. The cause and mechanism of landslides, design solution for remediation measures and experience during the execution of works are presented. Landslide remediation measures mainly consisted of pile walls with cap beams or retaining walls and geotechnical anchors or rod anchors where necessary. In addition, in the impact area of each landslide a reconstruction of stormwater drainage system was carried out. After the completion of remediation works, monitoring equipment was installed to monitor the geotechnical structure and to verify the design solution.

**Keywords** landslide, remediation measures, stability

## Description, cause and mechanism of landslides

State roads are public roads that have the function of connecting the territory of the Republic of Croatia into the European transport system as well as interconnecting regions within the Republic of Croatia (counties, larger cities) and enable traffic transit. Continuous and safe traffic is of significant interest to the country, and landslides are one of the dangers that can temporarily or permanently disable it. Landslides are common on roads, where the most common triggers are geologically unfavourable terrain structure, excessive traffic load, inadequately constructed or unmaintained road drainage,

inadequate drainage of surrounding terrain that directly affects the roads, clogged culverts, and drainage canals, etc.

When landslides occur on state roads, it is necessary to perform an inspection in the shortest possible time (up to 24 hours), and to start with geotechnical investigation works and preparation of the design documentation for the landslide remediation as soon as possible.

In the event of instability, the safe flow of traffic is endangered. One of the frequent requirements by the investors is to allow permanent or temporary traffic in at least one lane. These roads are often the only way for buses, supplies, firefighters, and ambulances to operate.

The paper presents four different landslides on state roads (Laz 18, Dedin, Vranja and Dubravci), and for each landslide the causes and mechanism, geological structure, and remediation solution are described.

## Description, cause and mechanism of landslides (comparison of different geological conditions and landslide initiators/triggers)

### Landslide Laz 18 on state road DC29 km 38+254

Laz 18 landslide was located on the northern edge of the City of Zagreb, south of Krapina-Zagorje, between the settlements of Kašina and Laz Bistrički. The landslide was formed on a forested unstable slope (approximately 30 - 35 °) to the southwest, while the left side of the landslide passes along the edge of state road DC 29, in section 38 + 254. The Suhopot stream flows in the toe of the landslide (Grošić 2019a). On the part of the unstable slope, along the northwestern edge of DC 29, a landslide of about 20-40 m wide and about 150 m long was started.

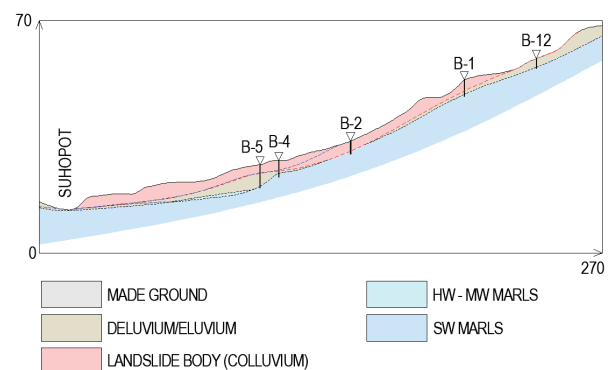


Figure 1 3D Engineering geological cross section of the landslide Laz 18 with marked investigation boreholes and Suhopot stream.

Elements of secondary sliding were determined within the investigated Landslide. There was a possibility of further expansion of the landslide on the sides, which directly affects the stability of the road embankment.

Detailed engineering geological and geotechnical investigation works were carried out. Investigation drilling was performed and 13 boreholes with a depth of 3.0 to 8.0 m (total of 66.0 m) were performed (Fig 1). In the boreholes, the groundwater level was continuously measured, and ranged from 0.4 m to 3.7 m from the ground level. Laboratory tests were performed on disturbed and undisturbed samples from boreholes.

The whole location consists of Miocene limestone marls covered with a continuous deluvial-eluvial cover (Fig. 1). Investigation works determined the leakage of groundwater at the contact between the landslide colluvium and the deluvium/eluvium or at the contact between the landslide colluvium and the substrate. A constant groundwater level was determined around the existing Suhopot stream on the southwestern edge of the landslide toe.

The landslide main body was defined by the contact of materials of different physical and mechanical characteristics. This was an active landslide that tended to expand in several directions: in the direction of the landslide movement (downwards), in the direction opposite to the direction of movement (upwards) and on both sides of the landslide.

Based on all conducted research as well as reinterpretation of previous investigations in the area, a geotechnical model of the landslide was developed, which was used for the analysis and development of a project solution for road rehabilitation.

#### **Landslide Dedin on state road DC3 (section 015) km 2+060**

The Dedin landslide was located in Dedin, which is part of the city of Delnice in the Primorje-Gorski Kotar County. The existing section DC 3 state road was constructed partly by cutting and backfilling on natural terrain – northeast part of the hill. The road structure is reinforced by stone supporting structure with existing culverts (at two locations).

Due to the landslide, the pavement was damaged by tensile cracks, which affected traffic safety. The location consists of deposits of upper triassic breccia conglomerates covered with cover material and deluvial-eluvial deposits.

Stormwater was drained by existing culverts, but mostly it naturally infiltrated into the ground through well-permeable gravel deposits and the deluvial-eluvial cover and very weathered substrate.

The landslide body is formed in the cover material and deluvial/eluvial deposits. The landslide is most likely triggered due to exceeding the strength of the near-surface materials, traffic vibrations (frequent heavy vehicle traffic) and local disturbance of physical and mechanical characteristics of deluvial-eluvial cover due to continuous atmospheric actions (Fig. 2).



Figure 2 Photo of the state road DC3 (section 015) at km 2+060 before remediation works. Tension cracks at the crown of the landslide Dedin are visible on the asphalt.

The landslide body passes through several different geotechnical units. The width of the sliding body was 15.0 m, the length was 10.0 m, and thickness was about 2.0 m. The volume of the sliding body was estimated to be about 300 m<sup>3</sup>.

Due to unfavourable hydrogeological and geomorphological conditions, as well as terrain and road configuration (part of the road was constructed in the slope and part of the road was on the embankment), further instabilities of cover deposits (deluvial/eluvial deposits and landslide deposits) were possible. Also, new landslides could be triggered on lateral and higher parts of the slopes due to unloading (Grošić 2018a).

#### **Landslide Vranja on state road DC500 (section 001) km 2+400**

The location of Vranja landslide was in the Istria County, on the state road DC500, at km 2+400. The area of Vranja landslide is located north of the settlement of Vranje and passes through an uninhabited area along its entire length of the road. In the southwestern part of the road, there were tensile cracks 40.0 m long and 2.50 m wide.

The landslide was approximately 45.0 m wide and approximately 80.0 m long and included the lower part of the state road. The landslide also affected the slope below the state road. The road has a slight slope to the northeast, while the terrain below the road has a steep slope of up to 30° to the southwest and is forested. On the north-eastern side of the road, there are surface outcrops of rock mass. Part of the road was constructed as embankment on the slope.

During the terrain inspection of the state road and surrounding area, the elements of the landslide were determined. The crown of the landslide was represented in the form of tensile cracks on the southwestern edge of the DC500 road, while the toe of the landslide, ridges and accumulation are not clearly visible due to the vegetation and forested terrain. The sliding surface along the slope is covered with landslides colluvium and is not clearly visible. On the natural slope below the road there are traces of landslides/soil creep (irregularly inclined trees,

irregular slope relief etc.). Frequent tensile cracks were observed within the road below the slope (Grošić 2020a).

According to the conducted geotechnical investigations, translational sliding of the slope southwest of the state road DC500 was determined, at km 2+400, in the part of the embankment and deluvium deposits with a sliding surface at the depth of approximately 4.5 - 9.0 m below the road embankment. This type of landslide (consequent landslide) includes deposits of cover material and deluvium whose sliding surface is formed within deluvial deposits, in contact with the bedrock made of alveolar limestones (Hungar et al. 2014). The landslide at the state road DC500 is retrogressive and the rupture surface could be extended in the direction opposite to the movement of the displaced material. Also, the deposits of the road embankment are additionally loading the landslide body. The sliding of the natural slope is conditioned by the destabilization of deluvial deposits and by the action of groundwater that seeps through at the contact of deluvial deposits and the rock base of alveolar limestones.

#### **Landslide Dubravci on state road DC3 (section 012) km 4+400**

The Dubravci landslide was located west of the Dubravci settlement, on the state road DC3, section 012 at km 4+400, Karlovac County. On the investigated part of the location, the DC3 road is passing in the general northwest-southeast direction and is formed by cutting transversely to a natural slope of approximately 25° to the southwest. The route of the road was made by partial cutting and partial filling of the existing terrain, which formed cuts along the left edge of the road and embankments along the right edge of the road. The existing embankments and cuts are unprotected, and no retaining structures are present at the location. At the left edge of the road, there are unregulated canals for drainage of rainwater, which redirect it towards the existing concrete culvert. There are numerous layers of asphalt and repaired cracks on the existing road, which indicate the systematic creeping of materials over a long period of time.

The earthquake in Banovina on 28<sup>th</sup> and 29<sup>th</sup> December 2020 caused the activation of the landslide of already potentially unstable material of the road and caused the opening of a tensile crack with a vertical height of approximately 3.5 m (Grošić 2021a).

After the terrain inspection and mapping of the location more signs of sliding were observed: open cracks, new tensile cracks in the asphalt, progress of the accumulation in the southwest direction, seepage of water at the bottom of the accumulation, dredging of the terrain and irregular sloping of the trees – Fig. 3.

The sliding body and accumulation of the material consisted of three cascade like terraces with a height of about 1.5 m between each terrace and was represented by light, water-soaked material which, due to the large mass of running material, causes the fall of trees at the base of the landslide (Fig. 4).



Figure 3 Aerial view of Dubravci landslide on the state road DC3 (section 015) at km 2+060.



Figure 4 Main scarp of the Dubravci landslide.

Geotechnical investigation works consisted of investigation drilling, engineering geological mapping of whole terrain and boreholes cores, and laboratory testing of samples.

On the existing road, tensile cracks were observed above and around the main crack of the landslide, inclined trees were observed on the slope below the road along the entire location, in the width of approximately 85.0 m. The width of the landslide was approximately 35.0 m and the length of the landslide was 35.0 m. Due to the weather conditions, it was possible that the landslide would further progress in the horizontal and vertical directions of the current landslide body. The depth of the sliding body at the deepest point was approximately 9.0 m from the level of the road and was located at the contact of deluvial-eluvial deposits and completely to highly weathered marls.

Based on the performed geotechnical investigation works at the location, a rotational landslide with a sliding surface of approximately 9.0 m depth was determined. The landslide included a part of the pavement structure and a part of the slope below the road. The sliding surface is formed at the contact or in the immediate vicinity of the deluvium/eluvium contact with high to medium weathered clastics. These types of landslides include deposits of cover material, cover layer and deluvial-eluvial deposits, and due to the action of water and the weight of the sliding mass, it deepens to the horizon of completely to highly weathered marls (Hungar et al. 2014). The cause

of the initial activation of terrain sliding is most likely inadequate slope drainage and overloaded high frequently traffic. After the earthquake the landslide progressed rapidly and there was a final failure of the whole terrain.

### Remediation measures design

Landslide remediation works along state roads need to be approached with increased attention and regarding requirements from investors. As these are state roads, they present the roads and connections of particular importance that connect the territory of the Republic of Croatia with the network of major European roads.

One of the conditions for remediation is to leave at least one traffic lane permanently or temporarily open (when it is possible), because these roads sometimes represent the only way for buses, supplies, firefighters, and ambulances to pass.

Following chapters of the paper, present stability analysis of the landslides and remediation measures (Popescu 2001) with a technical description of remediation works for each of the mentioned landslides.

#### Landslide Laz 18 on state road DC29 km 38+254

Remediation measures for the Laz 18 landslide were divided in two zones - zone I (includes remediation works of the upward part of the slope above the road curve) and zone II (includes protection of the side part of the road curve).

The stability analysis was carried out in Plaxis 2D software two phases and was carried out separately for the two zones. First, the current state was modelled, and a reverse stability analysis was performed to obtain the actual strength parameters of the geotechnical units. In the following phase, the proposed design solution was modelled and verified to confirm the stability and to determine the forces and moments for dimensioning of the structural elements (piles, walls, anchors). The model used for stability analysis of the remediation measures for zone I is presented in Fig. 5 (Bentley Systems 2020).

Remediation measures of zone I consisted of reinforced concrete bored piles, in two rows, with a diameter  $D = 600.0$  mm at a horizontal distance of 1.0 m. Designed pile length was from 5.0 m to 8.0 m. Above piles, a reinforced concrete "L" pile cap was constructed as foundation structure for a retaining wall – Figs. 5 and 6. Remediation measures of zone II consisted of a pile wall of bored piles in one row with a diameter of  $D = 600.0$  mm, length from 5.0 m to 8.0 m at a horizontal distance of 1.80 m each. A reinforced concrete pile cap was constructed above the piles. Self-drilling anchors with a length of 12.0 m at an axial distance of 3.60 m were installed through the pile cap (Grošić 2019b).

#### Landslide Dedin on state road DC3 (section 015) km 2+060

As a design solution for the remediation measures of the landslide Dedin, the construction of a reinforced concrete

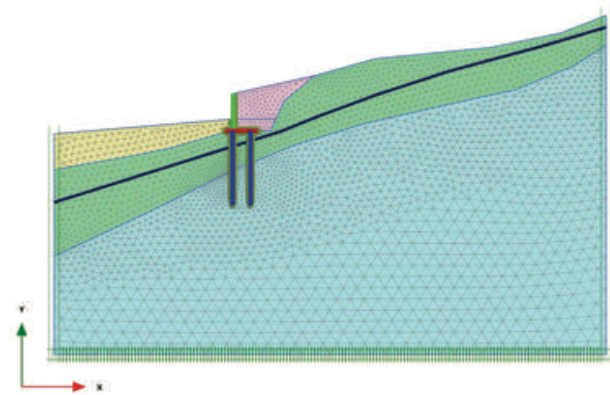


Figure 5 Numerical model used for geotechnical analysis of zone I (reinforced concrete wall with piles) for landslide Laz 18, performed in Bentley Plaxis 2D software.

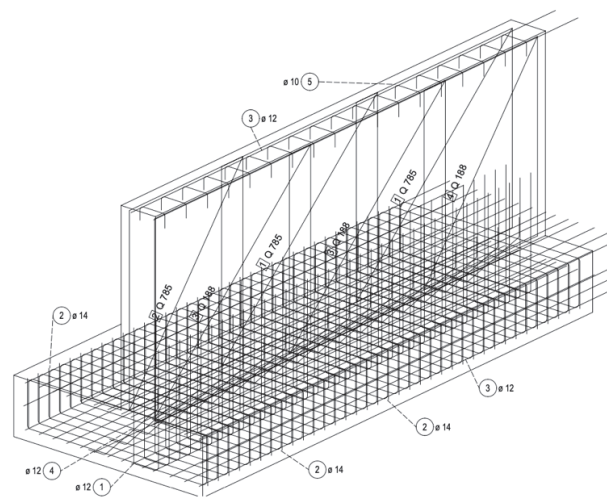


Figure 6 3D BIM model of reinforcement plan of the concrete pile cap and wall of zone I for landslide Laz 18 created in Allplan (Allplan Nemetscheck Group GmbH 2020).

retaining wall was chosen, which was constructed on bored piles. The pile wall was made of reinforced concrete bored piles with a diameter  $D = 400$  mm, pile lengths were  $L = 3.50$ ,  $4.50$  and  $5.0$  m respectively. The horizontal distance of the piles were 1.0 m and piles were embedded into the rock base at least 1.50 m. In this way, the stability of the retaining structure was ensured, and the pile wall was used not only for the foundation of the retaining wall but also for ensuring higher slip resistance of the whole geotechnical construction. Piles, with their whole length, passed through the landslide body and thus significantly contributed to the increase of the safety factors of the whole slope. Additional stability was provided by the construction of self-drilling rod anchors with a total length of  $L = 12.0$  m with an anchor bond length of  $L_b = 6.0$  m.

As part of the remediation measures works, the whole drainage system of the road (transverse and longitudinal slopes of the road, drainage channels) was completely reconstructed, and a new culvert was built. The outflow part of the new culvert with channels were constructed and water was drained from the impact area of the landslide area – Fig. 7 (Grošić 2018b).





Figure 7 Dedin landslide on state road DC3 (section 015) at km 2+060 after remediation works.

**Landslide Vranja on state road DC500 (section 001) km 2+400**

The length of the landslide remediation work was 65.0 m, and it consisted of bored piles  $D = 600$  mm in one or two rows (depending on the remediation zone and geological conditions of the site). At the start of work, a temporary barrier was installed (New Jersey bumpers) and temporary traffic control was established. Temporary excavation for the construction of a pile wall and retaining wall was excavated at a slope of  $V:H = 2:1$ .

Bored piles were installed through the cover material and embedded into the rock base. Piles of length  $L = 4.50$  and  $7.0$  m were constructed in one or two rows at an axial distance of  $1.80$  m – Fig. 8. The transverse distance of two rows of piles was  $1.20$  m. Request for minimal depth of embedding into the rock mass (limestones) was  $1.80$  m to ensure required load and moment transfer into the bedrock (Grošić 2020b).

**Landslide Dubravci on state road DC3 (section 012) km 4+400**

Remediation works on Dubravci landslide were performed by the combination of pile wall and a mechanically stabilized earth (MSE) retaining wall. Bored piles had a nominal diameter of  $D = 880.0$  mm and length of  $10.0$  m. An axial distance between the piles was  $2.50$  m in the longitudinal and transverse directions. For the proposed remediation solution stability analyses were performed – Fig. 9 (Bentley Systems 2020). As part of the preparation phase, temporary excavation was conducted for approaching of machines for piles installation. The excavation, and whole remediation works, were conducted in several phases to avoid further instabilities on the slope



Figure 8 Remediation works on pile wall at Vranja landslide.

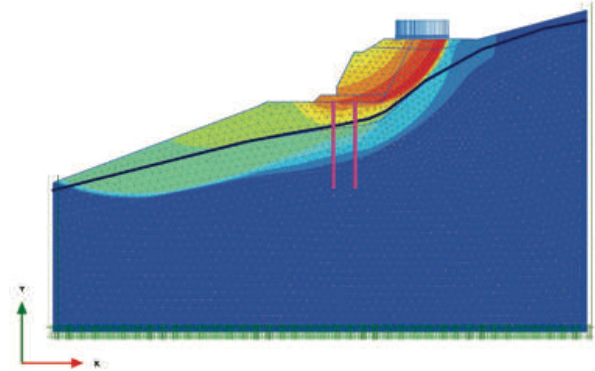


Figure 9 Results of stability analyses for factor of safety of proposed remediation solution for Dubravci landslide performed in Bentley Plaxis 2D software.

and road. After the excavation and construction of piles, the foundation of the soil was prepared and improved by mechanical compaction ( $M_s > 20.0$  MN/m<sup>2</sup>) and geotextile installation. Two layers of a mechanically stabilized granular stone material (granulation of  $\varnothing 0-63$  mm) was installed with a total thickness of  $75.0$  cm. Between two layers of mechanically stabilized granular stone material, the layer of geogrid was installed.

Above the mechanically stabilized granular stone material, a gabion support structure with tensile elements was constructed. An embankment of stone and mixed material with a final slope of  $V:H = 2:1$  was made behind the gabion retaining structure (Fig. 10). Hydro seeding was applied on the surface of the slope.

In the part of the location where there were no significant instabilities, the construction of a pile wall consisted of bored reinforced concrete piles with length  $L = 10.0$  m, nominal diameter  $D = 620.0$  mm in one row at an axial distance of  $2.25$  m, Piles are connected with a reinforced concrete pile cap  $0.50 \times 0.80$  m. Together with the landslide remediation works, the reconstruction of road layers and reconstruction of a stormwater drainage system was performed (Grošić 2021b).

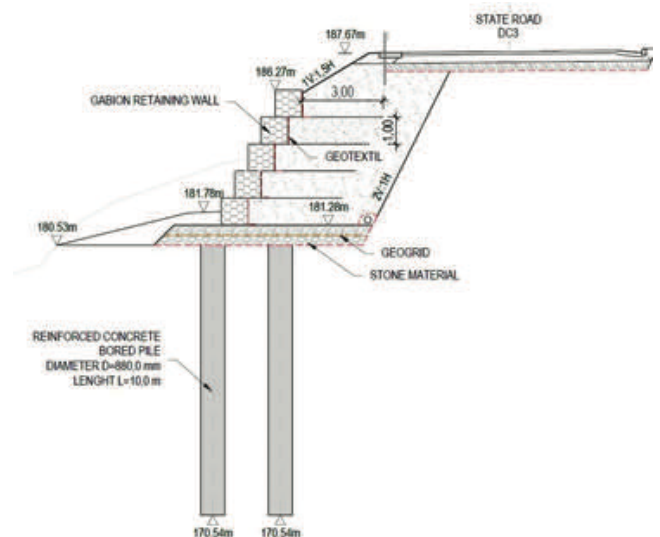


Figure 10 Characteristic cross section of remediation measures for Dubravci landslide.

## Discussion

The paper presents the geotechnical investigation works and remediation solutions for 4 landslides on state roads in Republic of Croatia: landslide Laz 18 on state road D29 in section 38+254, landslide Dedin on state road DC3, section 015 in section 2+060, landslide Vranja on state road DC500, section 001 in section 2+400, landslide Dubravci on state road DC3, section 012 in section 4+400.

The causes of landslides are conditioned by unfavourable geology, inadequate drainage systems, earthquakes, excessive traffic loads and usually a combination of these conditions. Among these landslides we also participated in the numerous remediation projects of state roads, and it can be concluded that a special and frequent trigger of landslides cannot be isolated. In most cases it is a combination of one or two unfavourable causes that trigger landslides.

For each of these landslides, detailed geotechnical investigation works were conducted to determine the landslide mechanism, the layout of geotechnical units and the parameters required for the geotechnical numerical analysis. Remediation measures mainly consisted of bored piles (diameter from 600 mm to 900 mm) in a combination with a pile cap or/and retaining wall. Sometimes, anchors are used for additional protection and safety. The pavement structure and complete reconstruction of drainage system in the impact area were always performed alongside the geotechnical remediation works. This type of reconstruction is most common along not only the state roads but also on the other roads because it has proven to be an ideal combination of performance technology and design solution.

## Acknowledgements

This landslide remediations case studies were made to protect and ensure stability of state roads and to ensure safe traffic for the investor Hrvatske ceste d.o.o., Vončinina 3, HR 10000 Zagreb. The geotechnical investigations, geotechnical report and slope protection design were carried out by Geotech d.o.o., Ciottina 21, HR 51000 Rijeka.

## References

- Allplan Nemetscheck Group GmbH (2020) Allplan Manual
- Bentley Systems (2020) Plaxis 2D Manual
- Grošić M (2018a) Geotechnical report for landslide Dedin at state road DC3, section 015, km 2+060. Geotech Ltd., Rijeka. (Project number: PR 18-059-02)
- Grošić M (2018b) Geotechnical design for landslide Dedin at state road DC3, section 015, km 2+060. Geotech Ltd., Rijeka. (Project number: PR 18-059-03)
- Grošić M (2019a) Geotechnical report for landslide Laz 18 at state road DC29, km 38+254. Geotech Ltd., Rijeka. (Project number: PR 18-127-01)
- Grošić M (2019b) Geotechnical design for landslide Laz 18 at state road DC29, km 38+254. Geotech Ltd., Rijeka. (Project number: PR 18-127-02)
- Grošić M (2020a) Geotechnical report for landslide Vranja at state road DC500, section 001, km 2+400. Geotech Ltd., Rijeka. (Project number: PR 20-027-01)
- Grošić M (2020b) Geotechnical design for landslide Vranja at state road DC500, section 001, km 2+400. Geotech Ltd., Rijeka. (Project number: PR 20-027-02)
- Grošić M (2021a) Geotechnical report for landslide Dubravci at state road DC3, section 012, km 4+400. Geotech Ltd., Rijeka. (Project number: PR 21-064-01-Rev0)
- Grošić M (2021b) Geotechnical design for landslide Dubravci at state road DC3, section 012, km 4+400. Geotech Ltd., Rijeka. (Project number: PR 21-064-02-Rev0)
- Hungr O, Leroueil S and Picarelli L (2014) The Varnes classification of landslide types, an update. *Landslides*. 11 (2): 167-194.
- Popescu M (2001) A suggested method for reporting landslide remedial measures. *Bull Eng Geol Env*, Vol. 60, pp 69–74.

# Deep landslide in the jointed flysch sediments on the Bar-Boljare Highway, Montenegro

Slobodan Živaljević<sup>(1)</sup>, Nikola Međedović<sup>(2)</sup>, Miodrag Bujišić<sup>(3)</sup>, Zvonko Tomanović<sup>(4)</sup>

1) University of Montenegro, Faculty of Civil Engineering, Podgorica, Cetinjski put 2, Montenegro, +38269388355 (sloboz@hotmail.com)

2) Geoprojekt ltd, Podgorica, Student street, Montenegro

3) University of Montenegro, Faculty of Civil Engineering, Podgorica, Cetinjski put 2, Montenegro

4) GeoT ltd, Podgorica, Djoko Mirasevic street 24, Montenegro

**Abstract** The subject of the paper is a case study of a deep landslide that formed in the jointed flysch sediments on the Bar-Boljare highway, Smokovac-Mateševo section, Montenegro. The landslide has affected 140 m of the left highway lane in the cut and has endangered the Uvač 4.1 bridge abutment. The landslide displacement first occurred in May 2019 and continued to intensify in early June of the same year. The cause of the instability occurrence is in the unsecured temporary subvertical cut (approximately 15 m high) constructed between left and right lane of the highway. The landslide was formed in the flysch formation, which consists of an alternation of sandstones and siltstones with a developed joints system. The landslide was initiated in the northern part of the site, where a wedge failure occurred (average block size 4 – 6 m), resulting in the formation of a 50 m wide unstable zone. The instability further propagated along the slope towards the southern part of the site, where a second sliding body was formed, the movement of which caused the displacement of the retaining wall and the bridge abutment. The total length of the landslide along the slope is about 80 m. This was further confirmed by a simple kinematic analysis. One of the unfavourable circumstances is the presence of a 2 to 3 m wide fault zone, so that the landslide zone partially propagated through this weakened zone. The whole mechanism of the process caused appearance of a clearly visible frontal scarp in the rock mass about 110 m long and a transverse crack separating two unstable masses (northern and southern) about 70 m long. Assessment based on the geotechnical investigation and inclinometer data suggests that the deepest points of sliding zone vary are between 17 and 22 m. Slope stability analysis was performed on typical cross-sections to confirm the assumed sliding mechanism and to obtain numerical parameters for design of remediation measures. The analysis was performed using Slide and RS2, Rocscience software. Based on the results of the geotechnical investigation, inclinometer data and numerical analysis it was concluded that the unfavourable position of discontinuities in the rock mass was a predisposing factor for the landslide occurrence. This refers primarily to the joint sets, since the orientation of

stratification is relatively favourable from the aspect of slope stability, which is atypical for this zone and is rarely the case for unstable flysch slopes. One of the characteristics of the landslide is also a high-quality rock mass composed mainly of sandstones and also affected by sliding. The landslide was remediated in 2021 through a combination of several types of remediation measures that included construction of bored piles with a diameter of 150 cm and a depth of 20 m with a cap beam, prestressed geotechnical anchors up to 30 m long connected with a reinforced concrete grid, 6 m long bolts, and surface and underground terrain drainage.

**Keywords** flysch, landslide, mechanism, remediation

## Introduction

The subject of the paper is a case study of a deep landslide formed in the jointed flysch sediments on the Bar-Boljare highway, Smokovac-Mateševo section, Montenegro. In flysch terrains, Quaternary layer usually slides over the bedrock (Živaljević et al. 2021), while in this case, due to the unfavourable orientation of discontinuities in the rock mass, sliding occurs through a more solid rock mass.

After a brief description of the site morphology and geologic conditions, the paper focuses on a detailed description of the key elements of the landslide and sliding mechanism. The paper presents the results of numerical analysis of the slope stability on a typical profile as evidence of the sliding mechanism that has been assumed based on the geotechnical investigations and inclinometer data. A brief description of the remediation solution is also provided.

## Study area

### Topography and landform

The landslide is located on the left slope of the open route of the Bar-Boljare highway, Smokovac-Mateševo section, on the chainage from km LK 33+280 to LK 33+420 (Fig. 1). The right lane extends along the bridge Uvač 4.1. The site

is located on the eastern mountainside of Vitanovica above the Tara river.

From the aspect of geomorphology, the overall terrain route is quite complex and rugged and can be generally classified as hilly and mountainous relief. At the micro location, morphometrically, it is a slope with an inclination of  $35^\circ$  to the east.

During the period of the landslide activation, the morphometry of the natural terrain changed due to the executed earth works for the construction of the highway. Seen from above, the following morphometry parts can be identified: a plateau at an elevation of about 1104 m a.s.l., from which the abutments of Uvač 4.1 bridge on right lane rise; a steep rock section formed between the left and the right lane with a height of 20 m; a 14-15 m wide plateau within the area of the left lane of the highway at the elevation of about 1124 m a.s.l.; a 7-8 m high retaining wall along the left edge of the left lane with an inclination of about 5:1. Three benches are constructed above the wall: first bench is 5 m high with an inclination of 3:1, and the other two benches are 5-7 m high with an inclination of 3:2. The berms are constructed between the benches; the slope crest is at an elevation of 1144 m a.s.l., followed by a natural slope with an inclination of about  $35^\circ$ .

#### Geological conditions

In the wider area of the landslide, the highway extends through flysch sediments of the Cretaceous-Paleogene age. The thickness of these sediments is about 500 m.

In terms of lithology, the micro location is dominantly featured by the engineering-geological (EG) unit 2d, which means that it has a similar ratio of sandstone and alevrolite.



Figure 1 Landslide position.

The prevailing presence of sandstone (EG unit 2a) is found at greater depths and eventually at lower thickness in the upper zone. The thickness of the silty-clayey materials varies from 0.5 m in the steeper parts of the slope to 4 m in the higher parts of the slope with lower inclination. The deluvium is absent from the large part of the micro location, because of the executed cut and major earthworks in this zone of the highway.

General bedding orientation is favourable from the aspect of the slope stability. This was further confirmed by EG mapping which registered bedding planes orientation of  $215-310/10-35$ , indicating a southwest-northwest orientation of bedding, sufficient for stability of the east-facing slope. Alevrolite (siltstone) is platy and tabular and sandstone is thin bedded to bedded. Where laminae occur in the rock mass texture, they have orientation of the bedding dip.

The joint system is clearly defined and shown on EG map (Fig. 2). According to the mapping, the bedding discontinuities are followed by two more dominant steep joint sets. A zone between boreholes BIP-5 and BIP-2 is typical and is considered to be the zone where the sliding process has been initiated, as two joint sets were registered with dip direction/dip angle (EP)  $40-55/55-70$  and a subvertical set which falls at very steep angle either on direction  $130^\circ$  or on  $310^\circ$ . The two joint sets can cause sliding of blocks down the slope; hence this occurrence is considered to trigger the slope instability. In addition to these two dominant joint sets, with deviations of up to  $20^\circ$ , there are also joint sets in the zone of the abutments of the Uvač 4.1 bridge of  $165/70$  and  $95/87$ , as well as  $325-335/35-50$  in the zone of BIP-7 and BI-1 boreholes. The geotechnical category P represents a deluvial-eluvial zone which is very thin, while category F represents the exceptionally poor flysch rock mass, i.e. a degraded and altered zone of the bedrock which is mainly present at the first (highest) bench of the slope excavation. Further on, the second and third benches are dominated by an E category rock mass, which is represented by clear texture properties of rock mass without zones that would characterise it as a rock to soil transition. Geotechnical categories F and E are related to the EG unit 2d.

Thereafter there is a dominant presence of sandstones (2c) that, due to their resistance, are automatically less fractured with two joint sets at larger distance and with a bedding plane also at larger distance. This is a D category of the rock mass.

#### Overview of the landslide and landslide mechanism

The information about the landslide development and the problem of slope instability was obtained from the Contractor of works. The first deformations occurred in May 2019 and intensified in early June.

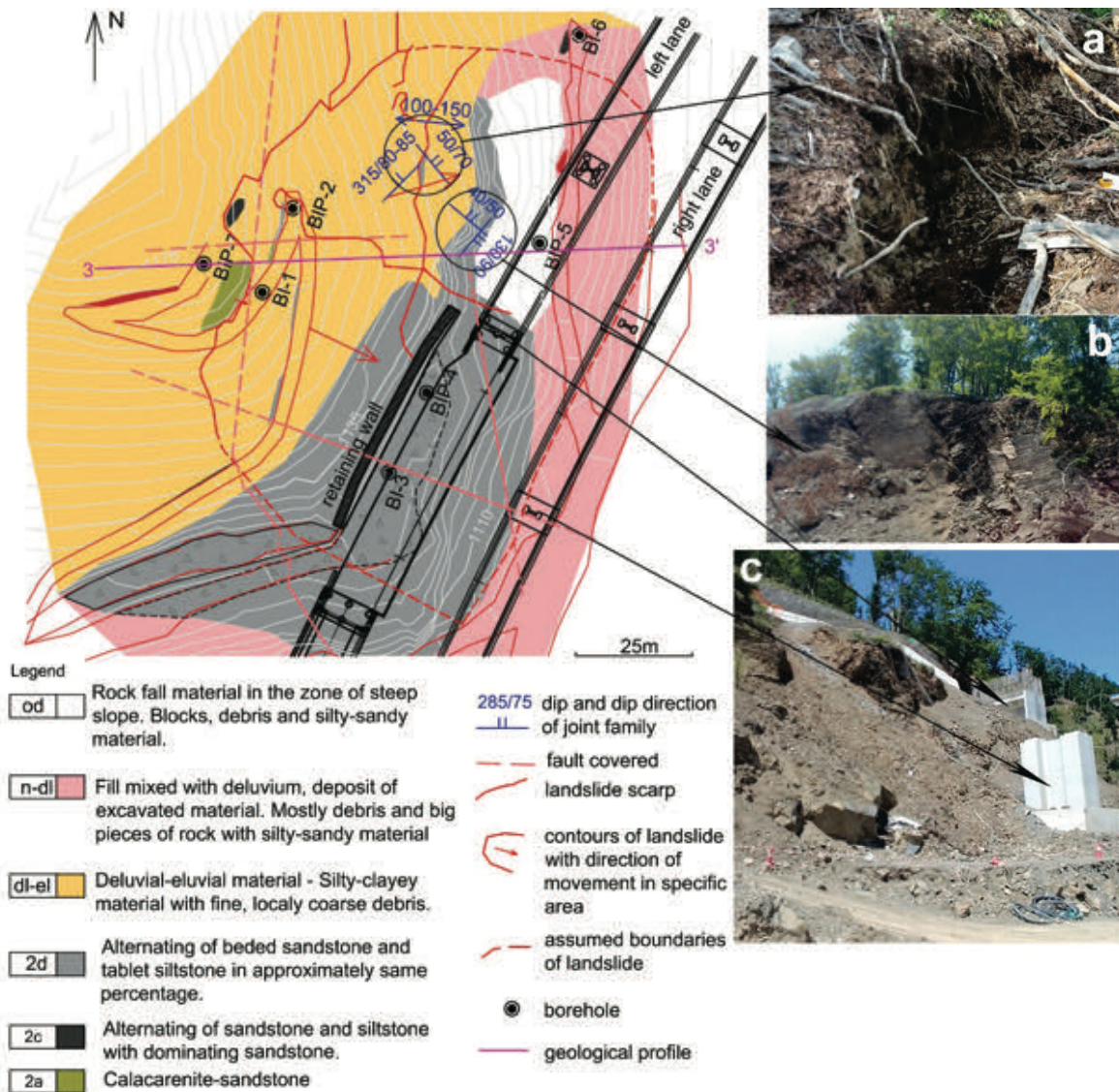


Figure 2 Simplified engineering-geological map with characteristic photos from the site: a Scarp, b Fallen rock blocks due to wedge failure, c Abutment of Uvač 4.1 bridge (Mededović 2019).

Based on the analysis of the data relating to the affected landslide, it can be said that the sliding of a rock mass with an estimated volume of about 50000 m<sup>3</sup> has started, which can be attributed to the unfavourable rock mass discontinuity set and inadequate cut-and-fill slopes, as well as the absence of any kind of terrain protection measures in the northern part of the micro location behind the retaining wall (Fig. 2) and also between the left and the right lane of the highway (Fig. 2c). The cause of the instability is not the cut in the open route, but the subvertical cuts between the left and right lane as well as the temporary cut in the northern part of the site. Namely, the cut between the left and right lane of the highway is steep to subvertical, with a height of about 15 m. The cut in the northern part of the location behind the retaining wall also has a similar geometry. The length of cut between the two lanes is approximately 70 m, while the length of cut-and-fill slope behind the retaining wall is

approximately 50 m. No support measures were provided for these two cuts. This means that the uncontrolled earthworks had crucial impact on activation of the sliding process, which endangered the slope, the retaining wall and the bridge abutment. About 25-35 m above the slope, a scarp is formed at the contact with the huge calcarenite block within flysch. The scarp is about 90 m long with locally clearly visible jump from 1.5 to 3.0 m and spreading of up to 1 m. Number of secondary scarps with a jump of up to 1.5 m is observed between the slope and the main scarps. Some vertical joints are visible on the third bench. A very significant scarp in the length of 70 m is registered at some 10 to 12 m from the top of the cut, beyond the highway zone (above borehole BIP-5), Fig. 2a. This scarp extends even to the retaining wall where it affects the last two benches that have displaced the most. A joint is clearly visible on the third bench of the slope.

Kinematic analysis of the rupture composition, inclination and orientation of the slope determined the wedge forming and rock block falling in this zone. The block falling because of the wedge forming is a common phenomenon, however, in this case blocks of enormous dimensions are formed, which would probably initiate the instability of the entire zone (Fig. 2b). Based on the kinematic analysis, the central part of the hillside and the slope is also prone to the block falling, which is further confirmed by the kinematic analysis in that zone.

Mapping the zone around the bridge abutment on the south hillside (abutment L1O2) recorded a fault zone extending from the abutment towards the top of the hillside. This fault zone can be tracked on all cut-and-fill slopes of the access road in the southern part of the hill. The zone width ranges from 2 to 3 m. The material consists of debris with dusty-sandy component. The elements of the fault dip are approximately 95/60. In addition to the instability that occurred in the northern part of the site, this fault also presented a very unfavourable situation in this part of the site, and it is considered that the sliding plane has partially formed through this weakened zone, as shown in the cross-section 3-3' (Fig. 3).

The south edge of the landslide is defined by subvertical joints with EP 20/90 that are formed on the

slope between the two lanes of the highway. These joints are located at about 15-20 m from the abutment towards north.

The EG terrain composition based on the investigation works is shown on the EG cross-section 3-3' (Fig. 3). The figure clearly shows the main and secondary scarps which have been determined by the EG terrain mapping. The toe area of the landslide is not defined considering this part of the site is covered with backfill material. Based on the geodetic monitoring and the inclinometer structures built in the boreholes, the slip surface has been interpreted as marked by the red line. Considering that the inclinometer BI-1 measured certain deformations (not necessarily suggesting the slip surface) at greater depth (approximately 20 m), the magenta colour has been used to mark the unfavourable slip surface at the greater depth, so that this input could be considered in the construction design as the unfavourable scenario when defining protection measures. Precise defining of these deformations required a longer period of time and additional inclinometer measurements. However, considering the urgent nature of the slope stabilisation subject to the timeline of the highway construction, the Designer was instructed to also consider the protection measures for the unfavourable scenario.

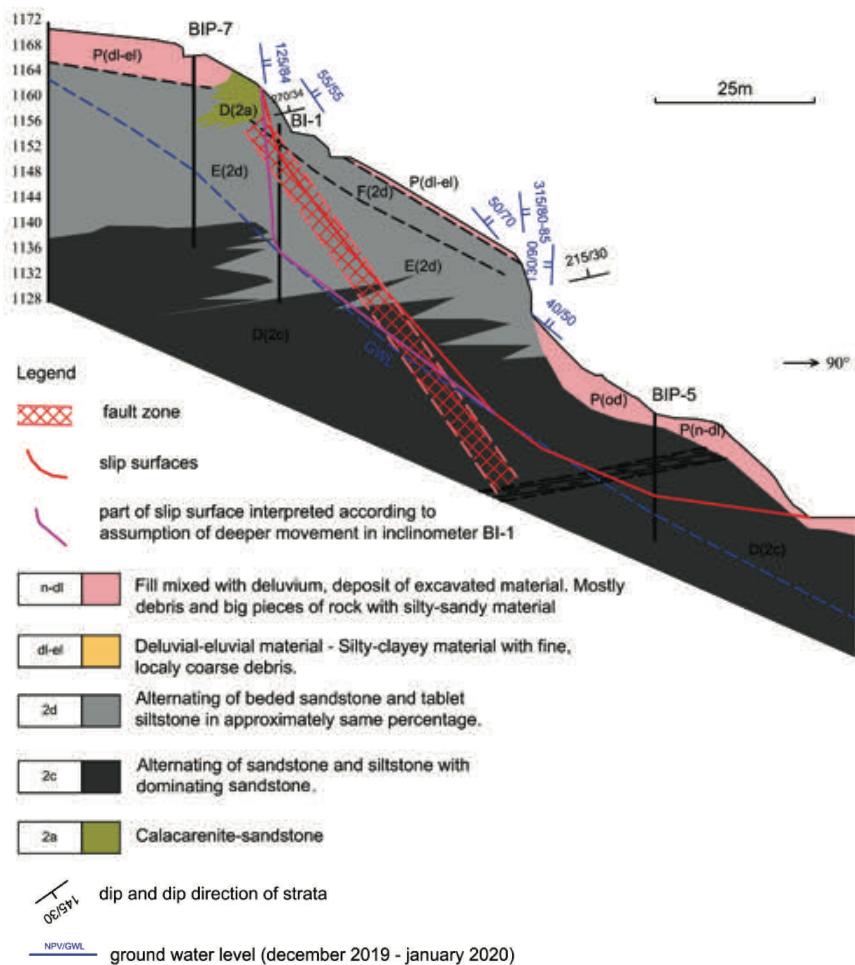


Figure 3 Engineering-geological cross-section 3-3' (Međedović 2019).

### Stability analysis

Slope stability analysis were performed on three typical cross-sections to confirm the assumed sliding mechanism and to obtain numerical parameters for design of remedial measures. The analysis was performed by using Slide and RS2, Rocscience software (Rocscience 2021). A standard back analysis based on the method of slices (Bishop simplified, Janbu simplified, Janbu corrected, Morgenstern-Price) with the unfavourable position of the sliding surface was used (Abramson et al. 2001, Rocscience 2021). The back analysis was conducted by varying the shear strength parameters for the slip surface until a factor of safety (FoS) of approximately 1 was obtained. The results of the analysis for profile 3-3' are shown in Fig. 4. It can be seen that the obtained average internal friction angle is about 30° while the adopted cohesion is 0 kPa. The RS2 programme was used to perform the back analysis on a 2D model consisting of linear triangular finite elements by using the shear strength reduction method (You et al. 2018). Tab. 1 shows the physical and mechanical parameters used for the corresponding rock masses. Joints have been modelled by the interface elements. The shear strength parameters for these elements have been varied until Strength reduction factor (SRF) (equivalent to FoS) of approximately 1 was obtained. The adopted joint system has been simplified and represented by 2 joint sets, one out of which with a downslope grade of 80° and the other with a downslope grade of 35°, corresponding to dominantly

unfavourable sets on the EG profile 3-3'. The results of the analysis indicate that the sliding mechanism of the trapezoid-shaped sliding surface over the adopted joint sets with the 35° inclined sliding surface and sliding surface depth of 13.80 m (Fig. 5).

### Landslide remediation

The landslide remediation was performed in 2021 through a combination of several types of remediation measures that included (Figs. 6 and 7):

- construction of bored piles with a diameter of 150 cm and a depth of 20 m with a cap beam,
- prestressed geotechnical anchors up to 30 m long connected with a reinforced concrete grid,
- 6 m long bolts,
- surface and underground terrain drainage.

Table 1 Computation parameters of rock masses (RS2 software).

Rock mass	$\gamma$ (kN/m <sup>3</sup> )	$\phi'$ (°)	$c'$ (kPa)	Young's modulus (kPa)
D (2c)	25.0	32	2500	2.5e+06
E (2d)	23.5	29	320	800000
F (2d)	23.0	26	50	60000
P3	21.0	30	10	40000
Fault	23.0	21	5	60000

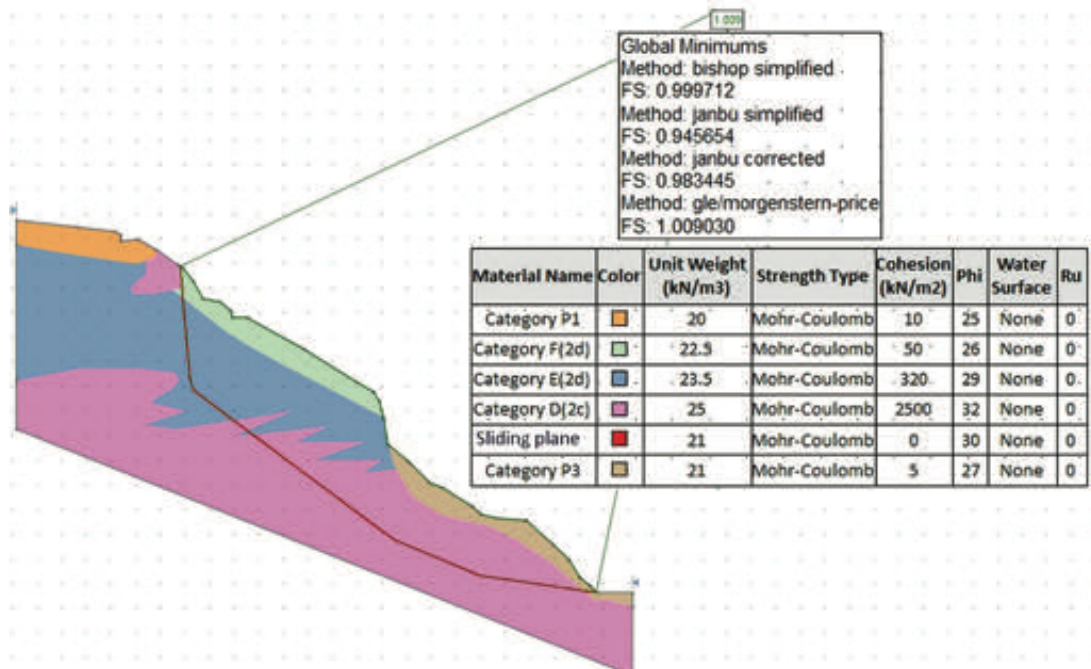


Figure 4 Results of the back-analysis conducted in Slide software.

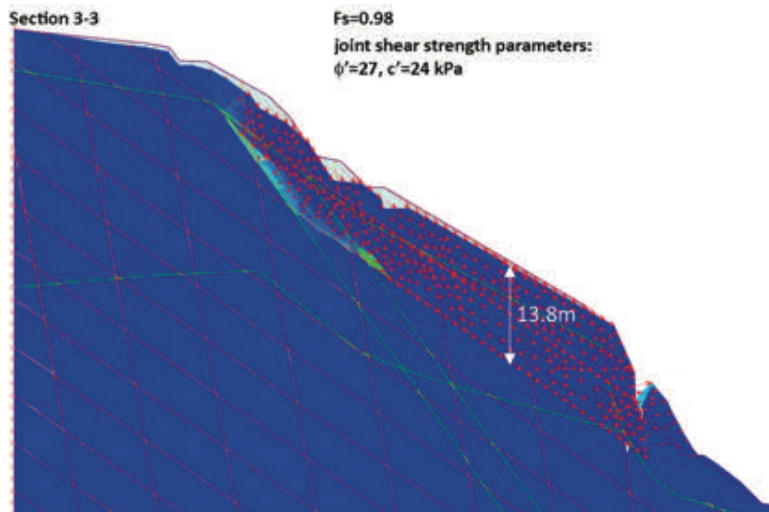


Figure 5 Results of back-analysis conducted in RS2 software.

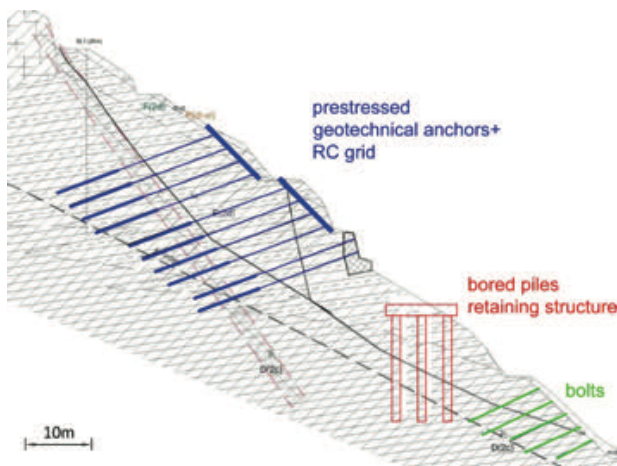


Figure 6 Cross-section with remediation measures.



Figure 7 Photo of remediation measures.

## Conclusions

Case study of a deep landslide formed in the jointed flysch sediments on the Bar-Boljare highway, Smokovac-Mateševo section, Montenegro was presented in this paper. Based on the results of geotechnical investigations, inclinometer data and numerical analysis it was concluded that the unfavourable position of discontinuities in the rock mass was a predisposing factor for the landslide occurrence. This primarily refers to the joint sets, since the orientation of stratification is relatively favourable from the aspect of slope stability, which is atypical for this zone and is rarely a case in unstable flysch slopes. Designed remediation measures are based on conducted stability analysis.

## References

- Abramson L W, Lee T S, Sharma S, Boyce G M (2001) Slope Stability and Stabilization Methods, 2nd edition, John Wiley & Sons.
- Međedović N (2019) Report on detailed geotechnical investigations for monitoring and rehabilitation of left hillside at km lk 33+280 to lk 33+420. Geoprojekt ltd, Podgorica.
- Roscience homepage, <https://www.roscience.com> [last accessed: 2021/06/14].
- You G, Mandalawi M A, Soliman A, Dowling K, Dahlhaus P (2018) Finite Element Analysis of Rock Slope Stability Using Shear Strength Reduction Method. In: Frikha W., Varaksin S., Viana da Fonseca A. (eds) Soil Testing, Soil Stability and Ground Improvement. GeoMEast 2017. Sustainable Civil Infrastructures. Springer, Cham. [https://doi.org/10.1007/978-3-319-61902-6\\_18](https://doi.org/10.1007/978-3-319-61902-6_18)
- Živaljević S, Tomanović Z, Radulović M (2021) Analysis of the triggering mechanism of landslide in the village Podi, Montenegro. Arab J Geosci. 56 (14). <https://doi.org/10.1007/s12517-020-06285-8>



## Author Index

Abolmasov, Biljana	125, 145, 237
Alcántara-Ayala, Irasema	157
Aleotti, Marco	19, 23
Apostolska, Roberta	119
Arbanas, Željko	87, 99, 171, 181, 187, 193, 201, 213, 225
Babaleku, Markel	119
Babović, Nemanja	29
Bernardi, Anna Rita	35
Bernardi, Matteo	35
Bernat Gazibara, Sanja	81, 87, 99
Berti, Matteo	35
Bezak, Nejc	7, 13, 75, 137
Bianchini, Silvia	47, 53
Biorac, Dajana	29
Blagdan, Ivana	243
Blažok, Lovro	131
Bogdanović, Snežana	145
Bojadjieva, Julijana	119
Bossi, Giulia	65, 71
Bozzoni, Francesca	119
Budimir, Vjekoslav	231
Bujišić, Miodrag	249
Calvello, Michele	165
Capparelli, Giovanna	157
Caputo, Giuseppe	35
Casagli, Nicola	53
Catelan, Filippo Tommaso	65
Cicareze, Giuseppe	19, 23, 35, 71
Confuorto, Perluigi	47, 53
Corsini, Alessandro	19, 23, 35, 71
Crescenzo, Luca	165
Critelli, Vincenzo	35
Cuomo, Sabatino	151
Čeh, Nina	171, 181, 187, 193
Damjanović, Vedran	87
Del Soldato, Matteo	47, 53
Di Meo, Antonella	119
Di Paola, Gianluigi	35
Đurić, Uroš	125, 145
Edip, Kemal	119
Festa, Davide	53
Fotopoulou, Stavroula	119
Gorin, Svemir	107
Grošić, Mirko	131, 243
Jaboyedoff, Michel	1
Jagodnik, Petra	87, 99
Jagodnik, Vedran	171, 181, 187, 193, 201, 213
Janža, Mitja	13
Jemec Auflič, Mateja	7, 13, 75, 113, 137
Jež, Jernej	13, 75, 137
Jocković, Sanja	125
Jordanova, Galena	59
Jovanovski, Milorad	107

---

Jurček, Timotej	207
Kobal, Milan	75
Kocijan, Valentina	131
Kralj, Polona	75
Krivic, Matija	113
Krkač, Martin	81, 87, 99
Krušić, Jelka	145
Kumelj, Špela	113
Lanter, Helene	231
Logar, Janko	13
Lukačić, Hrvoje	81, 87, 99
Maček, Matej	13, 207
Mair, Volkmar	71
Marcato, Gianluca	65, 71
Marjanović, Miloš D.	125, 145, 237
Marjanović, Miloš S.	125
Markelj, Anže	13
Marušić, Davor	225
Medici, Camilla	47
Međedović, Nikola	249
Mihalić Arbanas, Snježana	81, 87, 99
Mikoš, Matjaž	7, 13, 75, 137, 207, 219
Miladinović, Aleksandar	29
Milenković, Svetozar	237
Mulas, Marco	19, 23, 35, 71
Nedelkovska, Natasha	107
Novak, Ana	13
Oštir, Krištof	59
Pajalić, Sara	171, 181, 187, 193, 213
Papić, Jovan	107
Peranić, Josip	171, 181, 187, 193, 213
Peshevski, Igor	107
Peternel, Tina	13, 75, 113
Pitilakis, Dimitris	119
Plazonić, Davor	193
Radevski, Ivan	107
Radovanović, Janko	237
Raspini, Federico	53
Roduner, Armin	231
Ronchetti, Francesco	19, 23, 35
Ruiz-Cortés, Noemi Sharon	157
Schenato, Luca	71
Shalić, Radmila	119
Sheshov, Vlatko	119
Shkodrani, Neritan	119
Sinčić, Marko	81, 99
Skempas, Marinos	237
Sodnik, Jošt	13, 219
Spolverino, Gennaro	157
Steinlechner, Ronald	231
Stojmanovska, Marta	119
Strom, Alexander	41
Sušac, Maroje	225
Šegina, Ela	13, 75, 93
Šinigoj, Jasna	113
Tomanović, Zvonko	249
Tonidandel, David	71

Turković, Martina	201
Udovič, Dalibor	225
Verbovšek, Timotej	59
Vivoda Prodan, Martina	171, 181, 187, 193, 213
Volf, Ivan	243
Vrabc, Marko	59
Vugrinski, Mirjana	225
Zajec, Marjana	75
Zupa, Matija	13, 75
Žebre, Manja	75
Žibret, Gorazd	93
Živaljevič, Slobodan	249



# MONTERRA

PRVI KORAK STABILNOSTI

[www.monterra.hr](http://www.monterra.hr)


Zaštita  
od buke  
Zagrebački  
rotor

Armirano  
tlo Mineral  
Terramesh  
sustavom  
Rafinerija nafte  
Rijeka

Geotehnički  
radovi  
Pristupna  
cesta mostu  
Pelješac



# Projektiranje i stručni nadzor



Zaštite od buke  
(zidovi za zaštitu  
od buke svih  
namjena  
uključivo mjerenja  
razina buke)

Geotehničkih  
konstrukcija  
(sanacija pokosa,  
klizišta i potpornih  
zidova, zaštite  
građevnih jama)

Prometne  
infrastrukture  
(projektiranje i  
rekonstrukcija cesta  
svih razina, kružnih  
tokova, parkirnih  
površina)



Safety is our nature

**Reduce the number of inspections and increase safety at the same time with the Geobrugg GUARD.**

Developed for the toughest conditions the Geobrugg GUARD monitors your rockfall barrier, debris flow barrier, avalanche barrier or similar systems. No matter where they are.

Geobrugg GUARD provides the most important information to ensure the reliable functioning of your natural hazard mitigation measures. We supply everything - from the monitoring device to the online portal.

**More information:**

[www.geobrugg.com/guard](http://www.geobrugg.com/guard)



**Geobrugg GUARD remote monitoring**

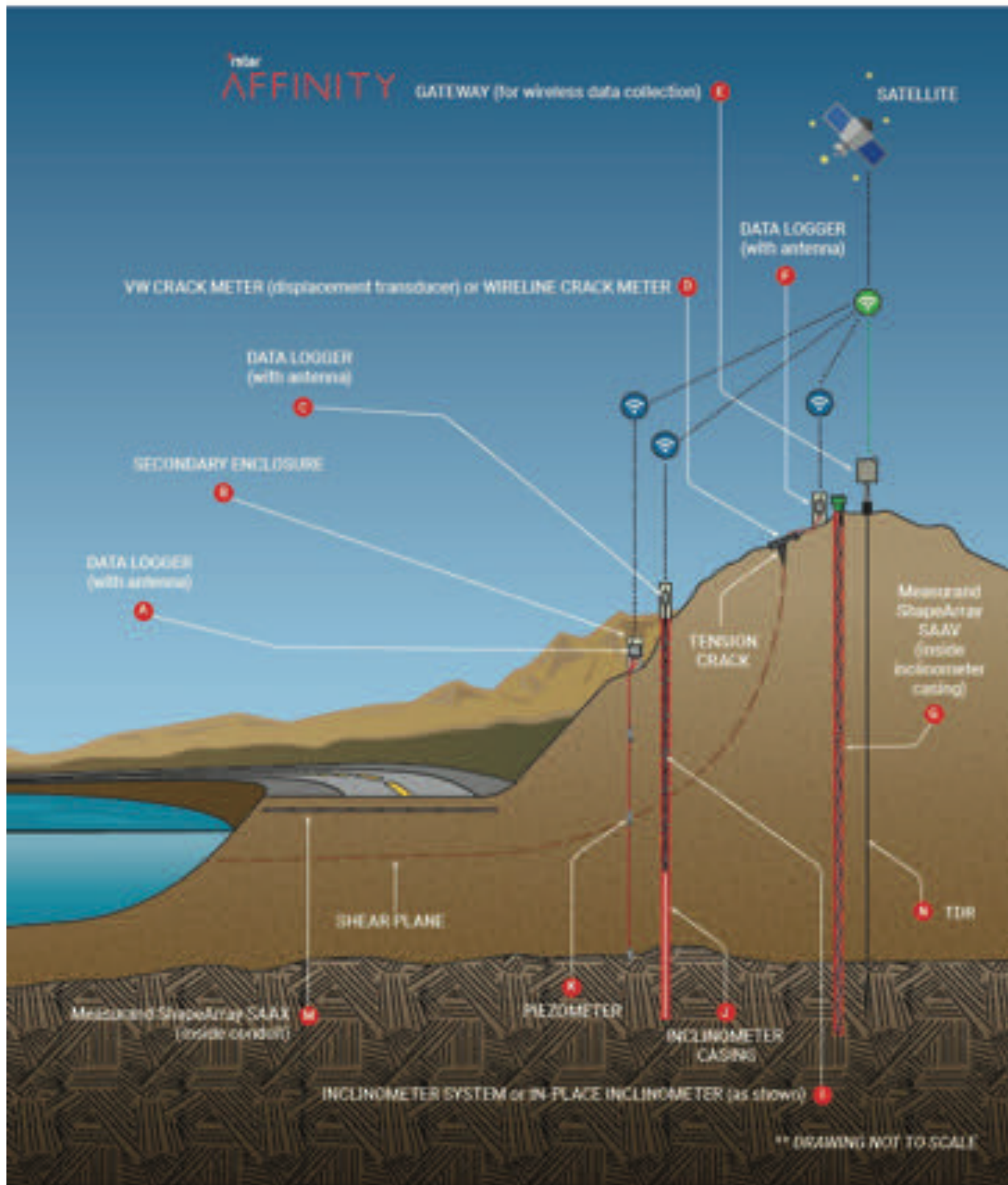
**THE GUARD STAYS WITH YOUR BARRIER - YOU STAY INFORMED**

Geobrugg AG | Aachstrasse 11  
8500 Romanshorn | Switzerland  
vjkoslov.budim@geobrugg.com  
M. +385 91 665 0845  
[www.geobrugg.com](http://www.geobrugg.com)



geotech 







## ***Proceedings of the 5th Regional Symposium on Landslides in Adriatic Balkan Region***

The Proceedings contains peer-reviewed and accepted papers submitted to the 5th Regional Symposium on Landslides in Adriatic Balkan Region. This book contains the followings:

Invited Lectures / Landslide Investigations / Landslide Monitoring / Landslide Mapping / Landslide Susceptibility / Laboratory Testing, Physical and Numerical Modelling of Landslides / Landslide case Studies / Landslide Investigations

**PhD Josip Peranić** is a postdoctoral researcher at the Faculty of Civil Engineering, University of Rijeka, Croatia. He has published several research papers in prestigious international journals, participated in a number of international conferences and contributed to several scientific research projects. His main research interests are rainfall-induced landslides and unsaturated soils. He is a lecturer in several undergraduate and graduate courses. He has received several recognitions for his scientific and educational achievements.

**PhD Sanja Bernat Gazibara** is a postdoctoral researcher at the Faculty of Mining, Geology and Petroleum Engineering, University of Zagreb, Croatia. The main subjects of her scientific research are landslide mapping, landslide susceptibility modelling, and regional analyses of rainfall-induced landslides. She was a member of several international and national scientific research projects related to landslide mapping and modelling for risk reduction. In addition, she is involved in the promotion of landslide scientific research through the organization of round tables, exhibitions and writing of popular science articles on the practical application of landslide maps in the system of spatial planning and civil protection.

**Professor Snježana Mihalić Arbanas** is Chair of ICL Network Committee and Co-coordinator of the Adriatic-Balkan Network. She is a Full Professor at the Faculty of Mining, Geology and Petroleum Engineering, University of Zagreb, Croatia. Field of her scientific work is related to engineering geology. The core subjects of her research are landslide investigation, landslide mapping, landslide susceptibility assessment and zonation. She was leader or project member in several international and national scientific research projects related to the application of landslide science for risk reduction.

**Assistant Professor Martina Vivoda Prodan** is a lecturer in several courses in graduate and undergraduate study at the Faculty of Civil Engineering, University of Rijeka. Area of her research interests are landslide remediation, landslide numerical modelling and laboratory testing of soil and rock mass with accent on ring shear test and flysch rock mass. She is involved in several scientific projects and has been contributed in many designs of geotechnical structures. She is Editor of International Journal Landslides.

**Associate Professor Martin Krkač** is a lecturer in several undergraduate and graduate courses at the Faculty of Mining, Geology and Petroleum Engineering, University of Zagreb, Croatia. The main subjects of his scientific research are landslide monitoring and remote sensing. He has been involved in several scientific projects related to landslides and in the establishment of the monitoring observatory of the biggest landslide in the Republic of Croatia, the Kostanjek Landslide in Zagreb, equipped with more than 30 geodetic, geotechnical, and hydrogeological sensors. He also contributes to the promotion of landslide scientific research through the organization of round tables, exhibitions and writing of popular science articles.

**Professor Željko Arbanas** is the Vice President of International Consortium on Landslides. He is a Full Professor of Faculty of Civil Engineering, University of Rijeka, Croatia. He is the Assistant Editor-in-Chief of International Journal Landslides. The subjects of his research are landslide investigation, physical and numerical modelling of landslides and landslide remediation. He contributed as a leader or project member in several international and national scientific research projects related to the landslide science.



University  
of Rijeka  
**Faculty of  
Civil Engineering**



University of Zagreb  
**FACULTY OF MINING,  
GEOLOGY AND PETROLEUM  
ENGINEERING**

